THE ROLE OF THE PROTEOGLYCANS OMD AND PRELP IN THE MAINTENANCE OF BRAIN VASCULATURE

By Hongorzul Davaapil

Thesis submitted to University College London

for the degree of Doctor of Philosophy

2017

UCL Institute of Ophthalmology

Faculty of Brain Sciences

Declaration

I, Hongorzul Davaapil, confirm that the work presented in this thesis is my own and does not exceed 100,000 words. Where information has been derived from other sources, I confirm that this has been indicated in the thesis.

Abstract

OMD and PRELP are proteoglycans belonging to the family of small leucine-rich repeat proteoglycans (SLRPs), whose members have been shown to modulate a variety of cellular processes, including migration, proliferation and differentiation. Abrogated expression of SLRP members has been linked to a multitude of developmental, age-related and inflammatory diseases. Previous work from the Ohnuma lab has shown that OMD and PRELP are strongly expressed in brain vasculature, and in this study, I aim to extend the understanding of OMD and PRELP in the context of vascular homeostasis.

The cellular localisation of OMD and PRELP was investigated and I determined that OMD is weakly expressed in neurons, whereas PRELP is expressed in pericytes, vascular smooth muscle cells, microglia and ependymal cells. I have shown that there is vascular dysfunction in PRELP$^{-/-}$ mice. There is increased blood vessel content in the brain, accompanied by blood brain barrier (BBB) breakdown. Analysis of BBB components indicates basement membrane components laminin and perlecan are down-regulated in addition to coverage by pericytes and astrocyte end-feet. PRELP$^{-/-}$ mice also exhibit weakened adherens- and tight-junctions between endothelial cells. I have determined that OMD$^{-/-}$ brain vasculature is comparable to that of wild-type.

I propose that PRELP has a role in maintaining vascular function. PRELP may modulate the stability of the BBB by acting as a bridging molecule for basement membrane proteins.

Acknowledgements

First, I would like to thank my supervisor, Prof Shin-Ichi Ohnuma, for the opportunity to undertake my PhD in his laboratory and for the support, patience and guidance over the past three years.

I would also like to extend my thanks to the members of the Ohnuma laboratory and the staff at the institute. A special thanks goes to Prof Stephen Bolsover for all his help with mouse experiments. I would like to thank Drs Noriaki Sasai, Ryohei Sekido and Patric Turowski for their scientific discussion and guidance. I am also grateful for the staff at the Pathology department – particularly David Essex and Hodan Jama for their help with cutting and staining tissue sections. Advice and guidance from Drs Matt Hayes and Peter Munro with regards to imaging using the confocal microscope have also been invaluable.

Further thanks goes to all of my friends who have supported me. To my friends at the institute – Brett, Moe, Megumi and Tomoko – talking with them has always lifted my spirits. A special thanks to Yan-Kay, Emma and Jeegar for their lasting friendship. Lastly, to my wonderful boyfriend Mark who is always there to cheer me up (and offer on-demand IT support).

Finally, I would like to thank my family. To my brother who has always been the rock in my life and always offers me very matter-of-fact advice. To my mother without whom any of this would be possible – through her hard work, she created the opportunity for me to pursue my dreams and ambitions.

Table of Contents

List of Figures

Chapter 1

Chapter 2

Chapter 3

Chapter 4

Chapter 5

Chapter 6

Appendix

List of Tables

Chapter 1

Chapter 2

Chapter 3

Chapter 4

Chapter 5

Chapter 6

Abbreviations

aco	Anterior commissure
alv	Alveus
AMD	Age-related macular degeneration
Ang	Angiopoetin
AQ	Cerebral aqueduct
AQP4	Aquaporin-4
arb	arbor vitae
BBB	Blood-brain barrier
BM	Basement membrane
BMP	Bone morphogenetic protein
BP	Biological process
BS	Brain stem
CA	Ammon's horn
CAM	Cellular adhesion molecule
CB	Cerebellum
CC	Cellular component
cc	Corpus callosum
chpl	Choroid plexus
CM	Conditioned media
CMV	Cytomegalovirus
CNS	Central nervous system
CNU	Cerebral nuclei
CP	Caudoputamen
CS	Chondroitin sulphate
CTX	Cortex
DAVID	Database for Annotation, Visualization and Integrated Discovery
DG	Dentate gyrus
Dll4	Delta-like 4
DS	Dermatan sulphate
ECM	Extracellular matrix
EGF	Epidermal growth factor
EHS	Englebreth Holm-Swarm
ENCODE	Encyclopedia of DNA Elements
ERANGE	Enhanced Read Analysis of Gene Expression
FAK	Focal adhesion kinase
FDG	Fluorescein di-β-D-galactopyranoside
FDR	False discovery rate
FGF	Fibroblast growth factor
FoxO1	Forkhead box factor
FPKM	Fragments Per Kilobase of transcript per Million mapped reads
fr	Fasciculus retroflexus
fx	Fornix
GAG	Glycosaminoglycan
GDNF	Glial-derived neurotrophic factor
GO	Gene ontology
gr	Granular
GSEA	Gene Set Enrichment Analysis
H&E	Haematoxylin and Eosin
HA	Hyaluronan
HEK	Human embryonic kidney
HIP	Hippocampus
HS	Heparin/heparan sulphate
HSPG	Heparan sulphate proteoglycan
HUVEC	Human umbilical vein endothelial cell
HY	Hypothalamus
IB	Immunoblotting

ICAM	Intercellular adhesion molecules
ICC	Immunocytochemistry
Ig	Immunoglobulin
IgG	Immunoglobulin G
IHC	Immunohistochemistry
Ihh	Indian hedgehog
int	Interal capsule
IP	Immunoprecipitation
IP	Intraperitoneal
IUM	Initially unmapped reads
IV	Intravenous
JAM-A	Junctional Adhesion Molecule-A
KEGG	Kyoto Encyclopedia of Genes and Genomes
KS	Keratan sulphate
LB	Luria broth
LDL	Low density lipoprotein
lot	Lateral olfactory tract
LPS	Lipopolysaccharide
LRR	Leucine-rich repeat
LV	Lateral ventricle
LVES	Large vessel endothelial supplement
MAS5	MicroArray Suite 5.0
MB	Midbrain
MBEC	Mouse brain endothelial cell
MSigDB	Molecular Signatures Database
MEF	Mouse embryonic fibroblast
MF	Molecular function
MM	Mismatch
mo	Molecular
MO	Motor area
MOp	Primary motor area
MUG	4-Methylumbelliferyl-β-D-galactopyranoside
MY	Medulla
NT	N-terminal
NVU	Neurovascular unit
OCT	Optimal cutting temperature
OLF	Olfactory region
OMD	Osteomodulin
ON	Optic nerve
opt	Optic tract
ORB	Orbital area
PBS	Phosphate-buffered saline
PDGF	Platelet-derived growth factor
PFA	Paraformaldehyde
PIGF	Placental growth factor
PIR	Piriform area
PM	Perfect match
po	Polymorph
PR	Proline and arginine
PRELP	Proline/arginine-rich and leucine rich protein
RINe	RNA integrity number
RMA	Robust Multi-Array Average
RNA seq	RNA sequencing
ROI	Region-of-interest
RT	Room temperature
SAM	Significance Analysis of Microarray
SEA	Sea urchin sperm protein-enterokinase-agrin
SEM	Standard error of the mean
Shh	Sonic hedgehog

SLRP	Small leucine-rich repeat proteoglycan
sm	Stria medullaris
Smo	Smoothened
SVP	Subventricular vascular plexus
TBS	Tris-buffered saline
TEER	Trans-endo/epithelial resistance
TGF	Transforming growth factor
TH	Thalamus
TLR	Toll-like receptor
TNF	Tumour necrosis factor
V3	Third ventricle
V4	Fourth ventricle
VCAM	Vascular cell adhesion molecules
VEGF	Vascular endothelial growth factor
vSMC	Vascular smooth muscle cell
ZO	Zonula occludens

Chapter 1 General Introduction

1.1 Preface

This PhD project investigates the role of extracellular proteoglycans OMD and PRELP in brain vasculature. These proteins belong to the small leucine-rich repeat proteoglycan (SLRP) family, whose members are implicated in regulating a variety of cellular processes, including angiogenesis. While other members of the SLRP family have been extensively studied, not much is known about OMD and PRELP, particularly regarding their role on vascular homeostasis. Following a description of the extracellular matrix, I will discuss the vascular system, the blood-brain barrier, SLRPs, current findings regarding OMD and PRELP and finally the aims of this project.

1.2 The extracellular matrix (ECM)

1.2.1 The extracellular matrix (ECM)

The extracellular matrix (ECM) is the 3-dimensional structure that surrounds cells. It is a network composed of a variety of macromolecules falling into two main classes –fibrous proteins and proteoglycans (Alberts et al., 2002), providing not only structural support for cells, but also creating a microenvironment conducive to tissue function.

Fibrous proteins, which include collagen, elastin and fibronectin have structural and adhesive functions, and are embedded within the hydrated polysaccharide microenvironment of proteoglycans. For example, collagens are abundant fibrous proteins and are a critical component of the ECM. Three collagen polypeptides, known as α-chains, form a long and sturdy triple-helix structure. Collagen fibrils form scaffolding for the binding of other proteins in addition to contributing to structures meant to resist tensile forces (Alberts et al., 2002).

Proteoglycans are proteins modified with sugar sidechains and consist of a protein core with covalently-bound glycosaminoglycan (GAG) chains. GAGs are long linear polysaccharides consisting of a repeating disaccharide unit, containing an amino sugar and a uronic acid or galactose (Esko et al., 2009), illustrated in Figure 1.1. As a result, GAGs are highly polar and can bind water. Glycosylation of the protein core occurs in the Golgi apparatus, and the modified protein is subsequently inserted into the plasma membrane or secreted into the ECM (Esko et al., 2009). GAGs include hyaluronan (HA), dermatan sulphate (DS), keratan sulphate (KS), chondroitin sulphate (CS), heparin and heparan sulphate (HS).

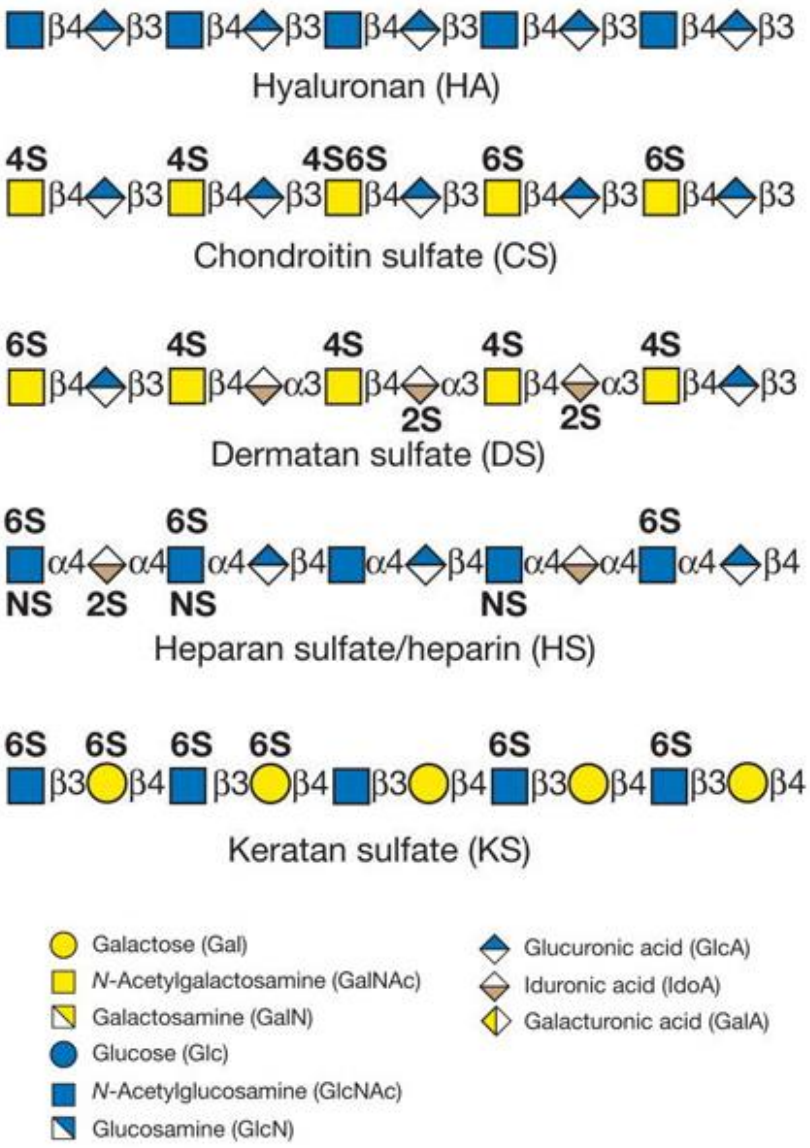

Figure 1.1. Structure of GAG polymers. Figure modified from (Esko et al., 2009).

ECM composition dictates the physical properties of the tissue and the activity of cells. It is a highly dynamic structure, and in addition to playing a structural role, it is an important regulator of cell and tissue behaviour by modulating signalling events. The ECM influences a variety of cellular processes, including differentiation, proliferation, survival, cell-cell communication, adhesion and migration (Alberts et al., 2002; Lu et al., 2011). Therefore, changes in the structure and/or composition of the ECM could lead to de-regulation of these biological processes and affect tissue homeostasis.

1.2.1.1 Cell adhesion

Cells adhere to the ECM via cell-surface adhesion receptors and these interactions are mainly mediated by integrins. Integrins are heterodimers formed by α- and β-subunits, which are both single-pass transmembrane proteins. They bind to ECM components, such as collagens, laminins and fibronectins, or adjacent cells to promote cell adhesion, migration over the ECM, differentiation and proliferation (Alberts et al., 2002; Harburger & Calderwood, 2009). Integrins are capable of bi-directional signalling; i.e. "outside-in" and "inside-out". They make connections to the actin cytoskeleton; after binding to its extracellular ligand, the cytoplasmic domain of the β-subunit binds to several intracellular anchor proteins, notably talin, α-actinin and filamin (Brakebusch & Fässler, 2003). These outside-in signalling functions lead to clustering of integrin receptors to ECM components to form nascent structures known as focal complexes (Nobes & Hall, 1995). These focal complexes can then mature and form larger structures – focal adhesions (C. Wu, 2007).

In addition to mechanical functions, outside-in signalling relays information to the cells regarding its environment, adhesive state and the composition of the ECM, and regulates processes such as migration, differentiation and motility. Early observations indicated that attachment to the ECM could also affect gene expression, even in the absence of growth factors (Haskill et al., 1988; Lee et al., 1984). It is now known that integrin signalling leads to mobilisation of actin and initiation of signalling cascades by activation of a non-receptor tyrosine kinase, focal adhesion kinase (FAK). Phospho-FAK in turn then phosphorylates other proteins to activate a variety of signalling pathways, including the Akt and MAPK pathways, as illustrated in Figure 1.2 (Berrier & Yamada, 2007).

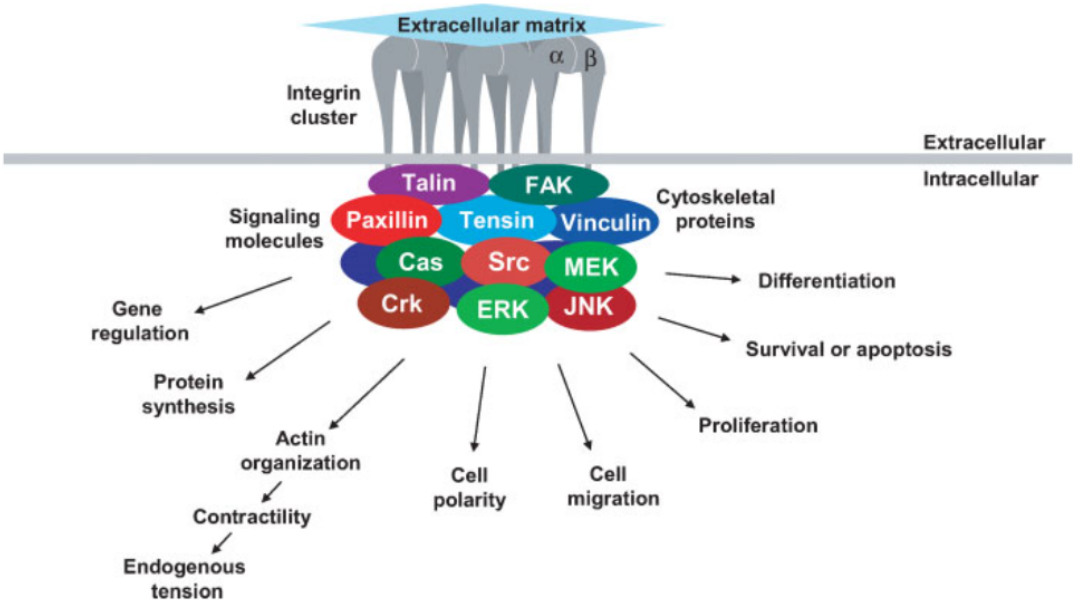

Figure 1.2. Schematic of the signalling pathways activated by integrins. Cytoplasmic components of integrin signalling recruit molecules to mediate other signalling pathways. Figure from (Berrier & Yamada, 2007).

Of particular interest to this study is the ability of integrins to regulate angiogenesis. Early studies of FAK signalling in endothelial cells demonstrated that there is an increase in the activation of FAK in migrating endothelial cells in an *in vitro* wound healing assay (Romer et al., 1994). FAK is strongly expressed in the vasculature during development (Polte et al., 1994), and FAK knock-out mice die *in utero* due to cardiovascular complications (Ilić et al., 1995). Evidence suggests that angiogenic growth factors regulate FAK; for example, there is increased association of FAK with PI3K upon vascular endothelial growth factor (VEGF) signalling through its receptor (VEGFR2) (Qi & Claesson-Welsh, 2001) and angiopoetin-1 signalling also induces FAK phosphorylation (Kim et al., 2000).

Integrins are therefore critical for the attachment of cells to the ECM but can also modulate a variety of signalling pathways and processes, including embryonic development, tissue repair and immunity.

1.2.2 Basement membrane

The basement membrane (BM) is a specialised flexible sheet of ECM proteins which separates cell monolayers, i.e. epithelia or endothelia, from surrounding connective tissues. The vascular BM is mainly composed of cross-linked laminin and type IV collagen, which are capable of self-assembly (Yurchenco & Ruben, 1987; Yurchenco et al., 1986). These insoluble laminin-collagen IV polymers are bound by nidogens (formerly known as entactins), aiding the structural integrity of the BM (Figure 1.3). Collagen IV triple helices

and laminin heterotrimers are assembled in the Golgi and transported to the ECM by vesicular transport along with perlecan and nidogen (LeBleu et al., 2007).

This solid matrix prevents cells from traversing the basement membrane. In addition, highly-hydrated proteoglycans such as perlecan and agrin, which contain HS GAGs, increase the volume of the BM and can attract and bind to growth factors. Other minor components of the BM, including different types of collagens, SPARC/osteonectin and agrin, confer its tissue specificity, however the core matrix composed of laminin, collagen and nidogen remains the same (LeBleu et al., 2007).

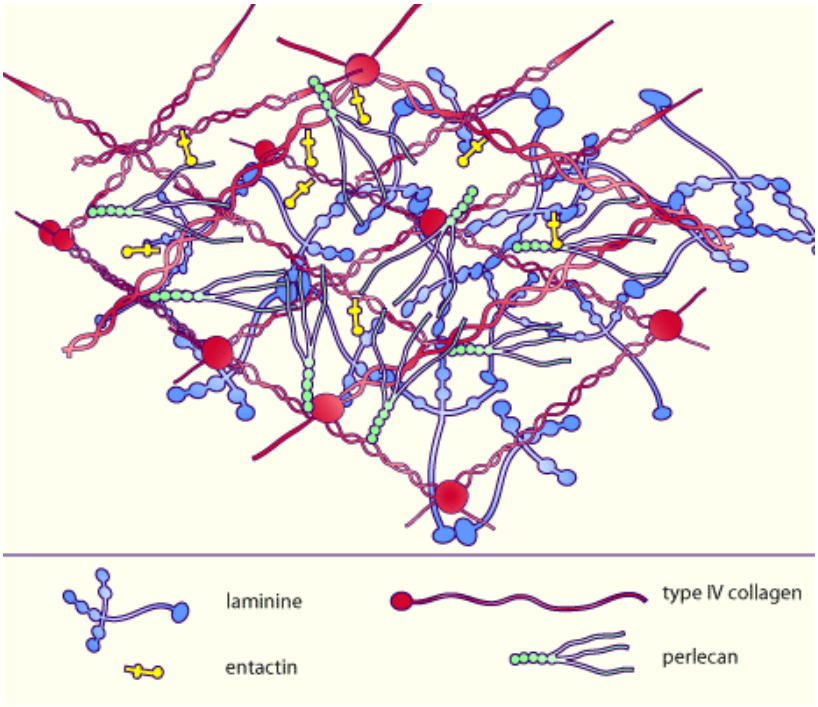

Figure 1.3. Structure of the BM. The BM is composed of laminin and collagen IV linked by nidogen (a.k.a. entactin) and perlecan. Image from the Université de Fribourg.

Initially thought to solely function as structural support, it is now known that the BM has a variety of functions. During development, the BM aids in the organisation of cell monolayers during tissue development; indeed knock-out mice for BM components often exhibit embryonic haemorrhaging (Costell et al., 1999; Gould et al., 2005; Thyboll et al., 2002). The BM can also sequester growth factors and store them until they are required; for example, proteoglycans containing HS chains in the BM bind to these growth and differentiation factors and create reservoirs (Bonnans et al., 2014). VEGF is a HS-binding, pro-angiogenic ligand which is stored in the BM of the vasculature and its bio-availability can be regulated by ECM proteases such as matrix metalloproteinases (MMPs) (Lee et al., 2005). Other sequestered growth factors include epidermal growth factor (EGF),

fibroblast growth factor (FGF), Wnts and transforming growth factor-β (TGF-β) (Bonnans et al., 2014), which are involved in growth, adhesion, cell division and differentiation.

1.2.2.1 Collagen

Collagen is the most abundant protein in mammals, making up 25% of all protein mass (Alberts et al., 2002). As mentioned above, collagen α-chains are wound around each other to form a triple-helix structure. They can be classified as fibrillar, fibril-associated and sheet-forming collagens. Collagen IV, composed of two α1- and one α2-chains, is the only sheet-forming collagen and is unique to the basement membrane (Alberts et al., 2002). Deletion of both α1 and α2 chains in mice led to relatively normal development up until E9.5; in addition, the deposition of BM proteins, such as laminins and nidogens, was not perturbed. However, around E10.5-11.5, embryos died due to defects in the basement membrane (Poschl et al., 2004).

While collagen IV sheets are a major constituent of the BM, collagens XV and XVIII are minor constituents (Amenta et al., 2005; Halfter et al., 1998). Collagen XV is thought to stabilise the BM; study of *Col15a1* knock-out mice indicated that although mice developed and mated normally, they exhibited collapsed capillaries and endothelial cell degeneration. In addition, exercise aggravated this phenotype to mimic early heart disease (Eklund et al., 2001). Collagen XVIII is unusual as it contains HS side-chains (Halfter et al., 1998). Analysis of *Col18a1* knock-out mice indicated that they developed hydrocephalus and dilation of the brain ventricles, due to abnormal thickening of the choroid plexus BM, indicating that collagen XVIII is important for the structural integrity of the BM (Utriainen et al., 2004).

A variety of proteins, including SLRPs bind to collagen, and are discussed below in Section 1.5.1 .

1.2.2.2 Laminin

Laminins are major constituents of the BM. Aside from collagen IV, which makes up approx. 50% of the BM, it is the most abundant protein in the BM (LeBleu et al., 2007). They provide structural rigidity due to cross-linking with collagen IV, but also have roles in a variety of processes including adhesion, differentiation and migration. They are large heterotrimeric proteins composed of three chains: α, β and γ (Figure 1.4); these chains are joined together by hydrophobic interactions of their coiled-coil domains (Beck et al., 1993).

Each protein chain has distinct isoforms, creating a large diversity of laminin proteins. Although the 12 mammalian chains can theoretically form 60 different trimeric proteins,

only 16 distinct combinations have been identified *in vivo* (Domogatskaya et al., 2012); this is likely due to charged residues in the coiled-coil region restricting the number of possible heterotrimers. Laminin heterotrimers are named after the constituent α, β and γ chains; for example, laminin-511 is composed of α5, β1 and γ1 chains. While the α subunits are mainly responsible for interactions with receptors and therefore can be considered to be have a more functional role, β and γ subunits have a more structural function (Durbeej, 2010).

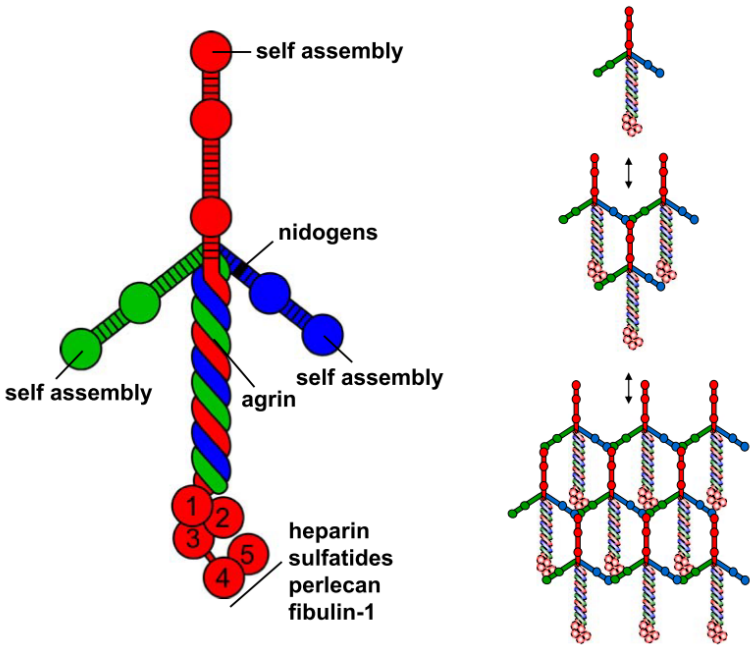

Figure 1.4. Structure and assembly of laminin heterotrimers. α-chains (red) mediate most of the interactions with receptors and other components of the BM, whereas β-chains (green) and γ-chains (blue) are mostly structural and aid in laminin self-assembly. Figure from (Durbeej, 2010).

Knock-out mouse models for different laminin subunits have shed light on the variety of functions of laminins. For example, laminin-α5 is the most abundant laminin, and its deletion caused several developmental defects in the neural tube, kidney and vasculature. Knock-out mice for more tissue-specific subunits survive until birth, but reveal defects in skeletal muscle, peripheral nerves, neuromuscular synapse and kidney glomerulus (Miyagoe et al., 1997; Noakes et al., 1995; Noakes et al. 1995b; Wallquist et al., 2005). In particular, deletion of laminin α4, which is enriched in vascular basement membranes, leads to defects in the microvasculature, notably leakage and disorganised vessels when investigated using the corneal angiogenesis model (Thyboll et al., 2002). While the mice were born with heavy haemorrhages seen in a variety of tissues, these defects disappeared in the adults possibly due to compensation by other laminin α chains. The authors performed a cornea angiogenesis assay (Rogers et al., 2007), where a pellet containing FGF-2 was inserted in the normally avascular cornea and the formation of

blood vessels assessed. The resulting vasculature was extremely leaky, indicating that laminin α4 has a role in vessel formation and maturation.

To my knowledge, there are three studies examining the effect of laminin isoform deletion in the context of the blood-brain barrier (BBB). One study examined knock-out of laminin α2 (*Lama2*$^{-/-}$), which would normally form the laminin-211 secreted by astrocytes and pericytes in the BBB (Menezes et al., 2014). *Lama2*$^{-/-}$ mice exhibit significant vascular permeability, pericyte loss, loss of astrocyte end-foot polarity and reduced tight junctions between endothelial cells. Yao and colleagues created an astrocyte-specific knock-out of laminin γ1 by crossing homozygous floxed laminin g1 (F/F) mice with Nestin-Cre transgenic mice. The resulting animals exhibit BBB dysfunction very similar to *Lama2*$^{-/-}$ mice (Yao et al., 2014). Finally, pericyte-specific ablation of laminin γ1 also resulted in BBB defects (Gautam et al., 2016), although the effects were notably more mild than in the laminin α2 knock-out and astrocyte-specific laminin γ1 knock-out. These studies strongly indicate that laminin is a critical component of the BBB.

1.2.2.3 Nidogen

In vertebrates, the nidogen family consists of two proteins, nidogen-1 and nidogen-2, which are sulphated monomeric glycoproteins present in BMs. Nidogens have three globular domains, denoted as G1-3, connected by linker regions; while the globular domains of nidogen-1 and nidogen-2 are quite similar, the differences occur in these linker regions (Ho et al., 2008). They bind a variety of proteins in the ECM, including collagen IV, laminin and perlecan and stabilise the structure of the BM. For example, nidogen and nidogen-laminin complexes have been shown to bind to collagen IV *in vitro*, whereas laminin alone could not (Aumailley et al., 1989). Nidogen was also shown to be able to bind to collagen IV, and together, nidogen was found to be required for the formation of the ternary complex formed of collagen IV, laminin and nidogen (Aumailley et al., 1993).

1.2.2.4 Perlecan

Perlecan is an extremely large secreted multi-domain HS-proteoglycan (HSPG) found in all BMs (Iozzo, 1998). It is composed of five connected domains with distinct folding modules, and its overall structure has been likened to train cars (Cabello et al., 2010) (Figure 1.5). Domain I contains the three attachment sites for HS GAG chains and the sea urchin sperm protein-enterokinase-agrin (SEA) module (Dolan et al., 1997). Domain II is homologous to the low-density lipoprotein (LDL) binding region of the LDL receptor and is capable of binding to calcium and LDL (Costell et al., 1996). Domain III contains laminin

B and EGF domains which act as substrates to integrins to promote cell adhesion (Chakravarti et al., 1995). Domain IV contains three immunoglobulin (Ig)-like domains (Hopf et al., 1999); these domains are typically found in cell adhesion molecules (Crossin & Krushel, 2000). Finally, domain V contains laminin and EGF-like repeats. In addition, it also has an alternate attachment site for a fourth HS GAG (Friedrich et al., 1999). Proteolytic cleavage of perlecan domain V releases an anti-angiogenic protein known as endorepellin which was found to inhibit several aspects of angiogenesis, discussed below (Mongiat et al., 2003).

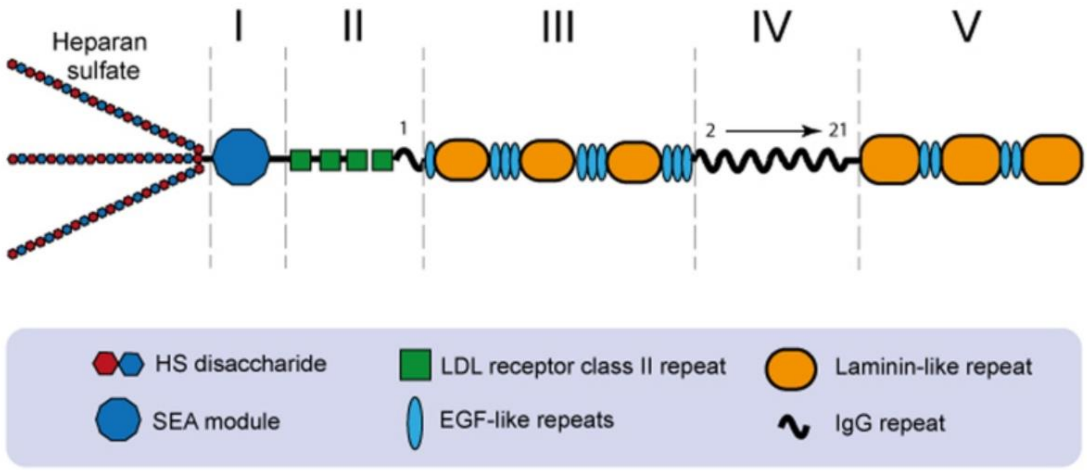

Figure 1.5. Perlecan is a multi-domain protein with HS chain covalently attached to Domain I. Figure from (Douglass et al., 2015).

Perlecan has been shown to bind to various ECM proteins through its HS chains and core protein, where a few examples are outlined in Table 1.1. Binding of perlecan to BM proteins laminin, nidogen and collagen IV has been shown to provide stabilising interactions. As explained above, since the BM is formed of two lattices formed by collagen IV and laminin which are brought together by nidogens, perlecan binds to all major BM constituents and stabilises the overall structure. Perlecan knock-out mice die *in utero* and perinatally due to defects in the BM (Costell et al., 1999). While the majority of BMs are relatively normal in knock-outs, tissues which incur mechanical stress, such as the myocardium, are strongly affected and embryos or neonates die of haemorrhaging. More recent studies involved the rescue of perlecan knock-out mice by restoring cartilage perlecan to circumvent embryonic and perinatal lethality. One study found that perlecan is essential for the vascularisation of endochondral bone (Ishijima et al., 2012), while others have found that the depletion of perlecan resulted in decreased levels of nitric oxide synthase leading to reduced endothelial relaxation in the aorta (Nonaka et al., 2015).

Perlecan has three to four HS chains and has been shown to bind to growth factors such as bFGF and VEGFA-165 (Table 1.1). HSPGs are also capable of binding growth factors at low affinity and presenting them to high-affinity cell-surface receptors (Klagsbrun & Bairdt, 1991), essentially acting as a co-receptor. This interaction was found to be vital, as removing or blocking HS proteoglycans ablated FGF signalling, despite the presence of high-affinity FGF receptors (Rapraeger et al., 1991; Yayon et al., 1991). Therefore, in addition to having a structural role to stabilise the BM, perlecan can also bind to growth factors and influence cellular processes.

Domain	Binding partner	Reference
I (HS)	Laminin	(Ettner et al., 1998)
I (HS)	PRELP	(Bengtsson et al., 2002)
I (HS)	VEGFA-165	(Zoeller et al., 2009)
I (HS)	bFGF	(Whitelock et al., 1999)
IV	Collagen IV	(Hopf et al., 1999; Whitelock et al., 1999)
IV	Laminin	(Hopf et al., 1999)
IV	Nidogen-1	(Hopf et al., 1999)
IV	Nidogen-2	(Hopf et al. 1999)
IV	Fibronectin	(Hopf et al., 1999)
V	α2β1 integrin	(Bix et al., 2004)
V	α5β1 integrin	(Nyström et al., 2009)

Table 1.1. Examples of perlecan binding partners.

Due to its multi-domain structure, perlecan has a multitude of roles, including cell adhesion and migration, lipid metabolism, cartilage homeostasis and angiogenesis (Douglass et al., 2015). In the context of angiogenesis, perlecan has two opposing roles. The complete perlecan protein is capable of binding to growth factors and modulating signalling. For example, perlecan was shown to regulate developmental angiogenesis via the VEGFA/VEGFR2 signalling axis (Zoeller et al., 2009). In addition, perlecan was able to stimulate angiogenesis by itself in the rabbit ear model for angiogenesis via bFGF (Aviezer et al., 1994). As alluded to above, perlecan also has anti-angiogenic ability; cleavage of domain V by Cathepsin L (Cailhier et al., 2008) results in the release of endorepellin which has been shown to have strong inhibitory effects on angiogenesis. Since endorepellin is derived from perlecan, its distribution is similar to that of perlecan.

Studies indicate that endorepellin acts to destabilise focal adhesions by binding to the collagen receptor α2β1 integrin resulting in sustained activation of FAK and ultimately

the disassembly of actin stress fibres and focal adhesions (Bix et al., 2004). Endorepellin can also bind to VEGFR1 and VEGFR2 in a discrete location separate from the VEGFA binding site (Goyal et al., 2011, 2012). As a result, endorepellin exerts regulatory effects on the Akt and JNK pathways. Finally, endorepellin has been shown to be pro-angiogenic after ischaemic stroke due to the lack of anti-angiogenic α2β1 integrin and the presence of pro-angiogenic α5β1 integrin receptor on endothelial cells (B. Lee et al., 2011), highlighting the complex role of perlecan and endorepellin in modulating angiogenesis.

1.3 The vascular system

1.3.1 Structure and function of blood vessels

The vascular system is a continuous network composed of blood vessels of differing sizes and structure depending on their function with the aim of transporting oxygen and nutrients in blood throughout the body (Figure 1.6). Arteries carry blood away from the heart, whereas veins carry blood back to the heart. Smaller arteries and veins are called arterioles and venules respectively, which then become capillaries enabling the exchange of nutrients and oxygen from the blood to tissues.

Endothelial cells under the BM form the inner lining of the vessel, and are surrounded by a type of mural cell; vascular smooth muscle cells (vSMCs) or pericytes (Ozerdem et al., 2001). Endothelial cells and mural cells secrete proteins which form the BM (Brachvogel et al., 2007; Gospodarowicz et al., 1981; Yousif et al., 2013). In addition to providing rigidity and structure to the vasculature, the BM also provides a platform onto which other cells can attach (Yurchenco, 2011).

Arteries and veins are the largest vessels; here, the endothelial cells are surrounded by vSMCs which form multiple concentric layers (Gaengel et al., 2009). There are additional layers of ECM depositions, the intima, separating endothelial cells and vSMCs. vSMCs regulate the vascular tone and contraction of these larger vessels, ultimately affecting blood flow.

In contrast, smaller vessels, capillaries, are composed solely of endothelial cells, surrounded by pericytes embedded within the basement membrane (Ozerdem et al., 2001). Pericytes are actively-signalling mural cells. They have roles in angiogenesis, maintenance of the blood-brain barrier, endothelial cell regulation, vessel stabilization and clearance of toxic products (Armulik et al., 2011).

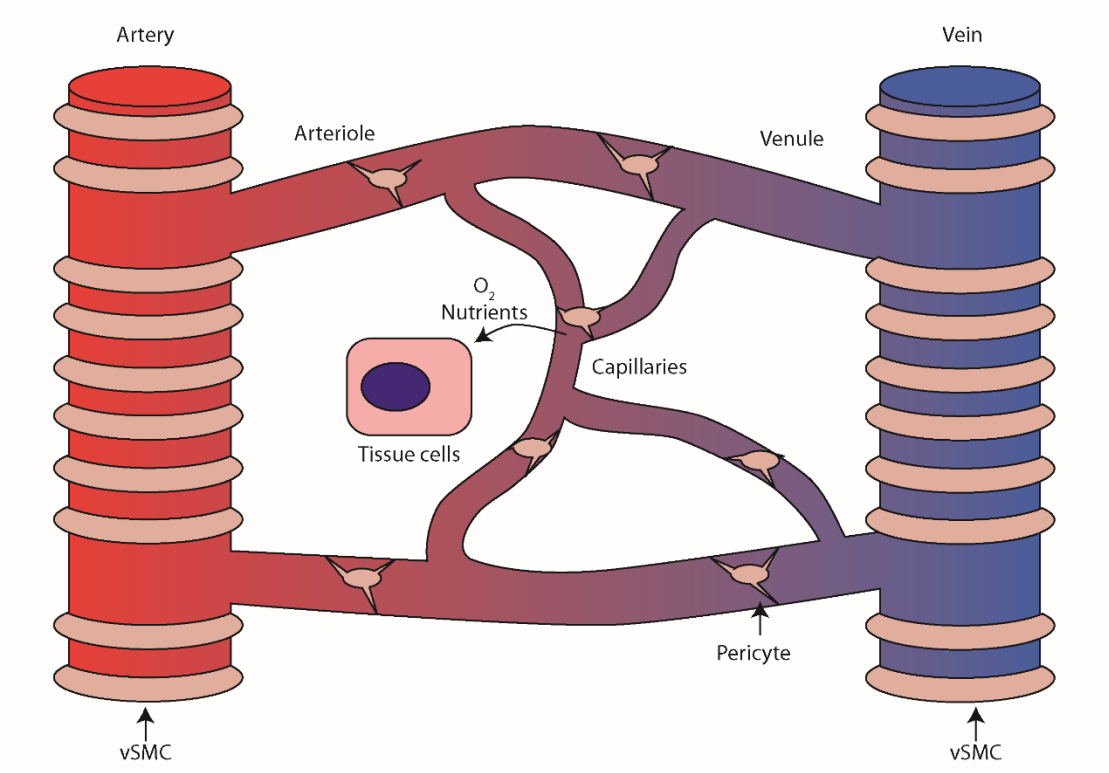

Figure 1.6. The vascular network is composed of larger arteries and veins and smaller arterioles, venules and capillaries. Arteries and arterioles contain oxygenated blood, whereas veins and venules carry deoxygenated blood back to the heart. Capillaries provide O_2 and nutrients to tissues.

1.3.1.1 Pericytes

Pericytes are mural cells associated with capillaries. Pericytes are embedded within the endothelial cells' BM and have a distinctive morphology: the cell body is round with an accompanying round nucleus and they also have processes which envelop blood vessels (Figure 1.7). Pericytes and endothelial cells are mostly separated by the shared BM, however there are discrete peg-socket type contacts (Armulik et al., 2011) which contain both gap (Cuevas et al., 1984) and N-cadherin-rich adherens junctions (Gerhardt et al., 2000). A single pericyte often contacts several endothelial cells through its cell processes. Pericytes not only provide structural support and regulate blood flow but also regulate angiogenesis, vessel permeability and maturation (Armulik et al., 2011; Bergers & Song, 2005).

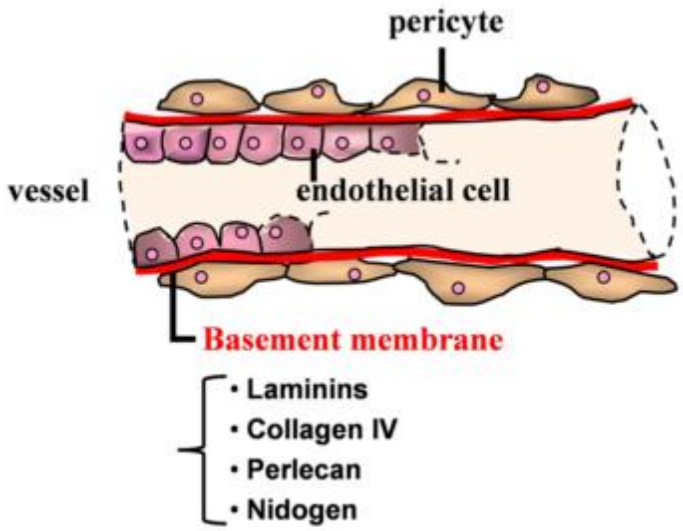

Figure 1.7. Pericytes are embedded in endothelial BM in microvasculature. Image from (Simon-Assmann et al., 2011).

The signalling events between pericytes and endothelial cells are crucial in maintaining healthy vasculature. Platelet-derived growth factor-B (PDGF-B) signalling has been shown to be required for pericyte recruitment to newly-formed blood vessels. PDGF-B secreted from angiogenic endothelial cells and binds to PDGF receptor-β (PDGFR-β) located on pericytes; this leads to proliferation and migration of pericytes along the growing vessel until PDGFR-β is down-regulated as the vessels progress into maturation (Armulik et al., 2005). Binding of PDGF-B to its receptor causes phosphorylation at tyrosine residues and the subsequent recruitment of mediators of a variety of pathways, including MAPK, Akt, PLCγ and Stats, leading to the activation of genes related to growth and motility (Heldin & Westermark, 1999).

A variety of knock-out mice, including *pdgfb* (Levéen et al., 1994; Lindahl et al., 1997), *pdgfr-β* (Soriano, 1994) and endothelium-specific conditional knock-out for *pdgfb* (Bjarnegård et al., 2004), have demonstrated that these signalling events are crucial; the knock-out animals die just before or shortly after birth. They all have very similar phenotypes, notably a lack of pericytes, vascular permeability and haemorrhage owing to the failing recruitment of pericyte progenitor cells.

PDGF-B expression along the endothelium is mainly localised in tip cells, rather than stalk cells (Gerhardt et al., 2003). Once endothelial cells secrete PDGF-B, a motif in the C-terminal, known as the retention motif, binds to HSPG (Ostman et al., 1991). As explained above, a mouse model for the deletion of this retention motif leads to pericyte loss (Lindblom & Gerhardt, 2003); however the phenotype is not as severe as in PDGFR-β or PDGF-B knockouts, as the retention motif mutants are viable. Notably, the authors

frequently observed partially-detached pericytes, highlighting the importance of the correct localisation and tethering of the PDGF-B ligand to the BM in pericyte recruitment.

Angiopoietin (Ang) and Tie receptor tyrosine kinase signalling is another paracrine interaction between pericytes and endothelial cells. They have been shown to be essential for vessel maturation and stabilisation. Angs are a family of secreted growth factors whose members all bind to the Tie receptors (Augustin et al., 2009). Ang-1 is mainly expressed in the mural cells, and binds to Tie2, which is itself expressed on the endothelium but also on haematopoietic cells, such as monocytes, and hence signalling events are mediated in a paracrine matter. In contrast, Ang-2 is secreted by endothelial cells and constitutively binds to Tie2 to signal in an autocrine manner. Ang-1-induced phosphorylation of Tie2 leads to activation of the PI3K/Akt survival pathway.

Transgenic mouse models have demonstrated that the deletion of Ang-1 or Tie-2 leads to embryonic lethality; the mice typically die *in utero* due to cardiovascular failure (Dumont et al., 1994; Suri et al., 1996). Analysis of their vasculature showed that the vasculature of knock-out mice was disorganised with fewer endothelial cells and branch points, as well as poor coverage of blood vessels by pericytes. The vessels had a disorganised BM and were leaky. In contrast, overexpression of Ang-1 induced the formation of more blood vessels and branch points. Interestingly, these vessels were particularly resistant to leakage; the effect of permeability-inducing inflammatory molecules was decreased compared to the wild-type littermates (Thurston et al., 1999).

Finally, TGF-β signalling has been shown to be important in vessel maturation by regulating ECM secretion, inhibition of endothelial cell proliferation and migration and induction of pericyte differentiation (Antonelli-Orlidge et al., 1989; Hirschi et al., 1998; Neubauer et al., 1999). The TGF-β superfamily includes TGF-βs, bone morphogenetic proteins (BMPs) and activins. TGF-β ligands bind to type I or type II receptors and result in the phosphorylation of Smad molecules which translocate to the nucleus to modulate gene expression (Weiss & Attisano, 2013). Both endothelial cells and pericytes secrete TGF-β and express TGF-β receptors. Two distinct receptors are present on both endothelial cells and mural cells, Alk-1 and Alk-5, which have seemingly opposing effects. Activation of Alk-1 leads to phosphorylation of Smad2/3 to promote pericyte differentiation (Chen et al., 2003). In contrast, Alk-5 activation leads to phosphorylation of Smad1/5 which induces the expression of genes promoting proliferation and migration (Goumans et al., 2003). It has been suggested that the fate of pericytes and endothelial cells with respect to TGF-β are determined by the relative expression levels of these TGF-β receptors in addition to length of signal (Armulik et al., 2011).

Signalling events between pericytes and endothelial cells goes in both directions; the PDGF-B/PDGFR-β interaction is from endothelial cells to pericytes, the Ang/Tie interaction is the opposite and TGF-β signalling occurs in both directions. Perturbations in the attachment and number of pericytes can lead to leakiness of the vasculature (discussed below), and hence changes in the signalling events can have consequences on the integrity of the circulatory system.

1.3.1.2 Vascular smooth muscle cells (vSMCs)

vSMCs are mural cells which surround large vessels, such as arteries, arterioles, veins and venules. They regulate the diameter of the vessels and blood flow, tissue remodelling after exercise or vascular injury and secrete growth factors and cytokines important for overall vascular function (Owens et al., 2004; Rensen et al., 2007).

There is a spectrum of vSMCs, ranging from synthetic and contractile cells (Owens et al., 2004). The synthetic phenotype is characterised by high proliferation, migration and secretion of ECM proteins. In contrast, the more mature contractile phenotype has a lower propensity for proliferation and higher expression of contractile proteins, particularly smooth muscle myosin heavy chain and elastin. vSMCs do not commit to a particular phenotype; they exhibit plasticity to revert to either phenotype (Owens et al., 2004). While synthetic vSMCs are essential in development and vascular remodelling, an excessive shift towards the synthetic phenotype has been associated with the development of vascular diseases, particularly atherosclerosis (Bennett et al., 2016).

The phenotype of vSMCs is determined by the action of signalling molecules. Signalling via PDGF-A and PDGF-B are critical for the recruitment and differentiation of vSMCs during the growth of new vessels. As a result, PDGF signalling generally induces a more synthetic phenotype by down-regulating the expression of α-smooth muscle actin (α-SMA), a marker for contractile cells, in rat aortic vSMCs and increasing proliferation and migration of pig coronary artery vSMCs (Hao et al., 2002; X. Li et al., 1997). These findings are supported by *in vivo* work, where inhibition of PDGF-B decreased vSMC proliferation and migration after arterial injury, reducing neointima formation (Deguchi et al., 1999).

In contrast, TGF-β signalling promotes the contractile phenotype. Treatment of cultured vSMCs with TGF-β1 and TGF-β2 results in the up-regulation of contractile proteins such as α-SMA and desmin (Hao et al., 2002; Hautmann et al., 1997). The expression of contractile proteins is also correlated with that of TGF-β, as demonstrated by qualitative immunostaining in rat arteries (Grainger et al., 1998).

The composition of the ECM seems to be important in specifying and maintaining the phenotype of vSMCs, either by modulating the availability of growth factors or by direct binding via integrins. For example, HSPGs such as perlecan seem to promote the maintenance of the contractile phenotype by sequestering mitogens such as FGF-2 and therefore reducing proliferation (Tran et al., 2004). Major components of the mature BM have been demonstrated to promote the contractile phenotype. In addition to collagen IV and laminin, fibrillar, but not monomeric, collagen I induces the contractile phenotype. In contrast, fibronectin and HA-containing proteoglycans stimulate cells towards the synthetic phenotype (Evanko et al., 1999; Forsberg et al., 1988; Ichii et al., 2001; Thyberg & Hultgårdh-Nilsson, 1994).

To summarise, a spectrum of vSMCs exist ranging from synthetic to contractile phenotypes. The specification of vSMCs is dependent on signalling molecules and the composition of the ECM. Deregulation of vSMCs phenotype has been associated with increased neointima formation and the development of atherosclerosis.

1.3.2 Growth of new vessels

The generation of new vessels is critical in embryonic and adult tissues. As the circulatory system is needed for the distribution of nutrients, it is the first functional organ system to be established during development (Patel-Hett & D'Amore, 2011). New vessels are also generated in adult tissues in the context of tissue repair for example. Vasculature is formed by *de novo* vasculogenesis and angiogenesis, described below.

1.3.2.1 Vasculogenesis

Vasculogenesis is the *de novo* formation of blood vessels from stem cells to establish primary vascular plexus. Vasculogenesis occurs both intra- and extra-embryonically; i.e. within the embryo and in the yolk sac, allantois and placenta (Reagan, 1915; Sabin, 1920). During murine development, at E6.5-7, progenitor cells in the yolk sac differentiate and associate in clusters of cells known as blood islands. Within these cell clusters, peripherally-located angioblasts further differentiate to form endothelial cells around E8.5. In contrast, the remaining cells, haematopoietic precursors, give rise to blood cells. Angioblasts then proliferate and migrate to form primitive cord-like structures. Angioblasts proceed to differentiate, deposit ECM, form of tight junctions between adjacent endothelial cells and recruit pericytes to form the mature vessel (Figure 1.8) (Drake, 2003; Patel-Hett & D'Amore, 2011).

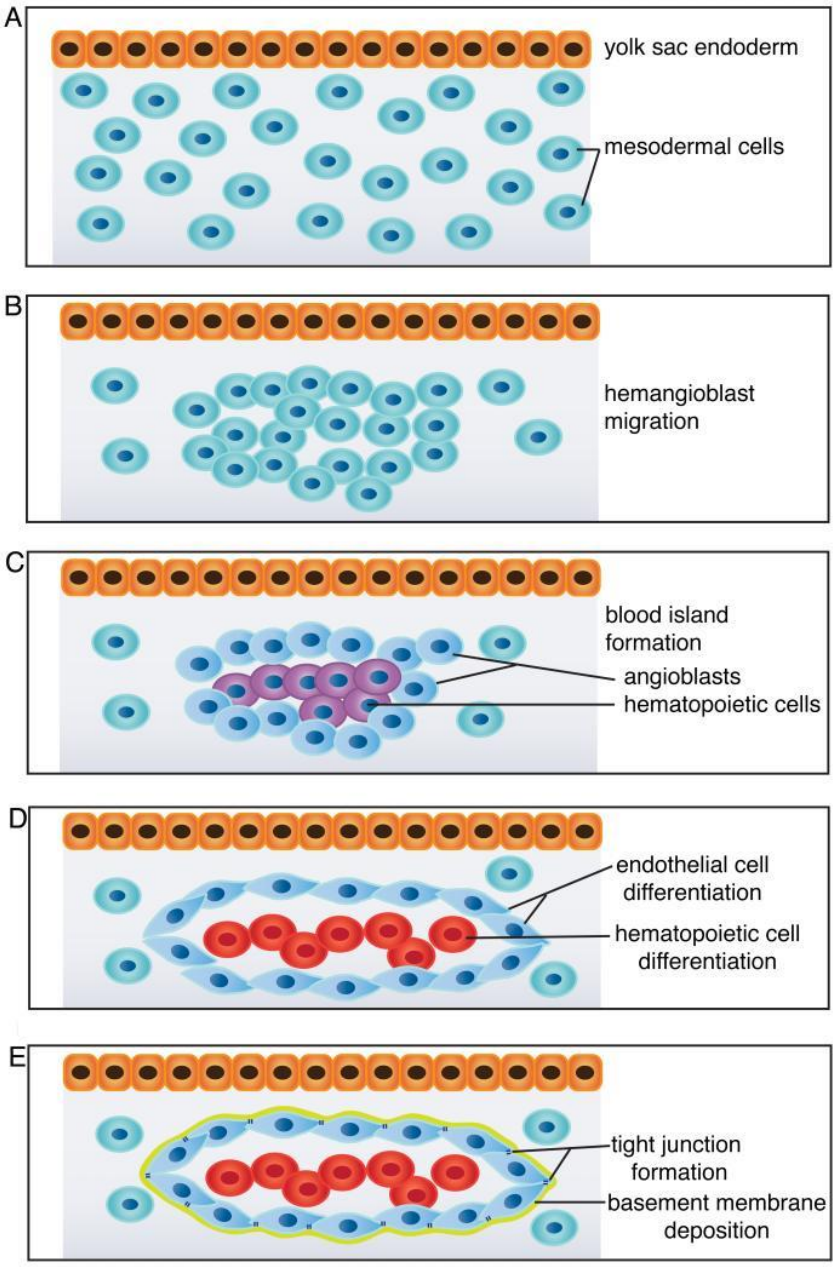

Figure 1.8. De novo formation of blood vessels. Mesodermal cells in the yolk sac **(A)** migrate **(B)** to form blood islands formed of angioblasts and haematopoietic precursor cells **(C)**. Cells differentiate **(D)** and form the mature vessel **(E)**. Figure from (Patel-Hett & D'Amore, 2011).

The signalling processes in vasculogenesis are not as well understood as those in angiogenesis. Members for the FGF family are thought to be involved. FGF-2 has been shown to be involved in the induction of angioblasts in quail embryos (Cox & Poole, 2000). Hedgehog morphogens signal through Patched to relieve repression of Smoothened and are strongly involved in developmental processes. In particular, Indian Hedgehog (Ihh) is required for proper blood island formation in the yolk sac and endothelial tube formation in the embryo (Dyer et al., 2001; Vokes et al., 2004).

VEGF signalling has clear roles in vasculogenesis and angiogenesis. There are many members of the VEGF protein family, including VEGFA, VEGFB, VEGFC, VEGFD and placental growth factor (PIGF) (Koch & Claesson-Welsh, 2012). VEGFA is the most widely-studied member and is implicated in both vasculogenesis and angiogenesis in addition to vascular permeability (Dobrogowska et al., 1998; Rosenstein et al., 1998). There are four main isoforms of VEGFA arising from differential splicing which differ in their binding affinities to HS and neuropillins due to incorporation of exons 6 and/or 7 (Park et al., 1993), as shown below in Table 1.2. VEGF proteins capable of binding to components of the ECM, notably HSPGs, can be anchored to the surrounding matrix and produce a stable VEGF gradient, guiding the formation of new vascular networks (Ashikari-Hada et al., 2005; Ono et al., 1999).

Isoform	HS binding	Neuropillin binding
121	No	No
165	Yes	Yes
189	Yes; strong	Yes
206	Yes; strong	Yes

Table 1.2. VEGFA isoforms generated as a result of alternate splicing.

VEGF members bind to three structurally-related receptors – VEGFR1, VEGFR2 and VEGFR3 (Koch & Claesson-Welsh, 2012). These receptors are receptor tyrosine kinases and trigger signalling cascades upon ligand binding. Binding of ligands to these receptors triggers homo- or heterodimerisation, autophosphorylation and the recruitment of adapter molecules for various signalling pathways, including the MAPK, Akt, Src and FAK pathways (Patel-Hett & D'Amore, 2011), as illustrated in Figure 1.9. VEGFA binds to VEGFR1 and VEGFR2. Although there is very high affinity between VEGFA and VEGFR1 (K_d = ~1-10 pM), activation of VEGFR1 has been shown to result in weak autophosphorylation (Shibuya, 2011). In contrast, VEGFR2 has been shown to have stronger activity, and its activation is responsible for pro-angiogenic signalling by VEGFA.

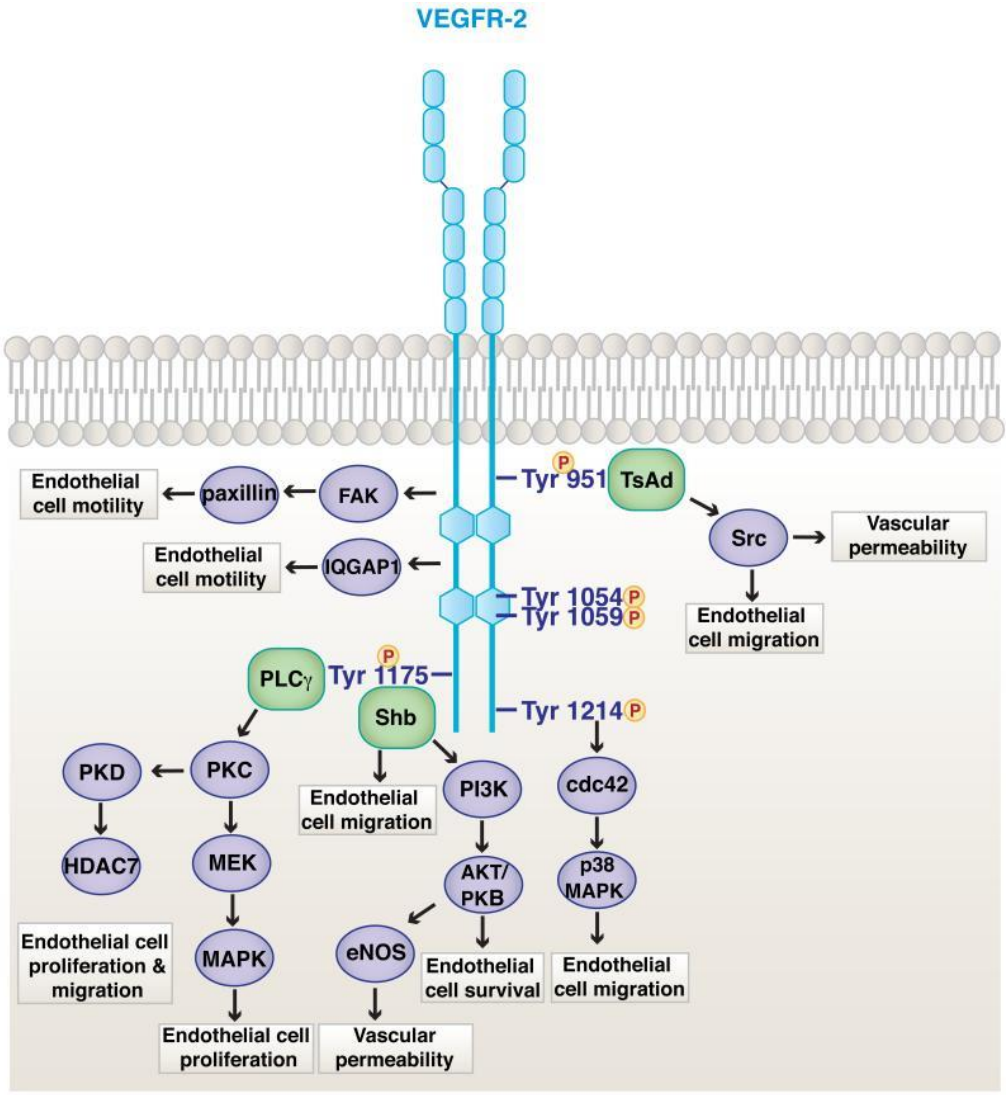

Figure 1.9. Signalling cascades triggered by VEGFR2 activity. Figure from (Patel-Hett & D'Amore, 2011).

VEGFA and its receptors are expressed early in development, starting from E8.5 (Patan, 2000). Genetic studies have highlighted the importance of VEGFA and VEGF receptors in development, as alterations in the expression of VEGFA and its receptors led to the formation of abnormal vasculature. Deletion of VEGFR1 led to vascular defects as a result of blood island angioblasts localising to the interior of the blood island, rather than the periphery (Fong et al., 1995). VEGFR2 knock-out mice die between E8.5 and E9.5 due to the absence of blood islands and lack of vasculogenesis (Shalaby et al., 1995). Similarly, deletion of VEGFA leads to death at E11 due to abnormalities in the vessels – authors noted that there were fewer endothelial cells lining the lumen of the dorsal aorta and the connections between embryonic vessels were defective (Carmeliet et al., 1996). In contrast, exogenous administration of VEGFA-165 in quail embryos led to excessive vasculogenesis and inappropriate fusion of adjacent vessels (Drake & Little, 1995).

In addition to VEGF receptors, VEGF molecules can signal through neuropillins, which are transmembrane glycoproteins which act as co-receptors for VEGF signalling (Koch & Claesson-Welsh, 2012). Two neuropillins exist in the vasculature – neuropillin-1 is located in the arterial endothelium, whereas neuropillin-2 is found in venous and lymphatic vessels (Herzog et al., 2001). VEGFA can bind to both neuropillin-1 and neuropillin-2, which can both form complexes with VEGFR1 and VEGFR2 (Fuh et al., 2000; Gluzman-Poltorak et al., 2001). Neuropillins were found to be important in vasculogenesis, as deletion of neuropillin-1 resulted in various vascular defects, including the development of a disorganised and insufficient vascular network in the yolk sac (Kawasaki et al., 1999). Mutants for neuropillin-2 did not exhibit any defects in the vasculature (Chen et al., 2000; Giger et al., 2000), yet deletion of both neuropillin-1 and neuropillin-2 resulted in embryonic lethality at E8.5 due to severely impaired yolk sac blood vessel formation (Takashima et al., 2002).

Finally, signalling through TGF-β seems to be important for regulating vasculogenesis. Endothelial cells express TGFβ1 and three receptors; Alk1 and Alk5 type I receptors and TGFRβII type II receptor (Lebrin et al., 2005). TGF-β1 knock-out mice either die *in utero* at E9.5 due to severe defects in yolk sac vascularisation (Dickson et al., 1995). Similarly, deletion of type I receptors Alk1 and Alk5 and type II receptor TGF-βRII results in embryonic lethality due to vascular defects (Larsson et al., 2001; Oh et al., 2000; Oshima, Oshima, & Taketo, 1996). Finally, as mentioned above, TGF-β signalling can be crucial for the maturation of the endothelium by promoting pericyte differentiation and secretion of ECM components.

To summarise, vasculogenesis is the *de novo* formation of blood vessels and mainly occurs during development. It is mainly regulated by VEGFA and TGF-β1, although there is evidence suggesting that other signalling molecules such as FGF-2 and Ihh are also involved.

1.3.2.2 Angiogenesis

The second mechanism allowing the growth of vessels is angiogenesis – the formation of new vessels from pre-existing ones. It occurs through two main mechanisms – sprouting angiogenesis, where endothelial cells from existing vessels migrate and sprout to form new vasculature, and intussusceptive angiogenesis where new vessels are formed by a splitting process (Figure 1.10). Angiogenesis begins at E9.5 in mice and both mechanisms of angiogenesis are responsible for the formation of most of the embryonic vasculature (Patel-Hett & D'Amore, 2011). While sprouting angiogenesis is more invasive and can therefore bridge gaps in vasculature, it is a relatively slow process as it relies on

proliferation of endothelial cells. In contrast, intussusceptive occurs much faster as it relies on remodelling and does not necessarily require proliferation (Burri et al., 2004).

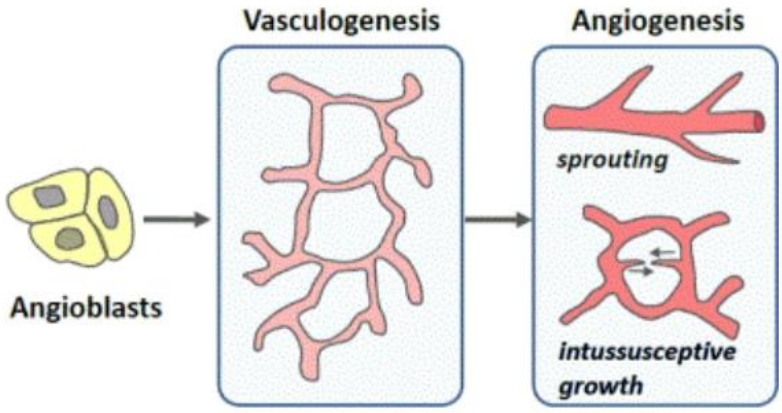

Figure 1.10. Mechanisms of blood vessel growth. Figure from (Adair & Montani, 2010).

Intussusceptive angiogenesis occurs through a remodelling process involving the insertion of tissue columns within existing vessels (Figure 1.11) (Burri et al., 2004; Makanya et al., 2009). Microvascular growth is initiated by the contact of endothelial cells on opposing sides of the vessel wall, which form the pillar core within the vessel. The cell-cell junctions between endothelial cells are then re-organised and the pillar core is invaded by vessel-associated cells such as pericytes. Basement membrane components are then synthesised to stabilise the structure (Patan, 2000). Depending on the tissue requirements, additional processes such as expansion of the vascular network or remodelling of vessel structure to meet perfusion requirements can occur (Makanya et al., 2009).

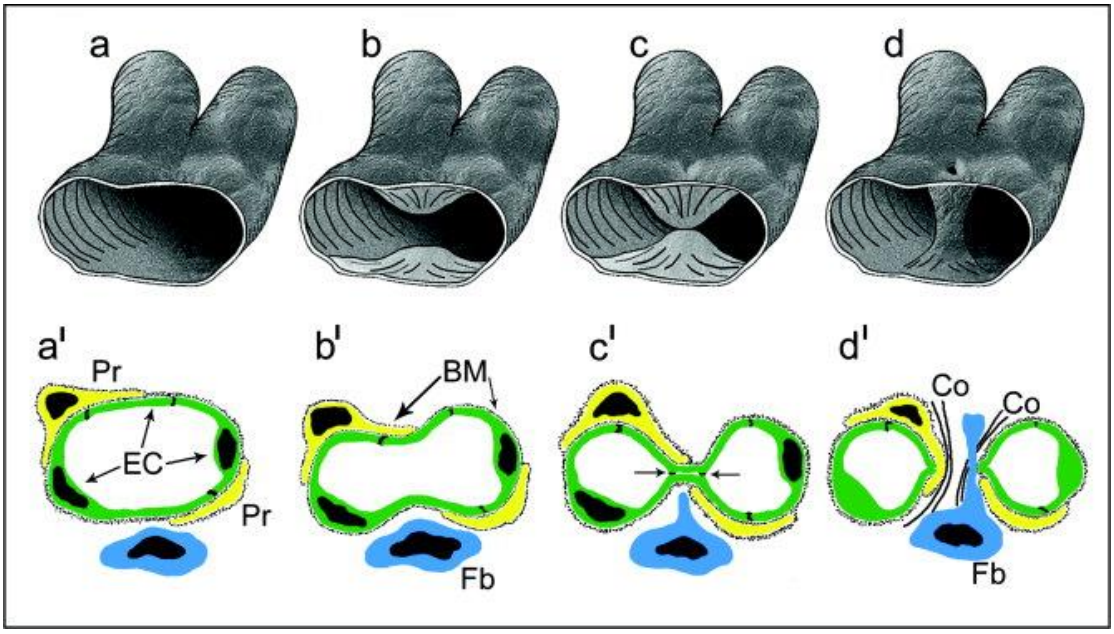

Figure 1.11. Schematic of steps which occur during intussusceptive angiogenesis. Figure from (Burri et al., 2004). Abbreviations: pericyte, Pr; fibroblast, Fb; Co, collagen.

Sprouting angiogenesis occurs in a step-wise manner – the degradation of the vessel ECM and BM, endothelial cell proliferation, migration, tube formation and vessel stabilisation (Figure 1.12) (Adair & Montani, 2010). Sprouting angiogenesis is led by specialised endothelial cells which are responsive the angiogenic stimuli – tip cells. After the destruction of the BM and dissociation of mural cells, tip cells migrate towards the angiogenic stimulus, e.g. VEGFA. Endothelial stalk cells proliferate and align to form a lumen. Attachment of mural cell and secretion of ECM components stabilise the newly-formed vessel (Neubauer et al., 1999).

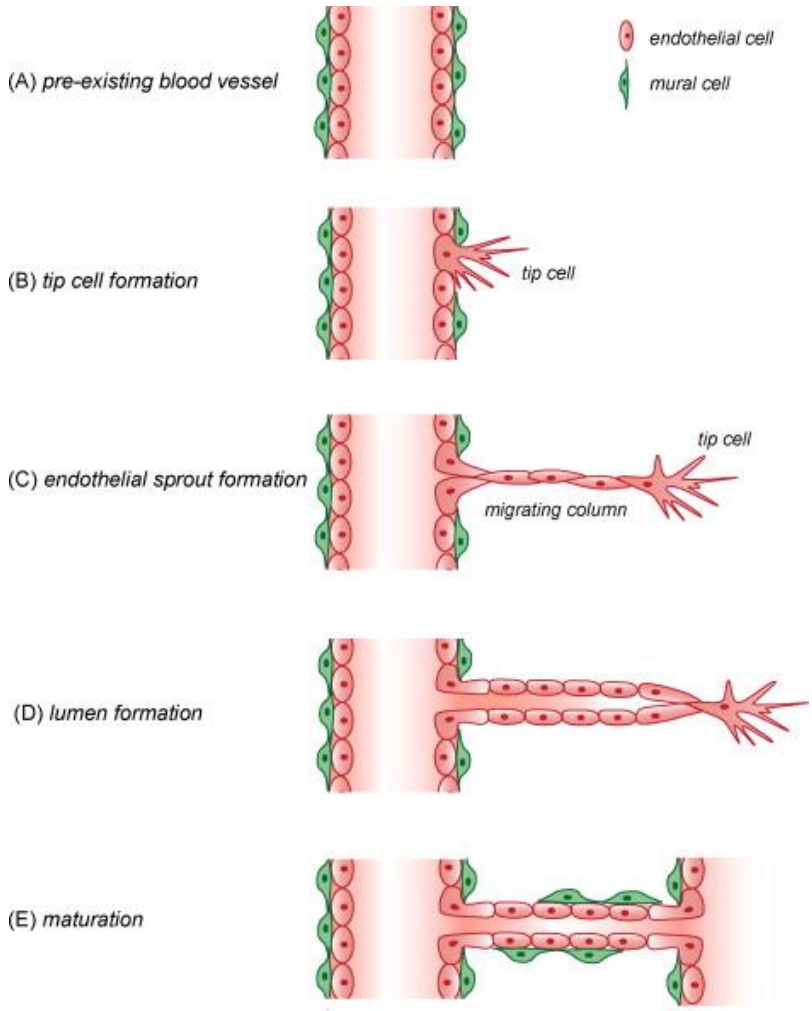

Figure 1.12. Sprouting angiogenesis. Figure from (Francavilla et al., 2009).

After the quiescent vessel is stimulated with an angiogenic signal, only a subset of endothelial cells are specified to become tip cells; the remaining endothelial cells form stalk cells. This specification of tip cells is regulated by the Notch pathway which is a known regulator for cell fate and patterning. Tip cells express higher levels of Delta-like 4 (Dll4), which is a transmembrane ligand for Notch, as a result of stimulation by VEGF. Activation of Notch signalling by Dll4 results in down-regulation of VEGF receptors VEGFR2 and VEGFR3, allowing the distinction between these two types of endothelial cells (Figure 1.13). Perturbations in Notch signalling lead to alterations in the resulting vascular network – for example, inhibiting Notch signalling results in the specification of a higher number of tip cells in the mouse retina (Hellström et al., 2007). The specification of tip and stalk cells is thought to be rather transient – upon completion of vascularisation, the tip cells would be incorporated in the newly-formed network and revert to a quiescent state after vessel stabilisation and maturation. In addition, changes in local gradients of VEGF or Notch signalling could convert tip cells into stalk cells and vice-versa (Eilken & Adams, 2010).

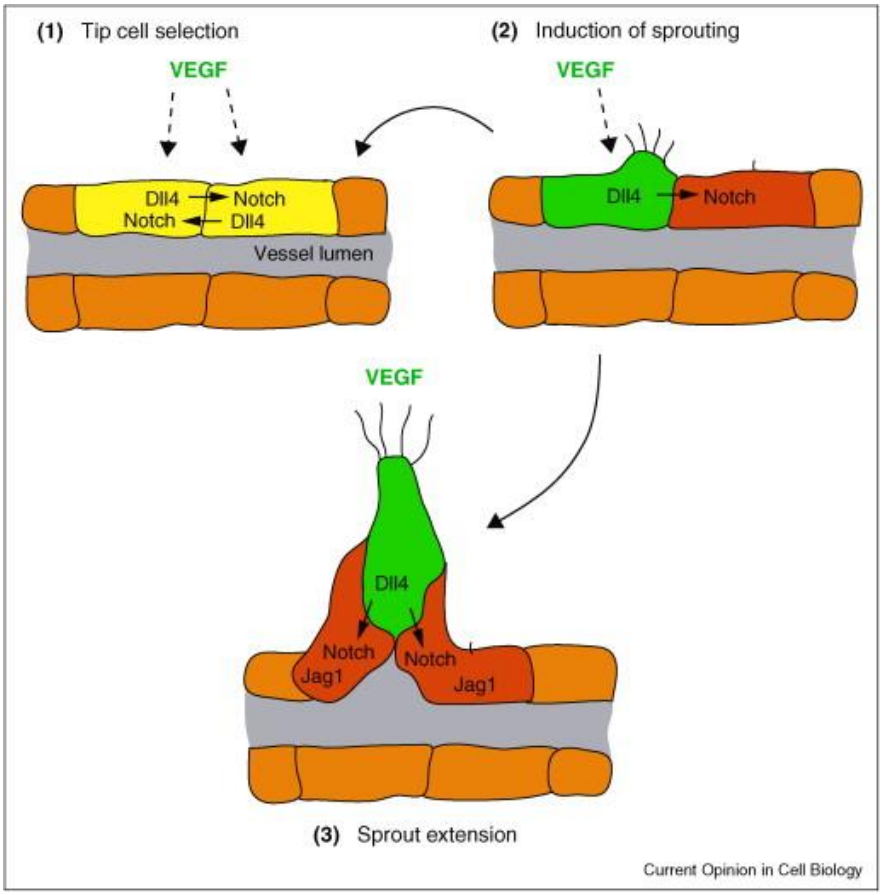

Figure 1.13. Dll4 and Notch signalling in tip cell specification. Figure from (Eilken & Adams, 2010).

Since tip cells have higher expression levels of VEGFR2 compared to stalk cells, they are able to sense VEGF gradients and guide sprouting. Tip cells possess filopodia which extend towards the angiogenic signal and respond to positive and negative cues to prevent random and aberrant vessel growth. Proteolytic enzymes are secreted by these filopodia to degrade the surrounding ECM, mainly mediated by metalloproteinases (Van Hinsbergh & Koolwijk, 2008). This allows the vessel sprout to proliferate and migrate towards other nearby sprouts or vessels. The assembly of new lumen-containing tubes is referred to as anastomosis.

During migration, the cell-cell contacts between endothelial cells are transiently abolished by VEGF signalling. After migration is completed, the nascent vessel is stabilised by the attachment of mural cells, the re-establishment of cell-cell junctions and the formation of a mature BM. Insufficient stabilisation of vessels leads to the formation of permeable vessels, which can lead to substantial consequences for tissue function, where examples of diseases caused by excessive or insufficient growth are listed in Table 1.3. As explained in Section 1.3.1.1 , paracrine signalling events between pericytes and endothelial cells via PDGF-B/PDGFR-β, Ang-1/Tie and TGF-β/Alk-1 are essential for

pericyte recruitment and attachment. During the initial phases of angiogenesis, pericytes become activated, shorten their processes, undergo intense proliferation and detach from the parent vessel. They are the first cells to invade the newly-vascularised tissue, and their re-attachment inhibits endothelial migration and proliferation, promoting the quiescent state of the newly-formed vessel (Ribatti et al., 2011).

Diseases caused by excessive growth of vessels	
Disease	References
Arthritis	(Luttun et al., 2002)
Psoriasis	(Heidenreich et al., 2009)
Diabetic retinopathy	(Enge et al., 2002)
Atherosclerosis	(Herrmann et al., 2006)
Various cancers	(Carmeliet, 2003)
Diseases caused by insufficient growth of vessels	
Disease	References
Hypertension	(Boudier, 1999)
Osteoporosis	(Martínez et al., 2002)
Nephropathy	(Kang et al., 2001)

Table 1.3. Examples of diseases caused by de-regulated vessel growth.

1.4 Blood-brain barrier (BBB)

1.4.1 Function of the BBB

The blood-brain barrier (BBB) is a specialised structure in the central nervous system (CNS) formed and maintained by a variety of different cells which separate the circulating blood from surrounding tissues in the brain. While the BBB permits exchange of water, gases and nutrients such as glucose and amino acids, which are essential for the functioning of the brain, it prevents access of neurotoxins and bacteria. Dysfunction of the BBB has consequences including neuroinflammation and can lead to neurodegenerative disorders.

The surface area of the vasculature is large (approx. 20m^2 endothelium per 1.3kg brain) and as a result, most neurons are in close proximity to blood vessels; the BBB is therefore critical in regulating the brain microenvironment (Abbott et al., 2006). Fluctuations in ions have to be regulated to prevent them affecting synaptic and axonal signalling after a meal for example. Molecules can cross the BBB in three manners; i) passive diffusion, ii) through selective transport proteins and iii) receptor-mediated transcytosis (Abbott et al., 2006). Small gases and lipophilic molecules can diffuse freely – this includes O_2, CO_2

and ethanol. Hydrophilic molecules, such as glucose, are unable to cross the BBB and require specific transporters expressed on luminal and abluminal surfaces of the brain endothelium to regulate nutrient entry and waste removal from the brain (Begley & Brightman, 2003). Finally, large polar molecules such as peptides are transported across the BBB by receptor-mediated endocytosis and transcytosis (Pardridge, 2005).

1.4.2 Neurovascular Unit (NVU)

The functional unit of the BBB is often referred to as the neurovascular unit (NVU), as it is composed of vasculature-specific endothelial cells, pericytes and their associated BM, but also CNS-specific astrocytes, microglia and neurons (Figure 1.14) (Obermeier et al., 2013). These cell types coordinate in establishing and maintaining the integrity of the BBB.

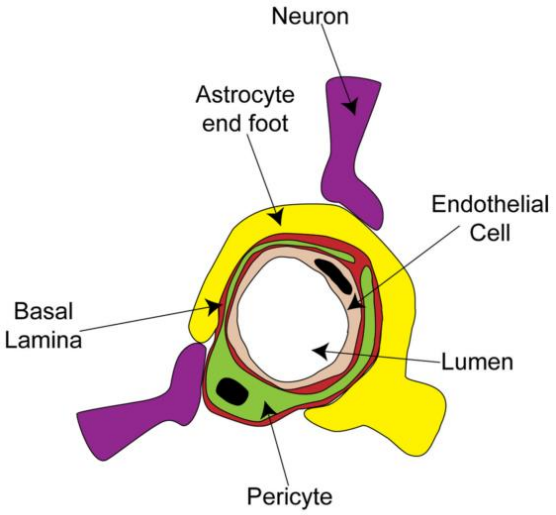

Figure 1.14. Structure of the NVU. Figure modified from (Hamilton et al., 2010).

1.4.2.1 Endothelial tight and adherens junctions

Endothelial cells form the first barrier of the BBB. Adjacent endothelial cell junctions are sealed with tight and adherens junctions. Adhesion mediated by tight and adherens junction proteins is maintained by transmembrane proteins, which are linked to intracellular scaffold proteins which anchor and link the junction to the actin cytoskeleton (Figure 1.15). Tight junctions are composed of integral membrane proteins notably occludin, claudins and Junctional Adhesion Molecule-A (JAM-A) as well as a variety of intracellular components including ZO-1 and cingulin (Gomperts et al., 2009). The transmembrane proteins are expressed on adjacent cells and are capable of making strong homophilic interactions, linking the two cells together. Intracellular proteins form a cytoplasmic plaque, which links membrane proteins to the actin cytoskeleton by recruiting structural proteins and signalling effectors (Furuse, 2010). Adherens junctions

between endothelial cells are organised in a similar manner to tight junctions. Vascular endothelial cadherin (VE-cadherin) transmembrane proteins on adjacent endothelial cells form homodimers. VE-cadherin is linked to the actin cytoskeleton via interactions with p120-catenin, β-catenin and plankoglobin (Giannotta et al., 2013).

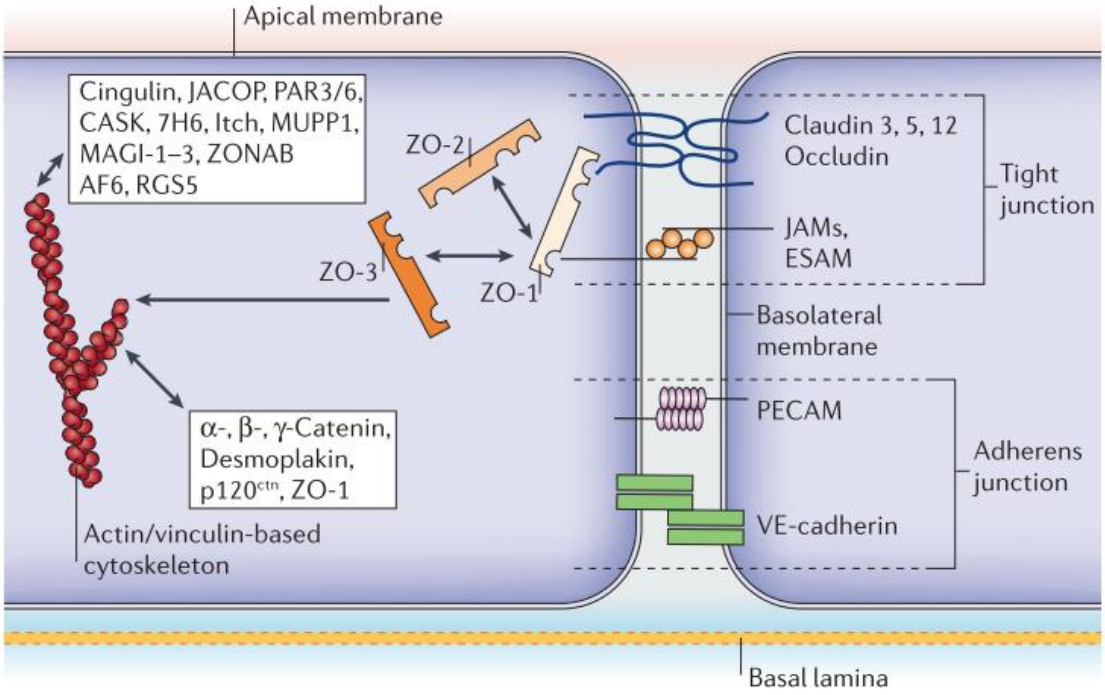

Figure 1.15. Architecture of cell-cell junctions. Adherens and tight junction complexes are found between neighbouring epithelial or endothelial cells. They are composed of homophilic transmembrane proteins and cytoplasmic adapters linked to the actin cytoskeleton. Modified from (Abbott et al., 2006).

Adherens and tight junctions have distinct functions. Tight junctions regulate the paracellular diffusion of molecules across the BBB and establish cell polarity by limiting movement of molecules from the apical to basal membranes; these are referred to as "gate" and "fence" functions respectively (Abbott et al., 2006; Tietz & Engelhardt, 2015). The formation of tight junctions generally requires the presence of adherens junctions. Adherens complexes initiate cell-cell adhesion and promote their maturation and maintenance (Tietz & Engelhardt, 2015). In particular, VE-cadherin is located at these cell-cell contacts. There is evidence that the signalling events which take place as a result of VE-cadherin's presence can affect the expression of claudin-5 (Taddei et al., 2008); VE-cadherin upregulated the expression of claudin-5 through PI3K/Akt pathway activation, preventing forkhead box factor (FoxO1)-mediated inhibition of transcription.

With respect to the gate function of the BBB, the presence of claudin homodimers were found to be a critical determinant for BBB function (Tsukita & Furuse, 2002). Occludin knock-out mice are viable, yet display a complex phenotype including hyperplasia of

gastric epithelia and calcification in the brain (Saitou et al., 2000). In contrast, claudin-5 knock-out mice died perinatally and had abnormalities in the BBB; size-selective changes in the BBB were present, where only small molecule tracers were able to cross the BBB (Nitta et al., 2003). Ablation of cytoplasmic components of tight junctions, such as ZO-1, results in embryonic lethality at E10.5 due to defects in vascular development, highlighting its importance in the formation of both adherens and tight junctions (Katsuno et al., 2008).

Perivascular contacts to the endothelium are crucial for the maintenance of the BBB phenotype by secreting ligands essential for the expression of cell-cell junction proteins. For example, canonical wnt signalling has been shown to be important in the maintenance of the BBB. Wnt ligands binding to Frizzled receptors leads to the destabilisation of the destruction complex, freeing β-catenin to translocate to the nucleus and initiate gene expression, including tight junction proteins claudin-3 and claudin-5 (Daneman et al., 2009; Liebner et al., 2008; Stenman et al., 2008; Zhou & Nathans, 2014). The Sonic hedgehog (Shh) pathway also seems to be involved in inducing the BBB phenotype. Shh released from astrocytes during brain angiogenesis bind to Smoothened (Smo) receptors on endothelial cells, ultimately leading to reduced expression of various junction proteins, including occluding, claudin-3, claudin-5, ZO-1 and p120-catenin (Alvarez et al., 2011). As expected, this change in gene expression was also accompanied by increased permeability of the vasculature. Lastly, *in vitro* data suggests that Ang-1/Tie-2 signalling between astrocytes and endothelial cells has been shown to increase the expression of occludin, claudin-1, ZO-1 and ZO-2, highlighting the importance of perivascular cells in the maintenance of the BBB (Lee et al., 2003).

In vitro models have been essential for studying the BBB. Primary endothelial cells are seeded onto a semi-permeable membrane in a cell culture insert, establishing apical and basal compartments. Additional cells, such as pericytes, astrocytes, can be added to the culture either by seeding on the bottom of the well or on the opposite side of the permeable membrane (Nakagawa et al., 2009) (Figure 1.16). The ease of movement of ions across an endothelial cell monolayer is measured by trans-endo/epithelial resistance (TEER), where high TEER is indicative of a highly impermeable cell layer. Cultures of endothelial cells on their own have a notably smaller TEER compared to double- or triple-cultures containing pericytes and/or astrocytes (Srinivasan et al., 2015). The mature endothelium of the BBB therefore has contacts to perivascular cells which contribute to the expression of tight junction proteins.

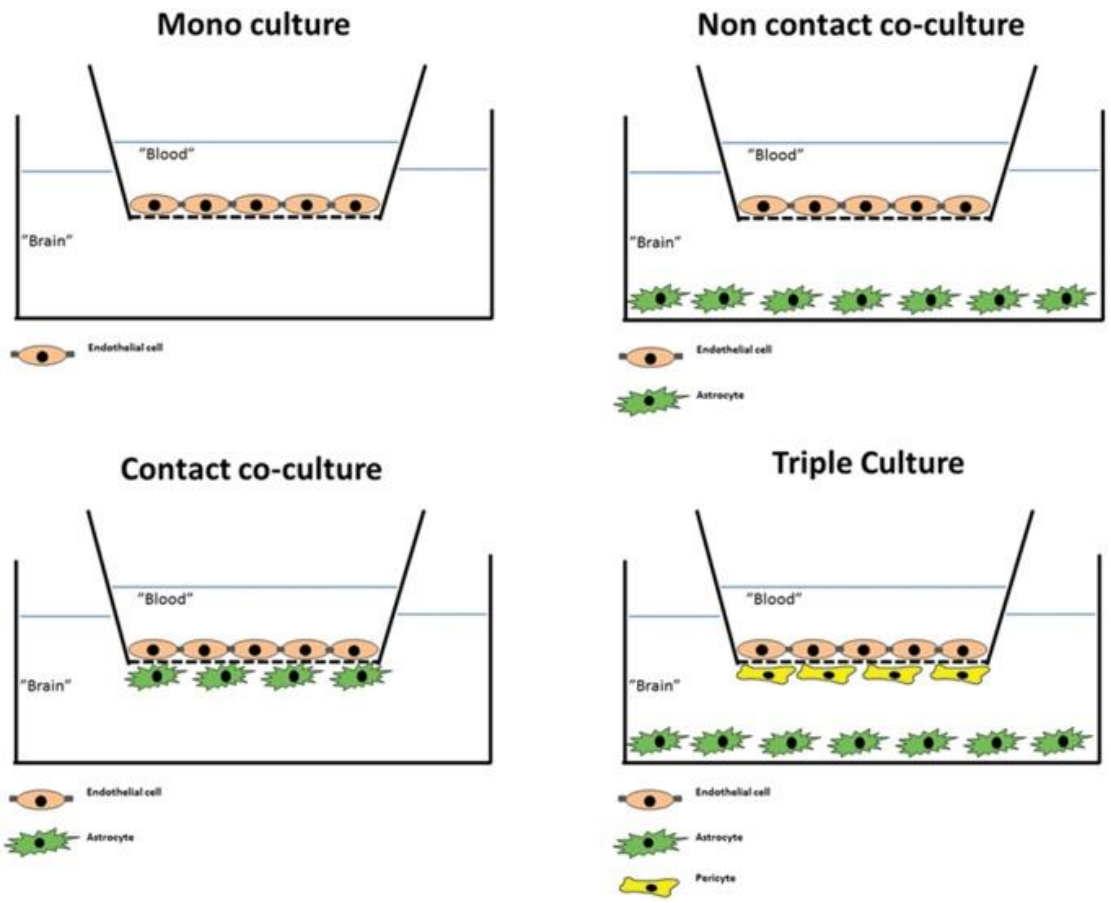

Figure 1.16. *In vitro* models for the BBB. Endothelial cells (orange) can be cultured with astrocytes (green) and pericytes (orange). Figure from (Helms et al., 2016).

1.4.2.2 Pericytes

I have described the general physiology and signalling of pericytes in Section 1.3.1.1 , and will be discussing CNS-specific features of pericytes and their contribution to the BBB in this section. Pericyte density varies between different tissues, with the central nervous system being the most pericyte-rich tissue, where approximately a third of the surface of small vessels are covered in pericytes (Mathiisen et al., 2010).

In addition to regulating blood flow and contractility, pericytes have been shown to be critical in the stability of the BBB. There are studies indicating that pericyte-deficiency is directly correlated to BBB breakdown and leakage. Manipulation of the PDGF-B/PDGFR-β pathway results in a decrease in pericyte coverage, loss of astrocyte end-foot polarity and increased vascular permeability (Armulik et al., 2010; Daneman et al., 2010). The authors of these studies suggest that the leakiness is caused by excess transcytosis, where macromolecules are transported across a cell in vesicles. In addition, loss of pericytes results in changes in gene expression, including an increase in permeability factor VEGFA and a decrease in maturation-promoting Ang-1 (Armulik et al., 2010). Finally, pericyte loss has been shown to exacerbate the progression of Alzheimer's disease (Sagare et al.,

2013). Pericyte-deficient mice were crossed with those harbouring a familial mutation in Aβ-precursor protein and were found to have an accelerated disease phenotype compared to Aβ-precursor protein transgenic mice.

To summarise, in addition to providing stabilising contacts through Ang-1/Tie-2 and TGF-β signalling, pericyte coverage seems to be essential in maintaining a healthy BBB. Pericyte loss frequently accompanies BBB breakdown and may affect other components of the BBB, such as astrocyte end-foot coverage.

1.4.2.3 Astrocytes

Astrocytes are stellate glial cells with long cytoplasmic processes which are important for maintaining a healthy CNS. Astrocytes interact with neurons and the vasculature, and secrete ligands modulating their function. In addition to modulating the BBB, astrocytes have roles in guiding development, regulating blood flow, maintaining fluid homeostasis and synapse function (Sofroniew & Vinters, 2010).

Astrocytes bind to the vasculature and provide stabilising interactions via specialised processes known as end-feet (Figure 1.17). These perivascular end-feet express channels and transporters, notably aquaporin-4 (AQP4) (Nagelhus et al., 1998) and Kir4.1 (Poopalasundaram et al., 2000) which regulate water and ion homeostasis, and also provide reliable markers for detection. In particular, AQP4 is widely-accepted as a key marker for the BBB, as its expression level seems to correlate positively with BBB function; decreased immunofluorescence of AQP4 occurs in many studies of BBB breakdown (Gautam et al., 2016; Isasi et al., 2014; Menezes et al., 2014; Yao et al., 2014). The polarity of astrocyte end-feet correlates with the levels of the HSPG agrin in the BM – loss of agrin results in loss of orthogonal clustering of end-feet (Noell et al., 2009).

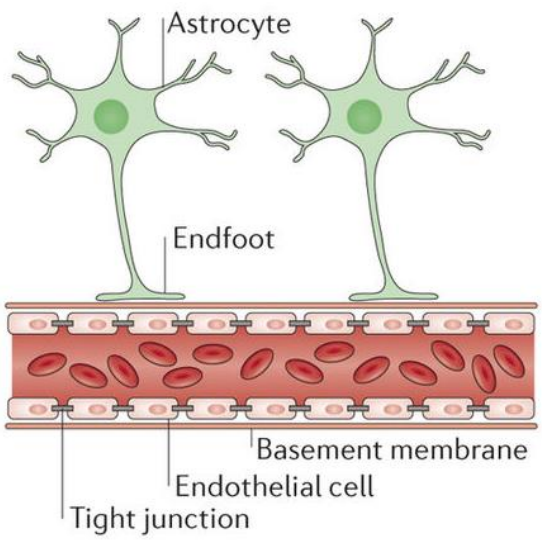

Figure 1.17. Astrocytes make contacts to the endothelium via specialised end-feet. Figure modified from (Cuddapah et al., 2014).

Astrocytes have been shown to be essential in inducing the BBB barrier phenotype (Janzer & Raff, 1987); in addition, the application of conditioned media from astrocytes to an endothelial cell culture has been shown to increase the TEER of the endothelial cell monolayer (Winger et al., 2014). *In vitro* studies have indicated that astrocyte secretion of maturation factors, such as TGF-β, Ang-1 and glial-derived neurotrophic factor (GDNF), can increase endothelial cell monolayer TEER and contribute to the induction of BBB properties (Abbott et al., 2006; Lee et al., 2003). This work indicates that astrocytes secrete these factors, but also that endothelial cells express matching receptors, allowing astrocytes to modulate the state of the BBB.

To summarise, astrocyte end-feet envelop the brain endothelium and provide stabilising interactions. Loss of end-foot attachment and/or polarity has been shown to result in changes in BBB integrity.

1.4.3 Implications of CNS vascular dysfunction

Changes in the CNS can lead to alterations in the BBB. For example, when there is trauma, there is an increase in the activity of bradykinin, a mediator of inflammation, which results in the release of pro-inflammatory interleukin-6 from astrocyte end-feet leading to an increase in BBB permeability (Schwaninger et al., 1999). Other inflammatory mediators include serotonin, histamine and nitric oxide (Abbott et al., 2006). Similarly, bacterial infections, such as meningitis, result in microglial secretion of tumour necrosis factor-α (TNF-α) and leads to increased expression of interleukin-6, interleukin-1β and reactive oxygen species capable of opening the BBB (Gaillard et al., 2003). Astrocytes were also shown to secrete VEGFA, which resulted in decreased expression of tight junction

proteins occludin and claudin-5 in endothelial cells in inflammatory models (Argaw et al., 2009). Increased permeability of the BBB results in leakage of plasma proteins into the brain parenchyma and inflammation characterised by a localised response from astrocytes and microglia; this is further described in Chapter 4.

BBB breakdown accompanies neurodegenerative disorders such as Alzheimer's disease, Parkinson's disease and Huntington's disease (Hirsch & Hunot, 2009; Politis et al., 2015; Streit et al., 2009). Studies have indicated that inflammation and BBB breakdown can exacerbate disease symptoms, but also precede their appearance (Dénes et al., 2011; Ujie et al., 2003). This indicates that changes in the BBB and neuropathology are linked and both contribute to disease progression.

1.5 Small Leucine-Rich Repeat Proteoglycans (SLRPs)

1.5.1 SLRP structure and function

Proteoglycans can broadly be categorised into four groups based on cellular localisation – intracellular, cell-surface, pericellular and extracellular (Iozzo & Schaefer, 2015). To my knowledge, the only intracellular proteoglycan is serglycin, expressed in mast cell granules (Douaiher et al., 2014). HSPGs tend to be closely associated with the cell surface or pericellular matrix via transmembrane domains or are GPI-anchored. CS- and DS-containing proteoglycans are located further away and are typically constituents of specialised matrices such as cartilage and bone. The final class of proteoglycans is found in the ECM and is mainly comprised of members of the small leucine-rich repeat proteoglycan (SLRP) family. The SLRP family is the largest class of proteoglycans comprising 17 members which function as both structural molecules and signal mediators to regulate migration, proliferation, immunity, apoptosis and angiogenesis (Dellett et al., 2012; Iozzo & Schaefer, 2015).

SLRP members have two main structural components: a relatively small protein core of 36kDa-42kDa, and attached GAGs. The protein core mediates protein-protein interactions, and is composed of tandem leucine-rich repeats (LRRs); the number of repeats varies greatly within the family. Based on the homology and chromosomal organisation, SLRPs are organised into five classes (Figure 1.18). Classes I to III are considered to be traditional SLRPs whereas classes IV and V are non-canonical, as most class IV and V SLRPs lack any GAG modifications, with the exception of chondroadherin, which contains KS GAGs (Neame et al., 1994). Of the canonical SLRPs, asporin, PRELP and opticin do not have GAG sidechains (Dellett et al., 2012).

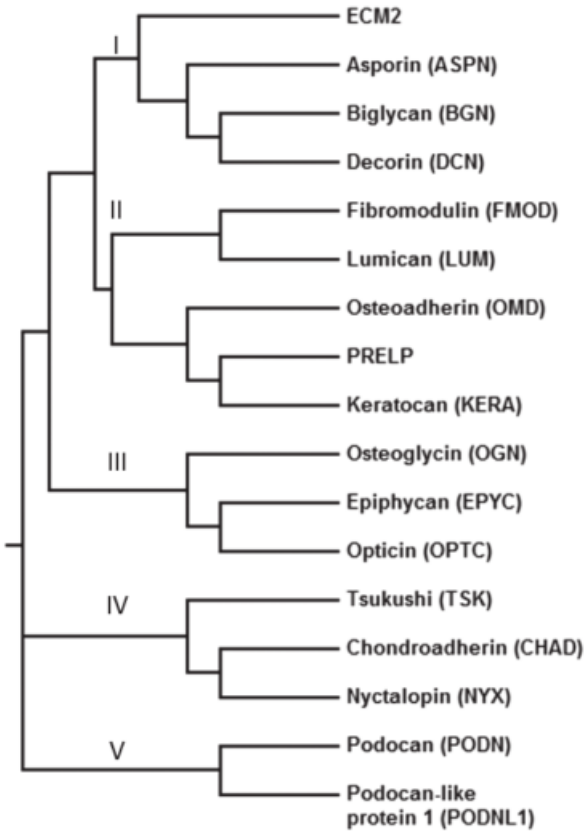

Figure 1.18. Classification of SLRP members. SLRP members are classified by homology of their protein cores. Image source (Dellett et al., 2012).

The core protein of SLRPs comprises LRRs and follow the consensus sequence LXXLXLXXNXL, where L is leucine, isoleucine or valine, N is aspargine, cysteine or threonine and X is any amino acid. The length of the LRRs vary between members, with 24 residues being the most common length (McEwan et al., 2006). Crystal structures of SLRP members indicate that these continuous LRRs form short, parallel β-sheet structures followed by β-turns and/or 3_{10}-helices dictated by repeat length (Figure 1.19). The LRRs are typically flanked by sequences containing four and two cysteine residues which form disulphide bonds at the N- and C-termini respectively; they are referred to as capping motifs, and are thought to contribute to the structural integrity of SLRPs by protecting the hydrophobic regions of LRRs (McEwan et al., 2006). The spacing of cysteine residues at the N-terminus is conserved within the class of SLRP (Dellett et al., 2012).

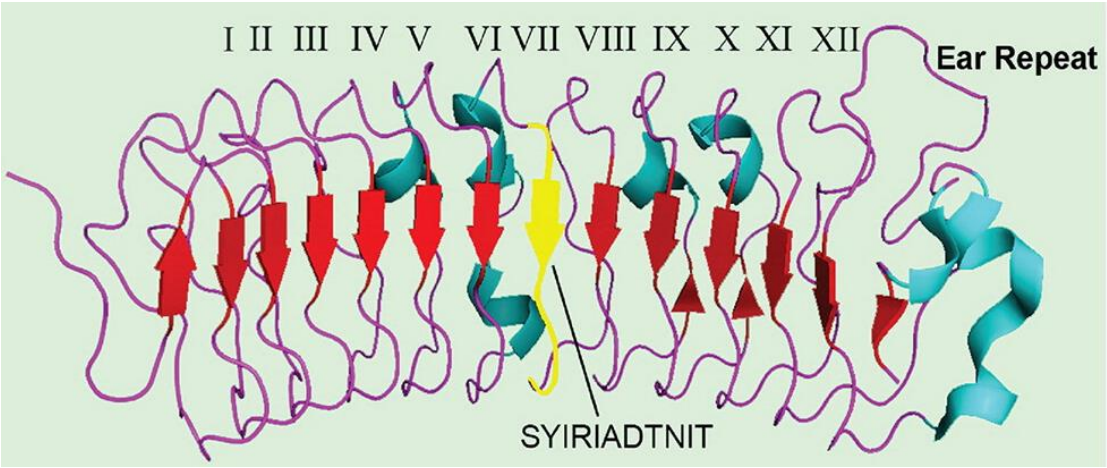

Figure 1.19. Structure of bovine decorin (PDB=1XKU). Arrows indicate β-strands, whereas α-helices are shown as ribbons. Figure modified from (Iozzo & Schaefer, 2015).

A classic feature of canonical SLRPs in classes I to III is the ear repeat, a long penultimate LRR. The ear repeat contains 30 or more residues including an unusual cysteine residue located shortly after the consensus LRR sequence and results in an LRR which extends away from the main structure before coming back to continue to form the final LRR (Figure 1.19) (McEwan et al., 2006). The function of the ear repeat is currently not well-understood. C-terminal truncation of decorin lacking the ear repeat results in congenital stromal corneal dystrophy in humans (Bredrup et al., 2005), and in mice (Chen et al., 2011).

Most SLRPs are modified with CS, DS or KS, as shown in Table 1.4. The exceptions are the non-canonical SLRPs in addition to asporin, PRELP and opticin. Instead of GAG chains, some members have unique N-terminal sequences: asporin has a stretch of aspartate residues and PRELP has a proline- and arginine-rich region (Bengtsson et al., 1995; Henry et al., 2001). Opticin also has sequences allowing covalent attachment of O-linked oligosaccharides (Reardon et al., 2000).

Class	SLRP	GAG modifications	References
I	Biglycan	CS/DS	(Fisher et al., 1989)
	Decorin	CS/DS	(Reed & Iozzo, 2002)
	ECM2	Not determined, but unlikely	(Iozzo & Schaefer, 2015)
	Asporin	Lacks GAG modifications	(Henry et al., 2001)
II	Fibromodulin	KS	(Lauder et al., 1995)

	Lumican	KS	(Chakravarti et al., 1995)
	Keratocan	KS	(Corpuz et al., 1996)
	OMD	KS	(Wendel et al., 1998)
	PRELP	May have short KS chain	(Bengtsson et al., 1995)
III	Epiphycan	DS	(Johnson et al., 1997)
	Osteoglycin	KS	(Funderburgh et al., 1997)
	Opticin	Lacks GAG modifications	(Reardon et al., 2000)
IV	Chondroadherin	KS	(Iozzo & Schaefer, 2015; Neame et al., 1994)
	Nyctalopin	Lacks GAG modifications	(Bech-Hansen et al., 2000; Pusch et al., 2000)
	Tsukushi	Lacks GAG modifications	(Ohta et al., 2004)
V	Podocan	Lacks GAG modifications	(Ross et al., 2003)
	Podocan-like 1 protein	Lacks GAG modifications	(Mochida et al., 2011)

Table 1.4. GAG modifications of SLRP members.

Many members contain hydrated GAG chains and are localised to the ECM and interact with ECM proteins. A classic example is that of decorin – decorin was given its name due to its ability to "decorate" collagen fibrils in a non-covalent manner (Scott & Orford, 1981). Decorin knock-out mice were viable and largely healthy, but had unusually fragile skin due to irregular collagen fibril formation (Danielson et al., 1997). It is now known that SLRP members can bind to collagen types I, II, III, V, VI and XI and regulate collagen fibrillogenesis (Iozzo & Schaefer, 2015). The binding of SLRPs to collagen fibrils has two main functions – first, to enable the association of collagen polypeptides into proper fibrils and second, to prevent fibril proteolysis by physically blocking access to collagenases.

SLRPs can modulate signalling pathways by binding to extracellular components such as ligands and receptors. As a result, they can modulate a variety of signalling pathways,

including the TGF-β, BMP, wnt, EGF, IGF and TNF-α pathways (Nikitovic et al., 2012). Decorin and biglycan are the most studied SLRPs. In addition to decorin's role in aiding collagen formation, it is known to inhibit the growth of cells. It has been shown to inhibit the TGF-β signalling pathway in Chinese hamster ovary cells by binding to and sequestering TGF-β from its receptor (Hildebrand et al., 1994; Yamaguchi et al., 1990). Exogenous decorin was also found to have an effect on the growth of cells – the decorin core protein could bind to EGFR and transiently trigger the MAPK cascade, resulting in the induction of cyclin-dependent kinase inhibitor $p21^{WAF1}$ and sustained down-regulation of EGFR itself (Luca et al., 1996; Moscatello et al., 1998).

Biglycan is the second-most studied SLRP, and with more than 65% overall homology, has a structure similar to that of decorin. Biglycan knock-out mice have an osteoporosis-like phenotype; bones grow more slowly and eventually have reduced bone mass (Xu et al., 1998). Biglycan can affect a number of pathways, including TGF-β, BMP-4 and canonical wnt signalling by modulating ligand bioavailability (Berendsen et al., 2011; Hildebrand et al., 1994; Moreno et al., 2005). In addition, biglycan is pro-inflammatory and can bind to toll-like receptors (TLR) as an endogenous ligand; as a result, biglycan knock-out mice have a much better survival rate compared to controls when injected with endotoxins such as LPS (Schaefer et al., 2005).

To summarise, SLRPs are a family of small proteoglycans found in the ECM. SLRP proteins have a small protein core and typically have GAG chains covalently attached. They provide structural support in addition to modulating a variety of signalling pathways regulating proliferation, migration, differentiation and immune response.

1.5.2 SLRPs in vasculature

Many members of the SLRP family have been shown to affect angiogenesis. As this project is focused on the roles of OMD and PRELP on the vasculature, I will review current knowledge of SLRP function in regulating vessel growth.

In addition to the roles of decorin in regulating the growth of cancer cells lines, there are many studies describing the effect of decorin on angiogenesis. Decorin is present in newly-formed vessels, but not in quiescent vessels (Bosse et al., 1993; Nelimarkka et al., 2001; Reich-Schupke et al., 2011). While decorin knock-out mice have no abnormalities in the vasculature under unstressed conditions, they exhibited impaired angiogenesis after corneal injury (Schönherr et al., 2004). Conditioned cell culture media was obtained from cancer cell lines transfected with decorin and applied to *ex vivo* rat aortic rings, resulting in inhibition of endothelial cell migration, attachment, tube formation and

capillary sprouting. In addition, the application of decorin to cancer cell lines resulted in a significant decrease in expression levels of VEGFA-165 (Grant et al., 2002). Finally, decorin induces endothelial cell autophagy through partial activation of VEGFR2 resulting in AMPKα and Vps34 activation to induce Peg3 expression, a master regulator for autophagy (Buraschi et al., 2013). In addition to affecting VEGFA signalling, decorin has been shown to bind and modulate the function of other pro-angiogenic growth factors, such as FGF-2, TGF-β and PDGF-B, by regulating ligand bio-availability (Baghy et al., 2013; Hildebrand et al., 1994; Sulochana et al., 2005). These studies collectively indicate that decorin is an inhibitor for angiogenesis.

Recent work has shown that decorin may have a role in BBB dysfunction and progression of neurodegenerative disorders. Decorin and biglycan were found in inflammatory lesions in patients with multiple sclerosis (Mohan et al., 2010). In a mouse model of inflammation, where BBB dysfunction was induced, decorin was found to accumulate in the ECM of leaking vessels. These results were replicated *in vitro* using primary brain endothelial cells, where the application of cytokines resulted in increased decorin deposition. Cells grown on surfaces coated with decorin exhibited increased permeability and decreased expression of claudin-5. Interestingly, the addition of collagen IV to the decorin coating reversed this effect, suggesting that free decorin may be pro-inflammatory and perpetuate BBB damage (Hoettels et al., 2017).

Increased levels of biglycan in a variety of cancers is associated with poor prognosis (Jacobsen et al., 2017; B. Wang et al., 2011; Zhu et al., 2013). Biglycan was found to be strongly expressed in tumour vessels and in the sera of cancer patients. Knock-down of biglycan in tumour endothelial cells resulted in decreased cell migration and impaired tubule formation (Yamamoto et al., 2012). Human colon cancer cell lines were transfected to overexpress biglycan and injected as xenografts in mice. Biglycan-overexpressing tumours had elevated levels of pro-angiogenic VEGFA and increased activation of the ERK signalling pathway compared to the vector control. Treatment with ERK inhibitor decreased the expression of biglycan-induced VEGFA (Xing et al., 2014). Another mechanism for the pro-angiogenic activity of biglycan may be associated with its interaction with endostatin, an inhibitor for angiogenesis produced by proteolytic processing of collagen XVIII (O'Reilly et al., 1997). The addition of endostatin to tubule formation assays inhibits cell migration and tubulogenesis. However, the addition of equimolar biglycan mitigates the inhibitory effect of endostatin (Myren et al., 2016). Taken together, these studies show that biglycan is an inducer of angiogenesis, particularly in the context of tumour vasculature.

Fibromodulin is important in wound healing. Knock-out mice have impaired blood vessel regeneration after injury. The addition of fibromodulin to human endothelial cells resulted in increased adhesion, spreading and tubulogenesis, accompanied by increased expression of collagen I and III, pro-angiogenic Ang-2 and VEGFA. These results indicate that fibromodulin is important in angiogenesis, but also in mobilising quiescent vessels into angiogenic vessels (Jian et al., 2013).

Incubation of lumican with human endothelial cells reduced cell migration and tubulogenesis. Mice were injected with bFGF-supplemented Matrigel plugs and injected with vehicle or lumican 72 hours after establishment of the plug. The extent of vascularisation of the Matrigel plug was determined after 12 days, and while the bFGF and vehicle plugs had extensive vascularisation, lumican-injected animals had markedly reduced blood vessel content. Lumican was found to interfere with pro-angiogenic α2β1 integrin activity, inhibiting angiogenesis (Niewiarowska et al., 2011). In addition, analysis of lumican knock-out mice indicated that tumours in knock-out animals had higher blood vessel content compared to tumours isolated from the wild-type. Surprisingly, *in vivo* angiogenesis assays in lumican knock-out mice did not indicate that lumican is anti-angiogenic (Sharma et al., 2013), possibly as a result of increased expression of other SLRPs with similar function.

Proline and arginine rich end leucine rich repeat protein (PRELP) is another class II SLRP which has been shown to inhibit the growth of blood vessels. PRELP was shown to inhibit complement activation and hence choroid angiogenesis in the eye. In contrast, in the same study, the authors found that PRELP application increased endothelial cell tubule formation (Birke et al., 2014). Thus, the role of PRELP in regulating the growth of new vessels is not clearly defined.

Using the chick chorioallantoic membrane *ex vivo* assay, opticin was found to reduce angiogenesis induced by FGF-2 and VEGFA. This was attributed to the ability of opticin to bind to collagen enabling it be a competitive inhibitor, preventing the activation of pro-angiogenic α1β1 and α2β2 integrins (le Goff et al. 2012a). In addition, opticin knock-out mice exhibited increased angiogenesis in a model of oxygen-reduced retinopathy (le Goff et al. 2012b). Taken together, these two studies indicate that opticin is an inhibitor for angiogenesis.

Finally, recent work has demonstrated that osteoglycin is an inhibitor of angiogenesis. Osteoglycin knock-out mice were found to recover more efficiently after induction of limb ischaemia compared to wild-type animals, owing to increased capillary density.

Vascularisation was assessed using the corneal angiogenesis and aortic ring assays; in both cases, osteoglycin knock-out tissues exhibited higher blood vessel content. Osteoglycin was found to abrogate VEGFA/VEGFR2 signalling by direct association with VEGFR2, enabling it to inhibit angiogenesis (Wu et al., 2017).

To summarise, with the exception of biglycan and fibromodulin, most SLRPs exhibit inhibitory functions with respect to angiogenesis, as summarised in Table 1.5. There seems to be no association with regards to GAG modification and effect on angiogenesis. SLRPs modulate angiogenesis by primarily affecting that VEGFA/VEGFR2 signalling axis in addition to acting as inhibitors for pro-angiogenic integrin activation. Finally, only decorin has been reported to have an effect on the BBB integrity.

Class	SLRP	GAG modifications	Effect on vasculature
I	Decorin	CS/DS	Potent inhibitor of angiogenesis Exacerbates BBB breakdown
	Biglycan	CS/DS	Activator of angiogenesis
II	Fibromodulin	KS	Activator of angiogenesis
	Lumican	KS	Inhibitor of angiogenesis
	PRELP	None	Inhibitor of choroid angiogenesis Activator of tubulogenesis
III	Opticin	None	Inhibitor of angiogenesis
	Osteoglycin	KS	Inhibitor of angiogenesis

Table 1.5. Summary of the role of SLRPs in the growth of new vessels.

1.5.3 Osteomodulin (OMD)

Osteomodulin (OMD; aka osteoadherin) is a class II, KS-containing SLRP. It contains 12 LRR repeats and contains an ear repeat of 31 amino acids (McEwan et al., 2006). It has an extended C-terminus of which roughly 60% is acidic residues (Sommarin et al., 1998).

OMD was first isolated from bovine bone matrix and its acidic nature enabled binding to hydroxyapatite, an abundant bone mineral (Sommarin et al., 1998). Current research indicates that, unlike other SLRPs, it is only expressed in mineralized tissues (Nikdin et al. 2012; Shen et al. 1999) and more specifically in osteoblasts via binding to αVβ3 integrin (Rehn et al., 2008; Sommarin et al., 1998).

Osteoblasts and osteoclasts have opposing roles in bone mineralisation. Osteoblasts deposit bone matrix and act to increase bone mass; in contrast, osteoclasts resorb bone matrix and undergo apoptosis, ultimately leading to a decrease in bone mass. The

activities of osteoblasts and osteoclasts are critical for bone homeostasis; diseases such as osteoporosis are often linked to an increase in osteoclast activity (Tanaka & Okada, 2005). Analysis of the OMD promoter sequence has indicated that there are binding sites for smad-3, smad-4 and AP-1, effectors of TGF-β signalling. Analysis has indicated that TGF-β1 down-regulates OMD expression, whereas BMP-2 signalling has the opposite effect, where both TGF-β1 and BMP-2 have roles in hard tissue development by regulating osteoblast proliferation, migration and differentiation (Rehn et al., 2006). *In vitro* cell culture studies have shown that OMD overexpression in osteoblasts accelerated osteoblast differentiation, whereas repression increased proliferation and migration; this effect is probably mediated by modulating the activity of EGFR (Rehn et al., 2008). Finally, work by our collaborator at the University of Tokyo has shown that OMD binds to collagen I fibrils, which are abundant in bone, and regulates their diameter (Tashima et al., 2015). Taken together, these studies show that OMD has a strong role in bone homeostasis. The signalling functions of OMD outside of bone mineralisation have not yet been reported.

1.5.4 Proline/arginine-rich and leucine rich protein (PRELP)

PRELP is also a class II SLRP. It contains 12 LRR repeats and a particularly long ear repeat of 39 amino acids (McEwan et al., 2006). In contrast to other class II SLRPs, it does not have covalently-attached GAG chains. Instead, as its name implies, it has a proline and arginine-rich region which is located to the N-terminus (Bengtsson et al., 1995).

PRELP was first isolated from bovine cartilage. Radioimmunology assays indicated that PRELP expression is also found in bone, lens, kidney, aorta, liver, skin, cornea and skeletal muscle (Heinegard et al., 1986). Since then, various research groups have demonstrated that PRELP is expressed in rodent developing and adult cartilage, in addition to human chondrocytes in cartilage (Grover & Roughley, 2001; Lui et al., 2010; Segawa et al., 2009). PRELP is also found in various BMs, including skin, kidneys and testis, consistent with early radioimmunology assays (Bengtsson et al., 2002). Finally, PRELP is detected in human sclera (Majava et al., 2014).

PRELP binds to both collagen I and II through its core protein (Bengtsson et al., 2002). In addition, its unique N-terminus rich in proline and arginine allows PRELP to bind HSPGs, including BM component perlecan (Bengtsson et al., 2000; Bengtsson et al., 2002). Given these two binding capabilities, it is thought that PRELP acts as an anchoring molecule to link basement membranes or cells to the surrounding ECM (Bengtsson et al., 2002). Mutations in PRELP have been associated with Hutchinson–Gilford progeria which causes rapid and premature aging shortly after birth (Lewis, 2003; Pollex & Hegele, 2004). This

rare genetic disorder is characterised by lack of collagen binding in the BM and cartilage, consistent with the structural role of PRELP described above.

Like OMD, PRELP has roles in skeletal remodelling. The addition of the heparin-binding domain of PRELP to mouse osteoblasts and osteoclasts resulted in impaired osteoclastogenesis and bone resorption. The heparin binding domain was found to be internalised and binds to the transcription factor NF-κB, where this interaction inhibits the expression of osteoclast-specific genes (Rucci et al., 2009). PRELP also induces the differentiation of osteoblasts. The expression of PRELP was found to be increased during osteoblast differentiation in cultured cells; knockdown of PRELP using siRNA resulted in decreased mineralised nodule deposition. This effect was found to be dependent on β-catenin (Li et al., 2016). Therefore, PRELP affects bone homeostasis by down-regulating genes in osteoclasts and inducing differentiation of osteoblasts.

PRELP also seems to have an effect on pathways involved in innate immunity. The complement system promotes inflammation and aids in the clearance of pathogens – unregulated complement activation is implicated in many diseases with chronic inflammation, such as rheumatoid arthritis (Okroj et al., 2007). SLRP members have been shown to be able to bind and activate or inactivate classic complement activators such as C1q (Groeneveld et al., 2005; Sjöberg et al., 2005; Sjöberg et al., 2009). PRELP was found to bind to C9, preventing its polymerisation to prevent complement activation and the formation of the membrane attack complex (Happonen et al., 2012). Furthermore, administration of PRELP prevented complement activation, neovascularisation and the formation of the membrane attack complex in mouse eyes, raising the possibility of using PRELP as treatment for age-related macular degeneration (Birke et al., 2014).

Finally, recent work has shown that the N-terminus of PRELP binds to other proteoglycans such as glypican-1, syndecan-1 and syndecan-4. In addition, treatment of fibroblasts with heparinase or the addition of exogenous heparin resulted in decreased attachment to PRELP. Finally, in concert with fibronectin, PRELP can induce the formation of focal adhesions by activating integrins (Bengtsson et al., 2016).

To summarise, PRELP has a unique and highly-conserved N-terminal domain which seems to mediate both structural and signalling functions. PRELP acts as a physical bridge between collagen and BM component heparin, in addition to regulating signalling by binding to NF-κB, β-catenin and C9.

1.5.5 Previous work in the Ohnuma lab

Previous members of the Ohnuma laboratory have investigated the functions of OMD and PRELP. I will briefly summarise their findings in this section. Using microarray gene expression studies, it was discovered that OMD and PRELP are down-regulated in several human cancers, with the most profound fall in bladder cancer. Work by Dr Julie Watson in the EJ-28 bladder cancer cell line indicated that the overexpression of OMD- and PRELP attenuated the cancer phenotype by inhibiting cell cycle progression and migration. Analysis of signalling pathways indicated that this was due to inhibition of the activities of various kinases, including ERK, MAPK, JNK and PI3K (unpublished), highlighting the role of OMD and PRELP as potential tumour suppressors.

OMD and PRELP knock-out mice were generated, where the respective genes were replaced by LacZ. Dr Vasiliki Papadaki stained tissues using X-gal and showed that OMD and PRELP are expressed in a variety of adult and embryonic tissues, including the bladder, brain, eye and bone. In particular, there was strong expression in brain vasculature. Dr Papadaki then analysed bladders from OMD and PRELP knock-out mice and found that these animals had spontaneous urothelial papillomas and disrupted tight junctions in the bladder epithelium (unpublished).

1.6 Project hypothesis and aims

X-gal staining of OMD and PRELP heterozygotes by previous members has shown that there is strong expression in the brain, particularly in brain vasculature. In this chapter, I have highlighted the importance of the ECM in the regulation of signalling pathways controlling processes integral to correct tissue function. ECM proteins such as SLRPs have been shown to have roles in tumour progression, angiogenic signalling and the regulation of inflammation. OMD and PRELP are currently poorly-studied members of the SLRP family. Given the strong expression of OMD and PRELP in brain vasculature, and the phenotype of weakened epithelial cell-cell junctions in the bladder in knock-out animals, I hypothesise that endothelial barrier function in OMD and PRELP knock-out mice may be impaired.

To this end, I will elaborate on the expression pattern of OMD and PRELP in the brain, characterise the vascular phenotype of knock-out mice, analyse changes in gene expression and finally use cultured endothelial cells to determine signalling pathways altered by OMD and PRELP.

Chapter 2 Materials and Methods

2.1 Preface

In this project, I aim to investigate the vascular phenotype of OMD and PRELP knock-out mice and determine deregulated pathways. I employed a variety of *in vivo* and *in vitro* methods. In this chapter, I outline solutions, reagents and methods utilised for this investigation. Note that all reagents were purchased from Sigma-Aldrich (USA), unless otherwise stated.

2.2 Materials

2.2.1 Standard Solutions

Solution	Composition
Phosphate Buffered Saline (PBS)	137mM NaCl, 2.7mM KCl, 10mM Na_2HPO_4, 1.8mM KH_2PO_4, pH7.4; all dissolved in ddH_2O
Phosphate Buffered Saline + Tween 20 (PBT)	PBS with 0.1% (v/v) Tween 20
Tris Buffered Saline (TBS)	50mM Tris-Cl, 150mM NaCl dissolved in ddH_2O and pH adjusted to 7.5
Tris Buffered Saline + Tween 20 (TBST)	TBS with 0.1% (v/v) Tween 20
4% Paraformaldehyde (PFA)	Diluted 32% PFA solution (Electronic Microscopy Sciences, USA) in PBS. Made fresh each time
X-gal stock solution	0.1g X-gal (Melford, UK) in 5ml dimethylformamide to make 20mg/ml stock Stored in the dark at -20 °C
X-gal staining solution	5.35mM $K_3Fe(CN)_6$, 5.35mM $K_4Fe(CN)_6.3H_2O$, 1.2mM $MgCl_2$, 0.01% Sodium deoxycholate (w/v), 0.02% (v/v) NP40 in 100mL PBS Stored in the dark at room temperature
Blocking buffer for IHC/ICC	10% goat serum + 0.03% (v/v) Triton X-100 in PBS Filter sterilized and stored at 4 °C
TAE buffer	40mM Tris, 20mM acetic acid, 1mM EDTA in ddH_2O and pH adjusted to 7.6

TN Buffer	150mM NaCl, 5mM KCl, 0.5% (v/v) Triton X-100, 10mM Tris-HCl in ddH_2O and adjusted to pH 7.8 Stored at 4 °C
Running buffer for western blot	5mM Tris, 190mM glycine, 3.5mM sodium dodecyl sulfate dissolved in ddH_2O
Transfer buffer for western blot	25mM Tris, 190mM glycine, 20% methanol (v/v) dissolved in ddH_2O
Blocking buffer for western blot	5% (w/v) non-fat milk powder dissolved in TBST
Blocking buffer for western blot (phospho-proteins)	5% (w/v) BSA in TBST
Luria Broth (LB) agar	LB agar powder dissolved in ddH_2O according to manufacturer's instructions
Luria Broth (LB) media	LB powder dissolved in ddH_2O according to manufacturer's instructions
TSS buffer	10% PEG 8000 (w/v), 30mM $MgCl_2$, 5% DMSO (v/v) in LB media

Table 2.1. List of standard solutions used throughout. All reagents purchased from Sigma-Aldrich unless otherwise stated.

2.2.2 Cell culture solutions

Solution	Composition
MEFs media	450ml DMEM, 50ml foetal bovine serum, 5ml 200mM L-glutamine, 5ml Penicillin/Streptomycin (10'000U/ml)
HEK293 media	450ml DMEM, 50ml foetal bovine serum, 5ml Penicillin/Streptomycin (10'000U/ml)
HUVECs media supplemented with LVES	489ml medium 200, 11ml 50x LVES
22% BSA	30% BSA solution diluted in PBS
Papain	Papain containing L-cysteine and EDTA (Worthington Biochemicals, USA) reconstituted in 5ml MEM-HEPES to yield 20U/ml

DNase I	DNase I (Worthington Biochemicals, USA) reconstituted in 500µl MEM-HEPES to yield 2000U/ml
MBEC media	450ml Nutrient Mixture F12 Ham medium (with sodium bicarbonate), 50ml foetal bovine serum, 5ml 200mM L-glutamine, 5ml Penicillin/Streptomycin (10'000U/ml), 30µg/ml endothelial cell growth supplement (Millipore, USA), 25µg/ml ascorbate, and 0.8% heparin
MBEC media with puromycin	MBEC media with 4µg/ml puromycin
Cryopreserving solution	9ml foetal bovine serum, 1ml DMSO

Table 2.2. List of solutions used for cell culture. All reagents listed in this table were purchased from Gibco, unless otherwise specified.

2.3 Mouse methods

2.3.1 Transgenic mice

All animal procedures were performed in accordance to the Animals (Scientific procedures) Act 1986 of the UK Government. Mice were kept in individually-ventilated cages with a 12-hour light-dark cycle. They were fed a complete pelleted mouse diet with constant access to water. All mice were housed in compliance with the Home Office Code of Practice.

The OMD and PRELP knock-out mouse lines were generated by the Takeda Pharmaceutical Company (Japan). The OMD and PRELP exons were replaced by exons of the LacZ gene, encoding β-galactosidase (Figure 2.1). The resulting mice have a C57BL/6J background.

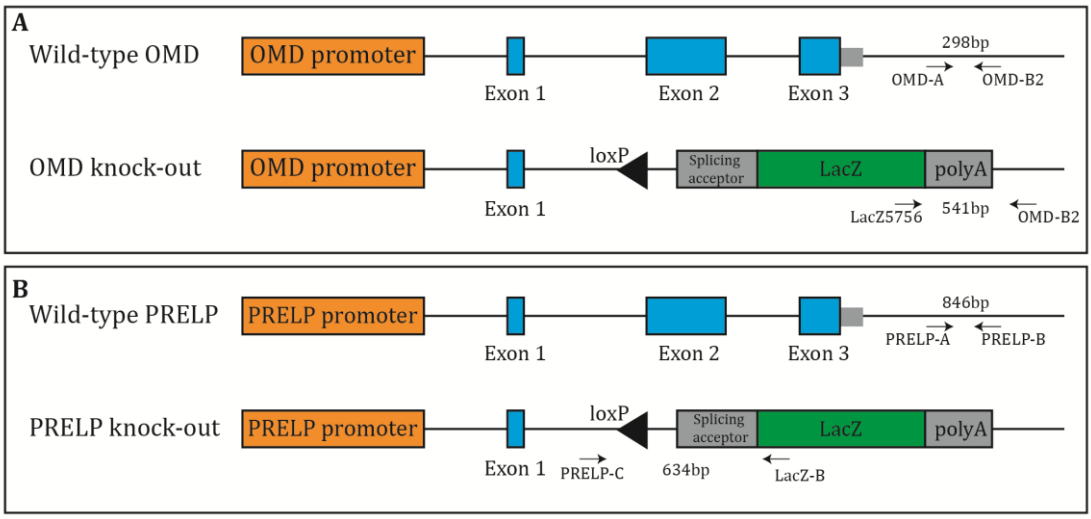

Figure 2.1. OMD (A) and PRELP (B) knock-out mice were generated by replacing Exons 2 and 3 with the LacZ gene. Primers used for genotyping are also displayed. For OMD genotyping, bands at 298bp and 541bp are expected for wild-type and OMD$^{-/-}$ respectively. For PRELP, band sizes are 846bp and 634bp for wild-type and PRELP$^{-/-}$ respectively.

2.3.1.1 Processing ear punches

Genotyping amplifies regions of the genome which correspond to wild-type and knock-out animals, as illustrated in Figure 2.1. Ear punches from transgenic mice obtained after weaning at 3-4 weeks. Ear punches were then digested in DirectPCR Lysis Reagent (Ear) (Viagen Biotech, USA) and 0.4mg/ml Proteinase K in a 55°C waterbath overnight. The following morning, the temperature of the water bath was increased to 85°C to inactivate proteinase K. Tubes were chilled on ice, spun briefly to pellet any debris, and supernatant transferred to fresh tubes. PCR reactions were set up immediately and digested ear samples were stored at -20°C.

2.3.1.2 Genotyping OMD mice

Wild-type and knock-out OMD bands were amplified in separate tubes. Taq polymerase PCR kit (Invitrogen, USA) was used and mixes were prepared (Table 2.3) and the PCR reaction was run according to the program (Table 2.5). 2% agarose gel (w/v) was prepared (see Section 2.6.4 for more details) with SYBR Safe DNA stain (Invitrogen; 1:10'000 dilution) and samples were run on the gel at 100V. Once the dye front reached the midway point on the gel, bands were visualised using the UV transilluminator. The wild-type band is 298bp and the knockout band is 541bp.

Reagent	Volume (µl)	
	Wild-type band amplification	Knock-out band amplification
10x PCR buffer minus Mg	2.5	2.5
10 mM dNTP mixture	0.5	0.5
50 mM MgCl2	0.75	0.75
Taq polymerase 5 U/µl	0.05	0.05
1% W1	1.25	1.25
ddH_2O	12.45	12.45
OMD-A	1.25	-
OMD-B2	1.25	1.25
LacZ_5756F	-	1.25
Genomic DNA	5	5
Total volume	25	25

Table 2.3. PCR mixture for genotyping OMD mice. Kit purchased from Invitrogen was used. A master mix containing all reagents except primers and genomic DNA was typically prepared before splitting and adding primers and template.

Primer name	Sequence (5' -> 3')
OMD-A	GGGAATGCTTTGACTTTCTGAGTTA
OMD-B2	TGAAGCATTGATGCCTGCTA
LacZ_5756F	CGGTCGCTACCATTACCAGT

Table 2.4. Primers used for genotyping OMD transgenic mice.

Temperature (°C)	Time	Number of cycles
95	3min	-
94	30s	35
61	90s	
72	90s	
72	10min	-
4	Indefinite	-

Table 2.5. PCR cycle used for genotyping OMD transgenic mice.

2.3.1.3 Genotyping PRELP mice

Both wild-type and knock-out PRELP bands can be generated from the same reaction mixture. Qiagen Multimix kit was utilised and PCR mixes were prepared (Table 2.6) and the PCR reaction was run according to the program (Table 2.8). 2% agarose gel (w/v) was prepared (see Section 5.4 for more details) with ethidium bromide (1:10'000 dilution) and samples were run on the gel at 100V. Bands were visualised using the UV transilluminator after the dye front reached the bottom of the gel. The wild-type band is 846bp and the knockout band is 634bp.

Reagent	Volume (µl)
Multimix master mix	12.5
Q solution	5
Water	3
PRELP-A	0.5
PRELP-B	0.5
PRELP-C	0.5
LacZ-B	0.5
Genomic DNA	2.5
Total volume	25

Table 2.6. PCR mixture for genotyping PRELP mice. PCR kit purchased from Qiagen. A master mix containing all reagents except primers and genomic DNA was typically prepared before splitting and adding primers and template.

Primer name	Sequence (5' -> 3')
PRELP-A	CACTGCAGGAAGAGTCATCTTTTCT
PRELP-B	TACACTTTCTCCCAGCTTCTATTCC
PRELP-C	GTTGAGCAGATTTTGGATGTCACT
LacZ-B	GGATAGGTCACGTTGGTGTAGATG

Table 2.7. Primers used for genotyping PRELP transgenic mice.

Temperature (°C)	Time	Number of cycles
95	15min	-
94	30s	40
63	90s	
72	90s	
72	10min	-
4	Indefinite	-

Table 2.8. PCR cycle used for genotyping PRELP mice.

2.3.2 Intraperitoneal (IP) injection

Mice were injected intraperitoneally to administer tracer dyes or Euthatal to euthanise animals according to Schedule 1 practices. Briefly, solutions were prepared beforehand, ensuring that the final pH is neutral as to avoid causing any excess pain during injection. Volume injected was determined by the animal's weight and was no more than 10ml/kg. Mice were picked up by the scruff and restrained to prevent any unwanted movement during the procedure and injected into the lower quadrant of the abdomen (Figure 2.2), ensuring the needle is kept horizontal to the animal to prevent accidentally injecting into organs. The substance was injected using a 40G needle attached to a 1ml syringe with the bevel facing up. Animals were then returned to their cage to allow tracer dye circulation or euthanasia to take effect.

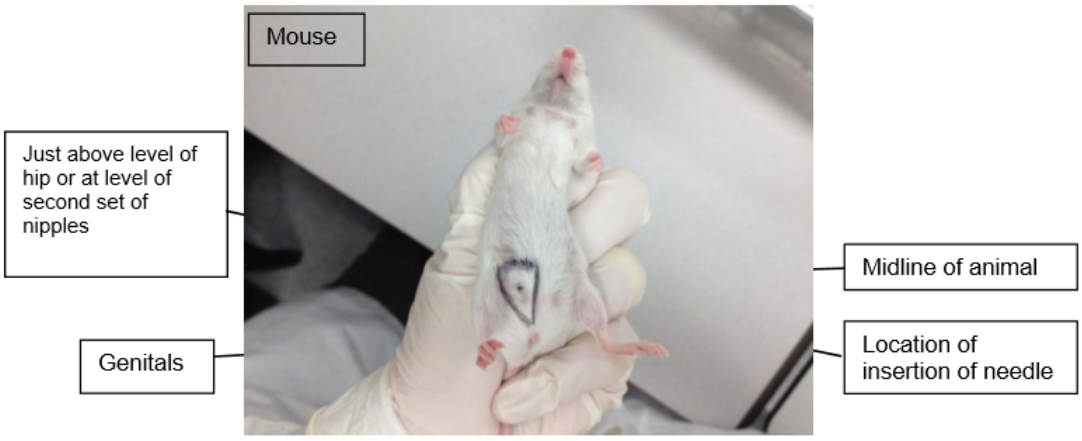

Figure 2.2. Location of IP injection. Needle should be injected in the center of a quadrant in the lower abdomen. Image from (Andrews, 2014).

2.3.3 Intravenous (IV) injection

Tracer dyes were administered to mice by intravenous (IV) injection into the tail vein. Solutions were prepared beforehand, ensuring that the final pH is neutral as to avoid causing any excess pain during injection. Volume injected was determined by the animal's weight and was no more than 10ml/kg. Mice were put into a heated chamber set to 37°C

for 15min prior to injection in the tail vein. Once the tail vein was sufficiently dilated, the animal was transferred to a tube restrainer. The tail vein was located and tracer dye was injected with the bevel facing up. A 34G needle and 0.1ml syringe were used. The animal was then returned to its cage to allow for the circulation of the dye. In initial experiments, animals were monitored for the full duration of the circulation period to confirm that the injection did not cause distress.

2.3.4 Perfusion

Animals were injected intraperitoneally with 0.1ml Euthatal and returned to its cage. Whilst waiting for the effect of the anaesthetic, the perfusion apparatus was set up, ensuring that the tubing was devoid of any air bubbles. The speed of perfusion was set to 3.33ml/min. Once the animal lost consciousness, its response to toe pinching was assessed, and once there was no longer a reaction, the mouse was pinned to a polystyrene board in the supine position using 24G needles. Using sharp scissors, abdomen was carefully cut open to reveal the ribcage. The ventral ribcage was then cut laterally and on the sides to fully allow access to the heart. The beating heart was then held in place with round forceps and a custom 40G needle with flowing PBS was inserted in the left ventricle; the needle was modified with an additional ring of material 2mm from the tip to prevent piercing the heart too deeply. Once the needle was inserted, an incision was made in the right atrium. Once the fluid exiting the right atrium ran clear, the perfusion solution was switched to ice-cold 4% PFA using a valve system. Perfusion with fixative continued until I observe movement and stiffening of the tail. Organs from the animal were then removed and processed for cryosectioning by cryoprotecting in 30% sucrose overnight and embedded for cryosectioning the following day (see Section 2.3.5.1 for more details).

2.3.5 Analysis of mouse tissue sections

2.3.5.1 Tissue harvest and preparation

Tissues were harvested from adult transgenic mice after termination using a rising concentration of CO_2, in accordance with Schedule 1 procedures. The tissues were fixed with 4% PFA at room temperature for 2 hours with gentle agitation. Tissues were then washed in PBS before cryo-protection in 30% sucrose until they sunk; typically, for brain tissues, overnight incubation with gentle agitation at 4°C was required. Cryo-protected tissues were then embedded in optimal cutting temperature (OCT) compound (Sakura Finetek, USA) before being snap-frozen on dry ice. Frozen embedded blocks were stored at -80°C. Sections were typically cut serially at 10µm using a Leica CM3050 cryostat.

Sections were mounted onto Superfrost Plus® glass slides (Fisher Scientific, UK) and stored at -80°C.

For immunostaining using certain antibodies, particularly antibodies against cell junction markers (listed in Table 2.9), fixation in PFA was detrimental. Therefore, some tissues were immediately immersed in 30% sucrose for cryoprotection. These unfixed tissues were then embedded in OCT, cut and stored just as described above.

2.3.5.2 Immunohistochemistry and immunofluorescence

Frozen sections were thawed at room temperature for 10 min. They were initially washed in PBS for 10 minutes. Sections were then outlined using a PAP pen (Vector Laboratories, USA) if necessary. If required, permeabilisation was done in PBS + 0.5% triton X-100 for 15 minutes. For HRP-based detection, endogenous peroxidase activity was quenched by room temperature incubation of BLOXALL™ (Vector Laboratories, USA) for 10 min. Sections were then blocked for 30 min in blocking buffer. The primary antibodies were then diluted in blocking buffer and applied to the sections and incubated overnight at 4°C. Sections were washed in PBS for 10 minutes. The secondary antibodies were diluted in blocking buffer, applied to the sections and incubated for 1 hour at room temperature. The sections were washed again in PBS. For immunofluorescence, nuclei were stained with Hoescht (Invitrogen, USA) diluted in PBS to 5µg/ml and mounted using VectaMount Acqueous Mounting Media (Vector Laboratories, USA). For HRP-based detection, the sections were incubated with the HRP substrate DAB chromogen (Pierce, USA) for 10min and mounted in glycerol.

For certain antibodies, listed in Table 2.9, unfixed tissue sections required fixation in ice-cold methanol, as PFA fixation prevented antibody binding. After thawing, slides were washed briefly in PBS for 1 min, before immersion in ice-cold methanol for 10 min at -20°C. These methanol-fixed sections were washed twice in PBS for 5 min each before blocking and primary antibody incubation.

In addition, non-antibody lectin reagents (Table 2.10) were used for labelling vasculature or vasculature and microglia – these are Isolectin IB4 (Ernst & Christie, 2006) and Tomato Lectin (Robertson et al., 2014; Villacampa et al. 2013) respectively. These could either be used on their own or simultaneously with antibody staining. After thawing slides and washing in PBS, lectin reagents were diluted in blocking buffer (with or without additional antibodies for double staining), applied to slides and incubated overnight at 4°C. Slides could then be washed in PBS and mounted, or any antibody staining could be continued as outlined above.

Antibody	Manufacturer	Catalogue number	Host IgG	Dilution	Methanol fixation?
PDGFR-β	Santa Cruz	Sc-432	Rabbit	1:300	-
β-galactosidase	Promega	Z3781	Mouse	1:100	-
Iba-1	Abcam	ab108539	Rabbit	1:300	-
Laminin	Abcam	ab11575	Rabbit	1:100	-
Collagen IV	Abcam	ab6586	Rabbit	1:100	-
α-Smooth Muscle Actin	Abcam	ab5694	Rabbit	1:100	-
NG2	Millipore	AB5320	Rabbit	1:200	-
Calbindin	Abcam	ab25085	Rabbit	1:100	-
GFAP	Abcam	ab7260	Rabbit	1:200	-
βIII Tubulin	Abcam	ab18207	Rabbit	1:1000	-
Perlecan	Abcam	ab2501	Rat	1:200	-
VE-cadherin	Abcam	ab33168	Rabbit	1:300	Required
ZO-1 (N-term)	Invitrogen	40-2300	Rabbit	1:100	Required
Claudin-5	Abcam	ab15106	Rabbit	1:100	Required
Rabbit IgG Alexa-488	Molecular Probes	A11034	Goat	1:1000	-
Rabbit IgG Alexa-594	Molecular Probes	A11012	Goat	1:1000	-
Rat IgG Alexa-488	Molecular Probes	A-11006	Goat	1:1000	-
Mouse IgG Alexa-488	Molecular Probes	A-11001	Goat	1:1000	-
Mouse IgG Alexa-594	Molecular Probes	A-11005	Goat	1:1000	-
Rabbit IgG HRP-linked	Vector Laboratories	PI-1000	Goat	1:500	-

Table 2.9. List of antibodies used for immunostaining of tissue slides.

Lectin	Conjugated-fluorophore	Manufacturer	Code	Dilution
Isolectin GS-IB4	Alexa-488	Thermo Fisher	I21411	1:200
Lycopersicon Esculentum (Tomato) Lectin	Alexa-488	Vector labs	DL-1174	1:500
Lycopersicon Esculentum (Tomato) Lectin	Alexa-594	Vector labs	DL-1177	1:500

Table 2.10. Lectin reagents used.

2.3.5.3 X-gal staining

Frozen sections were thawed at room temperature for 10 min. Sections were washed in PBS for 10 min, and PBS + 2mM $MgCl_2$ for 20 min. Sections were covered in X-gal staining solution (containing 1x X-gal, diluted from stock solution) and covered in a strip of Parafilm® to prevent slides drying. Slides were incubated in a dark humidity chamber for 2 hours to overnight at 37°C. Samples were washed with ddH_2O and PBS. Then, they were either stained with Nuclear Fast Red (Vector Laboratories, USA) as a counterstain and mounted or followed by IHC.

2.3.5.4 Image capture

Images were captured using bright field microscopy (Carl Zeiss Axioskop 2 Plus) with QICAM 12-bit Color Fast 1394 (Qimaging) and QCapture software (Qimaging). For fluorescent images, Hamamatsu ORCA-ER Digital Camera (Hamamatsu, Japan) and µManager software (Stuurman et al. 2011) were used for image acquisition. Images were then processed using Photoshop CS4 (Adobe Systems, USA). Measurements and quantification were done using ImageJ software (open source, developed by the National Institutes of Health, USA).

2.3.5.5 Quantification

Images from different fluorescence filters (for example, FITC and DAPI) were combined in Photoshop CS4. Quantification was carried out using ImageJ software using the following method: regions of interest (ROIs) were selected using the combined fluorescence image if appropriate. These ROIs were then stored and saved. The ROIs were opened and applied to the original single filter image intended for quantification, and mean grey value or integrated density (mean grey value x area) was measured. These

values were then entered into OriginLab (OriginLab Corp., USA) and statistical analysis was performed. p-values were calculated using a two-tailed student's T-test, assuming equal variance.

2.3.5.6 Quantification of microglial branch length

The method outlined by (Morrison & Filosa, 2013) was utilised with a few modifications. Images were pre-processed to remove background staining using a Gaussian blur and the Subtract Background function of ImageJ. A binary image was created and skeletonized using the *Analyze Skeleton* ImageJ plugin (Arganda-Carreras et al. 2010). The resulting skeleton was analysed using the *Analyze Skeleton* function and the sum of all branch lengths was obtained. Biological groups were then compared by performing two-tailed student's T-tests, assuming equal variance. The following macro was utilised to ensure that all images were processed in the same manner.

```
run("Gaussian Blur...", "sigma=1");
run("Subtract Background...", "rolling=50");
setAutoThreshold("Default dark");
//run("Threshold...");
//setThreshold(10, 255);
setOption("BlackBackground", false);
run("Convert to Mask");
run("Skeletonize (2D/3D)");
run("Analyze Skeleton (2D/3D)", "prune=none prune show");
```

2.3.6 Embryonic hindbrain vasculature analysis

2.3.6.1 Tissue harvest and preparation

Timed matings were set up by housing a male and female mouse overnight. Same genotype matings were set up in order to ensure the genotype of resulting embryos; i.e. wild-type x wild-type, $OMD^{-/-}$ x $OMD^{-/-}$ and $PRELP^{-/-}$ x $PRELP^{-/-}$ matings were set up. The next day, the females were checked for vaginal plug – if a plug was seen, that day was noted as being 0.5 day post-coitum (dpc). The pregnant mouse was then culled at 12.5 dpc using a rising concentration of CO_2.

Embryos were freed from their embryonic sacs and collected using a cut Pasteur pipette. They were then transferred to a dish containing cold PBS. Hindbrains were dissected according to a published protocol (Fantin et al. 2013) under a dissecting microscope. Briefly, using sharp forceps, embryos were decapitated above the forelimbs and the front of the heads were removed. The roof-plate above the hindbrain was ruptured at the level of the fourth ventricle and peeled away. Carefully, the pial membrane underneath the hindbrain was teased away. Each dissected hindbrain was transferred to a well in a 24-well cell culture plate and fixed with 4% PFA at 4°C for two hours.

2.3.6.2 Immunofluorescence

After fixation, hindbrains were washed in PBT and incubated with blocking buffer for 1 hour at room temperature (RT) with gentle agitation. Primary antibodies or lectin reagents (Table 2.9, Table 2.10) were diluted in blocking buffer and incubated overnight at 4°C. The following day, hindbrains were washed in PBT for 3 x 15 min. Secondary antibodies (Table 2.9) were then diluted in blocking buffer and incubated overnight at 4°C. Just as before, hindbrains were washed in PBT for 3 x 15 min.

Spacers were created on the slides using two thickness No. 1 (0.13mm to 0.16mm thickness) coverslips. These coverslips were attached to the slides using small drops of clear nail polish. A hindbrain was carefully pipetted onto the slides, in between the spacers, and using a fine-tip Pasteur pipette, excess solution was aspirated. A drop of VECTASHIELD Mounting Media (Vector Laboratories, USA) was applied to the hindbrain and then coverslipped. Clear nail polish was then used to ensure that the coverslips were secure.

2.3.6.3 Image capture

Images were captured on Zeiss Confocal Microscope 710 using the 10x and 40x water immersion lenses. After optimising the laser intensity settings, settings were recorded and unaltered for the imaging session Images were exported using Zen Black software (Zeiss, Germany).

2.3.6.4 Quantification

For quantifying vessel density, Tomato Lectin or Isolectin IB4-staining images were simplified and made into an ROI using the following macro:

```
run("16-bit");
run("Despeckle");
run("Subtract Background...", "rolling=50");
run("Median...", "radius=2");
run("Auto Threshold", "method=Huang white");
run("Create Selection");
roiManager("Add");
```

Briefly, images were de-speckled, background subtracted and applied with a median filter at 2px in order to remove all background noise. Huang auto-threshold was then applied, and the threshold was saved as an ROI. This ROI was then used as the "outline" of immunostaining to measure.

In order to quantify branches, branches were manually counted and drawn as dots over the image as a new layer in Photoshop CS4. The resulting new layer in Photoshop was saved as a separate image and opened in ImageJ – the Analyse Particles tool was used to

automatically count the number of dots, giving me a value for the number of branches I counted. Two-tailed student's T-tests, assuming equal variance, were then performed to identify any differences between groups.

In addition, the program AngioTool (Zudaire et al. 2011) was utilised to quantify parameters relevant to vasculature, such as percentage vessel area, junction density, vessel length, number of end-point and mean E lacunarity. Images were processed as above using ImageJ and opened in AngioTool. Using the overlay as a guideline, the slider controlling vessel intensity and diameter was moved to obtain the closest match to my image. In addition, depending on the nature of the image, the options to "Remove Small Particles" and/or "Fill Holes" were toggled. Results were saved as an annotated image and accompanying spreadsheet. Data was compiled and analysed for statistical significance using 2-tailed t-tests.

2.4 Cell culture methods

2.4.1 Basic cell culture set-up

Cell culture was performed inside a hood (Microflow II Biological Cabinet). A vacuum pump system was used to aspirate media, taking care to change the glass pipette if more than one cell line was being manipulated at one time. Cells were incubated in a humid 5% CO_2 37°C incubator (Sanyo, MCO-18AIC, Japan). Cells were monitored and viewed using an inverted microscope (Leica, Germany). Images were taken using the QICAM 12-bit Color Fast 1394 (QImaging, Canada) camera and QCapture software (QImaging, Canada).

2.4.2 Human Embryonic Kidney 293 (HEK293)

2.4.2.1 Harvesting HEK293

Human embryonic kidney HEK293 cells (ATCC number CRL-1753) were maintained in DMEM (Dulbecco's Modified Eagle's medium; Gibco, USA) supplemented with 10% Foetal Bovine Serum (Table 1.2). Cells were passaged when they reached 70% confluency, typically every 2-3 days; cells were washed in 1x PBS, and incubated in 0.025% trypsin-EDTA (Gibco, USA) for 5 min at 37°C. Trypsin was inactivated by the addition of serum-supplemented DMEM, and cells were spun at 2,500rpm for 5min, resuspended and seeded into the appropriate flasks, dishes or plates. Typically, cells were seeded into 25cm^2 flasks for maintenance, and in 10cm^2 dishes or 6-well plates for experiments. Cells were always kept in an incubator at 37°C with 5% CO_2.

2.4.2.2 Transfection of HEK293 cells and preparation of conditioned media

Plasmids with pCS2 backbone were used for transfections of HEK293 cells. The plasmid and Lipofectamine mixture was incubated at room temperature for 15 min. In parallel, cell media was replaced with Opti-MEM, washing cells with PBS to remove serum. The plasmid and Lipofectamine mixture was then added to the cells and they were returned to the incubator. 24 hours after transfection, the transfected cells' media was collected, centrifuged and used as necessary. Conditioned media was made fresh each time it was needed.

2.4.3 Mouse Embryonic Fibroblasts (MEFs)

2.4.3.1 Harvest of mouse embryonic fibroblasts (MEFs)

Timed matings were set up by housing a male and female mouse overnight. Same genotype matings were set up in order to ensure the genotype of resulting embryos; i.e. wild-type x wild-type, $OMD^{-/-}$ x $OMD^{-/-}$ and $PRELP^{-/-}$ x $PRELP^{-/-}$ matings were set up. The next day, the females were checked for vaginal plug – if a plug was seen, that day was noted as being 0.5 day post-coitum (dpc).

Mouse embryonic fibroblasts (MEFs) were created using an establish protocol (Jozefczuk et al. 2012). Briefly, prior to culling pregnant mice, T75 cell culture flasks were coated with 0.2% gelatin (gelatin from bovine skin, type B) for two hours. Then, pregnant mice were culled after 13.5dpc using a rising concentration of CO_2. Uterine horns were removed and rinsed briefly in 70% ethanol and immersed in PBS. In a tissue culture hood, uterine horns were placed in sterile petri dishes and using autoclaved tools, each embryo was freed from the placenta and its embryonic sac. Then, each embryo's head and red organs were removed. The remaining tissues were finely minced using a razor. 1ml 0.05% trypsin-EDTA (Gibco, USA) with 100 units DNase I (Stemcell Technologies, Canada) was added per embryo and then transferred to a 50ml tube and incubated at 37°C for 15min. During this incubation period, tissue was pipetted up and down using a serological pipette every 5min to help further dissociate the tissue. Trypsin was inactivated by adding 1 volume of warm MEFs media (Table 2.2). Cells were centrifuged at low speed for 5min and the resulting cell pellet was resuspended in MEFs media. The equivalent of 2-3 embryos was added to previously gelatin-coated T75 flasks and allowed to grow in the tissue culture incubator. Fibroblasts from these embryos are only cells capable of attaching to gelatin-coated flasks (Jozefczuk et al., 2012).

After 24 hours of culture, cells were checked; if confluent, cell stocks were made. Cells were harvested using 0.05% Trypsin/EDTA (Gibco, USA) and centrifuged at low speed for

5 min. Then, MEFs were resuspended in cryopreserving solution, aliquoted in cryotubes and frozen in Mr. Frosty (Nalgene, USA) at -80°C overnight. The next day, frozen tubes were put into a liquid nitrogen tank for long-term storage.

2.4.3.2 DNA extraction from MEFs

MEFs were grown in 60mm dishes until confluent. Then, AllPrep extraction kit (Qiagen, Germany) was used to extract genomic DNA following the manufacturer's instructions. Eluted DNA was used for genotyping by PCR (see Sections 2.3.1.2 and 2.3.1.3).

2.4.3.3 X-gal and FDG staining in MEFs performed by Dr Orita

X-gal staining was performed using the β-gal Staining Kit purchased from Invitrogen, which is optimized for detecting β-galactosidase enzyme activity in cultured cells. Staining was performed according the manufacturer's instructions. Briefly, cells were washed with PBS and fixed with Fixing Solution for 10min at RT. The Staining Solution containing 1mg/ml X-gal was prepared. Cells were washed twice with PBS and the Staining Solution applied to cells and incubated at 37°C for 2 hours in the dark. An alternative β-galactosidase substrate, Fluorescein Di-β-D-Galactopyranoside (FDG), was also utilized; when cleaved by β-galactosidase, a green fluorescent product is produced.

2.4.3.4 Treatment of MEFs with protein and subsequent protein extraction

MEFs were seeded in 24-well plates at 50,000 cells per well. The following day, cells were ready for treatment with protein. Cells were treated with 0, 5, 10 and 100ng/ml protein (Table 2.11) in serum-free media for 30 min at 37°C. Plates were then transferred onto ice and washed with cold PBS. Liquid was then aspirated and cells were lysed by incubation for 30 min at 4°C with 200µl RIPA buffer supplemented with phosphatase and protease inhibitor HALT (Thermo Fisher, USA). Protein samples were spun down, transferred to a new tube, denatured by the addition of reducing agent β-mercaptoethanol and incubated at 95°C for 5 min before being placed on ice. Protein samples were then analysed by western blotting (see Section 2.5.3 for more details)

Protein	Manufacturer	Code	Species
bFGF	R&D Systems	233-FB-025	Human
EGF	R&D Systems	236-EG-200	Human
PDGF-BB	R&D Systems	220-BB-010	Human
VEGFA-165	R&D Systems	293-VE-010	Human
TGF-β	R&D Systems	240-B-002	Human

Table 2.11. Proteins applied to MEF cells to study down-stream effects. Proteins were reconstituted in the buffer recommended by the manufacturer and stored in aliquots at -80°C.

2.4.4 Human Umbilical Vein Endothelial Cells (HUVEC)

2.4.4.1 HUVECs culture

Human umbilical vein endothelial cells (HUVECs; ATCC number PCS-100-010) were maintained in Medium 200 supplemented with Large Vessel Endothelial Supplement (LVES; Gibco, USA) (Table 2.2). Cell medium was changed every two days until cells were 80% confluent.

2.4.4.2 Passaging HUVECs

80% confluent HUVECs were washed with PBS and incubated with 0.5% Trypsin/EDTA solution (Gibco, USA). Trypsin treatment was monitored under the inverted microscope to ensure that cells were not exposed to trypsin for longer than necessary. After approximately 5 min, the cells would typically become round; the flask or dish was tapped gently to dislodge cells. HEK293 media, which contains 10% FBS (Table 2.2), was used to render the trypsin inert. The cells were collected in a 15ml tube, and the flask or dish was washed with supplemented Medium 200 in order to collect as many cells as possible. Cells were spun at 1,200rpm for 5 min and resuspended in the appropriate medium.

2.4.4.3 Thawing and freezing HUVECs

When initiating the culture of HUVECs, cells were seeded at a concentration of 1.25 x 10^4 per cm^2 cells in 75cm^2 flasks. Media was changed every two days until cells were 80% confluent; in order to maintain early passages of HUVECs, cells were frozen in early passages. Cells were suspended in FBS with 10% DMSO in cryo-tubes (PAA, UK). Cells were frozen overnight in a Nalgene Mr. Frosty Cryo 1°C Freezing Container; the following day, the tubes were transferred to liquid nitrogen for long-term storage.

2.4.4.4 Endothelial tube formation assay

GelTrex Matrix (Gibco, USA) basement membrane extract was thawed the night before or 2 hours before the experiment at 4°C. Geltrex Matrix irreversibly solidifies and gels rapidly above 15°C, and was therefore kept on ice at all times. Geltrex Matrix was applied

to the growth surface and spread using the pipette tip (Table 2.12). The coated plates were then incubated at 37°C for 30 min, ensuring that the Geltrex Matrix has fully solidified. Harvested HUVECs were diluted 1:1 in 0.4% Trypan Blue and numbers were counted and determined using a haemocytometer and then diluted to 4 x 10^4 cells/cm^2 in Medium 200 and applied to the Geltrex Matrix-containing wells. Supplemented Medium 200 was used as a positive control, as it contains growth factors required for endothelial cell growth. HUVECs formed tubules when grown at 37°C. As endothelial cells typically underwent apoptosis after 24 hours, images were taken 16 hours after the start of the incubation. To facilitate imaging, cells were labelled with Calcein AM (eBioscience, USA) by incubation with 3uM Calcein AM for 15 min. Images were taken using the 4x lens and green fluorescence FITC filter. HUVECs were then fixed in 4% PFA for 10mins, washed in PBS and stored at 4°C.

Growth surface	Area (cm^2)	Geltrex per cm^2 (µl)	Geltrex used (µl)
6-well plate	9.5	50	475
12-well plate	3.8	50	190
24-well plate	1.9	100	190
µ-Slide Angiogenesis (Ibidi)	0.1 (lower)	100	10

Table 2.12. Volume of Geltrex Matrix used for different growth surfaces.

2.4.4.5 HUVEC monolayers

24-well transwell inserts (Corning, USA) were coated with 25µg/ml fibronectin for 4 hours at 37°C or overnight at room temperature. HUVECs were harvested and suspended in Medium 200 + LVES before being counted and seeded at 70,000 cells per upper chamber of the transwell. The bottom compartment was filled with LVES and conditioned medium prepared from transfected HEK293 (see Section 2.4.2.2). Monolayers were allowed to form for 4 days thereafter.

2.4.5 Mouse brain endothelial cell (MBEC) isolation

Prior to MBEC isolation, 24-well transwell inserts were coated with 100µg/µl fibronectin and 500µg/µl collagen IV for 4 hours at 37°C or overnight at room temperature. MBECs were isolated and prepared according to a published protocol (Welser-Alves et al., 2014) with some modifications. 10-week old mice were sacrificed using a rising concentration of CO_2 and brains were removed. Brains were rolled on filter paper to remove the meninges and immersed in MEM-HEPES. A sterile blade was used to mince the tissue, ensuring that no large chunks remained. Minced tissue was collected in a 15ml tube and centrifuged at 300 x g for 5 min. The excess media was removed and tissue was

dissociated using papain and DNase I (Worthington Biochemicals, USA) for 1 hour and 10 min. The volume of papain and DNase I was determined depending on the number of brains used according to Table 2.13.

Number of brains	Volume of papain (µl)	Volume of DNase I (µl)
1	833.3	41.7
2	1,666.6	83.4
3	2,500.0	125.1µl

Table 2.13. Volume of papain and DNase I utilized for dissociating brain tissue.

Following tissue dissociation, tissue was gently titurated using a 18G needle and 1ml syringe. Ideally, vessels would be separated from surrounding tissue, but not entirely broken as isolated endothelial cells survive poorly in culture. 7ml 22% BSA was then added and mixed well. The BSA and tissue mixture was centrifuged for 10 min at 1,300 x g. Endothelial cells would be found in the pellet, whereas contaminating CNS cells in the myelin and BSA layer floating on top. The myelin-BSA layer was gently decanted in a new tube, mixed well, and spun again at 1,300 x g for 10 min. The pellets containing vessel fragments were pooled, washed with F12 media and spun at 300 x g for 5 min. Cells were resuspended in 1ml MBEC media per brain and seeded onto transwell inserts at 300µl per transwell.

The following day, transwell inserts were washed 3 times with F12 media to remove non-adherent cells and debris. Media was then replaced with MBEC media containing 4µg/µl puromycin for 3 days. After puromycin treatment, cells were washed with F12 media and grown in MBEC media without puromycin until monolayers were confluent. Confluency was determined using TEER measurements (see below).

2.4.6 Endothelial monolayer methods

2.4.6.1 TEER measurements

Since TEER values can fluctuate with temperature, cells were allowed to equilibrate to room temperature before resistance was measured using an EVOM Volt-Ohmeter (World Precision Instruments, USA). The STX2 "chopsticks" electrodes were disinfected using 70% ethanol and allowed to air-dry. Then, the longer electrode was inserted into the bottom compartment and the shorter electrode in the upper chamber as shown in Figure 2.3. Resistance was first measured for a blank – a coated transwell insert with the appropriate media; R_{Blank}. The resistance across the cell layer was then determined; R_{Total}. The resistance of the monolayer was therefore determined by the difference between Total and Blank resistance; i.e. $R_{Tissue} = R_{Total} - R_{Blank}$. Since resistance is inversely

proportional to area, TEER values reported were determined by multiplying raw resistance values by transwell growth area; i.e. TEER ($\Omega * cm^2$) = R_{Tissue} (Ω) * area (cm^2). Calculations were based on information provided by (Srinivasan et al., 2015).

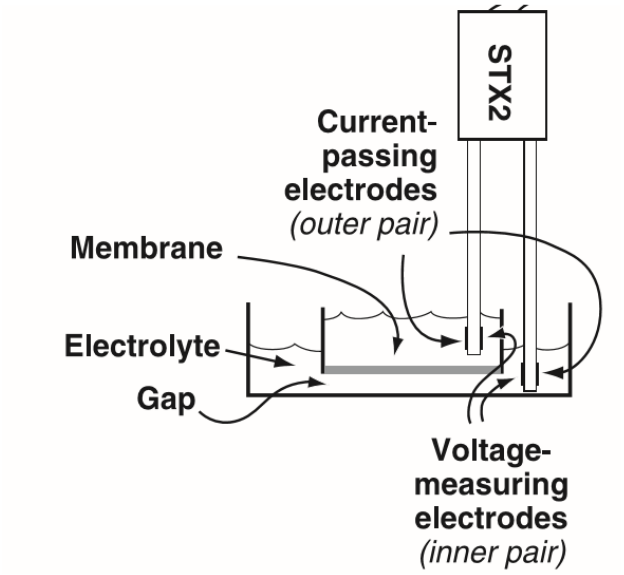

Figure 2.3. TEER measurement using STX2 "chopsticks" electrode. The longer electrode is immersed in the lower compartment, while the shorter electrode is in the upper compartment – the electrodes are therefore separated by the monolayer. Figure from World Precision Instruments manual.

2.4.6.2 Permeability measurements using FITC-Dextran

25mg/ml 70kDa FITC-Dextran (Life Technologies, USA) was diluted to 1mg/ml in the appropriate endothelial cell growth medium. The upper compartment of the transwell was replaced with 1mg/ml Dextran in media. After 1 hour, 100µl media from the lower compartment was collected and pipetted into an opaque black 96-well plate. Fluorescence was measured using a Modulus Microplate plate reader (Turner Biosystems, USA).

2.4.6.3 Immunofluorescence of cells grown on membrane

Transwell inserts were washed in PBS to remove excess media and fixed either with 4% PFA or ice-cold methanol/acetone 1:1 solution for 10 min at RT. Cells were washed with PBS three times and cells were stained directly on the transwell inserts. Cells were blocked using 10% goat serum for 1 hour at RT and primary antibodies (Table 2.14) were incubated for 1 hour at RT or overnight at 4°C. Transwell inserts were washed three times with PBS prior to incubation with secondary antibody. After washing with PBS, nuclei were stained using 5µg/ml Hoescht solution (Invitrogen, USA). Membranes were

carefully cut using a sharp scalpel and mounted on glass slides using VectaShield (Vector Laboratories, USA) cell-side up.

Antibody	Manufacturer	Code number	Host IgG	Dilution	Methanol fixation?
PECAM-1	Abcam	ab28364	Rabbit	1:50	-
VE-cadherin	Abcam	ab33168	Rabbit	1:200	Yes
Rabbit IgG Alexa-488	Molecular Probes	A11034	Goat	1:1000	-

Table 2.14. Antibodies used for endothelial cell monolayer staining.

2.5 Protein analysis methods

2.5.1 Immunoprecipitation

Protein G-Sepharose (GE Healthcare, USA) bead slurry was washed with TNEB. Excess buffer was removed using a 40G needle and 1ml syringe. Beads were resuspended in TNEB supplemented with protease inhibitor and incubated with conditioned media or cell lysate and the chosen antibody overnight at 4°C (Table 2.15). Beads were spun down and washed with TNEB three times and excess buffer was removed. 10µl TNEB and 10µl 2x Laemmli sample buffer (Bio-rad, USA) containing β-mercaptoethanol were added and the mixture heated at 95°C for 5min. Samples were then placed on ice for 5 min before loading onto polyacrylamide gels.

Antibody	Manufacturer	Host species	Dilution (IP)	Dilution (IB)
Myc tag	CST #2276	Mouse	1:1000	1:1000
FLAG tag	Sigma F3165	Mouse	1:1000	1:1000

Table 2.15. List of antibodies used in immunoprecipitation experiments. IP: Immunoprecipitation; IB: immunoblotting.

2.5.2 Preparation of cell lysates

Loosely-adherent cells, such as HEK293, were harvested using a cell-scraper, spun down and lysed using cold RIPA buffer supplemented with HALT protease inhibitor (Thermo Scientific, USA). Strongly-adherent cells, such as MEFs, were lysed by incubation of cells with RIPA buffer supplemented with HALT protease inhibitor for 30 min at 4°C with agitation. Cell lysates were spun at maximum speed for 10 min and supernatants transferred to a fresh tube. Samples were then mixed with 2x or 4x Laemmli sample buffer

(Bio-Rad, USA) with β-mercaptoethanol and frozen for later use or used immediately after heating at 95°C for 5 min.

2.5.3 Western blotting

2.5.3.1 Making acrylamide gels

Depending on the size of the protein of interest, different concentration acrylamide gels were made, according to Table 2.16. The reagents were added in order, paying special attention to make a fresh solution of ammonium persulfate each time. Bio-Rad glass plates were assembled and the separating gel was carefully pipetted in between glass plates. ddH_2O was then pipetted above the separating gel to help flatten the upper surface. Once the separating gel set, the stacking gel was prepared and pipetted just like before in between the glass plates. The comb was then inserted in between the glass plates and the stacking gel was allowed to set. At each step, a small amount of separating and stacking gel solution was kept to the side in order to assess when the gels were set.

Acrylamide percentage	10%	12%	15%	Stacking gel
Molecular weight range	20kDa – 300kDa	10kDa – 200kDa	3kDa – 100kDa	-
ddH_2O	3.8ml	3.2ml	2.2ml	3ml
Acrylamide (30%)	3.4ml	4ml	5ml	0.67ml
1.5M Tris-HCl, pH 8.8	2.6ml	2.6ml	2.6ml	-
0.5M Tris-HCl, pH 6.8	-	-	-	1.25ml
10% SDS	100µl	100µl	100µl	50µl
10% ammonium persulfate	100µl	100µl	100µl	50µl
TEMED	10µl	10µl	10µl	5µl
Total volume	~10ml	~10ml	~10ml	~5ml

Table 2.16. Separating and stacking gels for western blotting. Different acrylamide percentage separating gels were made depending on the molecular weight of the proteins I sought to detect. After polymerisation of the separating gel, the stacking gel was made and a comb inserted in between the glass plates.

2.5.3.2 SDS-PAGE, transfer, blocking and antibody incubations

Samples were loaded into the wells of the gel and run at 80V for 30 min initially and then at 100V for approximately 1 hour. The PVDF membrane was activated by rinsing in methanol, and the transfer chamber was set up, placed on ice and run at 60V for 2 hours.

The membrane was trimmed and blocked in blocking buffer (5% skimmed milk powder in TBST) for 1 hour and the primary antibody was diluted in TOYOBO Can Get Signal solution 1 (TOYOBO, Japan) and incubated overnight at 4°C (Table 2.17). However, if an antibody against a phosphorylated protein was going to be used, membranes were instead blocked in 5% BSA in TBST. The following day, the membrane was washed three times in TBST for 15 min before incubating the secondary antibody diluted in TOYOBO Can Get Signal solution 2. The membrane was washed three times in TBST for 15 min, and the ECL or ECL Plus (Pierce, USA) reagent was prepared and applied to the membrane for 1 min. Excess ECL reagent was then discarded and the membrane blotted dry slightly before being wrapped in clingfilm and adhered to the exposure cassette. The membrane was exposed to X-ray film (Fujifilm, Japan) in a dark room and developed using an X-ray developer. Films were typically exposed for 1 min and developed; the exposure time was then modified depending on this signal. The resulting films were then scanned at 300dpi and bands analysed in ImageJ. Integrated density of each band was measured (see Section 2.5.3.3).

Membranes were rinsed in TBST then stripped using stripping buffer (Thermo Fisher, USA) for 5 to 15 min and washed in TBST. The blocking step was repeated as above and a different primary antibody was incubated. Subsequent steps were the same as above. Membranes were stripped a maximum of 3 times.

Antibody	Manufacturer & catalogue number	Host species	Dilution	Expected MW
ERK1/2	CST #4695	Rabbit	1:1000	42kDa, 44kDa
pERK1/2 (Thr202/Tyr204)	CST #4370	Rabbit	1:1000	42kDa, 44kDa
p38 MAPK	CST #9212	Rabbit	1:1000	43kDa
p-p38 MAPK (Thr180/Tyr182)	CST #4511	Rabbit	1:1000	43kDa
Akt	CST #9272	Rabbit	1:1000	60kDa
pAkt (Ser 473)	CST #4060	Rabbit	1:2000	60kDa
Myc tag	CST #2276	Mouse	1:1000	-
FLAG tag	Sigma F3165	Mouse	1:1000	-
Anti-mouse IgG HRP-linked	CST #7076	Horse	1:2000	-
Anti-rabbit IgG HRP-linked	CST #7074	Goat	1:2000	-

Table 2.17. List of antibodies used for western blotting.

2.5.3.3 Quantification of bands using ImageJ

Scanned images were straightened using Photoshop, opened in ImageJ and converted to an 8-bit image (Figure 2.4A). Using the rectangular marquee tool, the first band of the western blot was selected (Analyse Gels; Select First Lane), ensuring that the selection was tall enough for an appropriate background reading and is wide enough to accommodate the band. The rest of the bands were selected (Analyse Gels; Select Next Lane) (Figure 2.4B) and a histogram was generated (Analyse Gels; Plot Lanes) (Figure 2.4C). A line was manually drawn to mark the baseline of the peak and area was measured by selecting the area using the wand tool (Figure 2.4D). The resulting value was then utilised for analysis. The expression of phosphorylated proteins was normalized to that

of total protein; for example, in the case of phospho-ERK (pERK), values were normalized to total-ERK (ERK). The final value is therefore the ratio of pERK/ERK.

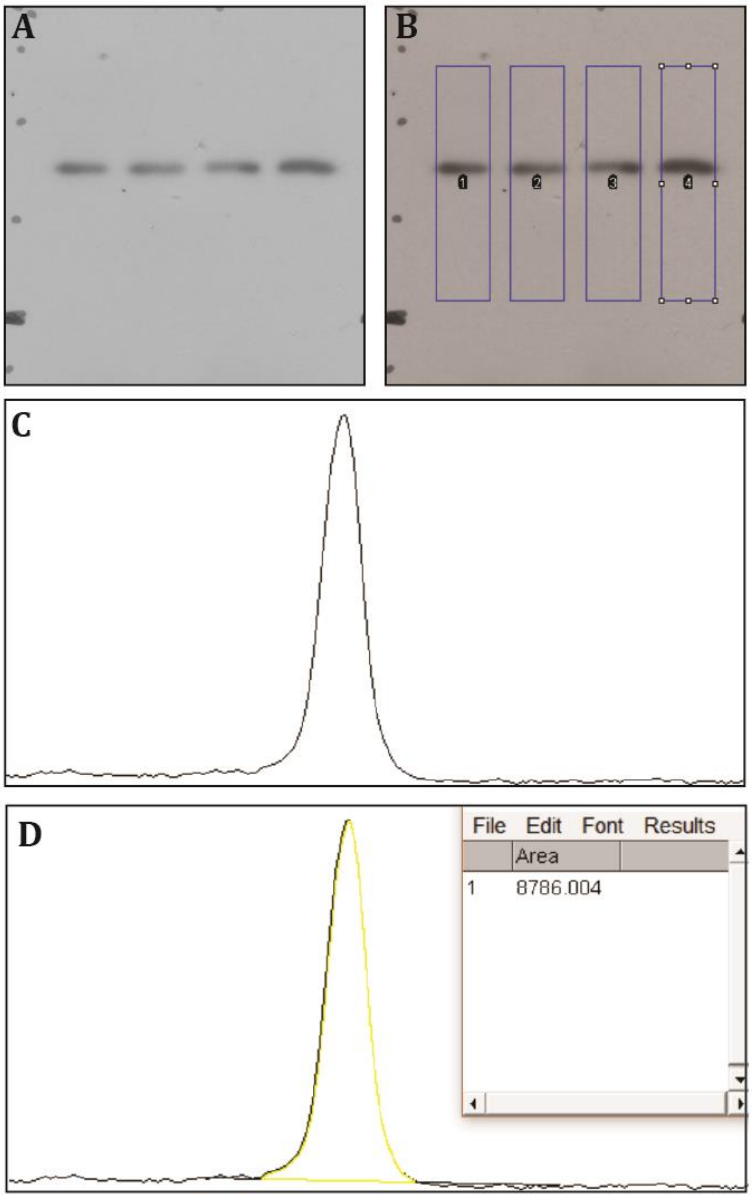

Figure 2.4. Quantification of western blot bands in ImageJ. A) Image converted to 8-bit mode and lanes were selected **(B)**. Histogram was created **(C)** and after manual assessment of the baseline, area of the peak was measured **(D)**.

2.6 DNA methods

2.6.1 Plasmids

A variety of plasmids were used throughout this project (Table 2.18). pCS2 plasmids were used for overexpressing proteins in HEK293 cells, as they are optimised for mammalian expression. The pCS2 vector contains a cytomegalovirus (CMV) promoter and SV40 late

polyA terminator. The vector also contains an ampicillin resistance cassette to propagate the plasmids in bacteria.

Plasmid name	Insert	Tag	Origin	Application
pCS2-MT	-	-	Acquired from RZPD	Empty vector
pCS2+MT	-	C-term Myc	Acquired from RZPD	Empty vector
pCS2-OMD	OMD (human)	-	Cloned by Dr Julie Watson	Mammalian expression
pCS2-OMDmyc	OMD (human)	C-term Myc	Cloned by Dr Julie Watson	Mammalian expression
pCS2-PRELP	PRELP (human)	-	Cloned by Dr Julie Watson	Mammalian expression
pCS2-PRELPmyc	PRELP (human)	C-term Myc	Cloned by Dr Julie Watson	Mammalian expression
pCS2 -PR PRELP	PRELP (human) Deleted aa 21-157	-	Cloned	Mammalian expression
ΔN-terminal-PRELP	PRELP (human) Deleted N-terminal	-	Gift from Dr Anders Aspberg	
pCS2 -NT PRELP	PRELP (human) Deleted aa 1-157	-	Cloned	Mammalian expression
pCS2-TGFβ1-FLAG	TGF-beta1 (porcine)	C-term FLAG	Cloned by Dr Noriaki Sasai	Mammalian expression

pPICZalphaA_VEGF-A121_Nhis	VEGFA 121 (human)	His	Gift from Dr Philipp Berger	Expression in *Pichia pastoris*
pCS2-VEGFA 121	VEGFA 121 (human)	-	Cloned	Mammalian expression
pCS2-VEGFA 121 FLAG	VEGFA 121 (human)	C-term FLAG	Cloned	Mammalian expression
pPIZAalphaA_hVEGF-A165_Nhis	VEGFA 165 (human)	His	Gift from Dr Philipp Berger	Expression in *Pichia pastoris*
pCS2-VEGFA 165	VEGFA 165 (human)	-	Cloned	Mammalian expression
pCS2-VEGFA 165 FLAG	VEGFA 165 (human)	C-term FLAG	Cloned	Mammalian expression
pPIZAalphaA_hVEGF-A165b_Nhis	VEGFA 165b (human)	His	Gift from Dr Philipp Berger	Expression in *Pichia pastoris*
pCS2-VEGFA 165b	VEGFA 165b (human)	-	Cloned	Mammalian expression
pCS2-VEGFA 165b FLAG	VEGFA 165b (human)	C-term FLAG	Cloned	Mammalian expression

Table 2.18. Plasmids used throughout project.

2.6.2 DNA purification

Bacterial colonies were picked and seeded into LB media containing ampicillin (100µg/ml). Cells were incubated at 37°C with agitation at 250rpm overnight and harvested the next day by centrifugation at 4,000 rpm for 5 min. Mini- and midi-prep kits (Qiagen, Germany) were used to purify plasmid DNA, according to the manufacturer's instructions. DNA concentration and purity was determined using the Nanodrop ND-1000 spectrophotometer (Thermo Fisher, USA).

2.6.3 Restriction enzyme digest

Restriction enzyme digests were performed in order to confirm the identity of a plasmid, or for the purposes of sub-cloning. Plasmid DNA was incubated with 10X reaction buffer containing BSA (NEB; New England Biolabs, USA) and restriction enzyme(s). Water was

used to adjust the final volume of the reaction (typically 10µl-15µl). In the case of double digests, the appropriate reaction buffer was determined using New England Biolabs' online Double Digest Finder tool. The restriction enzymes used in this project are listed in Table 2.19.

Depending on the purpose, a different amount of plasmid DNA was digested; for example, for preparing a vector backbone for sub-cloning, 2µg plasmid was digested.

Restriction enzyme	Manufacturer	Reaction buffer
EcoRI	NEB	NEB Buffer 3.1
XhoI	NEB	NEB Buffer 3.1
BamHI	NEB	NEB Buffer 3.1
ClaI	NEB	NEB Buffer 3.1

Table 2.19. Restriction enzymes used in this project.

2.6.4 Gel electrophoresis

1-2% (w/v) agarose gels were made by dissolving agarose (Fisher Scientific, UK) in 1X TAE and dissolved in the microwave, ensuring that the gel did not boil. SYBR Safe DNA gel stain (Invitrogen, USA) at 1X concentration was added to allow visualization of DNA. The gel was poured into the appropriate moulds and allowed to solidify before removing comb. The solidified gel was transferred to a gel tank and submerged in 1x TAE.

In the first well, 1kb DNA ladder (NEB, USA) was applied. 6x loading gel (NEB, USA) was added to each DNA sample, and loaded into subsequent wells. The gel was run at 100V for 30 min to 1 hour until the dye front reached the bottom of the gel. DNA was visualized and images were captured using a UV transilluminator.

2.6.5 Purification of DNA from agarose gel

DNA was purified from agarose gels for sub-cloning. Using a UV transilluminator, the desired DNA fragment was cut out and transferred to a pre-weighed microcentrifuge tube. The microcentrifuge tube was weighed again in order to determine the mass of the agarose gel fragment which was cut out. DNA was purified using NucleoSpin Gel and PCR Clean-up kit (Machery-Nigel, Germany) according to the manufacturer's instructions.

2.6.6 PCR for sub-cloning

PCR was used to amplify fragments of DNA used for sub-cloning. Template DNA and custom PCR primers were used with Phusion High-Fidelity DNA polymerase (NEB, USA). The reaction conditions are listed in Table 2.20, and the PCR cycle in Table 2.21.

Reagent	Volume (µl)	Final concentration
5x Phusion HF-buffer	20	1x
50mM $MgSO_4$	2	1mM
DMSO	5	5%
10mM dNTP	3	0.3mM
Phusion DNA polymerase	1	1.0units/50µl PCR
Template DNA	1	0.5mM
Primer (x2; 10uM each)	1 (x2)	0.1uM each
ddH_2O to 100µl	66	-

Table 2.20. PCR reaction conditions for 100µl total volume.

Temperature (°C)	Time	Number of cycles
96	5 min	-
96	30 s	40 cycles
55	30 s	
72	1 min 30 s	
72	10 min	-
4	Hold	-

Table 2.21. PCR cycle used.

2.6.6.1 Primers used for PCR

Custom primers were purchased from Sigma-Aldrich (USA) and are listed below in Table 2.22.

Primer	Sequence (5' -> 3')
VEGFA-121 FLAG fw EcoRI	TATAGAATTCGGTTCTCATCACCATCACCATCACGGTTCT
VEGFA-121 FLAG rev XhoI	TATACTCGAGTCATCACTTGTCGTCATCGTCTTTGTAGTCCCGCCT CGGCTTGTCACAATTTTCTTGTCT
VEGFA-165 FLAG fw EcoRI	TATAGAATTCGGTTCTCATCACCATCACCATCACGGTTCT
VEGFA-165 FLAG rev XhoI	TATACTCGAGTCATCACTTGTCGTCATCGTCTTTGTAGTCCCGCCT CGGCTTGTCACATCTGCAAGTACG
VEGFA-165b FLAG fw EcoRI	TATAGAATTCGGTTCTCATCACCATCACCATCACGGTTCT
VEGFA-165b FLAG rev XhoI	TATACTCGAGTCATCACTTGTCGTCATCGTCTTTGTAGTCGTCTTT CCTGGTGAGAGATCTGCAAGTACG
-NT PRELP fw EcoRI	TAGAATTCACACCCAGCTTTCCT
-NT PRELP rev XhoI	TACTCGAGATCCGGTGGCGGAG
-PR PRELP signal peptide fw EcoRI	TATAGAATTCAAATGAGGTCACCCCTCTGCTGGCTCCTCCCA
-PR PRELP signal peptide rev EcoRV	TATAGATATCCTGGCCTTGGGCCACTGAGGCCAAGATGAG
-PR PRELP LRR fw EcoRV	TATAGATATCAGCTTTCCTCAGCCTGATGAACCAGCAGAG
-PR PRELP LRR rev XhoI	TATACTCGAGCTAGATGACCACGGACTGCAGGAGGCGGAAGCA

Table 2.22. Sequences of primers used in PCR amplification. Sequences are written in 5' to 3' direction.

2.6.7 Ligation

Backbone and insert sequences were incubated with 2x ligation mix (Takara Clontech, Japan), and incubated for 2 hours at 14°C. Typically, 7µl purified insert and 1µl purified backbone were added to 7 µl 2x ligation mix. The ratio of insert to backbone was modified in subsequent experiments if the ligation and cloning did not succeed.

2.6.8 Bacterial transformation

The products of the ligation reaction were incubated with 30µl DH5α competent *E. coli* for 30 min on ice. The cells underwent heat shock treatment at 42°C for 40s before being returned onto ice for 5min. Cells were then plated on LB agar plates containing the appropriate antibiotic.

2.6.8.1 Producing chemically-competent cells

A starting culture of DH5α *E. coli* cells were grown overnight in LB media at 37°C with agitation at 250rpm. The following day the starting culture was diluted in a larger volume of fresh LB media in a conical flask to allow cells to enter the exponential phase of growth; cultures were typically diluted 1:100 at the least. After 1 hour, 500µl bacterial culture was removed and the absorbance at 600nm (i.e. OD_{600}) measured to determine the turbidity of the culture. Blank measurements were taken with LB media containing no bacteria. Culture was monitored until the OD_{600} measurement reached 0.4-0.6, where cells would be in the exponential phase. The culture was then split into 50ml tubes and chilled on ice for 10 min before spinning down at 3,000rpm for 10 min. While cells were spinning, microcentrifuge tubes intended to hold cell aliquots were chilled on ice. The supernatant was carefully poured out and cells were resuspended in 10ml TSS buffer per tube; if required, a vortex was used to ensure that cell clumps no longer remained. Cells were then split into 100µl aliquots and frozen at -80°C.

2.7 RNA methods

2.7.1 Meningeal blood vessel RNA extraction for RNA sequencing

Three mice from each genotype were culled using a rising concentration of CO_2. Meningeal blood vessels were dissected from brains under a dissecting microscope as described by (Bowyer et al., 2012). Briefly, brains were removed from mice and immersed in ice-cold PBS to ensure that the meninges remained well-hydrated to prevent adhesion to the surface of the brain. Meningeal vasculature was gently lifted from the surface of the brain starting with the Circle of Willis (Figure 2.5). Care was taken not to scrape the surface of the brain and introduce contaminants. Animals were not perfused with saline; this ensured that the vasculature was easily discernible.

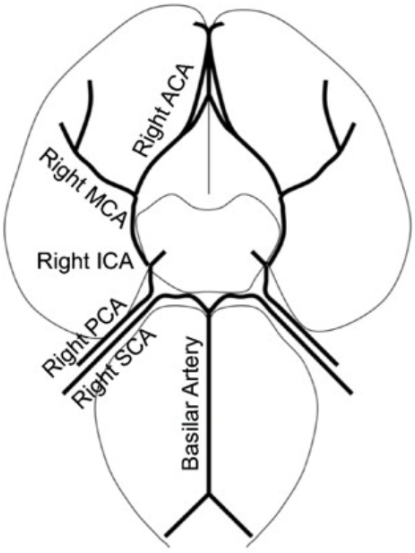

Figure 2.5. Circle of Willis (mouse). Schematic of ventral view of mouse brain, showing the major arteries forming the Circle of Willis. Anterior Cerebral Artery (ACA), Middle Cerebral Artery (MCA), Internal Carotid Artery (ICA), Posterior Cerebral Artery (PCA), Superior Cerebellar Artery (SCA). Modified from (Nuki et al., 2009).

Vessels were put in an RNase-free microcentrifuge tube containing 150µl Extraction Buffer (XB) from ARCTURUS PicoPure RNA Isolation Kit (Applied Biosystems, USA). The contents of the microcentrifuge tube were then transferred to a 1ml dounce homogenizer. The contents were homogenized at room temperature until the mixture had no easily-discernible solid tissue. Samples were transferred to an RNase-free microcentrifuge tube and incubated at 42°C for 30 min. Samples were centrifuged at 3,000 x g for 2 min and transferred to a new tube to eliminate any debris. 100µl RNase-free 70% Ethanol was added to each sample and this mixture was then added to a pre-conditioned spin column. RNA extraction was then performed according to the manufacturer's instructions and eluted each sample in 11µl elution buffer. Samples were then transferred to UCL Genomics for QC analysis, library preparation and RNA sequencing.

Chapter 3 Expression of OMD and PRELP in the brain

3.1 Preface

The function of SLRPs OMD and PRELP are not well understood compared to other members such as decorin or biglycan. As outlined in Chapter 1, many SLRPs have a role in modulating angiogenesis; it is therefore possible that OMD and PRELP may impact vascular function. In order to investigate the effect of OMD and PRELP *in vivo*, transgenic mice were generated. A previous member of the Ohnuma laboratory, Dr Vasiliki Papadaki, performed an initial investigation of OMD and PRELP expression pattern in these knock-out mice and found strong expression in the brain. The aim of this chapter is therefore to elaborate on this work and determine the cell-types expressing OMD and PRELP in the brain.

Many transgenic expression systems utilise reporter genes to facilitate the study of tissue-specific or cell-specific expression of the gene. This is done by replacing the studied gene with a reporter gene, whose expression would then be under the control of the studied gene's promoter (Figure 3.1). This is particularly useful for genes which have not yet been extensively studied, where expression pattern and the effect of gene knock-out can be studied in the same animals.

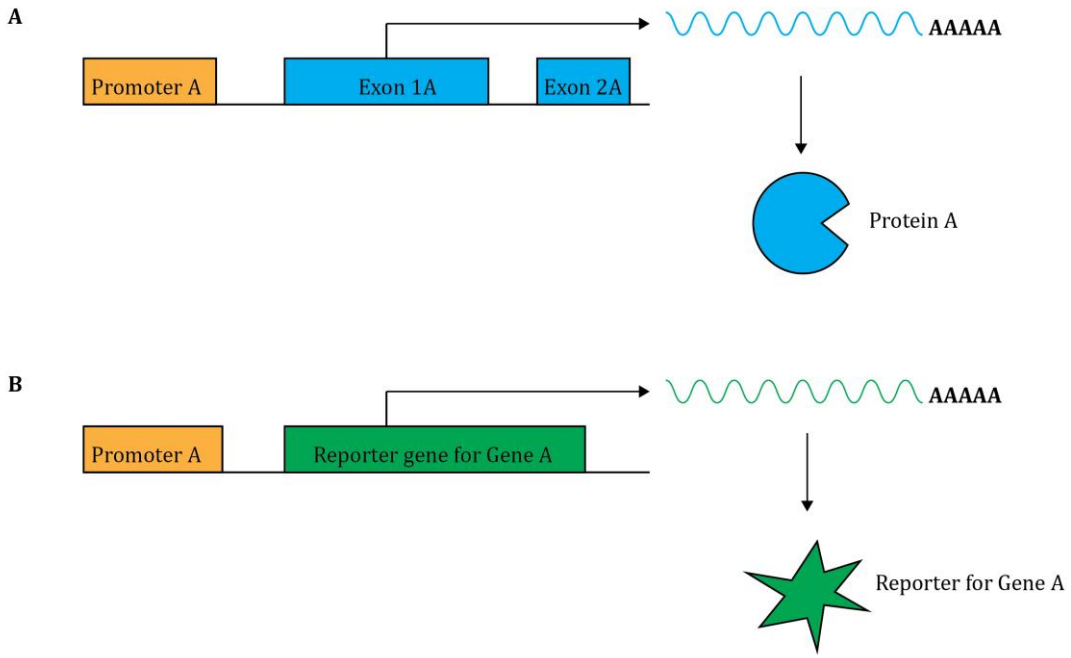

Figure 3.1. Reporter genes can be used to probe promoter activity. Since Gene A and Reporter Gene A are both transcribed from Promoter A, the reporter gene can therefore be used to determine which cells are transcriptionally active for Gene A.

To this end, several reporter systems exist, ranging from fluorescence to enzymes whose activity can be detected. In addition to straightforward knock-in mutations of the reporter gene, more sophisticated inducible systems are feasible; these are particularly relevant in the study of genes which lead to embryonic lethality, as the loss of the gene can be induced at particular stages of development or at any point after birth.

In our knock-out mice, exons encoding OMD or PRELP are replaced with *LacZ,* which itself encodes the *E. coli* enzyme β-galactosidase (Figure 3.2). This enzyme cleaves disaccharide lactose into monosaccharides glucose and galactose (Huber et al., 1976) and this catalytic activity can be exploited to determine areas of enzyme activity using the lactose analogues such as X-gal (Juers et al., 2012). X-gal itself is colourless, until it is cleaved by β-galactosidase where a blue precipitate is formed. Its activity is dependent on Na^+ or K^+ (Xu et al., 2004) and Mg^{2+} (Tenu et al., 1972), as these ions are crucial for its binding and catalytic activity. Mg^{2+} is particularly important and is required for maximum activity (Tenu et al., 1972) as ions bind to the substrate binding and catalytic sites of the enzyme in addition to stabilising the transition state (Juers et al., 2012).

This reporter gene will therefore be used to determine which cells express OMD and PRELP in order to understand the cells which are affected in the knock-out animals. All of the results presented in this chapter were consistently-observed in at least 3 animals unless otherwise stated.

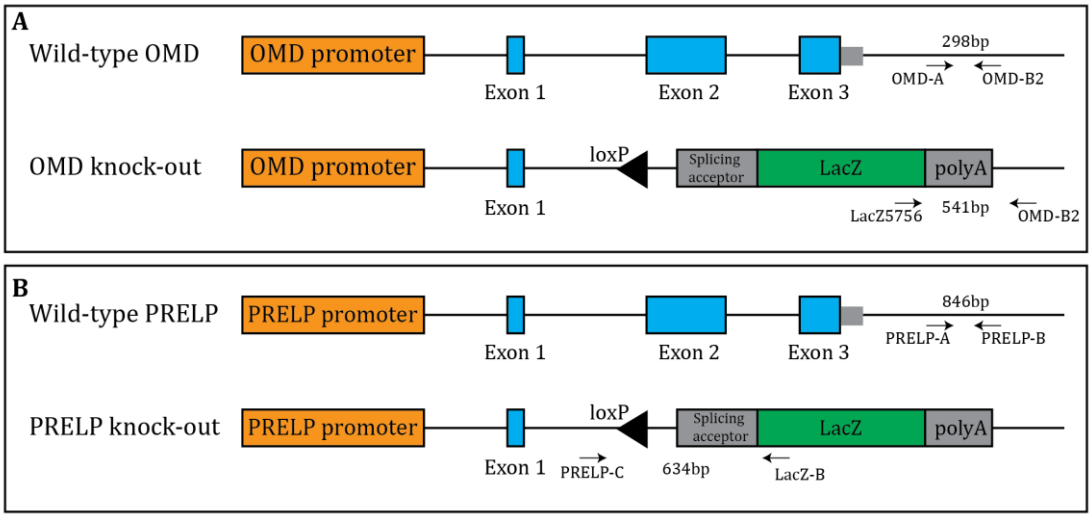

Figure 3.2. Gene structure in wild-type, OMD$^{-/-}$ (A) and PRELP$^{-/-}$ (B) mice. Exons 2 and 3 of OMD and PRELP knock-out mice have been replaced with the *LacZ* gene, where its expression is under the control of the OMD or PRELP promoters. Primers utilised for genotyping are displayed.

3.2 Determining background β-galactosidase staining in wild-type brain

3.2.1 β-galactosidase activity in wild-type brain

As the aim is to observe the expression pattern of OMD and PRELP by utilising β-galactosidase enzyme activity, I must first determine whether there is any background staining in wild-type animals. To this end, I stained for β-galactosidase using X-gal in whole-mount preparations and in sections.

Adult wild-type brains were cut sagittally to separate the hemispheres, fixed in 4% PFA and stained with X-gal overnight at 37°C. This sagittal orientation allows me to see a variety of tissues in the brain in order to have an overall view of the potential staining pattern. As shown in Figure 3.3, no blue precipitate was observed indicative of X-gal staining. Staining of OMD and PRELP heterozygote brains prepared in an identical manner exhibit staining (see Sections 3.3.1 and 3.4.1), indicating that the staining protocol is valid. This therefore demonstrates that there is no background β-galactosidase activity in the brain of wild-type mice, and that any staining observed in transgenic heterozygotes is indicative of exogenous catalytic activity.

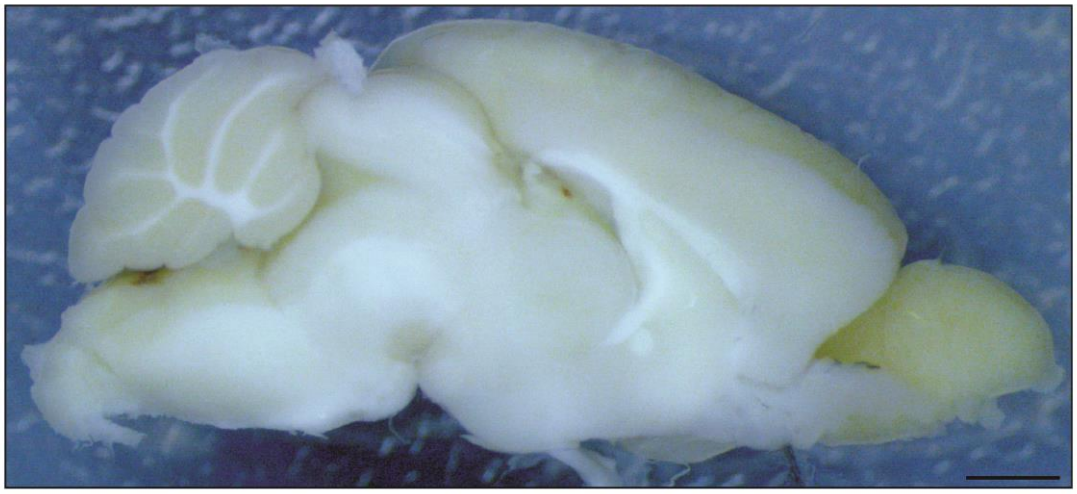

Figure 3.3. Whole-mount X-gal staining of wild-type mouse brain. Sagittal view of mouse brain shows no visible X-gal staining which would correspond to background staining. Scale bar 2mm.

In order to confirm that there is no background X-gal staining in the wild-type, brains were harvested, cut coronally and sections were stained with X-gal. Sections were counterstained with nuclear fast red, as I anticipated that there would be weak or no X-gal staining. Figure 3.5 shows that there was no staining in the cortex, hippocampus or cerebellum. In addition, I did not detect staining in the ventricles or vasculature. I therefore conclude that there was no detectable background β-galactosidase activity in

wild-type brains, indicating that any X-gal staining I observe in heterozygote animals is not as a result of background staining.

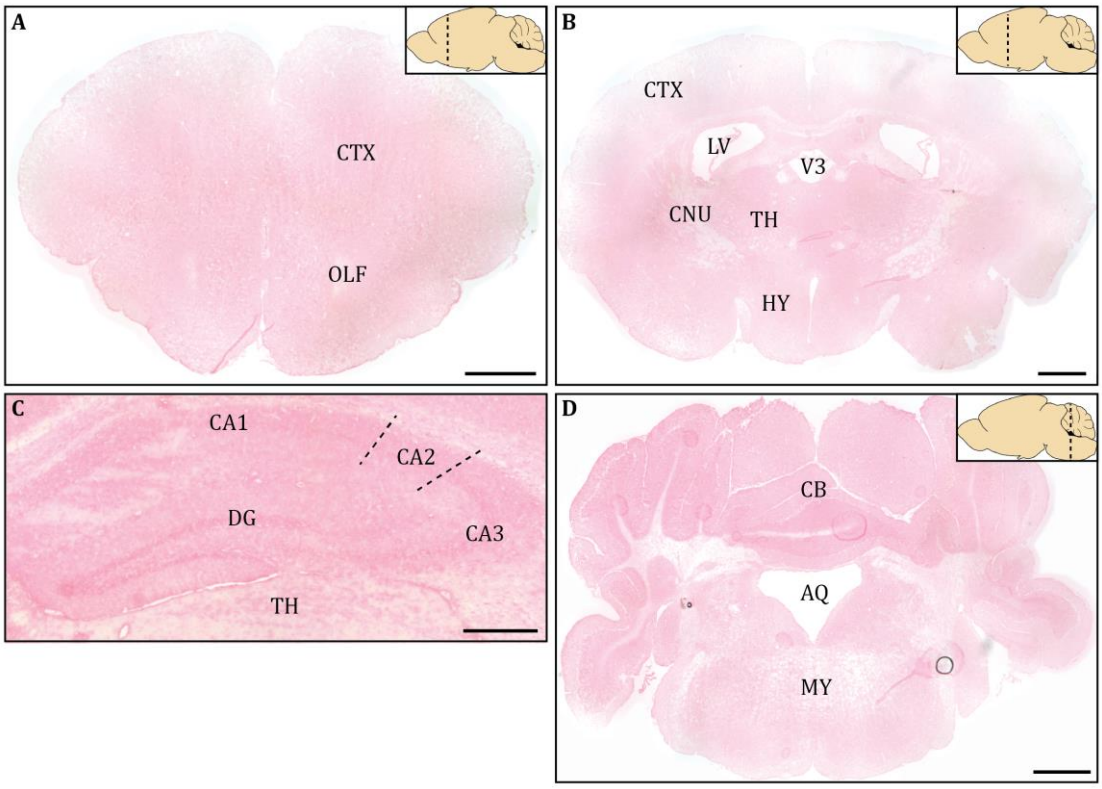

Figure 3.4. X-gal staining of wild-type brain sections counterstained with Fast Red. There was no staining detected in the cortex **(A)**, anterior cerebrum **(B)**, hippocampus **(C)** and cerebellum **(D)**. CTX, cortex; OLF, olfactory region; LV, lateral ventricle; V3, third ventricle; CNU, cerebral nuclei; TH, thalamus; HY, hypothalamus; CA1-3, Ammon's horn fields 1-3; DG, dentate gyrus; CB, cerebellum; AQ, cerebral aqueduct; MY, medulla. Scale bar 500um (A, B & D) and 200um (C).

3.2.2 β-galactosidase antibody staining in wild-type brain

The aim of experiments in this chapter is to identify the cell-types expressing OMD and PRELP. To this end, antibody staining against β-galactosidase will be used, and therefore the background staining of this antibody in wild-type sections must first be determined. Tissue from one animal was used in this experiment.

Figure 3.5 shows antibody staining of wild-type brain sections using the β-galactosidase antibody in the cortex, hippocampus, cerebellum and ventricles. No notable signal was observed in most tissues, with the exception of the ventricles – there is fluorescence detected in the choroid plexus capillaries. This therefore indicates that the β-galactosidase antibody I chose to utilise has limited background staining in the brain, with the choroid plexus being the only tissue displaying signal.

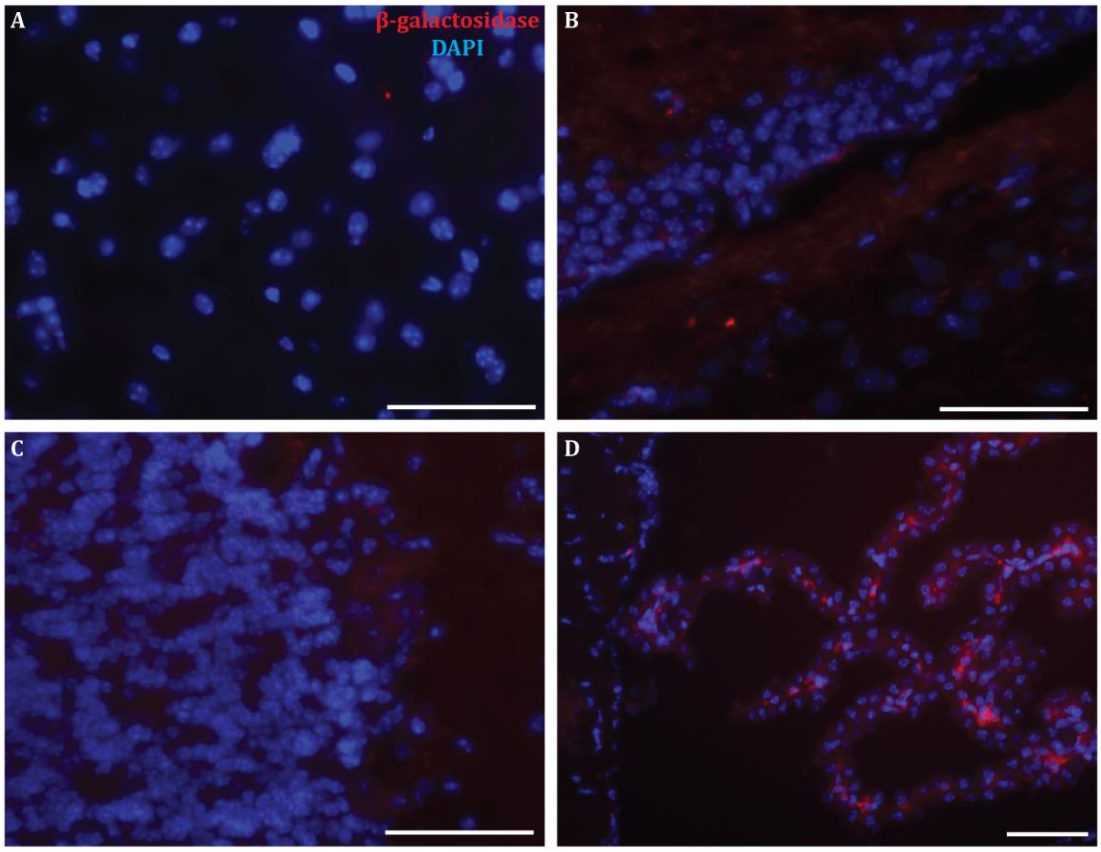

Figure 3.5. β-galactosidase antibody staining in wild-type A) cortex, B) hippocampus, C) cerebellum and D) ventricles. β-galactosidase is stained with Alexa-594; nuclear counterstain with DAPI. Note that the only signal detected was located in the choroid plexus of ventricles. Scale bars 50um.

3.3 Gene expression patterns of OMD in the brain

3.3.1 X-gal staining of OMD$^{+/-}$ brains

In order to have a broad understanding of the expression pattern of OMD in the brain, I performed X-gal whole-mount staining of adult heterozygote (OMD$^{+/LacZ}$; referred to hereafter as OMD$^{+/-}$) brains cut sagittally (Figure 3.6). There is intense staining in various regions of the cerebrum and cerebellum, with the exception of the olfactory bulbs. While the staining is widespread, with the exception of certain areas discussed below, a clear pattern is discernible in the cerebellum and hippocampus. In the cerebellum, there was intense staining of a layer of cells at the periphery of the granular and molecular layers (Figure 3.6B), potentially corresponding to Purkinje neurons. In the hippocampus, there was notable staining of cells in Amon's horn and dentate gyrus (Figure 3.6C). *LacZ* is therefore likely expressed in neurons.

White matter seemed to exhibit weaker or no X-gal staining. This was particularly visible in the fibre tracts near the hippocampus, thalamus and brain stem, as well as the arbor

vitae in the cerebellum. In addition, the optic nerve is also devoid of any staining. Weaker staining in the olfactory bulb allowed the visualisation of some vessels (Figure 3.6D; arrows). Staining of vessels is also visible in the cerebellum (Figure 3.6B; arrows). It is possible that OMD is expressed in vessels throughout the brain, although the intense staining in other regions may be masking staining in the vasculature in this whole-mount experiment.

To summarise, I have determined the broad expression pattern of the reporter gene judged by whole-mount X-gal staining. There is intense staining in the grey matter of the brain, notably in the cerebellum and hippocampus, and some staining found within blood vessels. To further identify the potential cells expressing the reporter gene, I stained analysed tissue sections.

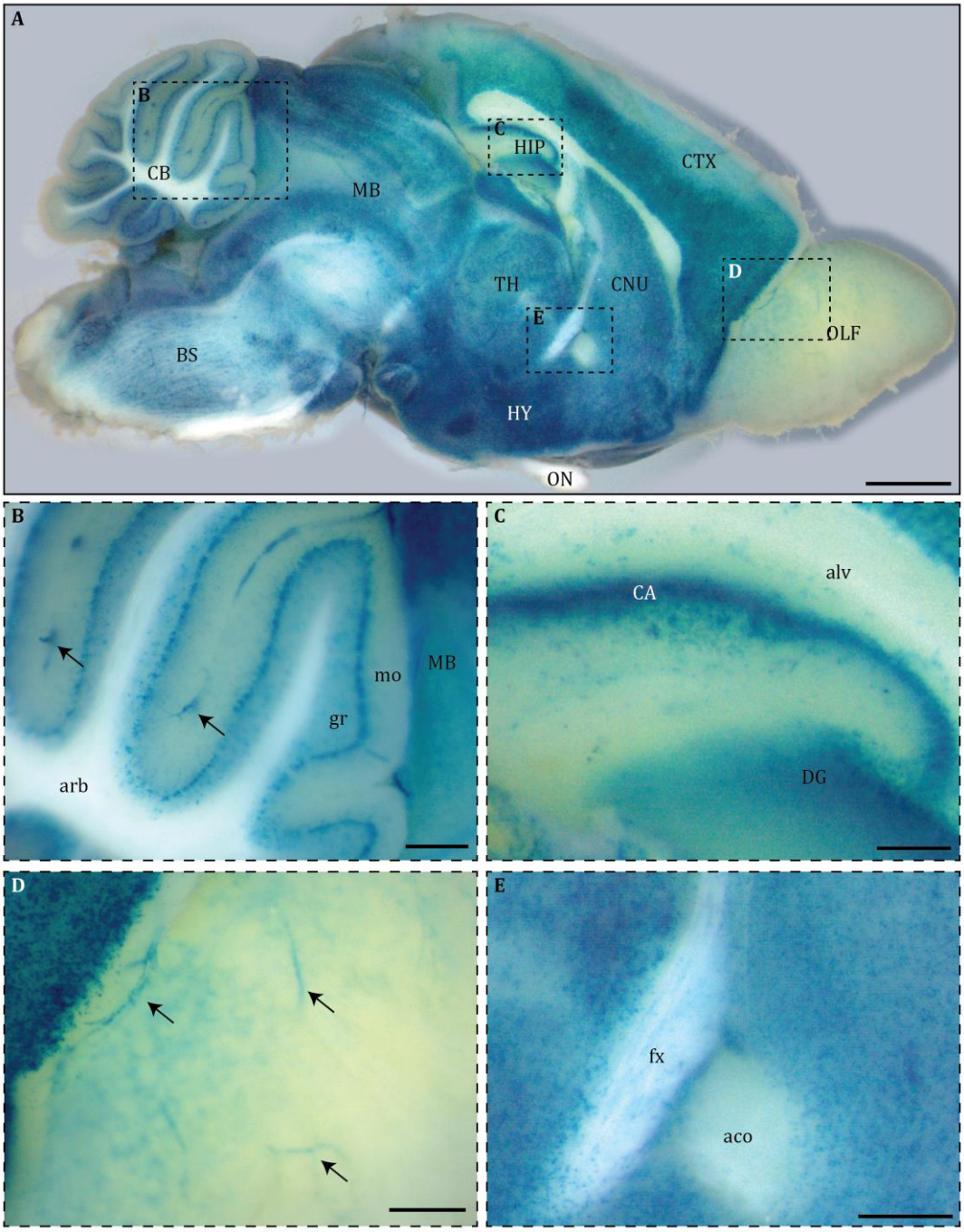

Figure 3.6. Whole-mount X-gal staining of OMD$^{+/-}$ brain. A) Overview of whole-mount stain. There is intense staining across the cerebrum and cerebellum with the exception of the olfactory bulbs and fibre tracts. **B)** Magnified view of the cerebellum; there is punctate staining in cells at the border between the granular and molecular layers. The abor vitae is devoid of staining. Arrows show staining in vasculature. **C)** Magnified view of staining in the hippocampus; there is intense staining Ammon's horn and the dentate gyrus. **D)** X-gal staining of the olfactory bulbs. Staining is notably weaker compared to other areas. Staining is also visible in the vasculature (arrows). **E)** Magnified view of staining of thalamus and hypothalamus. Note that the fibre tracts exhibit much weaker staining. CB, cerebellum; BS, brain stem; MB, mid brain; TH, thalamus; HY, hypothalamus; ON; optic nerve; HIP, hippocampus; CNU, cerebral nuclei; CTX, cortex; OLF, olfactory bulb; arb, arbor vitae; gr, granular; mo, molecular; alv, alveus; CA, Ammon's horn; DG, dentate gyrus; fx, fornix; aco, anterior commissure. Scale bar 2mm (A) and 500um (B, C, D & E).

Since X-gal penetrated whole-mount tissue poorly, coronal cryosections of $OMD^{+/-}$ brains were stained. Staining of the cortex, hippocampus and cerebellum are shown in Figure 3.7, Figure 3.8 and Figure 3.9.

The staining pattern was almost entirely punctate and present in all brain tissues, ranging from the cortex, midbrain and cerebellum. Staining in the cortex was spotty and seemed to be weaker in the outer regions, with staining being the strongest in the orbital and olfactory areas (Figure 3.7).

While the majority of the staining did not follow a particular pattern, staining in the hippocampus did show specificity (Figure 3.8), as staining was most intense in the pyramidal cell layers of all three fields of Ammon's horn, in addition to the granular cell layer of the dentate gyrus (Figure 3.8). In contrast, there is very little staining of the CA1, CA2 and CA3 oriens and the molecular layer of the dentate gyrus. This therefore suggests that OMD may be expressed in pyramidal and granular neurons.

Another tissue in the brain which exhibits an interesting staining pattern is the cerebellum. While there is strong staining in the medulla adjacent to the cerebellum (Figure 3.9C), there is staining in the molecular layer, and occasionally in the granular layer of the cerebellum (Figure 3.9B). The staining in the molecular layer of the cerebellum is most intense along the interface between the molecular and granular layers. This is where Purkinje cells reside, and could indicate that the reporter gene for OMD is expressed in Purkinje neurons. It should be noted that, just as mentioned previously, the arbor vitae fibre tract is devoid of β-galactosidase activity.

To conclude, X-gal staining of $OMD^{+/-}$ brains shows that the reporter gene in OMD mice is widely expressed throughout the brain in a spotty manner. Notably, there is expression in the cortex, thalamus, medulla, midbrain and cerebellum. Particularly strong staining was found in the hippocampus, especially along the pyramidal cell layer of Ammon's horn and the granule cell layer of the dentate gyrus. In the cerebellum, X-gal staining was organised between the molecular and granular layers, possibly indicating that the reporter gene may be expressed by Purkinje neurons. There was very weak or no staining in the fibre tracts throughout the brain.

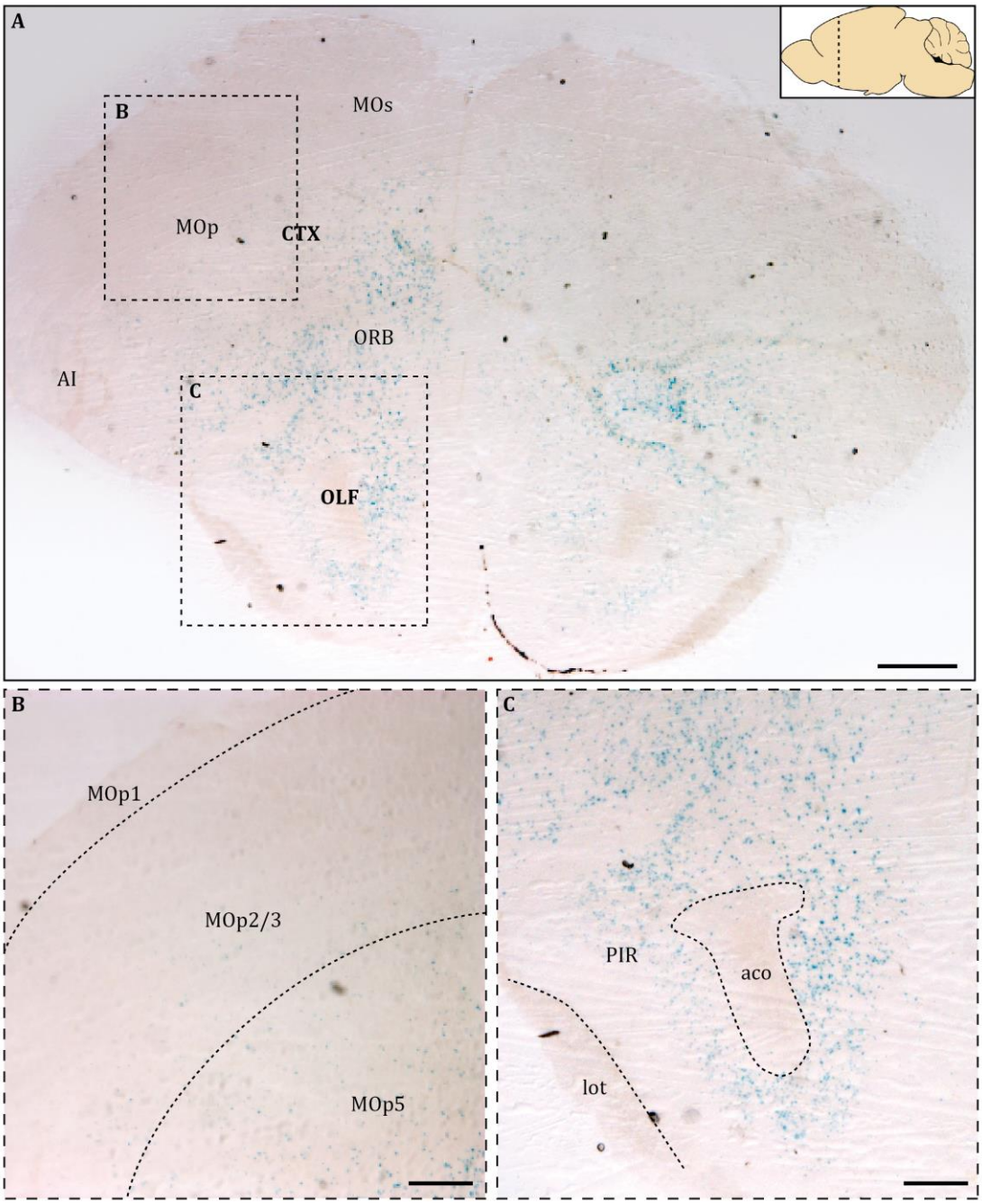

Figure 3.7. X-gal stain of OMD$^{+/-}$ in the anterior part of the brain. (A) Spotty X-gal staining found throughout the anterior cerebrum, with the exception of the outer-most layers of the cortex. **(B)** and nerve fibre tracts **(C**; lot and aco**)**. CTX, cortex; OLF, olfactory areas; MOp, primary motor area; MOs, secondary motor area; ORB, orbital area; MOp1-5, primary motor area layers 1-5; PIR, piriform area; aco, anterior commisure; lot, lateral olfactory tract. Scale bar 500um (A) and 300um (B & C).

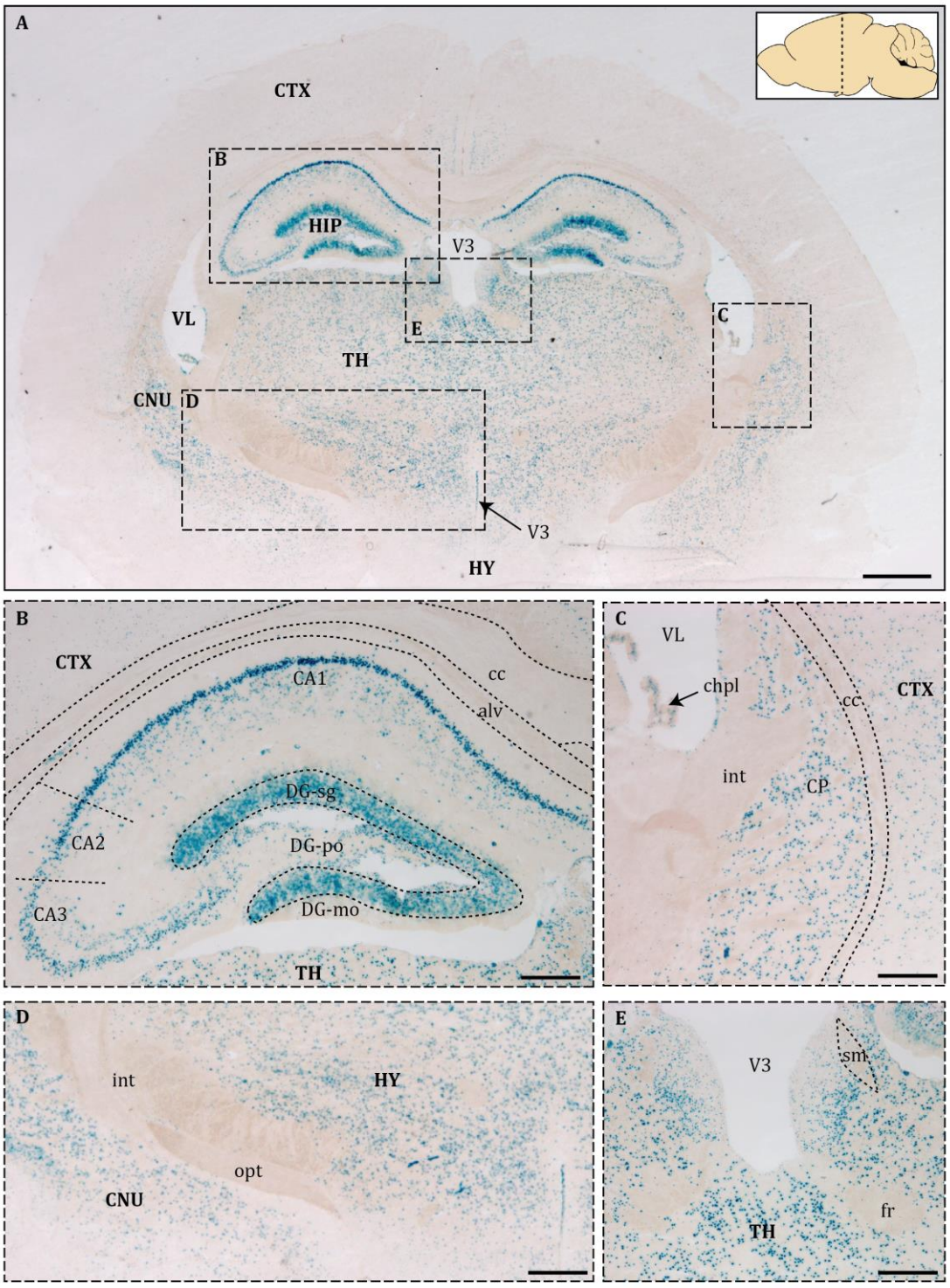

Figure 3.8. Strong X-gal staining in the hippocampus of OMD$^{+/-}$ brains. (A) Overview of X-gal staining, showing spotty staining in the thalamus, hypothalamus and cerebral nuclei. **(B)** Magnified view of hippocampus shows staining in both Ammon's horn and the dendate gyrus. **(C)** Caudoputamen and inner layers of the cortex exhibit staining, whereas fibre tract do not. There is also modest staining of the ependymal lining of lateral ventricles, as well as the choroid plexus. **(D)** Staining in the hypothalamus and caudoputamen. **(E)** Staining in thalamus. CTX, cortex; TH, thalamus; HY, hypothalamus; CNU, cerebral nuclei; VL, lateral ventricle; V3, 3rd ventricle; cc, corpus callosum; alv, alveus; CA1-3, Ammon's horn fields 1-3; DG-sg, dentate gyrus (DG) granule cell layer; DG-po, DG polymorph layer; DG-mo, DG molecular layer; CP, caudoputamen; chpl, choroid plexus;

int, internal capsule; opt, optic tract; sm, stria medullaris; fr, fasciculus retroflexus. Scale bar 1000um (A) and 300um (B, C, D & E).

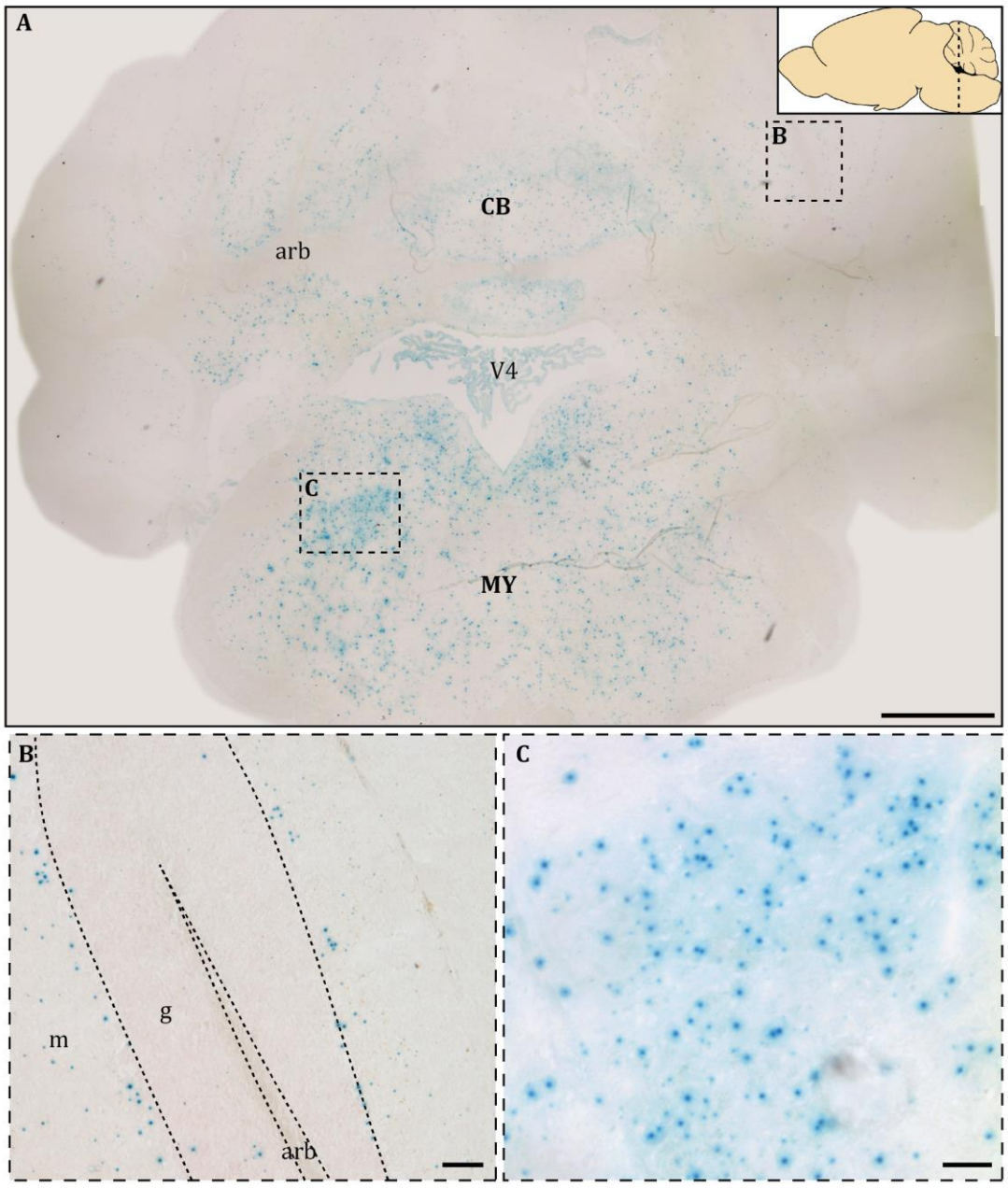

Figure 3.9. X-gal staining of OMD$^{+/-}$ cerebellum. (A) Overview of OMD$^{+/-}$ cerebellum X-gal staining. There is staining in the fourth ventricle, cerebellum and medulla. Staining shows spotty localisation of β-galactosidase in the molecular layer of the cerebellum **(B)**. There is strong, punctate, staining in the medulla **(C)**. CB, cerebellum; V4, 4th ventricle; MY, medulla; m, molecular layer (cerebellum), g, granular layer; arb, arbor vitae. Scale bars 500um (A) and 25um (B & C).

Staining was observed in the ventricles of the brain (Figure 3.10). There was staining in the lateral, third and fourth ventricles in both the ependymal linings and choroid plexuses. Staining of the lateral and fourth ventricles was the strongest, whereas staining in the third ventricle was notably weaker, especially in the choroid plexus, where only a few spots of X-gal were observed (Figure 3.10B; arrows). Staining of the ependymal cell layer

of ventricles was discontinuous, strongly suggesting that there is heterogeneity in the ependymal cells with respect to *LacZ* expression.

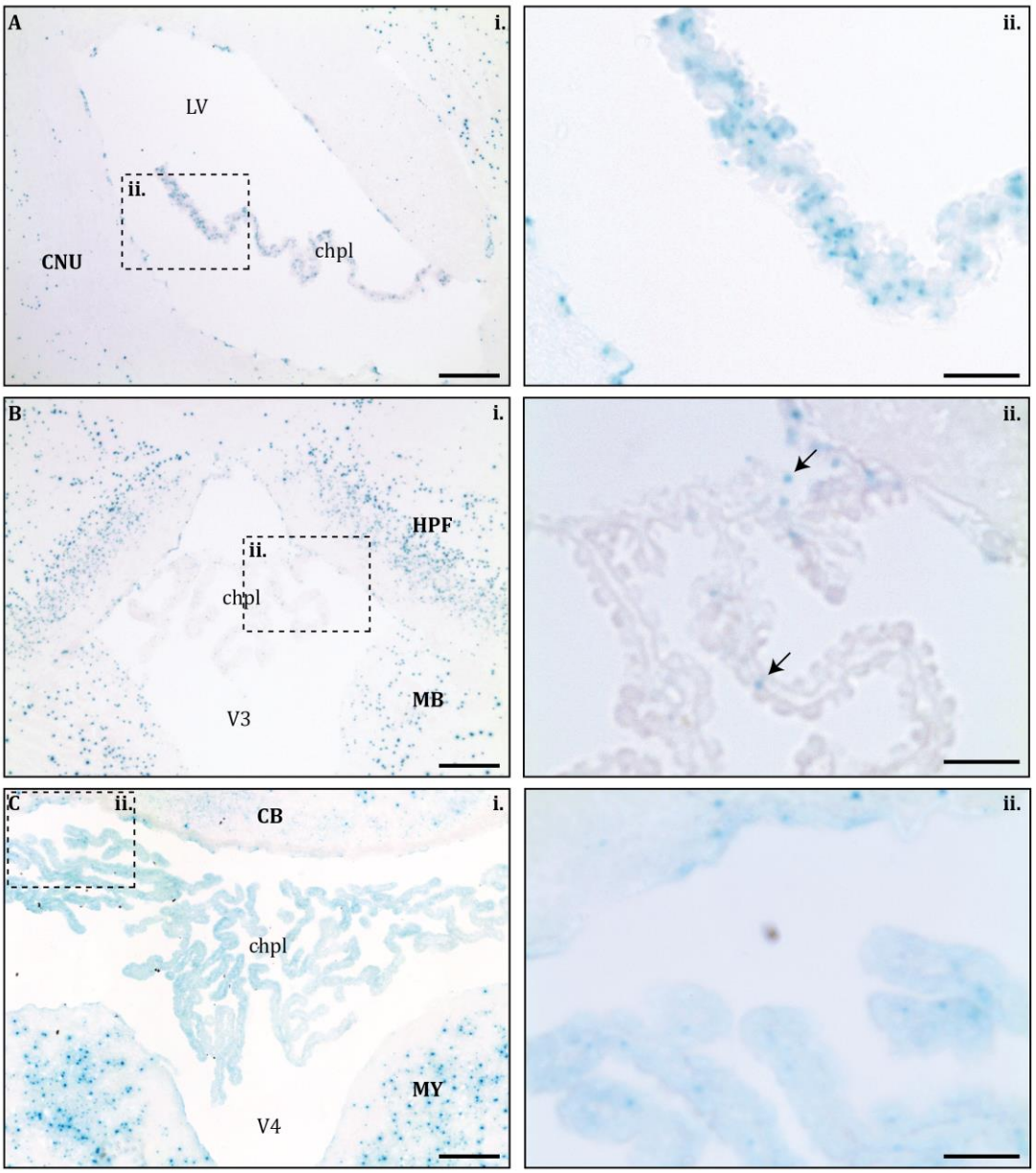

Figure 3.10. X-gal staining of OMD$^{+/-}$ ventricles. Staining was observed in lateral **(A)**, third **(B)** and fourth **(C)** ventricles. Both the ependymal linings and choroid plexuses were stained with X-gal, although staining in the third ventricle's choroid plexus was weakest (arrow). LV, lateral ventricle; chpl, choroid plexus; CNU, cerebral nuclei; V3; third ventricle; HFP, hippocampal formation; MB, midbrain; V4, fourth ventricle; CB, cerebellum; MY, medulla. Scale bars 100um (Ai, Bi & Ci) and 25um (Aii, Bii & Cii).

Finally, I also observed X-gal staining in capillaries and larger vessels in OMD$^{+/-}$ brain sections (Figure 3.11). From the X-gal staining alone, it is difficult to interpret which cell type is stained, as the staining pattern is rather diffuse; β-galactosidase antibody staining would therefore be required to determine the cell type expressing OMD in the vasculature.

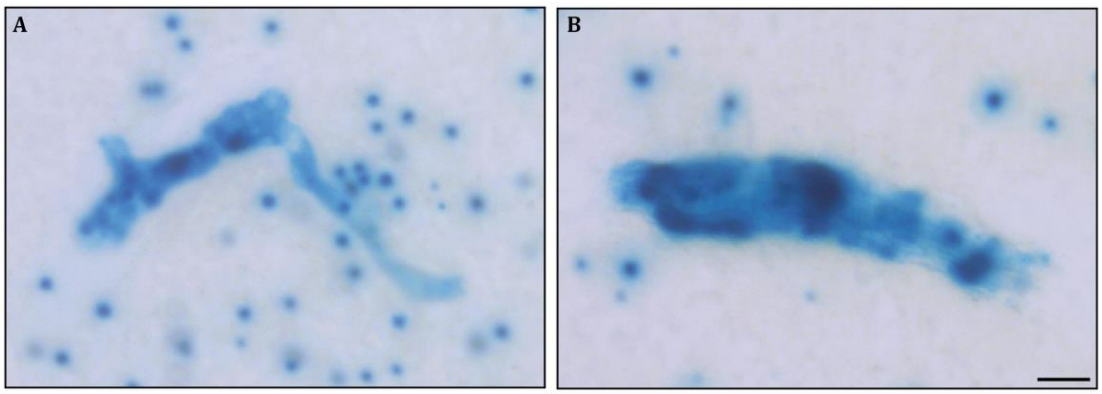

Figure 3.11. X-gal staining in OMD$^{+/-}$ vasculature. Intense, diffuse staining is observed in both smaller capillaries **(A)** and larger vessels **(B)**. Scale bar 10um.

To conclude, the reporter gene in OMD animals is expressed almost ubiquitously in the brain as judged by the punctate X-gal staining. Expression is most notable in Ammon's horn and dentate gyrus in the hippocampus in addition to an organised layer of cells in the cerebellum, possibly Purkinje cells. I have also determined that *LacZ* is expressed in the ventricles, choroid plexuses and vasculature.

3.3.2 X-gal and antibody double staining

I have established the general staining pattern of X-gal in OMD$^{+/-}$ brains. To determine which cell-type(s) express the reporter gene, I performed double staining of X-gal and antibody staining using an HRP-conjugated secondary antibody. Briefly, sections were stained with X-gal as done previously. After 2 hours of incubation at 37°C, I proceeded to antibody staining. Since I utilised an HRP-conjugated secondary antibody, it was critical to block endogenous peroxidase activity prior to blocking with serum. I then proceeded with the standard antibody staining protocol. Once the final wash was complete, the HRP substrate, DAB, was added to slides. Sites of primary and secondary antibody binding were marked with a brown precipitate. Slides were mounted and prepared for visualisation using a light microscope.

Given strong X-gal staining at the hippocampus and cerebellum, I were particularly interested in determining whether OMD is expressed in neurons. I therefore stained tissues with X-gal and an antibody against calbindin, a neuronal marker (Pfeiffer et al., 1989) (Figure 3.12). Staining revealed co-localisation of punctate X-gal staining with calbindin antibody, indicating that OMD is likely produced by neurons. In particular, clear staining was observed in neurons located in Ammon's horn in the hippocampus and Purkinje cells in the cerebellum as expected.

I also performed double-staining for astrocyte marker GFAP and microglial marker Iba-1 (Figure 3.13). Since the punctate nature of OMD$^{+/-}$ X-gal staining makes it challenging to ascertain colocalization at cell processes, I considered staining to be colocalised only if it occurred in the cell body, rather than the processes. As shown in Figure 3.13, X-gal staining is located within the cell bodies of astrocytes and microglia. It should be noted however that the majority of the X-gal "spots" corresponded to neuronal staining, whereas a smaller proportion were found within astrocytes and microglia.

Therefore, double staining of X-gal and cell markers suggests that the reporter gene is mainly produced by neurons but also by astrocytes and microglia to a lesser extent.

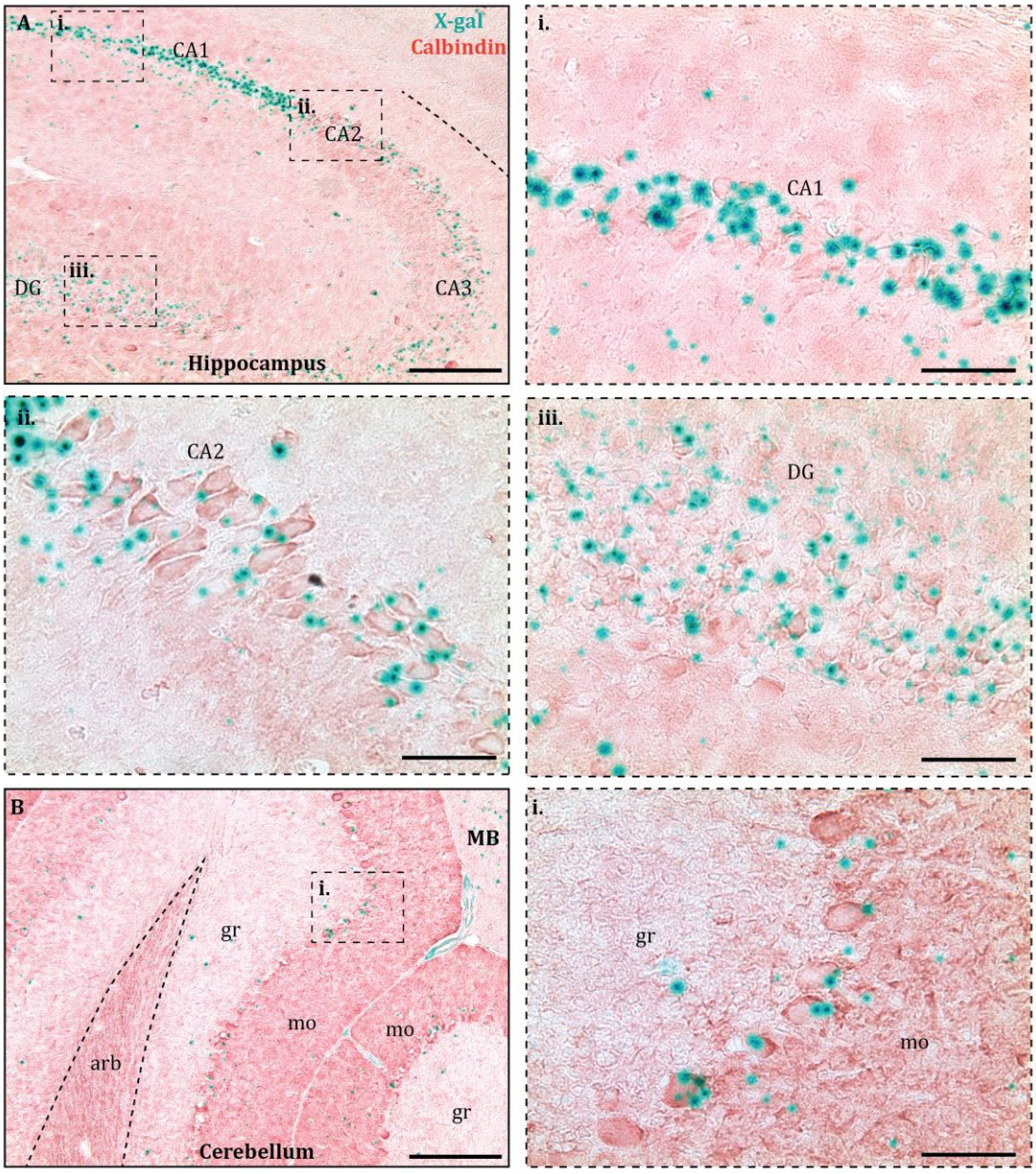

Figure 3.12. X-gal and calbindin double staining in OMD$^{+/-}$ brain. A) Strong expression of OMD in the hippocampus. **i)** Magnified view; CA1 neurons. **ii)** Magnified view; CA2 neurons. **iii)**

Magnified view; dendate gyrus. **B)** X-gal staining in cerebellum. **i)** Magnified view. CA1-3, Ammon's horn fields 1-3; DG, dentate gyrus; MB, midbrain; arb, arbor vitae; gr, granular layer; mo, molecular layer. Scale bars 100um (A & B) and 25um (magnified views).

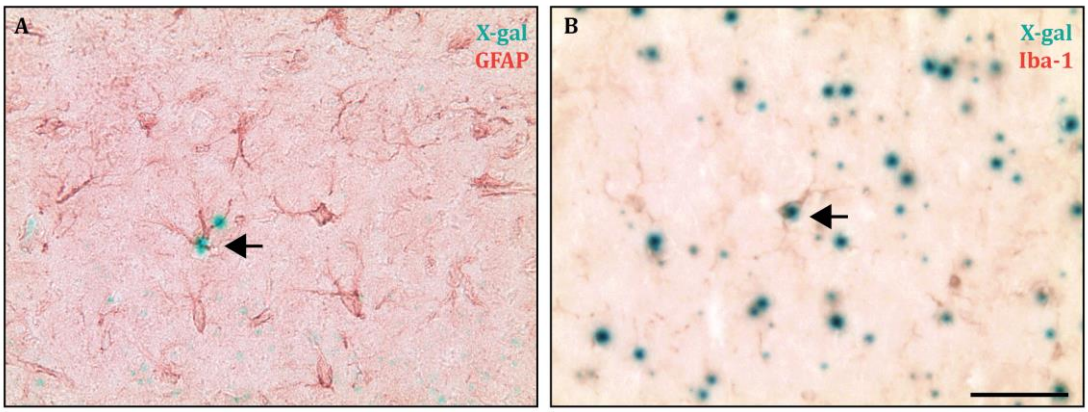

Figure 3.13. Double staining of X-gal with A) GFAP and B) Iba-1 antibodies in OMD$^{+/-}$ brain. X-gal expression is present in the cell bodies of astrocytes and microglia (arrows). Scale bar 25um.

3.3.3 Detection of OMD-expressing cells using β-galactosidase antibody staining

X-gal staining in OMD$^{+/-}$ was also found within the vasculature in the brain. Although I attempted to perform double staining as above using endothelial cell and pericyte/smooth muscle markers, the resolution I can obtain using X-gal was insufficient to discriminate between endothelial and mural cell staining. I therefore attempted to detect β-galactosidase protein using an anti-β-galactosidase antibody instead. As I aimed to obtain the strongest possible signal from β-galactosidase antibody staining, OMD$^{-/-}$ mice were used. Mice were perfused with PBS and then 4% PFA to wash out the blood and fix tissues. Brains were then processed, sectioned and stained with a mouse monoclonal antibody against β-galactosidase.

Surprisingly, despite the strong staining I observed when using X-gal, I was unable to detect any β-galactosidase antibody staining (Figure 3.14). The staining pattern was identical to that of the wild-type tissues, including non-specific staining in the choroid plexus. I attempted a variety of methods to improve the antibody staining, including utilising different antibodies from other manufacturers, increasing permeabilisation time/detergent concentration, altering antibody concentration and performing antigen retrieval in citrate buffer pH 6 and tris-EDTA buffer pH 9. All of the above methods did not change the outcome of the staining. In contrast, the standard protocol functioned well in PRELP$^{-/-}$ brain tissues (see Section 3.4.3).

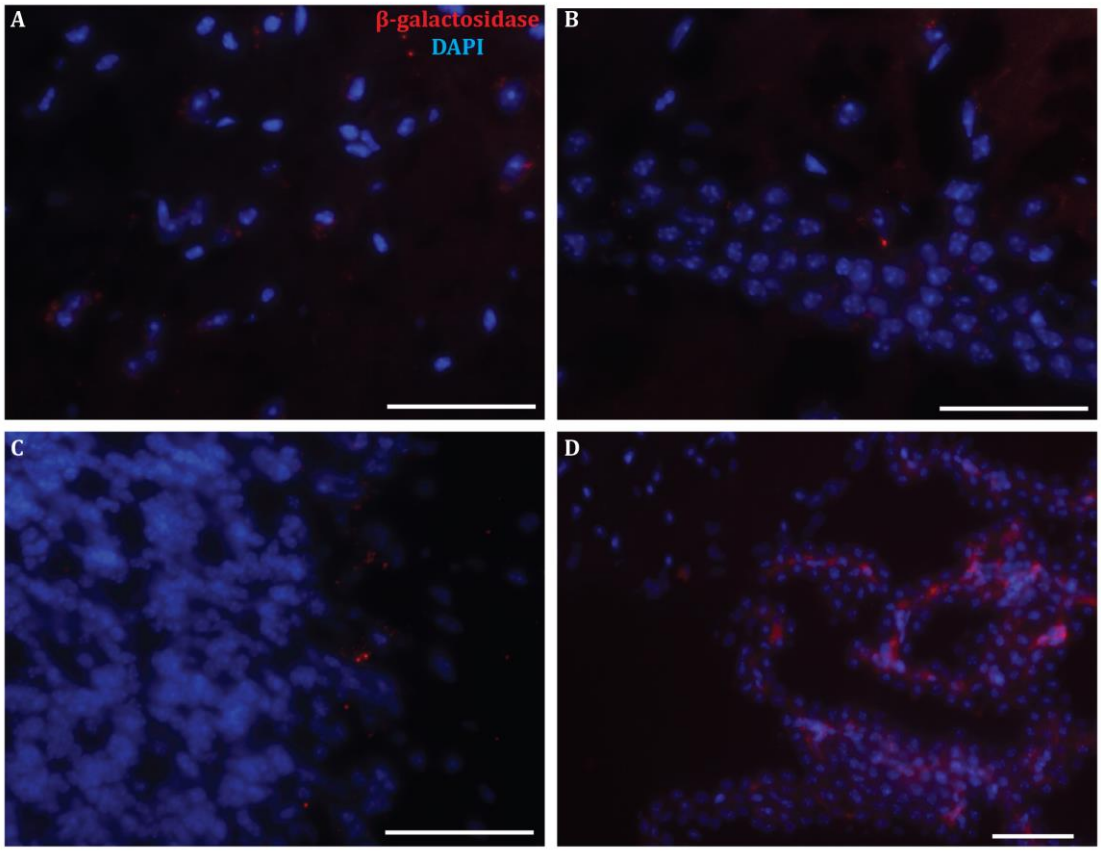

Figure 3.14. Antibody staining of β-galactosidase in OMD$^{-/-}$ brain. No staining was observed in the cortex **(A)**, hippocampus **(B)**, cerebellum **(C)** or choroid plexus and ependymal lining of ventricles **(D)**. Scale bar 50um.

I considered that there may have been an error in genotyping, and that perhaps the animals we thought were OMD$^{-/-}$ were potentially OMD$^{+/-}$ or OMD$^{+/+}$. Since processed ear punch samples were stored at -20°C, I was able to re-genotype the animals. I confirmed that the mice were OMD knock-outs and that there was no error in initial genotyping. In addition, my colleague Dr Ryohei Sekido isolated DNA from neighbouring tissue sections to those imaged and confirmed that the genotype of the sections was indeed OMD$^{-/-}$. Unfortunately, the failure to detect β-galactosidase protein using antibodies makes it impossible to verify findings from the double staining with antibodies to cell markers.

3.3.4 Staining of rat tissues with antibodies against OMD

Throughout this project, I have tested a variety of commercially-available OMD- and PRELP-antibodies with limited success. In some instances, I would observe staining in the wild-type brain sections, however, when using sections from knock-out animals as a negative control, the same staining pattern would be observed with comparable intensity indicative of non-specific staining.

Our collaborator, Mr Takumi Tashima at the University of Tokyo (Japan), has made a variety of OMD- and PRELP-antibodies. They were produced by injecting mice with fragments of human OMD and PRELP protein, and therefore have reactivity towards the human variants. Given the relatively high conservation of protein sequence between human, mouse and rat for both OMD and PRELP (see Figure A.1 and Figure A.2 for multiple sequence alignment), staining of rodent tissues using these antibodies should be possible.

Colleagues Dr Ryohei Sekido and Dr Byongsung Shim screened these academically-produced antibodies using eye and brain sections from one wild-type rat, kindly provided by the Institute of Ophthalmology Biological Resources Unit. OMD antibody #56 was found to have the strongest signal, and double staining with neuronal marker calbindin and astrocyte marker GFAP was performed (Figure 3.15). The anti-OMD staining was found to co-localise with neuronal staining using calbindin. From their observations, only neurons in the hypothalamus were positive for anti-OMD, indicating that OMD may be expressed by sub-populations of neurons in rat. In addition, no staining was observed in astrocytes or the vasculature. Due to the location of the tissue sections, brain ventricles were not visible and therefore the expression of OMD in ependymal cells is uncertain. This work performed by my colleagues therefore support my findings that OMD is expressed in neurons. Its expression in other cell types, however, is unclear. Given that rat sections were used, it is possible that discrepancy between X-gal and anti-OMD stains are due to species-specific differences.

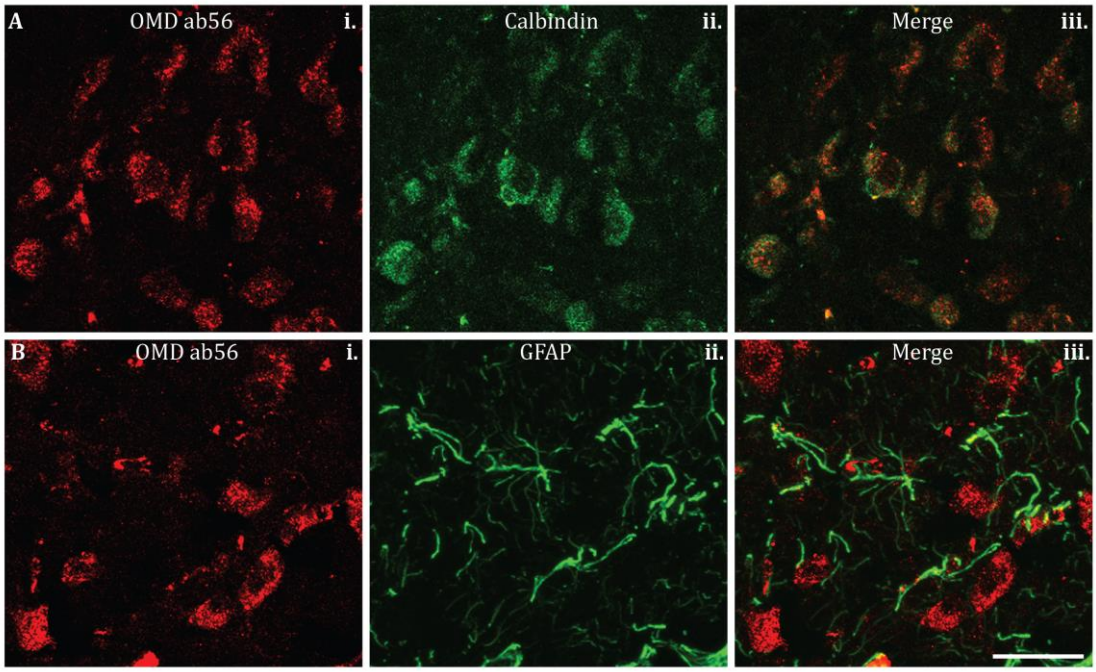

Figure 3.15. Staining of rat brain sections with OMD antibody #56 with neuronal marker calbindin (A) and GFAP astrocyte marker (B). Staining and image capture performed by Dr Ryohei Sekido and Dr Byongsung Shim. Scale bar 20um.

3.3.5 Single-cell analysis

In order to clarify the discrepancies between X-gal and antibody staining in $OMD^{+/-}$ or $OMD^{-/-}$ tissues, I analysed computational data. Single-cell RNA sequencing (RNA seq) of cortical and hippocampal mouse tissue was performed by researchers at the Karolinska Institute in Sweden and their data is available to view online (Zeisel et al., 2015). Somatosensory cortex and CA1 hippocampal tissues were harvested from young mice and dissociated to produce a single-cell suspension. This was then put into a C1 chip of a Fluidigm (USA) single-cell sorter, where individual cells were captured in specially-designed wells inside the chip. All cells were lysed and amplified cDNA was produced and utilised for RNA seq. 3,005 single-cell transcriptomes were compiled and genes clustered to reveal nine major classes of cells: interneurons, S1 pyramidal, CA1 pyramidal, mural, endothelial, microglia, ependymal, astrocytes and oligodendrocytes (Zeisel et al., 2015).

The research group has an online tool to investigate their single-cell data (Linnarsson, 2015). This tool was therefore used to investigate the expression of OMD in the brain (Figure 3.16). These results indicate that there is almost no expression of OMD in the cortex or hippocampus, aside from in subclasses of astrocytes (~3 copies) and oligodendrocytes (~3 copies). This data is surprising considering the strong X-gal staining in the $OMD^{+/-}$ hippocampus in particular. These findings are consistent with my

observations of β-galactosidase staining in OMD$^{-/-}$ sections, indicating that the expression of OMD may not be as strong and widespread in the brain, as suggested by X-gal staining.

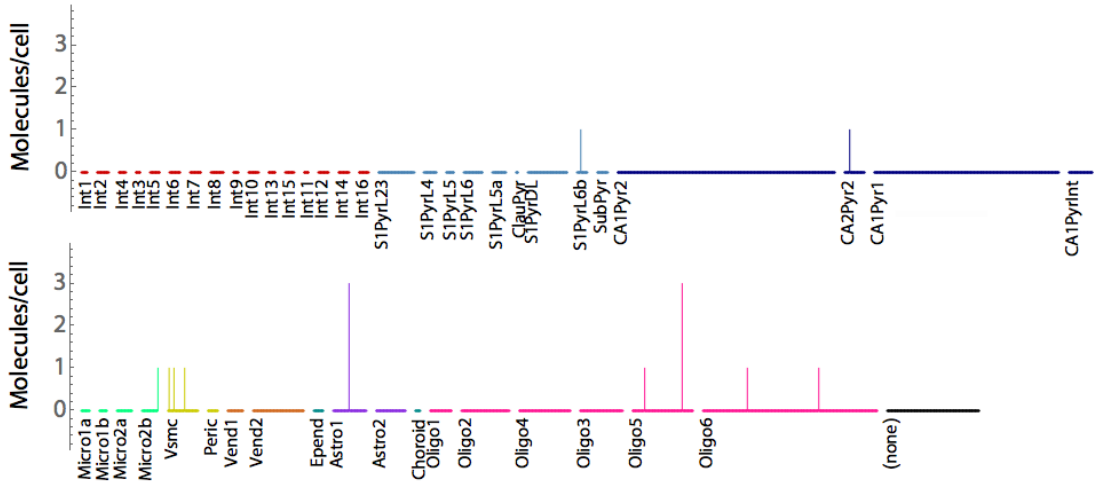

Figure 3.16. Expression of OMD in cortical and hippocampal cells based on single-cell RNA sequencing data. Zeisel et al. (2015) performed single-cell RNA sequencing in mouse cortex and hippocampus to identify different classes of cells. Int, interneurons; S1Pyr, S1 pyramidal neurons; CA1Pyr, CA1 pyramidal neurons; CA2Pyr, CA2 pyramidal neurons; ClauPyr, claustrum; Micro, microglia; VSMC, vascular smooth muscle cell; Peric, pericyte; Vend, vascular endothelial cell; Epend, ependymal cell; Astro, astrocyte; Oligo, oligodendrocyte. Figure generated from tool provided by group: http://linnarssonlab.org/cortex/.

3.4 Determining PRELP expression pattern in the brain

3.4.1 X-gal staining of PRELP$^{+/-}$ brains

As explained previously, PRELP knock-out mice were created by replacing exons 2 and 3 by the *LacZ* reporter gene (Figure 3.2). In order to determine the cells expressing PRELP, I performed X-gal staining in adult heterozygote animals (PRELP$^{+/LacZ}$; hereafter PRELP$^{+/-}$). To determine the overall staining pattern, I performed whole-mount X-gal staining (Figure 3.17).

It is immediately apparent that the staining pattern in PRELP$^{+/-}$ was very different from that seen in OMD$^{+/-}$. Staining was not as widespread and punctate; rather it seemed to be localised to the ventricles and vasculature. Staining was observed in the lateral ventricle, fourth ventricle and cerebral aqueduct (Figure 3.17A, D, E). The third ventricle was not clearly visible from this orientation and staining would have to be verified in cryosections. In addition, from this whole-mount staining, it was not clear whether the X-gal stain is present only in the ependymal lining of ventricles, choroid plexuses or both and would also have to be verified in tissue cryosections.

Staining was also visible in the vasculature in the cerebrum and cerebellum. There was staining of the vasculature in the olfactory bulbs, cortex, cerebral nuclei, thalamus,

hypothalamus, midbrain and cerebellum. There is limited staining of vasculature in the brain stem. Some vessels appeared to have a rather striated staining pattern reminiscent of the arrangement of mural cells, such as pericytes and smooth muscle cells (Figure 3.18C), but this would have to be verified in tissue sections.

To summarise, the reporter gene in PRELP animals is predominantly expressed in the ventricles and vasculature in the brain, however the precise cell types are not evident. It is possible that *LacZ* is expressed in other cells, however given the resolution of this whole-mount staining, it is difficult to determine whether its expression is completely restricted to the ventricles and blood vessels. Tissue sections were therefore analysed.

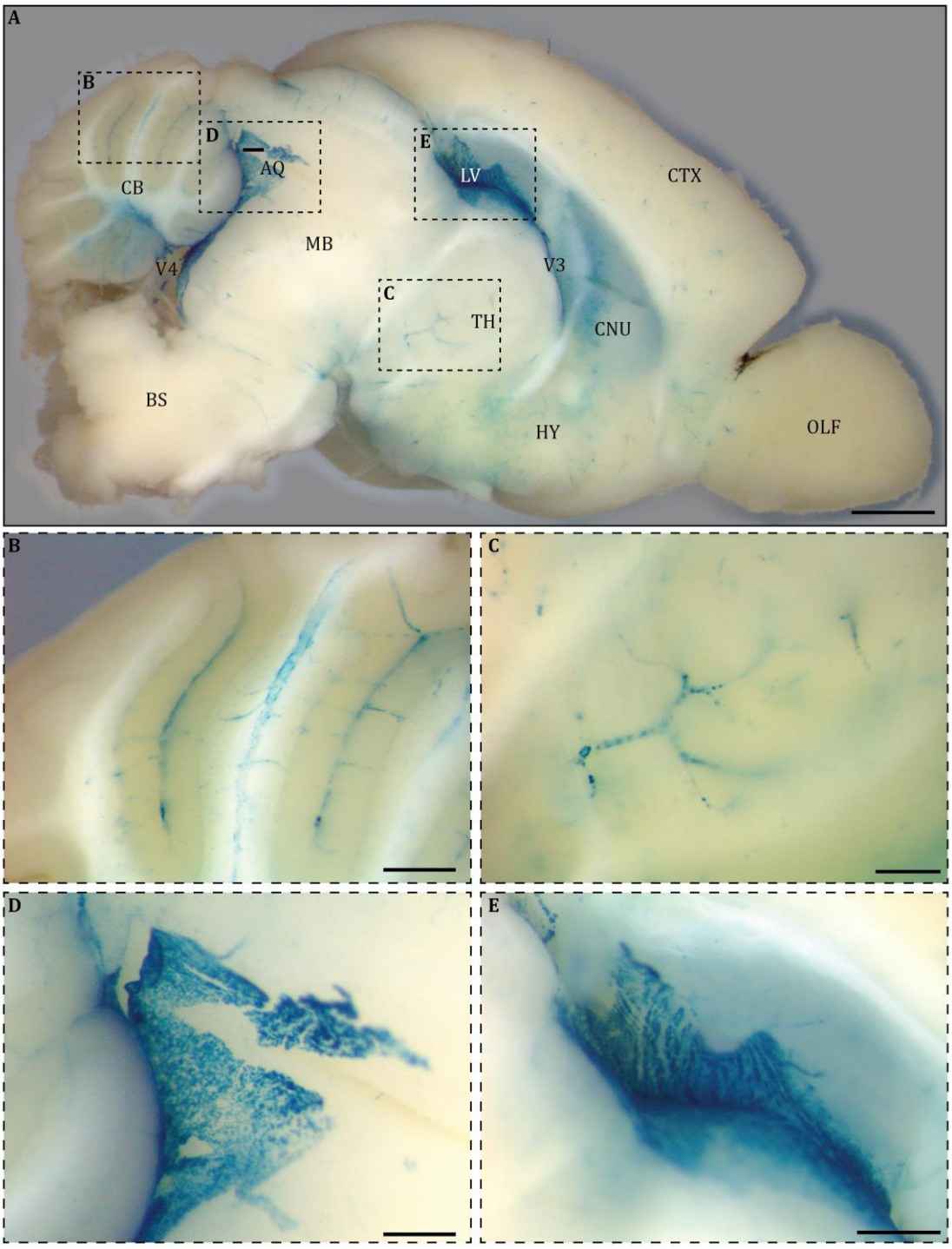

Figure 3.17 Whole-mount X-gal staining of PRELP$^{+/-}$ brain. Staining is observed in the vasculature **(A, B & C)** and ventricles **(A, D & E).** CB, cerebellum; BS, brain stem; MB, mid brain; TH, thalamus; HY, hypothalamus; CNU, cerebral nuclei; CTX, cortex; OLF, olfactory bulb; AQ, cerebral aqueduct; V4, fourth ventricle; LV, lateral ventricle; V3, third ventricle. Scale bar 2mm (A) and 500um (B, C, D & E).

Since there was poor penetration of X-gal into whole-mount tissue, individual coronal cryosections of PRELP$^{+/-}$ brains were stained. Staining of the cortex, hippocampus and cerebellum are shown in Figure 3.18, Figure 3.19 and Figure 3.20. Sections were counterstained with nuclear fast red.

There was limited X-gal staining in the cortex of PRELP$^{+/-}$ brains (Figure 3.18). Cortical tissues did not display X-gal staining, aside from a few small blood vessels. The most notable X-gal expression in the cortex was fairly strong staining in the anterior cerebral arteries located between the hemispheres of the brain (Figure 3.18B).

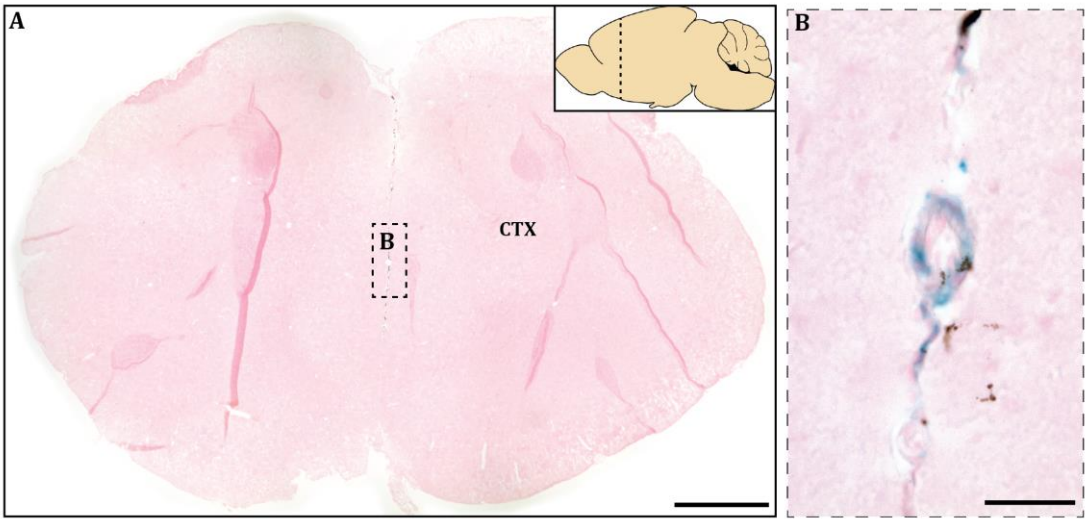

Figure 3.18. Expression of PRELP in the cortex assessed by X-gal staining in PRELP$^{+/-}$ brain. There is no obvious staining of X-gal in the cortex **(A)** aside from the large vessels separating the hemispheres **(B)**. CTX, cortex. Scale bars 500um (A) and 25um (B).

Staining of the hippocampus indicated no obvious β-galactosidase activity (Figure 3.19). Taking a closer look, I observed that there is weak punctate staining in the dentate gyrus granule cell layer of PRELP$^{+/-}$ brains in addition to staining in vasculature in the surrounding tissues (Figure 3.19B). This staining was similar to the expression pattern in OMD$^{+/-}$ dentate gyrus, albeit weaker.

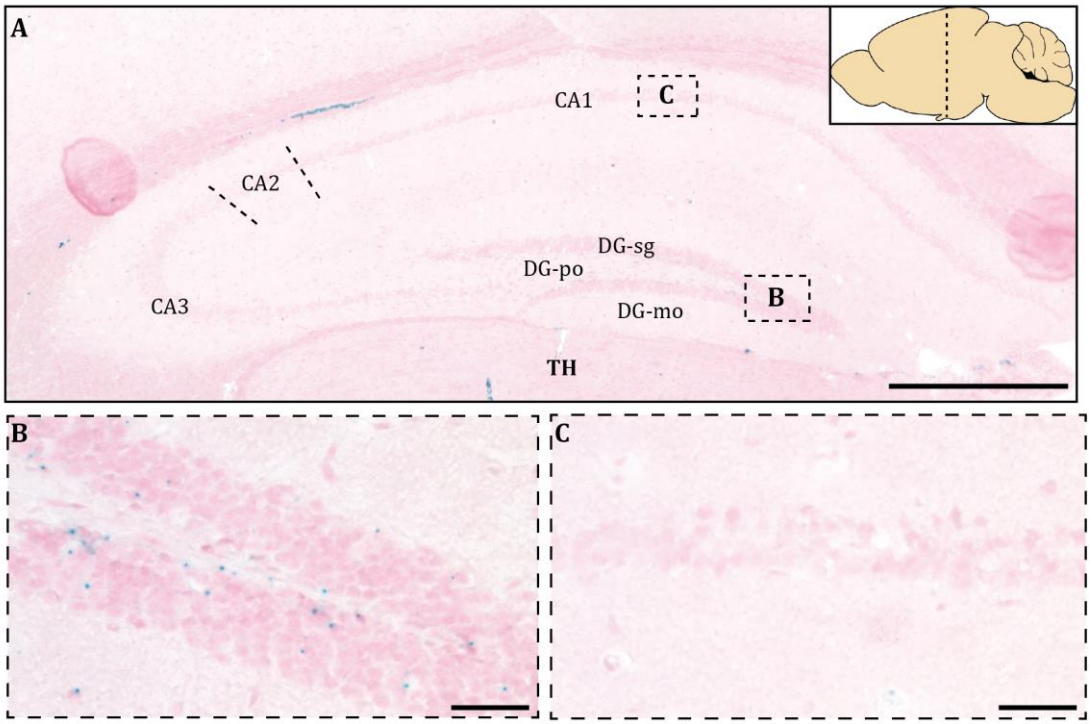

Figure 3.19. X-gal staining in PRELP$^{+/-}$ hippocampus is weak. A) X-gal staining in the hippocampus shows no obvious β-galactosidase activity. However, a magnified view of the dentate gyrus **(B)** shows weak punctate staining, although this was not visible in Ammon's horn **(C)**. CA1-3, Ammon's horn fields 1-3; DG-sg, dentate gyrus (DG) granule cell layer; DG-po, DG polymorph layer; DG-mo, DG molecular layer. Scale bars 500um (A) and 25um (B & C).

Staining of the PRELP$^{+/-}$ cerebellum with X-gal indicated that there is expressed in the lining of the cerebral aqueduct in addition to surrounding capillaries, veins and arteries (Figure 3.20A, C). In addition, I observed weak punctate staining in the granular and molecular layers of the cerebellum (Figure 3.20B).

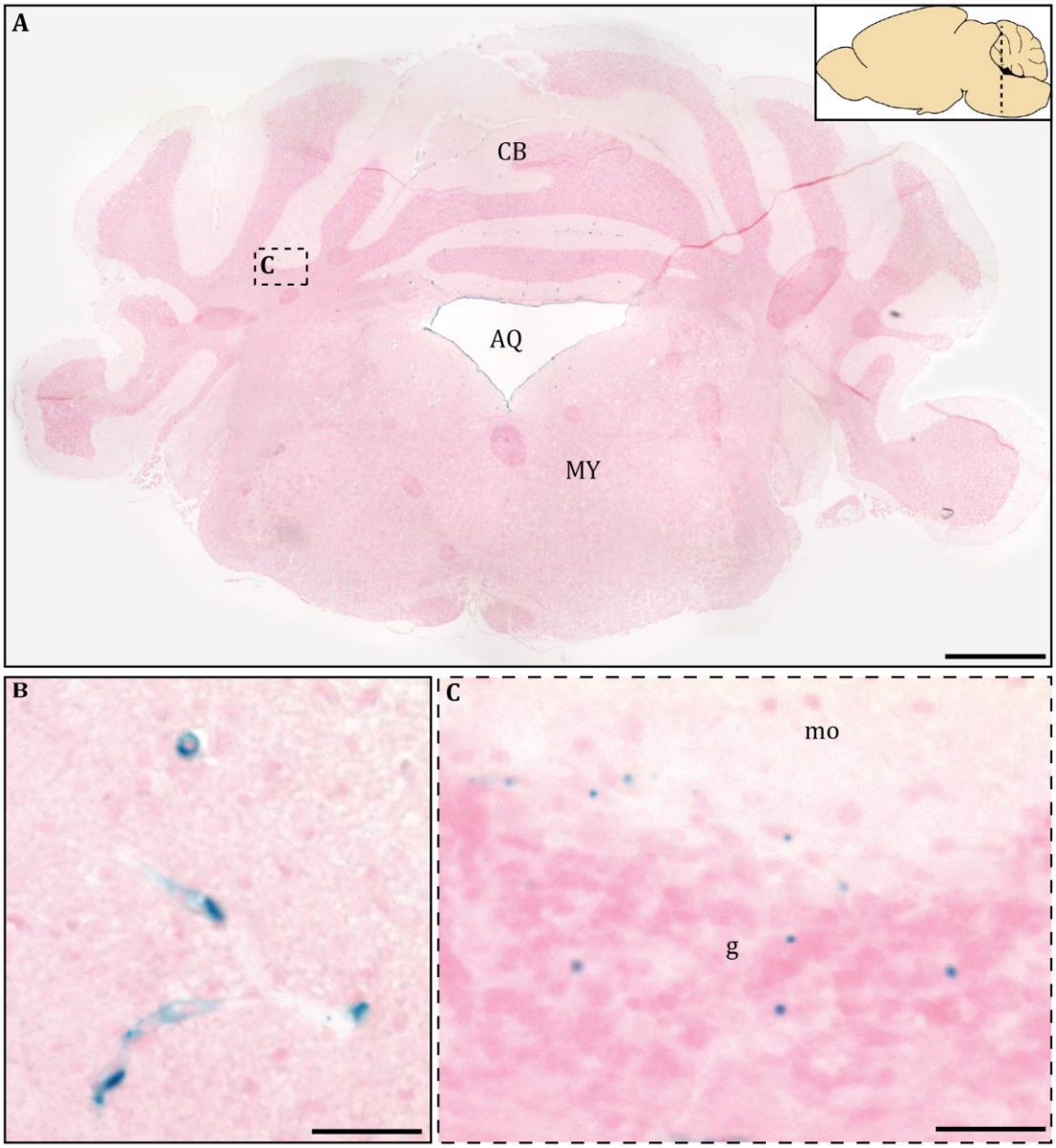

Figure 3.20. X-gal staining in PRELP$^{+/-}$ cerebellum. Staining observed in the lining of the cerebral aqueduct **(A)** and vasculature **(B)**. Spotty X-gal staining was detected in the granular layer of the cerebellum **(C)**. CB, cerebellum; MY, medulla; AQ, cerebral aqueduct; g, granular layer; mo, molecular layer. Scale bars 500um (A) and 25um (B & C).

Given the strong X-gal staining I observed in the ventricles in whole-mount brain (Figure 3.17), I verified the nature of this staining in tissue sections. I performed X-gal staining in sections containing the lateral ventricles, third ventricle and fourth ventricle (Figure 3.21). In all ventricles, staining was observed in the ependymal lining of the ventricles. Staining of the choroid plexuses was more variable (Figure 3.21; arrows). Overall staining appeared to be particularly strong in the lateral and fourth ventricles (Figure 3.21A, C). Staining in the choroid plexus was found in both the cuboidal epithelial cells and capillaries. The lateral and third ventricles' choroid plexuses exhibit staining mainly in the epithelial cells, whereas the fourth ventricle seems to display staining in both cell types.

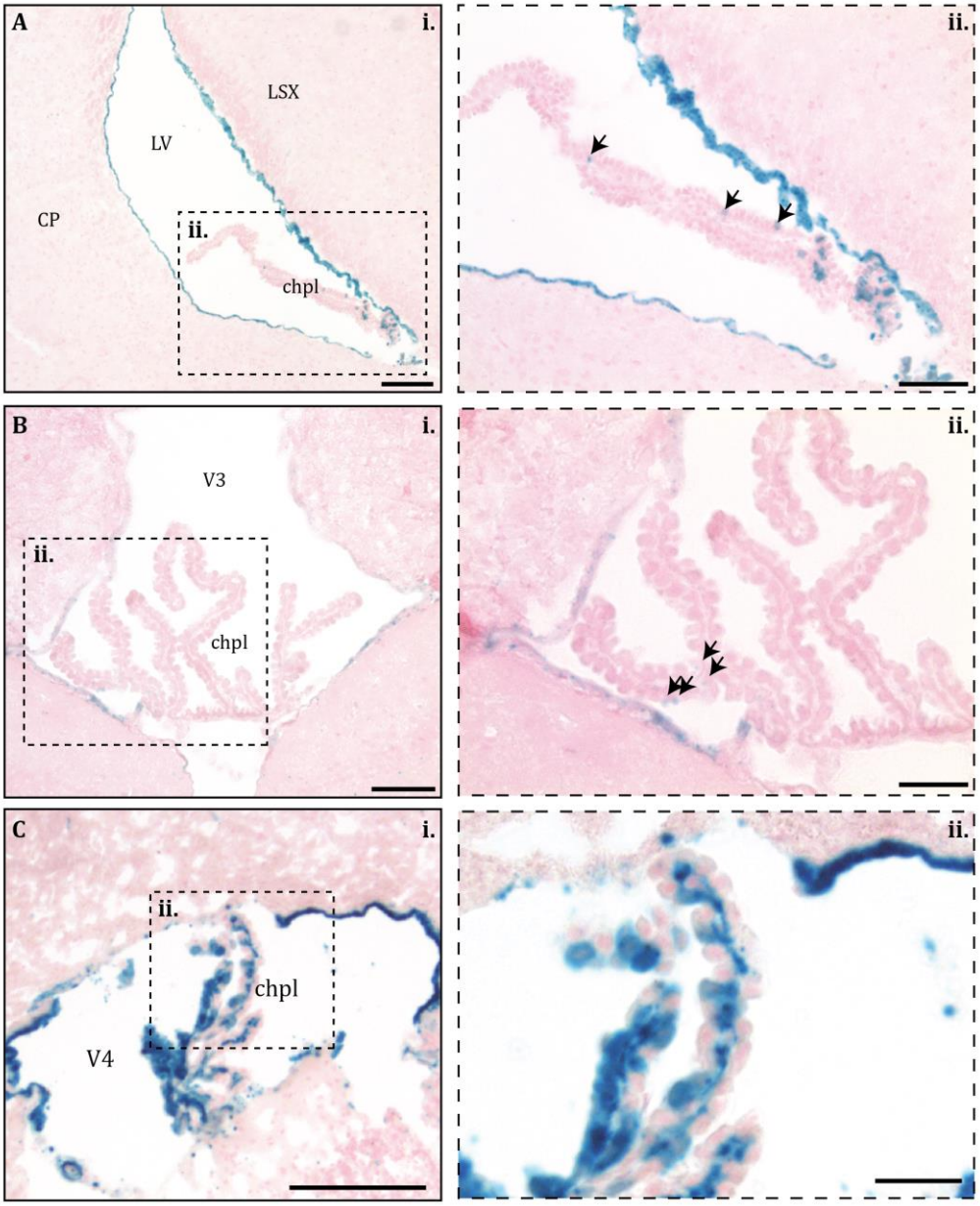

Figure 3.21. X-gal staining in the ventricles of PRELP$^{+/-}$ brain. Staining in the lateral ventricles **(A)** indicate expression of PRELP in the ependymal lining and choroid plexus (ii; arrows). The third ventricle **(B)** exhibits weaker staining the ependymal lining and choroid plexus (ii; arrows). The fourth ventricle **(C)** shows strong staining in both the choroid plexus and ventricle lining. CP, caudoputamen; LSX, lateral septal complex; LV, lateral ventricle; V3, third ventricle; V4, fourth ventricle ; chpl, choroid plexus. Scale bar 100um (Ai, Bi & Ci), 50um (Aii) and 25um (Bii & Cii).

X-gal staining was detected in both small capillaries (~5um diameter) and larger vessels (>10um diameter) (Figure 3.22) throughout the brain. Intense staining was localised in i) oval cells (Figure 3.22;arrows), ii) round cells (Figure 3.22A; arrowhead) and iii) striated cells (Figure 3.22C; arrowheads). The oval cells were likely to be endothelial cells, as they have a more elongated cell body and nucleus. The other two cell types are likely to be mural cells; pericytes can often be identified on the vasculature due to their round cell body, and smooth muscle cells wrap around vessels in a ring-like manner. However, these

findings would have to be verified by staining with antibodies specific to endothelial cells, pericytes and smooth muscle cells.

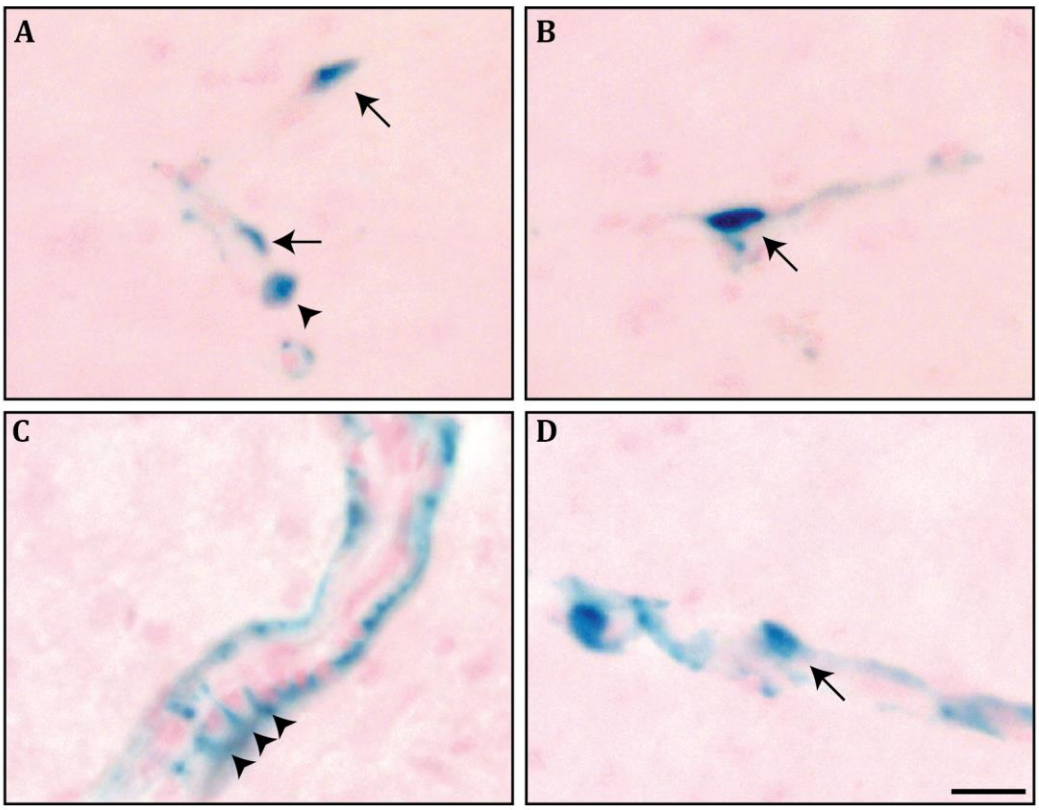

Figure 3.22. X-gal staining observed in PRELP$^{+/-}$ vasculature. PRELP is expressed on capillaries **(A & B)** and larger vessels **(C & D)**. X-gal staining is intense in the cell body of oval-shaped cell (arrows), round cells **(A**; arrowhead**)** and striated cells around the vasculature **(C**; arowhead**)**. Scale bar 10um.

I have confirmed that *LacZ* is likely to be expressed in the ventricles and vasculature in the brain as was suggested by whole-mount staining. X-gal staining was detected in all ventricles and found to be mainly localised to the ependymal lining, whereas there is weaker staining in the choroid plexuses. Staining of the vasculature indicated that the reporter gene is expressed in vessels in most regions of the brain, with the weakest staining in the cortex. X-gal staining of blood vessels showed that PRELP could be expressed by either endothelial cells or mural cells, such as pericytes and smooth muscle cells. In addition, I also observed weak, punctate staining in the hippocampal dentate gyrus and in the granular layer of the cerebellum.

3.4.2 X-gal and antibody double staining

In order to determine the identity of the cells expressing the reporter gene in a punctate manner in the hippocampus and cerebellum, I performed double staining using X-gal and an HRP-conjugated secondary antibody. As before, I performed double staining with GFAP

(astrocyte marker), Iba-1 (microglia) and calbindin (neuronal marker) after staining with X-gal.

Astrocytes are glial cells in the brain which act to maintain homeostasis by influencing a number of processes; they are highly abundant and essentially expressed in all tissues of the brain (Sofroniew & Vinters, 2010). I therefore probed whether punctate staining in the hippocampus and cerebellum corresponded to astrocytes using the astrocyte marker GFAP. Staining of X-gal and GFAP showed some possible co-localisation (Figure 3.23). Unfortunately, since the punctate staining was not as abundant as with $OMD^{+/-}$, staining in the cell body of astrocytes was difficult to identify. Co-localisation was identified with the elongated processes of astrocytes (Figure 3.23; arrows) and possibly in the cell body (Figure 3.23; arrowhead), indicating that there is expression in a sub-population of astrocytes in the hippocampus. In contrast, I was unable to detect any co-localisation in the cerebellum (Figure 3.23E).

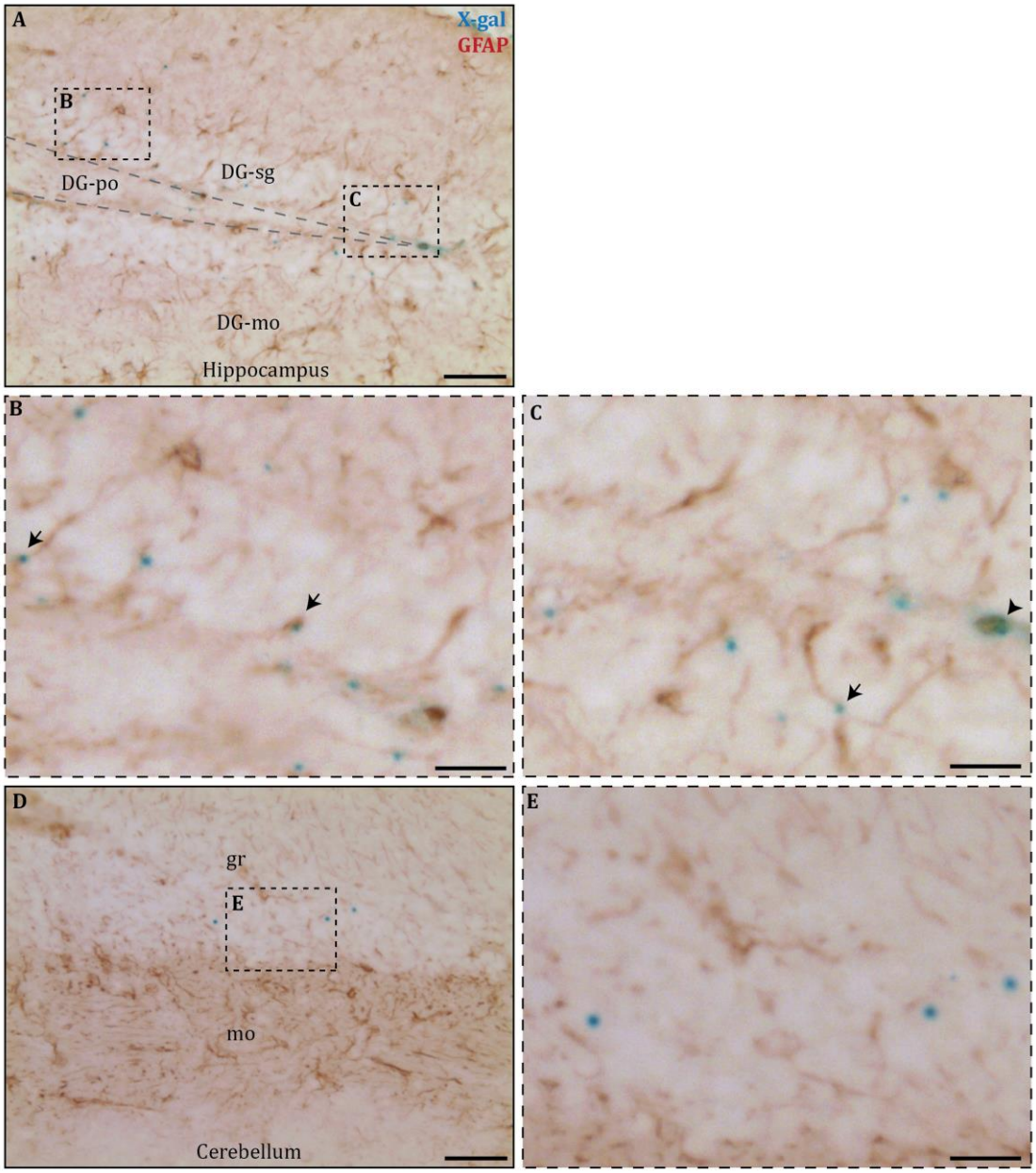

Figure 3.23. Double staining of X-gal and GFAP astrocyte marker in PRELP$^{+/-}$ brain. Staining in the hippocampus **(A, B & C)** shows that there may be colocalization of X-gal and GFAP stains in the cell processes (arrows) and cell bodies (arrowhead). Staining in the cerebellum **(D)** suggests that there is no colocalization **(E)**. DG-sg, dentate gyrus (DG) granule cell layer; DG-po, DG polymorph layer; DG-mo, DG molecular layer; gr, granular layer; mo, molecular layer. Scale bar 25um (A & D), 10um (B, C & E).

Microglia are the resident immune cells of the brain, and are expressed ubiquitously in brain tissues (Lawson et al., 1990). I performed double staining with X-gal and anti-Iba-1 microglial marker (Figure 3.24). I was unable to locate areas of co-localisation between X-gal and Iba-1 at the cell bodies of microglia. I noted that there may be co-localisation with respect to microglia cell processes in both the hippocampus (Figure 3.24B, C) and cerebellum (Figure 3.24E).

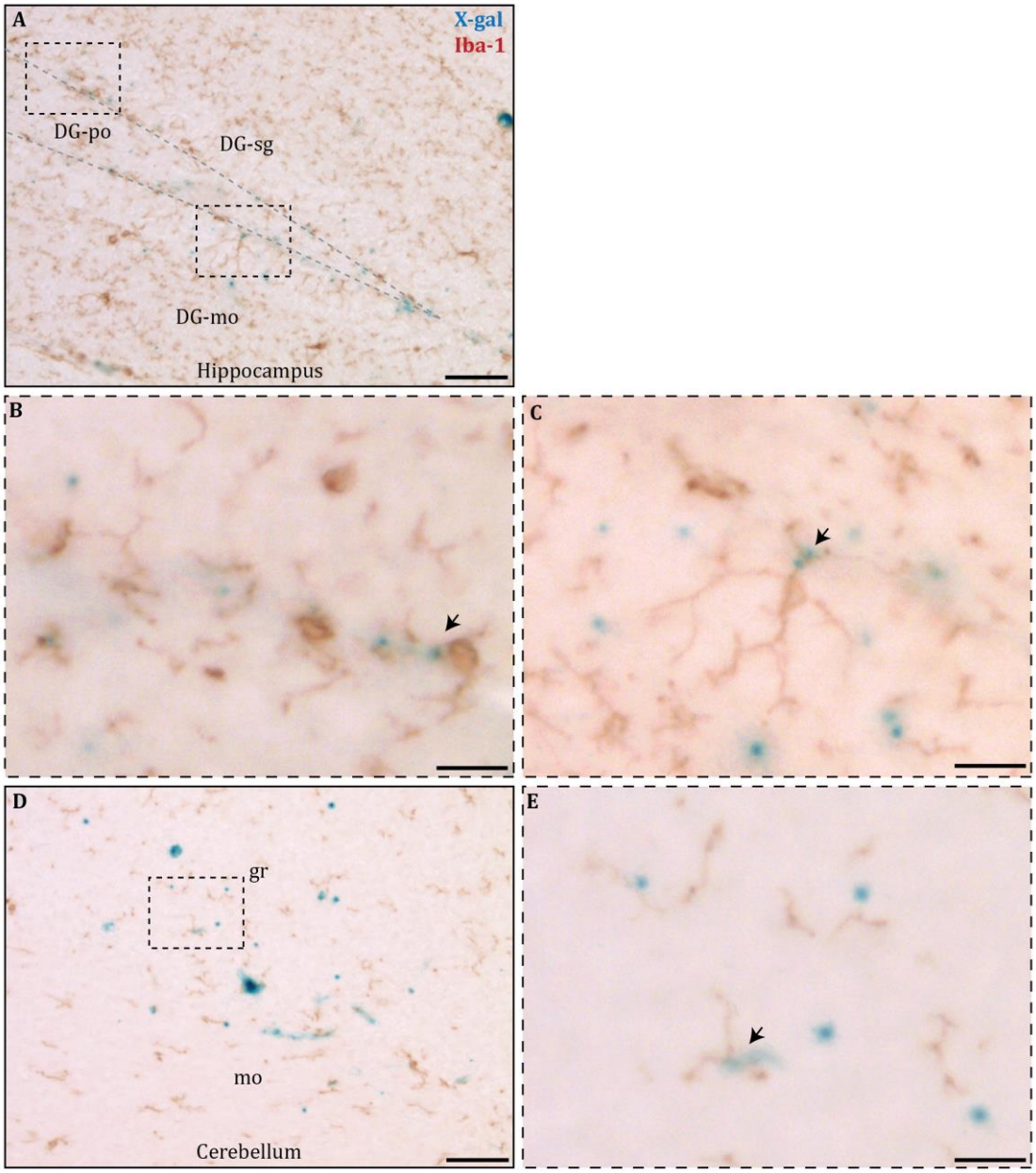

Figure 3.24. Double staining of X-gal and Iba-1 microglia marker in PRELP$^{+/-}$ brain. Staining in the hippocampus **(A,B & C)** shows that there may be colocalization of X-gal and Iba-1 stains in the cell processes (arrows). Staining in the cerebellum **(D, E)** suggests that there may be colocalization assessed in the cell processes (arrow). DG-sg, dentate gyrus (DG) granule cell layer; DG-po, DG polymorph layer; DG-mo, DG molecular layer; gr, granular layer; mo, molecular layer. Scale bar 25um (A & D), 10um (B, C & E).

Finally, I stained tissues with X-gal and anti-calbindin, a neuronal marker, as the granular layers of hippocampus and cerebellum are particularly rich in neurons (Figure 3.25). Staining in the hippocampus indicated that it is likely that there is co-localisation in the CA3 neuron field of Ammon's horn; these neurons are quite large and X-gal staining can be seen inside the cytoplasm or near the membrane (Figure 3.25B; arrows). Staining in the dentate gyrus was not as clear, however I can see potential co-localisation in dentate

gyrus neurons (Figure 3.25C; arrows). In contrast, staining in the cerebellum with calbindin indicates that there is no co-localisation of neurons and X-gal (Figure 3.25D, E).

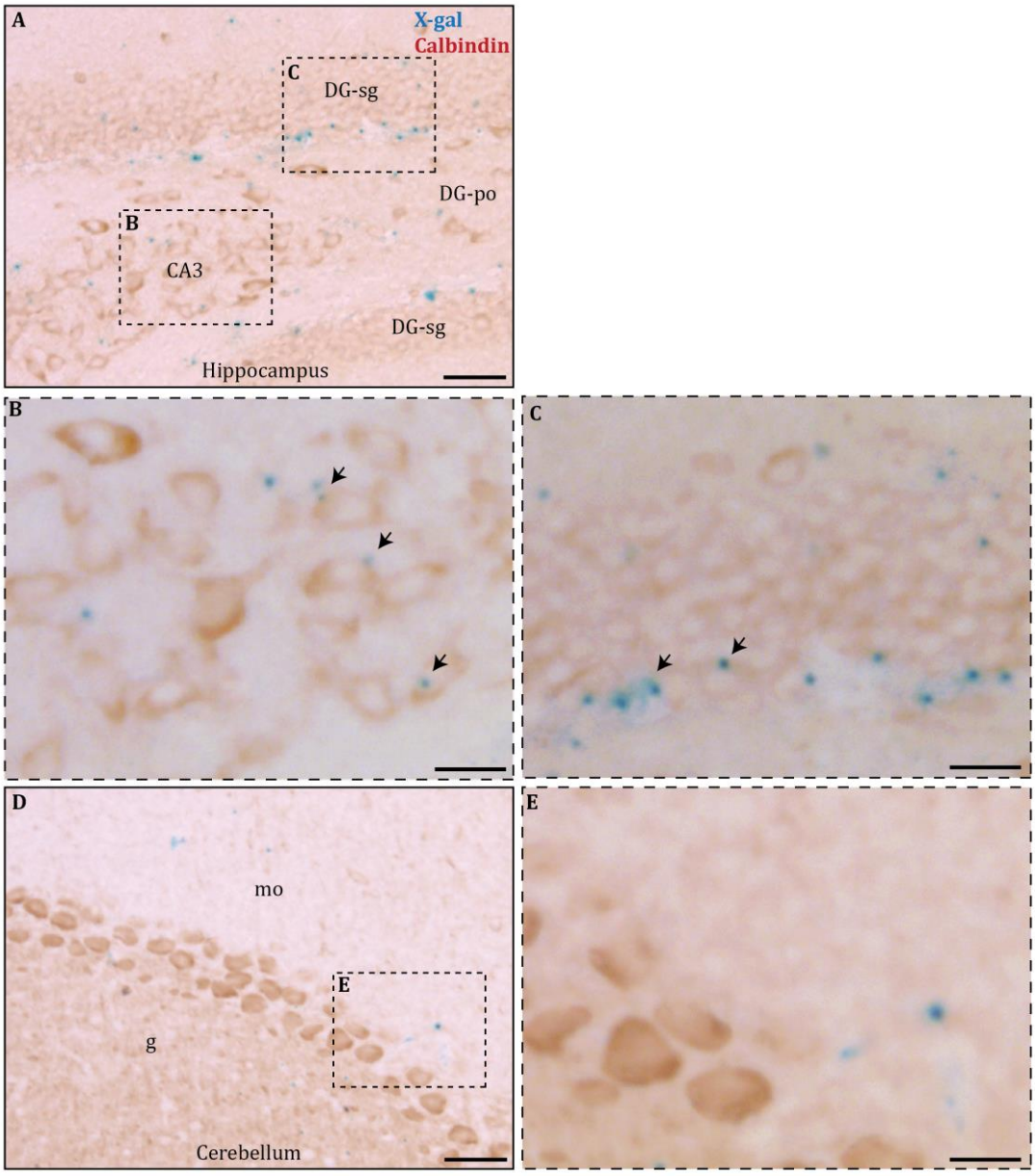

Figure 3.25. Double staining of X-gal and calbindin neuronal marker in PRELP$^{+/-}$ brain. Staining in the hippocampus **(A, B & C)** shows that there may be colocalization of X-gal and calbindin-positive neurons in Ammon's horn CA3 neuron field and the dentate gyrus granule cell layer; arrows. Staining in the cerebellum **(D & E)** shows that there no co-localisation of X-gal and calbindin stains in the cerebellar molecular layer. DG-sg, dentate gyrus (DG) granule cell layer; DG-po, DG polymorph layer; gr, granular layer; mo, molecular layer. Scale bar 25um (A & D), 10um (B, C & E).

Double staining of X-gal with cell markers therefore indicates that staining in the hippocampus potentially corresponds with astrocytes, microglia and neurons. In contrast, staining in the cerebellum seems to be restricted to microglia only. However, just as with

OMD, I was unable to identify the cell type expressing PRELP on the vasculature using this method.

3.4.3 Detection of PRELP-expressing cells using β-galactosidase antibody staining

Given that the double staining of X-gal and HRP-conjugated secondary antibody was inconclusive in PRELP$^{+/-}$, I decided to detect the expression of β-galactosidase protein instead of probing its catalytic activity. In order to obtain the strongest signal for β-galactosidase protein, tissue from knock-out animals was used instead of heterozygotes. Given the strong expression observed using X-gal in the vasculature, I perfused animals with PBS and then 4% PFA to remove blood and therefore a potential source of high background signal. Perfused brains were processed, sectioned and stained with a mouse monoclonal antibody against β-galactosidase.

β-galactosidase expression was detected throughout the brain, although staining in the cortex was slightly weaker. As expected, small and large blood vessels were strongly stained with β-galactosidase (Figure 3.26). I noted that not all vessels were positive for β-galactosidase antibody, indicating that the reporter gene is expressed in a subset of vessels. To my surprise, I also observed staining in cells with long, fine processes (Figure 3.26; arrows). While I detected potential non-vascular cell types expressing *LacZ* from X-gal staining previously, I only observed staining in the hippocampus and cerebellum. The cells that were stained for β-galactosidase, however, were found to be stained ubiquitously throughout the brain.

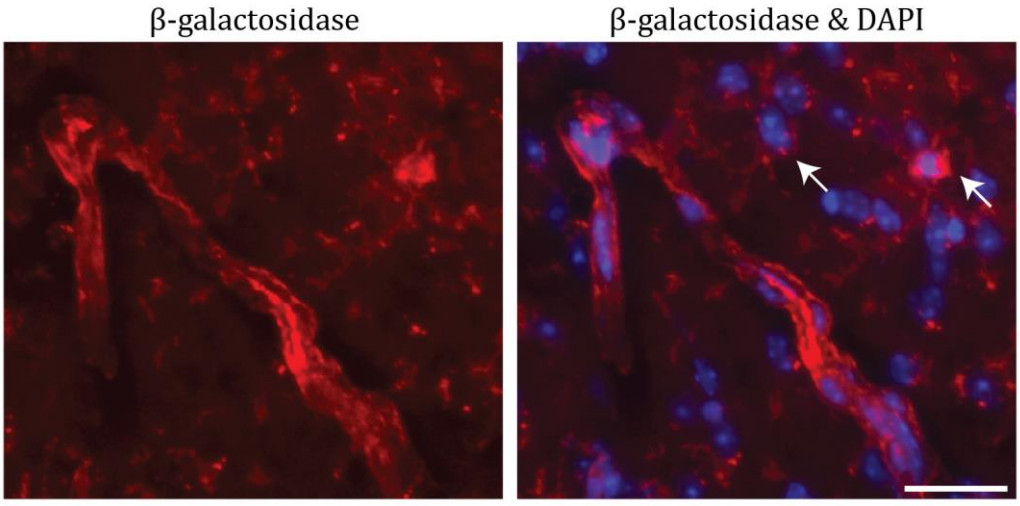

Figure 3.26. β-galactosidase antibody staining in PRELP$^{-/-}$. Staining was detected in vasculature in addition to cells with long fine processes (arrows). Scale bar 25um.

In order to determine PRELP-expressing cells by β-galactosidase antibody staining, I performed double staining with cell type markers. I first aimed to identify the cell type

with the long processes and therefore performed double-staining with GFAP and Iba-1, markers for astrocytes and microglia respectively. Co-staining with GFAP exhibited no co-localisation with β-galactosidase, indicating that the reporter gene is not likely to be expressed by astrocytes (Figure 3.27A). It should be noted that this is true for both astrocytes with processes attached to the vasculature and non-attached astrocytes. In contrast, β-galactosidase staining was found to co-localise entirely with Iba-1 microglial marker strongly indicating that PRELP is expressed in microglia (Figure 3.27B). This is therefore likely to be the cell type exhibiting β-galactosidase enzyme activity in the hippocampus and cerebellum that I observed previously.

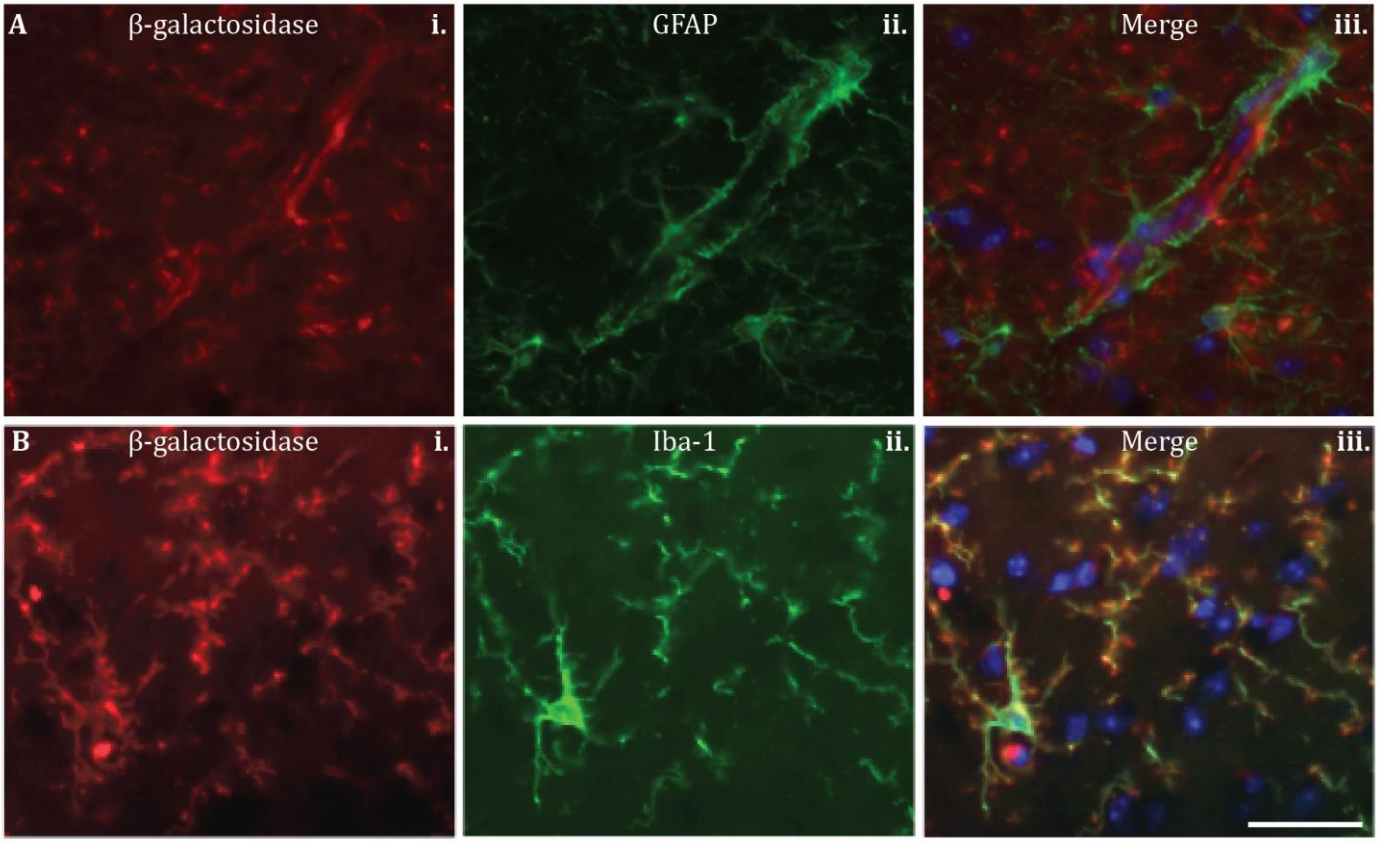

Figure 3.27. Double staining of β-galactosidase and GFAP (A) and Iba-1 (B) in PRELP$^{-/-}$ brain sections. Scale bar 25um for all images.

Given that β-galactosidase was detected on the vasculature, I performed double staining with pericyte marker NG2, smooth muscle marker α-smooth muscle actin and endothelial cell marker isolectin IB4. Co-staining with NG2 shows that there is no co-localisation with the pericyte cell body (Figure 3.28A; arrow). While NG2 is expressed on oligodendrocyte progenitor cells (Polito & Reynolds, 2005), it is also expressed on the surface of pericytes. Pericyte cell bodies can easily be distinguished from oligodendrocytes, as they are embedded in the basement membrane of blood vessels. There seems to be no co-staining

with smooth muscle marker α-smooth muscle actin (Figure 3.28B). Staining of the endothelial cell marker isolectin IB4 indicates that there is no co-localisation with the β-galactosidase antibody stain (Figure 3.28C). Despite performing these double-stains, it is still unclear which vascular cell type normally expresses PRELP.

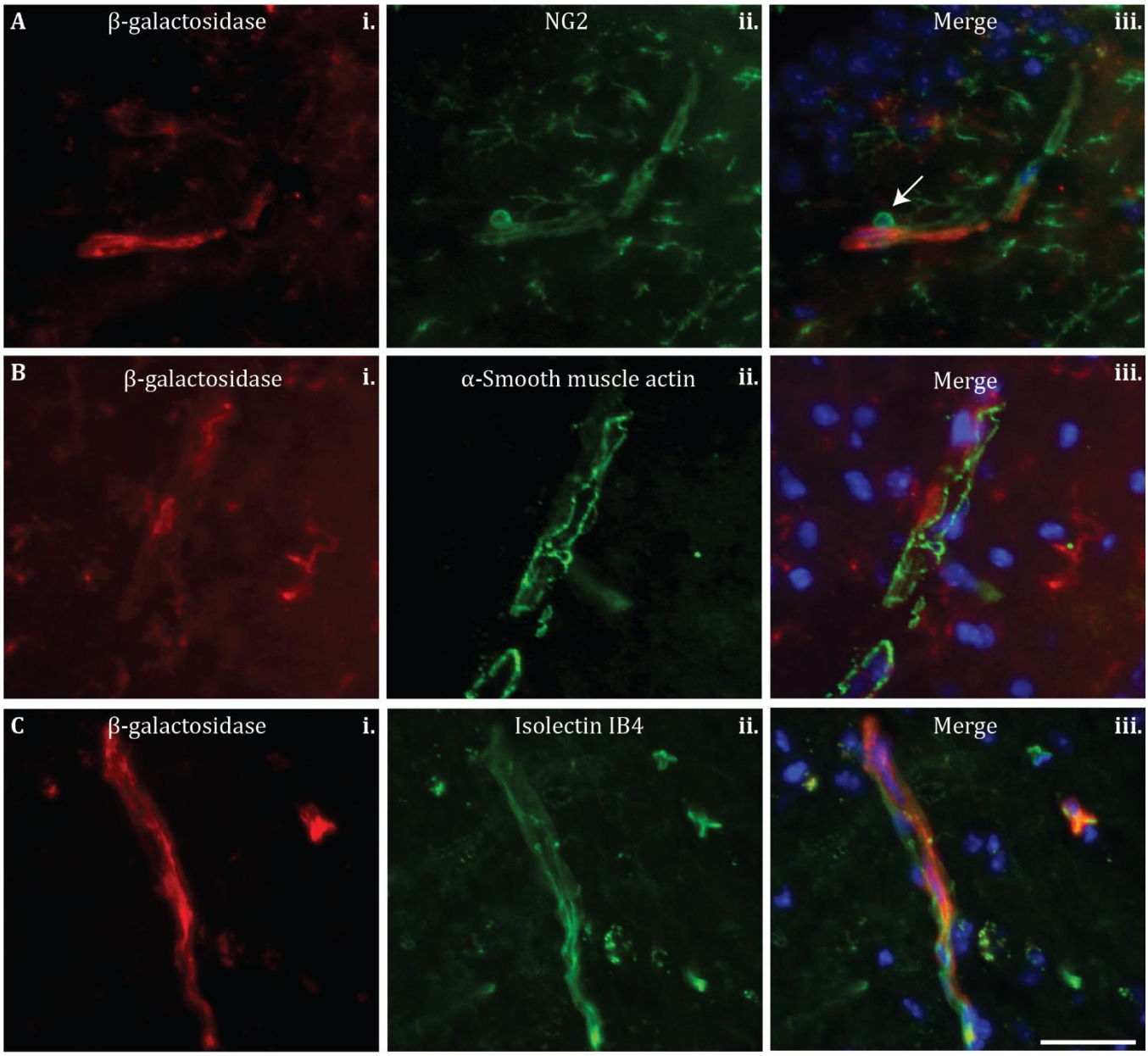

Figure 3.28. Double staining of β-galactosidase with NG2 (A), α-smooth muscle actin (B) and isolectin IB4 (C) in PRELP$^{-/-}$ brain sections. Arrow points toward pericyte on the abluminal surface of the vasculature. Scale bar 25um for all images.

I have previously demonstrated from X-gal staining that there is expression of PRELP in the ependymal lining of ventricles and choroid plexuses (see Section 3.4.1). In order to validate these findings, brain sections were stained with anti-β-galactosidase and the staining in the ventricles was assessed (Figure 3.29). There is staining of the ependymal lining and the choroid plexuses in all ventricles in PRELP$^{-/-}$ sections, consistent with my findings from X-gal staining. It should be noted that there is weak background staining of the choroid plexus only in wild-type sections; the ependymal cell layer does not exhibit background staining. The difference in staining intensity between wild-type and PRELP$^{-/-}$ choroid plexuses suggests the staining observed in PRELP$^{-/-}$ is not solely due to background staining, but rather that the reporter gene is expressed in choroid plexus capillaries and potentially in the epithelial cells. In addition, there is also clear staining of the ependyma, likely validating my conclusions from X-gal staining that PRELP is expressed in ependymal cells and the choroid plexus.

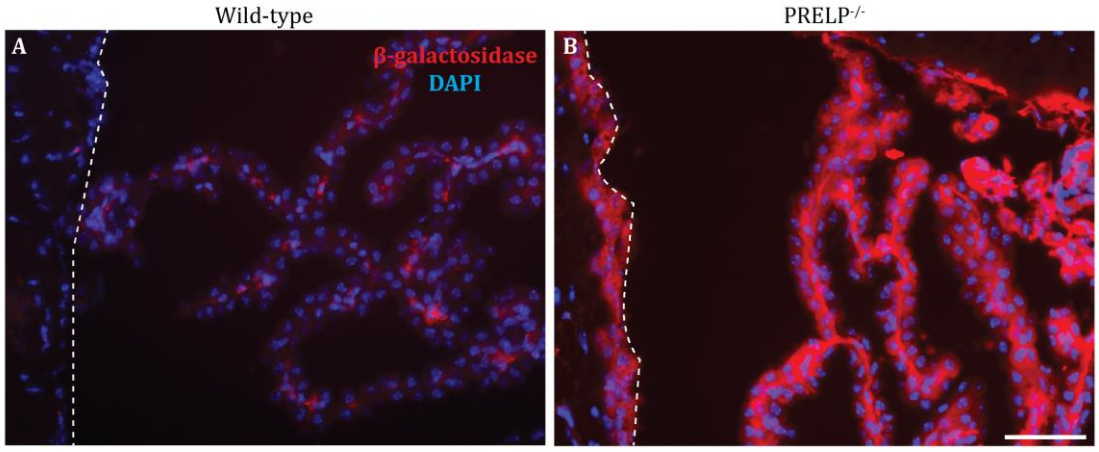

Figure 3.29. β-galactosidase staining of wild-type (A) and PRELP$^{-/-}$ (B) ventricles. There is weak staining in the wild-type choroid plexus, likely to be background staining. In contrast, the staining in PRELP$^{-/-}$ tissues is much stronger, indicating that PRELP is likely to be expressed in the choroid plexus and ependymal lining of the brain ventricles. White dotted line delimits the apical side of ependyma. Scale bar 50um.

To conclude, antibody staining detecting the β-galactosidase protein in PRELP$^{-/-}$ mice indicates that the cells likely to express *LacZ* in PRELP animals are microglia and ependymal cells and the choroid plexus of the brain ventricles. The cell expressing PRELP on the vasculature remains unclear.

3.4.4 Staining of rat tissues with antibodies against PRELP

As mentioned previously, we have attempted to stain tissues with commercially-available antibodies against OMD and PRELP with no success. Our collaborator, Mr Takumi Tashima at the University of Tokyo (Japan), has made antibodies against OMD and PRELP by injecting peptide fragments into mice.

Colleagues Dr Ryohei Sekido and Dr Byongsung Shim have screened the antibodies produced by Mr Tashima in eye and brain sections of one rat. Anti-PRELP #15 was found to have the strongest signal. Blood vessels were found to be stained using this antibody (Figure 3.30). Both arterioles/venules and capillaries were stained, although visual examination of tissue sections indicated that not all vessels are stained for anti-PRELP. No staining of microglia was detected using the PRELP antibody. Just as with OMD antibody staining, the expression of PRELP in the ventricles and choroid plexuses could not be confirmed in the rat sections. This experiment performed by my colleagues in rat tissues is in agreement with findings in mouse that PRELP is expressed in the vasculature. PRELP expression in rat microglia, however, is uncertain.

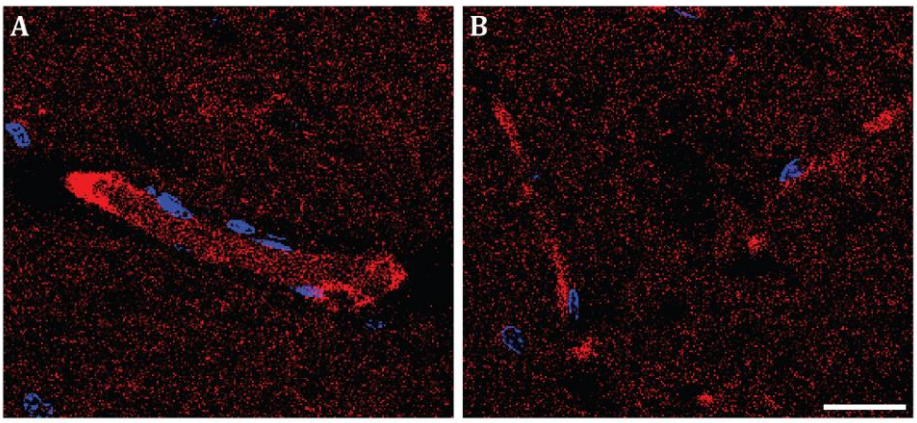

Figure 3.30. Staining of rat brain sections with PRELP antibody #15. Staining is visible in large arterioles/venules **(A)** and capillaries **(B)**. Staining performed by Dr Ryohei Sekido and Dr Byongsung Shim. Scale bar 20um.

3.4.5 Single-cell analysis

As explained above, a research group has done single-cell transcriptome analysis in cortex and hippocampal tissues (Zeisel et al., 2015). Using the online tool, the expression of PRELP in different cell types was examined (Figure 3.31). According to these data, PRELP is expressed in a sub-type of microglia identified by this research group (Micro1a; ~8 copies), vSMCs (~10 copies), ependymal cells (~12 copies), astrocytes (~4 copies), choroid plexus (~5 copies) and oligodendrocytes (~9 copies). These results support my findings that PRELP is expressed on microglia and ependymal cells.

The vascular cell type expressing PRELP according to these data is mainly vSMC and to a lesser extent pericytes. As shown throughout this chapter, PRELP seems to be expressed in a variety of vessels in the brain, ranging from capillaries to larger vessels. This therefore suggests that PRELP is expressed in both pericytes and vSMCs mural cells. The data presented in Figure 3.31, however, suggests that PRELP is mainly expressed in vSMCs. This may be attributed to the similarities between vSMCs and pericytes, as these mural

cells share common lineages, can be differentiated from common progenitor cells and have comparable gene expression profiles (Armulik et al., 2011; Chen et al., 2016). This is further explored in Section 3.5.3 . There is almost no expression of PRELP in endothelial cells, further supporting the idea that PRELP is expressed on mural cells.

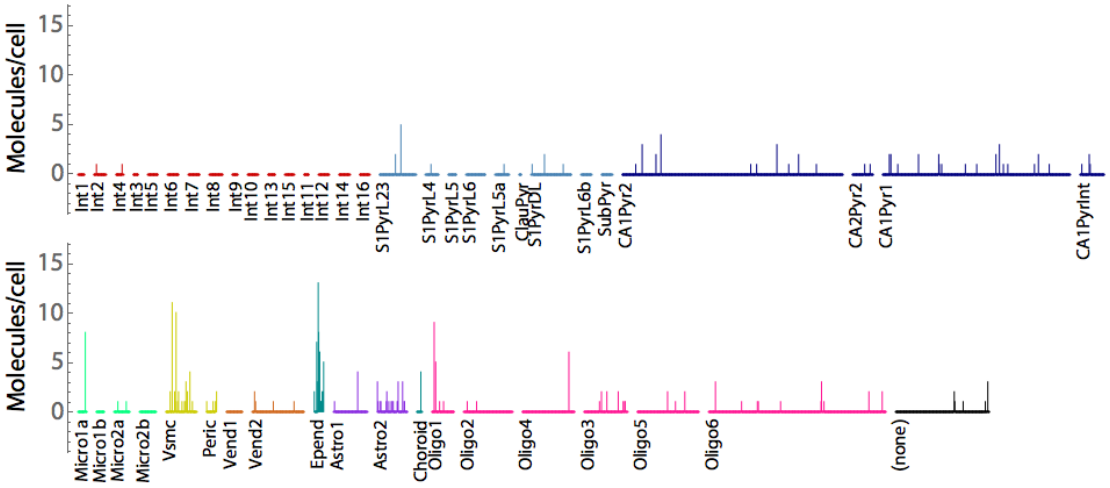

Figure 3.31. Expression of PRELP in cortical and hippocampal cells based on single-cell RNA sequencing data. Zeisel et al. (2015) performed single-cell RNA sequencing in mouse cortex and hippocampus to identify different classes of cells. Int, interneurons; S1Pyr, S1 pyramidal neurons; CA1Pyr, CA1 pyramidal neurons; CA2Pyr, CA2 pyramidal neurons; ClauPyr, claustrum; Micro, microglia; VSMC, vascular smooth muscle cell; Peric, pericyte; Vend, vascular endothelial cell; Epend, ependymal cell; Astro, astrocyte; Oligo, oligodendrocyte. Figure generated from tool provided by group: http://linnarssonlab.org/cortex/.

3.5 Discussion

3.5.1 Technical difficulties related to X-gal staining

I sought to determine the OMD- and PRELP-expressing cells in the brain. Given that the exons encoding OMD and PRELP are replaced by those of *E. coli LacZ*, β-galactosidase enzyme activity can be utilised for this purpose. Conventionally, I can use chromogenic substrate X-gal to probe β-galactosidase enzyme activity, whereby the product forms a blue insoluble precipitate. This staining is performed on individual tissue sections, given that the relatively large size and volume of the adult brain leads to incomplete penetrance of the X-gal substrate, where I only obtain X-gal staining on the surface of the tissues. Due to this technical limitation, I stained each slide containing tissue sections separately with X-gal, often performed overnight. This frequently led to staining heterogeneity; even if the staining was performed for the same amount of time, there was often variation in staining intensity, even on the same slide and was particularly notable when comparing staining intensity between different animals. The overall staining pattern, however, remained largely the same.

In order to determine which cell expresses OMD or PRELP, I attempted to combine X-gal staining with antibody staining. In initial attempts, I stained sections with X-gal and proceeded to incubate them with primary and fluorescent secondary antibodies. Unfortunately, I found that the X-gal signal completely masked the fluorescent signal, as shown in Figure 3.32. It therefore meant that combining X-gal and fluorescent antibody staining was challenging. Despite this, a member of the laboratory Dr Vasiliki Papadaki previously demonstrated that OMD and PRELP are expressed by a variety of cells using this method. Care must be taken when determining whether there is co-localisation of signals. In particular, it would potentially be possible to make such assessments provided that the stain is not too saturated and the pattern is punctate. In the brain, the majority of cells have long cell processes – therefore, to accurately determine co-localisation, the X-gal signal should be located in the cell body, rather than the cell processes, limiting the chance of false-positive results.

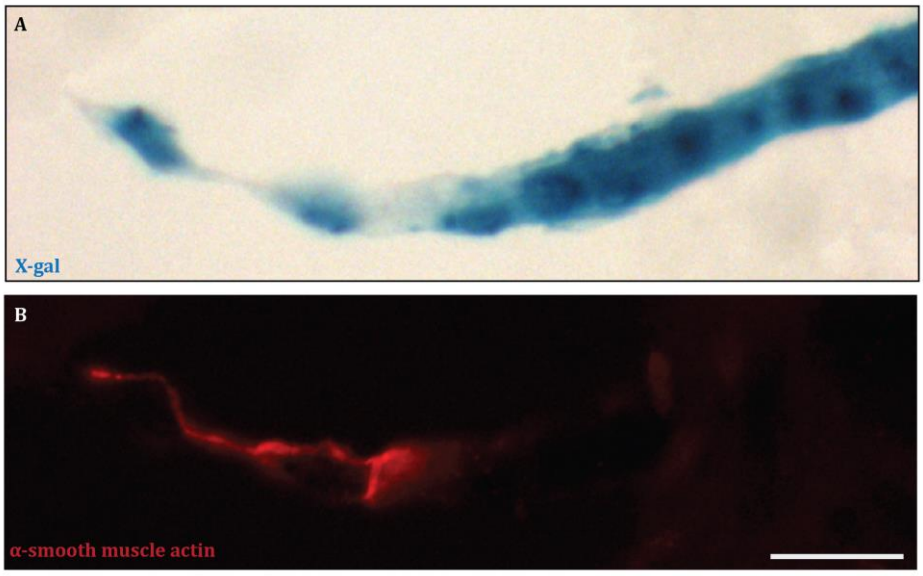

Figure 3.32. Strong X-gal staining can completely block signal from fluorescent antibody staining. A) X-gal staining of PRELP$^{+/-}$ large vessel. **B)** Staining of the same vessel using α-smooth muscle actin detected using a red fluorescent secondary antibody. Scale bar 40um.

A variety of substrates can be utilised by β-galactosidase, including those which produce fluorescent molecules upon enzymatic processing, and the use of these substrates would circumvent the issue I outlined above. I attempted to utilise two different reagents – 4-Methylumbelliferyl-β-D-galactopyranoside (MUG) and Fluorescein Di-β-D-Galactopyranoside (FDG). Cleavage of MUG by β-galactosidase produces methylumbelliferone, which has an emission maxima at 445nm (Strachan et al., 1961), which corresponds to UV. FDG is cleaved into fluorescein monogalactoside and has an emits at 515nm (Nolan et al., 1988), i.e. green fluorescence. Although there are

publications where reagents such as MUG and FDG have been successfully used to detect β-galactosidase enzyme activity, I was unable to obtain strong and consistent signal. It is possible that the binding affinity of these substrates and β-galactosidase is different from that of X-gal, and may have specific requirements for the reaction buffer. My colleague Dr Tomoko Orita later managed to use FDG to distinguish cells isolated from wild-type and knock-out mice using a protocol and kit optimised for cell culture; see Chapter 6 for more details. My attempts to optimise these reactions were unsuccessful; in the interest of time, I decided to use alternative methods.

Acknowledging the challenges of combining X-gal with fluorescent antibody staining, I attempted to combine X-gal staining with secondary antibodies conjugated to HRP. HRP catalyses the transfer of two electrons from a substrate to H_2O_2 to produce H_2O and an oxidised donor; reaction of DAB with HRP results in the formation of an insoluble brown precipitate. While it would be ideal to first perform antibody staining using HRP and then stain for X-gal, this was not found to be possible. When staining using an HRP system, the activity of endogenous peroxidases must be quenched prior to antibody staining – one could utilise a weak H_2O_2 solution or commercial reagents. While a weak H_2O_2 seemingly had no effect on subsequent X-gal staining, I often found that endogenous peroxidases were not completely quenched, leading to visible background staining. The commercial quenching reagent eliminated non-specific staining, but I found it to have a profound effect on the activity of β-galactosidase; i.e. when performing antibody staining followed by X-gal staining, there was no X-gal signal. I therefore had to first stain for X-gal, quench using commercial reagent and then proceed to antibody staining.

The disadvantage of this method was that certain antibodies were difficult to obtain strong signal with. Given that when staining with X-gal first, slides had to be incubated at 37°C first in the X-gal staining solution and then proceeded to antibody staining. I noticed that antibody staining was often weaker when performed after X-gal staining compared to antibody staining only. Combined with the strong X-gal staining in the vasculature, particularly in PRELP$^{+/-}$animals, it was challenging to use this staining system to determine which vascular cells displayed X-gal staining. When utilising HRP antibodies, I attempted to stain slides with X-gal for the shortest amount of time to see sufficient staining, however X-gal staining often still completely masked the DAB produced from antibody staining of vascular cells.

Therefore, while it is possible to utilise X-gal staining to determine whether there is co-localisation of β-galactosidase enzyme activity with antibody staining, these methods have limitations and are highly dependent on the nature of the X-gal staining. Determining

co-localisation would be more straightforward if the staining pattern was abundant and punctate as is observed in $OMD^{+/-}$; staining is not too clustered, yet sufficiently abundant to observe whether there is co-localisation in cell bodies. In the case of $PRELP^{+/-}$, the spotty staining in the hippocampus and cerebellum was unfortunately too sparse to clearly judge whether there is co-localisation. However, due to these drawbacks, I sought to utilise an alternative method to determine OMD- and PRELP-producing cells by staining for β-galactosidase protein.

3.5.2 Uncertainty over the cell type expressing OMD

X-gal staining of $OMD^{+/-}$ animals indicated that the reporter gene in OMD animals is expressed in a punctate manner throughout the brain grey matter, from the cortex to the cerebellum (Figure 3.6). X-gal staining was notably weaker or absent in the white matter. The strong expression in the hippocampus suggested that the β-galactosidase enzyme originated from neurons (Figure 3.8); in addition, there was distinct staining of cells between the granular and molecular layers of the cerebellum likely to be Purkinje neurons (Figure 3.9). There was weak staining of the ependymal lining of ventricles and choroid plexuses in addition to staining in the vasculature (Figure 3.10, Figure 3.11). X-gal signal in the blood vessels was quite diffuse and it was not possible to determine whether *LacZ* is expressed in endothelial cells or pericytes from staining morphology.

I combined X-gal and HRP-based antibody staining to determine the cell type expressing β-galactosidase. Staining was found predominantly in neurons as I had initially suspected (Figure 3.12); in addition, I also detected staining in the cell bodies of astrocytes and microglia, although co-localisation was detected less frequently (Figure 3.13). Therefore, it is likely from these experiments that the reporter gene is most strongly expressed in neurons and to a lesser extent in astrocytes and microglia. In parallel to these experiments, I also attempted to determine the vascular cell exhibiting X-gal staining, but were unsuccessful.

I stained sections with anti-β-galactosidase, but were unsuccessful in detecting β-galactosidase in $OMD^{-/-}$ animals (Figure 3.14); staining was identical to that of the wild-type despite the same protocol producing clear staining in $PRELP^{-/-}$ animals. Ear punches from these animals were re-genotyped, and my colleague Dr Ryohei Sekido also isolated DNA from the tissue sections I utilised for staining and determined that mice were correctly genotyped and identified as OMD knock-outs.

Staining with antibodies against OMD performed by Dr Ryohei Sekido and Dr Byongsung Shim in rat brain sections indicated that OMD is only weakly expressed in a subset of

neurons in the hypothalamus (Figure 3.15). There was no staining in other CNS-specific cell types or the vasculature. While the weak staining may be due to difficulties generating a good antibody against OMD, heterogeneous post-translational modifications, or simply differences in OMD expression between mouse and rat, these results indicate that there is probably weak expression of OMD in the brain. This is more consistent with my β-galactosidase antibody staining rather than the strong and widespread pattern of X-gal. There is therefore a considerable discrepancy between X-gal and antibody staining in OMD animals.

In order to resolve this conflict, I analysed data from a study of single-cells in the cortex and cerebellum (Figure 3.16). From X-gal staining, I would expect to see high expression of OMD in the hippocampal neurons and lower expression in other cell types such as microglia and astrocytes (Figure 3.12, Figure 3.13). The expression of OMD obtained from single-cell RNA seq analysis indicated that OMD is only expressed at the level of ~1-3 copies per cell in the cortex and hippocampus, clearly contradicting these X-gal staining patterns. These findings are therefore more consistent with the absent or weak staining using β-galactosidase and OMD antibodies. While OMD may exhibit stronger expression in other brain regions, as demonstrated by staining of anti-OMD in hypothalamus neurons, this seems unlikely. X-gal staining showed intense and widespread staining in almost all brain tissues. I therefore conclude that the activity of the reporter gene in OMD is not synonymous with OMD expression itself.

Finally, my colleague Dr Ryohei Sekido has very recently performed some *in situ* hybridisation experiments in paraffin sections to detect OMD mRNA. He found that the staining pattern obtained from *in situ* and X-gal staining were remarkably similar, suggesting that the results from X-gal staining are relevant. However, the fact that OMD was poorly-detected using anti-OMD antibodies and in single-cell analysis opens the possibility that its mRNA is unstable, providing a possible explanation for the discrepancy. Nonetheless, he noted that the staining signal was quite weak, supporting data that OMD is weakly expressed in the adult mouse brain.

To conclude, I initially attempted to identify cells reacting with X-gal using HRP-conjugated secondary antibodies and found co-localisation with markers against neurons, microglia and astrocytes. In order to confirm these findings, staining for β-galactosidase protein itself indicated that there is virtually no expression of OMD in the brain – a clear contradiction. My colleagues have performed staining against anti-OMD in rat tissue and only found weak staining in a subset of neurons. Single-cell RNA seq data clearly indicated that there is essentially no expression of OMD in the cortex and hippocampus. Finally,

recent *in situ* hybridisation experiments indicate that OMD mRNA may be unstable. Therefore, OMD has weak or no expression in the brain.

3.5.3 PRELP is expressed in mural cells, microglia and ependymal cells

X-gal staining in PRELP animals indicates that the staining pattern is more specifically localised to the brain ventricles and vasculature. From the whole-mount stain, I can clearly see strong staining in the ventricles and vasculature throughout the brain (Figure 3.17). Closer inspection of the X-gal staining pattern in cryosections confirms this finding. I see that the strong staining in the ventricles is mainly attributed to the ependymal lining of the ventricles and the choroid plexus to a lesser extent (Figure 3.21).

The staining in the vasculature indicated that the staining was located predominantly in endothelial cells, as the X-gal staining was concentrated in oval cell bodies along the vasculature (Figure 3.22). Occasionally, I would observe staining in round cells in capillaries, likely to be pericytes; I would also see striated staining across larger vessels thought to be vascular smooth muscle cells.

In order to circumvent the issues regarding X-gal staining and to identify the vascular cell and the source of the staining in the hippocampus and cerebellum, I relied on staining using an antibody against β-galactosidase. I was unfortunately unable to confidently assess whether there was co-localisation with markers NG2, α-smooth muscle actin and isolectin IB4 (Figure 3.28). I expected staining to co-localise with α-smooth muscle actin, as X-gal staining in larger vessels shows strong signal in striated cells surrounding the vasculature (Figure 3.33). However, double staining of β-galactosidase and α-smooth muscle actin indicated that there is no co-localisation.

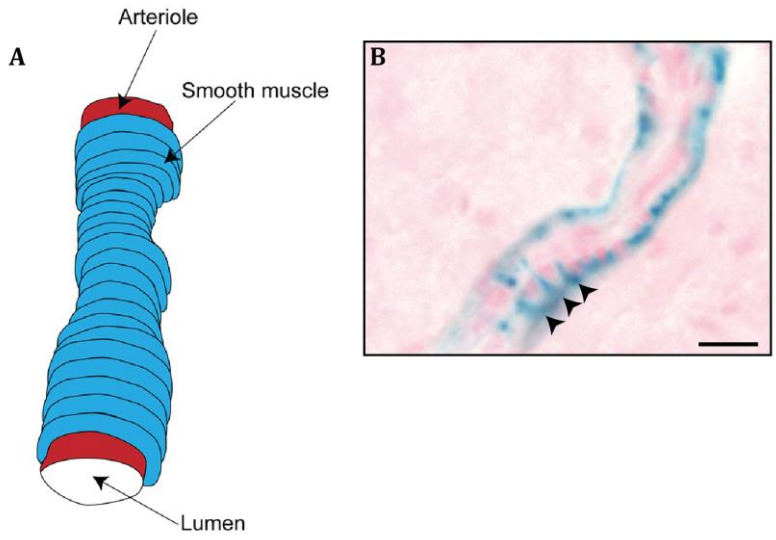

Figure 3.33. Smooth muscle cells surround the vasculature (A) and seems to be observed in PRELP$^{+/-}$ X-gal staining (B). Image (A) modified from (Hamilton et al., 2010). Scale bar 10um.

Data from single-cell analysis indicated that PRELP is strongly expressed in vSMCs, ~5-10 copies per cell was detected (Figure 3.31). Expression in pericytes and endothelial cells was much weaker. While the essentially-exclusive expression of PRELP in vSMCs is surprising and contradicts my observation that PRELP is expressed in capillaries in addition to larger vessels, it may be due to a number of factors. Single-cell analysis was performed using cortical and hippocampal tissues. I noted that there was weaker expression of PRELP in the cortex, although small vessels near the hippocampus were found to be stained with X-gal (as shown in Figure 3.19). The criteria for clustering genes to identify cell types, such as pericytes, may not be optimal. Pericytes and vSMCs are derived from common progenitors, and also have similar expression of genes (Armulik et al., 2011; Chen et al., 2016). From the heatmap shown in Figure 3.34, only ~25 genes were found to be specifically expressed in the pericyte cluster (orange box) compared to >120 in the vSMC clusters.

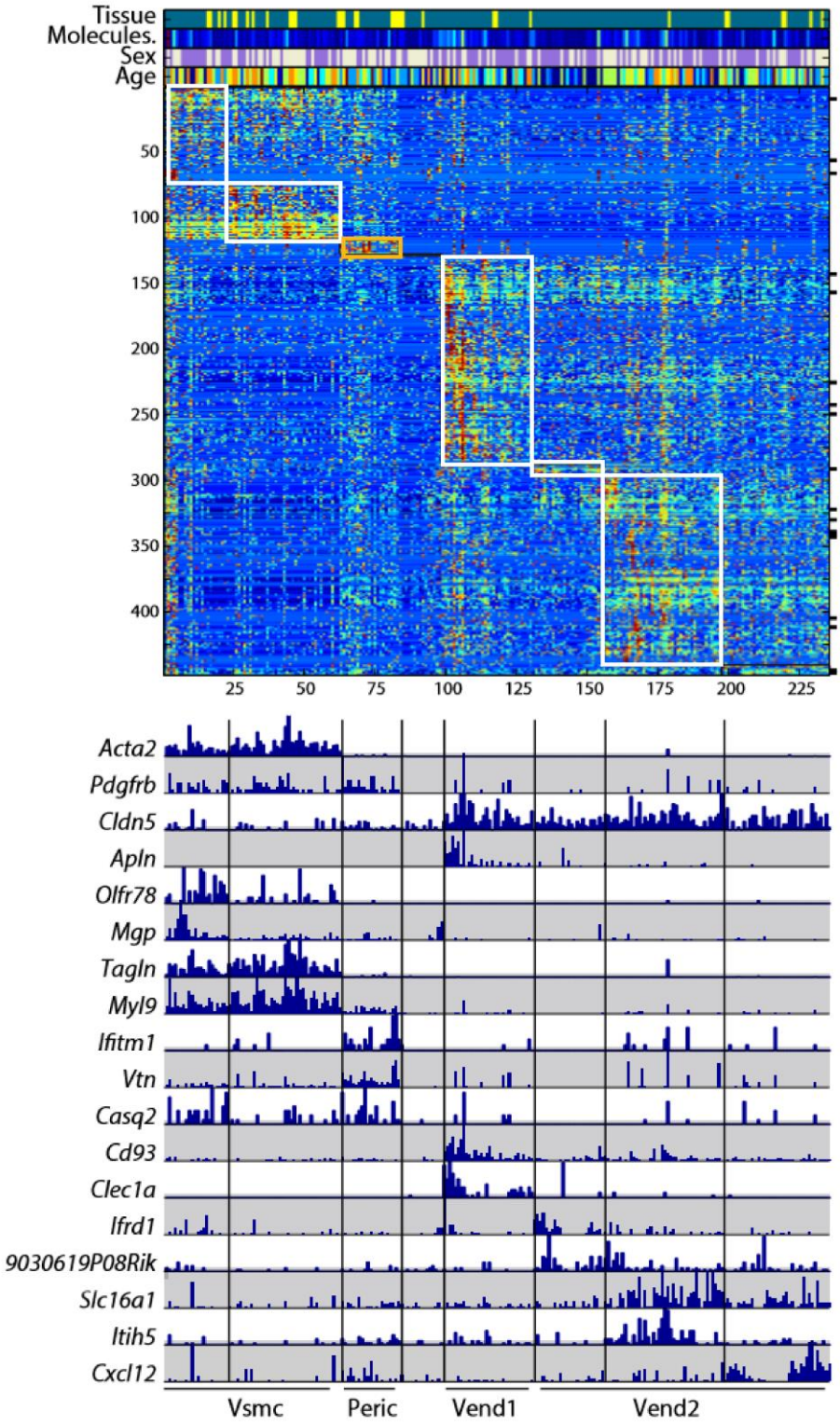

Figure 3.34. Clustering of vascular cells. From RNA seq, clusters of genes expressed in vSMCs, pericytes (outlined in orange) and two classes of endothelial cells (Vend1 and 2) were determined. The heatmap illustrates these clusters and the barplot below shows representative markers for the different vascular cells. Figure modified from (Zeisel et al., 2015) for clarity.

A recent brain pericyte-specific analysis of the transcriptome has identified 260 transcripts enriched in pericytes (He et al., 2016). Brain pericytes are known to express

PDGFR-β and NG2, and staining against these markers is a common way to detect pericytes in tissue sections (Armulik et al., 2011). Using transgenic mice harbouring two reporter genes, *Pdgfrb-eGFP* and *NG2-DsRed*, double-positive cells were isolated using fluorescence-activated cell sorting (FACS), their gene expression profiles were analysed. A total of 856 mural-cell specific genes were identified. This dataset was trimmed by comparing it with four other studies aiming to elucidate pericyte-specific gene expression profiles, including work by Zeisel and colleagues (above), and focused on genes which were identified in at least two studies, leading to the identification of 260-pericyte-specific genes. The authors noted that a significant number of genes were localised to the ECM. After studying this list of genes, I found that many SLRPs were detected, as shown in Table 3.1 with their relative gene count expressed in Fragments Per Kilobase of transcript per Million mapped reads (FPKM). This analysis confirms that PRELP is expressed in pericytes in addition to vSMCs, although its expression is not as strong as other detected SLRP members.

SLRP member	FPKM
Biglycan	345.2
Asporin	59.4
Osteoglycin	16.8
PRELP	8.7

Table 3.1. Expression of SLRP members in pericytes determined by the tailored list provided by (He et al., 2016)**.** Relative expression level is denoted by FPKM.

Combining results from my staining experiments and transcriptome data available online, I conclude that PRELP is expressed in both vSMCs and pericytes. X-gal, anti-β-galactosidase and anti-PRELP staining showed that arterioles/venules and capillaries were stained, suggesting that mural cells associated to vessels of various sizes were stained in these experiments (Figure 3.22, Figure 3.30). This is confirmed by data obtained from transcriptome experiments performed by (Zeisel et al., 2015) and (He et al., 2016).

Neither X-gal or antibody stained all the vessels of the brain. While many arterioles/venules and capillaries exhibited X-gal, β-galactosidase or PRELP staining, this is not the case for all brain vasculature, suggesting that PRELP is expressed in sub-types of mural cells. This may also contribute to the relatively-low expression of PRELP cited by (He et al., 2016) (Table 3.1), as not all vessels express PRELP. I observed that the number of vessels which are positive for X-gal or β-galactosidase was highest in posterior regions of the brain, such as the cerebellum, and staining is weakest in the cortex (Figure 3.18,

Figure 3.20). This should therefore be a consideration when selecting a region of the brain to study for a potential phenotype in PRELP$^{-/-}$.

In addition, further work could be performed to understand the conditions of PRELP expression in mural cells. Methods such as laser microcapture dissection could be used to uncover differences in PRELP-positive and PRELP-negative vessels (Figure 3.35). For example, after brief X-gal staining and a nuclear counterstain, PRELP-positive and PRELP-negative vessels in close proximity could be captured and analysed using RNA seq. Differences in the transcriptomes may be detected to understand the differences in gene expression patterns between PRELP-positive and -negative vessels.

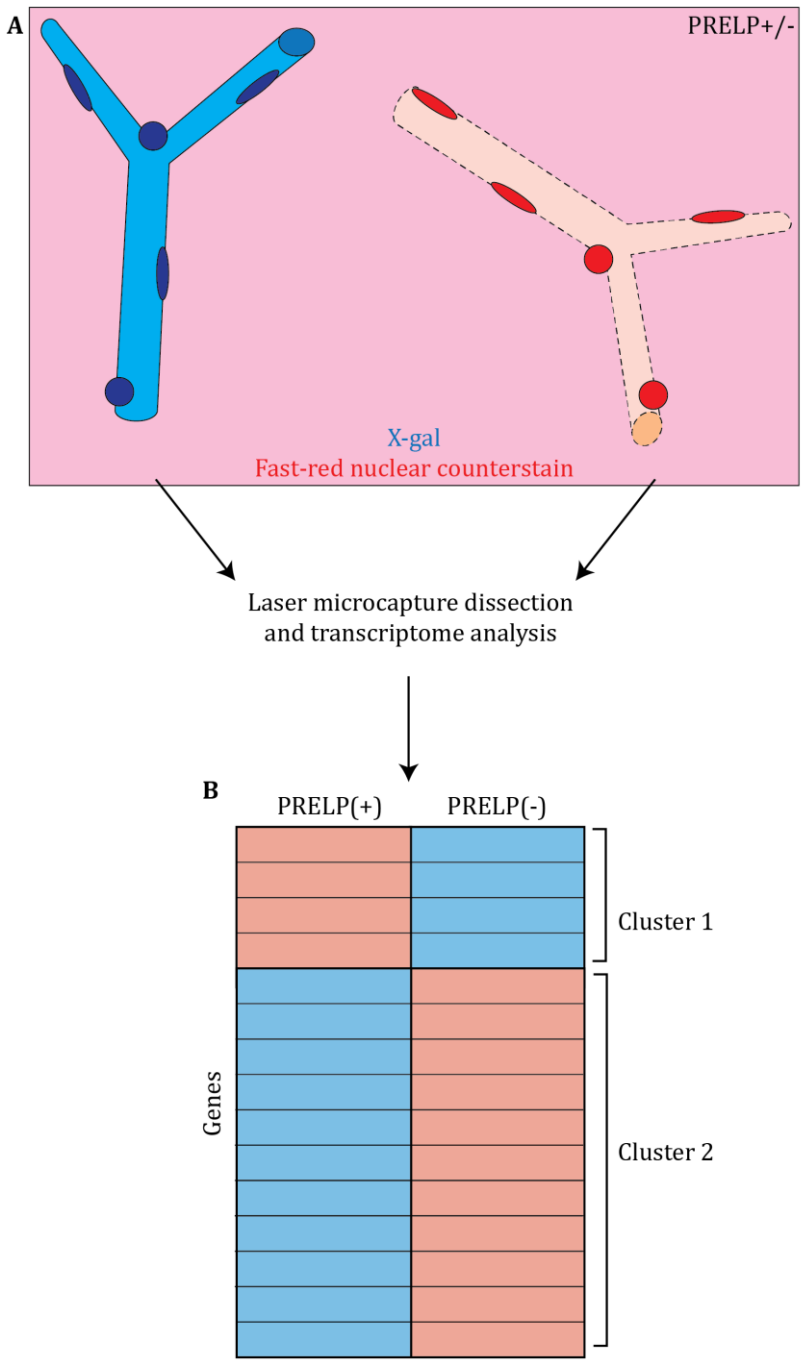

Figure 3.35. Schematic diagram of potential laser microdissection capture experiment to determine differences between PRELP-positive (+) and PRELP-negative (-) vessels. Brief X-gal staining of PRELP$^{+/-}$ tissues would be performed with a counterstain such as fast red. PRELP(+) and PRELP(-) vessels in close proximity could then be cut out using laser microdissection **(A)** and transcriptome analysis performed. Heatmaps could illustrate differences between these vessels **(B)**.

β-galactosidase antibody staining indicated that PRELP is expressed in microglia (Figure 3.27). Double staining with pan-microglial marker Iba-1 indicated that all Iba-1-positive cells were also stained with β-galactosidase, suggesting that all microglia express PRELP. Antibody staining of PRELP performed by colleagues also did not identify staining in

microglia (Figure 3.30), although, as mentioned previously, this could be due to a number of factors related to antibody production, post-translational modifications and differences within species. When observing data from single-cell analysis, however, it seems that PRELP is only expressed in a sub-type of microglia at ~8 copies per cell. Other cells types express PRELP from single-cell RNA seq – astrocytes and oligodendrocytes. From staining experiments, I was unable to confirm that PRELP is expressed by astrocytes and oligodendrocytes.

Finally, from X-gal and β-galactosidase staining experiments and analysis of single-cell data, PRELP is expressed in ependymal cells and in the choroid plexus (Figure 3.21, Figure 3.29 and Figure 3.31). The choroid plexus hangs from the root of ventricles in the brain and are composed of fenestrated capillaries ensheathed by cuboid ependymal cells. Cerebrospinal fluid is produced from blood plasma filtered through the epithelial cells, where an osmotic gradient is created by the transport of sodium and chloride ions into the ventricles. The expression of PRELP in ependymal cells and choroid plexus capillaries suggests that the production of cerebrospinal fluid could be altered in PRELP$^{-/-}$ animals, although this aspect was not investigated in this project.

To conclude, X-gal staining in PRELP seems to be more specific than what was observed in OMD$^{+/-}$ animals. I have determined by X-gal, β-galactosidase antibody staining and analysis of transcriptome data that PRELP is likely to be expressed in vSMCs, pericytes, microglia, ependymal cells and choroid plexus capillaries. In addition, PRELP may also be expressed in astrocytes and oligodendrocytes.

3.5.4 Potential roles of OMD and PRELP based on expression patterns in the brain

Based on the expression patterns of OMD and PRELP presented in this chapter, their potential roles in the brain are discussed below.

Other members of the SLRP family share similarities in their expression pattern with OMD and PRELP in the brain. Decorin was found to be expressed in the hippocampus, thalamus, Purkinje cells, neurons in the cortex and brainstem, in addition to blood vessels and choroid plexuses of the rat brain (Hanemann et al., 1993; Kappler et al., 1998). Decorin was also found to be expressed in astrocytes in the glia limitans (Stichel et al., 1995). Staining of biglycan in the rat brain also suggests that it is expressed by neurons "*in most brain areas*", endothelial cells, vSMCs and ependymal cells (Stichel et al., 1995). In addition, biglycan expression was detected in cultured astrocytes (Koops et al., 1996).

Numerous studies describe the roles of decorin and biglycan in fibrosis and inflammation in the brain. Both decorin and biglycan expression were found to be up-regulated in

astrocytes located in brain lesions, persisting for as long as 6 months after injury (Stichel et al., 1995) and between the basement membrane and astrocyte end-feet in multiple sclerosis Decorin has been shown to attenuate the accumulation of ECM and glial scar formation in the brain and spinal cord (Davies et al., 2004; Logan et al., 1999) by inhibiting signalling through TGF-β1/2 in astrocytes, inhibiting the formation of CSPG-rich scars (Davies et al., 2004) and attenuating the responses of astrocytes and microglia to injury (Ahmed et al., 2014; Davies et al., 2006). In addition, when short-term hydrocephalus was induced in rats, there was a mild increase in the expression levels of decorin in neurons located in the compressed cortex (Del Bigio & Enno, 2008; Mohan et al. 2010). These studies suggest that decorin has a role in modulating inflammation and tissue homeostasis.

Given the similar expression pattern of PRELP in the brain compared to decorin and biglycan, and their effect on glial scar formation and inflammation in the cerebrum and spinal cord, PRELP may also be involved in regulating the inflammatory response.

From double staining experiments, I have determined that PRELP is probably expressed in cells forming and maintaining the BBB, including pericytes and microglia and possibly astrocytes.

There is increasing evidence that microglia and endothelial cell cross-talk can influence barrier opening and inflammation. For example, using a co-culture system of model of rat brain endothelial cells and microglia to model the BBB, the application of lipopolysaccharide (LPS) to the culture resulted in barrier function loss, directly dependent on the presence of number of microglia in culture (Sumi et al., 2010).

In addition, microglia have a role in modulating brain angiogenesis. During development, microglia migrate into the CNS before vessels, allowing them to regulate aspects of angiogenesis. Depletion of microglia in transgenic systems or by administering clodronate liposomes resulted in decreased vascular density in the brain (Fantin et al., 2010; Markovic et al., 2005; Rigato et al., 2011).

There is a recent study on the role of decorin in BBB dysfunction (Hoettels et al., 2017). In murine models of inflammation accompanied by BBB breakdown, the authors noted that there is increased deposition and expression of decorin in the basement membrane. *In vitro* experiments suggest that decorin is detrimental for barrier properties of primary endothelial cells. Given that PRELP has similar staining patterns in the brain to decorin, it is possible that these proteins may have equally similar and redundant function, opening up the possibility that PRELP may be able to regulate properties of the BBB.

3.6 Conclusions

In this chapter, I have investigated the expression pattern of OMD and PRELP by probing the expression of the reporter gene *LacZ*. Initial experiments suggested that there may be strong expression of OMD in the brain. There is, however, considerable discrepancy between X-gal and antibody staining in OMD animals. In addition, single-cell RNA seq indicated that there is virtually no OMD expression in the cortex and hippocampus, indicating that reporter gene enzyme activity in OMD animals is not an indication of OMD localisation. I conclude that OMD expression in the brain is probably weak. Using X-gal, antibody staining and analysis of transcriptome data, I have determined that PRELP is expressed in vSMCs, pericytes, microglia and ependymal cells. From single-cell RNA seq data, it may also be expressed in astrocytes and oligodendrocytes.

These findings are summarised below in Table 3.2 and Table 3.3. In addition to endothelial cells and pericytes, the functional unit of the BBB, the NVU, is also composed of astrocytes and microglia. Based on the cells expressing PRELP, I hypothesise that PRELP may affect properties of the BBB and will be examined in the following chapter.

Method	Neurons	Astrocytes	Microglia	Endothelial cells	Pericytes	vSMCs	Ependymal cells
X-gal staining	Yes	Yes	Yes	Unclear	Unclear	Unclear	Yes
β-gal antibody staining	No	No	No	No	No	No	No
OMD antibody staining*	Yes	No	No	No	No	No	N.D.
Single-cell analysis**	~1 copy per cell	~2 copies per cell	~1 copy per cell	No expression	No expression	~1 copy per cell	No expression

Table 3.2. Summary of findings regarding OMD localisation in the brain. *OMD antibody staining was performed by Dr Ryohei Sekido and Dr Byongsung Shim. **Data obtained from (Linnarsson, 2015). N.D., not determined.

Method	Neurons	Astrocytes	Microglia	Endothelial cells	Pericytes	vSMCs	Ependymal cells
X-gal staining	No	Unclear	Unclear	Yes	Yes	Yes	Yes
β-gal antibody staining	No	No	Yes	Unclear	Unclear	Unclear	Yes
PRELP antibody staining*	No	No	No	Unclear	Unclear	Unclear	N.D.
Single-cell analysis**	~5 copies per cell	~5 copies per cell	~8 copies per cell	~2 copies per cell	~2 copies per cell	~10 copies per cell	~12 copies per cells

Table 3.3. Summary of findings regarding PRELP localisation in the brain. *PRELP antibody staining was performed by Dr Ryohei Sekido and Dr Byongsung Shim. **Data obtained from (Linnarsson, 2015). N.D., not determined.

Chapter 4 Vascular Phenotype and Blood Brain Barrier Integrity in OMD$^{-/-}$ and PRELP$^{-/-}$ mice

4.1 Preface

Many members of the SLRP family, including other class II members, have been shown to have an impact on angiogenesis. Given the expression of PRELP in brain vasculature, as demonstrated in the previous chapter, I aimed to examine the effect of PRELP on angiogenesis using the *in vivo* embryonic hindbrain assay.

X-gal and β-galactosidase antibody staining in PRELP animals indicated that PRELP is strongly expressed in vSMCs, pericytes and microglia. The BBB is a specialised interface restricting the unregulated movement of ions and molecules across the brain endothelium. It is composed of endothelial cells, pericytes, astrocyte end-feet and microglia. Since I observed expression of PRELP in these cell types, I considered the impact on the BBB in their absence. I therefore decided to determine whether there were any differences between wild-type and knock-out BBB.

4.2 Effect of OMD and PRELP on brain angiogenesis

4.2.1 Embryonic hindbrain vasculature model for assessing angiogenesis

Angiogenesis is the formation of new blood vessels from pre-existing ones; endothelial cells of existing vessels are stimulated by growth factors to form sprouts and migrate towards the surrounding tissue (Ozerdem et al., 2001). From my X-gal stains, I have determined that PRELP is expressed on the vasculature. Hence the first question I would like to address is whether OMD and PRELP have an impact on the architecture of blood vessels in the brain.

My initial impression of the vasculature was assessed by observing paraffin sections of the adult brains stained with H&E. I noted that the vascular content in PRELP$^{-/-}$ in particular seemed to be increased when compared to the wild-type. Initial efforts included counting vessels, measuring vessel length and branch points manually from Haematoxylin and Eosin (H&E) stains and fluorescent immunostaining images. This effect was unfortunately challenging to assess in a scientifically-sound manner – given that I was observing 2-dimensional sections of vessels growing in all directions, it was possible that the effect I observed was purely based on the cutting angle of the sections and the location of the images captured.

I therefore opted to utilise the embryonic hindbrain as a flat-mount model for angiogenesis. Hindbrain vasculature is established early in development, where vessels begin sprouting from the perineural vascular plexus around E9.75 and grow towards the ventricular zone (Figure 4.1; E9.75). Critically, from E10, vessels sprout perpendicularly to the plane of the ventricular surface (Figure 4.1; E10.0); these vessels meet and anastomose to form a perfused and homogenous capillary network – the subventricular vascular plexus (SVP) (Figure 4.1; E10.5) (Fantin et al., 2010). As a result of this growth pattern, the vessels of the embryonic hindbrain are mainly growing in a single orientation parallel to the ventricular surface, facilitating imaging and quantification. In addition, the embryonic hindbrain is a model which is typically used for mice harbouring mutations which are embryonically lethal, such as mutations in the VEGF (Carmeliet et al., 1996) or notch pathways (Xue et al., 1999). While our mice do not exhibit any embryonic lethality, as heterozygote matings result in typical Mendelian ratios, the hindbrain provides an easily accessible *in vivo* model for angiogenesis. I will therefore utilise the embryonic hindbrain as a model for angiogenesis in our transgenic animals.

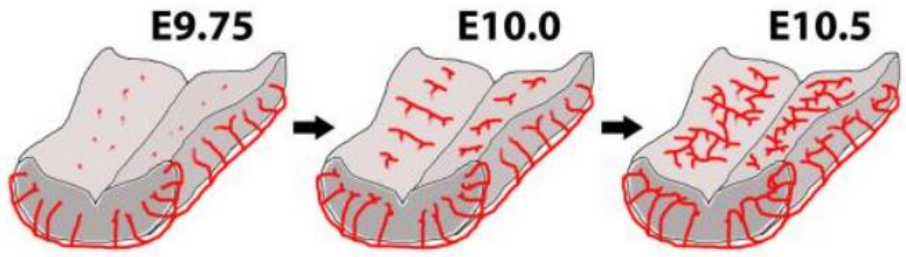

Figure 4.1. Vascularisation of the embryonic hindbrain. Vessels sprout from the perineural vascular plexus at E9.75, where vessels migrate towards the ventricular surface. Vessels then grow at right angles and form a vascular network. Figure from (Fantin et al., 2013).

Hindbrains of embryos between ages E10.5 and E12.5 can be utilised for analysis of vascular parameters, such as vascular network complexity and pericyte coverage (Fantin et al., 2013). Beyond E13.5, hindbrain tissue becomes too thick and hinders staining and imaging methods. I opted to utilise hindbrains at E12.5; the removal of the pial membrane from the hindbrain is a critical step in the dissection protocol and is much easier to perform in older hindbrains without damaging the tissues.

4.2.2 Effect of OMD and PRELP on hindbrain vascularisation

Using the embryonic hindbrain vasculature as a model to assess angiogenesis, I prepared hindbrains from E12.5 wild-type, $OMD^{-/-}$ and $PRELP^{-/-}$ embryos. Hindbrains were stained with various vascular markers, including Isolectin IB4 and Tomato Lectin. In order to maintain consistency, I only captured images of the SVP. Images were processed in ImageJ

to remove background noise as described in Chapter 2, and AngioTool was utilised for the analysis of vascular networks.

I first sought to determine whether there is an increase in vascular content in OMD$^{-/-}$ and PRELP$^{-/-}$ hindbrains (Figure 4.2). I compared the vessel area and junction density between OMD$^{-/-}$ and wild-type and found that there were no statistically significant differences. Indeed, when observing the images, the differences between wild-type and OMD$^{-/-}$ were minimal, indicating that OMD is not likely to have a role in angiogenesis in the hindbrain model.

I then compared wild-type and PRELP$^{-/-}$ vasculature. There was an increase in the vascular content of PRELP$^{-/-}$ hindbrains compared with that of wild-type. In addition, analysis of branch point density indicates that this also increases in PRELP$^{-/-}$. These results together indicate that it is likely that PRELP$^{-/-}$ embryonic hindbrains have increased vascular content.

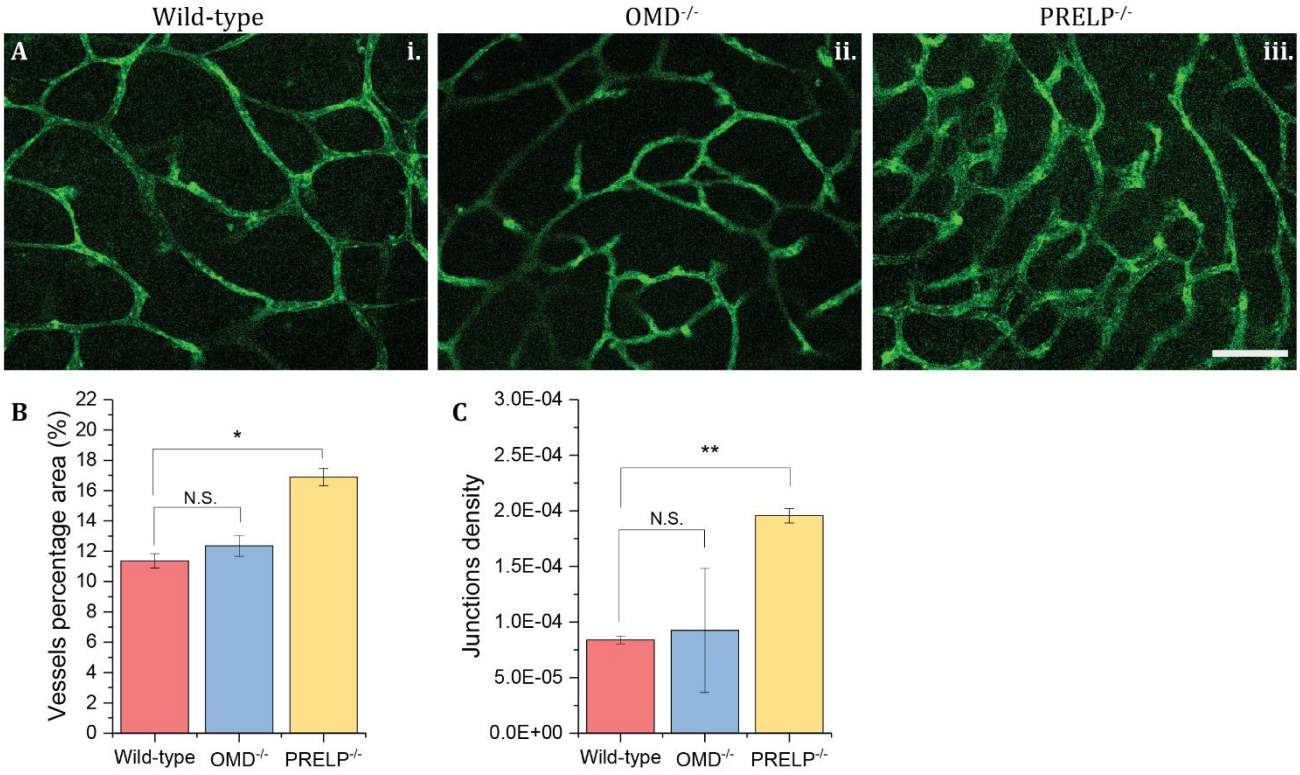

Figure 4.2. Analysis of vascular content of embryonic hindbrains from E12.5 wild-type, OMD$^{-/-}$ and PRELP$^{-/-}$ mice. Hindbrains were stained with Isolectin IB4 and the SVP was imaged **(A).** Parameters vessels percentage area **(B)** and junctions density **(C)** were quantified using AngioTool using identical parameters. 2-tailed student's t-test was performed and p-values < 0.05 were considered significant (*; 0.01 < p-value < 0.05 and **; 0.001 < p-value < 0.01). 4-5 fields were imaged per animal. Error bars are the SEM where n=3. Scale bar 100um.

It has been demonstrated that microglia have an impact on developmental angiogenesis in the brain (Fantin et al., 2010). I therefore investigated whether there was a significant increase in microglia surrounding vessels in PRELP$^{-/-}$. Note that due to the nature of these experiments, where female pregnant mice were sacrificed in order to obtain embryos, I did not proceed with experiments comparing wild-type and OMD$^{-/-}$ as I did not observe any differences in vascular density. By performing double staining of isolectin IB4 and tomato lectin, I was able to label microglia, as tomato lectin labels both microglia and vasculature (Figure 4.3). Manual counting of the number of tomato lectin-positive cells in contact with the vasculature indicated an increase in PRELP$^{-/-}$ hindbrains, however this value was not significant (p-value = 0.6).

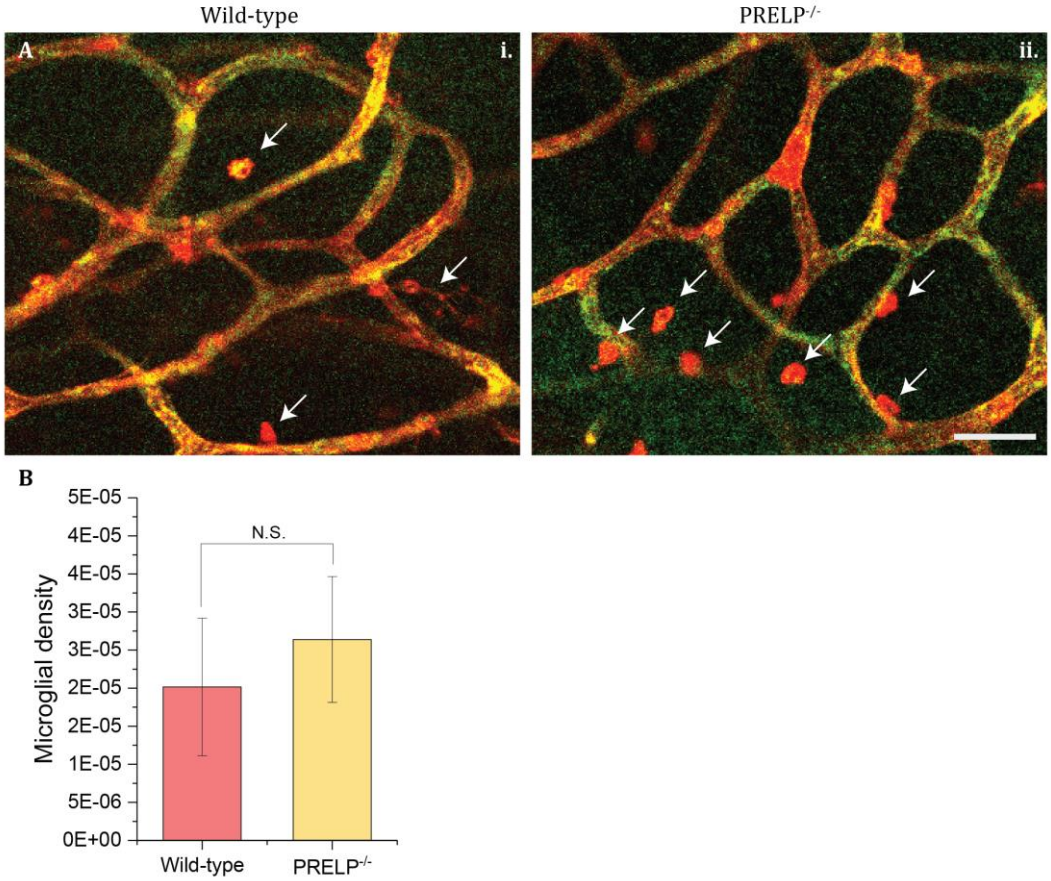

Figure 4.3. There is no significant change in density of microglia in PRELP$^{-/-}$ embryonic hindbrains at E12.5. Hindbrains were stained with Isolectin IB4, green, and Tomato Lectin, red (A). While isolectin IB4 only labels vessels, tomato lectin labels both vasculature and microglia (arrows). Microglia were manually quantified and found to be non-significant in PRELP$^{-/-}$. 2-tailed student's t-test was performed and p-values < 0.05 were considered significant. 4-5 fields were imaged per animal. Error bars are the SEM where n=3. Scale bar 50um.

The attachment of pericytes to the endothelium can regulate angiogenesis. In the initial stages of angiogenesis, pericytes detach and undergo intense proliferation. After tubulogenesis, pericytes attach to the nascent vessel to provide stabilising contacts

(Ribatti et al., 2011). Given that I observe a phenotype regarding angiogenesis in PRELP$^{-/-}$, I attempted to stain tissues with NG2, a pericyte marker. While I was unable to confidently identify pericytes along the hindbrain vasculature, I noted that there is a decrease in staining intensity of NG2 along the vasculature in PRELP$^{-/-}$, although this was not found to be statistically significant (Figure 4.4).

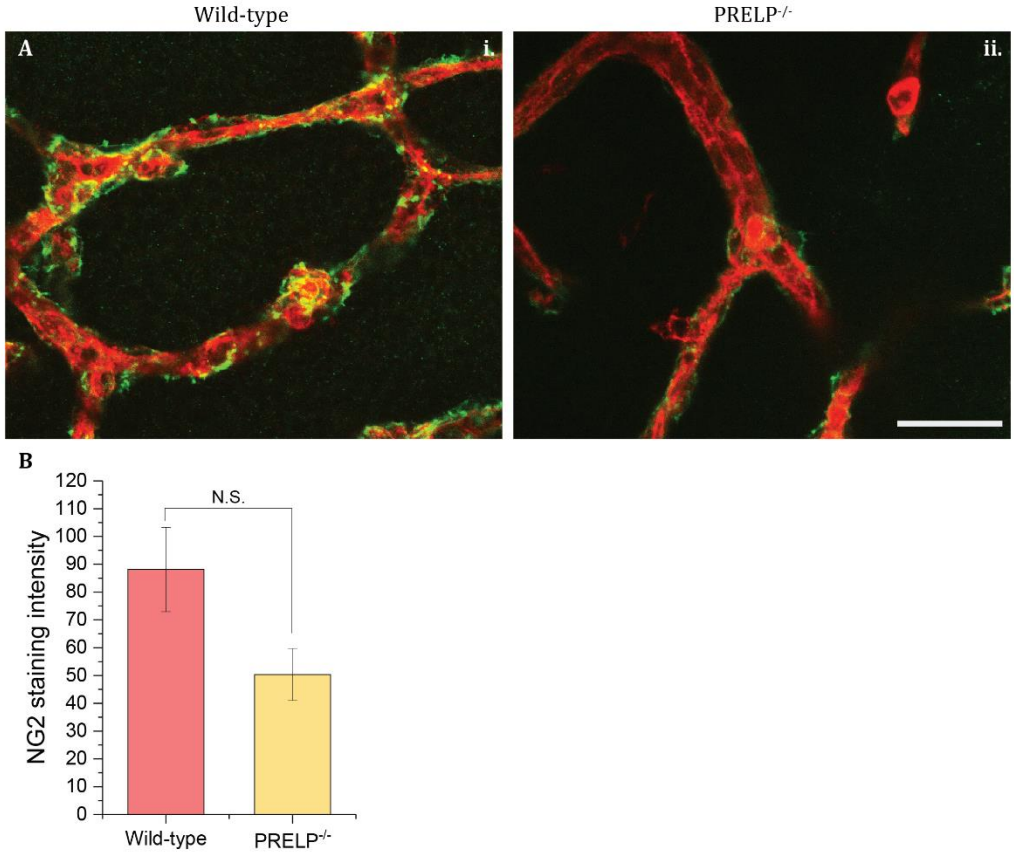

Figure 4.4. Staining of NG2 pericyte marker of E12.5 wild-type and PRELP$^{-/-}$ hindbrains. A) Staining with tomato lectin vascular marker, red, and NG2 pericyte marker, green. B) Quantification of staining intensity reveals that there is a statistically insignificant decrease in PRELP$^{-/-}$. 2-tailed student's t-test was performed and p-values < 0.05 were considered significant. 4-5 fields were imaged. Error bars are the SEM where n=4. Scale bar 40um.

These results indicate that PRELP may have an effect on angiogenesis, as assessed by the embryonic hindbrain although I was unable to detect significant differences in microglia coverage and NG2 staining intensity. In contrast, there were no notable differences between wild-type and OMD$^{-/-}$ vasculature.

4.3 Effect of OMD and PRELP on the Blood Brain Barrier (BBB)

4.3.1 Blood brain barrier disruption

The BBB is a barrier formed by a variety of cell types. It prevents contact of the circulating blood with neural tissues and ensures the proper function of the brain. It is formed of

endothelial cells sheathed in a BM, which contacts pericytes and astrocytes. Integrity of the BBB is critical for brain homeostasis and the disruption of the BBB has been shown to be implicated in a variety of CNS disorders such as Alzheimer's disease and multiple sclerosis (Obermeier et al., 2013).

I have determined that PRELP is expressed in pericytes and microglia, both important for the maintenance of the BBB. I therefore decided to characterise the BBB of our transgenic animals compared to the wild-type. One-year old mice were used for all experiments described below, where three animals were used from each genotype. All images are taken of the cortex of the cerebellum, unless otherwise stated.

BBB integrity can be assessed using a variety of methods; a common method is to stain for immunoglobulin G (IgG). IgG is a 160kDa protein which is abundant in blood plasma. An intact BBB would prevent solutes such as IgG from passing through the vasculature and coming into contact with neural tissues. Hence, when the BBB is disrupted, it would be possible to detect plasma solutes in the tissues surrounding the vasculature.

Using anti-mouse IgG (Alexa Fluor 594), which is normally used as a secondary antibody, I stained for plasma IgG in wild-type, $OMD^{-/-}$ and $PRELP^{-/-}$ mice (Figure 4.5). IgG staining was found not only inside blood vessels, but also along the walls of the blood vessels in a regular striated pattern perpendicular to the length of the vessel. This latter is presumably staining of Ig-like domain-containing cellular adhesion molecules (CAMs) such as intercellular adhesion molecules (ICAMs) and vascular cell adhesion molecules (VCAMs) (Acton, 2013). Wild-type brain sections showed that the BBB is intact; there is no evidence of IgG outside of the vasculature (Figure 4.5Ai).

In contrast, in $OMD^{-/-}$ and $PRELP^{-/-}$ brains, vessels show perturbations (Figure 4.5ii and iii). Plasma IgG is found outside of blood vessels (Figure 4.5) in a diffused pattern. The extent of perturbation in $OMD^{-/-}$ seems to be extremely mild and was found to be statistically insignificant; only a few vessels exhibit IgG staining outside of the vasculature. In contrast, the extent of IgG located outside of the vasculature in $PRELP^{-/-}$ is much greater, and the regular pattern and expression of CAMs seen in the wild-type tissues is also perturbed.

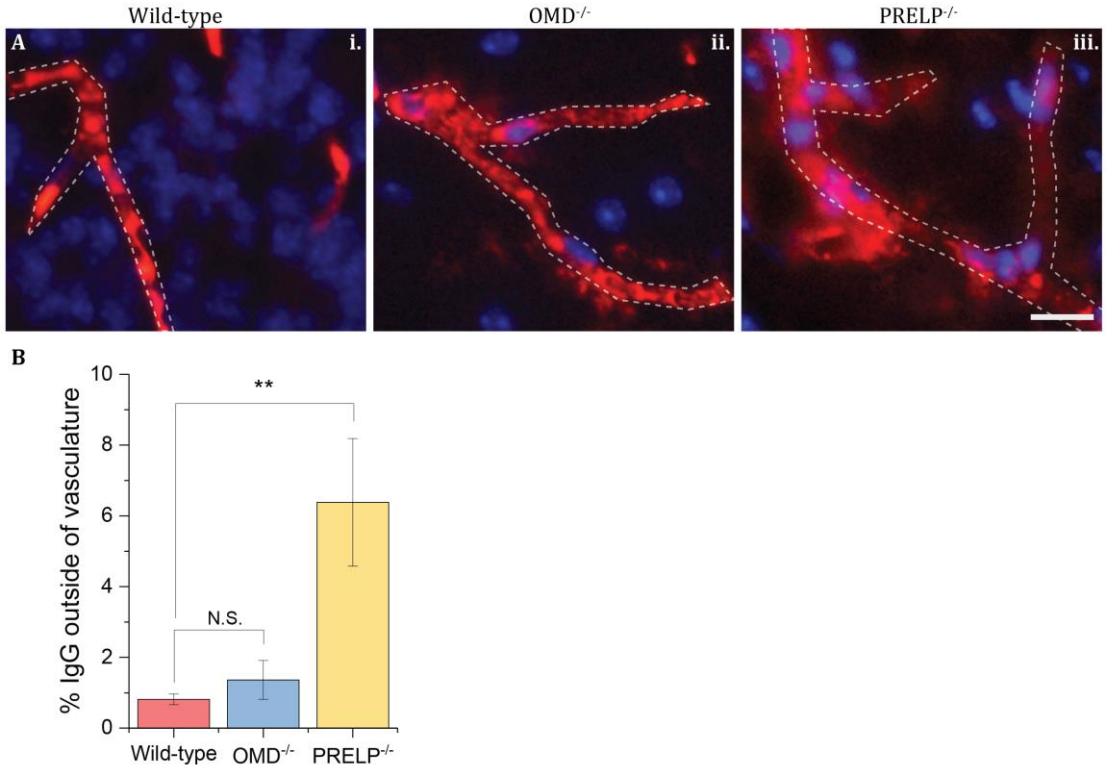

Figure 4.5 Assessment of BBB integrity in the cerebellum by IgG staining in adult wild-type, OMD$^{-/-}$ and PRELP$^{-/-}$. Immunofluorescence was performed using anti-mouse IgG conjugated with Alexa Fluor A594 fluorophore **(A)**. DAPI was used as a nuclear stain. IgG signal outside blood vessels was quantified **(B)**; there is a small non-significant increase in IgG leakage in OMD$^{-/-}$, and a much greater increase in PRELP$^{-/-}$. 2-tailed student's t-test was performed and p-values < 0.05 were considered significant (**; 0.001 < p-value < 0.01). 5 fields were randomly imaged per animal. Error bars are the SEM where n=4. Scale bar 10um.

In addition, I also found that the disruption of PRELP$^{-/-}$ BBB was most intense in the midbrain and cerebellum. While there was perturbation of the BBB in the cerebellum, vessels in the cortex were entirely intact in the same animal (Figure 4.6). This demonstrates that although the BBB in the entire brain seems to be affected, the posterior regions are more heavily affected. This could potentially be a reflection of PRELP localisation in the brain, where β-galactosidase antibody staining was most notable in deep tissues of the brain and cerebellum (see Chapter 3 for more details).

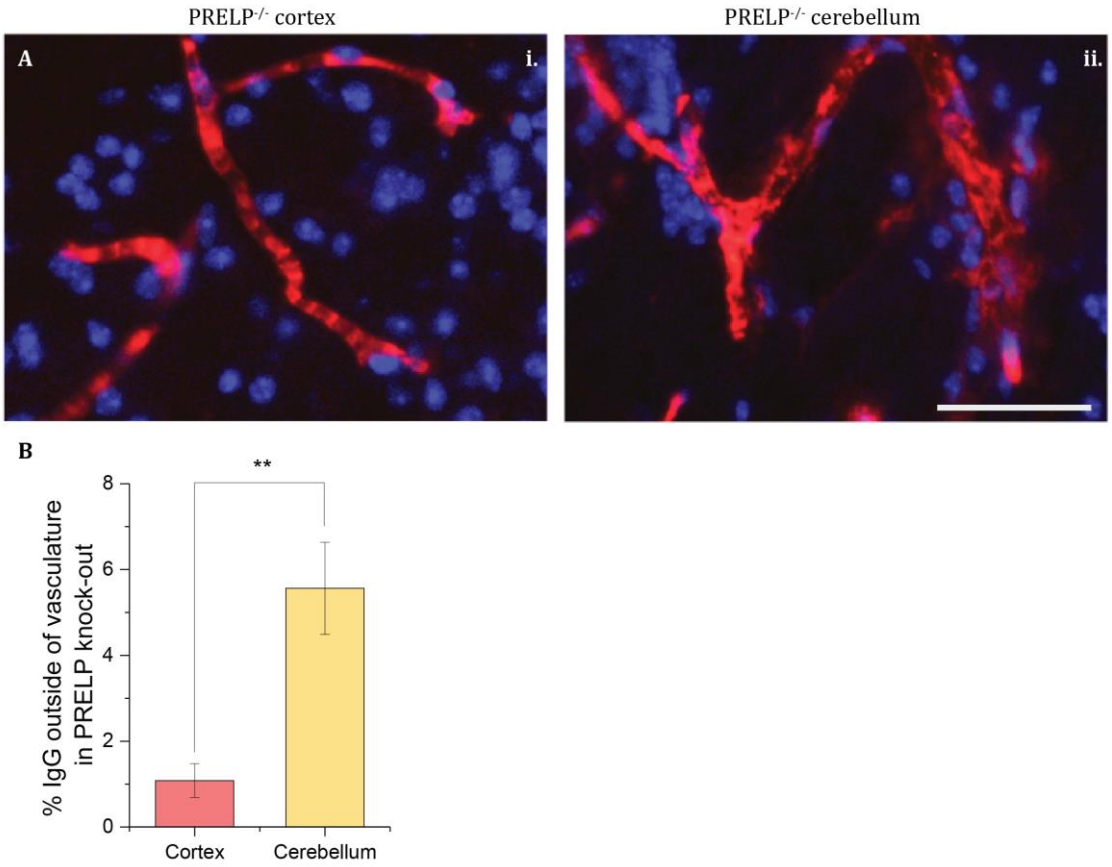

Figure 4.6. BBB disruption in adult PRELP$^{-/-}$ is more apparent in the cerebellum. IgG and DAPI staining of PRELP$^{-/-}$ cortex **(Ai)** and cerebellum **(Aii)**. 2-tailed student's t-test was performed and p-values < 0.05 were considered significant (**; 0.001 < p-value < 0.01). 5 fields were randomly imaged per animal. Error bars are the SEM where n=3. Scale bar 40um.

While IgG staining is a published method to determine whether there is vascular leakage, I also opted to verify this finding by injecting animals with 70kDa-Dextran conjugated with Texas Red. We initially attempted to inject animals in the tail vein for intravenous administration (Figure 4.7) – injection of wild-type and OMD$^{-/-}$ animals was successful, however we were unsuccessful on several occasions when injecting the PRELP$^{-/-}$ (Figure 4.7iii). A member of staff of the Biological Resources Unit noted that the veins of PRELP$^{-/-}$ seem to "*be very poor*" when attempting to perform intravenous injections, perhaps reflecting poor venous architecture in the systemic circulation in PRELP$^{-/-}$ animals.

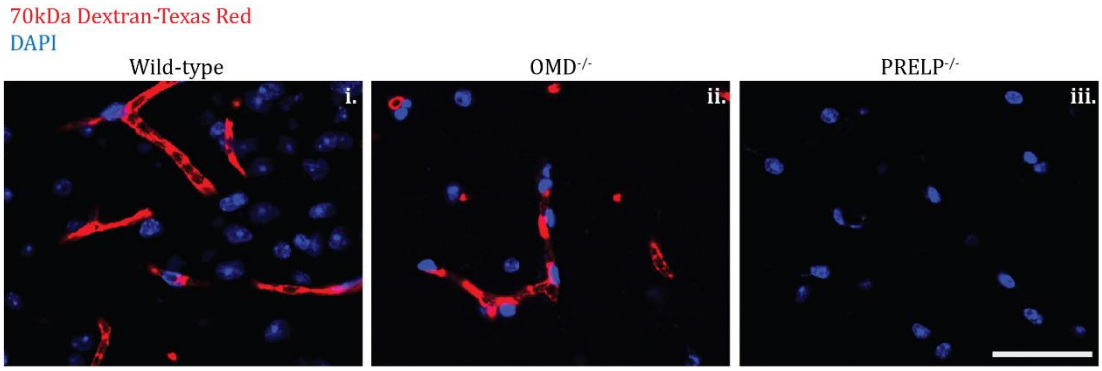

Figure 4.7. Sections of the cerebellum after intravenous administration of 70kDa Dextran-Texas Red in adult mice. While the vessels of wild-type **(i)** and OMD$^{-/-}$ **(ii)** were clearly perfused with 70kDa Dextran-Texas Red, the procedure was unsuccessful in PRELP$^{-/-}$ **(iii)**. Scale bar 40um.

Since the intravenous injection of fluorescently-labelled 70kDa Dextran was unsuccessful, we attempted to administer the tracer dye by intraperitoneal injection. While the perfusion of the dye was not as clear as with the intravenous injection in the wild-type, I was able to detect dye within the vasculature. Consistent with my IgG staining and analysis, I detected areas of the posterior brain where dye was detected outside of the vasculature in PRELP$^{-/-}$, confirming that PRELP$^{-/-}$ animals have a perturbed BBB (Figure 4.8).

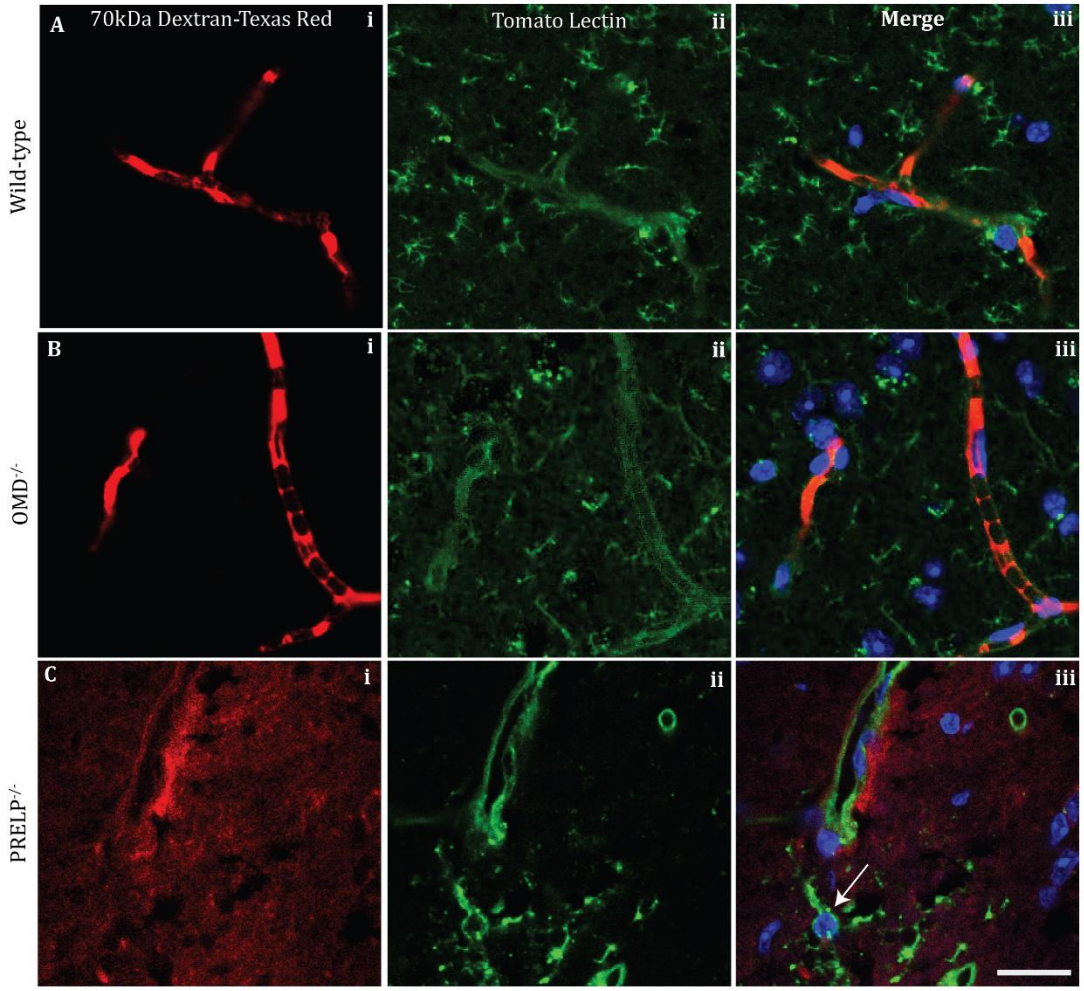

Figure 4.8. IP injection of 70kDa Dextran confirms BBB leakage in adult PRELP$^{-/-}$ cerebellum. Wild-type **(A)**, OMD$^{-/-}$ **(B)** and PRELP$^{-/-}$ **(C)** mice were injected with 70kDa Dextran-Texas Red. Tissues were processed and stained with tomato lectin to stain vessels and microglia. PRELP$^{-/-}$ sections indicate that there is leakage of dextran in addition to microglia with thickened processes (arrow). Scale bar 20um.

4.3.2 Analysis of BBB components

Having determined that there is BBB dysfunction in PRELP$^{-/-}$, I sought to analyse the individual components of the BBB in order to understand the nature of this breakdown.

BM-associated protein markers, as discussed below, were quantified. Since the BM surrounds the vasculature, staining intensity can be quantified in a relatively simple manner, illustrated in Figure 4.9. In essence, the aim of the quantification would be to omit staining found outside of the vessel and within the lumen of the vessels, and only retain staining associated with the BM. To this end, the lumen of the vessel was manually outlined in ImageJ and saved; this region-of-interest (ROI) was saved as $Vessel_{IN}$. The abluminal side of the vessel was outlined in the same manner and saved as $Vessel_{OUT}$. Using the measurement tool in ImageJ, the integrated density of $Vessel_{IN}$ and $Vessel_{OUT}$ were determined; where integrated density = mean grey value * area, which describes

both staining intensity and thickness of the stain. The difference between $Vessel_{OUT}$ and $Vessel_{IN}$ was calculated and the value normalised by the length of the vessel, as shown in the equation below. Five randomly-selected areas of the cerebellum were analysed per animal. To avoid bias, the genotype of the animal was masked.

$$Staining\ intensity\ (A.U.) = \frac{Vessel_{OUT} - Vessel_{IN}}{Length}$$

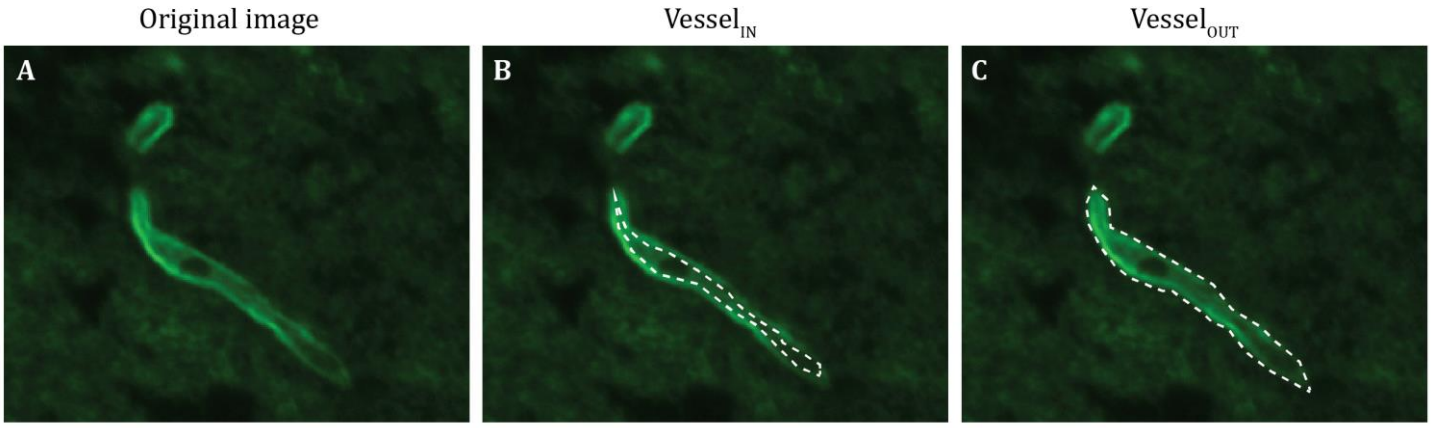

Figure 4.9. Quantification method utilised to determine signal intensity of immunostains of proteins associated with the vascular BM. The original image **(A)** was opened in ImageJ, the luminal **(B)** and abluminal **(C)** portions of a stained vessel were outlined and integrated density measured. Staining intensity was then calculating by the difference between luminal and abluminal staining, which was then normalised to the vessel's length.

4.3.2.1 Basement membrane

The BM is a relatively thick layer of secreted proteoglycans which underlies not only endothelia, but also epithelia. It is composed of laminin, fibronectin and collagen IV. It completely envelops blood vessels and is an intermediate layer of the BBB; pericytes are embedded in the inner layer of the BM, and astrocyte end-feet make contacts with its outer portion. Hence, the BM is a key structure of the BBB.

4.3.2.1.1 Laminin

I performed a double stain of laminin and IgG; the latter is to visualize blood vessels and detect any disruptions of the BBB (Figure 4.10). Laminin staining in wild-type and OMD$^{-/-}$ is intense, and clearly surrounds the blood vessels (Figure 4.10A and B). However, in PRELP$^{-/-}$, not only is the staining weaker, but it also seems that the thickness of laminin around blood vessels is reduced (Figure 4.10C). It is also interesting to note that although most blood vessels in PRELP$^{-/-}$ exhibit weaker laminin staining, there are some blood

vessels which display more intense staining resembling that of wild-type mice (Figure 4.10C.iii; white arrow).

Quantification of laminin signal (Figure 4.10D) shows that there is a statistically-significant reduction in laminin expression and thickness in PRELP$^{-/-}$. I also observed that in PRELP$^{-/-}$, areas of the vessel with intense IgG leakage also exhibit decreased laminin expression suggesting that BBB dysfunction and reduction of laminin are closely linked. There was no difference in laminin intensity of OMD$^{-/-}$ vessels.

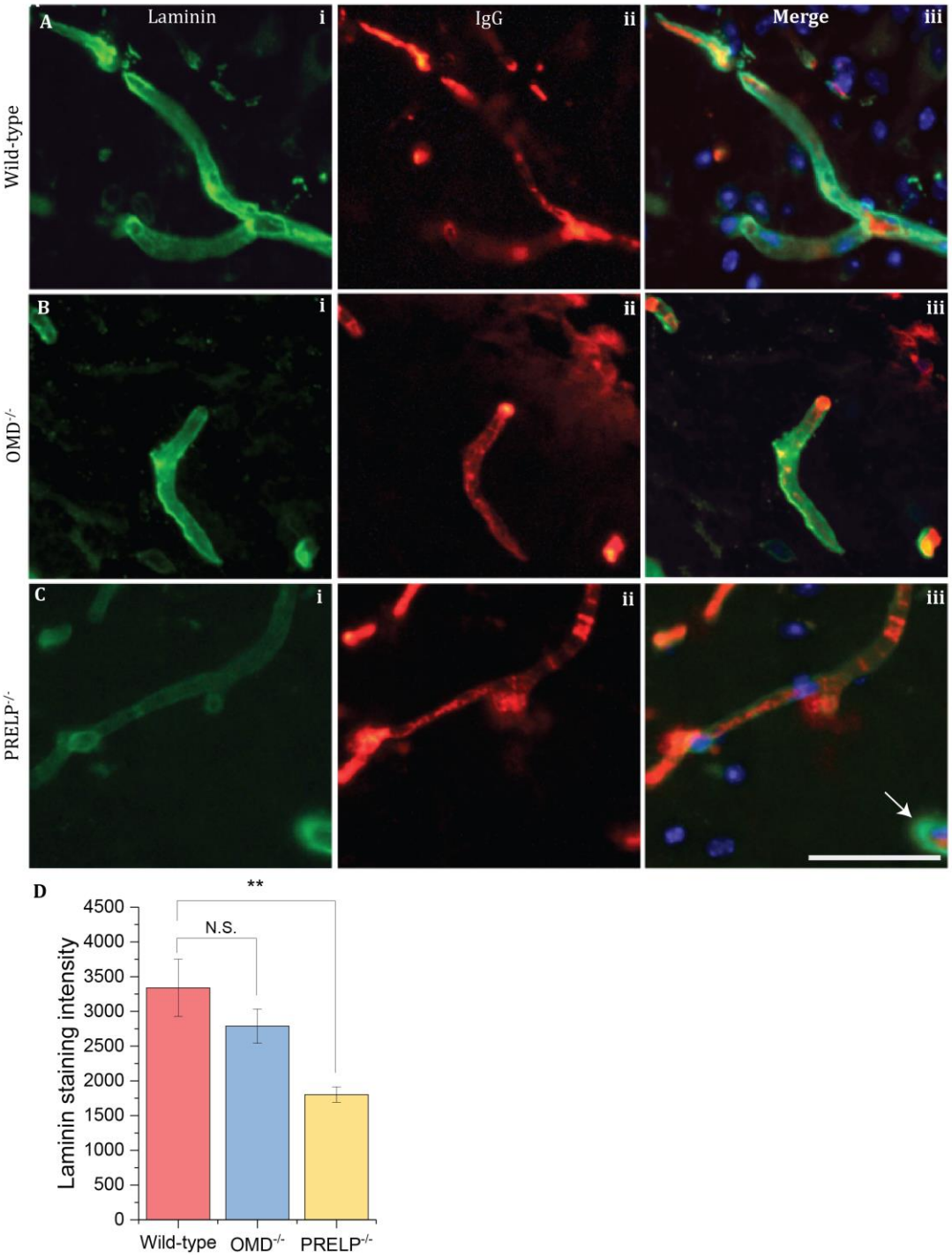

Figure 4.10 Reduction in laminin in adult PRELP$^{-/-}$ cerebellum. Wild-type **(A)**, OMD$^{-/-}$ **(B)** and PRELP$^{-/-}$ **(C)** tissues were stained for laminin **(i)**, IgG for leakages **(ii)** and DAPI to detect nuclei **(iii)**. Quantification is shown in **(D)**. In PRELP$^{-/-}$, I can occasionally see blood vessels with laminin signal intensity resembling that of wild-types (white arrow). 2-tailed student's t-test was performed and p-values < 0.05 were considered significant (**; 0.001 < p-value < 0.01). 5 fields were randomly imaged per animal. Error bars are the SEM where n=3. Scale bar 40um.

4.3.2.1.2 Collagen IV

Given that there was specific down-regulation of laminin in PRELP$^{-/-}$, I sought to find whether the entire BM has become thinner, or whether there was specific down-regulation of laminin. I therefore stained for collagen IV, a major component of the BM (Figure 4.11).

This staining revealed that there was no difference between wild-type and knock-out tissues. It is also interesting to note that collagen IV expression does not seem affected by the leakiness of the vasculature. This is most obvious in PRELP$^{-/-}$, where there are many disrupted blood vessels (Figure 4.11C; arrows), yet collagen IV deposition in the BM is comparable to regions which show no permeability.

The fact that there was no change in collagen IV indicates that laminin is specifically down-regulated in PRELP$^{-/-}$. As for OMD$^{-/-}$, there were no detectable differences in laminin or collagen IV expression, suggesting that the BM of OMD$^{-/-}$ is largely unaffected.

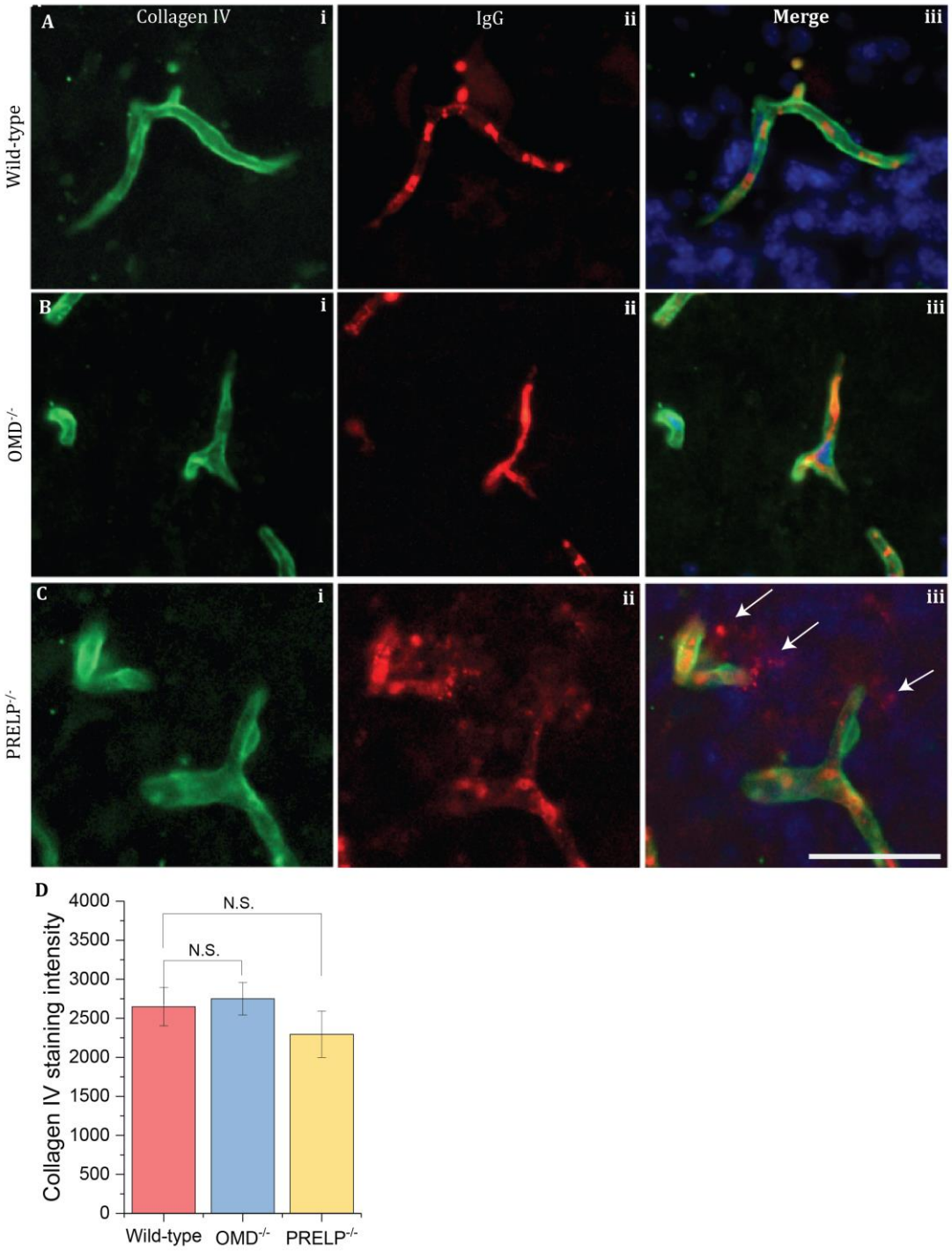

Figure 4.11 OMD and PRELP do not affect collagen IV expression in the cerebellum in adult mice. Tissues were stained for collagen IV and IgG. There is no visible difference between wild-type **(A)**, OMD$^{-/-}$ **(B)** and PRELP$^{-/-}$**(C)**, as shown by the quantification **(D)**. Areas of IgG are indicated with the white arrow. 2-tailed student's t-test was performed and p-values < 0.05 were considered significant. 5 fields were randomly imaged per animal. Error bars are the SEM where n=3. Scale bar 40um.

4.3.2.1.3 Perlecan

Perlecan is a large, multi-domain heparin/heparan sulphate proteoglycan found in BMs in many organs. By binding to a variety of extracellular proteins in addition to providing a reservoir for growth factors such as bFGF, perlecan can regulate a multitude of cellular processes, such as angiogenesis and vascular BM maintenance. Critically, PRELP can bind to perlecan heparin/heparan sulphate moieties; it has been hypothesised that binding of PRELP to both perlecan and collagen enables PRELP to anchor perlecan to the BM.

Given the importance of perlecan in the BM, I stained sections with perlecan and quantified its staining intensity (Figure 4.12). I found that while there were no differences between wild-type and $OMD^{-/-}$, there was a statistically-significant decrease in the immunostaining of perlecan in $PRELP^{-/-}$.

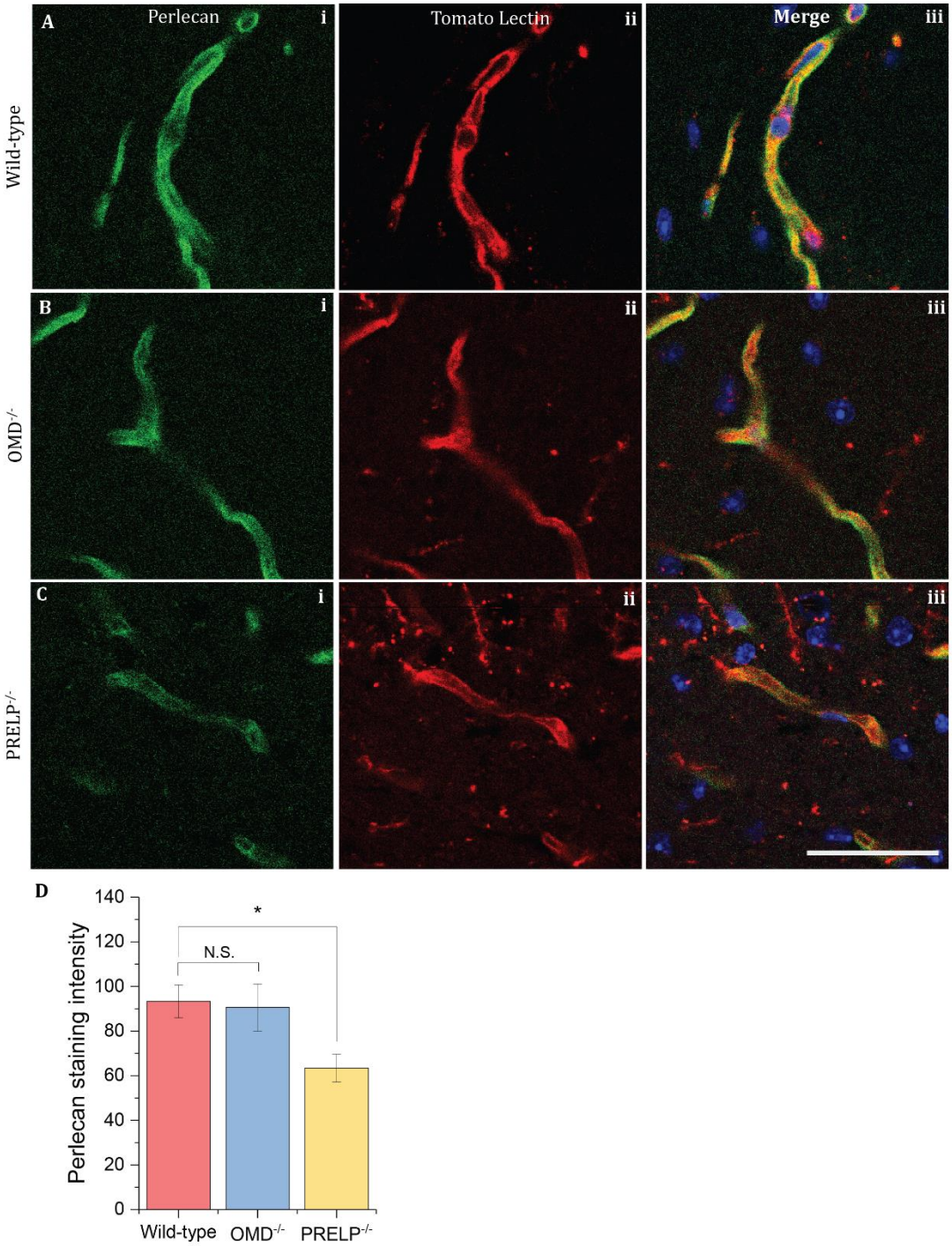

Figure 4.12. Decrease in perlecan staining around PRELP$^{-/-}$ vessels in the cerebellum. Adult wild-type **(A)**, OMD$^{-/-}$ **(B)** and PRELP$^{-/-}$ **(C)** cerebellum sections were stained with perlecan and tomato lectin. Staining intensity was quantified **(D)**. 2-tailed student's t-test was performed and p-values < 0.05 were considered significant (*; 0.01 < p-value < 0.05). 5 fields were randomly imaged per animal. Error bars are the SEM where n=3. Scale bar 40um.

These results therefore indicate that the composition of the BM of PRELP$^{-/-}$ is altered compared to the wild-type and may have strong implications for the integrity of the BBB.

4.3.2.2 Astrocyte end-feet

Another vital component of the BBB are astrocytes; namely, the astrocyte perivascular end-feet. These end-feet make contacts with the BM of the vasculature and stabilize the BBB. AQP4 is a water channel found on astrocyte end-feet and is a common marker for astrocyte end-feet. I performed a double stain with AQP4 and IgG in wild-type, $OMD^{-/-}$ and $PRELP^{-/-}$ cerebellum (Figure 4.13). Quantification revealed that there is a significant decrease in aquaporin-4 signal around the vasculature in $PRELP^{-/-}$, whereas no difference was observed in $OMD^{-/-}$.

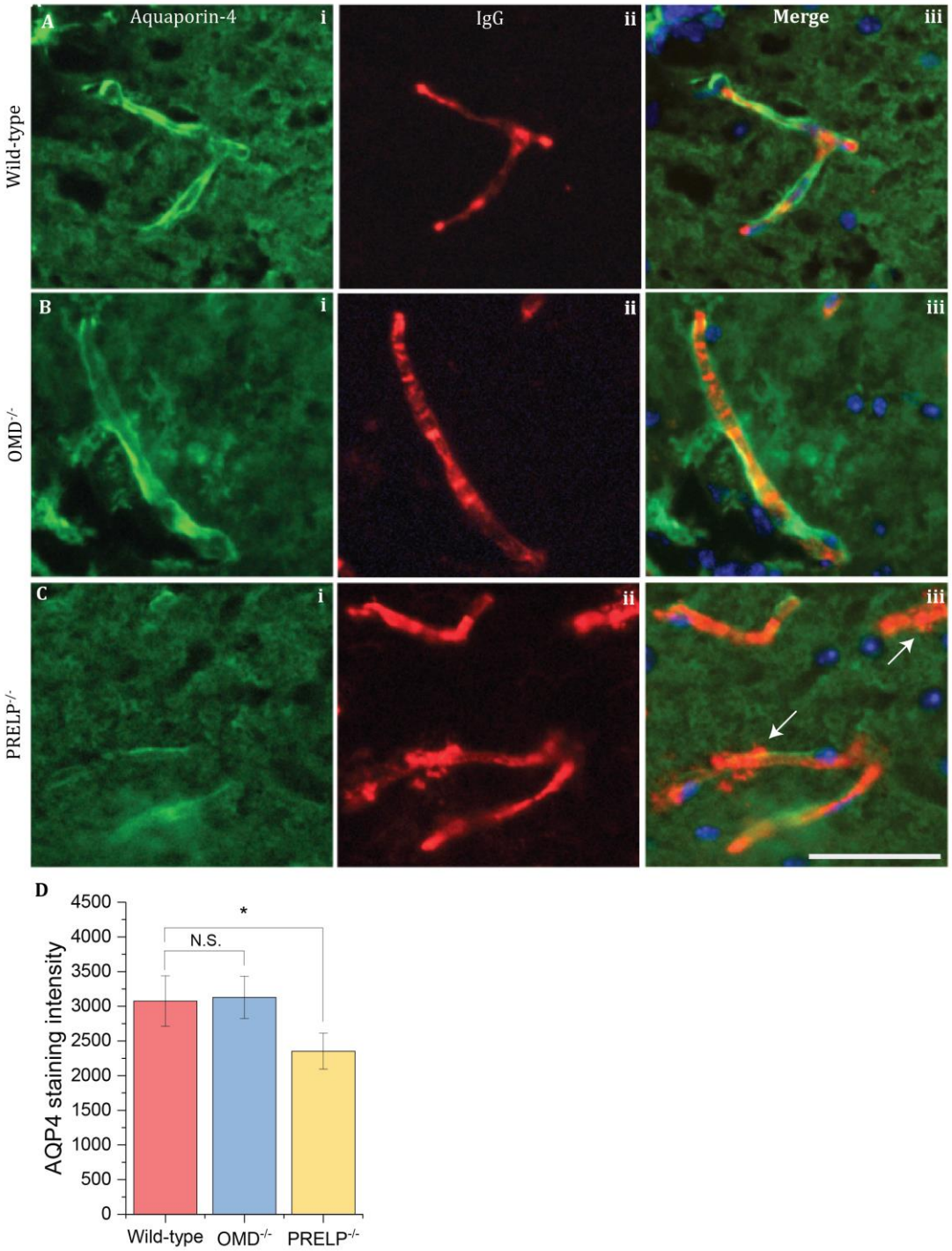

Figure 4.13. AQP4 staining reveals fewer astrocyte end-feet in contact with vasculature in PRELP$^{-/-}$. Double staining of Aquaporin-4 and IgG in adult wild-type **(A)**, OMD$^{-/-}$ **(B)** and PRELP$^{-/-}$ **(C)** cerebellum. White arrows show areas of IgG leakage. Quantification reveals that there is reduced aquaporin-4 staining around blood vessels in PRELP$^{-/-}$ **(D)**. 2-tailed student's t-test was performed and p-values < 0.05 were considered significant (*; 0.01 < p-value < 0.05). 5 fields were randomly imaged per animal. Error bars are the SEM where n=3. Scale bar 40um.

4.3.2.3 Pericytes

Another key component of the BBB is pericytes. Pericytes are mural cells which envelop endothelial cells. They can be morphologically distinguished from endothelial cells by their characteristically round nucleus; in contrast, endothelial cells have a more elongated nucleus. Pericytes participate in key signalling functions to maintain the integrity of the BBB. A decrease in pericytes has been linked to BBB dysfunction, but also to a number of diseases, such as Alzheimer's disease (Sagare et al., 2013) and diabetic retinopathy (Wisniewska-Kruk et al., 2014).

In order to quantify pericyte coverage of vessels, I initially attempted to stain pericytes with NG2, a frequently-used marker (Armulik et al., 2011). Unfortunately, I found that NG2 staining in PRELP$^{-/-}$ in particular was unreliable; the deposition, stability or retention of NG2 around pericytes is possibly affected by the absence of PRELP as they are both secreted proteins (Ozerdem et al., 2001). I therefore opted to use an antibody against PDGFR-β. While PDGFR-β staining was not as clear as NG2, I observed no heterogeneity in staining pattern between wild-type and knock-outs and therefore opted to continue using PDGFR-β to quantify pericyte coverage.

I performed a double stain of PDGFR-β and fluorescently-labelled tomato lectin (Figure 4.14). Tomato lectin is a polysaccharide isolated from tomato which binds to the BM and microglia (Nachbar & Oppenheim, 1982). I used tomato lectin as a method to clearly outline blood vessels. I quantified the number of pericytes found along blood vessels in the cerebellum of wild-type, OMD$^{-/-}$ and PRELP$^{-/-}$ mice by manually counting pericytes per image. Since I previously described an increase in blood vessels in both PRELP$^{-/-}$ (see Section 4.2.2), pericyte density was expressed as pericytes per blood vessel in order to consider the increase in vascular content of PRELP$^{-/-}$. Pericytes were distinguished from endothelial cells by their morphology and staining pattern of PDGFR-β; endothelial cells have an oval nucleus (Figure 4.14; arrowheads), whereas pericyte nuclei are round (Figure 4.14; arrows).

Quantification of pericyte coverage indicated that there were no differences when comparing wild-type and OMD$^{-/-}$. In contrast, PRELP$^{-/-}$ vessels had decreased pericyte coverage and occasionally harboured detaching pericytes (Figure 4.14C). Pericyte projections usually wrap around endothelial cells, and this contact is important for proper pericyte function. However, I observed pericytes in PRELP$^{-/-}$ have projections which point away from the blood vessel, suggesting that they are in the process of detaching entirely. This was a rare observation, and therefore the % detachment could not be quantified. This

suggests that the signalling activities between pericytes and endothelial cells, perhaps through PDGF-B (Bjarnegård et al., 2004), may be affected.

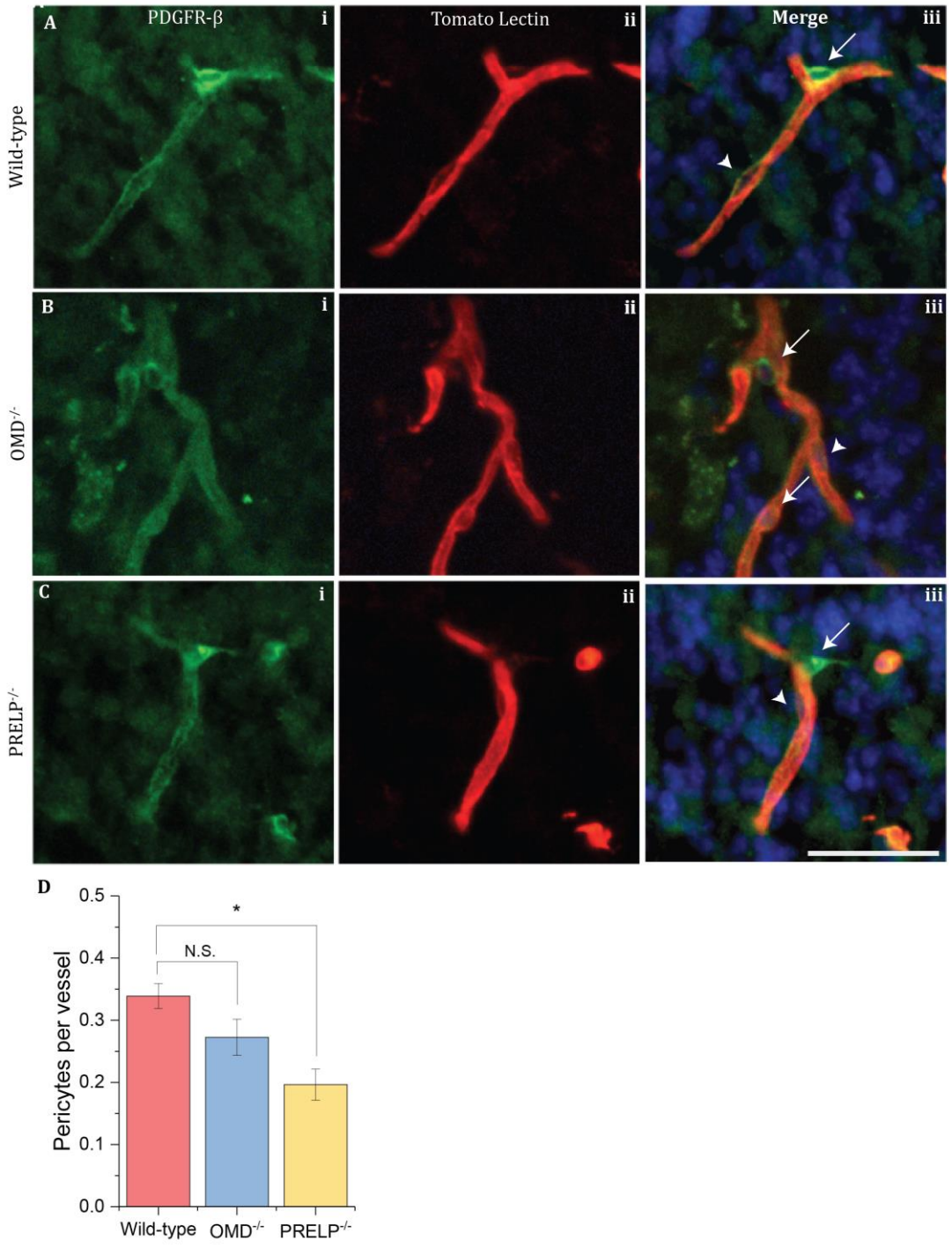

Figure 4.14 Reduction in pericytes in PRELP$^{-/-}$. PDGFR-β and tomato lectin double stain allows the visualisation of pericytes and blood vessels in adult wild-type **(A)**, OMD$^{-/-}$ **(B)** and PRELP$^{-/-}$ **(C)** cerebellum. Pericytes (arrow) can be distinguished from an endothelial cell (arrowhead) by its rounder nucleus. Quantification of pericytes per vessel revealed a significant decrease in PRELP$^{-/-}$ **(D)**. 2-tailed student's t-test was performed and p-values < 0.05 were considered significant (*; 0.01 < p-value < 0.05). 5 fields were randomly imaged per animal. Error bars are the SEM where n=3. Scale bar 40um.

4.3.3 Cell-cell integrity

I have demonstrated that there is BBB dysfunction in PRELP$^{-/-}$, with the bleeding being more significant in PRELP$^{-/-}$ animals, especially in the cerebellum. I have investigated some of the potential causes of BBB breakdown by investigating individual components of the BBB; the BM, pericytes and astrocyte end-feet. Indeed, I have demonstrated that there are perturbations in these BBB components.

Although changes in the expression or distribution of these BBB constituents is an important indicator on BBB function, cell-cell junctions of the vasculature would also need to be analysed to further understand the impact of PRELP loss in brain capillaries. To this end, I have performed a variety of immunostains against adherens and tight junction markers and quantified their signal.

In contrast to BM or BM-associated proteins, cell-cell junction markers would not typically display a clear and predictable pattern around the vessels (as shown in Figure 4.9). I therefore used an alternative method, where the entire vessel was outlined in ImageJ and saved as an ROI. Instead of measuring integrated density, I simply measured mean grey value and normalised it to the length of the vessel, essentially calculating mean grey value per length vessel (Figure 4.15). Slides were also stained with tomato lectin to provide a reliable and consistent means to outline the exterior of the vessel unambiguously. As before, five randomly-selected regions of the cerebellum were quantified per animal, and animal genotypes were masked when performing quantification.

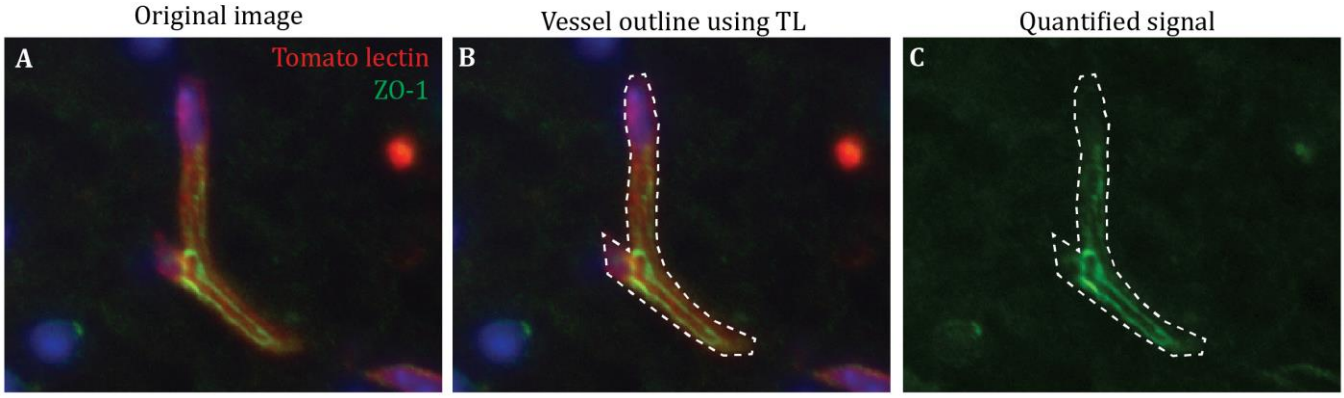

Figure 4.15. Quantification method for assessing staining intensity of cell-cell junction markers. The original image **(A)** stained with Tomato lectin and tight junction marker ZO-1 was utilised to make an outline of the entire vessel and was saved as a ROI **(B)**. The saved ROI was then overlayed onto the image of cell-cell junction staining **(C)** and mean grey value was determined.

4.3.3.1 Adherens junctions

The predominant adherens junction protein found at cell-cell junctions between endothelial cells is VE-cadherin (Navarro et al., 1998). I performed immunostaining using an anti-VE-cadherin antibody and quantified signal intensity in the vasculature (Figure 4.16).

Quantification of VE-cadherin signal revealed that there was no difference in VE-cadherin signal in $OMD^{-/-}$. In contrast, when examining $PRELP^{-/-}$ vessels, I noted that staining was absent in some areas of the vessel (Figure 4.16C; arrows). The overall staining intensity of VE-cadherin in $PRELP^{-/-}$ was significantly lower. This indicated that there may be perturbations in VE-cadherin localisation in $PRELP^{-/-}$ capillaries.

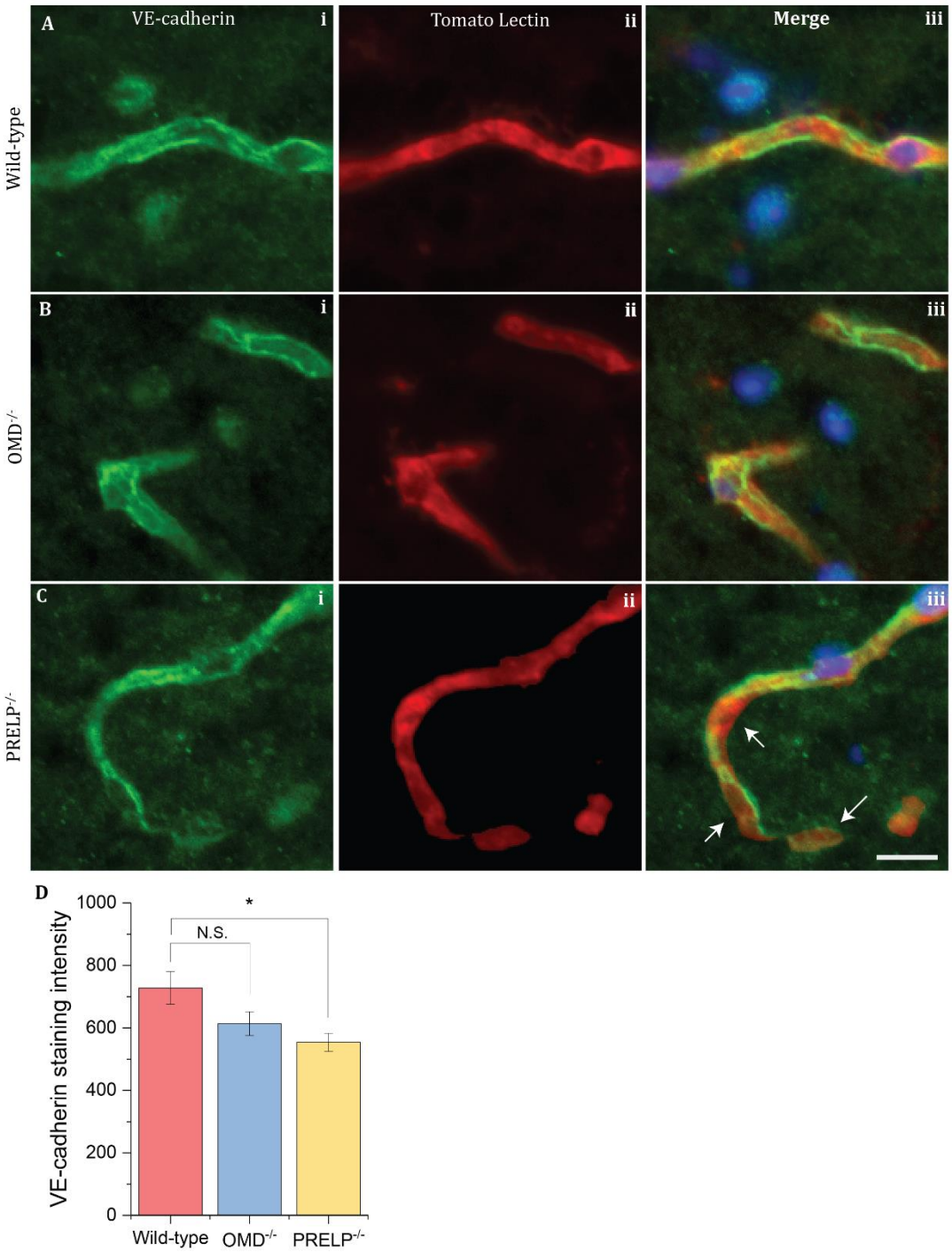

Figure 4.16. Reduced VE-cadherin coverage of PRELP$^{-/-}$ vessels. Sections of adult wild-type **(A)**, OMD$^{-/-}$ **(B)** and PRELP$^{-/-}$ **(C)** cerebellums were stained with VE-cadherin and tomato lectin. Staining of PRELP$^{-/-}$ vessels was found to be less consistent (arrows). VE-cadherin staining intensity was quantified **(D)**. 2-tailed student's t-test was performed and p-values < 0.05 were considered significant (*; 0.01 < p-value < 0.05). 5 fields were randomly imaged per animal. Error bars are the SEM where n=3. Scale bar 10um.

4.3.3.2 Tight junctions

Since adherens junctions in PRELP$^{-/-}$ seem to be abnormal, I sought to investigate the state of tight junctions in the vasculature. In order to assess the integrity of tight junctions, I utilised two different antibody markers: zonula occludens 1 (ZO-1) and claudin-5. Both ZO-1 and claudin-5 are tight junction markers, however they have different cellular localisations (Furuse, 2010); ZO-1 is a peripheral membrane protein, expressed in the cytoplasmic face of cells while claudin-5 is a transmembrane protein.

Slides were stained with ZO-1 and tomato lectin and staining intensity was quantified (Figure 4.17). Staining revealed that there were no differences in staining intensity or pattern in OMD$^{-/-}$. In contrast, the staining pattern in PRELP$^{-/-}$ was visibly more punctate (Figure 4.17C; arrow) and the overall staining intensity per vessel was found to be decreased, indicating that the adapter protein ZO-1 expression or localisation is perturbed in PRELP$^{-/-}$.

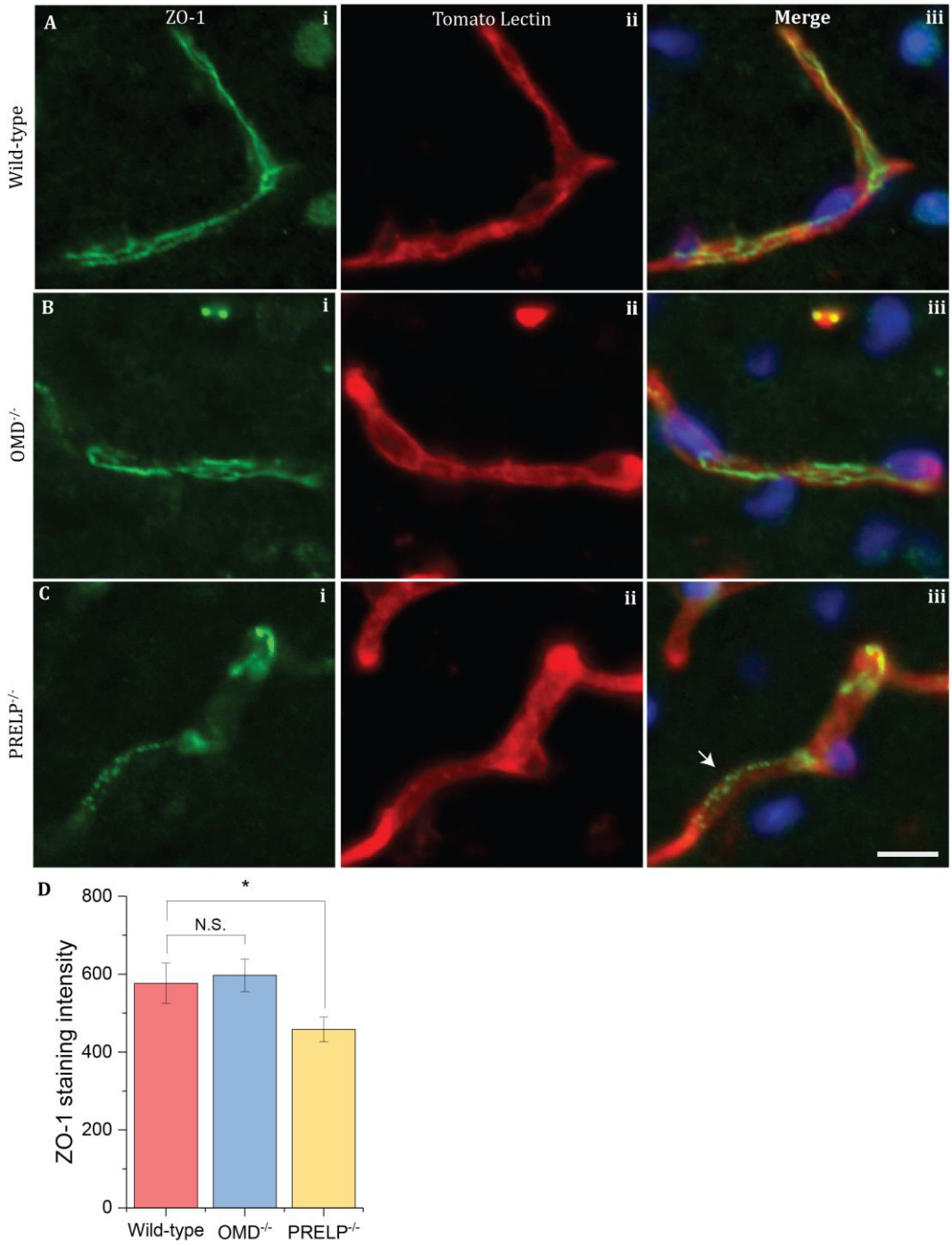

Figure 4.17. ZO-1 staining intensity is reduced in PRELP$^{-/-}$. Adult wild-type **(A)**, OMD$^{-/-}$ **(B)** and PRELP$^{-/-}$ **(C)** brain sections were stained with ZO-1 and tomato lectin. Staining along vessels in PRELP$^{-/-}$ were found to be punctate (arrow). Staining intensity was quantified **(D)**. 2-tailed student's t-test was performed and p-values < 0.05 were considered significant (*; 0.01 < p-value < 0.05). 5 fields were randomly imaged per animal. Error bars are the SEM where n=3. Scale bar 10um.

I then analysed claudin-5 staining (Figure 4.18). Antibody staining and quantification revealed that, just as before, there were no discernible differences between OMD$^{-/-}$ and wild-type. Claudin-5 staining along PRELP$^{-/-}$ vessels was found to be less continuous when

compared to the wild-type and quantification of overall staining intensity indicated a decrease in claudin-5 in PRELP$^{-/-}$ indicative of disrupted tight junctions.

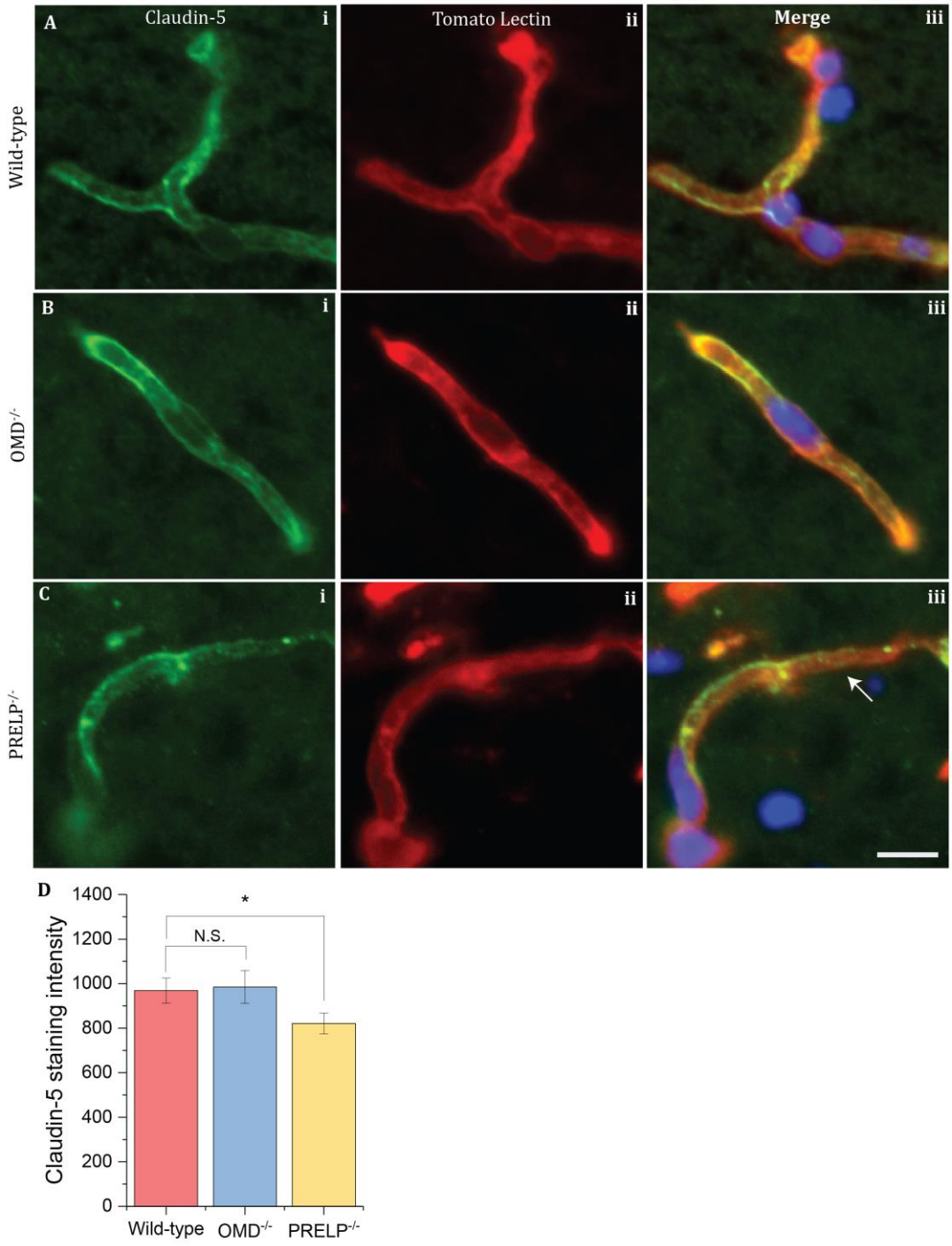

Figure 4.18. Weaker claudin-5 staining in PRELP$^{-/-}$ vessels. Claudin-5 and tomato lectin staining was performed in adult wild-type **(A)**, OMD$^{-/-}$ **(B)** and PRELP$^{-/-}$ **(C)** cerebellum sections. Staining in PRELP$^{-/-}$ vessels was found to be more discontinuous (arrow). Quantification of staining intensity was performed **(D)**. 2-tailed student's t-test was performed and p-values < 0.05 were considered significant (*; 0.01 < p-value < 0.05). 5 fields were randomly imaged per animal. Error bars are the SEM where n=3. Scale bar 10um.

4.3.4 Summary

I found the BBB of PRELP$^{-/-}$ mice to be dysfunctional, as assessed by IgG staining and tracer dye injection. I then examined the individual components of the BBB to determine the cause of this BBB dysfunction. I analysed the BM, pericytes and astrocyte end-feet and found these components to be down-regulated in PRELP$^{-/-}$. Analysis of cell-cell junction proteins also indicated that they are down-regulated in PRELP$^{-/-}$ vessels, consistent with my findings so far. No changes were observed in OMD$^{-/-}$ vessels. These results are summarised in Table 4.1.

	OMD$^{-/-}$	PRELP$^{-/-}$
BBB breakdown		
IgG	N.S. p = 0.9	Leakage observed (**) p = 0.004
70kDa Dextran	No leakage observed	Leakage observed
BBB components		
Laminin	N.S. p = 0.08	Decrease (**) p = 0.002
Collagen IV	N.S. p = 0.7	N.S. p = 0.4
Perlecan	N.S. p = 0.8	Decrease (*) p = 0.03
Pericytes	N.S. p = 0.06	Decrease (*) p = 0.01
Astrocyte end-feet	N.S. p = 0.6	Decrease (*) p = 0.04
Cell-cell junctions		
VE-cadherin	N.S. p = 0.3	Decrease (*) p = 0.02
ZO-1	N.S. p = 0.7	Decrease (*) p = 0.04
Claudin-5	N.S. p = 0.8	Decrease (*) p = 0.04

Table 4.1. Summary of findings regarding the BBB in OMD$^{-/-}$ and PRELP$^{-/-}$.

4.4 Effect of OMD and PRELP on inflammation in the brain

4.4.1 Microglial activation

Microarray analysis that was previously completed in the Ohnuma lab showed that there were several pathways involved in inflammation and immunity upregulated in EJ-28 bladder cancer cells transfected with siRNA against OMD and PRELP. Gene expression profiling of HEK293 cells overexpressing OMD and PRELP also support these findings (Ohnuma, unpublished). In addition, leakage of plasma proteins is often accompanied by not only an increase in microglial density, but also more abundant activated microglia (Menezes et al., 2014). A study has also demonstrated that the activation state of microglia can be a determinant for regulating endothelial cell proliferation; conditioned media from resting microglia containing TGF-β1 inhibited proliferation, whereas conditioned media from activated microglia promoted endothelial cell proliferation, probably though TNF-α signalling (Welser et al., 2010). I therefore investigated whether there is an increase in microglia and/or microglial activation in $OMD^{-/-}$ and $PRELP^{-/-}$.

Brain sections were stained with Iba-1 and the number of microglia per field of view was manually counted; only cells exhibiting staining within the cell body were counted. Cells were counted irrespective of whether processes were visible or not; these values therefore reflect the total number of microglia. Quantification revealed that there was an increase in the number of microglia stained with Iba-1 in $PRELP^{-/-}$ sections, while there was no change with in $OMD^{-/-}$.

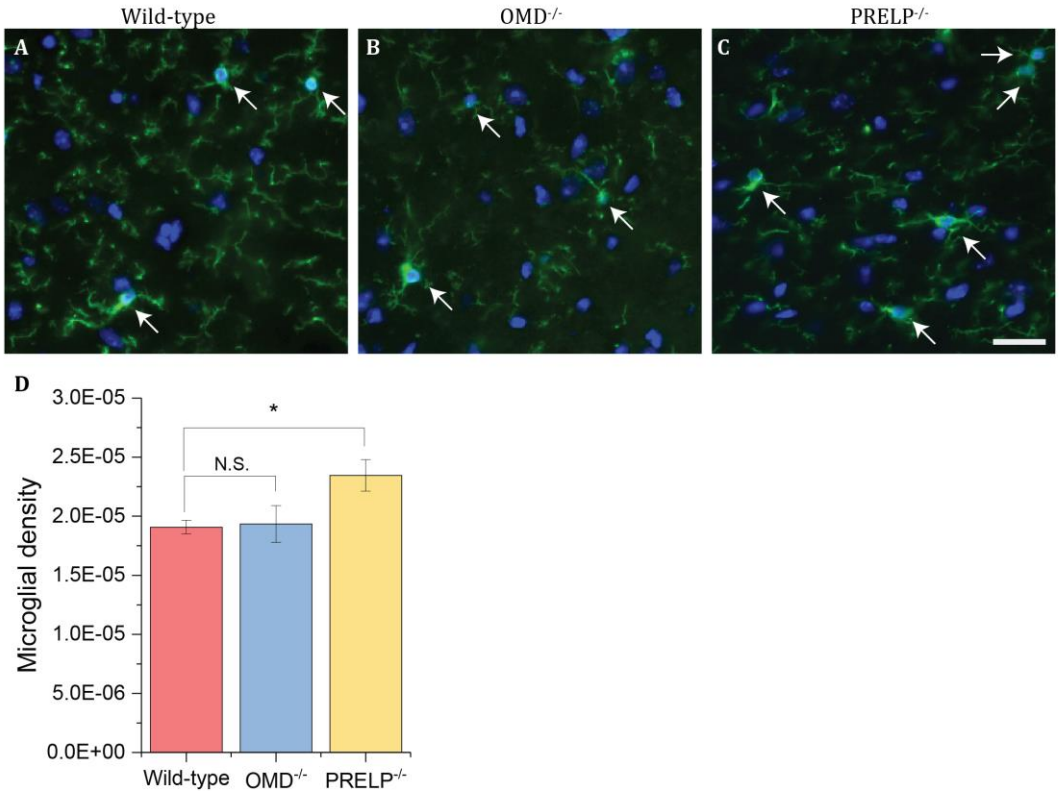

Figure 4.19. Iba-1 staining of adult wild-type (A), OMD$^{-/-}$ (B) and PRELP$^{-/-}$ (C) cerebellum sections. Microglia were manually counted based on Iba-1 and nuclear staining (arrows). Microglial density was quantified (D) and there was an increase in total microglia in PRELP$^{-/-}$. 2-tailed student's t-test was performed and p-values < 0.05 were considered significant (*; 0.01 < p-value < 0.05). 5 fields were randomly imaged per animal. Error bars are the SEM where n=3. Scale bar 25um.

In order to determine whether microglia are resting or activated, I utilised the protocol suggested by (Morrison & Filosa, 2013) with some minor modifications. Briefly, images of Iba-1 staining were processed to remove noise and any background staining. A threshold was applied to produce a binary image; this binary image was then skeletonised using the plugin Analyze Skeleton (Arganda-Carreras et al., 2010) in ImageJ. The simplified image (Figure 4.20) was then analysed and the sum of the branch lengths were extracted and utilised for quantification. A macro was written so that all images were processed using the same parameters (see Chapter 2). Branch lengths were normalised by number of microglia per area; the resulting value was therefore expressed as branch length per microglial density.

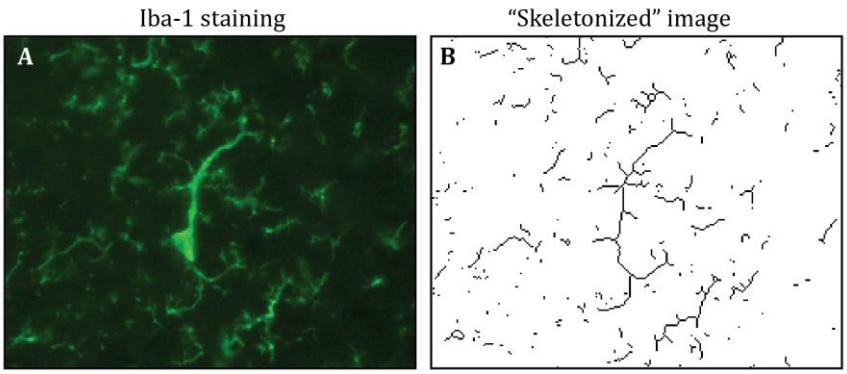

Figure 4.20. Skeletonizing images of Iba-1 staining to quantify microglial branch length. The original image of Iba-1 staining **(A)** was made into a binary image which was then skeletonized **(B)**. The sum of the lengths of the branches was utilised in quantification.

Resting microglia have fine ramified processes and therefore return a higher value for branch length. In contrast, activated microglia have a more amoeboid morphology and have a smaller value. Quantification of branch length per microglial density revealed that there is a statistically significant decrease in PRELP$^{-/-}$ (Figure 4.21). This suggests that there is a higher proportion of microglia which have an amoeboid morphology in PRELP$^{-/-}$, indicative of increased microglial activation in PRELP$^{-/-}$.

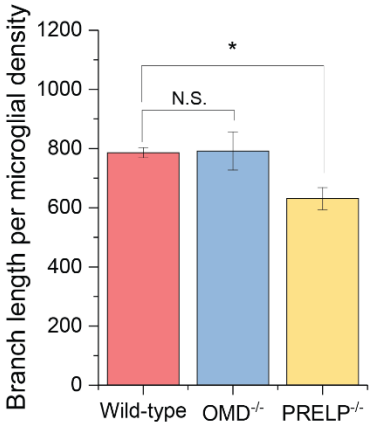

Figure 4.21. Quantification of branch length per microglial density in adult wild-type, OMD$^{-/-}$ and PRELP$^{-/-}$ cerebellum. Images of Iba-1 staining were processed, simplified and analysed. Values were normalised to microglial density. 2-tailed student's t-test was performed and p-values < 0.05 were considered significant (*; 0.01 < p-value < 0.05). 5 fields were randomly imaged per animal. Error bars are the SEM where n=3.

4.4.2 Reactive astrocytes

CNS insults trigger astrogliosis including the upregulation of intermediate filaments GFAP and vimentin. In addition, astrocyte morphology changes with hypertrophy of the cell body and processes (Figure 4.22). Reactive gliosis is a common downstream effect of BBB disruption. Given that I have determined that there is BBB breakdown in PRELP$^{-/-}$ mice

and an increase in activated microglia, I sought to determine whether there was an increase in astrogliosis in PRELP$^{-/-}$.

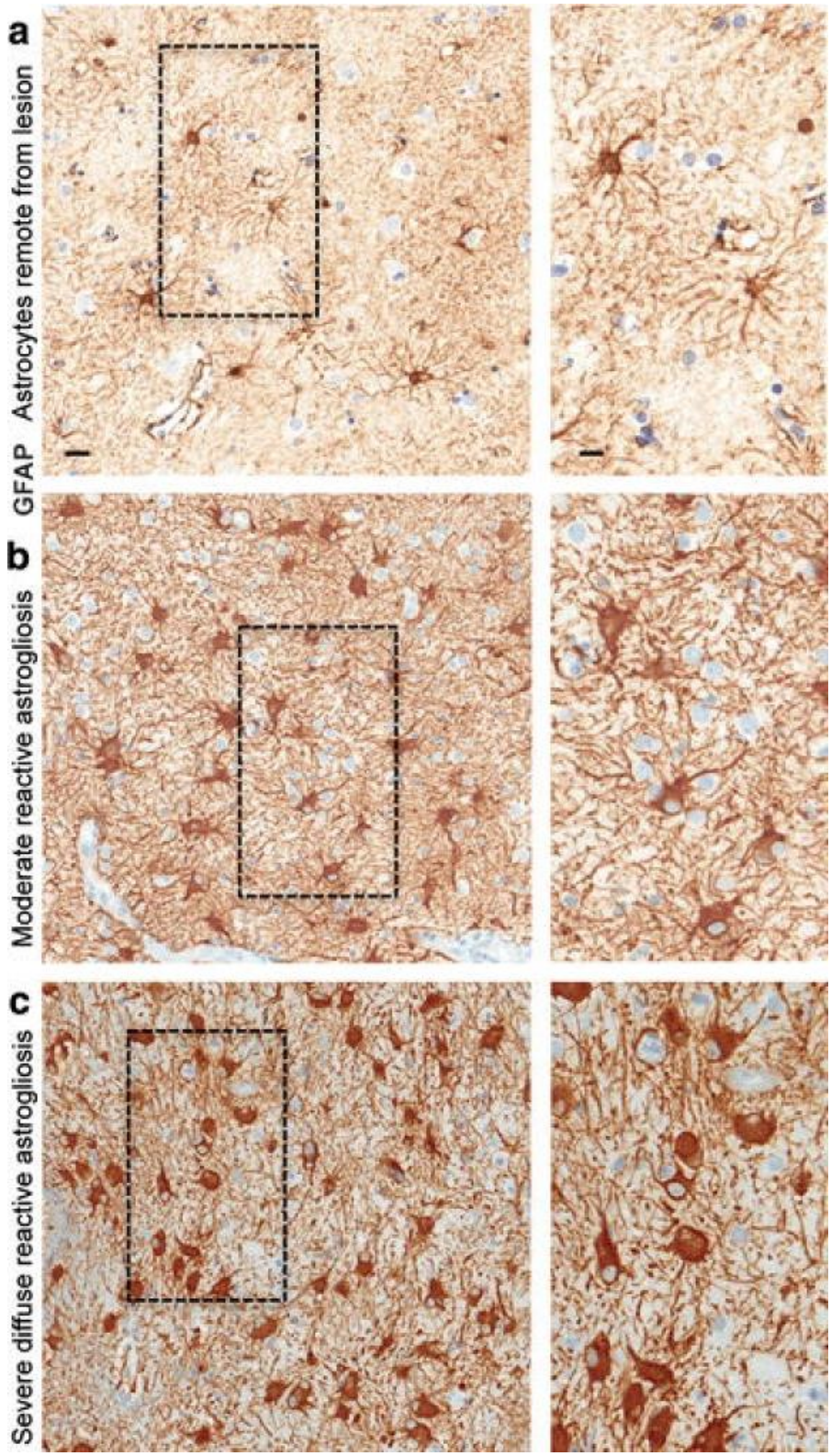

Figure 4.22. Changes in expression of GFAP and morphology of astrocytes in the absence (A) and presence of CNS injury (B & C). Image from (Sofroniew & Vinters, 2010).

Wild-type, OMD$^{-/-}$ and PRELP$^{-/-}$ brain sections were stained with GFAP, and the number of astrocytes were manually counted. Only cells displaying staining within the cell body were counted. In addition, in order to determine whether there is an increase in GFAP expression in knock-out astrocytes, the mean grey value of the entire image was measured. There were no changes in astrocyte number or staining intensity between wild-type and both OMD$^{-/-}$ and PRELP$^{-/-}$ mice (Figure 4.23). In addition, I did not observe any notable changes in astrocyte morphology, indicating that astrocytes, unlike microglia, are not affected by knock-out of OMD or PRELP.

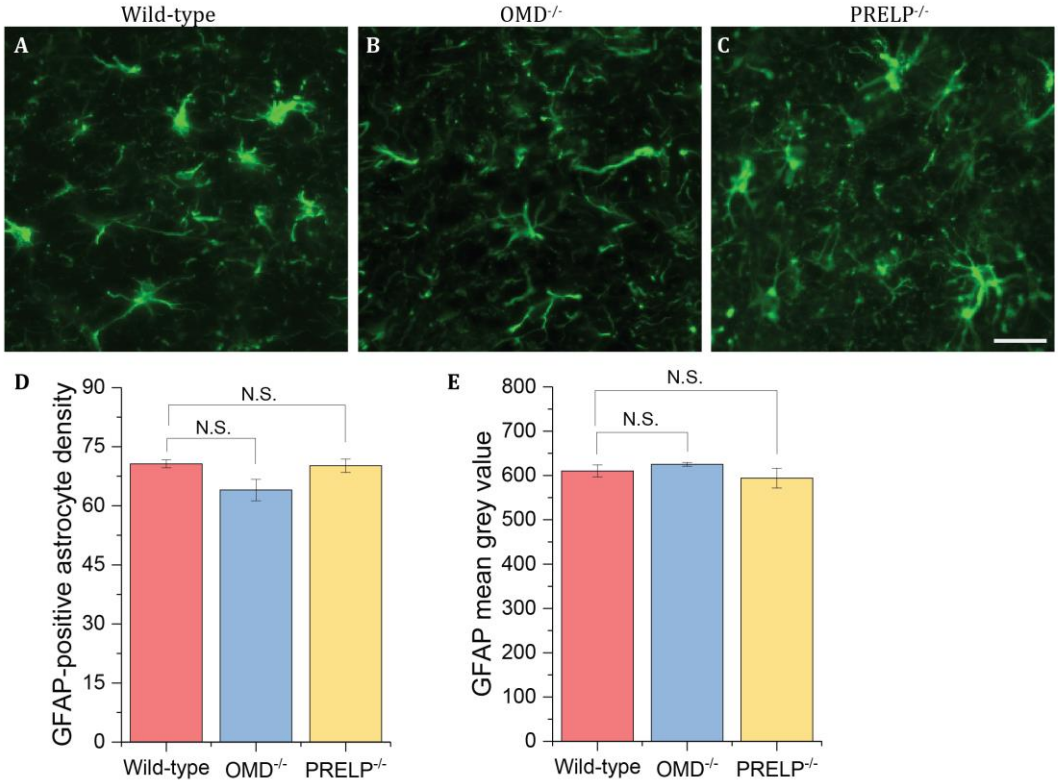

Figure 4.23. No change in GFAP-positive astrocytes in knock-out animals. Adult wild-type (A), OMD$^{-/-}$ (B) and PRELP$^{-/-}$ (C) cerebellum sections were stained with GFAP. Astrocyte count and mean grey value were quantified (D) and were found to be non-significant. 2-tailed student's t-test was performed and p-values < 0.05 were considered significant. 5 fields were randomly imaged per animal. Error bars are the SEM where n=3. Scale bar 25um.

4.4.3 Summary

I have observed differences in the number and branching of microglia between wild-type and PRELP$^{-/-}$, where my results suggest that there are more activated microglia in the PRELP$^{-/-}$ cerebellum. No differences were observed between wild-type and OMD$^{-/-}$ microglia. In contrast there were no differences in the extent of gliosis between wild-type and both OMD$^{-/-}$ and PRELP$^{-/-}$. These results are summarised below in Table 4.2.

	OMD$^{-/-}$	PRELP$^{-/-}$
Microglial activation		
Total number of microglia	N.S. p = 0.9	Increase (*) p = 0.04
Branch length per microglial density	N.S. p = 0.9	Decrease (*) 0.02
Reactive astrocytes		
Astrocyte density	N.S. p = 0.3	N.S. p = 0.9
GFAP mean grey value	N.S. p = 0.4	N.S. p = 0.9

Table 4.2. Summary of findings related to microglial activation and astrogliosis in OMD$^{-/-}$ and PRELP$^{-/-}$.

4.5 Discussion

4.5.1 The effect of PRELP on hindbrain angiogenesis

I ensured that the embryos did not need to be genotyped by mating two animals of the same genotype; i.e. wild-type x wild-type, OMD$^{-/-}$ x OMD$^{-/-}$ and PRELP$^{-/-}$ x PRELP$^{-/-}$. Although in the end the timed matings did work and I was able to obtain embryos, there were difficulties in determining whether the female was plugged the next morning. I frequently culled female mice assessed to be plugged 12 days prior only to find that mating had been unsuccessful. In addition, I also encountered problems with the plug not being identified at all; female who had been used for timed matings but were unplugged later gave birth to pups. These difficulties in obtaining pups therefore meant that fewer hindbrain experiments were performed than hoped.

I dissected embryonic hindbrains at E12.5 from wild-type, OMD$^{-/-}$ and PRELP$^{-/-}$ mice. No phenotype was observed in OMD$^{-/-}$ hindbrains with respect to angiogenesis. In contrast, I observed an increase in blood vessel content in PRELP$^{-/-}$ compared to wild-type (Figure 4.2). Both vessel percentage area and junction density were increased, indicating that PRELP$^{-/-}$ vessels have a higher propensity for angiogenesis in the brain.

As mentioned previously, I have observed that PRELP$^{-/-}$ adult mice have more vasculature in the brain. H&E-stained paraffin sections were analysed, and results suggested increase total length of vessels and branches in PRELP$^{-/-}$. These results have been omitted from this chapter as their reliability was questionable, given that these findings could be strongly influenced by cutting angle, manual detection of microvessels and location of image capture. Although results from the embryonic hindbrain are consistent with initial

observations in the adult brain, I was unable to determine whether PRELP is expressed in the vessels and/or microglia at E12.5. A previous member, Dr Vasiliki Papadaki studied the localisation of OMD and PRELP in embryonic stages and adult mice using X-gal and did not detect any expression of OMD and PRELP in the brain at these stages. There seemed to be sufficient penetration of X-gal into the tissue, as cartilage was stained with X-gal. As was discussed in Chapter 3, there are discrepancies between X-gal and β-galactosidase antibody staining. Therefore, it is possible that PRELP is expressed at E12.5 in the vasculature, microglia or another cell type entirely and was not detected using X-gal in Dr Papadaki's experiments. The single-cell analysis performed by (Zeisel et al., 2015) was done in post-natal mice, and their results may not reflect PRELP expression *in utero*.

Images of the SVP of embryonic hindbrains were analysed using AngioTool, software which was specifically designed with flat-mount models of angiogenesis in mind (Zudaire et al., 2011). Briefly, the program detects edges of vessels, branch points and end-points and computes a variety of parameters describing the vascular network. I found that the fidelity of the edge detection to be satisfactory; the program did not over- or under-estimate the size of vessels (Figure 4.24). The findings obtained using AngioTool therefore reflect the vascular phenotype of the animals, and are not due to variations in analysis.

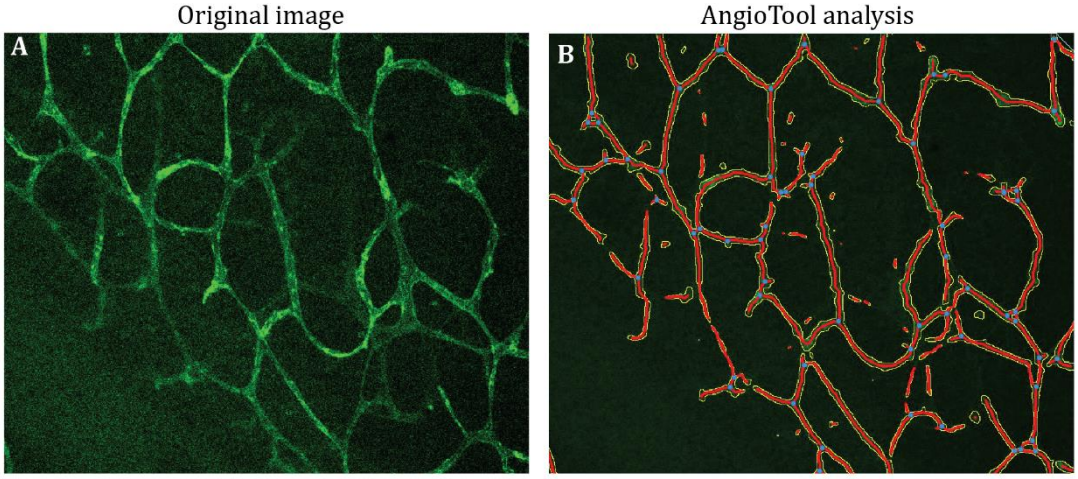

Figure 4.24. Use of AngioTool for analysing vascular networks. Isolectin IB4-stained images **(A)** were analysed using AngioTool, resulting in a skeleton of the vascular network **(B)**.

The increase in vascular content in PRELP$^{-/-}$ suggests that pathways prominent in developmental angiogenesis are affected. Vasculogenesis is initiated by the formation of endothelial cells from progenitor mesodermal angioblasts, which then form a small network of blood vessels known as the primary vascular plexus (Risau, 1997). In the case of brain vasculature, angioblasts migrate into the head early in development to form the

perineural vascular plexus, which covers the entire neural tube (Risau & Wolburg, 1990). Angiogenesis then occurs from the vascular plexus to develop the vascular network, including vasculature in the embryonic hindbrain (Eilken & Adams, 2010; Fantin et al., 2013). Nascent vessels undergo sprouting angiogenesis, whereby a leading endothelial tip cell guides the sprouting vessel through the ECM. In parallel, endothelial stalk cells proliferate behind the tip cell, allowing the capillary to grow and depositing a provisional BM (Park et al., 2014). Finally, the vessels are stabilised by the recruitment of mural cells by secretion of PDGF-B from endothelial cells (Lindblom & Gerhardt, 2003) and a specialised extracellular matrix is induced by TGF-β (Verrecchia et al. 2001). Many members of the SLRP family are able to modulate TGF-β signalling typically by binding to TGF-β and regulating its bio-availability (Dellett et al., 2012). PRELP may therefore be able to affect TGF-β signalling and therefore matrix maturation after the formation of new vessels.

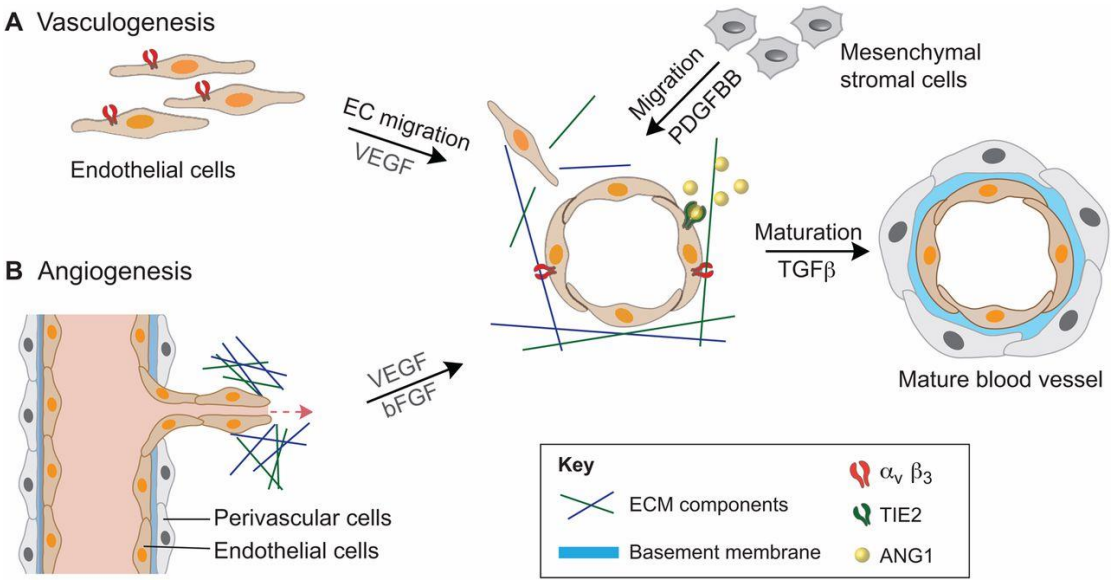

Figure 4.25. Formation of vascular networks during development. Figure from (Park et al., 2014).

The notable molecule responsible for regulating developmental vascularisation is VEGF acting through VEGFR2. VEGF-VEGFR2 signalling has been shown to be critical for the differentiation of angioblasts into endothelial cells; VEGFR2 (Flk-1)-knock-out mice die between E8.5 and E9.5 due to the absence of blood islands and vessels (Shalaby et al., 1995). VEGF is also a regulator for angiogenesis; in particular, VEGF was found to alter the behaviour of tip and stalk cells by cross-talk with the notch signalling pathway to inhibit tip cell formation. Studies inactivating notch signalling found an increase in the number of tip cells and a decrease in stalk cells, indicating that VEGF regulates the relative numbers of tip and stalk cells, thus regulating angiogenesis. The exposure of VEGF to

embryonic, neonate and adult cortical slice explants resulted in dramatic increases in vessel growth (Figure 4.26) – this effect was correlated to the dose of VEGF administered, demonstrating the impact of increased VEGF signalling (Rosenstein et al., 1998).

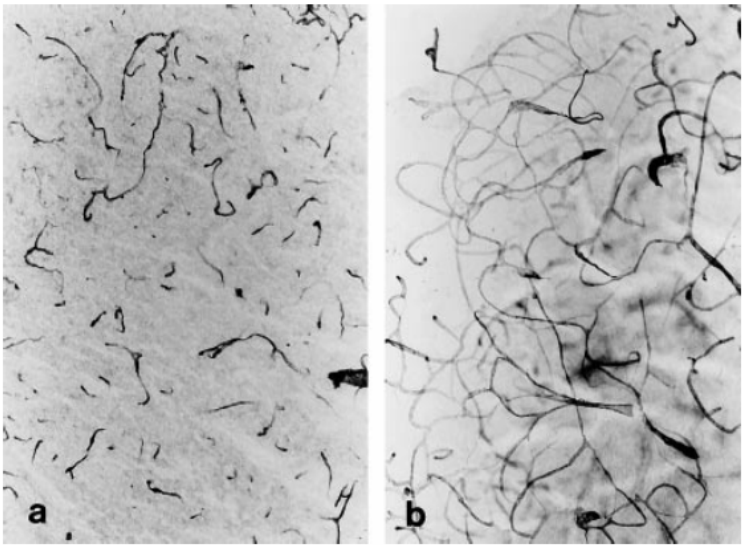

Figure 4.26. Cortical explants without (a) and with (b) 25ng/ml VEGFA-165 stimulation. Figure from (Rosenstein et al., 1998).

The structure and composition of the extracellular matrix of endothelial cells could have an impact on the retention and diffusion of signalling ligands. In particular, ligands capable of influencing angiogenesis, such as VEGF, TGF-β and bFGF, are able to bind to heparin/heparan sulphate moieties (Dougher et al., 1997; McCaffrey et al., 1992; Ornitz et al., 1992; Yayon et al., 1991). In addition, *in vitro* studies have demonstrated that heparin is essential for the mitogenic activity of VEGFA-165, an isoform of VEGF with mediocre heparin-binding capabilities (Ashikari-Hada et al., 2005; Ono et al., 1999). These experiments evaluated the proliferation and tubule formation capabilities of HUVECs, a common *in vitro* model for angiogenesis. These authors found that the effect of VEGFA-165 was strongly enhanced by the addition of heparin/heparan sulphate, strongly hinting at the role of the extracellular milieu in regulating cellular processes such as angiogenesis.

There is one study describing the role of PRELP in angiogenesis in the context of age-related macular degeneration (AMD) (Birke et al., 2014). AMD is a leading cause of blindness among the elderly population and is caused by abnormal angiogenesis or neovascularisation in the eye. An experimental model of AMD in mice can be utilised by inducing choroidal neovascularisation using a laser; investigators found that choroidal neovascularisation was reduced in mice treated with PRELP (Figure 4.27). These results are consistent with my observations from the embryonic hindbrain – PRELP acts to inhibit angiogenesis.

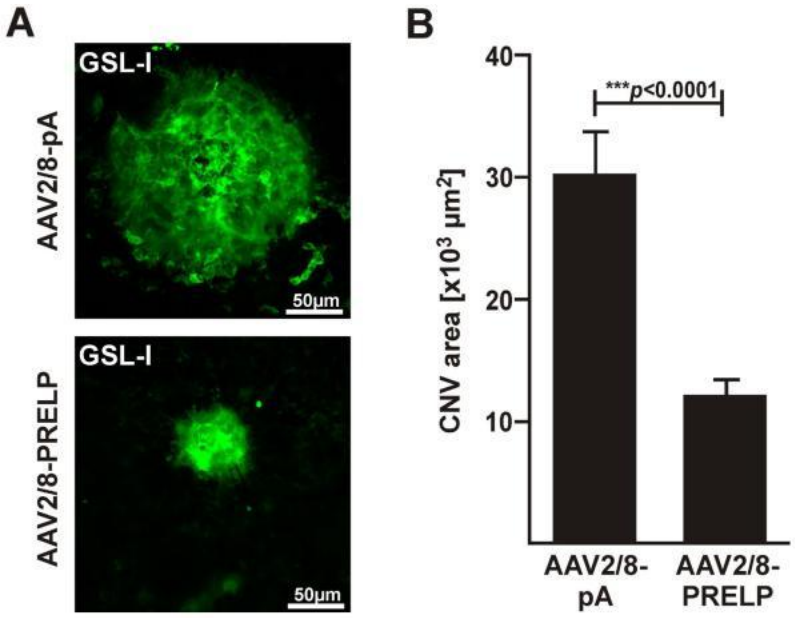

Figure 4.27. PRELP inhibits neovascularisation in the eye. Figure from (Birke et al., 2014).

The increase in vascular content in PRELP$^{-/-}$ could therefore be due to an increase in VEGF signalling. VEGF isoforms, such as VEGFA-165, can bind to heparin/heparan sulphate and their binding can strongly influence their impact on angiogenesis. Therefore, it is possible that in the absence of PRELP, there are changes in the composition of the extracellular matrix, leading to differences in vascular phenotype.

Other *in vivo* models of angiogenesis could be utilised to investigate the effect of PRELP on angiogenesis in different tissues and conditions. The corneal micropocket assay could be utilised where the growth of vessels in an otherwise avascular tissue is measured (Rogers et al., 2007). Briefly, the mouse is anaesthetised and a small incision is made in the cornea to create a micropocket A pellet containing growth factors is inserted in the corneal micropocket and vessels from the limbus undergo angiogenesis. Other more general assays using Matrigel plugs (Kragh et al., 2003) or sponge/matrix implants (Andrade & Ferreira, 2016) could also be used to probe angiogenesis in non-CNS tissues. However, the major disadvantage of utilising such implants would be the compositional heterogeneity of Matrigel/matrix; as the effect of an extracellular proteoglycan is investigated, I would ideally use plug or matrix of known composition (Norrby, 2006). In addition, cell culture-based systems can also be utilised – endothelial tubule formation assays are particularly popular in this regard. In Chapter 6, I have utilised HUVECs to investigate the effect of PRELP on tubule formation. Finally, *ex vivo* methods such as the aortic ring assay could be utilised. Thoracic aortas from our knock-out mice could be harvested, prepared and embedded in a BM extract – the sensitivity of these organ cultures to angiogenic factors could then be tested (Bellacen & Lewis, 2009).

Next, I considered the impact of microglia on the developmental angiogenesis. While developmental brain angiogenesis occurs around E9.5 in mice (Ruhrberg & Bautch, 2013), progenitor microglia can be detected at a slightly earlier timepoint – E9 (Alliot et al., 1999). Analysis of developing vasculature indicates that nascent vessels are closely associated with microglia, suggesting a role for microglia in the formation of vasculature (Cuadros et al., 1993; Dalmau et al., 1997). Studies by various groups have indicated that the depletion of microglia, whether chemical or genetic, results in a reduction of vascular density in the brain and retina, as shown in Figure 4.28 (Checchin et al., 2006; Fantin et al., 2010; Kubota et al., 2009; Rymo et al., 2011). Interestingly, mouse embryos lacking microglia had similar numbers of tip and stalk cells compared to wild-type counterparts, suggesting that microglia act to facilitate angiogenesis downstream of initial steps of angiogenesis (Kubota et al., 2009). The number of branches in the vascular network was correlated with the number of microglia, suggesting that microglia act as a bridge between vascular sprouts in the CNS (Fantin et al., 2010). These findings are reinforced by *in vitro* studies; microglia co-culture with mouse aortic rings indicated that microglia actively migrate towards the aortic ring and increased the number of branches (Rymo et al., 2011).

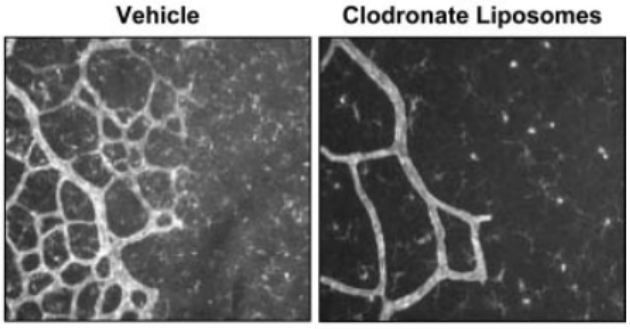

Figure 4.28. The effect of microglia depletion by clodronate liposomes on retinal angiogenesis. Figure from (Checchin et al., 2006).

Manual counting of microglia in the SVP of the embryonic hindbrain showed only a small statistically-insignificant increase in microglia in PRELP$^{-/-}$ (Figure 4.3). While an increase in microglia in PRELP$^{-/-}$ could provide a possible explanation for the increased vascular density, the results are inconclusive. As is done in various publications, staining of a microglial marker such as Iba-1 in parallel with a vascular marker would have been ideal. I have attempted to use an antibody against Iba-1 to stain microglia, however staining was not successful. Due to the limited number of knock-out embryos in particular, I opted to use tomato lectin, as I had previously found it to be a reliable stain and papers indicate that it labels microglia, including prenatal microglia (Dalmau et al., 1997; Robertson et al., 2014). Since tomato lectin also labels the vasculature, errors may have been made when

identifying microglia despite double staining with a vasculature-only marker such as isolectin IB4. Therefore, to confirm whether an increased infiltration of microglia in development is responsible for the increased vascular content in PRELP$^{-/-}$, staining using an antibody against microglia would be ideal.

Next, I attempted to determine whether there were any changes in the recruitment of pericytes in PRELP$^{-/-}$. Pericytes are mural cells which provide contractile and stabilising contacts to the endothelium and are recruited by PDGF-B-secreting endothelial cells. Pdgf-b-null mice die *in utero*, just before birth, due to excessive haemorrhaging (Levéen et al., 1994). Ablation of endothelium-specific PDGF-B results in a viable mouse line; analysis of adult vasculature suggests that the reduced pericyte coverage results in decreased vascular density, increased bleeding and increased vessel diameter (Bjarnegård et al., 2004). I noted that PRELP$^{-/-}$ vessels seemed to be more dilated compared to the wild-type and considered whether there were changes in pericyte distribution. PDGF-B contains a retention motif which is required for binding to heparin/heparan sulphate; deletion of the retention motif results in reduced pericyte coverage in *Pdgf-b*$^{ret/ret}$ mice (Lindblom & Gerhardt, 2003). *Ndst*$^{-/-}$ mice have abnormal heparin/heparan sulphate with reduced N-sulphation and this mutation has been shown to prevent appropriate binding of pericytes to the vasculature during development (Abramsson et al., 2007). In both mutations regarding pericyte attachment, authors have noted abnormal morphology of pericytes, where processes typically do not wrap around the endothelium in a tight manner. In my experiment, I observed no statistically-significant differences between wild-type and PRELP$^{-/-}$ (Figure 4.4).

To summarise, I observed an increase in vascular content in PRELP$^{-/-}$ and attempted to analyse microglial and pericyte coverage of the vasculature which could possibly cause changes in vascular density. Difficulties regarding antibody staining were encountered and would have to be optimised for future experiments.

4.5.2 Challenges in utilising tracer dyes to assess BBB integrity

I initially detected BBB breakdown using anti-mouse IgG staining (Figure 4.5). While this method has been used in numerous publications (Armulik et al., 2010; Bell et al., 2010; Gautam et al., 2016; McKittrick et al., 2015; Yao et al., 2014), I aimed to validate whether PRELP$^{-/-}$ mice have a disrupted BBB by injecting them with a tracer dye, 70kDa Dextran. 40-70kDa Dextran are the most commonly used size of tracer dye in recent literature; smaller dextrans can be used for the quantification of extravasation by fluorometry, they are typically difficult to visualise in tissue sections (Hoffmann et al., 2011). In addition, even in recent research, Evans Blue is still utilised as a dye to assess the integrity of the

BBB. Tracer dyes are typically administered directly into the tail vein of animals, however there are alternative routes which have been reported, summarised in Table 4.3.

Tracer dye	Route	Concentration	Dosage	Reference
Evans Blue	IP	1%	800ul	(Morrey et al., 2008)
Evans Blue	Tail vein (IV)	0.5% and 2%	4ul per g	(Armulik et al., 2010)
70kDa Dextran-TRITC	Tail vein (IV)	25mg/ml	0.1mg per g	(Armulik et al., 2010)
Evans Blue	Tail vein (IV)	2%	500ul	(Hoffmann et al., 2011)
40kDa Dextran-FITC	Tail vein (IV)	100mg/ml	500ul	(Hoffmann et al., 2011)
70kDa Dextran-FITC	Tail vein (IV)	100mg/ml	500ul	(Hoffmann et al., 2011)
Evans Blue	IP	2%	4ul per g	(Manaenko et al., 2011)
Evans Blue	Tail vein (IV)	2%	4ul per g	(Manaenko et al., 2011)
70kDa Dextran-FITC	Tail vein (IV)	5mg/ml	N.R.	(Errede et al., 2012)
70kDa Dextran	Left ventricle (IC)	25mg/ml	0.25mg per g	(Schellenberg et al., 2012)
70kDa Dextran-Texas Red	Tail vein (IV)	25mg/ml	0.2mg per g	(Sagare et al., 2013)
Evans Blue	IP	2%	10ul per g	(Yao et al., 2014)
500kDa Dextran-FITC	Tail vein (IV)	10mg/ml	100ul	(Yao et al., 2014)
10kDa Dextran-FITC	Tail vein (IV)	10mg/ml	250ul	(Naito et al., 2014)
Evans Blue	IP	2%	15ul per g	(Menezes et al., 2014)
Evans Blue	Carotid artery (IV)	5mg/ml	500ul	(McMillin et al., 2015)

Table 4.3. Summary of typical methods of administering tracer dyes in adult rodents in recent research. IP, intraperitoneal; IV, intravenous; IC, intracardial; N.R., not reported.

Our initial efforts included tail vein injection, i.e. intravenous injection, a number of times with poor success in the PRELP$^{-/-}$, whereas the procedure was successful in wild-type and OMD$^{-/-}$ (Figure 4.7). The technician from our Biological Resources Unit, Mr Wells, performed these injections and noted that these injections are generally trickier to perform in black mice and that the veins of PRELP$^{-/-}$ mice were "*very poor*", suggesting that peripheral vessels in PRELP$^{-/-}$ are affected; perhaps there are differences in the contractility or rigidity of PRELP$^{-/-}$ vessels.

Since we had difficulties with injection of 70kDa Dextran in the tail vein, we opted to use a different method of administration. The easiest way was to inject intraperitoneally – while this is not as ideal as intravenous injection, there are publications demonstrating that intraperitoneal injections could be utilised in assessing BBB integrity with Evans Blue (Table 4.3). There is also a study comparing the method of administration on Evans Blue extravasation visible in tissue sections (Manaenko et al., 2011); the authors found that there are no changes in Evans Blue outside of the vasculature when comparing IP and IV injections, suggesting that IP injections of tracer dyes could be a viable method of administration. To my knowledge, there are no publications where dextrans are injected intraperitoneally in adult mice; IP injections are typically used in assessing BBB integrity in neonates.

Prof Bolsover injected animals intraperitoneally and we allowed the circulation of the tracer dye for 3 hours prior to culling using CO_2. After harvesting, processing and cutting the brains, I observe that the dye injected into the peritoneal space was taken into circulation and reached the vessels of the brain. I did note, however, that the perfusion was not as complete as with intravenous injection – there were occasionally vessels which did not contain any dye. This is possibly due to the long circulation time prior to culling; it is possible that the concentration of fluorescent Dextran circulating decreased with time as the Dextran was degraded. Nonetheless, detection of 70kDa Dextran-Texas Red outside of the vasculature was successful in PRELP$^{-/-}$ brains, confirming that there is indeed BBB breakdown (Figure 4.8).

Unfortunately, given the poor perfusion of vessels with dextran, it was not possible to accurately quantify the extent of BBB breakdown, as not all vessels had detectable fluorescence inside the lumen. I judge that the presence of dextran outside of the vessels detected only in PRELP$^{-/-}$ is sufficient to indicate that there are perturbations in the BBB, however a means of accurate quantification would be important. To this end, mice could

be administered fluorescent dextran and perfused with saline after the circulation period, removing all dextran from the vessels. Brains would then be harvested, homogenised and fluorescence measured using a spectrophotometer. The read-out would provide a quantifiable measurement of the extent of BBB breakdown. It should be noted that Dextran should be administered directly into the blood stream for most accurate quantification; any variation in the uptake of dextran through the peritoneum would be eliminated. Since tail vein injection seems to be technically challenging to perform in PRELP$^{-/-}$, other vessels such as the carotid artery could be targeted.

In addition to providing a reliable means of quantification, this method could also allow me to characterise the extent of BBB breakdown. For example, if the perturbations to the BBB are assessed to be mild, I would expect smaller dextrans to cross the barrier while large dextrans would remain in the lumen. Unfortunately, due to time constraints, I was unable to perform these experiments.

To conclude, I have determined that there is BBB breakdown, as initially assessed by IgG staining. This finding was confirmed after tracer dye injection into the peritoneal after failed attempts to inject the dye directly into the tail vein. Further work could be pursued to improve the administration of dextran, followed by perfusion by saline and fixative to more clearly visualise areas of leakage. In addition, the severity of BBB breakdown can be assessed by determining the penetration of dextrans molecules of different sizes.

4.5.3 BBB breakdown in PRELP$^{-/-}$ could be related to a decrease in laminin deposition

In this chapter, I have demonstrated that there is BBB breakdown in PRELP$^{-/-}$ animals. This was initially discovered using IgG staining of endogenous circulating IgG molecules (Figure 4.5). This effect was found to be particularly strong in the cerebellum of PRELP$^{-/-}$ brains. Further analysis using tracer dyes demonstrated that 70kDa Dextran was found outside of the vasculature in PRELP$^{-/-}$ only (Figure 4.8). In order to determine whether a specific feature associated with the BBB was down-regulated, I quantified the intensity of staining of BM components laminin (Figure 4.10), collagen IV (Figure 4.11) and perlecan (Figure 4.12). Perivascular contacts to astrocytes were quantified using antibody staining against AQP4 (Figure 4.13). In addition, pericyte coverage of vessels was also quantified and expressed as pericytes per vessel (Figure 4.14). Note that from previous observations of intensity of IgG leakage and PRELP localisation by β-galactosidase, I opted to focus on cerebellum vessels.

I determined that BM components laminin and perlecan in addition to astrocyte end-feet and pericyte coverage were all decreased in PRELP$^{-/-}$ vessels. There was no change in levels of collagen IV.

There are multiple publications describing the importance of laminin isoforms in the stability of the BBB. Laminins are trimeric proteins containing α-, β- and gamma-subunits; for example, laminin-411 is formed of laminin α4, β1 and γ1 chains. They form an integral part of the BM of blood vessels; endothelial cells, astrocytes and pericytes contribute to the formation and maintenance of the BM by secreting isoforms of laminin (Gautam et al., 2016). Studies of transgenic mice lacking specific isoforms of laminin strongly point to the importance of laminin proteins in regulating vascular permeability. A summary of laminins involved in the BBB is found in Table 4.4.

Source	Laminin isoform	Effect on BBB	References
Endothelial cells	411	- Permissive for T-cell transmigration - Important for vessel maturation in development	(Frieser et al., 1997; Sixt et al., 2001; Thyboll et al., 2002)
Endothelial cells (post-natal)	511	- Restrictive for T-cell transmigration - Involved in BBB repair after hypoxic injury*	(Kangwantas et al., 2016; Sixt et al., 2001; Sorokin et al., 1997)
Astrocytes	111	- Stabilises the BBB - Prevents pericyte differentiation to BBB-disrupting contractile stage - Maintains polarity of astrocyte end-feet	(Sixt et al., 2001; Yao et al., 2014)
Astrocytes, pericytes	211	- Stabilises the BBB - Prevents pericyte differentiation to BBB-disrupting contractile stage - Regulates pericyte coverage - Maintains polarity of astrocyte end-feet	(Jucker et al., 1996; Menezes et al., 2014; Sixt et al., 2001; Yao et al., 2014)

Table 4.4. Effect of various isoforms of laminin on the BBB. All data derive from *in vivo* experiments unless marked with *.

The antibody I utilised for detecting laminin is a polyclonal antibody generated from laminin protein purified from Englebreth Holm-Swarm (EHS) mouse sarcoma. According to the manufacturer, "*This source of laminin used to generate the antibody will contain alpha, beta and gamma types of laminin and is probable that this polyclonal antibody will react against all three types, but this has not been fully characterized*". The predominant isoform of laminin isolated from EHS is laminin-111 (Aumailley, 2013); although the α1 chain is only expressed by astrocytes, both the β1 and γ1 chains are expressed by laminins secreted by endothelial cells, astrocytes and pericytes (Table 4.4). Therefore, the antibody I have utilised can be used to determine global changes in laminin expression and deposition in the BBB, since β1 and γ1 chains are expressed. In order to determine whether endothelial, pericytic or astrocytic laminin is affected by the absence of PRELP$^{-/-}$, monoclonal antibodies raised against specific isoforms should be utilised, as was done by (Sixt et al., 2001).

While there has not been much work done on elucidating the effect of endothelial laminins in the context of the BBB, there is considerable evidence of the importance of astrocytic and pericytic laminins in the integrity of the BBB. Mutants lacking laminin α2 (Lama2$^{-/-}$),

a component of laminin-211 secreted by astrocytes and pericytes, display significant abnormalities in the integrity of the brain vasculature (Menezes et al., 2014). It should be noted that in this study, both astrocytic and pericytic laminin α2 were knocked-out. Other groups have created more specific knock-outs and analysed the effect on the BBB; a neural- and glial-specific knock-out of laminin γ1 was generated and found to have a highly perturbed BBB, including reduced astrocyte end-feet coverage and disrupted endothelial tight junctions (Yao et al., 2014). In contrast, a study using a pericyte-specific inducible knock-out of laminin γ1 found that only 10% of mutant animals exhibit hydrocephalus and BBB breakdown (Gautam et al., 2016). Taken together, this indicates that astrocytic laminin is more crucial in the maintenance of the BBB.

The extent of BBB dysfunction in a global laminin α2 knock-out, Lama2$^{-/-}$, was much more severe than the phenotype I observed in PRELP$^{-/-}$ mice (Figure 4.29). While I observed IgG leakage mainly in the cerebellum, Menezes and colleagues have detected Evans Blue leakage in the cortex, striatum, hippocampus and cerebellum. In response to the disrupted BBB, there was an increase in microglial density and the authors noted a more amoeboid morphology of microglia, although no quantification was performed. Morphology of astrocytes was also found to be consistent with the induction of astrogliosis. Analysis of astrocyte end-foot coverage of vessels found that mutant vessels have reduced staining of vessels, consistent with data obtained from PRELP$^{-/-}$. Pericyte coverage in numerous regions was also reduced in Lama2$^{-/-}$. Staining of junction proteins VE-cadherin, ZO-1, claudin-5 and occludin was performed and found to be abnormal or greatly decreased in Lama2$^{-/-}$ mice. Therefore, the phenotypes observed in PRELP$^{-/-}$ and Lama2$^{-/-}$ are similar, and therefore the mechanisms of BBB breakdown in these transgenic mice may be related. The key difference is that the BBB breakdown in the absence of laminin α2 seems to result in a more severe phenotype – extravasated dye was observed in multiple tissues of the brain, evidence of astrogliosis, the extent of the reduction of AQP4 and junction protein staining seemed to be greater.

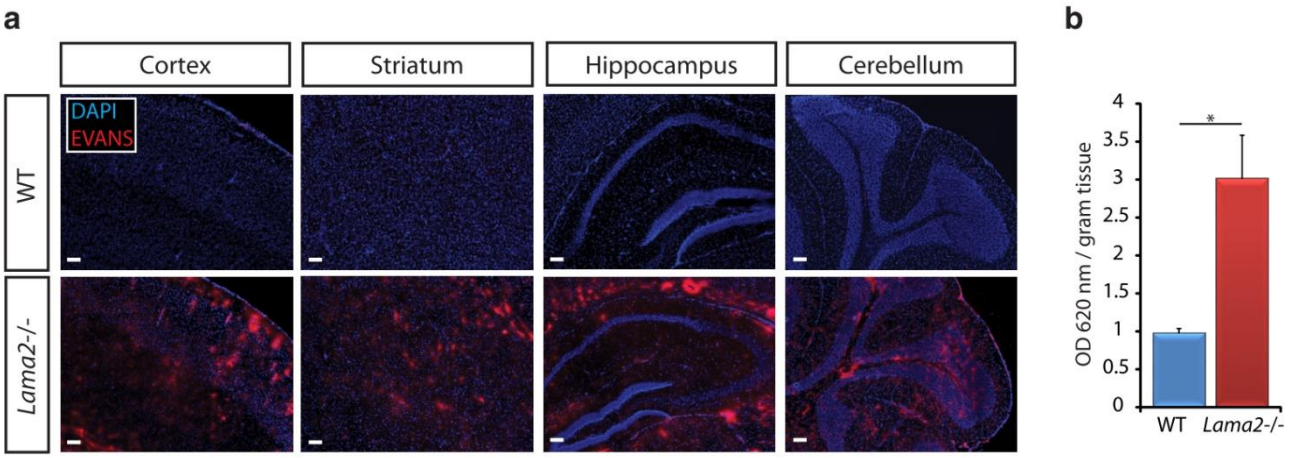

Figure 4.29. BBB in Lama2$^{-/-}$ mice. Wild-type and Lama2$^{-/-}$ mice were injected with Evans Blue dye, perfused and various regions of the brain were analysed **(a)**. The extent of leakage was quantified by measuring Evans Blue remaining in the brain after perfusion **(b)**. Figure modified from (Menezes et al., 2014).

Glial-specific knock-out of laminin γ1 resulted in animals with BBB breakdown; Evans Blue leakage was quantified and IgG staining was employed to further indicate a disrupted BBB (Yao et al., 2014). The authors describe the extent of BBB breakdown to be restricted to the deep brain regions, and rarely in the cortex and hippocampus. I do note that the degree of IgG leakage in their Nγ1-KO animals to be quite similar to what I have observed in PRELP$^{-/-}$ (Figure 4.30). While the study described decreased staining of astrocyte end-feet marker AQP4 and junction markers, one of the key findings of their research was that astrocytic laminin affected pericyte differentiation via integrin α2. They observed that PDGFR-β-positive pericytes in control animals did not exhibit staining for α-smooth muscle actin, whereas Nγ1-KO PDGFR-β-positive pericytes were positive for α-smooth muscle actin, suggesting that astrocytic laminin would normally prevent pericytes from differentiating to a more contractile state. While I have not analysed the state of pericyte differentiation in PRELP$^{-/-}$, the phenotype of Nγ1-KO and PRELP$^{-/-}$ are similar, providing further evidence that the loss of laminin in the BM may be a relevant mechanism.

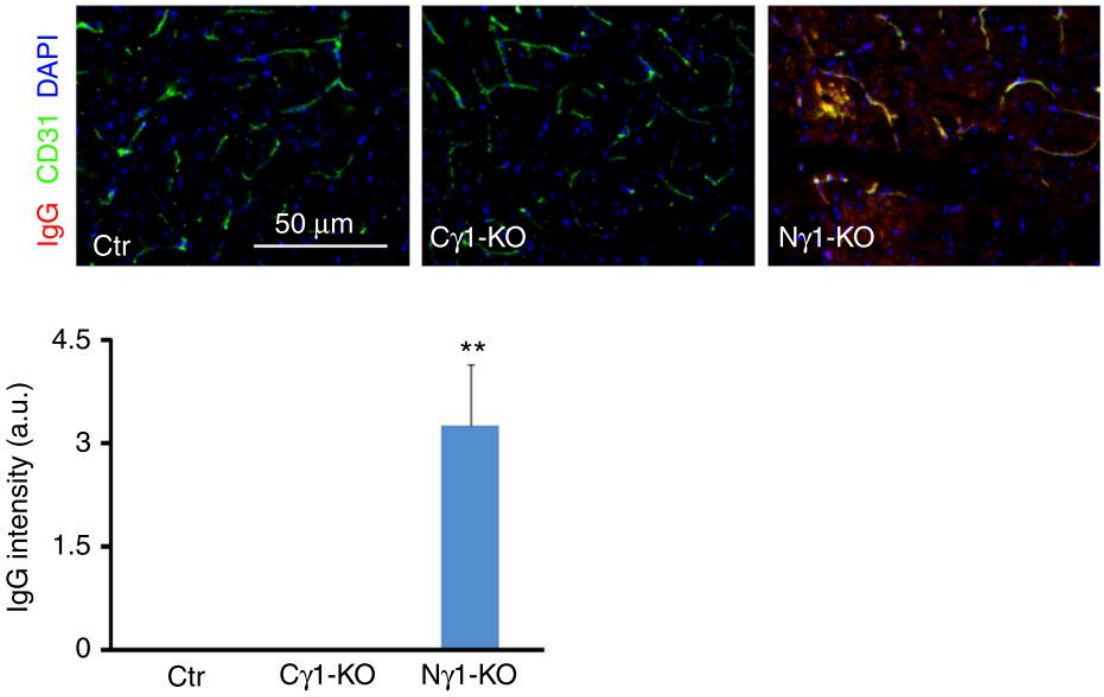

Figure 4.30. BBB breakdown in Nγ1 determined by IgG leakage. Figure modified from (Yao et al., 2014).

Finally, mice harbouring a pericyte-specific knock-out of laminin γ1, PKO, also display an abnormal BBB (Gautam et al., 2016). Interestingly, only 10% of mutants exhibit any notable phenotype, and those which do display BBB breakdown almost always have hydrocephalus (Figure 4.31). PKO mice which have a disrupted BBB display reduced coverage of AQP4 and pericytes along with decreased staining of junction proteins ZO-1. Anecdotally, throughout this project I have had the impression that PRELP$^{-/-}$ brains were slightly larger, possibly directly linked to BBB disruption, I have no reliable evidence. I have attempted to determine differences in the water content of the brain (Figure 4.32); the results were unfortunately unreliable due to inaccurate mass measurements. It would be valuable to re-assess whether there is swelling in the PRELP$^{-/-}$ brains, to determine whether it is possible that BBB breakdown accompanies hydrocephalus, possibly an indication of the involvement of pericytic laminin.

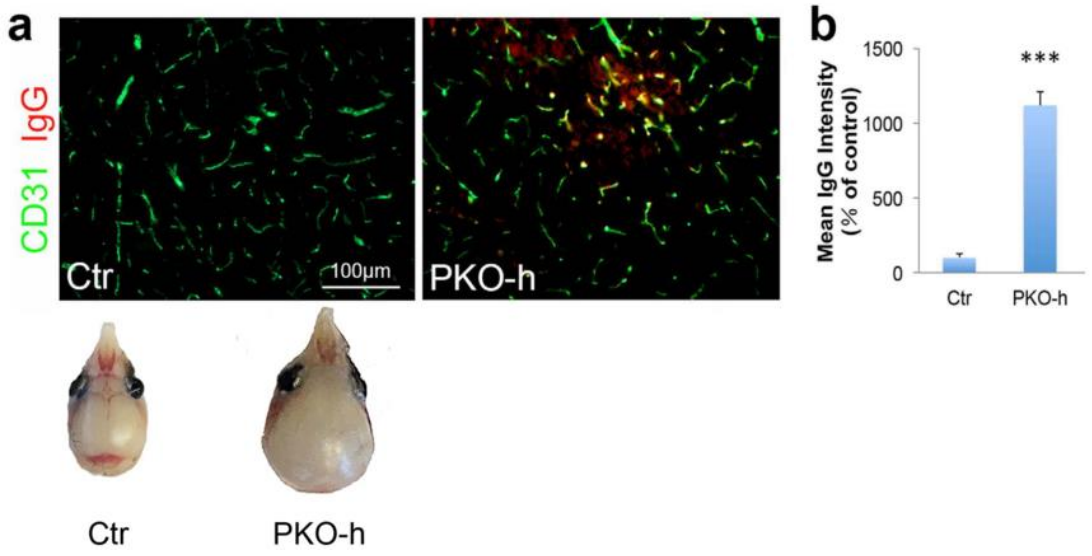

Figure 4.31. PKO-h mice have enlarged brains and BBB dysfunction as assessed by IgG leakage. Figure modified from (Gautam et al., 2016).

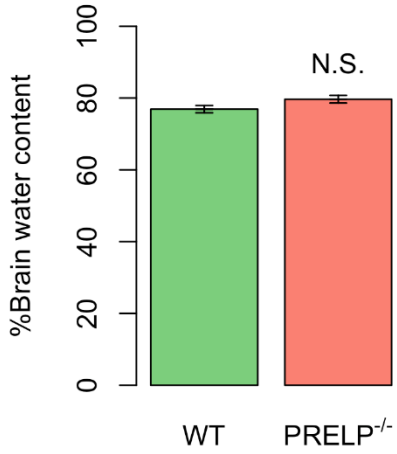

Figure 4.32. No change in % brain water content in PRELP$^{-/-}$. Brain water content was determined by measuring wet and dry mass. The % difference was then calculated. Error bars are the SEM where n=3.

I have demonstrated above that astrocytic laminin in the BM is a critical factor in the integrity of the BBB. The phenotype I observe in PRELP$^{-/-}$ seems to be most similar to Nγ1-KO mice, suggesting that the secretion or deposition of astrocytic laminin is disrupted in PRELP$^{-/-}$. The parallels in the phenotypes are striking and I have shown in Chapter 3 that PRELP is expressed by pericytes, suggesting that pericytic laminin deposition may be altered in PRELP$^{-/-}$. I have performed double staining of β-galactosidase and astrocyte marker GFAP and found no co-localisation. While not directly related to the BBB, I am aware of a recent publication suggesting that laminin-511 secreted by endothelial cells is capable of affecting leukocyte transmigration and stabilising VE-cadherin (Song et al., 2017). It would therefore be valuable to fully understand which isoform(s) of laminin are reduced in PRELP$^{-/-}$.

The deposition and stabilisation of laminin is strongly regulated by extracellular receptors and proteoglycans. Nidogens are secreted proteoglycans that have been shown to stabilise components of the extracellular matrix. Nidogen-1, for example, has been shown to be able to bind to the γ1 subunit of laminin (Hamill et al., 2009). Nidogen-1 and nidogen-2 single knock-out mice are viable and have a relatively normal life-span, with the only abnormality being over-expression of the other nidogen protein (Murshed et al., 2000; Schymeinsky et al., 2002). In contrast double knock-out of both nidogen-1 and -2 die shortly before birth or soon after and have a disrupted BM notably lacking laminin-411 (Bader et al., 2005), highlighting the importance of nidogen family members in the stabilisation of the BM. Since the nidogen-1 and -2 double knock-outs die just before or after birth, it would suggest that nidogens do not have a strong role in development, but rather the maintenance of tissues.

HSPGs perlecan and agrin have also been shown to have a role in the stabilisation of secreted laminin trimers. Perlecan is a multi-domain protein capable of binding a variety of ECM components including PRELP, laminin, nidogens, collagen IV and dystroglycan (Cabello et al., 2010). Despite a ternary complex between perlecan, laminin and nidogen-1 existing (Hopf et al., 1999), the role of perlecan in the deposition/stabilisation of laminin is unclear. Analysis of epidermal BM fractions indicated that perlecan is present in both laminin-enriched and collagen IV-enriched fractions, acting as a bridge between laminin and collagen IV networks (Behrens et al., 2012).

Perlecan knock-out mice die between E10-E12 and perinatally, despite having a mostly normal BM, aside from tissues suffering from mechanical stress, such as cardiac muscle cells leading to intrapericardial haemorrhages (Costell et al., 1999). This suggests that the function of facilitating BM assembly can be compensated for by another protein, such as agrin (Hohenester & Yurchenco, 2013). Agrin is another HSPG and is likely to be involved in linking laminin and collagen IV. Agrin has been shown to bind to laminins-111, -211 and -221 and its function particularly important in neuromuscular junctions (Samuel et al., 2012). Agrin is present in the vascular BM (Burgess et al., 2000), and was found to be important in the integrity of the BBB. For example, in glioblastoma, agrin was absent in the BM (Rascher et al., 2002); vessels lacking agrin exhibited weakened tight junctions and altered immunostaining of astrocyte end-foot marker AQP4, which I will discuss below.

It is known that PRELP binds to both perlecan and BM collagen (Bengtsson et al., 2002) and my analysis has indicated that there is a decrease in perlecan immunoreactivity in PRELP$^{-/-}$ brain vessels. Perlecan has heparin/heparan sulphate GAG chains in Domains I

and V (Farach-Carson & Carson, 2007); both laminin (Ettner et al., 1998) and PRELP (Bengtsson et al., 2002) interact with perlecan via binding to heparin/heparan sulphate moieties with similar affinities (Cabello et al., 2010). Therefore, it is possible that PRELP can act as an additional bridging molecule, bringing perlecan and laminin into close proximity to the collagen lattice of the BM (Figure 4.33). In addition, since agrin contains HS sidechains, PRELP may be able to bind to agrin and provide a similar function.

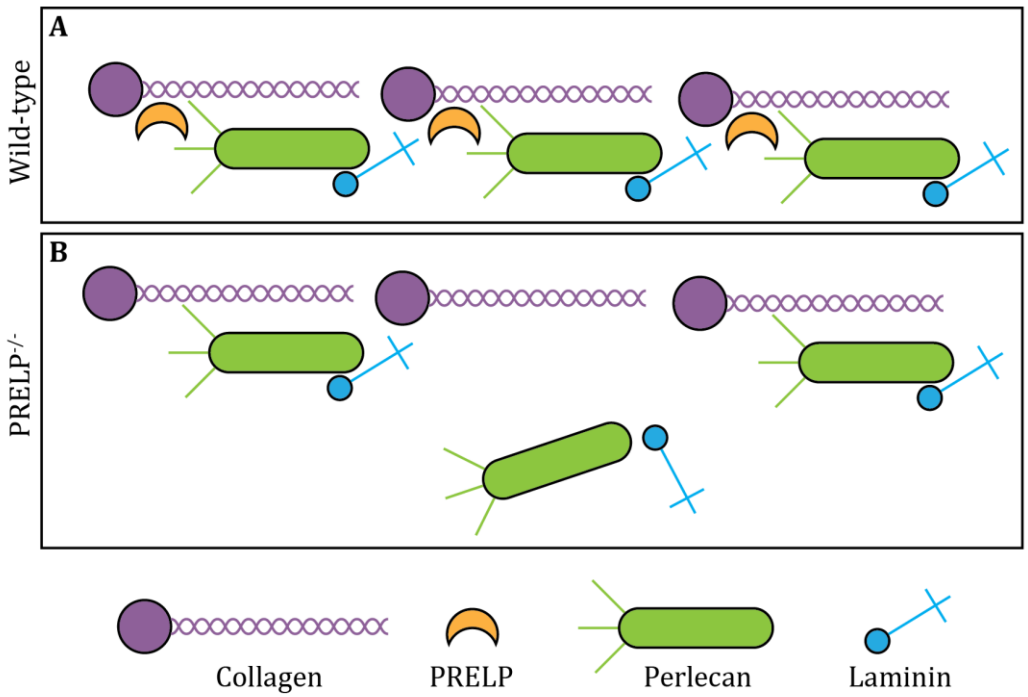

Figure 4.33. Schematic diagram illustrating the possible role for PRELP in the maintaining the integrity of the BM. In wild-type BMs **(A)**, PRELP acts to link perlecan and laminin to the collagen lattice. In contrast, in the absence of PRELP **(B)**, there is loss of perlecan and laminin.

PRELP is expressed by pericytes, which have direct contacts to the BM and endothelial cells. It is therefore possible that in the absence of PRELP, other components of the extracellular milieu are altered and could therefore have an effect on laminin deposition, providing a rationale for the phenotype I observe in PRELP$^{-/-}$ mice. Furthering our understanding of the changes in the extracellular environment of PRELP$^{-/-}$ BM would be necessary.

I observed a decrease in the intensity of astrocyte end-feet staining in PRELP$^{-/-}$. Astrocytes have been demonstrated to being critical in the induction of BBB properties in endothelial cells, in addition to other functions such as regulating cerebral blood flow. The permeability of an endothelial monolayer in culture is greatly decreased by co-culture with astrocytes (Wang et al., 2015). Conditioned medium from astrocyte culture applied to endothelial cells can also improve their barrier properties (Winger et al., 2014),

suggesting that this effect is mediated by soluble factors secreted by astrocytes. It is now known that astrocytes secrete growth factors such as GDNF, bFGF and Ang-1 (Alvarez et al., 2013).

Astrocyte end-feet are enriched with the water and potassium channels AQP4 and Kir4.1. The exclusive distribution of AQP4 to astrocyte end-feet is dependent on agrin (Noell et al., 2009), where agrin directly influences the insertion of AQP4 into the end-foot membrane. From the results in this chapter, I have only determined that the immunoreactivity of end-foot marker AQP4 is decreased. It is unclear whether there is decreased gliovascular contact, or whether there are disruptions in the insertion of AQP4 into end-feet. Nonetheless, other publications studying BBB breakdown have noted that AQP4 immunostaining is frequently decreased in their models (Gautam et al., 2016; Isasi et al., 2014; Menezes et al., 2014; Yao et al., 2014). Of note, Menezes and co-workers noted that the distribution of AQP4 is perturbed in their *Lama2*$^{-/-}$ mice, since the decrease in AQP4 immunoreactivity was accompanied by no change in global AQP4 protein levels, as assessed by western blotting. In contrast, work by Yao and colleagues have noted a decrease in AQP4 immunoreactivity and protein levels by western blotting. Loss of organised clusters of AQP4 channels in end-feet have been linked to BBB breakdown in experimental autoimmune encephalomyelitis (Wolburg-Buchholz et al., 2009). Therefore, it would be valuable to extract protein from our transgenic animals and determine whether there are global changes in AQP4 protein expression. As mentioned previously, HSPG agrin can affect astrocyte polarity, and therefore it is possible that the phenotype observed is due to decreased AQP4 insertion in end-feet as a result of altered ECM architecture.

The final component of the BBB I analysed was pericytes. Pericytes act to protect the BBB by providing stabilising interactions via pericytic processes. As discussed above, pericyte-specific loss of laminin leads to mild BBB perturbation (Gautam et al., 2016), and therefore a loss of overall pericyte coverage probably decreases the deposition of pericytic laminin. Gene expression analysis of vessels lacking pericytes identified changes in expression of key genes implicated in vascular permeability, notably an increase in *vegfa* expression (Armulik et al., 2010).

I determined that there is a decrease in pericyte coverage in PRELP$^{-/-}$. Initial attempts to label pericytes using NG2 were unsuccessful as PRELP$^{-/-}$ pericytes often exhibited poor staining. An alternative marker was used to label pericytes; PDGFR-β. While PDGFR-β is also frequently used in the literature as a means to label pericytes, I found that clear immunostaining was difficult to obtain. As a result, double staining of PDGFR-β and

tomato lectin was performed. Pericytes were manually identified by staining with PDGFR-β in conjunction with their morphology, and values were normalised by vessel length. While there may have been errors in manual discrimination of pericytes versus endothelial cells, the use of a pericyte-specific marker and the fact that the nuclei of pericytes and endothelial cells are quite different, I am confident that errors were kept to a minimum. I found the pericyte coverage of wild-type brain vessels to be close to literature-cited values of approximately 30% (Mathiisen et al., 2010). Therefore, the results obtained from manual quantification of pericyte numbers should be reliable.

Immunostaining of cell-cell junction proteins indicated that there is a small overall decrease in their expression levels along the vessels in PRELP$^{-/-}$ mice (Figure 4.16, Figure 4.17, Figure 4.18). It was evident that the distribution of junction proteins was different between PRELP$^{-/-}$ and wild-type, where staining in PRELP$^{-/-}$ was found to be more discontinuous. Analysis of total protein levels by western blotting would be interesting – for example, data from laminin knock-out animals have indicated that there is a reduction in total VE-cadherin, claudin-5 and occludin (Menezes et al., 2014; Yao et al., 2014). In addition, analysis of specific phosphorylated forms of junction proteins could also be interesting; for example, phosphorylation of VE-cadherin Y685 has been shown to regulate vascular permeability; knock-in Y685F mice have reduced BBB breakdown compared to wild-type upon stimulation with VEGF (Wessel et al., 2014).

Overall, my data indicates that there is BBB breakdown in PRELP$^{-/-}$.

4.5.4 BBB breakdown in PRELP$^{-/-}$ is likely to be mild

BBB breakdown often leads to inflammation, notably microglial and astrocytic activation. Since I have demonstrated that there is BBB in PRELP$^{-/-}$, I sought to examine whether there is increased inflammation.

Analysis of total microglia indicated that there is an increase in the number of microglia (Figure 4.19). While I had previously attempted to manually distinguish ramified and amoeboid microglia, assessing microglia in between those distinct states was challenging. Manual analysis was unreliable, as I found that analysis of the same image on separate days could result in slightly different findings. By utilising an automated method of skeletonising microglial processes (Figure 4.20), I have analysed microglia in a more consistent manner. The results indicate that on average, microglia in PRELP$^{-/-}$ have fewer ramifications, indicative of an increased population of amoeboid cells (Figure 4.21).

Since PRELP is expressed on microglia, it is possible that the absence of microglial PRELP has an effect on the microglia, regardless of the state of the BBB. A study has suggested

that microglial heparin/heparan sulphate is critical for the inflammatory response (O'Callaghan et al., 2015). Using transgenic mice overexpressing heparanase (Hpa-tg), the authors have demonstrated that the response to LPS is attenuated in Hpa-tg mice compared to the wild-type. LPS interacts with CD14, which activates the TLR4/MD2 inflammatory pathway, resulting in the release of TNF-α and IL1β (Allan et al., 2005; Godowski, 2005). LPS treatment of Hpa-tg mice resulted in a reduction of TNF-α release and limited IL1β. It should be noted that in this study, mice were exposed to LPS for 24 hours, whereas no stress was introduced in my experiments.

Therefore, it is possible that PRELP binding to heparin/heparan sulphate molecules on the surface of microglia can regulate their inflammatory state by masking HS sidechains. In the case of PRELP$^{-/-}$ mice, these heparin/heparan sulphate moieties would be more exposed, making the animals more susceptible to inflammation. Nonetheless, the increase in microglial activation is consistent with my findings regarding BBB breakdown.

Next, I analysed the number of astrocytes labelled with GFAP and measured the overall staining intensity of GFAP (Figure 4.22, Figure 4.23). An increase in astrocytes in addition to increased expression of GFAP are indicative of astrogliosis. My results indicate that there were no differences between either OMD$^{-/-}$/PRELP$^{-/-}$ and wild-type with respect to GFAP. This finding was rather surprising, and perhaps indicates that BBB breakdown is a relatively mild stressor. The induction of astrocytes typically occurs when neuronal death occurs, where astrocytes proliferate to fill the gaps left by dead neurons. These results therefore suggest that the leakage of plasma proteins is not sufficient to cause notable neuronal death.

To summarise, investigation of the inflammatory state of the PRELP$^{-/-}$ brain suggests that the BBB breakdown is relatively mild, as only microglia were activated. There was no evidence of up-regulation of GFAP or any changes in the number of GFAP-positive astrocytes.

4.5.5 No phenotype observed in OMD$^{-/-}$

OMD$^{-/-}$ embryonic hindbrains were compared to wild-type, and I did not observe any differences between them in terms of vascular density. As explained above, I did not pursue this line of experiments, given that pregnant mice had to be culled each time embryos were required for analysis.

I analysed the BBB of OMD$^{-/-}$ mice. As I demonstrated in Figure 4.5, I occasionally see vessels exhibiting leaked IgG, however a more systematic quantification of IgG in the

parenchyma indicated that this is not significant. This is indeed confirmed when using tracer dyes to confirm BBB leakage; I observed no areas of 70kDa Dextran leakage.

Since several phenotypes were observed in PRELP$^{-/-}$, I opted to continue analysis of the BBB and included OMD$^{-/-}$ tissue sections in this analysis. Since I quantified cells associated with the BBB of the cerebellum in PRELP$^{-/-}$, the same set of experiments was mirrored in OMD$^{-/-}$. As expected, I did not observe any changes in the components of the BBB in OMD$^{-/-}$, nor in the tight junctions of the endothelium. Finally, I did not observe any changes related to an increase in inflammation by analysing microglia and astrocyte number and morphology in OMD$^{-/-}$.

To conclude, I did not observe any difference between OMD$^{-/-}$ and wild-type brain vasculature.

4.6 Conclusions

To summarise, PRELP$^{-/-}$ animals have numerous abnormalities with respect to brain vasculature. Using the embryonic hindbrain, I have shown that PRELP$^{-/-}$ has increased blood vessel content. With regards to adult brain vasculature, I have demonstrated that PRELP$^{-/-}$ have a disrupted BBB by IgG staining and presence of 70kDa Dextran in the brain parenchyma. Analysis of BBB components indicated that the absence of PRELP in capillaries results in decreased BM components laminin and perlecan, reduced attachment of astrocyte end-feet and sparser coverage by pericytes. Analysis of the cell-cell junction proteins VE-cadherin, ZO-1 and claudin-5 in PRELP$^{-/-}$ indicated that the staining patterns were abnormal compared to the wild-type. Microglia in PRELP$^{-/-}$ were found to be more numerous and had fewer branches, indicative of a higher proportion of activated microglia. No differences were detected in the activation state of PRELP$^{-/-}$ astrocytes.

Chapter 5 Gene expression analysis of OMD$^{-/-}$ and PRELP$^{-/-}$ using microarray and RNA sequencing

5.1 Preface

I have previously determined that PRELP is expressed by pericytes in brain vasculature. Upon further examination of the characteristics of this vasculature, I have demonstrated that PRELP brain vasculature is abnormal. In order to identify the signalling pathways which are disrupted, transcriptome analysis using microarrays and RNA sequencing was performed. In contrast, no differences were found in OMD$^{-/-}$ vessels; transcriptome analysis was therefore utilised to discover pathways which may be regulated by OMD.

5.2 Microarray study

5.2.1 Comparing the transcriptomes of adult wild-type, OMD$^{-/-}$ and PRELP$^{-/-}$ ventral arteries

Prior to the commencement of this PhD project, a previous member of our laboratory Dr Noriaki Sasai extracted RNA from a large vessel in the abdomen (ventral artery) from adult OMD$^{-/-}$, PRELP$^{-/-}$ and wild-type mice. The microarray experiment was performed by our collaborator Dr. Ryuji Hamamoto, University of Chicago (USA), using Affymetrix mouse 430A2 chips. Two samples per genotype were analysed. The raw output files were received and processed and analysed using R to compile a list of significant and differentially-expressed genes; see Appendix 1 for the full R script.

To begin with, microarray data needs to be pre-processed before a meaningful list of genes can be compiled. In general, for gene expression analysis, I need to ensure that noise is reduced as much as possible without interfering with potential and biologically-relevant outliers. To do this, I assume that when comparing different samples, most genes are unchanged and only relatively few genes are over- and under-expressed in one array relative to others. In particular, for the Affymetrix platform, normalisation is critical in order to obtain probe values which accurately represent gene expression levels. Affymetrix provides one-colour data, where one specific set of probes, known as a probe set, is used to assess each gene. Each probe set consists of 10 to 20 probe pairs, where each probe pair consists of one perfect match (PM) and one mismatch (MM) probe (Figure 5.1).

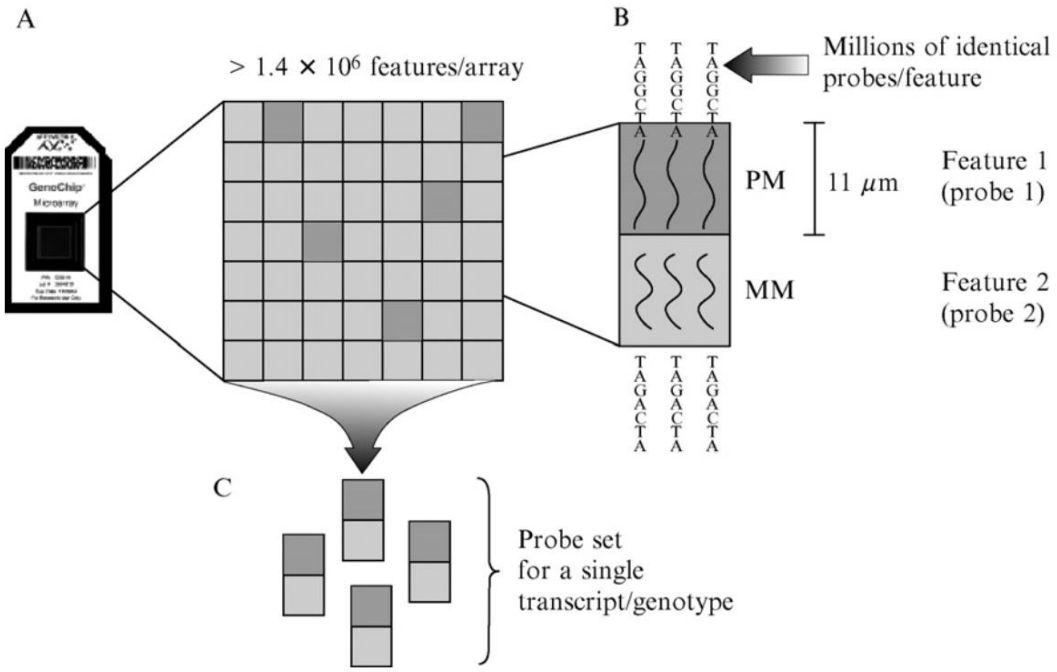

Figure 5.1. Affymetrix probe sets are comprised of perfect match (PM) and mis-match (MM) probes. Figure from (Dalma-Weiszhausz, Warrington, Tanimoto, & Miyada, 2006).

PM and MM probes are almost identical, apart from a single nucleotide difference in the MM probes (Dalma-Weiszhausz, Warrington, Tanimoto, & Miyada, 2006). The MM probes are designed to estimate the amount of non-specific signal given by a probe of this sequence. Therefore, in order to obtain information on the expression levels of genes, PM and MM data must be combined in order to obtain the summary of probe sets; i.e. obtain an aggregate estimate of the abundance of a sequence. To this end, there are three main normalisation methods which are typically used: MAS5, RMA and gcRMA (Liu, Milo, Lawrence, & Rattray, 2005).

In order to remove background intensity, normalisation methods rely on subtracting MM data from PM to determine an estimate average signal (i.e. signal = PM – MM). In the case of MAS5 (MicroArray Suite 5.0) normalisation, MM values are subtracted from PM intensities and an overall intensity value is estimated using a single-step Tukey's biweight statistic (Hubbell et al., 2002). Tukey's biweight functions by associating a weight to each value according to its distance to the median, correcting for non-specific binding of probes but also introducing noise. The main problem with MAS5 normalisation is the loss of probe-level information and increased noise at low intensity levels due to subtraction of MM probe data (Irizarry et al., 2003; Stafford & Brun, 2007) – the presence of noise is particularly troublesome in large gene expression datasets.

The RMA (Robust Multi-Array Average) normalisation method subtracts MM data according to the MAS5 method (above), correcting for non-specific hybridisation but also increasing noise in the dataset. RMA also employs background correction which functions by assuming that PM data is a combination of background and signal; i.e. PM = signal + background. In addition, it also summarises probe sets by median polishing whereby each gene's probes are normalised to its median and repeated until medians converge (Irizarry et al., 2003). The advantage of RMA is that it is robust – this is particularly important in order to detect potential outliers in large datasets.

This is demonstrated in Figure 5.2, where MAS5-normalised data shows increased noise at lower intensities due to subtraction of MM data. Such plots are useful in determining whether there is any probe intensity-dependent variation within the dataset. MVA plots compare the log ratio and mean of probe sets. Log ratio on the y-axis is denoted as M (M; from "minus" on the log scale) and mean values (A; average) are on the x-axis. These are easily done in two-colour experiments, where M = log2(red) – log2(green) for example. In the case of one-colour experiments, at least two arrays are required to draw an MVA plot.

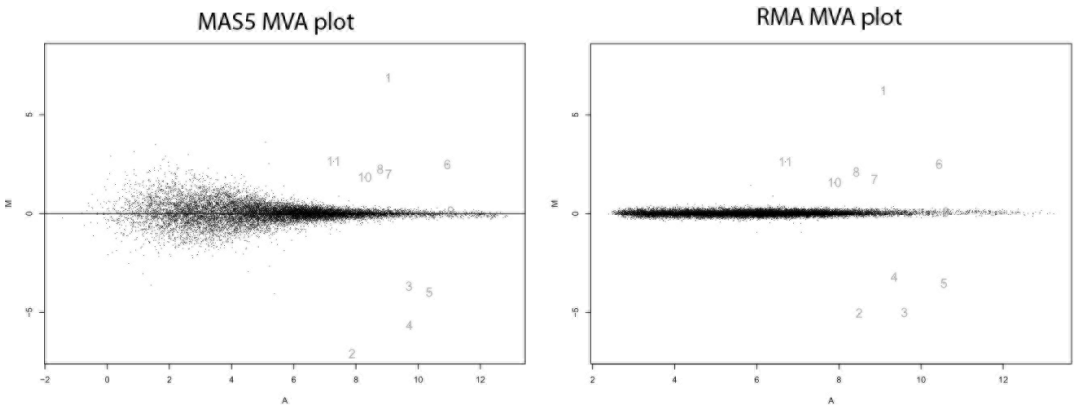

Figure 5.2. MVA plots demonstrating the differences between MAS5 and RMA normalisation. Modified from (Irizarry et al., 2003). Note that after MAS5 normalisation, there is noise at lower probe intensities. This is not the case for RMA normalisation, where there doesn't seem to be any intensity-dependent effects.

Finally, GC-RMA is another widely-used method. It is very similar to RMA, however it calculates background noise differently. MM probe data is adjusted based on thermodynamic properties of nucleic acids (Stafford & Brun, 2007); i.e. GC-RMA weights stronger G:C bonds differently to the comparatively weaker A:T bonds. Hence, probe affinity is determined and then subtracted from PM data, instead of simply being subtracted like in the case of standard RMA normalisation.

Since normalisation is such a critical step in microarray experiments, I performed all of the above normalisations and compared the results in order to determine which normalisation method is most appropriate for the dataset. Please refer to Appendix 2 for R codes related to microarray analysis.

To begin with, I produced boxplots and histograms in order to visualise the distribution, range and median of the data before and after normalisation (Figure 5.3, Figure 5.4). It is immediately apparent that the data has a relatively even distribution – this can be seen in the boxplots, where the range and median are very similar. The exception is PRELP$^{-/-}$ (1), where the third quartile of probe intensities is slightly smaller than for probe intensities from other gene chips (Figure 5.3). Note that after MAS5 normalisation, the range of the data is from approx. 0 to 100,000; this is because this normalisation method changes the overall distribution of the dataset such that it is completely different from raw, RMA- or GC-RMA normalisations. I can clearly see that there is quite a lot of variation in the maximum intensity values after MAS5 normalisation, suggesting that RMA or GC-RMA may be more appropriate. From these boxplots alone, however, it is impossible to determine whether RMA or GC-RMA should be utilised.

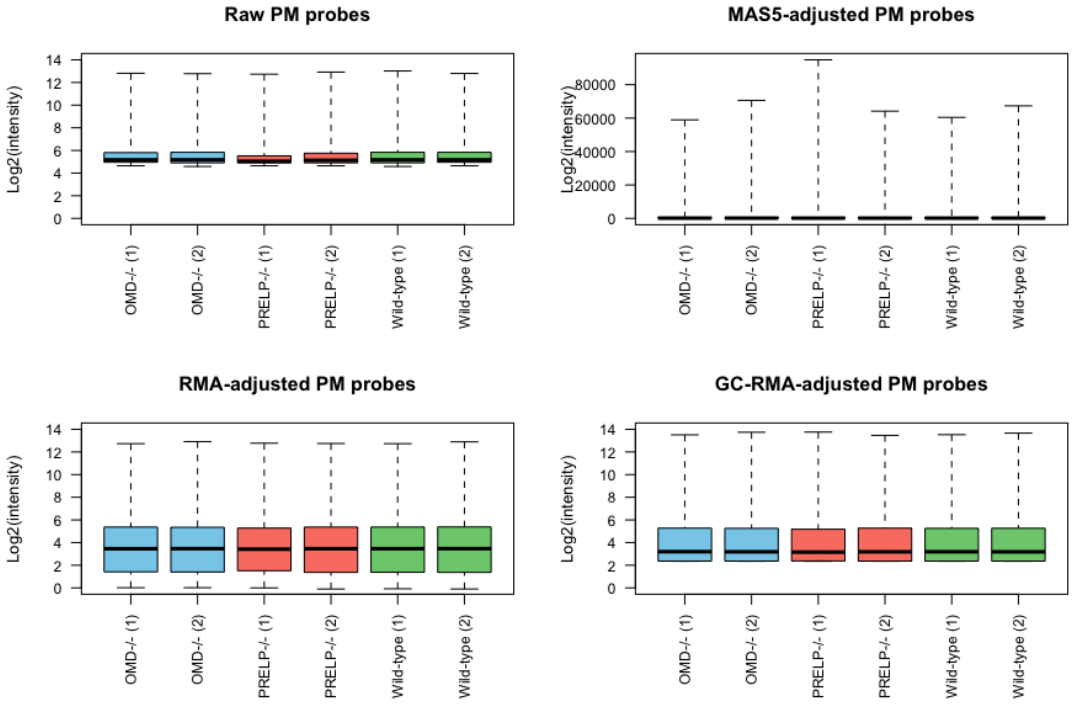

Figure 5.3. Boxplots of PM probe intensities before and after applying normalisation methods.

I therefore plotted histograms to visualise the distribution of the data in more detail (Figure 5.4). Visually, I determine that the raw PM intensities are quite similar, with the

exception of a single gene chip set corresponding to sample PRELP$^{-/-}$ (1), whereby there is an increase in probe intensities at approximately $\log_2 5$. I can also see that this irregularity is still present in the distribution obtained after MAS5 normalisation; therefore, MAS5 normalisation is not appropriate for this dataset. In the case of RMA normalisation, the same gene chip data is shifted slightly to the right. This is not the case when GC-RMA normalisation is applied; in fact, the distributions of all curves are extremely similar. Hence, it seems likely that GC-RMA is the most appropriate normalisation method to utilise.

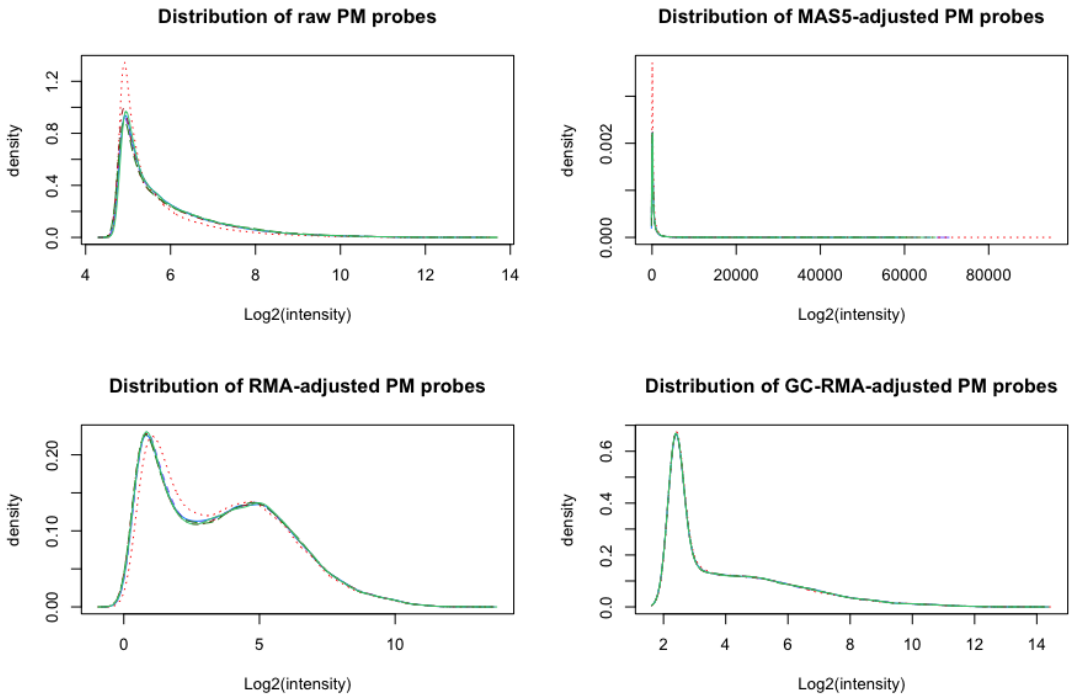

Figure 5.4. Distribution of probe intensities before and after applying normalisation methods. Note that one gene chip (red; corresponds to PRELP$^{-/-}$ (1)) conforms poorly with the rest of the dataset in the raw, MAS5 and RMA-adjusted probes.

MVA plots were plotted to determine whether there were any intensity-dependent effects that arose from the normalisation procedure. In Figure 5.5, I can visually see the relationship between log ratio and average probe intensities in the MVA plots. In addition, statistical parameters median and IQR (inter-quartile range) were also calculated; IQR is a measure of variability of the dataset. MAS5-normalised data clearly has skewed intensity-dependent artefacts (assessed by the red fit line; it is not even close to x=0). Comparing RMA versus GC-RMA, I can also see that RMA data has a higher level of noise, as assessed by its higher IQR values. I therefore conclude that GC-RMA is likely to be the best normalisation method for my microarray experiment.

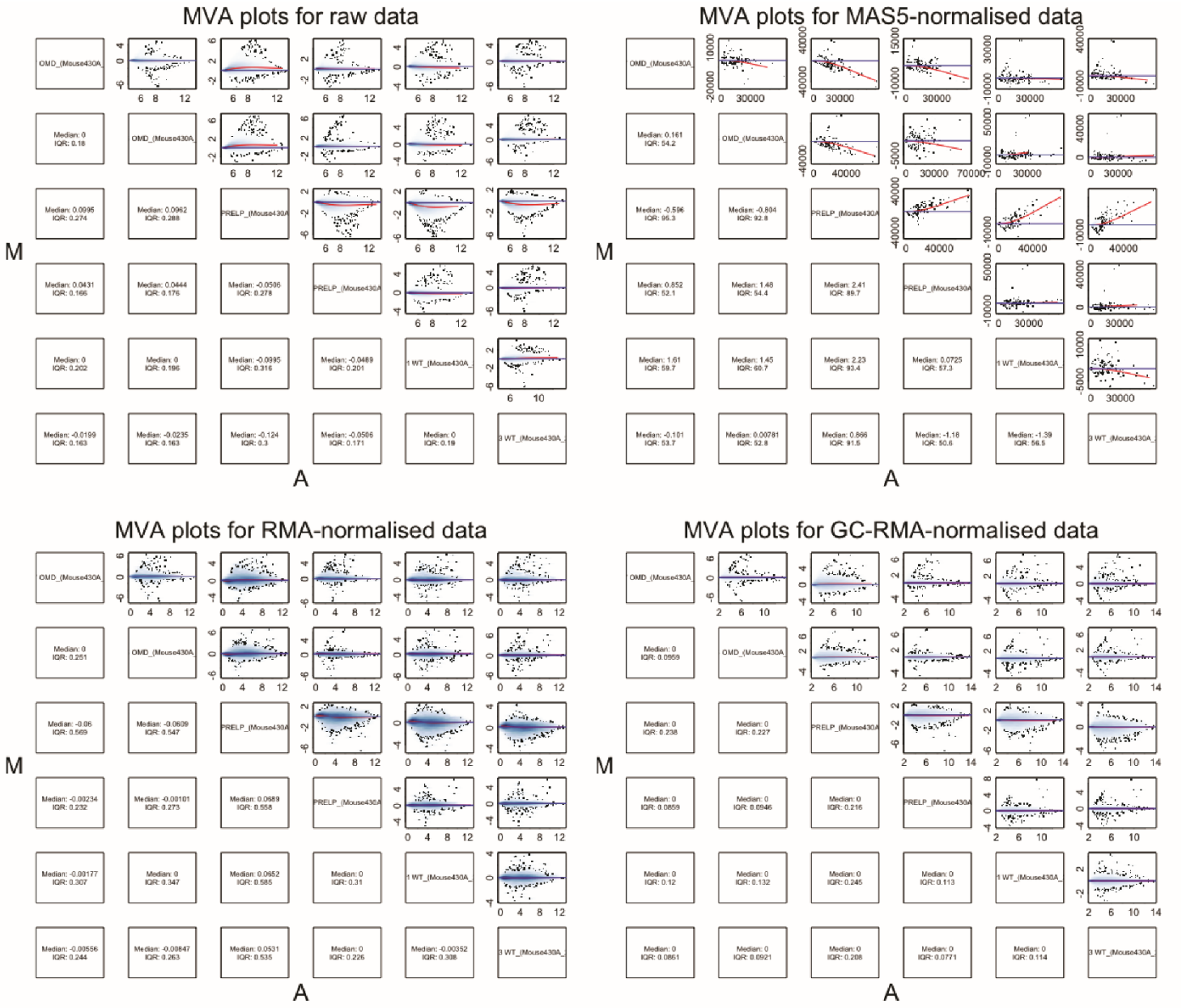

Figure 5.5. MVA plots before and after normalisation. Statistical parameters median and IQR (inter-quartile range) were also calculated.

Now that I have identified the normalisation method which is most appropriate with this dataset, I then proceeded to determine a list of significantly altered genes, comparing wild-type to OMD$^{-/-}$ and wild-type to PRELP$^{-/-}$. In essence, raw .CEL files were extracted and converted to a series of data frames, which could easily be manipulated. Since I only had 2 samples per genotype, I performed an unpaired 2-tailed Student's t-test assuming unequal variance to calculate unadjusted p-value for each gene. I then plotted the distribution of p-values, shown in Figure 5.6, where red bars indicate p-values less than 0.05. It is evident that the majority of genes in this dataset are not statistically significant, and only a very small portion where $p < 0.05$, particularly when comparing PRELP$^{-/-}$ to

wild-type. This could be due to the small sample size of n=2, poor RNA preparation or genuinely subtle differences between wild-type and mutant samples.

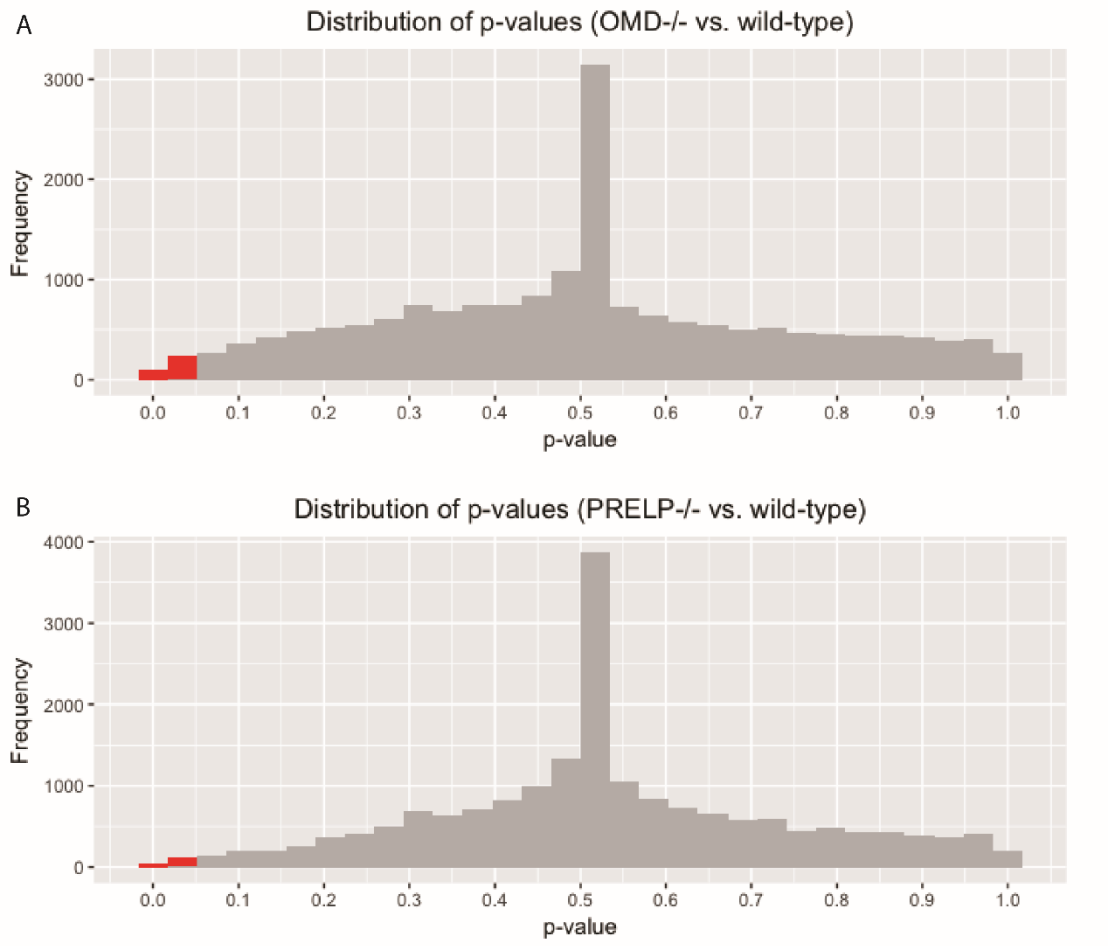

Figure 5.6. Distribution of p-values across microarray dataset. A) p-values obtained from comparison of OMD$^{-/-}$ and wild-type. **B)** p-values obtained from comparison of PRELP$^{-/-}$ and wild-type. Values $p<0.05$ are in red.

From the list of significant genes, I drew heatmaps comparing OMD$^{-/-}$ to wild-type and PRELP$^{-/-}$ to wild-type (Figure 5.7). It is evident when visualising this data that the differences in gene expression are rather small, and that many genes could potentially be false-positives; i.e. found to be statistically-significant purely by chance.

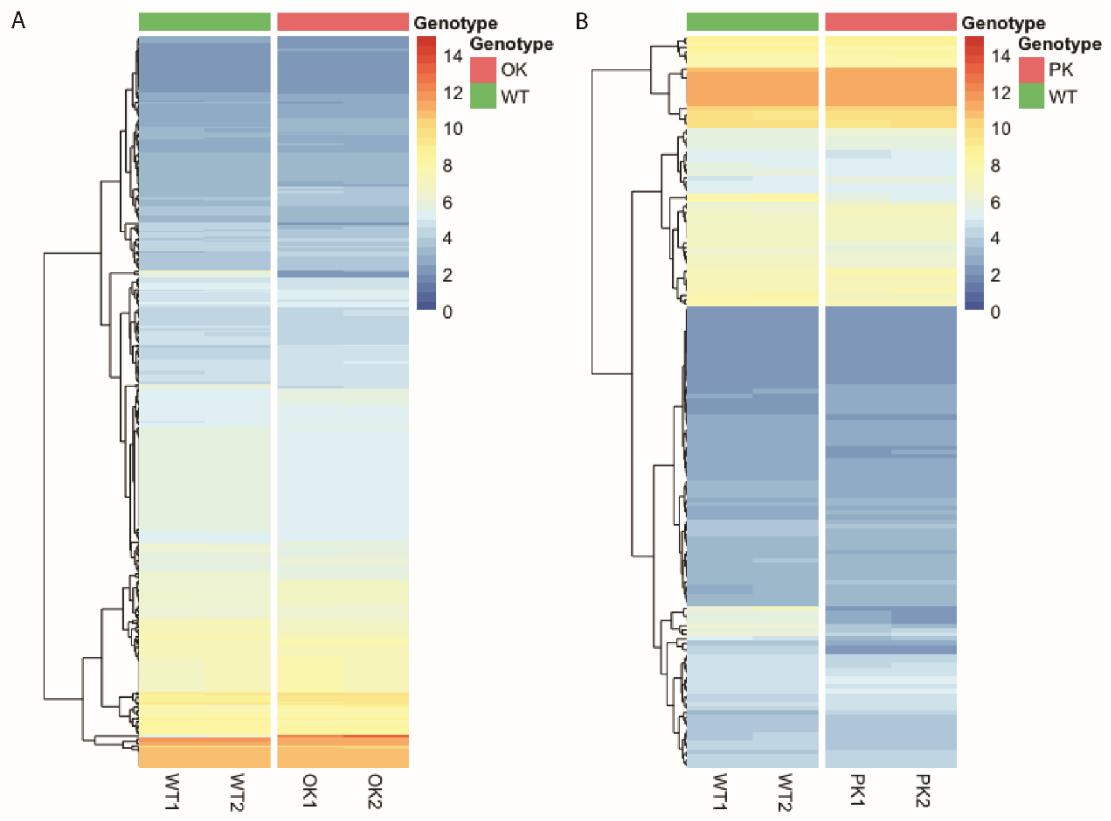

Figure 5.7. Heatmaps for differentially-expressed genes (where p<0.05) for OMD$^{-/-}$ and PRELP$^{-/-}$ datasets. Gene expression values are expressed as log2. Rows are clustered according to expression levels, and similarity is shown as a dendrogram.

Given the poor distribution of p-values when conducting t-tests, I sought to use a different statistical test to determine significant genes. To this end, I performed Significance Analysis of Microarray (SAM) which was developed specifically to detect differentially expressed genes with fewer false positives (Tusher, Tibshirani, & Chu, 2001). SAM works by performing a series of t-tests and assigning a score to each gene based on the standard deviation of repeated measurements. If the score is higher than a threshold (Δ), it is deemed to be a significant gene. Unlike standard t-tests, SAM uses non-parametric statistics which do not rely on the dataset following a normal distribution.

In practice, SAM analysis is performed and before a list of significant genes is extracted, the researcher consults a table corresponding to the tuning value Δ and an estimated False Discovery Rate (FDR). Based on this table of values, an appropriate value for Δ is selected based on the FDR and I can obtain the list of significant genes. FDR is arguably a much more appropriate parameter to utilise for cut-offs of large transcriptome datasets; FDR = 0.1 indicates that, at most and in expectation, 10% of the genes in the list would be false positives.

I performed this analysis on my datasets and obtained a table of Δ and local FDR values (Table 5.1). From these data, I can clearly see that even at high values of Δ, the FDR remains extremely high; 0.492 for wild-type vs. $OMD^{-/-}$ and 0.481 for wild-type vs. $PRELP^{-/-}$. This indicates that almost half of detected genes are potentially false-positives and is particularly detrimental given the number of detected genes at these high Δ levels is very low – 18 and 9 for $OMD^{-/-}$ and $PRELP^{-/-}$ respectively. Again, this situation is quite similar to when I attempted to extract a list of significant genes from p-value (above); this could be due to the small sample size, poor RNA quality or minimal biological differences between wild-type and knock-out samples. Given that there are only 2 samples per genotype, it is quite likely that this is the source of the extremely high FDRs calculated in this analysis.

	Wild-type vs. OMD$^{-/-}$			Wild-type vs. PRELP$^{-/-}$		
Δ	FALSE	Called	FDR	FALSE	Called	FDR
0.5	258.333	304	0.766	10.167	11	0.924
1.0	63.833	80	0.719	10.167	11	0.924
1.5	45.833	61	0.677	10.167	11	0.924
2.0	41.5	59	0.634	7	10	0.7
2.5	36.667	52	0.636	7	10	0.7
3.0	28.667	45	0.574	7	10	0.7
3.5	28.667	45	0.574	7	10	0.7
4.0	23.5	37	0.572	7	10	0.7
4.5	22	36	0.551	7	10	0.7
5.0	21	35	0.541	7	10	0.7
5.5	21	35	0.541	7	10	0.7
6.0	14	23	0.549	7	10	0.7
6.5	13.167	22	0.539	7	10	0.7
7.0	11.667	20	0.526	7	10	0.7
7.5	11.667	20	0.526	7	10	0.7
8.0	11.667	20	0.526	4.333	9	0.481
8.5	11.667	20	0.526	4.333	9	0.481
9.0	10.5	19	0.498	4.333	9	0.481
9.5	10.5	19	0.498	4.333	9	0.481
10	9.833	18	0.492	4.333	9	0.481

Table 5.1. Relationship between Δ tuning value and FDR for datasets of differentially-expressed genes for wild-type and OMD and PRELP knock-outs. For each value of Δ, the number of estimated false-positive (FALSE) and true-positive (Called) genes is determined to calculate an estimated local FDR.

Despite the high FDR, I chose Δ = 10 and constructed a heatmap to visualise these significant genes detected using SAM (Figure 5.8). Even when using a much more stringent method to remove non-significant genes, the heatmaps reveal that the differences in gene expression remain extremely subtle. In addition, SAM analysis of the PRELP$^{-/-}$ dataset did not even detect PRELP itself as being a differentially-regulated gene. Finally, given that there are so few significant genes detected, ontology analysis would not be meaningful in this instance.

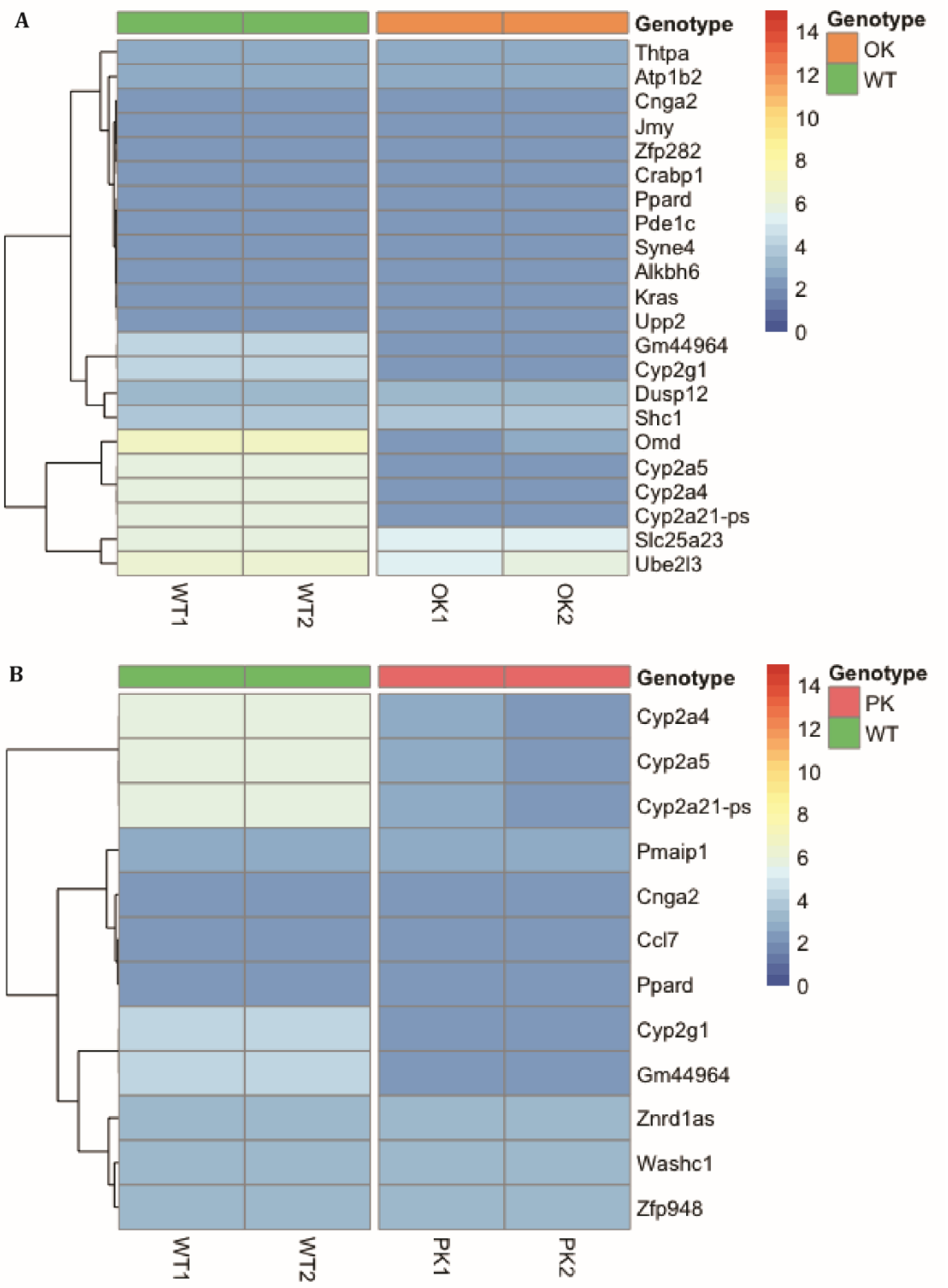

Figure 5.8. Heatmaps of differentially-expressed genes in OMD$^{-/-}$ (A) and PRELP$^{-/-}$ (B) as assessed by SAM analysis. Rows are clustered according to expression levels, and similarity is shown as a dendrogram.

To conclude, I have explored the microarray dataset of RNA extracted from a large ventral vessel from wild-type, OMD$^{-/-}$ and PRELP$^{-/-}$. I attempted to normalise the dataset using MAS5, RMA and GC-RMA and have determined that GC-RMA normalisation is the most

appropriate. Using t-tests and a p-value cut-off at $p < 0.05$, I have detected 449 and 169 significant genes for $OMD^{-/-}$ and $PRELP^{-/-}$ respectively. However, upon further inspection of the heatmaps obtained as well as the distribution of significant p-values, I have concluded that the data is not ideal. Statistically-significant genes show very small differences between wild-type and knock-out samples and the distribution of p-values was also found to be unexpected, where most p-values were found to be around $p = 0.5$. In addition, I utilised an alternative method, SAM, to detect significant genes. This analysis indicated that there is an extremely high estimated FDR in the dataset, and even at very high threshold values ($\Delta = 10$), only a small list of significant genes could be determined. This is likely a consequence of the small sample size, where I only analysed two samples per genotype.

5.2.2 Ontology analysis of differentially-expressed genes in $OMD^{-/-}$

As described above, although the dataset is not ideal, I attempted to perform ontology analysis. To this end, the DAVID (Database for Annotation, Visualization and Integrated Discovery) (Huang et al., 2009) resource was probed to determine whether any pathways are differentially-regulated using the t-test dataset, as the SAM dataset does not return enough genes for meaningful ontology analysis. I therefore input the probe IDs into DAVID and extracted the list of KEGG (Kyoto Encyclopedia of Genes and Genomes) pathways deemed to be significantly-enriched. Acknowledging that these data derived from a large abdominal vessel is not ideal for my study, I hoped to uncover the larger trends of pathways affected by OMD and PRELP, rather than focusing on smaller details.

The results of analysis using DAVID are shown in Table 5.2 for the data comparing significantly-altered genes between $OMD^{-/-}$ and wild-type, with a total number of pathways of 42.

There are clearly results which are related to others; for example, there are several specific classes of cancer: Chronic myeloid leukaemia, Thyroid cancer, Acute myeloid leukaemia, Endometrial cancer and Colorectal cancer in addition to more general entries such as Pathways in cancer and Proteoglycans in Cancer. The presence of chronic and acute myeloid leukaemia is interesting; the literature suggests that certain SLRP members are expressed in particular in chronic myeloid leukaemia, including opticin (Mikaelsson et al., 2013), PRELP (Mikaelsson et al., 2015) and fibromodulin (Mikaelsson et al., 2005). In addition, ontology analysis also detected B-cell and T-cell receptor pathways, and numerous pathways involving immunity against pathogens, indicating that OMD may have a role in the adaptive immune system.

Pathway	KEGG code	Count	p-value	FDR
cAMP signaling pathway	mmu04024	12	0.001	0.0045
Melanogenesis	mmu04916	8	0.001	0.0142
Chemokine signaling pathway	mmu04062	10	0.005	0.0578
Estrogen signaling pathway	mmu04915	7	0.005	0.0644
B cell receptor signaling pathway	mmu04662	6	0.006	0.0687
HTLV-I infection	mmu05166	12	0.006	0.0692
Chronic myeloid leukemia	mmu05220	6	0.006	0.077
Thyroid cancer	mmu05216	4	0.011	0.1361
Pathways in cancer	mmu05200	14	0.013	0.1487
Acute myeloid leukemia	mmu05221	5	0.013	0.1531
Sphingolipid signaling pathway	mmu04071	7	0.016	0.1827
MAPK signaling pathway	mmu04010	10	0.022	0.2505
Choline metabolism in cancer	mmu05231	6	0.024	0.2708
Tight junction	mmu04530	7	0.026	0.285
T cell receptor signaling pathway	mmu04660	6	0.027	0.2978
Wnt signaling pathway	mmu04310	7	0.028	0.3002
Natural killer cell mediated cytotoxicity	mmu04650	6	0.028	0.307
Prolactin signaling pathway	mmu04917	5	0.031	0.3316
Salmonella infection	mmu05132	5	0.038	0.3924
Oxytocin signaling pathway	mmu04921	7	0.044	0.4393
Antigen processing and presentation	mmu04612	5	0.045	0.4422
Proteoglycans in cancer	mmu05205	8	0.048	0.4666
Neurotrophin signaling pathway	mmu04722	6	0.049	0.4734
Gap junction	mmu04540	5	0.052	0.492
Endometrial cancer	mmu05213	4	0.053	0.4987
Herpes simplex infection	mmu05168	8	0.053	0.5043
Rap1 signaling pathway	mmu04015	8	0.060	0.5492
cGMP-PKG signaling pathway	mmu04022	7	0.061	0.5502
Influenza A	mmu05164	7	0.061	0.5502
Regulation of lipolysis in adipocytes	mmu04923	4	0.066	0.5806

Maturity onset diabetes of the young	mmu04950	3	0.071	0.6106
VEGF signaling pathway	mmu04370	4	0.074	0.627
Long-term depression	mmu04730	4	0.077	0.6419
Insulin signaling pathway	mmu04910	6	0.079	0.6483
Ras signaling pathway	mmu04014	8	0.080	0.6573
Colorectal cancer	mmu05210	4	0.086	0.6847
Chagas disease (American trypanosomiasis)	mmu05142	5	0.087	0.6894
Pyrimidine metabolism	mmu00240	5	0.087	0.6894
Glioma	mmu05214	4	0.090	0.6983
Hepatitis B	mmu05161	6	0.090	0.7009
Renal cell carcinoma	mmu05211	4	0.096	0.7244
Fc epsilon RI signaling pathway	mmu04664	4	0.099	0.737

Table 5.2. DAVID pathway analysis for OMD$^{-/-}$ dataset. Pathways with p-value < 0.05 are highlighted in orange.

Heatmaps from the genes involved in select pathways were generated (Figure 5.9). Visually, I can see that the majority of the genes illustrated from these select pathways have quite low expression levels. Importantly, these heatmaps nicely illustrate that there isn't a large difference in log2(intensity) between OMD$^{-/-}$ and wild-type transcriptomes based on these data. This is likely due to the relatively poor dynamic range of microarray experiments in general in addition to the poorly-stringent significance cut-off limit I utilised in the analysis. As such, it is likely that most of these genes are false-positives. Given the permissive settings I used on DAVID, where only 3 genes associated to a pathway are considered to be enriched, it is also evident that a few select genes are present in duplicate across the different pathway results; for example, genes such as *Map2k2* and *Kras* are found in several datasets despite having a very small difference in log2(intensity) between knock-out and wild-type. Unfortunately, when I attempted to use the more stringent SAM analysis, I only detected a handful of significant genes.

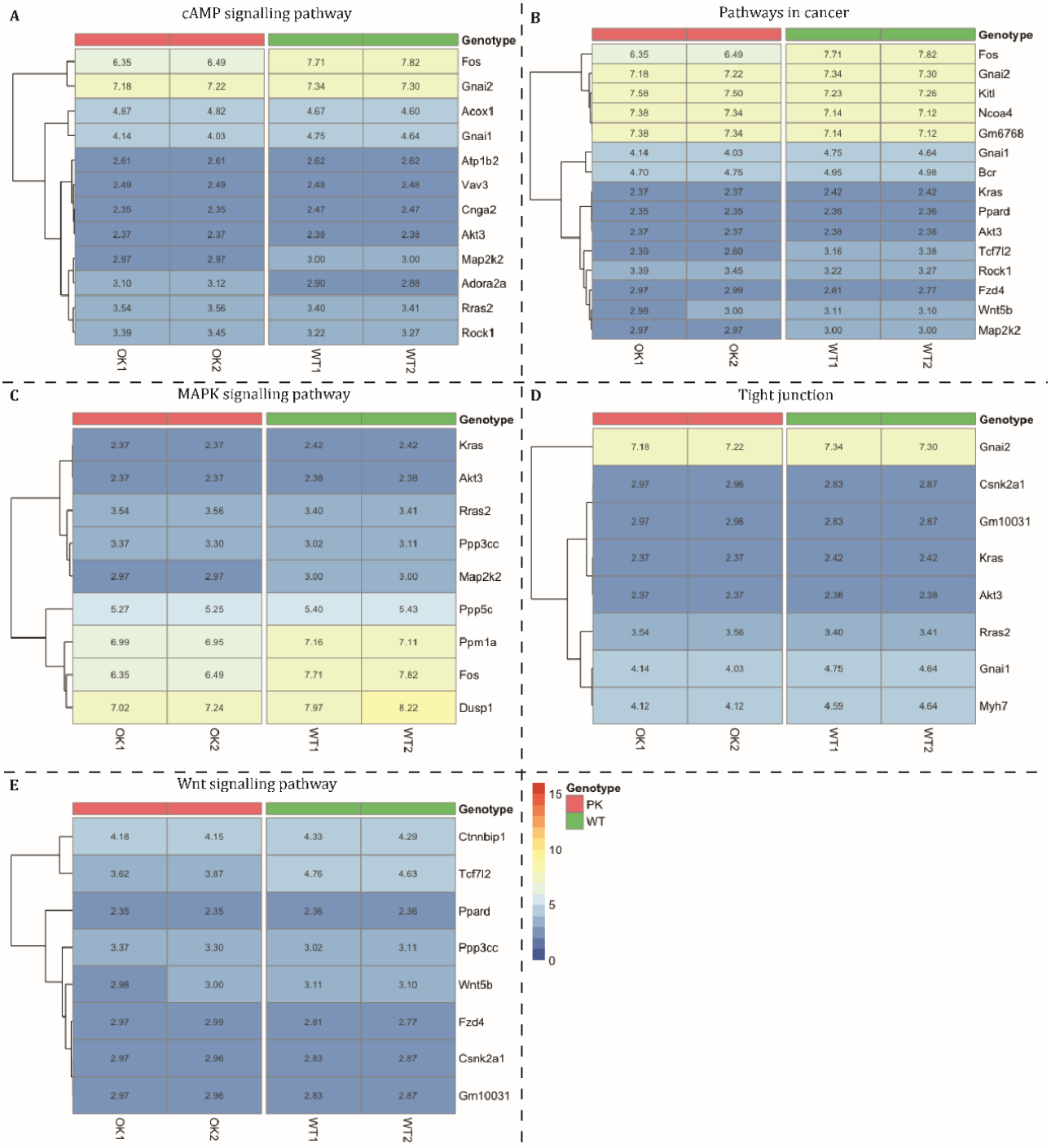

Figure 5.9. Heatmaps of pathways detected using DAVID. A) cAMP signalling pathway, **B)** Pathways in Cancer, **C)** MAPK signalling pathway, **D)** Tight junction and **E)** Wnt signalling pathway. Rows are clustered according to expression levels, and similarity is shown as a dendrogram.

Despite the fact that interesting pathways were flagged in this enrichment analysis, such as Pathways in cancer (mmu05200), only very small differences were detected amongst individual genes and it is extremely difficult to determine whether a given pathway is up- or down-regulated purely from these gene expression values. In addition, even if it was possible to determine the impact of these changes have on pathways, these small variations in log2(intensity) could very well be due to noise and chance.

5.2.3 Ontology analysis of differentially-expressed genes in PRELP$^{-/-}$

As before with the OMD$^{-/-}$ dataset, I input the significant genes detected by the student's t-test into DAVID in order to probe the KEGG database. The results are shown in Table 5.3. Despite the poorly-stringent p-value cut-off, there was a limited number of genes detected to be significant when comparing the wild-type and PRELP$^{-/-}$ datasets. I also utilised very permissive settings when utilising DAVID, allowing pathways to be deemed "enriched" if more than 3 genes from the list was found in a given pathway. Of the six pathways I have detected, only one of them, the MAPK signalling pathway, has a p-value < 0.05, albeit with a large FDR.

Pathway	KEGG code	Count	p-value	FDR
MAPK signaling pathway	mmu04010	6	0.038	0.3719
Acute myeloid leukemia	mmu05221	3	0.064	0.5465
FoxO signaling pathway	mmu04068	4	0.076	0.6116
Colorectal cancer	mmu05210	3	0.081	0.6346
p53 signaling pathway	mmu04115	3	0.087	0.6647
Melanoma	mmu05218	3	0.096	0.7023

Table 5.3. DAVID pathway analysis for PRELP$^{-/-}$ dataset. Pathways with p-value < 0.05 are highlighted in orange.

I therefore created a heatmap of the genes involved in the MAPK signalling pathway from the PRELP dataset (Figure 5.10). Again, just like with the OMD$^{-/-}$ dataset, the magnitude in differences in gene expression between wild-type and PRELP$^{-/-}$ is rather small. The only genes showing a large difference in gene expression are *Nr4a1* and *Fos*. *Nr4a1* encodes the nuclear receptor Nur-77 which is often found over-expressed in a variety of cancer cells (Hanna et al., 2011) and seems to have a role in mediating inflammation in macrophages by binding to NF-kB (Pei et al., 2006). Interestingly, there have been reports linking Nur-77 to angiogenesis and vessel permeability – Nur-77 transcriptional activity has been shown to be activated in response to the potent angiogenic factor VEGF-A (Zeng et al., 2006) as well as histamine- and serotonin-induced vascular permeability (Qin et al., 2013). *Fos* encodes the proto-oncogene c-Fos which dimerises with Jun family proteins and modulates pathways involved in proliferation, differentiation and survival (Angel & Karin, 1991; Tulchinsky, 2000). c-Fos has been shown to induce the expression of VEGF-D, a pro-angiogenic protein capable of binding to VEGFR2 and 3 in HUVECs (Marconcini et al., 1999).

Both *Nr4a1* and *Fos* are down-regulated in PRELP$^{-/-}$, however the significance of this is uncertain. Given their roles in mediating angiogenesis, I would have expected to see an

increase in *Nr4a1* and *Fos* expression in PRELP$^{-/-}$ in light of my *in vivo* data. However, given the limitations of this microarray experiment, it is uncertain whether these genes are truly down-regulated in PRELP$^{-/-}$ or whether their detection was accidental.

There also seems to be upregulation of *Fgf14*. It has been reported that treatment of human and murine sarcoma cell lines with various members of the FGF family, including FGF14, leads to their consequent upregulation (Ding et al., 2002). Although this is interesting, I would expect to see higher levels of mRNA of other FGF family members if that were the case. This may therefore be a false-positive I obtained by pure chance or that this positive-feedback loop is not present in the tissue that I have analysed.

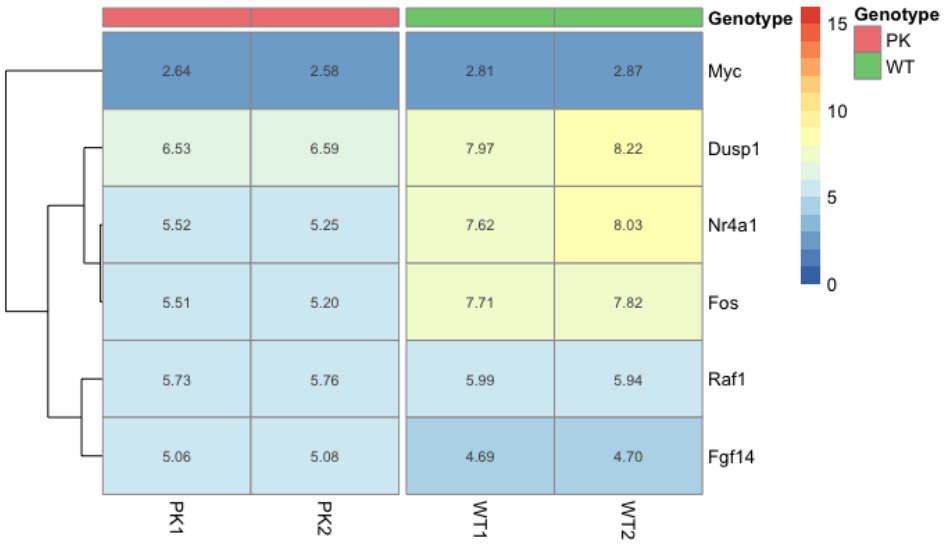

Figure 5.10. Heatmap of genes involved in the MAPK signalling pathway as detected by KEGG. Rows are clustered according to expression levels, and similarity is shown as a dendrogram.

5.2.4 Summary

I performed a microarray experiment in the hopes of detecting changes in gene expression between OMD$^{-/-}$, PRELP$^{-/-}$ and wild-type vasculature. RNA samples were prepared from mice prior to the commencement of this PhD project and were extracted from a large vessel in the abdomen of these animals. Given the focus of this project is to study CNS micro-vasculature in these transgenic mice, this dataset derived from a large abdominal vessel is not ideal with regards to both the size and nature of the vessel but also localisation of this vasculature. Smaller vessels obtained from the brain would therefore be more appropriate.

Using the statistical programming language, R, I have successfully managed to normalise the data by the GC-RMA method and obtained a list of significant genes, either from a student's t-test ($p<0.05$) or SAM ($\Delta=10$), a more rigorous method. From this list of

significant genes, I subset the original matrices of log2(expression values) and constructed heatmaps. Ontology analysis was performed by probing the KEGG database via DAVID, returning a list of significantly-altered genes within enriched pathways. Although my workflow seems to be valid, I have unfortunately not managed to detect any significant changes in gene expression which may explain, in part at least, the phenotype I observe in these animals *in vivo*. In the case of wild-type vs. $OMD^{-/-}$, I have detected multiple pathways involved in immunity and cancer. However, upon further inspection of the heatmaps that I generated, the differences in gene expression between wild-type and $OMD^{-/-}$were minimal. Similarly, the only significant pathway detected when comparing wild-type and $PRELP^{-/-}$ was MAPK signalling. Very few genes were detected and therefore I cannot draw any concrete conclusions as to whether the pathway is positively or negatively affected by PRELP.

From my analysis of the microarray data, it is apparent that the experiment was rather limited, as will be further elaborated in Section 5.4.1 .

5.3 RNA sequencing

5.3.1 RNA seq theory

In light of the weaknesses of the microarray experiment, I decided to then analyse changes in gene expression using RNA seq. The development of high-throughput next-generation sequencing methods gave rise to sequencing-based approaches to analyse gene expression, circumventing many of the problems which plague hybridisation methods, such as arrays (Mantione et al., 2014). Since sequencing-based methods directly determine cDNA sequences, they do not rely heavily on pre-existing knowledge of the genome, in contrast to microarrays. In addition, the dimension of high background noise and normalisation is entirely eliminated when performing RNA seq experiments since sequenced fragments can be mapped to unique regions of the genome rather unambiguously (Wang et al., 2009). Finally, given that transcript number is determined and due to its digital nature, the resolution and range of RNA seq is more impressive, where low-abundance transcripts and splice variants can be detected (Zhao et al., 2014).

Briefly, I will summarise RNA and cDNA preparation and sequencing (Figure 5.11). RNA is extracted from the tissue of choice and abundant transcripts, such as rRNA, are typically removed. This can be done by isolating mRNA by purifying RNA containing polyA-tails (Murata et al., 2014) or by depleting rRNA by hybridisation of oligonucleotides specific to rRNA (O'Neil et al., 2013). In order to be compatible with high-throughput sequencing, long RNA molecules are fragmented and converted to a cDNA library by random priming.

These cDNA fragments have adapters conjugated to one or both ends and are then sequenced from one end (single-end sequencing) or both ends (pair-end sequencing) to produce reads which typically range from 30-400 bp, depending on the DNA sequencing technology used (Wang et al., 2009).

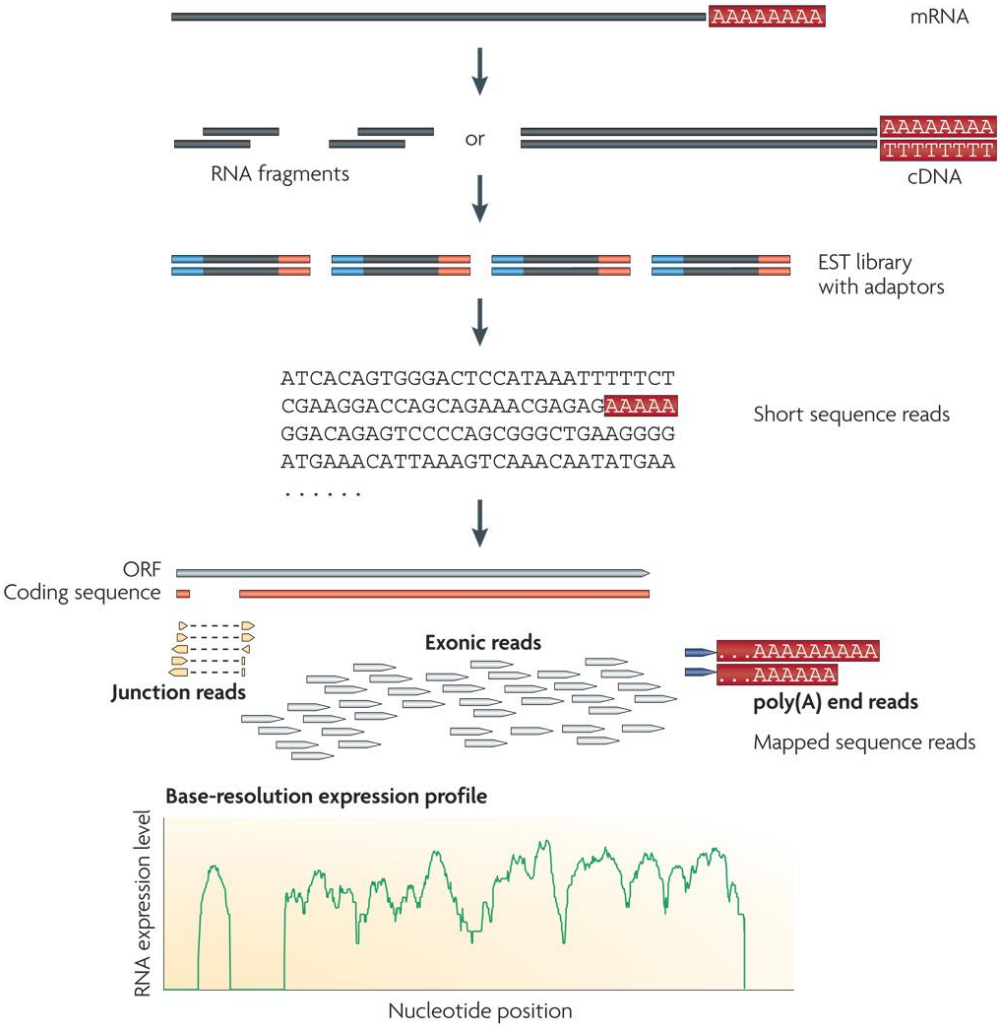

Figure 5.11. Overview of sample preparation and sequencing for RNA seq. RNA is converted to cDNA with specific adapters for sequencing. Short reads are sequenced, mapped to a reference genome and expression levels of genes are calculated. Figure from (Wang et al., 2009).

The "depth of sequencing" refers to the number of sequences reads for a given sample (Conesa et al., 2016). Careful consideration must be taken when selecting a sequence depth which is appropriate for the experiment. While gross changes in gene expression can be detected using relatively few reads, the detection of low-abundance transcripts require much deeper sequencing. However, the cost of deeper sequencing is also higher. In addition, for larger and more complex genomes, deeper sequencing is necessary than for more simple organisms (Wang et al., 2009). The depth of sequencing that is chosen is therefore dependent on the aims of the experiment.

With this information, what would be an appropriate depth of sequencing for an RNA seq experiment with tissues from our mice? There are two notable studies examining the relationship of sequencing depth and detection of transcripts (Mortazavi et al., 2008; Myers et al., 2011). RNA pooled from a variety of mouse tissues was used to create the cDNA library and generated 25bp single-end reads to sequence at depths of 0.82 million to 41million reads (Figure 5.12A). This study highlighted that the abundant transcripts could be detected at approximately 16 million reads, yet this has to be increased to approximately 32 million reads for rarer transcripts (Mortazavi et al., 2008).

The Encyclopedia of DNA Elements (ENCODE) consortium (Feingold et al., 2004) has conducted a similar study to address the number of reads required to quantify genes, but now in human cells (Myers et al., 2011). Using RNA extracted from H1 human embryonic stem cells, they generated 100bp paired-end reads at different depths of sequencing, ranging from 9 million to 214 million reads (Figure 5.12B). This study demonstrates that approximately 36 million reads is enough accurately detect 80% of most transcripts. In order to have the same confidence in detecting low-abundance transcripts, a sequencing depth of approximately 80 million would be required, highlighting a significant difference in the requirements of analysis between murine and human RNA samples.

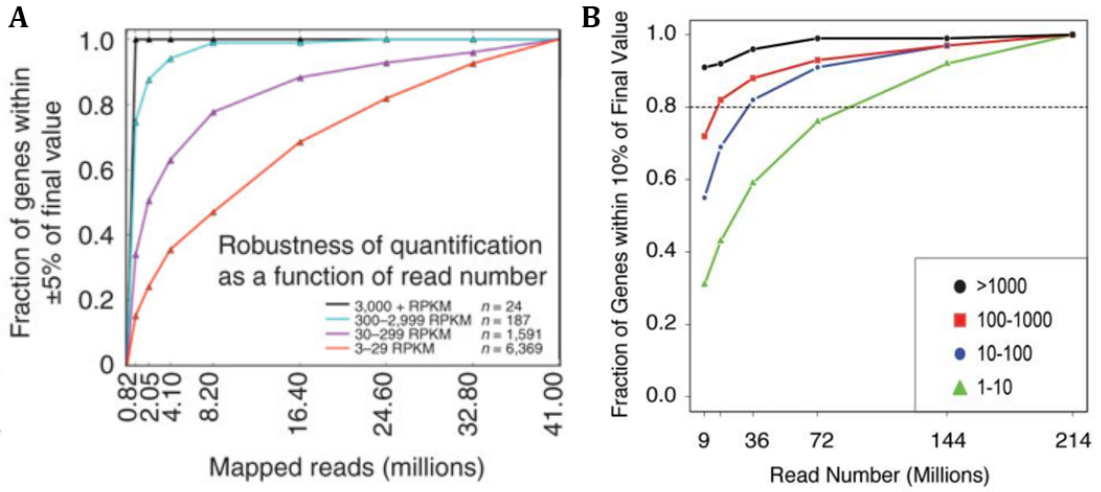

Figure 5.12. Saturation analysis on the depth of sequencing required to detect transcripts of different abundance. A) Analysis of RNA extracted from a variety of mouse tissues. Transcripts were divided into four classes of abundance; black being the most abundant and red being the rarest. **B)** Analysis of RNA extracted from human H1 embryonic stem cells. Transcripts were divided into four classes of abundance; black (O) being most abundant and green (Δ) being the rarest. Figure adapted from (Mortazavi et al., 2008) and (Myers et al., 2011).

The sequences are then aligned to a reference dataset (e.g. reference genome or particular set of transcripts) in order to obtain information on the transcriptome. Short-read mappers such as Maq (Li et al., 2008) and Bowtie (Langmead et al., 2009) both utilise

indexing methods to quickly map short reads to exons. While programs such as these would be appropriate for the analysis of relatively simple genomes, due to the short reads generated, the analysis of complex mammalian genomes would be hindered owing to difficulties mapping reads found at exon-exon junctions. This is illustrated in Figure 5.13, where short-read mappers would only be able to align the black reads found within exons but fail to properly align blue reads which are found at exon-exon junctions and typically return an error.

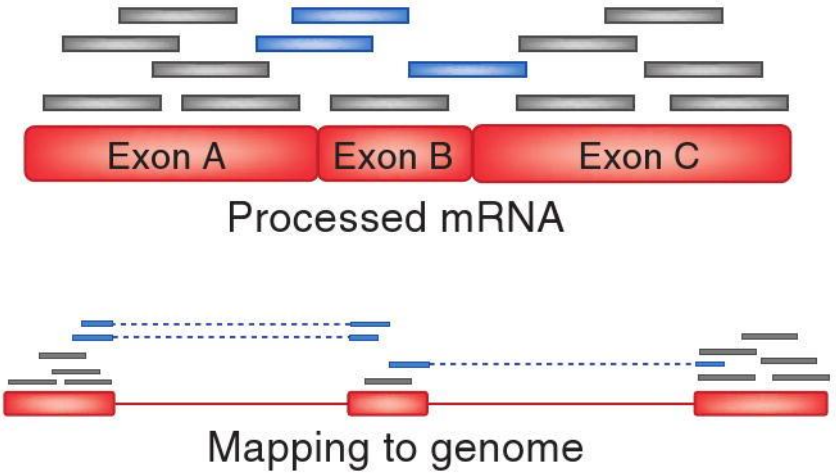

Figure 5.13. Alignments created solely by short-read mappers are imperfect for analysing complex genomes. Programs such as Maq and Bowtie would typically only align the black reads to the reference genomes. The alignment of blue reads, found at exon-exon junctions, would require other methodologies. Figure from (Trapnell et al., 2009).

Spliced-read mappers such as Enhanced Read Analysis of Gene Expression (ERANGE) (Mortazavi et al., 2008) and TopHat (Trapnell et al., 2009) are commonly used to address the problem mapping reads to spliced genes. ERANGE functions by utilising available genome annotation to create sequences likely to be produced after introns are removed. The hypothetical sequences are then used as a reference and RNA seq reads are aligned to this new reference genome using a short-read mapper. ERANGE is therefore reliant on having an annotated genome available to the researcher. In contrast, TopHat first relies on Bowtie to align reads which are fully found within exons and all the reads that are unaligned, i.e. possibly found at junctions, are set aside as "initially unmapped reads" (IUM reads). IUM reads are then mapped to the reference genome again, however this time, allowing for mismatches to occur, allowing a single read to have multiple alignments. Using Maq's *assemble* function, TopHat predicts putative exons by assembling "islands" of adjacent sequences, circumventing the need to have an annotated genome.

Once the majority of sequenced fragments are aligned to the reference dataset, RNA abundance needs to be determined. To this end, a common method is to utilise the Cufflinks suite (Trapnell et al., 2010), a collection of programs to enable the analysis of RNA seq data, illustrated in Figure 5.14. Essentially, Cufflinks collects aligned fragments from TopHat, which includes fragments that span exon-exon junctions, and assembles overlapping fragment alignments. The probable arrangement of exons and introns is then determined by excluding incompatible fragments – these are fragments which must have originated from distinct isoforms. According to their methodology, "*two reads are not compatible if their overlap contains the exact same implied introns or none*" (Trapnell et al., 2010). Sequenced fragments are matched to the transcripts from which they originate and transcript abundance is then estimated, assuming that the probability of encountering a fragment is linearly proportional to the relative abundance of the original transcript. The resulting dataset can now be utilised for downstream analysis.

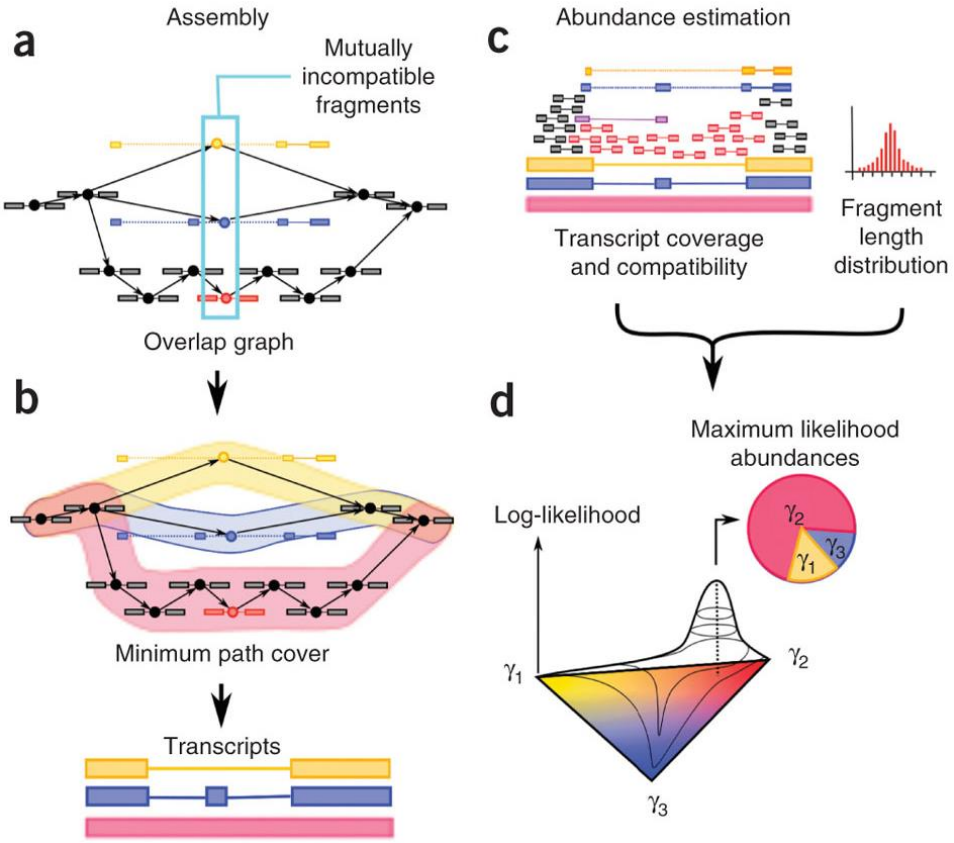

Figure 5.14. Overview of Cufflinks for determining relative transcript abundance. A) Removal of incompatible fragments. **B)** Determination of likely topology of transcripts. **C & D)** Estimation of transcript abundance based on fragment abundance. Modified from (Trapnell et al., 2010).

5.3.2 Experimental design

Given the information above, I have determined that RNA seq would be an appropriate method to detect differences in gene expression between wild-type and knock-out mice in the hopes that it would clarify the differences observed *in vivo*.

One of the key issues of the microarray experiment was that RNA was extracted from vasculature which did not originate from the brain. In addition, Dr Noriaki Sasai informed me that the vessel he cut from the abdomens of the mice used for the microarray study was large. Therefore, I aimed to obtain RNA from smaller brain vasculature. To this end, I considered performing microvessel isolation, where whole brains would be harvested, homogenised and endothelial cells purified. There are two possible methods to purify capillary endothelial cells – either by incubating the brain homogenate with endothelial cell-specific antibodies or treatment with puromycin. Puromycin is a protein synthesis inhibitor which functions by prematurely terminating translation (Azzam & Algranati, 1973); this method relies on the abundance of ABC transporters on brain endothelial cells preventing puromycin's action whereas the other cells would quickly die. However, my concern with this experimental design is that gene expression could change quite drastically during this fairly lengthy isolation process, where cells would be exposed to mechanical stress and/or exposure to a cytotoxic drug.

Therefore, in order to obtain brain vasculature in a relatively short period of time, I have decided to harvest vessels present on the surface of the brain, i.e. meningeal vessels (Figure 5.15), notably those on the ventral side. The meninges is a group of membranes surrounding the brain and spinal cord and is made up of three distinct layers: the dura, arachnoid and pia maters (Peeters et al., 1991). There is a rich network of arteries and veins embedded within the arachnoid mater, in direct contact with the pia mater (Hutchings & Weller, 1986). These arteries and veins branch into the brain via perivascular space and form the network of vessels inside the brain. Meningeal vessels differ from those located in the brain parenchyma by their lack of contact with astrocyte end-feet. As described previously, contact with astrocyte end-feet seems to be critical in maintaining the BBB (Janzer & Raff, 1987). Despite this, a recent study has demonstrated that these meningeal arteries, veins and capillaries have very comparable distribution of tight junction proteins to brain parenchyma capillaries (Hanske et al., 2016). Hence, given that i) meningeal vessels have comparable tight junctions to BBB vasculature, ii) both OMD and PRELP seem to be expressed on meningeal vessels and iii) a more rapid isolation of tissue is possible, I have decided to perform RNA seq using meningeal vasculature RNA.

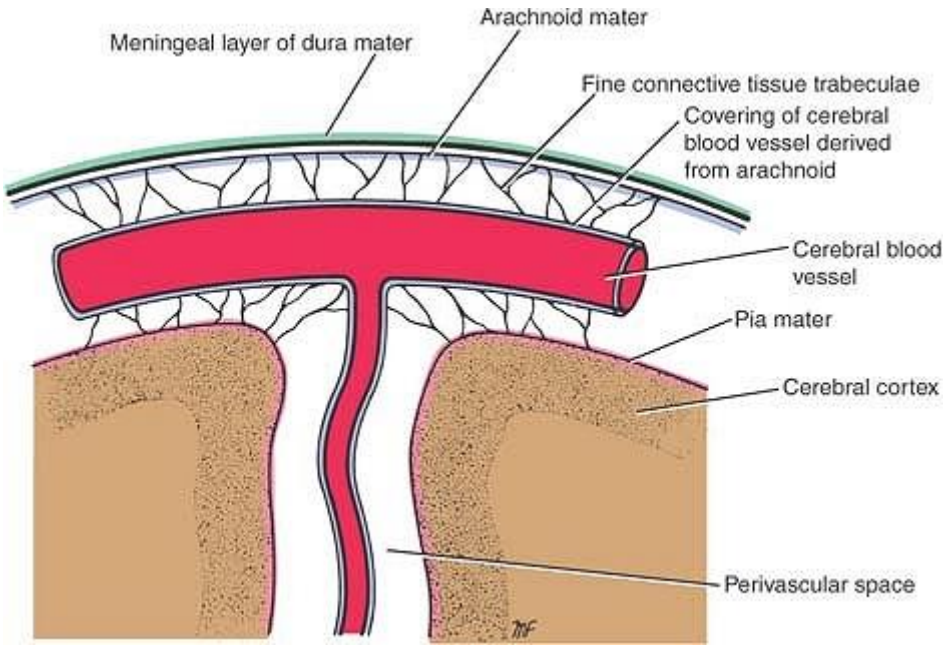

Figure 5.15. Structure of the meninges surrounding the brain. Figure from (Michael, 2012).

Given considerations for number of animals available and the cost of library preparation/sequencing, I opted to have three samples per genotype; i.e. 9 samples in total. Meningeal vessel isolation was performed as described by (Bowyer et al., 2012). Initial efforts to extract RNA indicated that RNA extraction itself was very poor. Meningeal vessels were very tough and elastic in texture, making it difficult to lyse cells adequately. I sought to improve the homogenisation method; I found that tissue homogenisation was best done using a small glass dounce homogeniser. Special care was taken to ensure that the homogeniser was very thoroughly washed between samples. However, even with improved homogenisation of tissue, I had difficulties obtaining enough RNA to make the cDNA library using the Qiagen RNA extraction kit that Dr Noriaki Sasai had previously used for the preparation of microarray samples. Therefore, as detailed in Chapter 2, I performed the RNA extraction using the PicoPure RNA extraction kit which enabled me to obtain a much higher RNA yield.

Figure 5.16 shows the quantification of the RNA which I submitted initially as a test (Figure 5.16A) and the final samples used for cDNA library preparation (Figure 5.16B). RNA integrity was assessed by UCL Genomics using an Agilent Tapestration 2200 instrument, where the RINe (RNA integrity number) value was determined. This is a measure of RNA integrity dependent on the electrophoretic profile of RNA bands ranging from 0 (degraded) to 10 (high-quality) (Schroeder et al., 2006). RINe values ranged from 7.2 to 8.4, indicating that RNA is intact. For RNA seq, UCL Genomics accepts samples with RINe values ≥ 7 (personal communication). Analysis of RNA peaks indicates that samples

have some DNA contamination, however this would not impact the library preparation as mRNA molecules were enriched by polyA capture. These samples were therefore of appropriate quality for RNA seq.

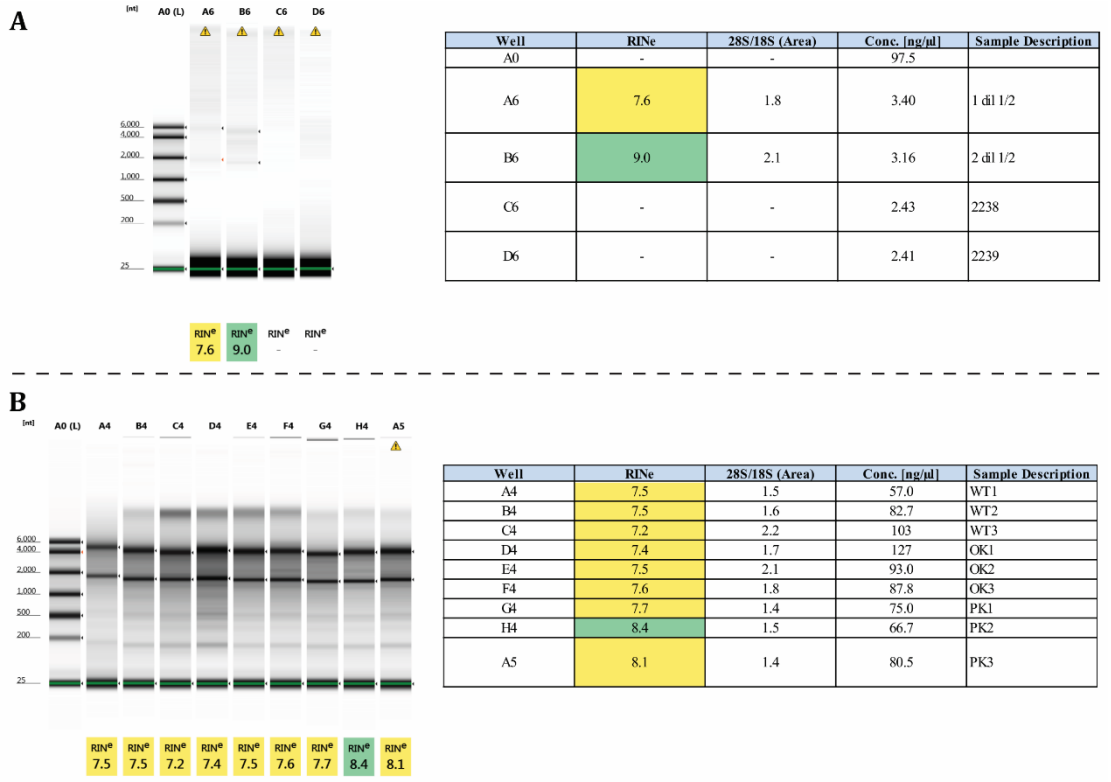

Well	RINe	28S/18S (Area)	Conc. [ng/µl]	Sample Description
A0	-	-	97.5	
A6	7.6	1.8	3.40	1 dil 1/2
B6	9.0	2.1	3.16	2 dil 1/2
C6	-	-	2.43	2238
D6	-	-	2.41	2239

Well	RINe	28S/18S (Area)	Conc. [ng/µl]	Sample Description
A4	7.5	1.5	57.0	WT1
B4	7.5	1.6	82.7	WT2
C4	7.2	2.2	103	WT3
D4	7.4	1.7	127	OK1
E4	7.5	2.1	93.0	OK2
F4	7.6	1.8	87.8	OK3
G4	7.7	1.4	75.0	PK1
H4	8.4	1.5	66.7	PK2
A5	8.1	1.4	80.5	PK3

Figure 5.16. QC analysis of RNA submitted for cDNA library preparation. A) Initial test of RNA extracted using typical RNA extraction kit. Note that RNA concentration and quality are very poor. **B)** Samples used for RNA seq analysis. Concentration of RNA is adequate and RNA is not degraded.

As discussed in Section 5.3.1 , the depth of sequencing is a critical factor to consider in RNA seq experiments. From the data provided by (Mortazavi et al., 2008), it is clear that approximately 32 million reads is sufficient to detect ~80% of rare transcripts in addition to more abundant ones and this would need to be increased to 41 million or more reads to obtain information on virtually all transcripts. Given the implication in cost, I aimed to obtain a depth of sequencing around 30 million reads, providing information of most transcripts for a more reasonable price. Samples were submitted to UCL Genomics, where they performed the library preparation, sequencing and alignment to the reference genome Mus musculus UCSC mm10 (Dec 2011). The number of reads and alignment of those reads are summarised in Table 5.4. The number of reads ranged from 27.5 million to 33.3 million reads, appropriate for my purpose. In addition, more than 95% of all reads were mapped to the reference, indicating that the sequencing and alignment processes were successful.

Sample	Number of Reads	Total Aligned Reads (% Reads)	Unaligned Reads (% Reads)
Wild-type 1	33.3 mil	95.49%	4.51%
Wild-type 2	30.2 mil	96.09%	3.91%
Wild-type 3	28.7 mil	95.98%	4.02%
$OMD^{-/-}$ 1	27.5 mil	96.17%	3.83%
$OMD^{-/-}$ 2	32.0 mil	95.88%	4.12%
$OMD^{-/-}$ 3	28.5 mil	96.13%	3.87%
$PRELP^{-/-}$ 1	29.2 mil	95.85%	4.15%
$PRELP^{-/-}$ 2	32.4 mil	95.92%	4.08%
$PRELP^{-/-}$ 3	33.1 mil	95.41%	4.59%

Table 5.4. Summary of reads and alignment for all samples.

The final normalised gene counts were obtained from UCL Genomics and I performed analysis of the data using DeSeq2 (Anders & Huber, 2010). Genes counts were loaded into the R interface along with required packages. The comparisons of $OMD^{-/-}$ vs. wild-type and $PRELP^{-/-}$ vs. wild-type were performed separately to ensure no error was produced in the code by mistake. The same code was utilised for the analysis of $OMD^{-/-}$ and $PRELP^{-/-}$, but the source data frame was simply changed to ensure that both datasets were treated in the same manner. Once the dataframe containing gene counts was split, 2-tailed student's t-test was performed on all rows. The resulting p-values and p-values adjusted for multiple correction using the Benjamini-Hochberg procedure (p-adj) were calculated, the data was subsetted based on the chosen cut-off. This final list of significant genes was then utilised for ontology or enrichment analyses.

The significance of results prior to this chapter have been determined using uncorrected p-values. Due to the small sample size (n=3), the number of datapoints and statistical tests performed were minimal and I assumed the incidence of false-positive p-values was limited. In contrast, the chance of making such Type I errors is much higher when comparing the expression of thousands of genes. I therefore opted to correct for this using the Benjamini-Hochberg procedure to calculate p-values adjusted for conducting multiple comparisons. Briefly, unadjusted p-values are ranked in ascending order and assigned a rank. To calculate p-adj, the largest p-value would be multiplied by the number of genes within a given test. The second largest p-value would be multiplied by the number of genes, minus 1, and so on. Once all of the p-values have been adjusted, the dataset can be subsetted based on a cut-off.

In order to discover trends in the RNA seq data, three bioinformatics tools were utilised. First, I aimed to discover gene ontologies (GOs) which were overrepresented in the differentially expressed dataset. GO terms are manually- and electronically-assigned keywords describing a protein's function and cellular localisation (Carbon et al., 2017). GO terms are split into three main categories – Biological Processes, Cellular Component and Molecular Function. While Cellular Component describes where a gene product localises to in the cell, for example the cytoplasm, functional annotation is described by Biological Processes and Molecular Function. Biological Processes describes the overall role of the protein in molecular events in tissues or in the organism, for example the regulation of angiogenesis, whereas Molecular Function describes the function of the protein at a molecular level, such as binding or kinase activity. The enrichment analysis itself was performed using the GO consortium's enrichment tool, PANTHER (Mi et al., 2017). Next, the tool STRING was used to visualise protein-protein interaction networks (Szklarczyk et al., 2015). STRING computes estimated scores for protein interactions, based on experimental and predicted data, and generates a map of protein interactions. Finally, I explored the curated database Molecular Signatures Database (MSigDB) to identify biological processes which may be affected by OMD and PRELP. The MSigDB is composed of collections, where genes are annotated and grouped based on published work (Liberzon et al., 2011). It is intended for use with Gene Set Enrichment Analysis (GSEA) analysis (Subramanian et al., 2005) to discover whether a user-defined set of genes is associated with a biological state. In particular, I investigated the overlap between my dataset and the Hallmark gene sets, a highly-curated collection of gene sets which correspond to specific biological processes (Liberzon et al. 2015).

5.3.3 RNA seq comparing the transcriptomes of wild-type and OMD$^{-/-}$ meningeal vessels

Upon initial analysis of my data, I was surprised to not find any differences between wild-type and OMD$^{-/-}$ samples. When further examined, I noticed that one of the animals labelled as being a knockout was likely to be a heterozygote, i.e. OMD$^{+/-}$, since OMD mRNA transcripts were detected; the likely explanation is that a mistake was made during the genotyping process. Although a third OMD$^{-/-}$ sample was prepared and sequenced afterwards, I decided not to include it in the analysis; see Section 5.4.2 for more details. Therefore, the following analysis of RNA seq is based on 5 samples (3 wild-type and 2 OMD$^{-/-}$).

After p-value and p-adj calculations, I detected 189 genes at p-value < 0.01 and 56 genes at p-adj < 0.05. In order to reduce the chance of false-positive results, genes detected with p-adj < 0.05 were used for ontology analysis. All detected genes were up-regulated in

OMD$^{-/-}$, with the exception of OMD, as expected, and *Gdf10,* which encodes Growth/differentiation factor 10 – an inhibitor for osteoblast differentiation (Matsumoto et al., 2012). GO analysis was performed using the tools provided by the GO consortium, where Biological Process was selected. 40 GO classifications were detected, and the top 10 results are shown below in Table 5.5. In addition, enrichment analysis was also performed with respect to Cellular Component to determine whether any changes occurred in the ECM in the absence of OMD. Analysis indicates that queried genes localise to the cytoplasm, aside from *Omd* and *col15a1*.

GO Biological Process	Input	Expected	Fold enrich.	p-value
Defense response to virus (GO:0051607)	16	0.38	41.77	6.30E-18
Response to virus (GO:0009615)	17	0.5	34.07	8.46E-18
Response to interferon-beta (GO:0035456)	11	0.11	97	2.74E-15
Response to other organism (GO:0051707)	23	2.03	11.31	6.41E-15
Response to external biotic stimulus (GO:0043207)	23	2.04	11.28	6.77E-15
Response to biotic stimulus (GO:0009607)	23	2.11	10.88	1.50E-14
Defense response to other organism (GO:0098542)	20	1.38	14.46	2.04E-14
Cellular response to interferon-beta (GO:0035458)	10	0.1	> 100	6.05E-14
Defense response (GO:0006952)	24	2.95	8.13	1.49E-12
Innate immune response (GO:0045087)	19	1.54	12.36	2.94E-12

Table 5.5. Top 10 GO Biological Processes enriched from OMD$^{-/-}$ RNA seq dataset. p-values listed above were corrected for multiple testing using Bonferroni.

It is clear that processes related to immunity and response to foreign molecules are altered in OMD$^{-/-}$ animals. The table above shows that all GO classes are parent and child terms related to immune response. The GO class with the most input genes, Defense response (GO:0006952), was selected and the input genes extracted. These genes were then collated to produce a heatmap (Figure 5.17). All genes extracted from Defense response (GO:0006952) are shown to be up-regulated in OMD$^{-/-}$. The genes with the largest changes are *Oasl1*, *Ccl2* and *Oas3*, where Oasl1 and Oasl3 are interferon-induced anti-viral enzymes and Ccl2 is a chemokine responsible for monocyte recruitment (Eskildsen et al., 2003; Raghu et al., 2017).

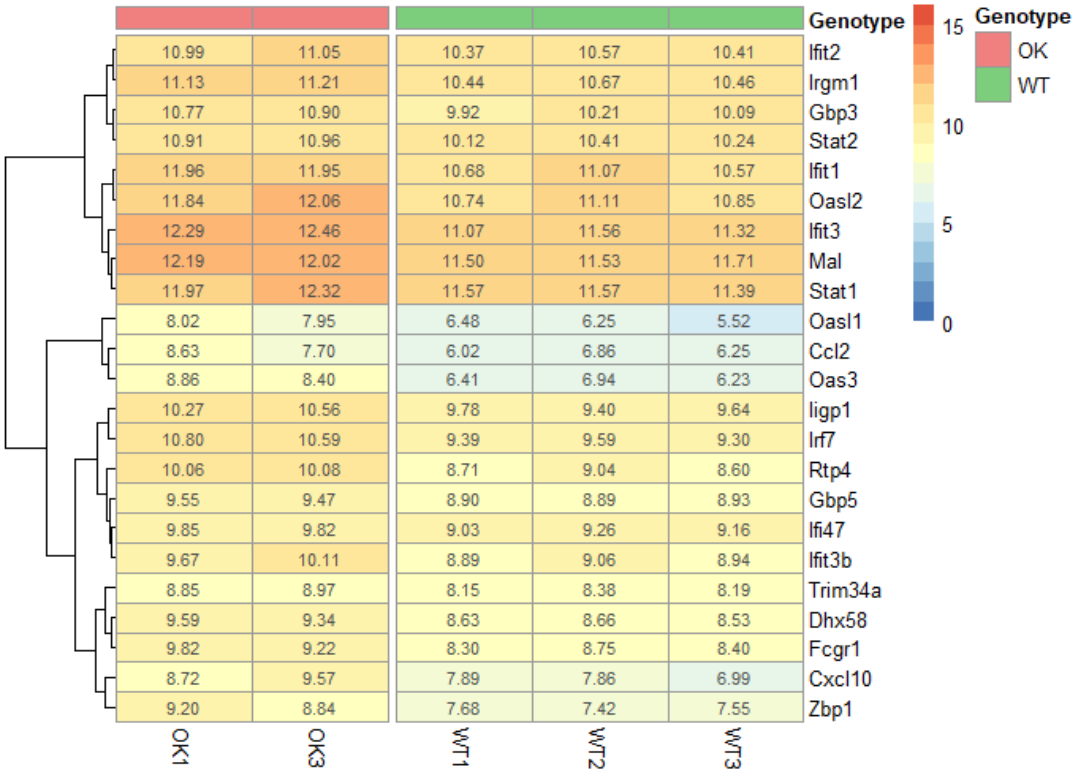

Figure 5.17. Heatmap of Defense response (GO:0006952). Rows are clustered according to expression levels, and similarity is shown as a dendrogram.

In order to determine whether there is a notable central hub responsible for the changes in gene expression, I utilised STRING to visualise protein-protein interactions. Initial inputs resulted in a highly-saturated network, where almost all gene nodes had interacting partners. Using highly-stringent settings and only visualising known interactions, as opposed to both known and predicted interactions, I generated a map of protein-protein interactions (Figure 5.18). There is a notable cluster of interactions involving *Stat1*, *Stat2*, *Stat3*, *Jak2* and *Crebbp*. Interferon activation results in the activation of Jak kinases and subsequent phosphorylation and formation of the trimeric transcription factor complex formed of Stat1, Stat2 and IRF9, resulting in changes in gene expression in response to pathogens (Au-Yeung et al., 2013). Stat3 mediates responses induced by interleukins (Yu et al., 2002). Therefore, from GO term analysis, there is an up-regulation of cytokine-induced signalling mediated by an increase in expression of genes induced by interferons and interleukins.

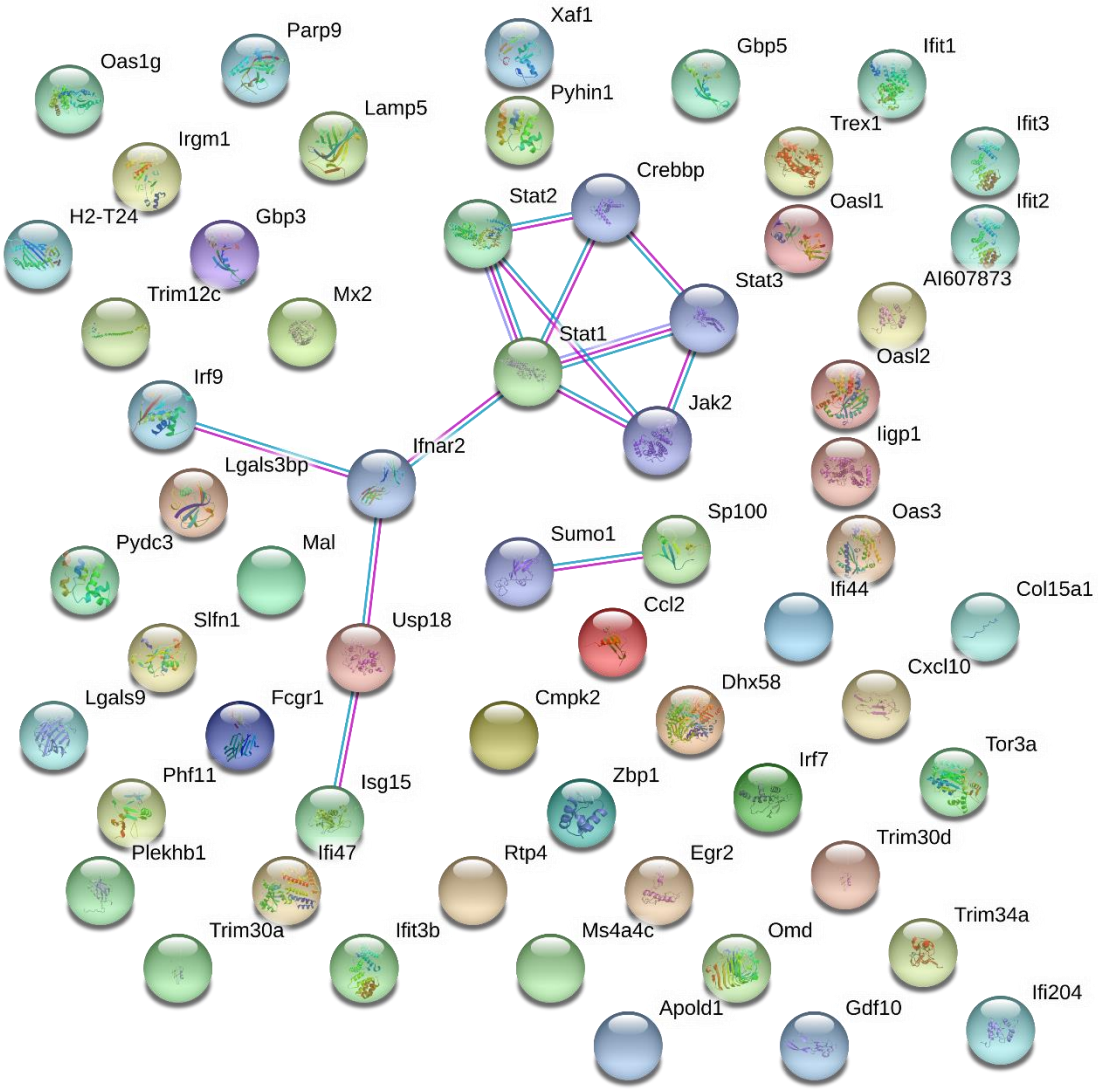

Figure 5.18. Protein interaction network of genes differentially-expressed in OMD$^{-/-}$. Analysis performed using STRING. Highest confidence settings were used and only known interactions are shown. Data from curated databases are shown in cyan and experimental data in magenta.

Finally, I also performed enrichment analysis using GSEA and the results are summarised below in Table 5.6. Differentially-expressed genes were enriched in six hallmark gene sets – interferon-γ response, interferon-α response, IL6-JAK-STAT3, inflammatory response, TNF-α signalling via NF-κB and allograft rejection. Consistent with ontology analysis, gene sets related to inflammation were detected in many genes up-regulated in OMD$^{-/-}$, suggesting a strong role for OMD in immunity and inflammation. In contrast, only a few down-regulated genes were associated with gene sets.

Hallmark Gene Set Name	Description	Input	p-value	p-adj
Interferon Gamma Response	Genes up-regulated in response to IFNG	22	1.63E-42	8.17E-41
Interferon Alpha Response	Genes up-regulated in response to alpha interferon proteins	16	1.53E-33	3.82E-32
IL6-JAK-STAT3 Signaling	Genes up-regulated by IL6 via STAT3, e.g. during acute phase response	4	9.37E-7	1.56E-5
Inflammatory Response	Genes defining inflammatory response	4	2.54E-5	2.54E-4
TNFA signaling via NF-kB	Genes regulated by NF-kB in response to TNF	4	2.54E-5	2.54E-4
Allograft Rejection	Genes up-regulated during transplant rejection	3	6.61E-4	5.51E-3

Table 5.6. Enriched Hallmark Gene Sets up-regulated in OMD$^{-/-}$. Analysis was done using the tools available online (http://software.broadinstitute.org/gsea/msigdb/annotate.jsp).

To conclude, analysis of OMD$^{-/-}$ meningeal RNA seq suggests a role for OMD in mitigating inflammatory pathways such as interferon, interleukin and TNF-α inflammatory pathways as assessed by ontology and enrichment analyses. Unfortunately, analysis was only performed using two OMD$^{-/-}$ samples, as one sample was likely to be OMD$^{+/-}$.

5.3.4 RNA seq comparing the transcriptomes of wild-type and PRELP$^{-/-}$ meningeal vessels

After p-value and p-adj calculations, I detected 288 genes at p-value < 0.01 and 37 genes at p-adj < 0.05. Ideally, in order to reduce the chance of type I errors, adjusted p-values should be utilised. Unfortunately, ontology or enrichment analyses using genes detected at p-adj < 0.05 was unsuccessful – no GO classifications or hallmark gene sets were found to be enriched. Therefore, although not ideal, differentially expressed genes at p-value < 0.01 were utilised for analysis.

As before, GO term analysis was performed using the tools provided by the GO consortium. The top ten significant Biological Processes are shown below in Table 5.7. The two most significant GO classes are related to macrophage activation and immune system processes, similar to results obtained from OMD$^{-/-}$ RNA seq. In addition to cell-cell and cell-matrix adhesion, genes encoding proteins in involved in transport processes are

also enriched. The only process which directly references the vasculature is blood circulation.

GO Biological Process	Input	Expected	Fold enrich.	p-value
Macrophage activation (GO:0042116)	8	1.43	5.59	1.15E-04
Immune system process (GO:0002376)	17	6.34	2.68	2.65E-04
Cell-cell adhesion (GO:0016337)	9	2.29	3.92	5.84E-04
Sulfur compound metabolic process (GO:0006790)	7	1.42	4.94	6.38E-04
Extracellular transport (GO:0006858)	4	0.42	9.54	9.07E-04
Intracellular protein transport (GO:0006886)	22	10.48	2.1	9.82E-04
Lipid transport (GO:0006869)	6	1.18	5.07	1.35E-03
Protein transport (GO:0015031)	22	10.76	2.04	1.37E-03
Blood circulation (GO:0008015)	7	1.64	4.27	1.47E-03
Cell-matrix adhesion (GO:0007160)	5	0.81	6.14	1.48E-03

Table 5.7. Top 10 GO Biological Processes enriched from PRELP$^{-/-}$ RNA seq dataset. p-values listed above were not corrected for multiple testing using Bonferroni.

None of the Biological Processes detected using ontology analysis is clearly linked to the phenotype observed in PRELP$^{-/-}$ animals, although there is some interesting information. For example, macrophage activation (GO:0042116) has the child term microglial cell activation (GO:0001774) – as described in Chapter 4, an increase in the activation state of microglia was detected in PRELP$^{-/-}$, as assessed by average branch length per microglia. In addition, treatment of endothelial cell monolayers *in vitro* with cytokines has been shown to increase their permeability. Finally, cell-cell and cell-matrix adhesion are

important for the various steps in angiogenesis, where both endothelial cells and mural cells undergo migration (Ramjaun & Hodivala-Dilke, 2009).

I observed that many genes encoding extracellular proteins are differentially-regulated. Of the 288 genes found to be differentially expressed in PRELP$^{-/-}$ at p-value < 0.01, 89 of these were found to encode proteins which localise to the extracellular region.

GO Cellular component	Input	Expected	Fold enrich.	p-value
Proteinaceous extracellular matrix (GO:0005578)	17	4.3	3.95	2.94E-03
Extracellular matrix (GO:0031012)	21	6.29	3.34	2.65E-03
Cell projection part (GO:0044463)	31	13.75	2.25	3.23E-02
Plasma membrane bounded cell projection part (GO:0120038)	31	13.75	2.25	3.23E-02
Plasma membrane bounded cell projection (GO:0120025)	46	24.54	1.87	3.60E-02
Cell projection (GO:0042995)	49	26.67	1.84	3.17E-02
Extracellular exosome (GO:0070062)	57	31.42	1.81	8.53E-03
Extracellular vesicle (GO:1903561)	57	31.6	1.8	1.02E-02
Extracellular organelle (GO:0043230)	57	31.69	1.8	1.10E-02
Extracellular region part (GO:0044421)	79	48.57	1.63	5.65E-03

Table 5.8. GO Cellular component over-representation analysis using PRELP$^{-/-}$ RNA seq dataset. Analysis was corrected from multiple testing using Bonferroni.

Observations from many knock-out models of SLRP members indicate that deletion of one member often results in up-regulation of others with similar function (Ameye & Young, 2002; Zhang et al., 2009). I therefore exported the list of genes found within the GO

classification Extracellular matrix (GO:0031012) and created a heatmap to visually observe the changes which occur (Figure 5.19). In addition to PRELP, the expression levels of three other SLRPs are altered in the knock-out: osteoglycin, OMD and opticin. The expression levels of osteoglycin and OMD are increased in PRELP$^{-/-}$, whereas that of opticin is decreased. In addition to SLRPs, there are changes in other interesting genes. There are changes in the expression levels of genes encoding BM components – perlecan (*hspg2*), laminin (*lamb2*) and collagen VI (*col6a5*). Finally, there is altered expression of signalling molecules, notably BMP1 (*bmp1*), angiogenin (*ang*) and angiopoietin-related protein 4 (*angptl4*). Both angiogenin and angiopoietin-related protein 4 (Angptl4) are implicated in regulating angiogenesis. Angiogenin is an RNase and binds to the surface of endothelial cells, where it is endocytosed and translocated to the nucleus where it stimulates rRNA production to promote cell growth. It was found to vascularise both normal and malignant tissues (Gao & Xu, 2008). Angptl4 is a hypoxia-driven pro-angiogenic factor found to disrupt cell-cell junctions in endothelial cells in cancer to promote metastasis (Huang et al., 2011). While changes in angiogenin and Angptl4 are not necessarily meaningful on their own, it is clearly interesting to note that the ECM of wild-type and PRELP$^{-/-}$ vessels are different.

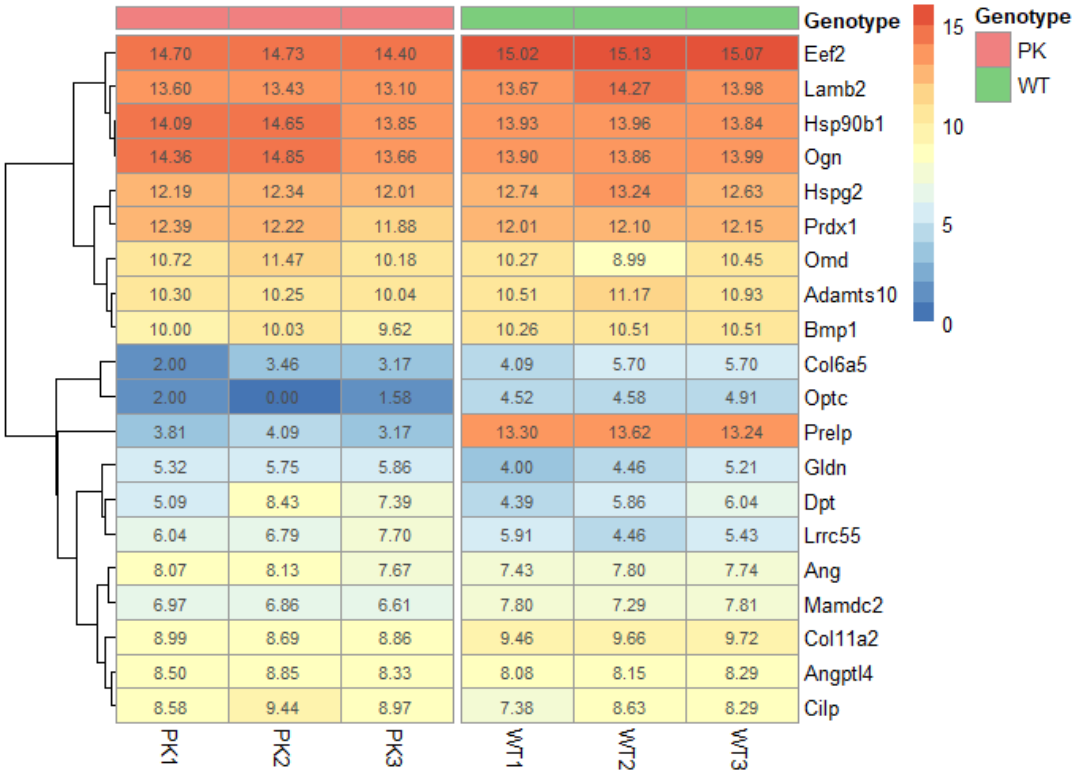

Figure 5.19. Heatmap of Extracellular matrix (GO:0031012). Rows are clustered according to expression levels, and similarity is shown as a dendrogram.

Finally, I utilised GSEA to perform enrichment analysis. I analysed up-regulated and down-regulated genes separately, and top 10 enriched gene sets are shown in Table 5.9 and Table 5.10 respectively. Interestingly, gene sets related to inflammation have been detected to being up-regulated in PRELP$^{-/-}$ samples. In contrast, the number of genes found to be enriched in gene sets in the list of down-regulated genes is smaller, suggesting that the absence of PRELP generally causes an increase in the transcription of genes.

Hallmark Gene Set Name	Description	Input	p-value	FDR
Interferon Gamma Response	Genes up-regulated in response to IFNG	22	4.24E-16	2.12E-14
Interferon Alpha Response	Genes up-regulated in response to alpha interferon proteins	16	6.93E-15	1.73E-13
Complement	Genes encoding components of the complement system, which is part of the innate immune system	18	6.37E-12	7.96E-11
Myc Targets v1	A subgroup of genes regulated by Myc – version 1 (v1)	18	6.37E-12	7.96E-11
mTORC1 signaling	Genes up-regulated through activation of mTORC1 complex	16	5.47E-10	5.47E-11
Inflammatory Response	Genes defining inflammatory response	15	4.59E-9	3.82E-8
Xenobiotic Metabolism	Genes encoding proteins involved in processing of drugs and other xenobiotics	14	3.58E-8	2.56E-7
UV Response up	Genes up-regulated in response to ultraviolet radiation	12	1.4E-7	8.73E-7
Apoptosis	Genes mediating programmed cell death (apoptosis) by activation of caspases	12	1.72E-7	9.53E-7
Estrogen Response Late	Genes defining late response to estrogen	13	2.6E-7	1.3E-6

Table 5.9. Enriched Hallmark Gene Sets up-regulated in PRELP$^{-/-}$. Analysis was done using the tools available online (http://software.broadinstitute.org/gsea/msigdb/annotate.jsp).

Hallmark Gene Set Name	Description	Input	p-value	FDR
Myogenesis	Genes involved in development of skeletal muscle (myogenesis)	9	7.02E-5	3.51E-3
Heme Metabolism	Genes involved in metabolism of heme and erythroblast differentiation	8	3.91E-4	9.77E-3
UV response DN	Genes down-regulated in response to ultraviolet (UV) radiation	6	1.68E-3	2.41E-2
Epithelial Mesenchymal Transition	Genes defining epithelial-mesechymal transition, as in wound healing, fibrosis and metastasis	7	1.93E-3	2.41E-2
Bile Acid Metabolism	Genes involved in metabolism of bile acids and salts	5	3.02E-3	2.85E-2
Hedgehog Signaling	Genes up-regulated by activation of hedgehog signaling	3	3.75E-3	2.85E-2
Cholesterol Homeostasis	Genes involved in cholesterol homeostasis	4	3.99E-3	2.85E-2
Apical Junction	Genes encoding components of apical junction complex	6	8.33E-3	4.16E-2
mTORC1 Signaling	Genes up-regulated through activation of mTORC1 complex	6	8.33E-3	4.16E-2
Xenobiotic Metabolism	Genes encoding proteins involved in processing of drugs and other xenobiotics	6	8.33E-3	4.16E-2

Table 5.10. Enriched Hallmark Gene Sets down-regulated in PRELP$^{-/-}$. Analysis was done using the tools available online (http://software.broadinstitute.org/gsea/msigdb/annotate.jsp).

5.3.5 Summary

I have analysed RNA seq data in the hopes to determine which signalling pathways are affected in $OMD^{-/-}$ and $PRELP^{-/-}$ mice. Although only two $OMD^{-/-}$ samples were analysed, enrichment analysis suggests that cytokine signalling is affect in $OMD^{-/-}$ mice. For PRELP, differentially expressed genes determined using p-values adjusted for multiple tests did not yield any ontology or enrichment results. Unadjusted p-values were used, and ontology analysis indicated that a variety of biological processes included macrophage activation and cell adhesion were altered in $PRELP^{-/-}$. Taking a closer look, a large portion of genes deregulated in $PRELP^{-/-}$ were found to localise to the ECM – these were found to be other members of the SLRP family, BM components and angiogenic signalling molecules among others.

5.4 Discussion

5.4.1 Limitations of the microarray study

A microarray experiment to determine differential gene expression in $OMD^{-/-}$ and $PRELP^{-/-}$ vessels was performed by colleagues and collaborators before the beginning of this project. After obtaining the raw files, I attempted to analyse the data using R and found it challenging to extract meaningful data from.

By considering the distribution of p-values, I can see that the dataset is not ideal, where there are very few significant genes, even at quite a permissive p-value cut-off of p-value<0.05 (Figure 5.6). In particular, the peak of p-values at around 0.5 for both datasets is quite unexpected; it's possible that these genes may be differentially regulated, but because I have such a small samples size (n=2), they are regarded as being insignificant. Indeed, the ideal distribution of p-values would display an anti-conservative distribution (Figure 5.20). In this distribution, a high number of genes would have a low p-value, and the rest of the histogram would be rather flat.

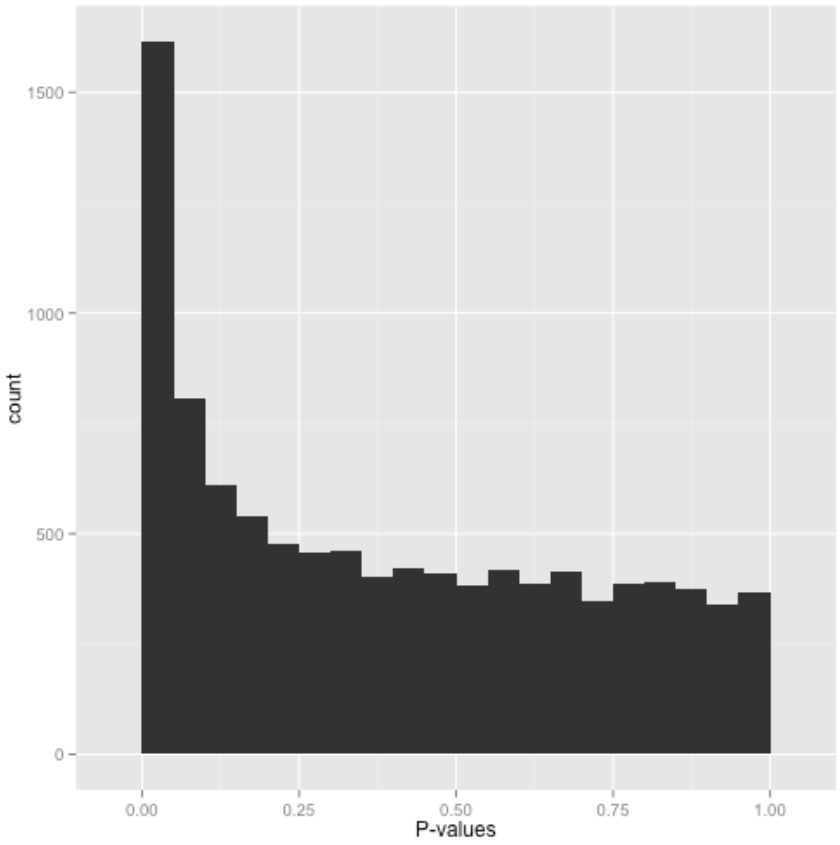

Figure 5.20. Histogram of ideal, anti-conservative distribution of p-values. (Robinson, 2014)

In addition, given that there are approximately 20'000 probes in an Affymetrix GeneChip Mouse 430A2 chip, at a p-value cut-off of $p<0.05$, there is a huge possibility of false-positive results. Indeed, analysis using SAM indicated that there is a very high estimated FDR in the dataset. Ideally, with a larger dataset with at least 3 samples per genotype, I would correct for multiple testing, e.g. using a Bonferroni correction. The adjusted p-values would also have a more stringent cut-off, where significant genes have p-value (adjusted) < 0.01.

Microarray experiments also have a number of theoretical and technical issues in general. They are dependent on target sequences hybridising to a premade set of probes, and hence can only probe known information. Although this is particularly cumbersome for researchers studying unconventional model organisms, microarray technology still has drawbacks for well-studied genomes. For example, given that the probe sequences are pre-determined, it does not allow exploratory work, looking at new, undiscovered RNA molecules.

Although various normalisation methods exist to correct for non-specific binding, as I saw previously, each normalisation method can have quite a dramatic effect on the dataset,

sometimes even changing the values quite drastically in the case of MAS5 normalisation for example (Figure 5.3). However, it should be noted that there are a few studies highlighting the issues with pre-processing techniques. Of particular note is a study where the authors examined a spiked-in experiment, where a set of control genes are spiked in at known concentrations, and found that raw data was more reliable in detecting these spiked-in genes compared to MAS5- or RMA-normalised data (Deandrés-Galiana et al., 2016). Another study showed that normalisation in cancer datasets could lead under-estimation of the magnitude of the changes in genes expression (Wang et al., 2012). Reports such as these demonstrate a major flaw in microarray data analysis – it is extremely difficult to know whether it is appropriate to apply normalisation at all, and which method would be the most appropriate.

Finally, since most microarray chips are scanned for fluorophores and hence fluorescence intensity, the dynamic range of microarray experiments is dictated very strongly by the limits of the sensitivity of fluorescence detection. For example, two probes may exhibit maximum fluorescence intensity due to binding of multiple cDNA molecules and have a very similar log2(intensity) expression value. However, in reality, it's possible that one of these transcripts is actually expressed at a much higher level than the other – however this difference is not detected due to the nature of scanning chips to detect fluorescence intensity.

Given the technical limitations of this experiments, where I had a very small sample size, I was unable to perform reliable statistical analysis. By enabling a particularly generous significance threshold for such a large dataset (over 20'000 probes), I detected differentially-expressed genes. However, upon viewing the heatmaps created from log2(intensity) values of these significant genes, I can visually determine that there aren't obvious differences between knock-out and wild-type transcriptomes. This is likely to be a combination of a high number of false-positives due to the p-value cut-off and small sample size. The nature of microarray experiments could also have contributed to this experimental noise. Although I probed three of the most widely-used normalisation methods and selected what I deemed to be the most appropriate, it's been well-documented that the normalisation method applied to the dataset could have a profound effect on the resulting list of significant genes.

5.4.2 RNA seq of OMD$^{-/-}$ samples

As mentioned previously, I have detected that one of the samples did not originate from an OMD$^{-/-}$ mouse and was likely a heterozygote. Gene expression analysis above was therefore performed with 2 OMD$^{-/-}$ samples compared to 3 wild-type samples. Whilst analysing the RNA seq data, I also prepared another OMD$^{-/-}$ sample prepared in the same manner to complete the dataset. Unfortunately, when comparing all 6 samples together, it is clear that the most recent sample is wildly different from the others. The heatmap produced clearly shows that sample OK2's gene counts are completely different from OK1 and OK3 (Figure 5.21). The fact that gene counts obtained from separate library preparations produced different results is a concern. From the heatmaps, I can see that the expression levels of genes from OK2 are generally higher than all other samples. I suspect that the trend remains the same, where there is an increase in genes related to immunity and inflammation. These differences observed could be due to differences in library preparation, but may also be variation in that particular sample. Therefore, in order to perform RNA seq analysis of OMD$^{-/-}$ meningeal vessels, six new samples should be prepared and sequenced simultaneously to prevent variation in gene counts due to library preparation and sequence batch.

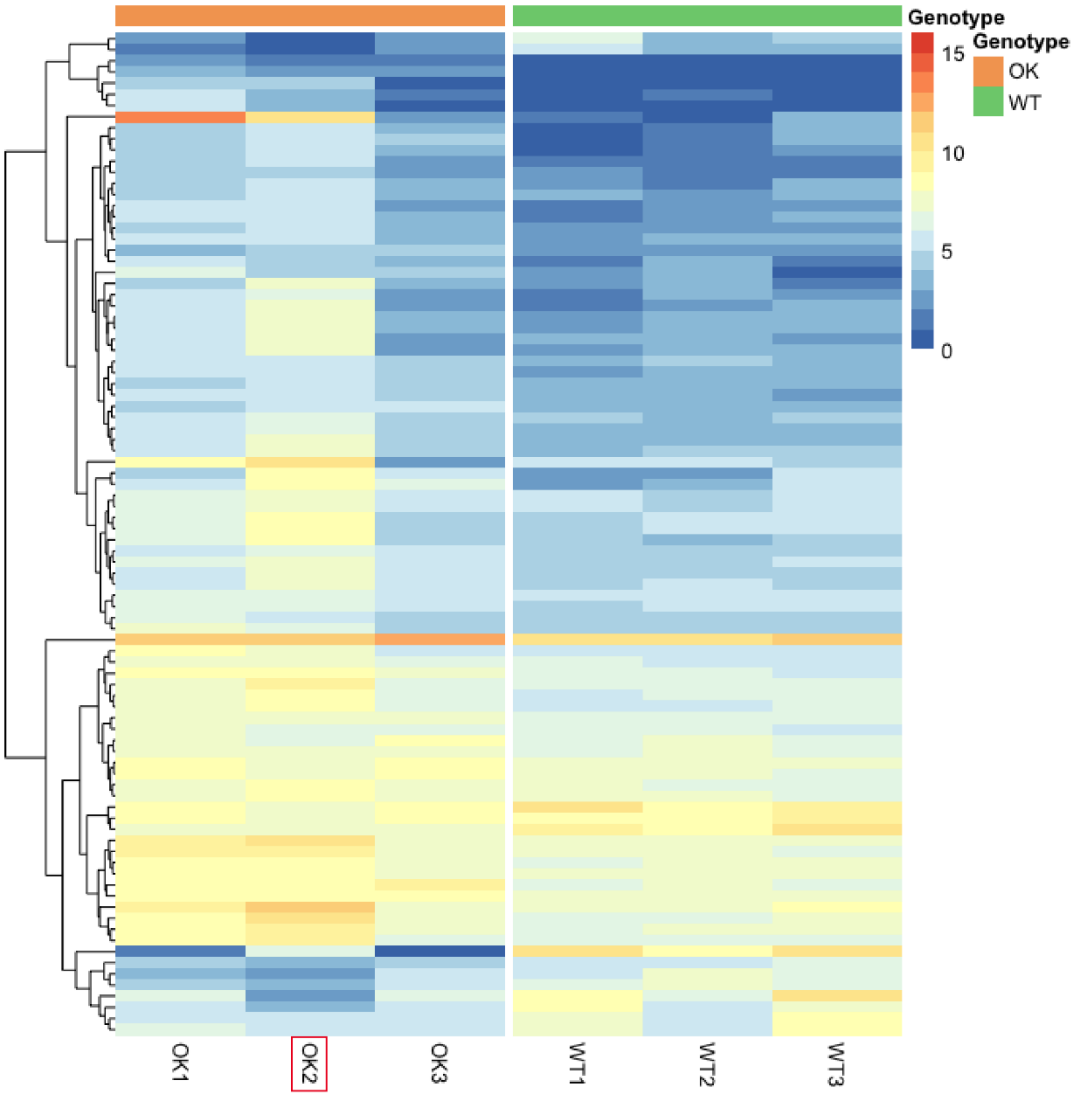

Figure 5.21. Heatmap of genes detected at p-value < 0.01 when comparing OMD$^{-/-}$ and wild-type datasets. Sample OK2 (red) was prepared separately from the others to replace the sample originating from OMD$^{+/-}$.

Enrichment analysis of differentially-expressed genes from the two OMD$^{-/-}$ samples strongly suggests that OMD has a role in inflammation (Table 5.5, Table 5.6 and Figure 5.18). Interferon signalling seems to be the most strongly affected by the absence of OMD. Interferons are critical components of the innate and adaptive immune system, particularly against viral infections. It is produced primarily by activated T cells and natural killer cells, leading to an up-regulation of pro-inflammatory molecules such as interleukins and TNF-α (Tau & Rothman, 1999). I observed that genes associated with interleukin and TNF-α signalling were also up-regulated. Finally, visualisation of the protein-protein interaction network of differentially expressed genes in OMD$^{-/-}$ using the default settings in STRING indicates that the majority of proteins act in concert (Figure 5.22). OMD may therefore affect immunity and inflammation.

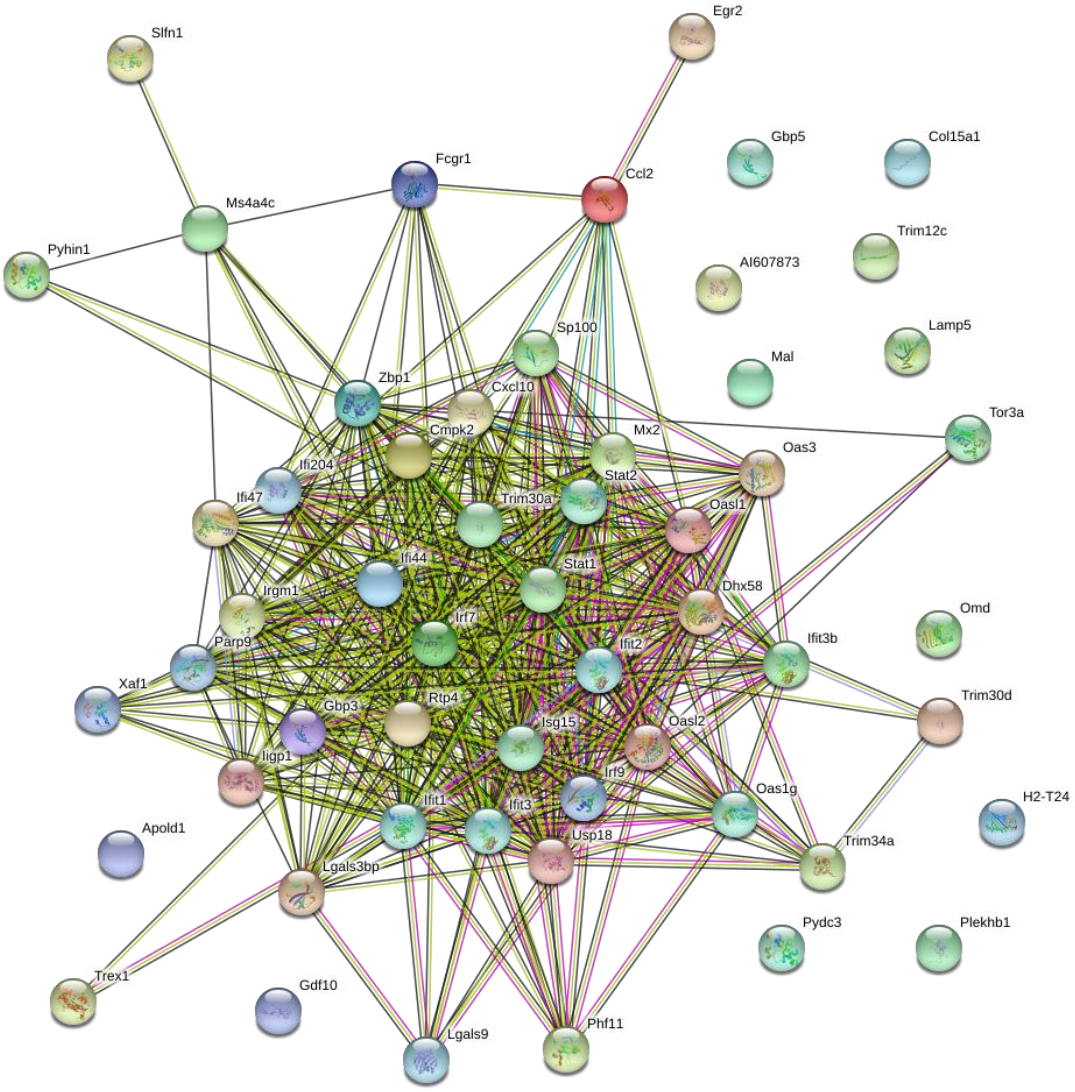

Figure 5.22. Visualisation of protein-protein interactions of differentially-regulated genes in OMD$^{-/-}$ using the default settings in STRING.

5.4.3 RNA seq of PRELP$^{-/-}$ samples

When viewing the heatmap of global changes in gene expression between PRELP$^{-/-}$ and wild-type, it is clear that the differences between knock-out and wild-type are subtle in this experiment. This was highlighted by the fact that enrichment analysis using a cut-off of adjusted p-values yielded no significant results. Analysis was therefore performed using an unadjusted p-value of 0.01 – the dataset is much larger, 288 genes at p-value < 0.01 as opposed to 37 genes at p-adj < 0.05. Due to lack for multiple testing, the incidence of type I errors was much larger.

GO analysis of Biological Processes did not yield any results which seem to be directly relevant to the disrupted BBB of PRELP$^{-/-}$ animals, aside from perhaps macrophage activation and immune response (Table 5.7). Instead, using GO: Cellular Component, many differentially expressed genes were found to encode ECM proteins. Of the 288 genes

found to be statistically-significant at p-value < 0.01, 69 genes were found to be associated with the ECM (Table 5.8). There were changes in components of the basement membrane, including collagens, laminin β2 and perlecan (Figure 5.19). As discussed in Chapter 4, laminin β2 is not a component of the BBB basement membrane; it was found to be expressed in smooth muscle, skin, kidneys (Durbeej, 2010; Iivanainen et al., 1995; Noakes, Miner, et al., 1995). However, the down-regulation of a laminin subunit does suggest a possibility that the expression of BBB laminins may also be decreased.

The decrease in perlecan expression is also very interesting. In Chapter 4, staining of brain capillaries with perlecan indicated that there was a decrease in perlecan around the vasculature in PRELP$^{-/-}$. Clearly the loss of vascular BM perlecan is relatively small; if PRELP loss induced a large change in the expression of perlecan, I would expect a more severe phenotype; as discussed previously, perlecan knock-out mice die at E10-12 or shortly after birth due to haemorrhaging (Costell et al., 1999).

There were also changes in ECM proteins implicated in the regulation of angiogenesis. For example, the expression of osteoglycin was found to be up-regulated in PRELP$^{-/-}$. As discussed in Chapter 1, deletion of an SLRP often leads to the up-regulation of other members with similar function. Osteoglycin is a class III SLRP with anti-angiogenic activity, capable of preventing VEGFA/VEGFR2 signalling (Wu et al., 2017). In Chapter 3, when I investigated the expression of PRELP and SLRP members in a mural-cell specific gene set, osteoglycin was also detected (He et al., 2016). Given its up-regulation in PRELP$^{-/-}$, it is possible that PRELP and osteoglycin have overlapping functions and osteoglycin was up-regulated to compensate for PRELP loss.

Other pro-angiogenic factors such as Angiogenin and Angptl4 are up-regulated too, supporting my hypothesis that PRELP is important for vascular homeostasis. Aside from osteoglycin, there were changes in OMD and opticin. OMD has no known angiogenic function according to the literature and the results presented in Chapter 4. Opticin has been shown to also be an inhibitor for angiogenesis, and seems to be expressed rather weakly in brain vessels. When comparing knock-out and wild-type, its expression level is decreased in PRELP$^{-/-}$.

Although the changes in the transcription of genes encoding proteins in the ECM do not necessarily rationalise the phenotype observed in PRELP$^{-/-}$, they do indicate that PRELP can affect the structure and/or composition of the ECM, which in turn may affect the regulation of signalling pathways.

Genes implicated in increased IFN-γ signalling were found to be up-regulated in PRELP$^{-/-}$ using GSEA (Table 5.9). *In vitro* studies have demonstrated that the addition of IFN-γ to endothelial monolayers led to changes in morphology and an increase in monolayer permeability (Huynh & Dorovini-Zis, 1993), suggesting that increased IFN-γ activity can be detrimental for the integrity of the BBB. Infection of mice with a variety of viruses was found to lead to an increase in IFN-γ as expected, and this was accompanied by BBB breakdown (Chai et al., 2014; Too et al., 2014). In these studies, infection of IFN-γ knock-out animals or those treated with antibodies against IFN-γ were found to have less severe BBB permeability. It is therefore possible that if there is an up-regulation of inflammation-related molecules in PRELP$^{-/-}$, viral infection would strongly exacerbate the existing phenotype of a weakened BBB.

Inflammation and BBB breakdown accompany many neurodegenerative disorders, including Alzheimer's disease, Parkinson's disease and Huntington's disease (Hirsch & Hunot, 2009; Politis et al., 2015; Streit et al., 2009). Studies in inflammation mouse models have indicated that acute inflammation can lead to BBB breakdown which can aggravate or precede the appearance of symptoms, suggesting that inflammation and BBB breakdown are not simply consequences of disease progression (Dénes et al., 2011; Ujie et al., 2003). Treating purified human pericytes with IFN-γ was found to increase PDGFR-β internalisation and subsequent degradation (Jansson et al., 2016). Consistent with these findings, pericyte loss has also been implicated in BBB dysfunction in Alzheimer's disease (Sagare et al., 2013) and diabetic retinopathy (Enge et al., 2002). Therefore, given the increase in transcription of genes related to inflammation and the phenotype of BBB breakdown, it is possible that PRELP$^{-/-}$ mice could develop neurodegenerative disorders more readily than wild-type. It is unclear whether inflammation precedes BBB breakdown or vice versa in PRELP$^{-/-}$.

Finally, another hallmark gene set found to be up-regulated in PRELP$^{-/-}$ is complement activation (Table 5.9) – the complement system is part of the innate immune system and aids the clearance of pathogens. PRELP, among other SLRP members, affects the complement system. *In vitro* evidence indicates that PRELP binds to C9 and prevents the formation of the membrane attack complex (Happonen et al., 2012). This was demonstrated *in vivo* too, where PRELP was found to be a potent inhibitor of complement-mediated damage in mouse eyes (Birke et al., 2014). While these findings are not directly linked to the BBB breakdown I observed in PRELP$^{-/-}$ mice, this does indicate that the RNA seq data is consistent with findings in the literature.

To summarise, using RNA extracted from meningeal vessels, I discovered an enrichment in Biological Processes which may be linked to the phenotypes observed in PRELP$^{-/-}$, including macrophage activation and cell-cell adhesion. In addition, ontology analysis for Cellular Compartment indicated that PRELP affects many genes encoding ECM proteins, including other SLRPs and BM components. Enrichment analysis using GSEA has indicated that pathways involved in inflammation are up-regulated in PRELP$^{-/-}$ and may have a role in affecting vessel stability in PRELP$^{-/-}$ and possibly progression towards neurodegenerative diseases. Further work would have to be pursued in order to identify the processes involved in BBB breakdown.

5.4.4 Technical difficulties regarding RNA extraction from meningeal vessels

I have detected that there is an up-regulation of immune processes in OMD$^{-/-}$ and PRELP$^{-/-}$ mice. Although inflammation has been linked to BBB breakdown in many circumstances, the prevalence of immune processes detected from my datasets may be attributed to contamination from lymphatic endothelial cells, which are located in close proximity to meningeal vessels (Figure 5.23) (Raper et al., 2016). According to the protocol I utilised for the dissection of the meninges, "*less than 5% of the RNA harvested should be of blood origin*" (Bowyer et al., 2012). Despite this, from a practical point of view, the amount of contamination is probably higher – particularly when isolating the meningeal vessels near the olfactory bulb, where tissue was more likely to peel alongside the meninges. Therefore, it is highly likely that the RNA seq dataset contains information from a variety of cell types, possibly masking differences gene expression related to changes specifically in the vascular system.

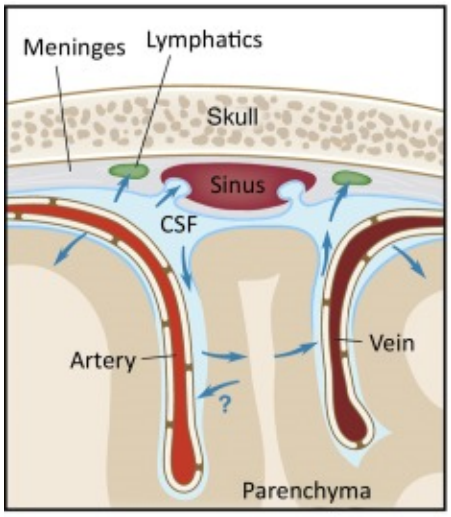

Figure 5.23. Proximity of the lymphatic endothelium to the meningeal vessels on the surface of the brain. Figure from (Raper et al., 2016).

As hinted to above, there is a technical aspect to removing meningeal vessels. Brains were submerged in cold PBS and the meningeal vessels carefully peeled off. Each isolation, even after practice, could take up to 20 minutes prior to RNA isolation. RNA was extracted from meningeal vessels sequentially – i.e. mice were culled, and RNA extracted immediately after death as I was concerned that there may be rapid post-mortem changes in the transcriptome, completely independent of genotype. Although I attempted to perform the procedure consistently, there may have been variations in the purity of each sample as the procedure proved to be quite technically challenging in order to prevent excess contamination from the brain itself. As a result of this, there may also be more noise introduced than expected by slightly varied sample preparation.

In order to reduce contamination in these meningeal RNA samples, animals could be perfused with saline and a dye. The use of a dye, such as Evans Blue, is to facilitate the visual identification of vessels on the surface of the brain.

5.5 Conclusions

I analysed microarray data of ventral arteries. After normalising the data, I attempted to perform ontology analysis using DAVID and KEGG but did not obtain clear data. I then isolated RNA from brain meningeal vessels and analysed the data. First, enrichment analysis was performed based on Biological Processes and Cellular Component GO terms. Then enrichment in curated gene sets was performed to further understand the genes which are differentially-regulated in OMD and PRELP. I found that there was up-regulation of many genes involved in immune processes, particularly in $OMD^{-/-}$. I found that many genes in $PRELP^{-/-}$ encoded ECM proteins, including BM components, other SLRPs and signalling molecules. These results therefore suggest that the phenotype observed in $PRELP^{-/-}$ is due to changes in the composition of the ECM and BM, and an increase in inflammatory signalling causing BBB breakdown. In order to further investigate signalling pathways which may be altered in $PRELP^{-/-}$, the next chapter will discuss experiments performed in cultured cells.

Chapter 6 Signalling functions of OMD and PRELP

6.1 Preface

I have analysed OMD and PRELP knock-out mice, and have determined that there is vascular dysfunction in PRELP$^{-/-}$ mice. Using RNA seq, I found hints of pathways and processes which may be affected in PRELP$^{-/-}$, however they are not entirely clear. I must therefore use *in vitro* systems to probe any effect exerted by OMD and PRELP. To this end, I attempted to utilise mouse embryonic fibroblasts (MEFs), human umbilical vein endothelial cells (HUVECs) and isolated mouse brain endothelial cells (MBECs). In addition, immunoprecipitation experiments were performed to determine binding of OMD and PRELP to TGF-β and VEGFA isoforms.

6.2 Molecular cloning

6.2.1 VEGFA isoform constructs

PRELP$^{-/-}$ animals in particular exhibit signs of BBB breakdown. One of the most important growth factors regulating vascular permeability is VEGFA. Of the many VEGFA isoforms, VEGFA-165 is the most strongly implicated in vascular permeability (Dobrogowska et al., 1998). I aimed to create FLAG-tagged VEGFA isoform constructs to determine whether there is direct binding of OMD or PRELP. VEGFA-121, VEGFA-165 and VEGFA-165b encoding plasmids were kindly provided by Dr Phillipp Berger, Paul Scherrer Institute (Switzerland). After sequencing the plasmids, I designed PCR primers for amplifying the cDNA molecules with the appropriate restriction enzyme sites on the 5' and 3' ends (see Chapter 2). Tools such as ExPASy (Gasteiger et al., 2003), Clustal Omega (Sievers et al., 2011) and Serial Cloner (Perez, 2013) were used to verify sequences and strategies. I then sub-cloned the PCR amplicons into pCS2 vectors, appropriate for mammalian cell expression. See Appendix for detailed sequences and rationale behind primer design.

6.2.1.1 Validating VEGFA-FLAG constructs

After amplification by PCR, I obtain strong bands around ~400, ~500 and ~500bp for VEGFA-121, VEGFA-165 and VEGFA-165b respectively (Figure 6.1; shown in red), consistent with the sizes of cDNA molecules. I then proceeded with the cloning protocol and transformed chemically-competent bacteria. Since the pCS2 vector contains an ampicillin resistance cassette, bacteria were plated on ampicillin agar plates. The following day, colonies were picked and seeded into liquid media containing ampicillin overnight. Potential plasmids were then purified and sent for sequencing.

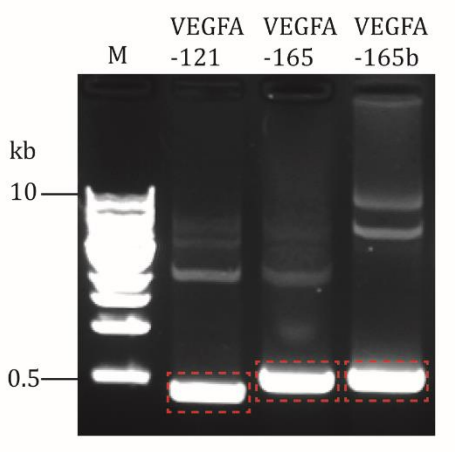

Figure 6.1. PCR amplification of VEGFA isoforms. PCR products were run on a 1% agarose gel stained with SYBR Safe. The PCR amplicons are surrounded in red. 1kb DNA ladder was run alongside samples. Expected sizes: ~399 bp (121), ~531 bp (165), ~531 bp (165b).

Once I obtained the correct sequences, I then proceeded to transfect HEK293 cells with pCS2-VEGFA-FLAG constructs. Since the VEGFA cDNA does not contain the signal peptide targeting the proteins for secretion, I aimed to detect VEGFA-FLAG in the cell lysate. To this end, 48h after transfection, I determined the expression of VEGFA-FLAG by western blotting (Figure 6.2). Low molecular weight proteins were detected using an anti-FLAG antibody, thereby confirming that the pCS2-VEGFA-FLAG constructs allow the cells to produce FLAG-tagged VEGFA isoforms.

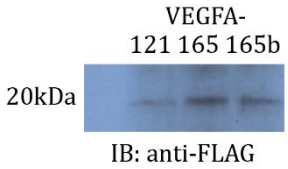

Figure 6.2. Detection of FLAG-tagged VEGFA constructs by western blotting. Western blot of proteins extracted from transfected HEK293 cells. Immunoblotting was performed using anti-FLAG tag antibody.

6.2.2 PRELP constructs -PR and -NT

Given the importance of PRELP in the maintenance of the BBB and its ability to bind to HS, I was interested in determining whether the HS-binding domain of PRELP is important for its function. I have therefore decided to make a construct of PRELP lacking its critical proline and arginine (PR)-rich domain; -PR PRELP. In addition, I also utilised a construct of PRELP lacking its N-terminal signal peptide to act as an additional negative control in experiments where the conditioned media was utilised; -NT PRELP. This construct could also be used to determine whether there are any changes in the secretome when cells are exposed to higher concentrations of cytoplasmic PRELP.

6.2.2.1 -NT PRELP

A PRELP plasmid lacking the N-terminal GAG-binding domain was kindly provided by Dr Anders Aspberg, Lund University (Sweden). While this plasmid was initially used to probe the HS-binding capabilities of PRELP, given that it lacks the entire N-terminus (Bengtsson et al., 2002), it as a result also lacks the signal sequence required for protein secretion. I obtained the PCR primer sequence used to amplify this plasmid from their publication (Bengtsson et al., 2000) and modified the restriction enzyme sites to suit the cloning vector. I aimed to produce untagged and C-terminal myc-tagged constructs.

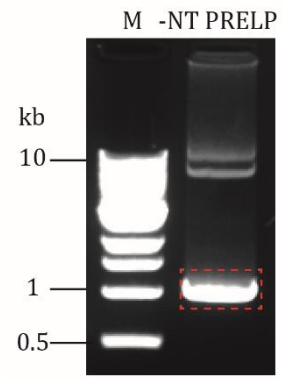

Figure 6.3. PCR amplification of -NT PRELP. PCR products were run on a 1% agarose gel stained with SYBR Safe. The PCR amplicons of -NT PRELP is surrounded in red. 1kb ladder was run alongside sample. Expected band size: ~1kb.

6.2.2.2 -PR PRELP

I aimed to produce a protein with an intact N-terminal signal sequence, but lacking the N-terminal HS-binding domain. Box 6.1 shows the protein sequence of human PRELP; I sought to conserve the signal peptide (green) and LRR domains (blue) whilst removing the PR-rich region (red). This should therefore produce a secreted, PR-deficient version of PRELP.

MRSPLCWLLPLLILASVAQGQPTRRPRPGTGPGRRPRPRPRPTPSFPQPDEPAEPTDLPPPLPPGPPSIFPDCP
RECYCPPDFPSALYCDSRNLRKVPVIPPRIHYLYLQNNFITELPVESFQNATGLRWINLDNNRIRKIDQRVLEK
LPGLVFLYMEKNQLEEVPSALPRNLEQLRLSQNHISRIPPGVFSKLENLLLLDLQHNRLSDGVFKPDTFHGLKN
LMQLNLAHNILRKMPPRVPTAIHQLYLDSNKIETIPNGYFKSFPNLAFIRLNYNKLTDRGLPKNSFNISNLLVL
HLSHNRISSVPAINNRLEHLYLNNNSIEKINGTQICPNDLVAFHDFSSDLENVPHLRYLRLDGNYLKPPIPLDL
MMCFRLLQSVVI

Box 6.1. Protein sequence of human PRELP (Uniprot P51888). Signal peptide in green, PR-rich region in red and LRR domains in blue.

To this end, I designed primers to amplify the signal sequence and LRR domain of PRELP. The strategy was to ligate the signal sequence fragment to the LRR domain fragment before ligating the entire -PR PRELP sequence into the pCS2 vector (Figure 6.4). Three restriction enzymes were utilised; EcoR1 and EcoRV on the 5' and 3' ends of the signal

sequence fragment and EcoRV and XhoI on the LRR domain fragment. The two DNA fragments could then be ligated via the sticky ends produced by digestion by EcoRV to produce -PR PRELP. Critically, EcoRV was chosen specifically to produce sticky ends between the signal peptide and LRR fragments as it is not present in the multiple cloning site of the pCS2 vector.

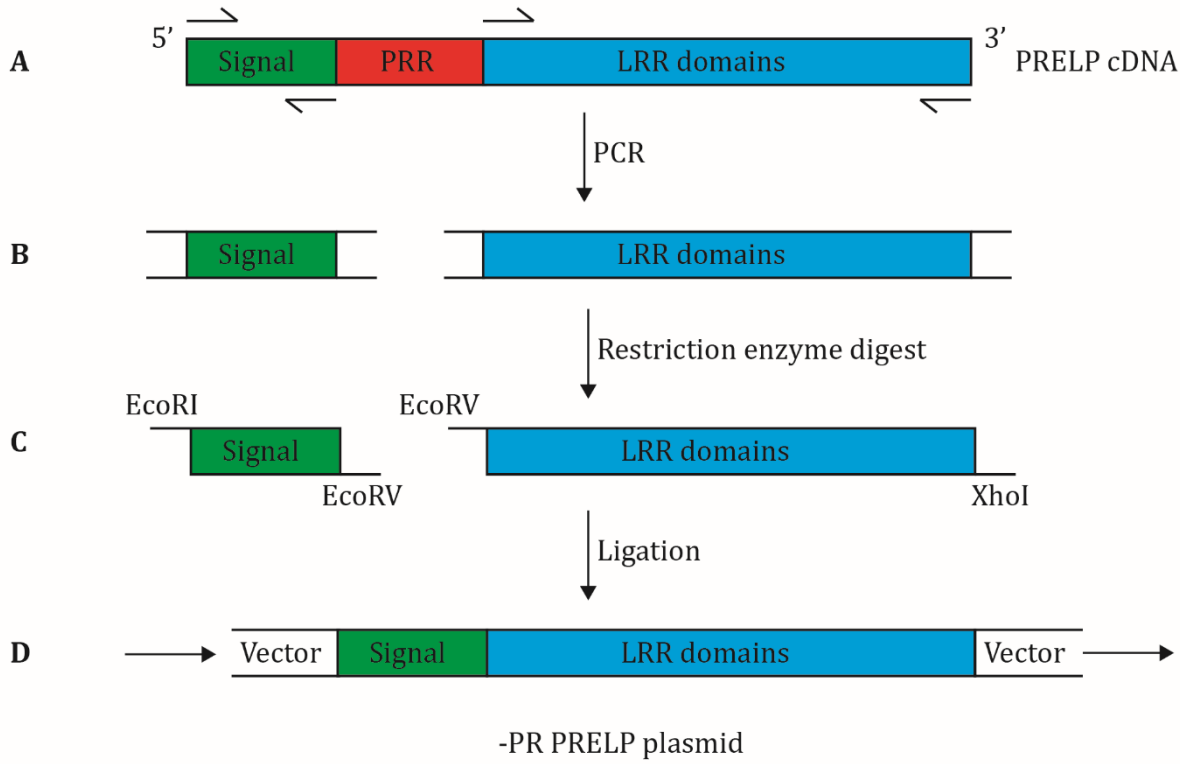

Figure 6.4. Cloning strategy to produce -PR PRELP plasmid. The signal peptide and LRR domains were amplified using PCR **(A)** to create two cDNA fragments **(B)**. These cDNA fragments were then digested using EcoRI, EcoRV and XhoI **(C)** before being ligated to the vector **(D).**

I simulated this cloning strategy in the program Serial Cloner. I obtained a nucleotide sequence of 1086bp (Box 6.2) and translated it to obtain the protein sequence (Box 6.3). I noted that two additional residues, aspartate and isoleucine, would potentially be incorporated into the protein sequence between the signal peptide and LRR region. Given that the strategy seems to work *in silico*, I proceeded with the outlined experiment. Just as before, I aimed to produce untagged and C-terminal myc-tagged constructs.

5'atgaggtcacccctctgctggctcctcccacttctcatcttggcctcagtggcccaaggccaggatatcagc
tttcctcagcctgatgaaccagcagagccaacagacctgcctcctcccctccctccaggccctccatctatctt
ccctgactgtccccgcgaatgctactgccccctgatttcccatctgccctctactgtgatagccgcaacctgc
gaaaggtccctgtcatcccgccccgcatccattacctctatctccagaacaacttcatcactgagctcccggtg
gagtccttccagaatgccacaggcctgcgatggattaacctggacaacaaccgaatccgcaagatagaccagag
ggtgctggagaaactgcccggcctggtgttcctctacatggagaagaaccagttggaagaggtcccctcggccc
tgccccggaacctggagcagctgaggctgagccagaaccacatctccagaatcccgcctggtgtcttcagcaag

ctggagaacctgctgctcctggatctccagcacaacaggctgagcgacggcgtcttcaagcccgacaccttcca
tggcctcaagaacctcatgcagctcaacctggcccacaacatcctgagaaagatgccgcccagggtccccaccg
ccattcaccagctctacctggacagtaacaagattgagaccatccctaacggatacttcaagagctttcccaat
cttgccttcattcggcttaactacaacaagctgacagacaggggactccccaagaactcctttaatatctccaa
cctgcttgtgctccacctgtcccacaacaggatcagcagtgtgcccgccatcaacaacaggctggaacacctgt
acctcaacaacaatagcatcgagaaaatcaacggaacccagatttgccccaacgacctagtggcgttccatgac
ttctcctcggacctggagaacgtgccacacctgcgctacctgcggctggatggaaactacttgaagccgcccat
cccgctggacctcatgatgtgcttccgcctcctgcagtccgtggtcatctag **3′**

Box 6.2. Nucleotide sequence of putative -PR PRELP construct.

MRSPLCWLLPLLILASVAQGQ**DI**SFPQPDEPAEPTDLPPPLPPGPPSIFPDCPRECYCPPDFPSALYCDSRNLR
KVPVIPPRIHYLYLQNNFITELPVESFQNATGLRWINLDNNRIRKIDQRVLEKLPGLVFLYMEKNQLEEVPSAL
PRNLEQLRLSQNHISRIPPGVFSKLENLLLLDLQHNRLSDGVFKPDTFHGLKNLMQLNLAHNILRKMPPRVPTA
IHQLYLDSNKIETIPNGYFKSFPNLAFIRLNYNKLTDRGLPKNSFNISNLLVLHLSHNRISSVPAINNRLEHLY
LNNNSIEKINGTQICPNDLVAFHDFSSDLENVPHLRYLRLDGNYLKPPIPLDLMMCFRLLQSVVI*

Box 6.3. Translated protein sequence of putative -PR PRELP construct. Signal sequence in green and LRR domains in blue. Note that two residues have been incorporated between the signal peptide and the LRR domains (bold).

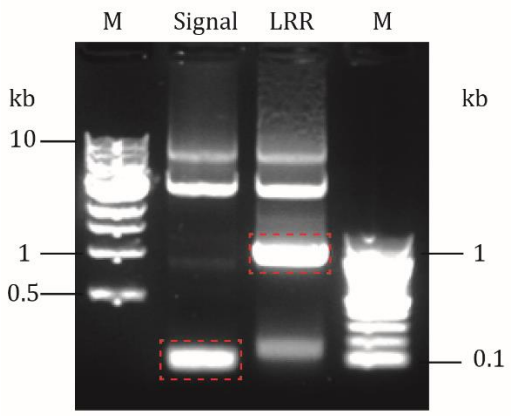

Figure 6.5. PCR amplification of signal sequence and LRR domains of PRELP. PCR products were run on a 1% agarose gel stained with SYBR Safe. The PCR amplicons are surrounded in red. Two ladders were utilised; 1kb (left) and 100bp (right). Expected sizes: 77bp (signal) and 1029bp (LRR).

6.2.2.3 Validating the PRELP constructs

After obtaining bacterial colonies with putative constructs, DNA was isolated and sent for sequencing. Sequencing of -NT PRELP has confirmed that it lacks N-terminal amino acids 2-157 (Box 6.4). Sequencing of -PR PRELP has also confirmed that there was a deletion although more amino acids than expected were deleted; amino acids 21-157 (Box 6.5; compare Box 6.1 with Box 6.5). Analysis in Pfam has indicated that the additional amino acids form a "low complexity region" and part of an LRR domain. Critically, however, the signal peptide in the -PR PRELP construct is intact. While this is not the construct outlined

above, I proceeded with this putative -PR PRELP construct nonetheless, as the cloning proved to be time-consuming and challenging.

```
>-NT PRELP

MEKNQLEEVPSALPRNLEQLRLSQNHISRIPPGVFSKLENLLLLDLQHNRLSDGVFKPDTFHGLKNLMQLNLAH
NILRKMPPRVPTAIHQLYLDSNKIETIPNGYFKSFPNLAFIRLNYNKLTDRGLPKNSFNISNLLVLHLSHNRIS
SVPAINNRLEHLYLNNNSIEKINGTQICPNDLVAFHDFSSDLENVPHLRYLRLDGNYLKPPIPLDLMMCFRLLQ
SVVI
```

Box 6.4. Protein sequence of -NT PRELP construct produced by pCS2-NT-PRELP plasmid. N-terminal sequence is in green and LRR sequence in blue. Amino acids 2-157 were deleted.

```
>-PR PRELP

MRSPLCWLLPLLILASVAQGQEKNQLEEVPSALPRNLEQLRLSQNHISRIPPGVFSKLENLLLLDLQHNRLSDG
VFKPDTFHGLKNLMQLNLAHNILRKMPPRVPTAIHQLYLDSNKIETIPNGYFKSFPNLAFIRLNYNKLTDRGLP
KNSFNISNLLVLHLSHNRISSVPAINNRLEHLYLNNNSIEKINGTQICPNDLVAFHDFSSDLENVPHLRYLRLD
GNYLKPPIPLDLMMCFRLLQSVVI
```

Box 6.5. Protein sequence of -PR PRELP construct produced by pCS2-PR-PRELP plasmid. N-terminal sequence is in green and LRR sequence in blue. Amino acids 21-157.

Source	Domain	Start	End
sig_p	n/a	1	20
low_complexity	n/a	4	13
disorder	n/a	18	66
low_complexity	n/a	21	43
low_complexity	n/a	48	66
Pfam	LRR_8	102	162
Pfam	LRR_8	171	233
low_complexity	n/a	193	206
Pfam	LRR_8	242	303
Pfam	LRR_1	312	340

Figure 6.6. Pfam analysis of PRELP domain structure. Amino acids 21-157 deleted in -PR PRELP (red box) correspond to low complexity and disorders regions in addition to part of an LRR domain.

Finally, in order to validate the use of -NT and -PR PRELP constructs for *in vitro* assays, HEK293 cells were transfected with the plasmids and cells were lysed after 48 hours. Protein samples were analysed by western blotting using a primary antibody against the myc tags on the pCS2+MT vector. Detection of blotting of PRELP and its mutant forms was challenging, where there are multiple bands (Figure 6.7). This may be due to various post-translational modifications of PRELP, but also indicative that PRELP may not be a very stable protein. This is a consideration which should be taken into account when interpreting results. Nonetheless, there seems to be adequate expression of mutant PRELP, particularly -PR PRELP, which I will use in subsequent experiments.

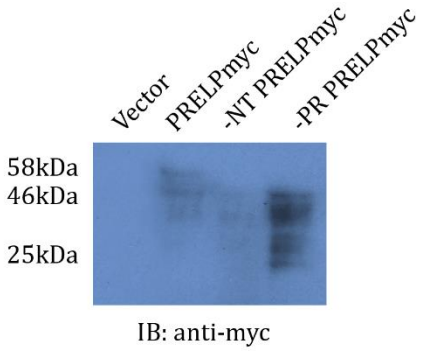

Figure 6.7. IB to detect -NT and -PR PRELPmyc constructs. -NT and -PR PRELPmyc were detected in cell lysates at lower molecular weight than PRELPmyc.

6.3 Effect of signalling ligands in mouse embryonic fibroblasts (MEFs)

6.3.1 Isolation of MEFs

In order to determine the signalling pathways affected by OMD and PRELP, I decided to generate MEFs from our wild-type and knock-out animals. Along with the relatively straightforward isolation procedure, these cells proliferate quickly and are easy to culture and maintain. Fibroblasts are derived from the mesodermal layer and are the major cell-type in connective tissues and secrete a variety of ECM components, including collagens and GAGs (Van Gansen & Van Lerberghe, 1988). Given that OMD and PRELP are secreted proteins, I hoped to be able to see differences in cellular response to signalling as a result of an altered ECM.

I therefore set up timed matings and culled the pregnant female mouse at E13.5 and isolated MEFs as described in Chapter 2. Critically, the homogenised mixture of cells derived from the embryos were cultured in gelatin-coated flasks – according to a published protocol, fibroblasts are the only cells capable of attaching to gelatin-coated flasks (Jozefczuk et al., 2012).

In order to confirm that these MEFs are knock-outs for OMD and PRELP, I extracted DNA and performed genotyping alongside a known heterozygote control (Figure 6.8). The results of genotyping indicated that the MEFs I isolated were the correct genotype. Note that in Figure 6.8B, the heterozygote control for PRELP genotyping only shows the knock-out band. This is due to the observation that PRELP ear samples must be processed and genotyped immediately for the most accurate genotyping. Storage at 4°C or -20°C reduces the quality of genomic DNA sufficiently for PCR reactions to fail. Nonetheless, I can confirm the genotype of the cell lines successfully.

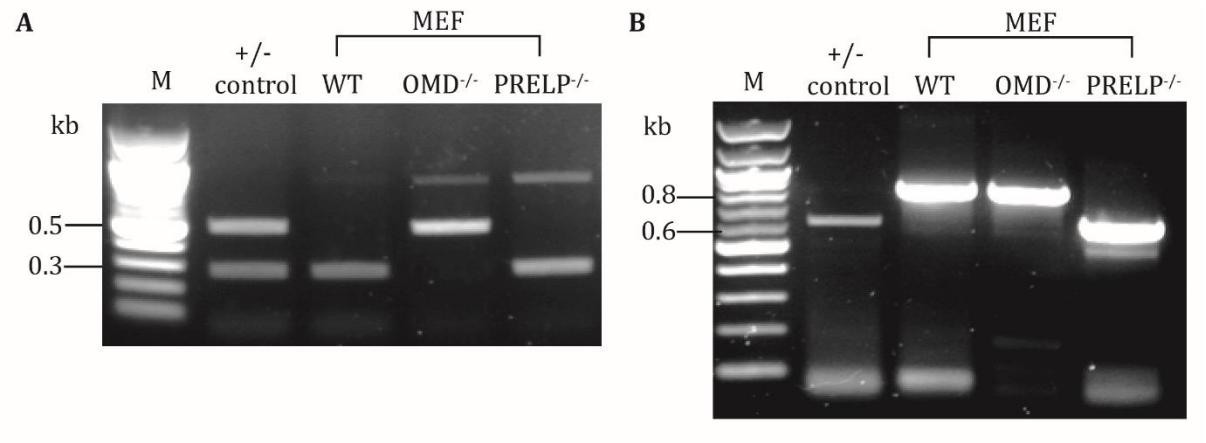

Figure 6.8. Genotyping of MEFs to detect OMD PCR bands (A) and PRELP PCR bands (B). PCR products were run on a 1% agarose gel stained with SYBR Safe. 100bp ladder was run alongside samples. As a positive control, I also genotyped a known heterozygote animal ($^{+/-}$ control). Expected band sizes: 298bp (OMD wild-type), 541bp (OMD knock-out), 846bp (PRELP wild-type), 634bp (PRELP knock-out).

In addition, our former colleague Dr Tomoko Orita confirmed by western blotting and β-galactosidase enzyme activity that the cell lines express β-galactosidase. Cell lysates were prepared and analysed by western blotting with an anti-β-galactosidase antibody. In addition, β-galactosidase enzyme activity was tested using X-gal and FDG, a fluorescent β-galactosidase substrate. While X-gal staining was difficult to detect in cells, the more sensitive fluorescent analogue FDG shows that there is weak β-galactosidase enzyme activity in the wild-type MEF cell line (Figure 6.9).

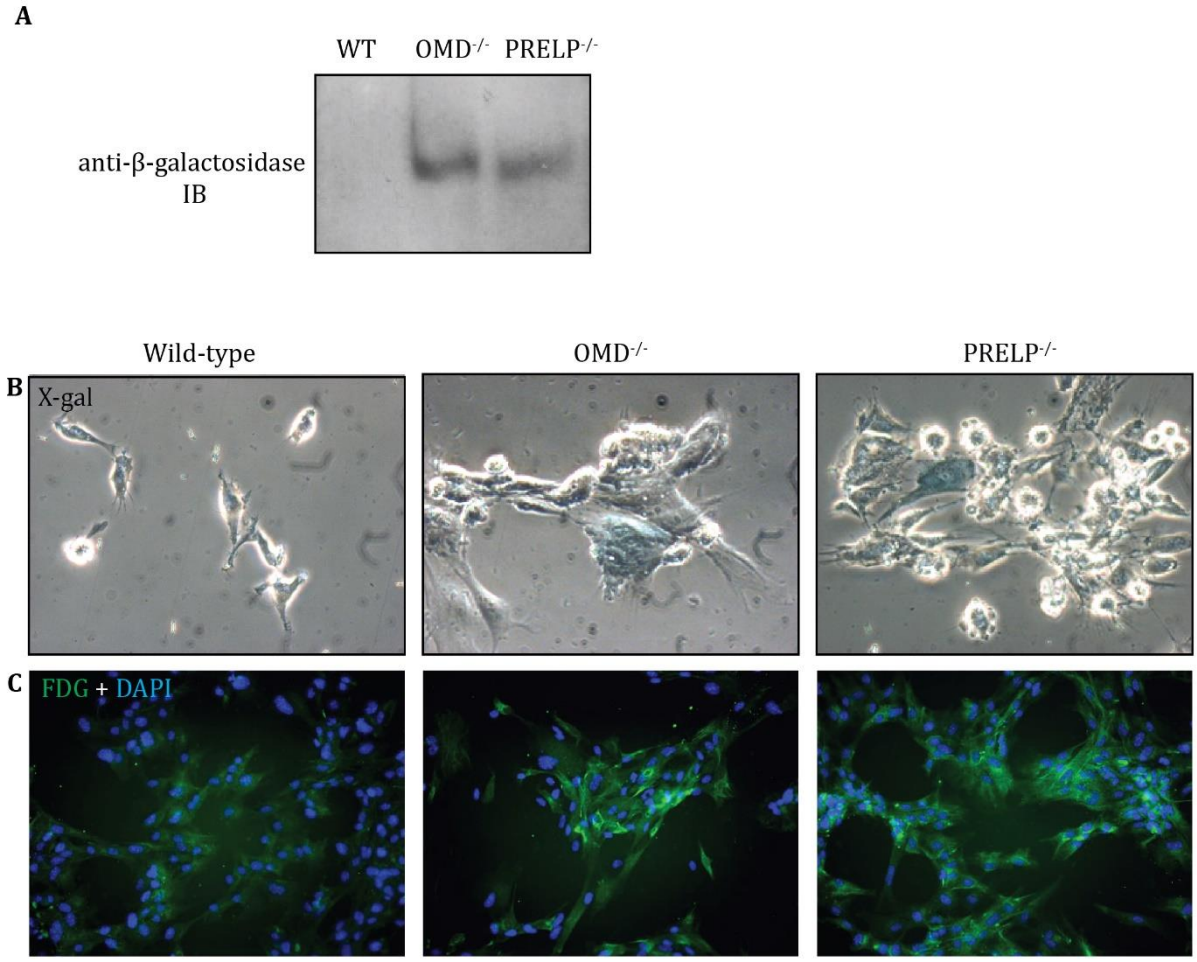

Figure 6.9. Detection of β-galactosidase protein (A) and β-galactosidase enzyme activity (B & C) in newly-established MEF cell lines. Images taken and experiments performed by Dr. Tomoko Orita.

From the genotyping and detection of β-galactosidase protein and enzyme activity, we determine that the cell lines have been established as planned. I have therefore proceeded to probe the effect of signalling molecules in OMD$^{-/-}$ and PRELP$^{-/-}$ cell lines. Cells were treated with growth factors and cell lysates were prepared. The phosphorylation of down-stream proteins was assessed. The ratio of band intensity of phosphorylation/total protein was determined, as outlined in in Chapter 2.

6.3.2 Effect of bFGF on MEFs

FGFs are growth factors involved in many processes including angiogenesis. FGFs are particularly interesting given that they are capable of binding to heparin (Arakawa et al., 1994). Given the finding using embryonic hindbrain vasculature that PRELP$^{-/-}$ mice have increased blood vessel content, I was interested to determine whether signalling downstream of bFGF are altered. Upon FGF binding, FGFR dimerisation occurs in the presence of heparin (Schlessinger et al., 2000) and leads to trans-phosphorylation at

tyrosine residues (Mohammadi et al., 1996). FGFR phosphorylation then triggers PLCγ, MAPK and PI3K-Akt signalling (Beenken & Mohammadi, 2009). Therefore, to this end, I examined the effect of bFGF by determining the extent of phosphorylation of ERK1/2 and Akt (Figure 6.10). Analysis of protein bands indicated that there is no change in bFGF downstream signalling in OMD$^{-/-}$ and PRELP$^{-/-}$ MEFs compared to wild-type (Figure 6.10).

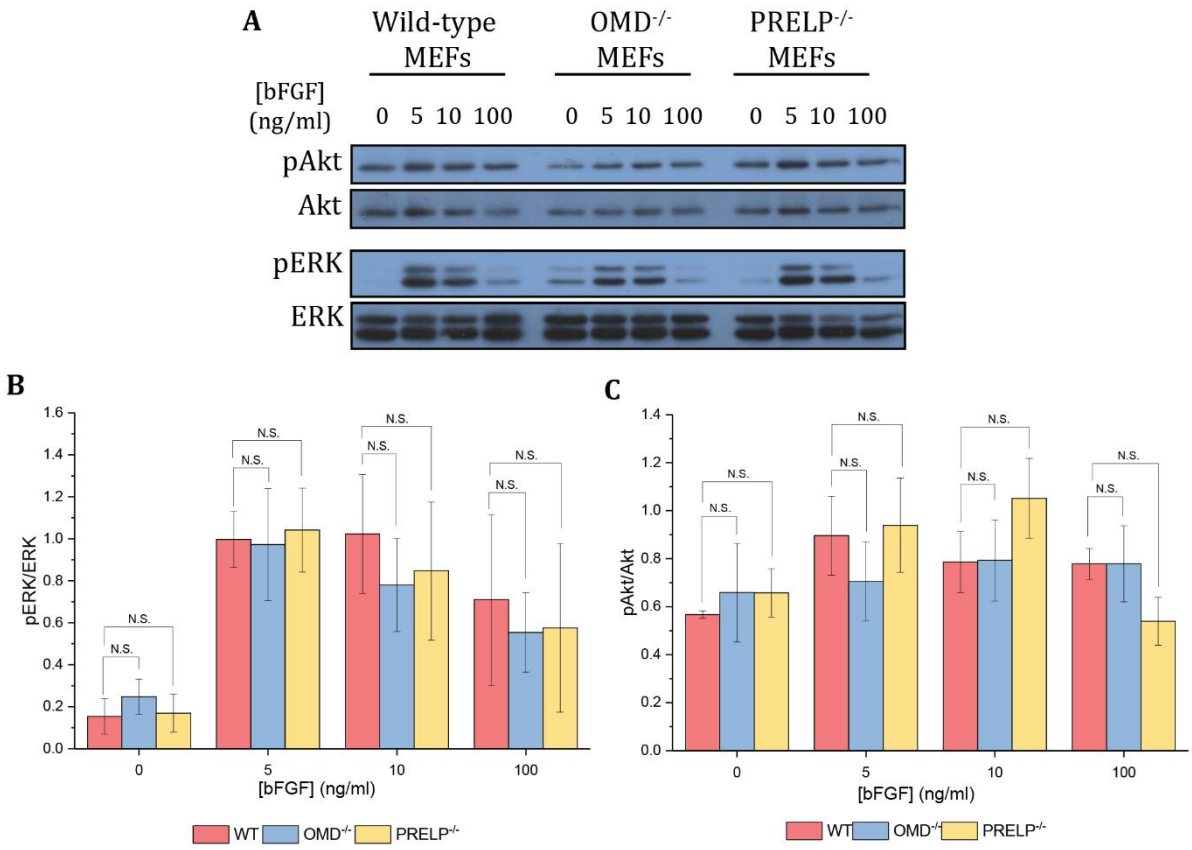

Figure 6.10. Effect of bFGF on MEFs isolated from wild-type, OMD$^{-/-}$ and PRELP$^{-/-}$ mice. A) Immunoblotting of pAkt, Akt, pERK and ERK. **B & C)** Quantification of band intensity. 2-tailed student's t-test was performed and p-values < 0.05 were considered significant. Error bars are the SEM where n=3.

6.3.3 Effect of EGF on MEFs

I then decided to assay the effect of EGF on transgenic MEF cells. EGF is particularly relevant for OMD and PRELP because previous work in the Ohnuma lab in the context of bladder cancer has suggested that OMD and PRELP act to protect tight junctions by inhibiting the action of EGF (unpublished). In the vasculature, various cell types in the blood vessels express EGFR receptors and ligands (Makki et al., 2013). In addition, it has been demonstrated that the inhibition of EGF signalling attenuates vascular leakage in diabetic retinopathy (Sugimoto et al., 2013). EGF can affect a number of pathways by activating required transcription factors; in particular, there is evidence that EGF and VEGF pathways are linked – application of EGF to malignant glioma cells stimulates the

production of VEGF and therefore increases the extent of tumour vascularisation (Goldman et al., 1993). It was later discovered that EGF can modulate the expression of VEGF through PI3K and MAPK cascades by activating key transcription factors such as STAT3 (Niu et al., 2002), Sp1 (Pore et al., 2006) and hypoxia-inducible factors (Peng et al., 2006) leading to the stimulation of angiogenesis. Therefore, given the importance EGF in the regulation of tight junctions from previous data from our laboratory and other published work, I decided to test the effect of EGF ligand signalling on the MEF cells.

Binding of a ligand to ErbB receptors causes them to form homo- or heterodimers with other members of the ErbB family (Holbro & Hynes, 2004). Upon dimerization, its tyrosine kinase domain is activated and leads to autophosphorylation at its C-terminal domain (Schlessinger, 2000). Adapter proteins bind to these phosphorylated residues and initiate downstream signalling pathways, notably PI3K/Akt (Soltoff & Cantley, 1996) and ERK/MAPK (Rozakis-Adcock et al., 1993) pathways. I therefore probed the PI3K/Akt and ERK/MAPK pathways using antibodies against pAkt, Akt, pERK and ERK (Figure 6.11). Visually, I can see that there is no change in pAkt when increasing concentrations of EGF was applied to cells, indicating that the proteins required for the PI3K/Akt signalling from EGFR are likely to not be expressed in MEFs. In contrast, cells were responsive with respect to the ERK/MAPK pathway, as shown by increased pERK when EGF was applied. Quantification of band intensity shows that there are no differences in sensitivity to EGF when comparing knock-out and wild-type MEFs (Figure 6.11).

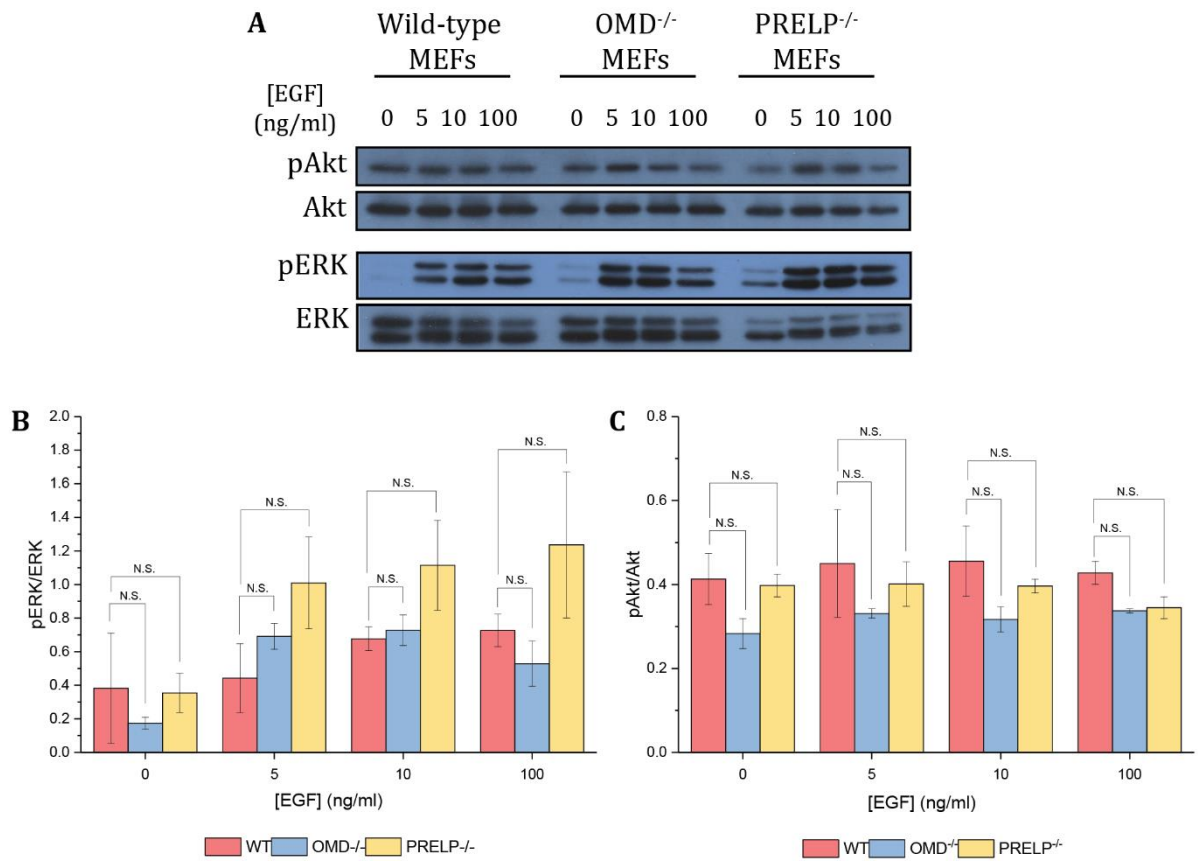

Figure 6.11. Effect of EGF on MEFs isolated from wild-type, OMD$^{-/-}$ and PRELP$^{-/-}$ mice. A) Immunoblotting of pAkt, Akt, pERK and ERK. **B & C)** Quantification of band intensity. 2-tailed student's t-test was performed and p-values < 0.05 were considered significant. Error bars are the SEM where n=4.

6.3.4 Effect of PDGF-B on MEFs

PDGF-B is a member of the platelet-derived growth factor family. In blood vessels, it is produced and secreted by endothelial cells and act on pericytes in a paracrine manner (Armulik et al., 2011). Binding of PDGF dimers such as PDGF-BB results in the activation of PDGFRβ, which leads to recruitment of adapter molecules leading to the activation of a variety of cascades, notably PI3K/Akt and ERK/MAPK (Heldin, 2013).

In Chapter 3, I have rationalised that PRELP is most likely to be secreted by pericytes. In PRELP$^{-/-}$ animals, I observe a decrease in pericytes surrounding the vasculature. Studies have shown that mice lacking PDGF-B or its receptor PDGFRβ also exhibit a marked decrease in pericyte coverage of microvessels (Levéen et al., 1994; Soriano, 1994). I therefore attempted to treat MEFs with PDGF-B to determine whether there is a decrease in signalling molecules in response to PDGF-B in PRELP$^{-/-}$ cells. I treated MEFs with an increasing concentration of PDGF-B and blotted for pERK, ERK, pAkt and Akt. Quantification of western blot bands demonstrates that there are no significant

differences in the responsiveness to PDGF-B between wild-type and knock-out MEFs (Figure 6.12).

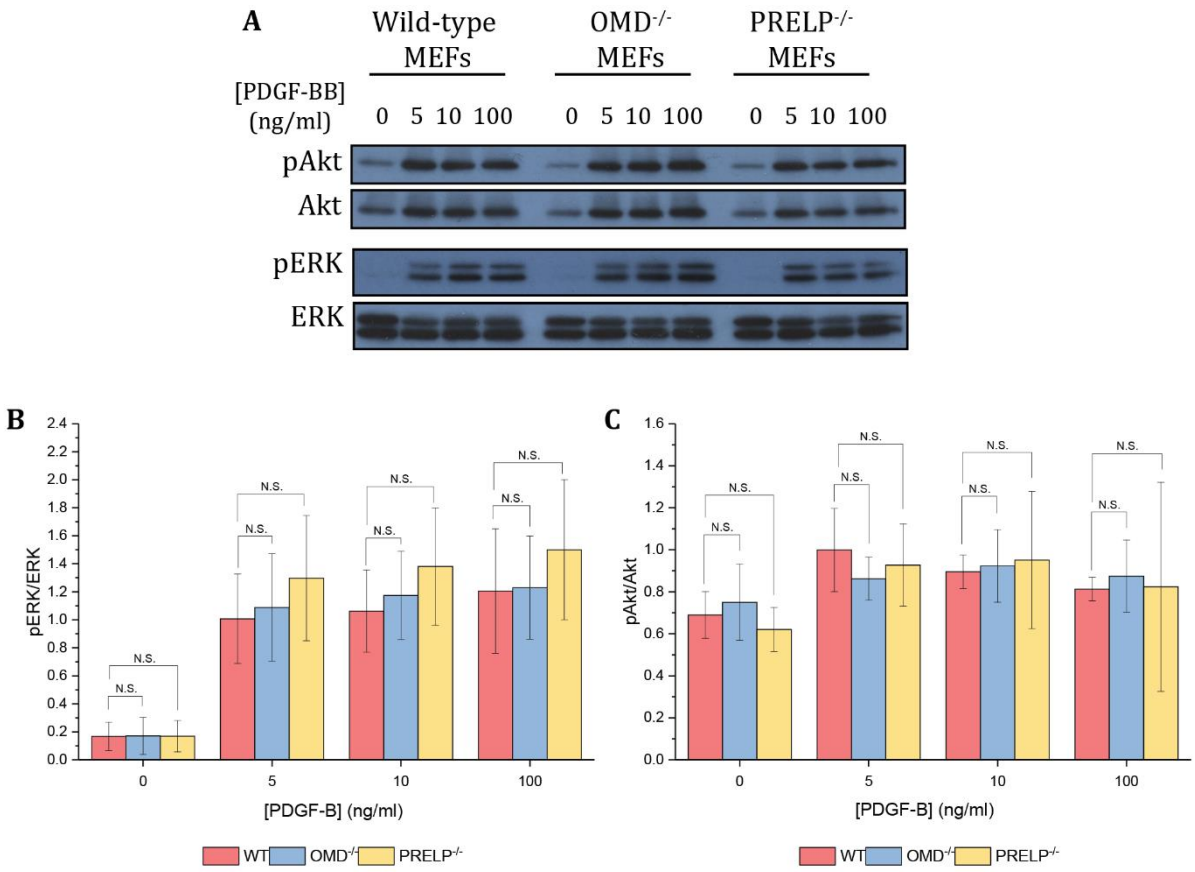

Figure 6.12. Effect of PDGF-B on MEFs isolated from wild-type, OMD$^{-/-}$ and PRELP$^{-/-}$ mice. A) Immunoblotting of pAkt, Akt, pERK and ERK. **B & C)** Quantification of band intensity. 2-tailed student's t-test was performed and p-values < 0.05 were considered significant. Error bars are the SEM where n=3.

6.3.5 Effect of TGF-β on MEFs

Many members of the SLRP family have been shown to bind to TGF-β and related proteins (Dellett et al., 2012). The binding of TGF-β to a Type II receptor leads to the recruitment and subsequent phosphorylation of a Type I receptor, forming a hetero-tetrameric complex (Wrana et al., 1992). Receptor-regulated Smad proteins, such as Smad2 and 3 in the case of TGF-β (Nakao et al., 1997), are then phosphorylated by the Type I receptor and form a complex with other co-Smads such as Smad4 (Nakao et al., 1997) which can then enter the nucleus and activate the transcription of target genes.

The action of TGF-β has been associated with changes in the distribution and expression of tight junction proteins. Studies suggest that TGF-β decreases permeability of the BBB (Dohgu et al., 2004; Ronaldson et al., 2009) whereas others have shown that TGF-β is detrimental to the integrity of the BBB (McMillin et al., 2015). Given the phenotype I

observe in PRELP$^{-/-}$ animals, I have decided to treat transgenic MEF cells with TGF-β and determine whether there are changes in the phosphorylation of Smad2. Western blotting to detect pSmad2 and Smad2 and the quantification of band intensity indicate that there are no significant differences between wild-type and knock-out MEFs with respect to TGF-β (Figure 6.13).

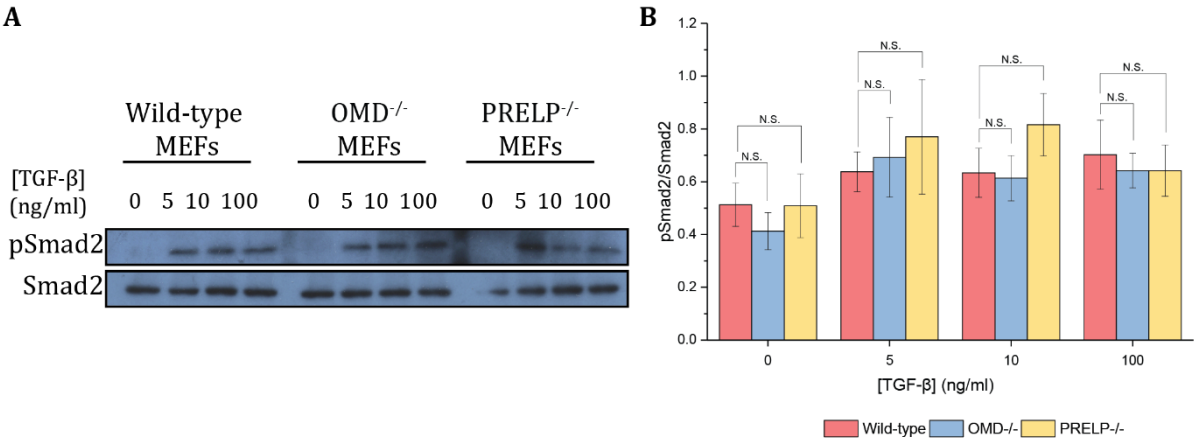

Figure 6.13. Effect of TGF-β on MEFs isolated from wild-type, OMD$^{-/-}$ and PRELP$^{-/-}$ mice. A) Immunoblotting of pSmad2 and Smad2 **B)** Quantification of band intensity. 2-tailed student's t-test was performed and p-values < 0.05 were considered significant. Error bars are the SEM where n=3.

6.3.6 Effect of VEGFA-165 on MEFs

VEGFA-165 is a critical regulator for vascular permeability and angiogenesis (Senger et al., 1983; Zhang et al., 2000). It functions by binding to VEGF receptors with the main receptor on endothelial cells being VEGFR2 (Gerhardt et al., 2003). VEGFA-165 binds to VEGFR2 and promotes receptor dimerization, which subsequently leads to trans- and auto-phosphorylation of tyrosine residues in the intracellular domain of VEGFR2. Adapter molecules bind to specific phosphor-tyrosine residues and initiate intracellular signalling pathways, notably PI3K/Akt and ERK/MAPK (Koch & Claesson-Welsh, 2012).

Given the increased blood vessel content and vascular leakage in PRELP$^{-/-}$, VEGFA proteins may be candidates for the induction of this phenotype. I therefore treated transgenic MEFs with VEGFA-165 recombinant protein at various concentrations and determined the relative expression levels of pERK, ERK, pAkt and Akt. Quantification of western blot bands indicate that there is no change in the levels of phosphorylated proteins upon treatment with VEGFA-165, demonstrating that MEF cells are unlikely to express the required components of this signalling pathway (Figure 6.14). I must therefore utilise a more appropriate and specific *in vitro* system to probe the effect of PRELP$^{-/-}$ on VEGFA-165.

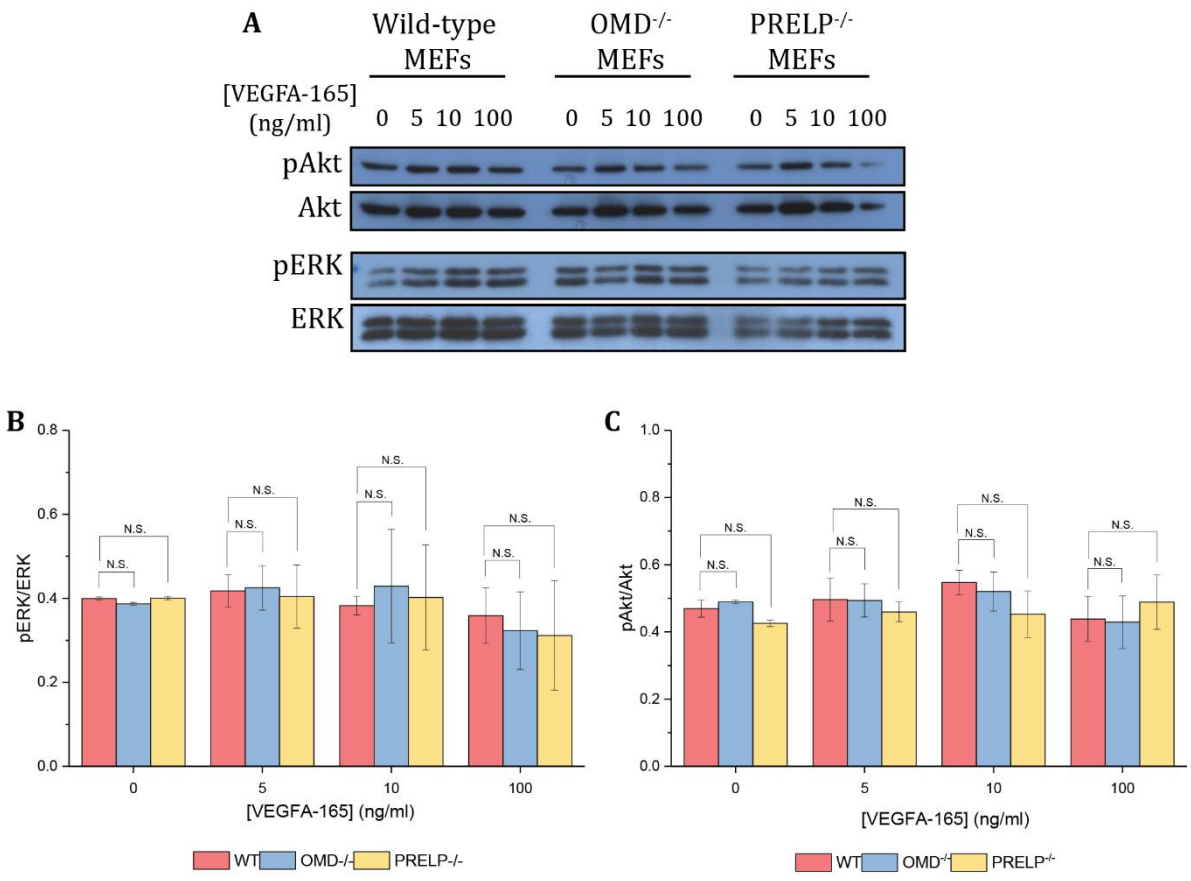

Figure 6.14. Effect of VEGFA-165 on MEFs isolated from wild-type, OMD$^{-/-}$ and PRELP$^{-/-}$ mice. **A)** Immunoblotting of pAkt, Akt, pERK and ERK. **B & C)** Quantification of band intensity. 2-tailed student's t-test was performed and p-values < 0.05 were considered significant. Error bars are the SEM where n=3.

6.4 HUVECs to elucidate signalling functions

6.4.1 Effect of OMD and PRELP on HUVEC tubule formation

Angiogenesis requires the correct assembly of endothelial cells to form tubules. HUVECs have the ability to form tubules in BM extract (BME), which is essentially the BM isolated from EHS mouse sarcoma cells (Kleinman et al., 1986). These tubules typically form within 12 hours and undergo apoptosis after 24 hours. Wells were photographed before the induction of apoptosis and morphogenesis is typically assessed by measuring length or area of formed tubules. Given that the effect of angiogenic mediators or inhibitors can be determined using this tubule formation assay, I have decided to probe the function of OMD and PRELP in angiogenesis using HUVECs.

To begin with, I optimised the conditions for the HUVECs tube formation assay, from seeding density to tubule incubation time and BME thickness/dilution. Figure 6.15A shows the initial conditions I used for tubule formation, whereas Figure 6.15B shows the optimized conditions. I found that 4 x 10^4 cells/cm^2 was ideal to obtain tubules without

excessive clustering of cells. Various protocols recommended different incubation times, ranging from a mere 4 hours to 20 hours. I found that after 4 hours, the tubules have not properly formed. However, after 20 hours, I notice that many tubules retract and cells begin to cluster, probably when apoptosis begins to become apparent. Images were therefore taken after 16 hours of incubation. Finally, I have also determined that passage number is critical for the formation of tubules. Later passage cells did not form extensive networks and tended to show early signs of apoptosis, such as clustering and retraction of tubules, at 16 hours. I therefore opted to use only passage 3-4 HUVECs for all experiments.

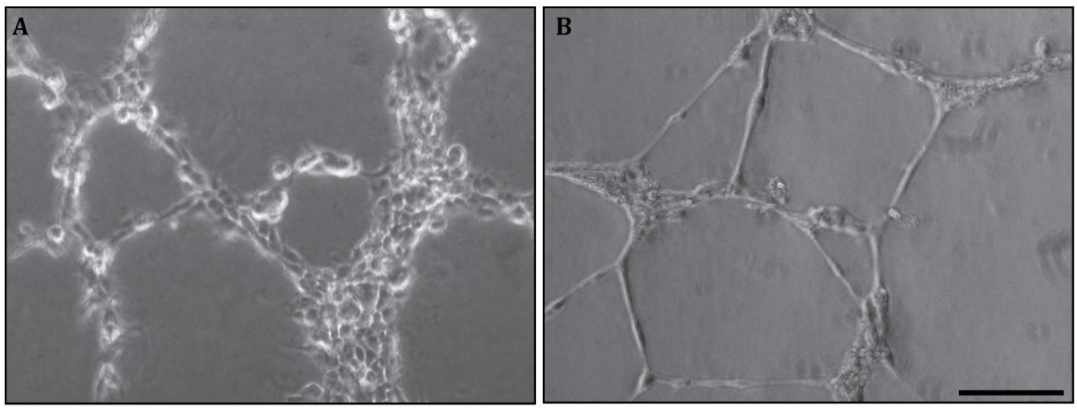

Figure 6.15. Optimisation of HUVECs tubule formation assay. (A) Initial attempts at tubule formation assay; there are clumps of HUVECs which have aggregated together, and the tubules have not properly formed. **(B)** After optimizing the culture conditions (BME, cell density, incubation time), tubules are well-formed with few clumps. Scale bar: 200um.

While initial work was performed in standard tissue culture plates (6-well, 12-well, 24-well and 96-well), I opted to utilise the μ-Slide Angiogenesis from Ibidi. These slides have the advantage of using very little Matrigel (10ul per well) and reducing the formation of a meniscus due to its "well-in-well" design (Figure 6.16). This is especially important given the cost of growth-factor reduced BME. The absence of a notable meniscus also facilitated the imaging of tubules, where one focal plane was typically sufficient to obtain a clear image. In addition, there was an even distribution of cells in each well, allowing more accurate quantification of the extent of tubule formation.

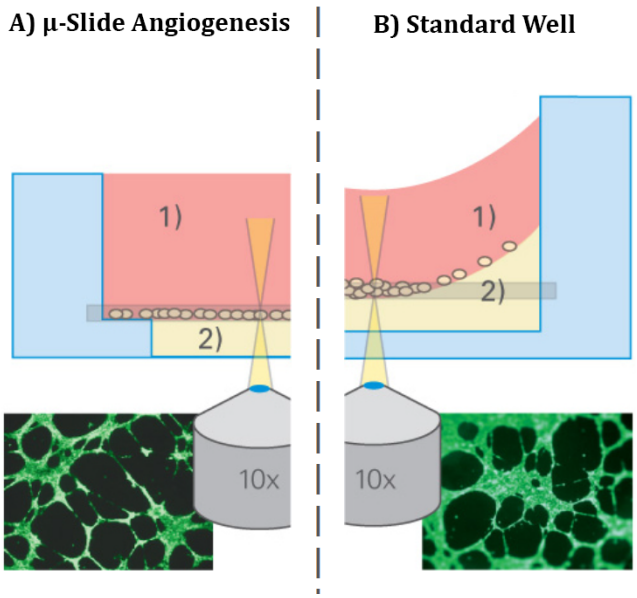

Figure 6.16. Difference between µ-Slide Angiogenesis (Ibidi) and standard tissue culture wells for tubule assay. A) µ-Slide Angiogenesis utilises a "well-in-well" system preventing the formation of a meniscus of the BME. **B)** BME pipetted into a standard tissue culture dish would lead to the formation of a meniscus and uneven dispersion of cells. Image modified from Ibidi online catalogue.

I aimed to provide HUVECs undergoing tubule formation with OMD and PRELP by using conditioned media (CM) from transfected HEK293 cells. Cells were transfected using pCS2-vector, pCS2-OMDmyc and pCS2-PRELPmyc plasmids using Lipofectamine 2000. The following day, media was replaced with serum-free Opti-MEM. Cells were allowed to secrete OMD and PRELP for an additional day before the CM was harvested. I tested whether the CM contains myc-tagged OMD and PRELP by western blotting (Figure 6.17). While OMD and PRELP were detected in the cell lysates (Figure 6.17; left), they were difficult to detect directly from CM; I therefore opted to concentrate OMD and PRELP using anti-myc antibody-conjugated beads (Figure 6.17; right). Using this method, I managed to detect myc-tagged OMD and PRELP and therefore decided to utilise CM for HUVECs tubule formation assay. Note that OMD and PRELP are tagged with 6 x myc-tags; the molecular weights of their protein cores would therefore equate to 57kDa and 51kDa respectively, consistent with the molecular weights of the bands from the cell lysates. As explained in Section 6.2.2, the detection of OMD and PRELP is particularly poor by western blotting. There are multiple bands above and below the expected molecular weight for the core protein. This could be due to post-translational modifications, but also due to degradation and/or aggregation of these SLRPs resulting in these banding patterns, reflecting poor quality protein being produced.

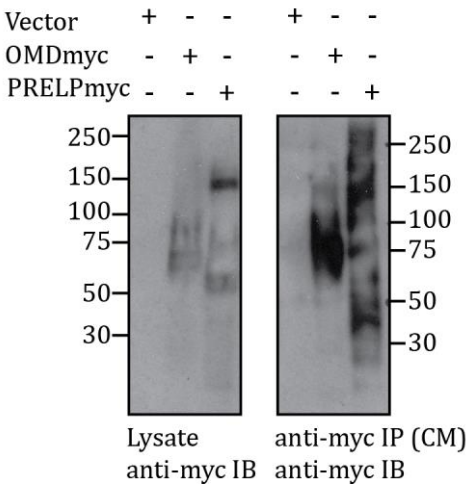

Figure 6.17. Detection of myc-tagged OMD and PRELP proteins in HEK293. HEK293 cells were transfected with pCS2+MT (vector), pCS2-OMDmyc and pCS2-PRELPmyc. Cell lysates were prepared 48 hours after transfection and myc-tagged proteins detected using anti-myc antibody (left). In addition, the CM from these cells were incubated with beads conjugated to anti-myc antibody and used to pull-down myc-tagged proteins. Myc-tagged proteins were then detected using anti-myc antibody (right).

I utilised CM from HEK293 overexpressing i) Vector, ii) OMD or iii) PRELP. When preparing the cell suspension for the tubule assay, I mixed LVES-supplemented HUVEC media and CM 1:1 and allowed tubules to form for 16-hours before labelling and imaging. Images were analysed with AngioTool and morphological parameters such as vessel percentage area and junction density.

I assayed the effect of OMD and PRELP on bFGF, EGF, TGF-β and VEGFA-165 (Figure 6.18). Tubule networks were quantified using AngioTool and vessel percentage area and junction density were determined (Figure 6.19). Since multiple comparisons were made, I normalised values to vector-CM for each growth factor and adjusted the p-values using Bonferroni correction, where the significance threshold is increased to reduce false-positive results. This was done by calculating a new α value, based on the number of tests (α adj = α /number of tests).

I have determined that while OMD-CM had no statistically-significant effect on tubule formation. In contrast, PRELP-CM seems to negatively affect tubule formation regardless of the growth factor, however this effect was found to be significant when incubated with TGF-β and VEGFA-165. The addition of PRELP-CM to TGF-β-driven tubule formation indicated that there is a decrease in junction density. Similarly, vessel percentage is decreased with regards to VEGFA-165. When no adjustments were made to p-values, both vessel percentage area and junctions density were found to be statistically significant when tubules were incubated with TGF-β, VEGFA-165 and PRELP-CM. This is reflected in adjusted p-values which were almost statistically-significant (summarised in Table 6.1).

Finally, when unadjusted p-values were used, tubule formation driven by EGF was also inhibited by PRELP-CM with regards to vessel percentage area, but not junction density.

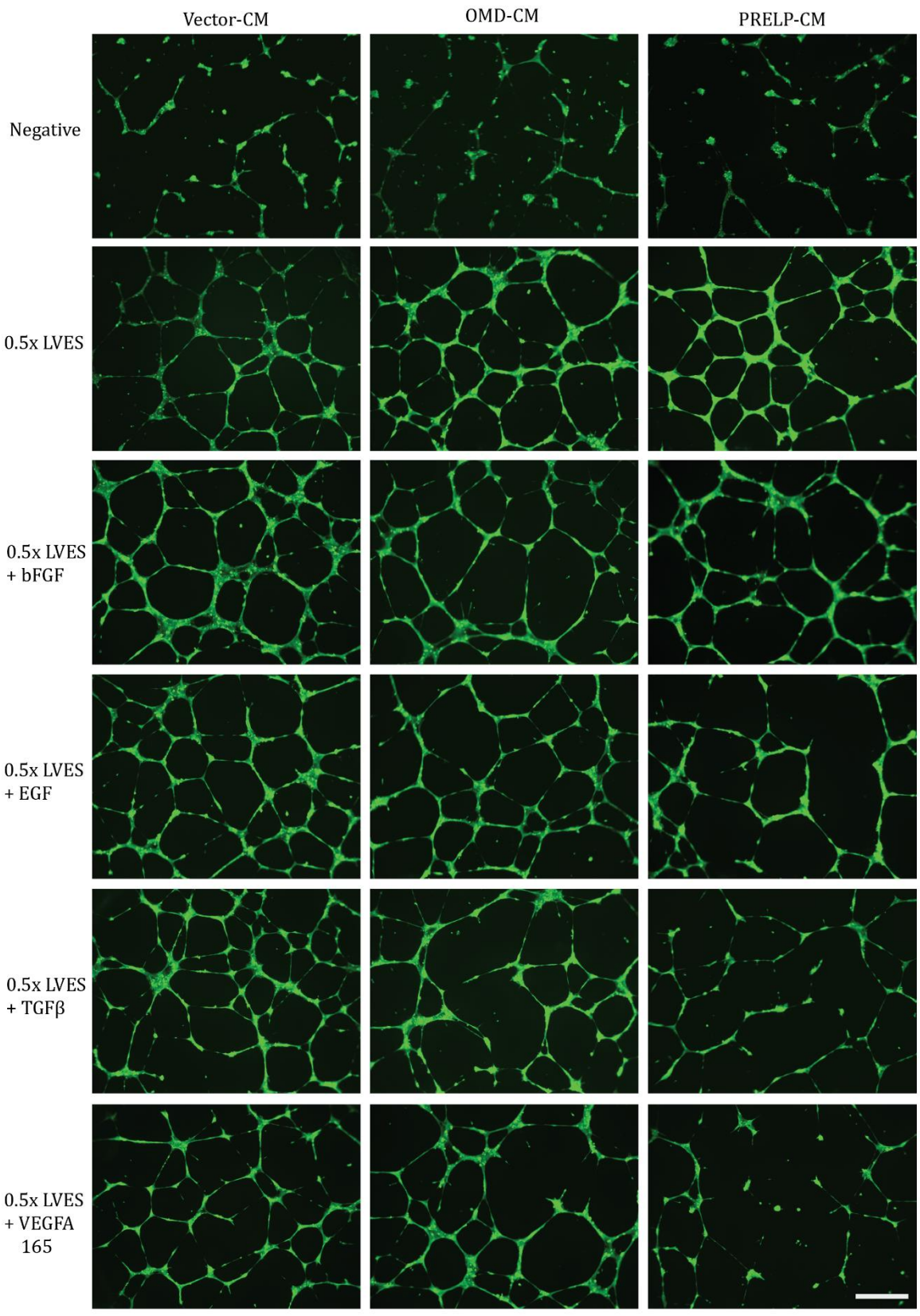

Figure 6.18. Effect of OMD and PRELP on HUVEC tubule formation. HUVECs were incubated with 0.5x LVES, conditioned media and specific growth factors at 20ng/ml. Tubules were allowed to form for 16 hours before incubation with Calcein AM and image acquisition.

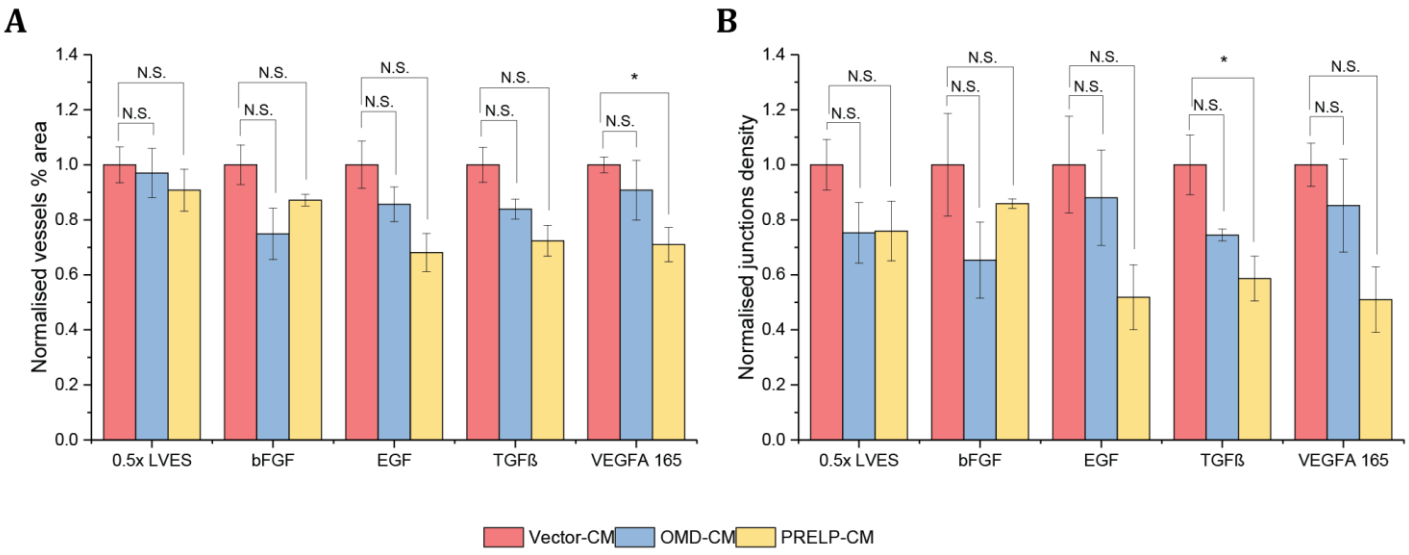

Figure 6.19. Quantification of HUVEC tubule formation assay parameters Vessels percentage area (A) and Junctions density (B). Images were analysed in AngioTool using the same parameters. 2-tailed student's t-test was performed and adjusted p-values < 0.05 were considered significant (*; 0.01 < p-value < 0.05). Error bars are the SEM where n=3-4.

In an attempt to determine the domain of PRELP responsible for interfering with TGF-β and VEGFA-165, I performed the same tubule formation assay with conditioned media obtained from HEK293 overexpressing -NT PRELP and -PR PRELP constructs (see Section 6.2.2). I found no statistically-significant differences between vector-CM and -NT or -PR PRELP constructs (Figure 6.20, Figure 6.21). Therefore, it seems that the PR-rich region responsible for HS binding is critical for the ability of PRELP to affect TGF-β and VEGFA-165 signalling.

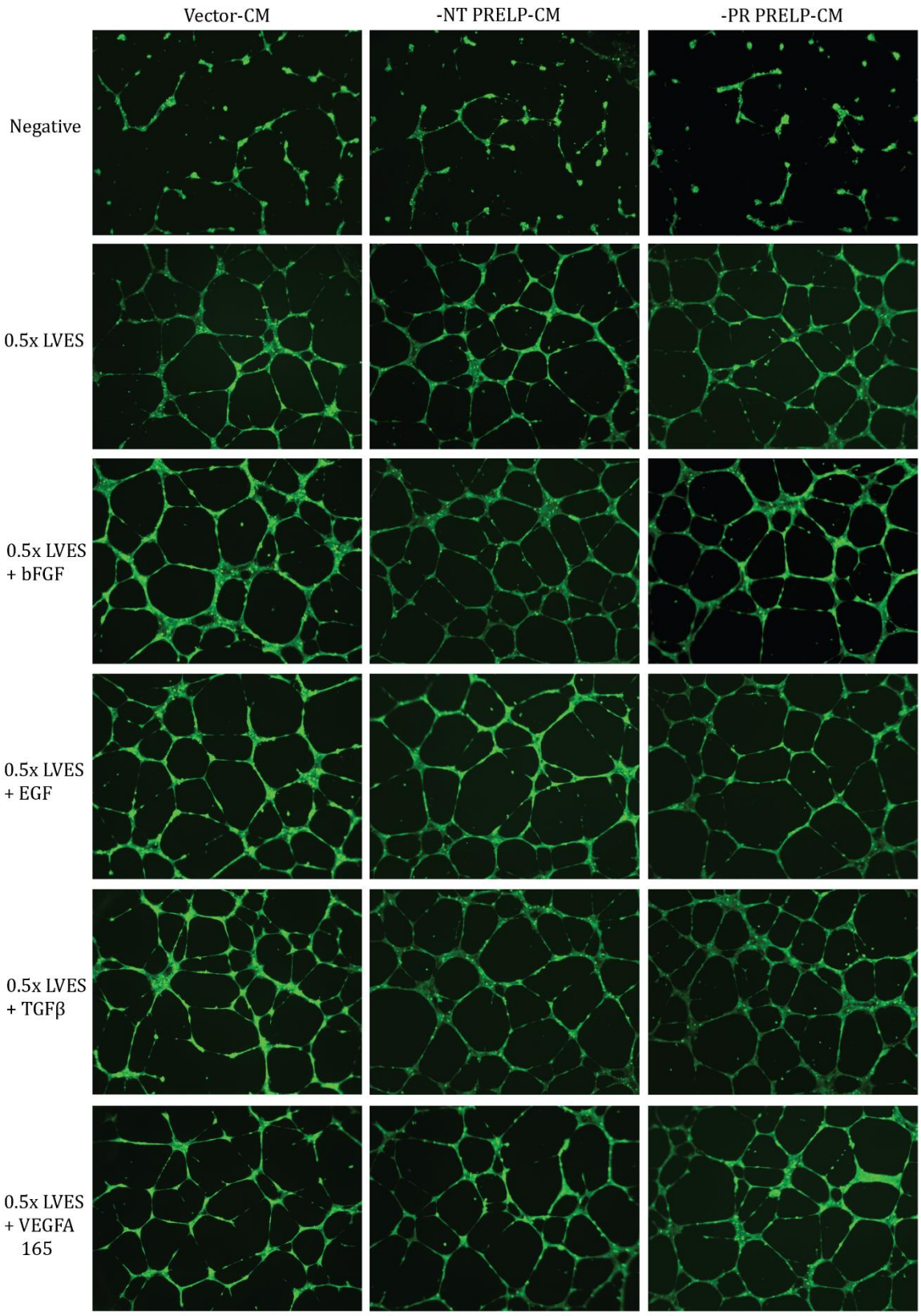

Figure 6.20. Tubule formation assay using CM from -NT and -PR PRELP-expressing cells. HUVECs were incubated with 0.5x LVES, conditioned media and specific growth factors at

20ng/ml. Tubules were allowed to form for 16 hours before incubation with Calcein AM and image acquisition.

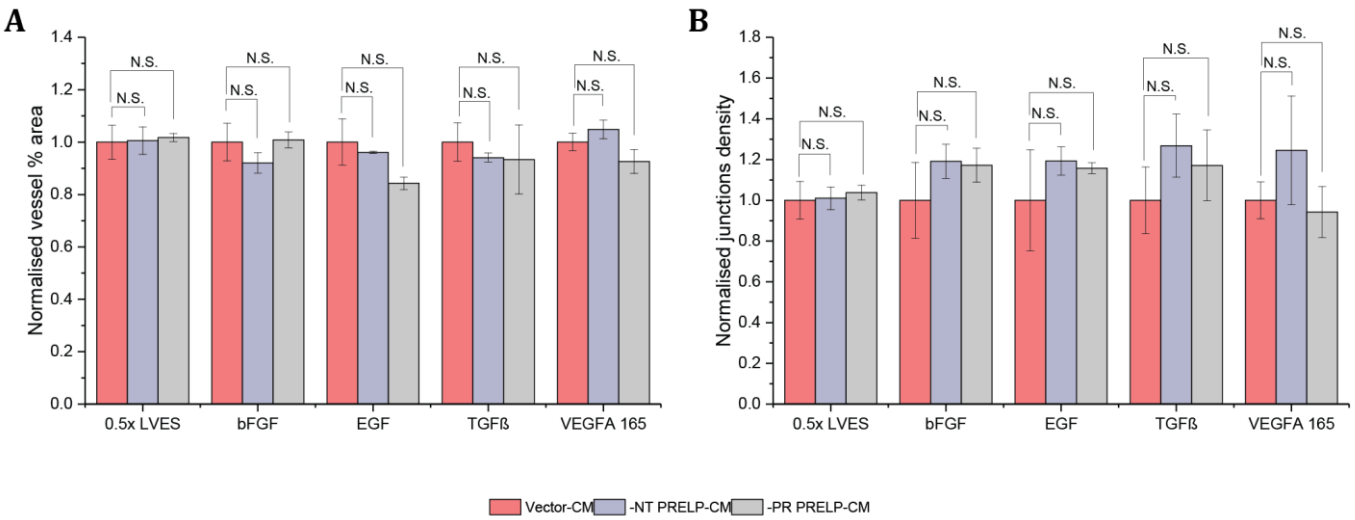

Figure 6.21. Quantification of HUVEC tubule formation assay using -NT and -PR-PRELP constructs. Parameters Vessels percentage area **(A)** and Junction density **(B)** were quantified. Images were analysed in AngioTool using the same parameters. 2-tailed student's t-test was performed and adjusted p-values < 0.05 were considered significant (*; 0.01 < p-value < 0.05). Error bars are the SEM where n=3-4.

The results of the tubule formation assay are summarised in Table 6.1. From this preliminary data, PRELP seems to act as an inhibitor of angiogenesis. This effect is most evident when cells were treated with TGF-β and VEGFA-165. This inhibition was found to be dependent on the PR region of PRELP, since tubule formation with the addition of CM from -PR PRELP-expressing cells had no effect. Although interesting, the concentration of PRELP and its mutant forms applied to cells is unknown; it is impossible to know solely from these experiments whether the inhibition is due to a physiological function of PRELP or an artificial effect due to overloading HUVECs with a high-concentration of aggregated or partially-degraded protein. Finally, as shown by Figure 6.7, the expression of -NT PRELP and -PR PRELP is not optimal.

		OMD-CM		PRELP-CM		-NT PRELP-CM		-PR PRELP-CM	
		Adj. p-val.	Sig.	Adj. p-val.	Sig.	Adj. p-val.	Sig.	Adj. p-val.	Sig.
0.5x LVES	% area	1.6	N.S.	0.8	N.S.	1.9	N.S.	0.6	N.S.
	J.D.	0.3	N.S.	0.3	N.S.	1.9	N.S.	1.5	N.S.
bFGF	% area	0.2	N.S.	0.3	N.S.	0.9	N.S.	1.9	N.S.
	J.D.	0.4	N.S.	1.0	N.S.	1.0	N.S.	0.9	N.S.
EGF	% area	0.9	N.S.	0.1	N.S.	1.4	N.S.	0.3	N.S.
	J.D.	1.4	N.S.	0.1	N.S.	1.0	N.S.	1.1	N.S.
TGF-β	% area	0.2	N.S.	0.06	N.S.	1.0	N.S.	1.4	N.S.
	J.D.	0.07	N.S.	0.04	*	0.6	N.S.	1.0	N.S.
VEGFA-165	% area	1.0	N.S.	0.03	*	0.8	N.S.	0.5	N.S.
	J.D.	1.04	N.S.	0.06	N.S.	0.9	N.S.	1.5	N.S.

Table 6.1. Summary of results of tubule formation assay in HUVECs. Tabulated view of results, indicating the growth factor, conditioned medium utilised alongside measured parameters and their associated p-values and significance levels compared to vector-CM control. Value is determined to be significant if adjusted p-value < 0.05 (*; 0.01 < p-adj < 0.05). J.D., junction density; sig. significance.

6.4.2 Binding of OMD and PRELP to TGF-β

It has been demonstrated that many members of the SLRP family bind to TGF-β and related proteins (Dellett et al., 2012). In addition, I have demonstrated that PRELP may affect TGF-β signalling in HUVECs, as determined by the tubule formation assay. I investigated whether OMD and PRELP can bind to TGF-β by immunoprecipitation (IP). HEK293 cells were transfected with a plasmid encoding TGF-β-FLAG with signal sequence in addition to vector, OMDmyc or PRELPmyc constructs. Since all constructs encode secreted proteins, CM from HEK293 was collected after 48 hours and incubated with Protein G-Sepharose beads and anti-myc antibody overnight at 4°C. The following day, samples were analysed by western blotting, where I attempted to identify TGF-β-FLAG using an anti-FLAG antibody. Immunoblotting (IB) with anti-FLAG detected a band around 12kDa, likely to be TGF-β (Figure 6.22.; arrow). This band was not present when the membrane was stripped and probed for the myc-tag. OMD and PRELP therefore bind to TGF-β.

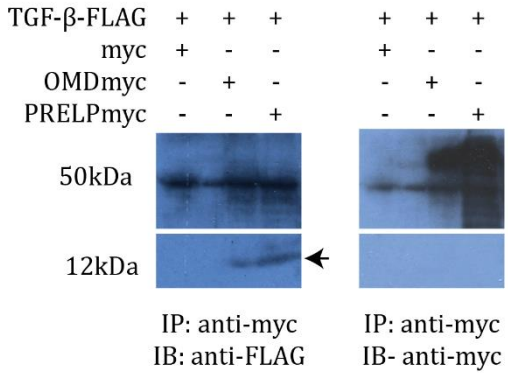

Figure 6.22. IP of TGF-β with OMD and PRELP. CM was prepared from HEK293 cells transfected with FLAG-tagged TGF-β and vector encoding myc, OMDmyc and PRELPmyc and incubated with Protein G-Sepharose beads conjugated to anti-myc. FLAG-tagged proteins were detected by western blotting. ~12kDa FLAG-tagged protein was detected in CM containing TGF-β and OMD and PRELP.

Since I have determined that TGF-β binds to PRELP, I performed another IP experiment using the -NT and -PR PRELPmyc constructs, however instead of using CM, cell lysates were incubated with beads since -NT PRELP is not secreted (Figure 6.23). I detected no FLAG-tagged proteins pulled down with either construct, suggesting that the N-terminal HS-binding domain of PRELP may be important in mediating its binding with TGF-β. As discussed in Section 6.2.2, the expression of mutant PRELP is particularly poor – this result is therefore unreliable.

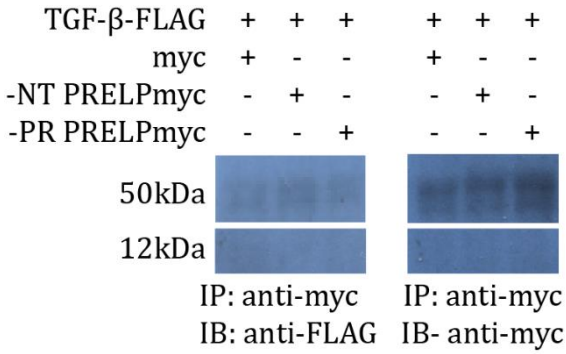

Figure 6.23. IP of TGF-β with -NT and -PR constructs of PRELP. Cell lysates were prepared from HEK293 cells transfected with FLAG-tagged TGF-β and vector encoding myc, -NT PRELPmyc and -PR PRELPmyc and incubated with Protein G-Sepharose beads conjugated to anti-myc. FLAG-tagged proteins were detected by western blotting. TGF-β was not pulled-down by -NT or -PR constructs of PRELP.

6.4.3 Binding of OMD and PRELP to VEGFA isoforms

I have previously demonstrated that PRELP seems to inhibit VEGFA-165 signalling in HUVECs. Using the FLAG-tagged constructs of VEGFA isoforms, as described in Section 6.2.1 , I performed IP experiments to determine whether there is direct binding of OMD/PRELP to VEGFA-121, -165 and -165b. To this end, HEK293 cells were co-transfected with FLAG-tagged VEGFA and vector encoding the myc peptide, OMDmyc or PRELPmyc. After 48 hours, cell lysates were prepared and incubated with Protein G-Sepharose beads conjugated with anti-myc antibody. Protein samples were then analysed by western blotting (Figure 6.24). These results indicate that there is no binding of VEGFA isoforms to OMD or PRELP.

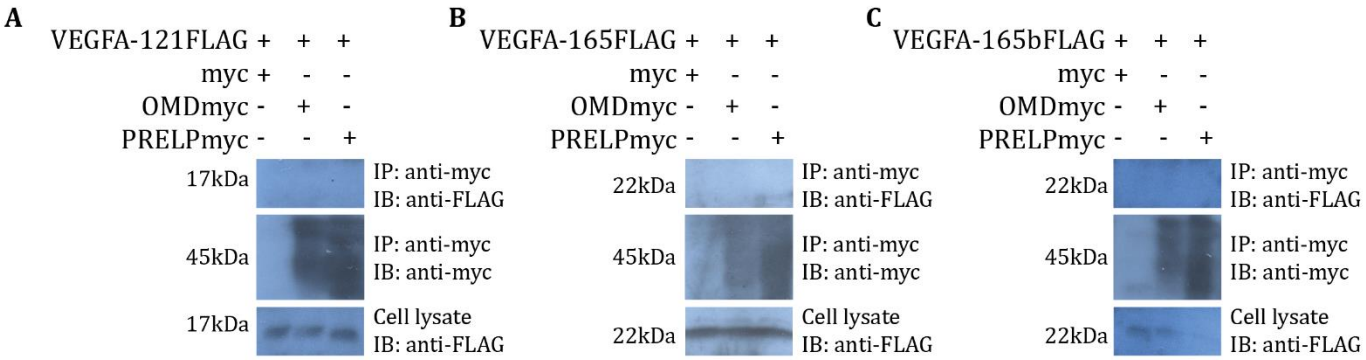

Figure 6.24. IP of OMD and PRELP binding to VEGFA isoforms -121 (A), -165 (B) and -165b (C). Cell lysates of HEK293 cells transfected with VEGFA and vector encoding myc, OMDmyc or PRELPmyc were incubated with beads conjugated to anti-myc. IB was performed using anti-FLAG to detect any bound VEGFA protein and anti-myc to confirm that OMDmyc or PRELPmyc were present in the cell lysate.

6.4.4 Effect of OMD and PRELP on the integrity of HUVEC monolayers

Given that PRELP in particular seems to be able to affect the morphology of HUVEC tubule, I was also interested in determining whether OMD and PRELP can affect HUVEC monolayers. Briefly, HUVEC monolayers were grown on transwell inserts, creating basal and apical compartments. I measured the trans-epithelial/endothelial resistance (TEER) to determine the integrity of HUVEC monolayers. In addition, I attempted to study the integrity of the monolayer by determining its permeability to fluorophore-tagged 70kDa dextran.

I optimised the conditions for growing HUVECs in a monolayer. I compared gelatin, collagen I and fibronectin transwell coatings. I found that fibronectin provided the best substrate for cell attachment. Next, I proceeded to determine the optimal seeding density and culture time. I opted to seed 70,000 cells per 24-well transwell insert and allow them to grow for 4 days. TEER was measured to confirm that the monolayer was confluent – values obtained of approx. 25Ω * cm^2 were consistent with literature values, which typically range between 20-30Ω * cm^2 (Dewi et al., 2004; Minami et al., 2015). As with the

tubule formation assay, passage number strongly affected the cells' ability to form a confluent monolayer, so I only used HUVECs passage 3-4. Figure 6.25 shows PECAM-1 staining of a confluent HUVEC monolayer using the conditions described above.

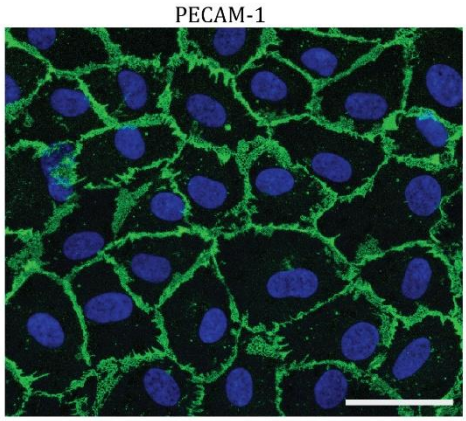

Figure 6.25. HUVEC monolayer stained with PECAM-1. Cells were grown on fibronectin-coated transwell inserts for four days prior to fixation and antibody staining. Scale bar 40um.

After optimising the conditions for obtaining a confluent monolayer of HUVECs, the effect of OMD- and PRELP-CM on their integrity was measured. Once HUVECs were harvested, they were resuspended in 1x LVES media and seeded onto a coated transwell membrane. The bottom chamber was filled with 0.5x LVES with CM from vector-, OMD-, PRELP-, -NT PRELP- or -PR PRELP- expressing cells, as illustrated in Figure 6.26A. HUVECs were allowed to form a monolayer for 4 days and TEER values were measured. Statistical analysis of TEER indicated that PRELP has an effect on HUVEC monolayer integrity. Interestingly, when the experiment was performed using CM derived from -NT or -PR PRELP-expressing cells, no differences were found when compared to vector CM. This strongly indicates that the ability of PRELP to affect TEER is dependent on its HS-binding domain.

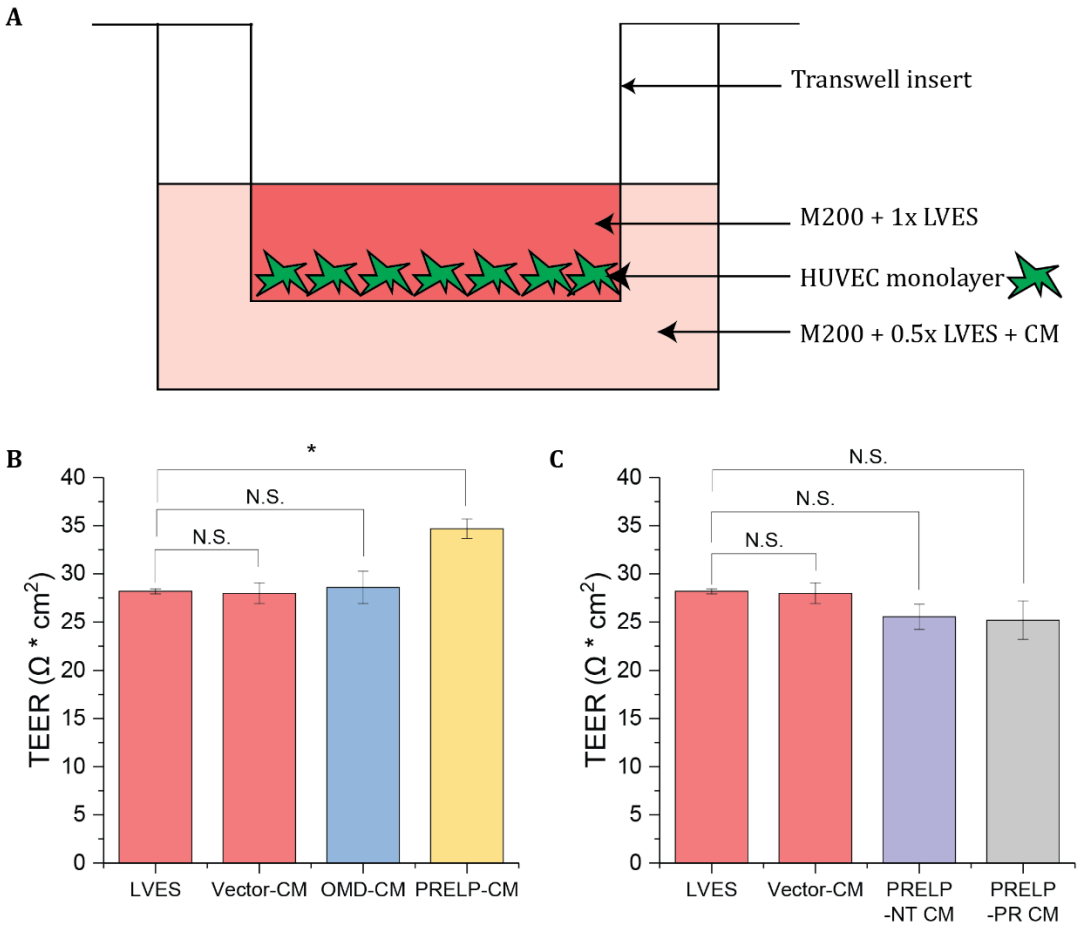

Figure 6.26. PRELP influences HUVEC monolayer TEER. Conditioned media was applied to the basal compartment of the transwell insert **(A)**. Once the HUVEC monolayer was confluent, TEER was measured **(B & C)**. PRELP-CM, but not -NT or -PR PRELP-CM affected HUVEC TEER values. 2-tailed student's t-test was performed and p-values < 0.05 were considered significant (*; 0.01 < p-value < 0.05). Error bars are the SEM where n=5.

Next, I determined whether there were any changes in the permeability of HUVEC monolayers to 70kDa dextran. After HUVECs had formed a monolayer, the media in the upper chamber was replaced with 1mg/ml 70kDa dextran-Texas Red (Figure 6.27A). Media from the lower compartment was collected after 1 hour and the relative amount of dextran measured using a fluorescence plate-reader, as done by (Miao et al., 2014). Quantification of values indicates that there are no differences in the permeability of monolayers to 70kDa dextran (Figure 6.27B & C).

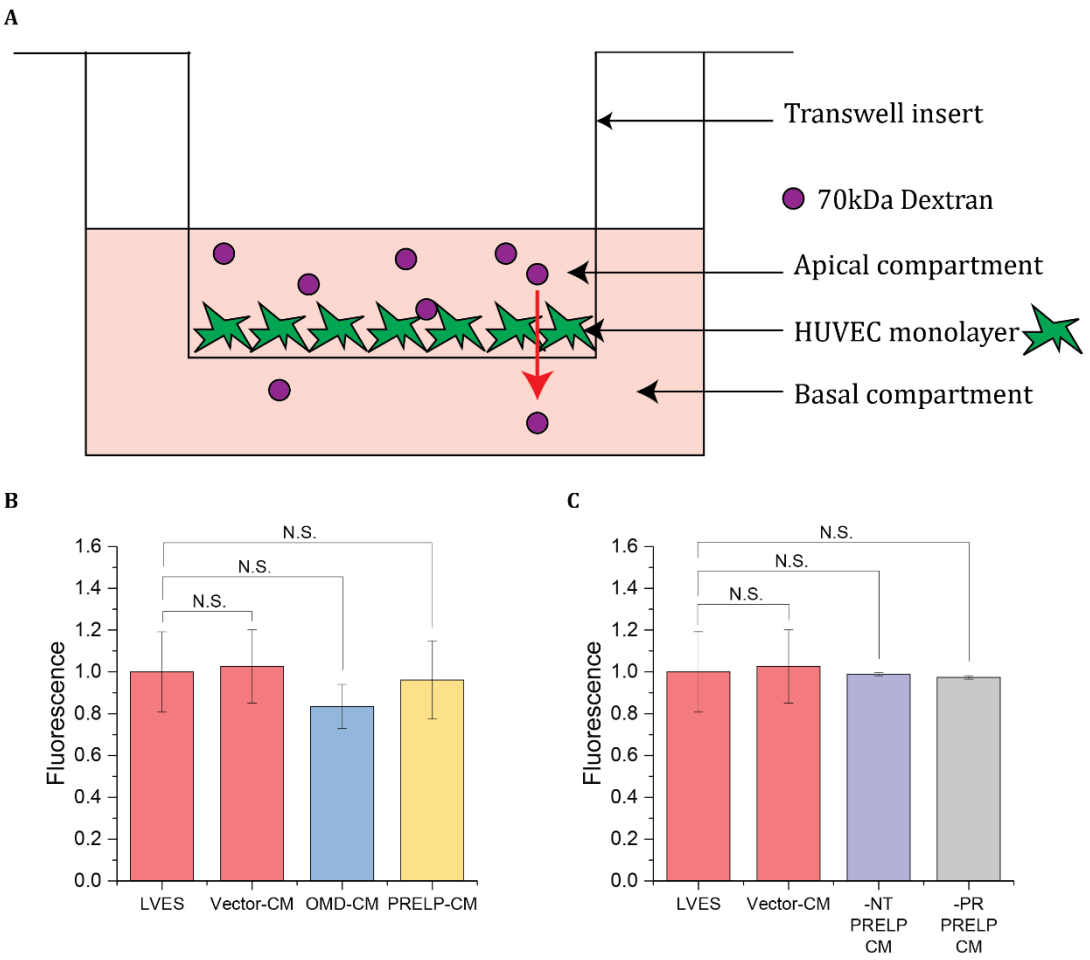

Figure 6.27. No change in HUVEC monolayer permeability to 70kDa dextran. The HUVEC monolayer was grown on the transwell membrane and 70kDa Dextran added to the upper compartment and allowed to diffuse to the lower compartment (red arrow) for one hour **(A)**. Media from the basal compartment is then analysed to detect 70kDa dextran. Quantification of relative fluorescence indicates that there are no differences in the permeability of HUVEC monolayers grown with CM **(B & C)**. 2-tailed student's t-test was performed and p-values < 0.05 were considered significant. Error bars are the SEM where n=3.

To conclude, I utilised CM produced from HEK293 cells to determine whether OMD or PRELP could affect HUVEC morphogenesis or monolayer properties. The effect of PRELP from CM on HUVECs should be interpreted with caution – as discussed, the quality of protein produced from HEK293 is likely to be poor, as assessed by western blotting images. Nonetheless, the results presented in this section indicate that PRELP had a minor effect on tubule formation with respect to EGF and TGF-β, but a more pronounced inhibition on VEGFA-165 signalling. HUVEC monolayers grown with PRELP-CM had increased TEER values, indicating that monolayers were more intact in response to PRELP. Finally, I observed no changes in the permeability of monolayers to labelled 70kDa dextran.

6.5 Properties of brain endothelial cells isolated from OMD$^{-/-}$ and PRELP$^{-/-}$ mice

6.5.1 Isolation and purification of MBECs

While I obtained interesting data using HUVECs, I aimed to utilise a more relevant *in vitro* model for the BBB. To this end, I decided to purify mouse brain endothelial cells (MBEC) directly from our transgenic mice. MBECs on transwell inserts mimic the *in vivo* condition of brain vasculature. Cells maintain polarity with the presence of basal and apical compartments created by the use of transwell inserts.

Briefly, age- and sex-matched mice were sacrificed and brains harvested. Tissue was homogenised and separated using a BSA gradient before being plated onto transwell inserts. Puromycin was utilised to kill any contaminating cells, as brain endothelial cells have high expression of ABC transporters which actively pump out any toxins.

Initial efforts were aimed at optimising the yield, attachment and formation of confluent MBEC monolayers from wild-type mice. I determined that fibronectin- and collagen IV-coated transwells were ideal for growing MBECs as it provides the natural substrate for brain endothelial cells to attach to. In addition, published work suggests that using fibronectin in particular allows the formation of higher-quality monolayers (Nooteboom et al., 2000). Since MBECs tend to have poor survival when seeded too sparsely, the amount of cells plated into transwell inserts is critical. As my aim was to isolate MBECs from our transgenic mice, I hoped to optimise the protocol for isolating cells from one mouse brain at a time. I found that one mouse brain should ideally be used in two 24-well transwell inserts. In order to confirm that the monolayer is confluent, TEER was measured. I obtained TEER values of 70-80Ω * cm^2, which is consistent with literature values for endothelial cell culture without supplementation (Banks et al., 2008; Nishitsuji et al., 2011). Figure 6.28 shows PECAM-1 staining of a confluent monolayer of purified MBECs using the conditions outlined above.

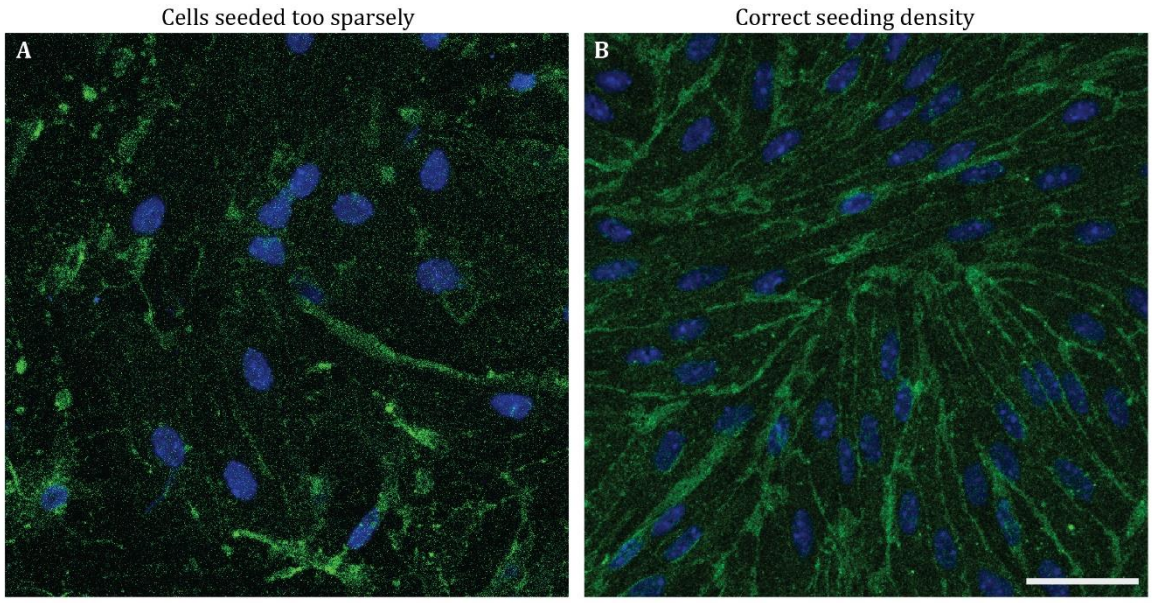

Figure 6.28. Optimisation of MBEC monolayer stained with PECAM-1. A) MBECs were seeded too sparsely on the membrane and do not form a confluent monolayer in contrast to MBECs seeded at the appropriate density **(B)** and form a PECAM-1-positive monolayer. Scale bar 40um.

Unfortunately, I attempted the isolation of MBECs from PRELP$^{-/-}$ brains five times but were always unsuccessful. When isolating and purifying wild-type and PRELP$^{-/-}$ MBECs in parallel, confluent monolayers were only formed by wild-type cells. Efforts to improve the culture of PRELP$^{-/-}$ MBECs were unsuccessful. In particular, I noted that the survival of PRELP$^{-/-}$ MBECs was poor after treatment with puromycin, suggesting that PRELP$^{-/-}$ MBECs have poor puromycin tolerance.

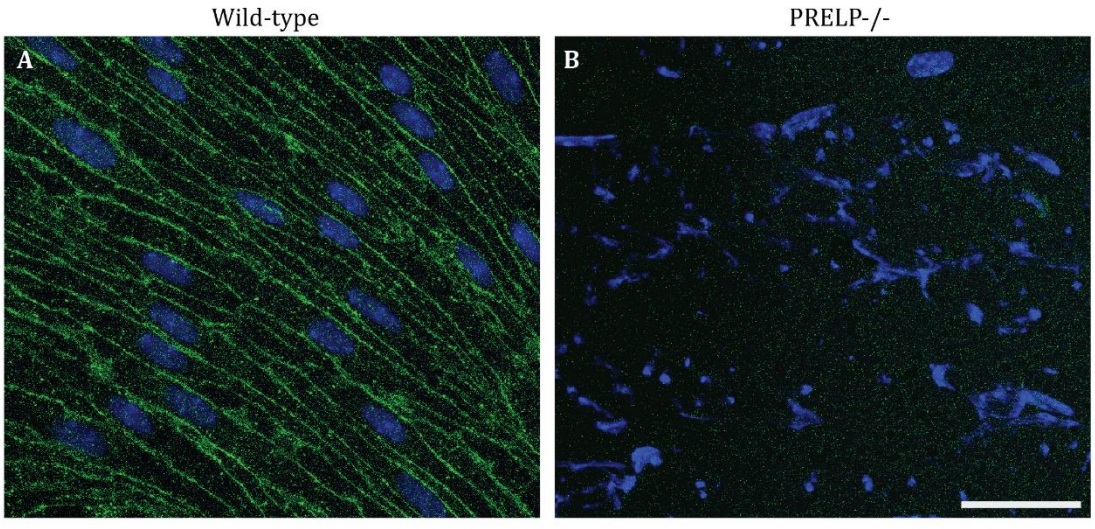

Figure 6.29. PRELP$^{-/-}$ MBECs do not form a monolayer. MBECs were isolated and purified from wild-type **(A)** and PRELP$^{-/-}$ **(B)** mice and stained with VE-cadherin. While wild-type MBECs form a monolayer, PRELP$^{-/-}$ cells did not survive the purification process. Scale bar 40um.

To conclude, I optimised the formation of confluent MBEC monolayers using wild-type cells. Unfortunately, despite my efforts, the isolation and purification of MBECs from PRELP$^{-/-}$ was unsuccessful.

6.6 Discussion

6.6.1 No difference between wild-type and knock-out MEFs

I have successfully created three cell lines based on our transgenic mice – wild-type, OMD$^{-/-}$ and PRELP$^{-/-}$. With the help of our colleague Dr Orita, we have verified that these cells originate from the intended mice by genotyping, β-galactosidase protein and enzyme activity. The advantage of using MEFs was that I would have a primary cell line with deletions in OMD or PRELP.

From my experiments and those of Dr Orita, it seems likely that OMD and PRELP are not highly-expressed in MEFs. First, I probed the responses to different growth factors using these cell lines. Phosphorylated and total protein bands were quantified and compared. No significant differences were detected between the three cell lines when stimulated with a variety of ligands. Second, Dr Orita noted that X-gal staining of MEF cells was difficult to visualise, perhaps indicative of poor β-galactosidase expression. Strong β-galactosidase enzyme activity was only detected when using FDG, a fluorescent substrate of β-galactosidase.

Finally, MEFs are not specialised vascular cells and may not express the ECM components and/or receptors relevant to angiogenesis and vascular permeability and therefore there are no differences between wild-type and knock-out cell lines when examining pathways triggered by molecules such as VEGFA. Nonetheless, these unsuccessful experiments led me to utilise a more specific *in vitro* model for exploring the phenotype I observe *in vivo*.

6.6.2 The effect of PRELP on tubule formation and HUVEC monolayer integrity

After utilising MEFs, I opted to probe OMD and PRELP activity using HUVECs. Although these are not CNS-derived endothelial cells, they are widely used as a model for angiogenesis. Since there is evidence that PRELP affects angiogenesis from the results of the hindbrain angiogenesis assay, I opted to utilise HUVECs.

The first difficulty I had was optimising the tubule formation assay. Initial attempts were performed in conventional cell culture plates and dishes and imaged using an inverted light microscope. Imaging was challenging as I was required to create a panorama of images taken using the 10x lens. As a result, the resulting images were heterogeneous in terms of location in the dish and size of field of view. The location of imaging was

particularly important when using conventional cell culture plasticware; the formation of a meniscus of ECM gel led to cells accumulating in the middle of the well or dish. I would therefore quantify a higher number of tubules in the middle of a well compared to the outer areas. I also had difficulties quantifying tubule formation reliably from light-microscope images. I was unable to find an automated method to quantify tubules and attempted to quantify angiogenesis parameters manually. Unfortunately, I was unable to obtain consistent results using the method described above.

Use of the μ-slide Angiogenesis yielded more consistent results. Since the meniscus formed when using these slides is less pronounced, cells were more evenly-dispersed. Well size was also much smaller, allowing me to readily image an entire well easily using an upright microscope. In addition, I decided to use Calcein AM to stain cells, allowing the capture of high-contrast images. These images could then easily be converted in a binary black-and-white image. Quantification was simplified by using a program called AngioTool, originally developed for quantifying vascular networks in *in vivo* models for angiogenesis (Zudaire et al., 2011). The advantage of utilising AngioTool over manual quantification was time and consistency of the quantification. While AngioTool was excellent in providing information on vessel area, junction density, vessel length and disorder, it did have drawbacks. Notably, the program had difficulties handling variable vessel diameters or clumps of cells (Figure 6.30). Clusters of HUVECs would mistakenly be identified as multiple smaller vessels, leading to an artificial inflation in tubule number and junction density. However, since all images analysed were subject to the same quantification conditions, I deemed that this is unlikely to affect the overall results of the experiment.

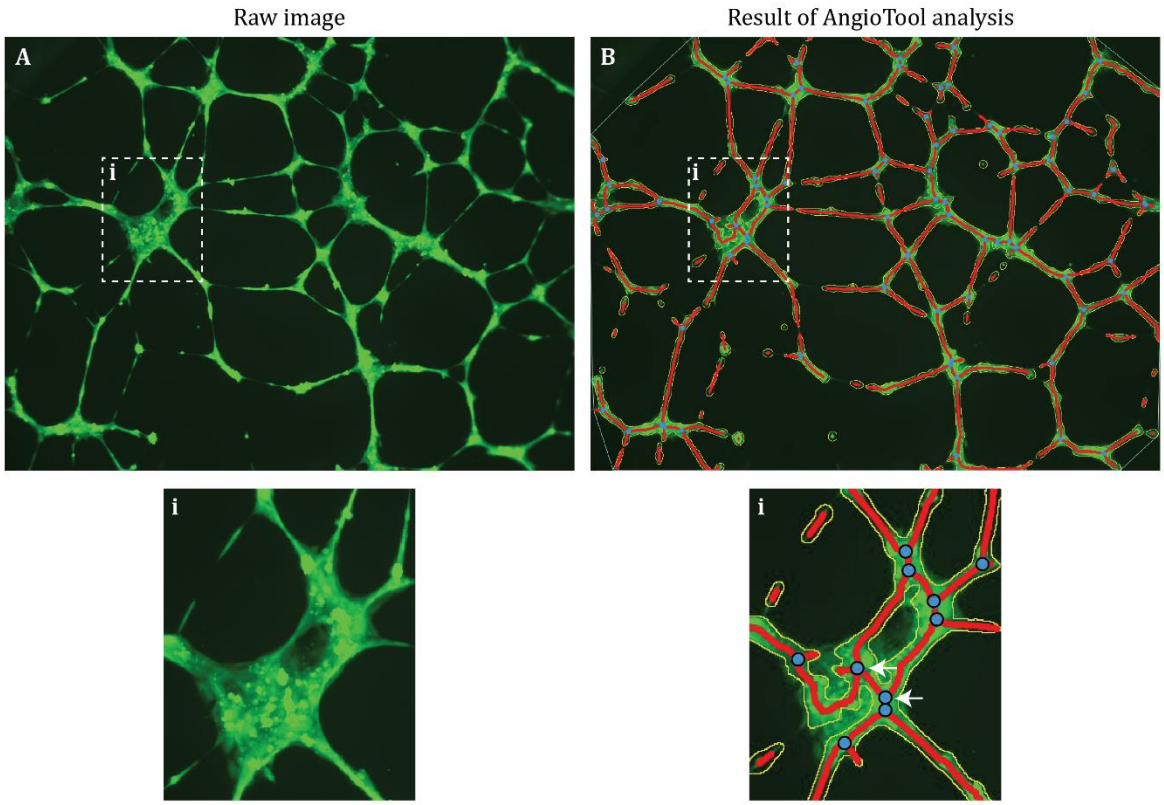

Figure 6.30. Difficulty handling vessels of varying diameters. A) Raw image used for processing with AngioTool. **B)** Resulting image after AngioTool analysis. **Ai & Bi)** Magnified views of cluster of cells. Note how this cluster of cells is treated as multiple vessels with two additional junctions within the cluster (arrows). AngioTool colours: vessel outline in yellow, skeleton in red and junctions as blue dots.

PRELP was found to affect tubule formation driven by TGF-β and VEGFA-165. Initial analysis using un-adjusted p-values indicated that EGF was also affected with respect to vessel percentage area. The tubule formation assay was then repeated with CM from -NT PRELP and -PR PRELP to determine whether overexpression of cytoplasmic PRELP resulted in secretion of anti-angiogenic factors and whether the HS-binding region of PRELP is important for its inhibition of VEGFA-165 activity respectively. Critically, I failed to observe the same inhibition of VEGFA-165 using CM from -NT or -PR PRELP-expressing cells. This would therefore indicate that the effect I observe using PRELP-CM is not due to the function of the LRR domain. It is therefore possible that PRELP inhibits VEGFA-165 in this experiment via the HS-binding domain.

Although these results of this experiment are consistent with *in vivo* data, such as the embryonic hindbrain assay, this data should be interpreted with caution. Firstly, the direct application of CM from HEK293 to HUVECs means that there was no quality-control of the amount or quality of PRELP protein. This means that there was probably some variation in the amount of protein produced between experiments. As a result, I do not know whether the effect of angiogenic inhibition is due to a function of PRELP at

physiological concentrations. In addition, western blotting of PRELP proteins (Figures 6.7 and 6.17) indicates that PRELP protein is probably quite unstable. Multiple bands above and below the molecular weight of the core protein suggests that it is significantly degraded and/or aggregated. Repeating these tubule formation assays with proper quality controls would be valuable. In particular, determining the dose-responsiveness of HUVECs to PRELP would be important to understand whether the role of PRELP inhibiting angiogenesis is relevant. To this end, utilising commercially-produced OMD and PRELP protein would be ideal.

I performed immunoprecipitation experiments to determine whether there is binding of VEGFA isoforms 121, 165 and 165b to OMD and PRELP. I was unable to detect such interaction under these experimental conditions. This therefore suggests that PRELP affects VEGFA-165 in an indirect manner. One possibility is that since VEGFA-165 is also a HS-binding protein, VEGFA-165 and PRELP compete to bind to the same HS sites on the cell surface (illustrated in Figure 6.31A). For example, if PRELP is already bound to 90% of the available HS sites on a given cell's surface, VEGFA-165 would only be able to bind to the remaining 10%, resulting in reduced signalling from VEGFR2.

Alternatively, it is possible that PRELP binds to VEGF receptors and either acts to directly block VEGFA-165 binding or cause a conformational change in the receptor upon binding which decreases the affinity of binding between the receptor and ligand (Figure 6.31B). Osteoglycin, another member of the SLRP family also expressed in brain pericytes has been shown to bind directly to VEGFR2 to block signalling (Wu et al., 2017). Finally, it is also possible that VEGFA-165 and PRELP have a direct interaction but is not detected under my experimental conditions (Figure 6.31C). For future studies, other methods to detect protein interactions could be essential.

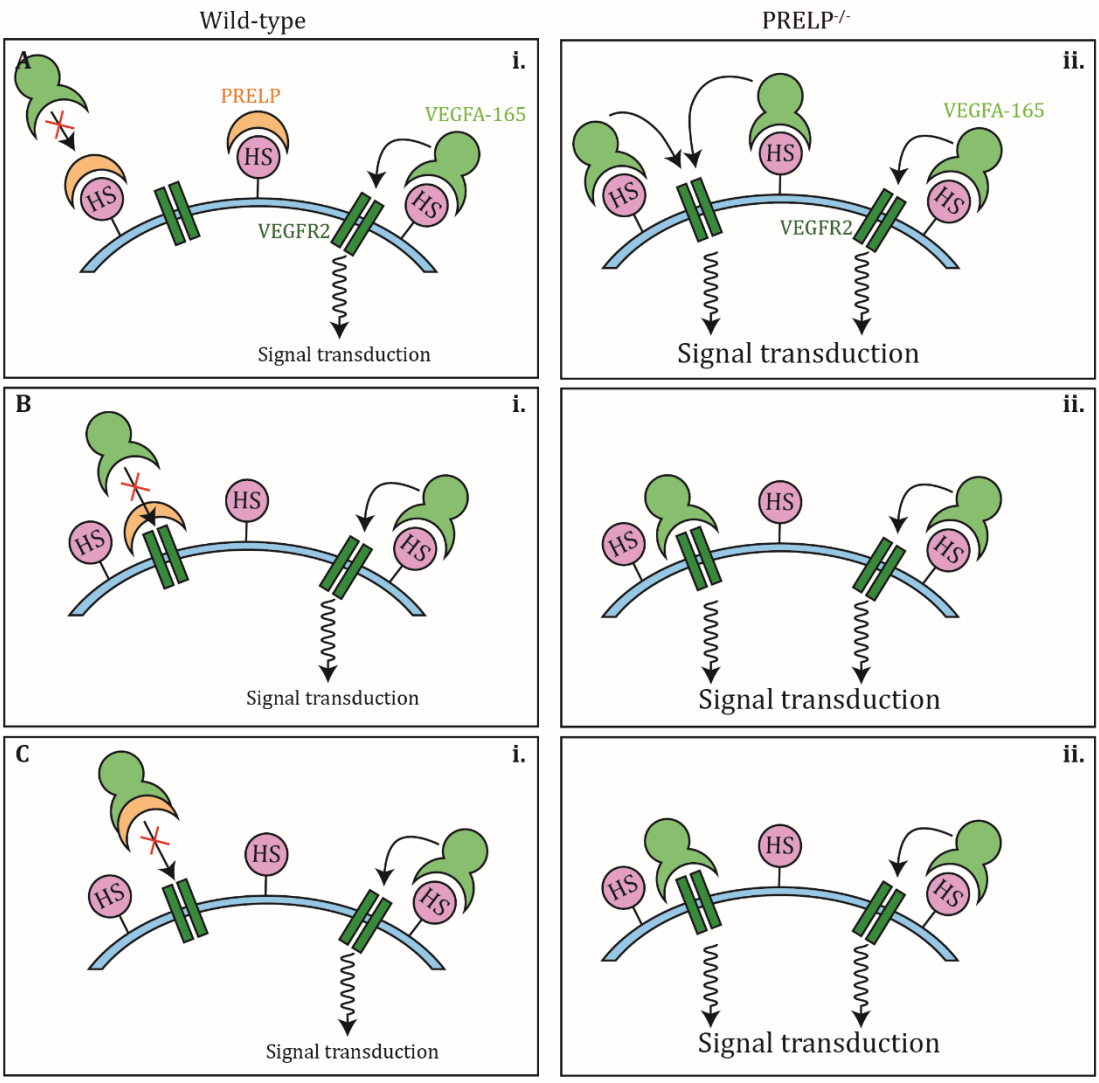

Figure 6.31. Possible mechanisms of PRELP inhibition of VEGFA-165 signalling. PRELP may act to inhibit VEGFA binding to HS sidechains on the cell surface, thereby reducing its concentration on the cell surface **(A)**, by binding to the VEGF receptors **(B)** or by binding directly to VEGF **(C)**.

Finally, I investigated the effect of PRELP on HUVEC monolayer integrity using TEER measurements and monolayer permeability to 70kDa dextran. After optimising the conditions to form a confluent monolayer, as assessed by PECAM-1 staining, TEER of these monolayers was measured. The addition of PRELP-CM in the basal chamber for the duration of monolayer formation resulted in a small increase in electrical resistance across the monolayer, indicative of an increase in barrier properties, although the validity of using PRELP-CM from HEK293 is not ideal. Next, I attempted to utilise 70kDa dextran to determine whether there are differences in the permeability of the monolayer, but found no statistically-significant changes based on CM. It is possible that the change in permeability as assessed by TEER is rather subtle and that 70kDa dextran is not appropriate for this study. A smaller size dextran, such as 10 or 40kDa may be more

suitable. Nonetheless, despite the technical concerns of using CM, these assays performed using HUVECs support my findings in PRELP$^{-/-}$ animals. Repeating these experiments using a proper source of OMD and PRELP protein would be valuable.

6.6.3 PRELP binds to TGF-β and may inhibit its function

There are many interactions of SLRPs with TGF-β. Biglycan, decorin, asporin and fibromodulin have been shown to bind to TGF-β and act to inhibit TGF-β signalling by sequestering free TGF-β (Hildebrand et al., 1994; Kizawa et al., 2005). I therefore utilised the secreted TGF-β-FLAG construct made by our former colleague Dr Noriaki Sasai to determine whether OMD and PRELP also share the ability to bind to TGF-β. These results indicate that OMD and PRELP are both capable of binding to TGF-β and may therefore affect TGF-β signalling in a similar manner to other members of the SLRP family.

Interestingly, I did not detect binding of the PRELP construct lacking its HS-binding domain. While the binding of PRELP may be dependent on N-terminal domains, it is not the case for decorin; using immobilised peptide fragments, a study has demonstrated that the core protein of decorin, i.e. the LRR domain, is responsible for its binding to TGF-β (Schönherr et al., 1998). In addition, since multiple SLRP members share this ability to bind to TGF-β, it is likely to be due to common structural motifs, notably the LRR core protein. In addition to concerns regarding the quality of mutant PRELP protein produced, it is possible that the deletion of the HS-binding domain of PRELP resulted in changes in the overall protein conformation, abrogating binding to TGF-β. This also has implications for the experiments regarding VEGFA (above).

Finally, PRELP-CM had an effect on TGF-β-induced tubule formation on HUVECs. Combined with the binding of PRELP directly to TGF-β, it would be interesting to further investigate the effect of PRELP on TGF-β signalling both *in vivo* and *in vitro*.

6.6.4 Problems encountered when isolating and purifying MBECs from PRELP$^{-/-}$

I was successful in optimising the isolation and purification of MBECs from wild-type brains. I determined that a mixture of collagen IV and fibronectin was important for the adhesion of wild-type MBECs in addition to the minimum seeding density needed to grow a confluent monolayer. Despite performing the optimised purification protocol five times to isolate PRELP$^{-/-}$ MBECs, I was unable to obtain a confluent monolayer.

The fact that endothelial cells isolated from wild-type mice formed monolayers but not those from PRELP$^{-/-}$ mice indicates that there are clear differences in the properties of wild-type and PRELP$^{-/-}$ MBECs. It could be due to a number of factors, notably the composition of the extracellular matrix of PRELP$^{-/-}$ MBECs and the expression of

endothelial transporters responsible for pumping out puromycin. While I was able to confirm that PRELP$^{-/-}$ blood vessel fragments were able to attach to the transwell membranes, almost all cells died after puromycin treatment. This strongly indicates that there is a reduction in the expression or activity of ABC transporters. When RNA seq data was initially analysed by probing DAVID and KEGG resources, I observed that members of the ABC transporters were down-regulated in a statistically-significant manner in PRELP$^{-/-}$ (Figure 6.32), supporting this hypothesis. ABC transporter expression is dependent on the activation of β-catenin (Lim et al., 2008). There is a study showing that PRELP may be able to affect osteoblastic differentiation by affecting β-catenin stability – knockdown of PRELP resulted in decreased expression of β-catenin target genes in osteoblast cell lines (Li et al., 2016). It is therefore possible that the expression of ABC transporters in PRELP$^{-/-}$ vessels was affected by decreased β-catenin levels.

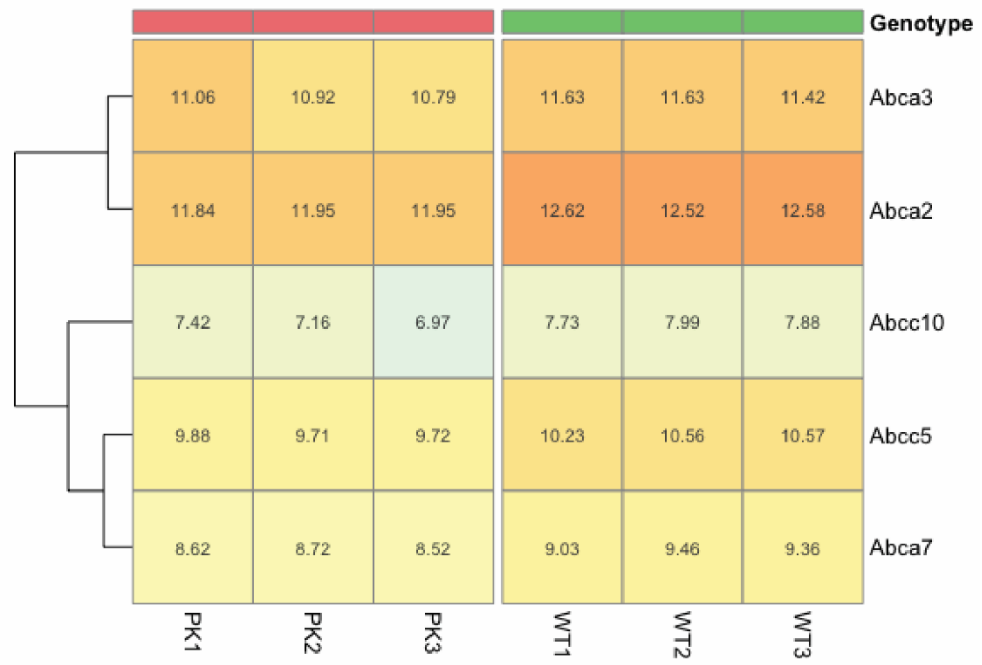

Figure 6.32. Heatmap of ABC transporters differentially expressed in PRELP$^{-/-}$. Analysis of meningeal RNA from PRELP$^{-/-}$ and wild-type mice. Differentially expressed genes at p-value < 0.01.

If it is correct that the failure to isolate MBECs from PRELP$^{-/-}$ brains was due to puromycin toxicity, alternative methods to purify endothelial cells from mouse brains would have to be employed. Antibody-based purification could be utilised, where single cell suspensions are mixed with endothelial cell-specific antibodies and purified by FACs or magnetic beads (Figure 6.33) (van Beijnum et al., 2008).

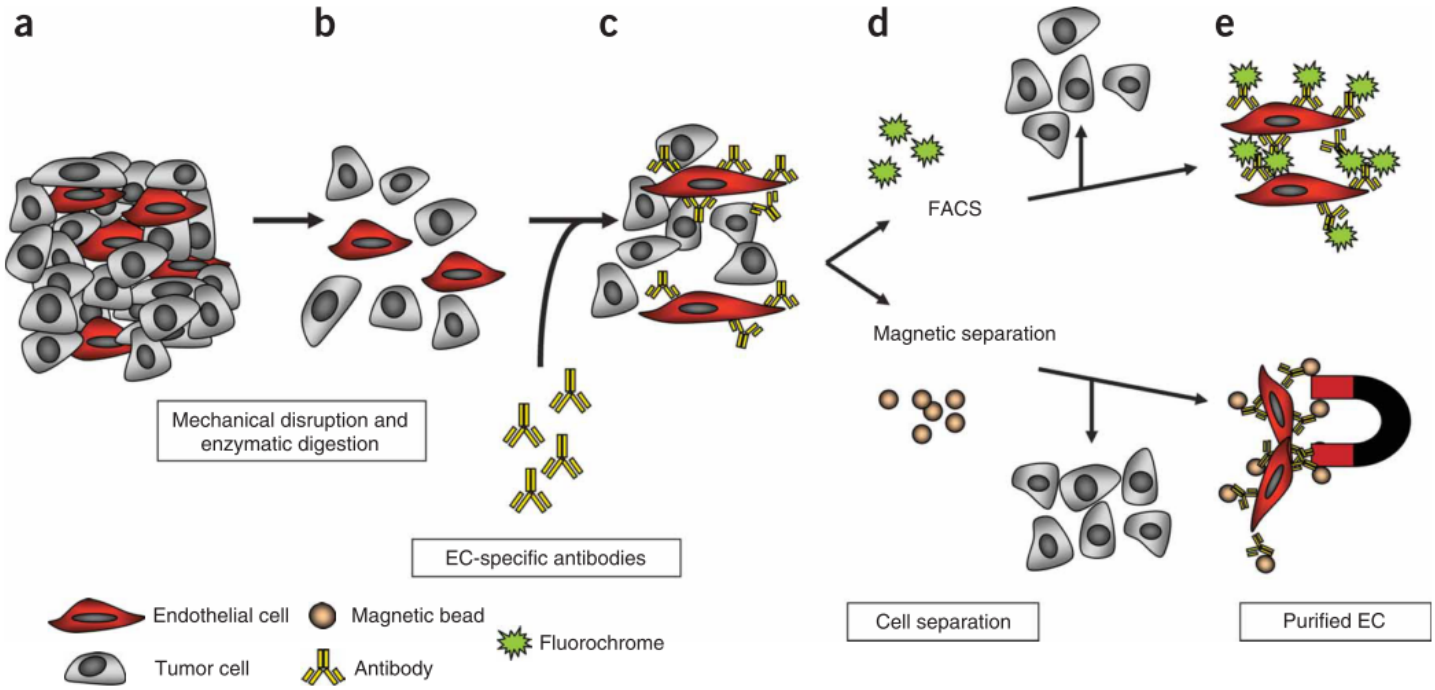

Figure 6.33. Schematic of antibody-based purification of brain endothelial cells using FACS or magnetic beads. Figure from (van Beijnum et al., 2008).

6.7 Conclusions

To conclude, I successfully created a variety of constructs encoding VEGFA isoforms and PRELP lacking various N-terminal sequences. Unfortunately, it was evident that there were issues with the quality of PRELP mutant constructs secreted by HEK293 cells. I was successful in establishing cell lines derived from OMD$^{-/-}$ and PRELP$^{-/-}$ fibroblasts and did not detect any differences in the response of the cell lines when stimulated with growth factors. I then optimised the HUVECs tubule formation assay and investigated the cells' propensity to form tubules when stimulated with growth factors and crude conditioned media containing OMD or PRELP protein, and found that there was a notable inhibition of VEGFA-165 signalling when incubated with PRELP-CM. This was dependent on the proline/arginine-rich HS-binding domain, as assessed by the -PR PRELP construct, although unfortunately the validity of this result is questionable given the problems expressing these proteins by HEK293 cells. I determined that both OMD and PRELP bind to TGF-β; binding of PRELP was dependent on the HS-binding domain. In contrast, there

was no binding of OMD or PRELP to VEGFA isoforms, suggesting that the inhibition of VEGFA-165 signalling by may be indirect by modulating cells' sensitivity to VEGFA-165 or by binding to its receptor. Next, HUVECs grown on transwell membranes exhibited an increase in TEER when incubated with PRELP-CM, but not -PR PRELP-CM. In order to assess the permeability of endothelial cells directly from our transgenic mice, I optimised the purification and growth of MBECs on transwell inserts. Unfortunately, PRELP$^{-/-}$ MBECs did not form a monolayer using the same experimental conditions, likely due to differences in the expression of ABC transporters.

Chapter 7 General Discussion and Conclusions

7.1 Summary of findings

7.1.1 Chapter 3

Since the exons encoding OMD and PRELP were replaced by those of *LacZ*, I used X-gal staining as a means to identify the cell types which would express OMD and PRELP. Initially, the intense and wide-spread staining of $OMD^{+/-}$ brains indicated that the reporter gene is expressed by a variety of cells in the brain, including the vasculature. However, staining of OMD tissues with anti-β-galactosidase and anti-OMD indicated that there is little or no expression of OMD in the brain. This was supported by single-cell RNA seq data, where OMD was only detected at ~1-2 copies per cell.

In contrast, the staining pattern of $PRELP^{+/-}$ was more specific and localised to the ventricles and blood vessels. In addition to X-gal staining, using antibodies against β-galactosidase and PRELP, I have determined that PRELP is expressed in mural cells in a variety of vessels. This finding is supported by data obtained from transcriptome analyses, where PRELP gene expression was detected in vSMCs and in pericytes. Finally, from β-galactosidase staining, I have determined that PRELP is also expressed in ependymal cells and microglia.

7.1.2 Chapter 4

Given the expression pattern of PRELP in particular, I sought to determine whether there were differences in the brain vasculature compared to wild-type. Using the embryonic hindbrain as a model for angiogenesis, I determined that there is an increase in blood vessel content in $PRELP^{-/-}$. Next, using staining for endogenous mouse IgG, I identified vascular leakage in $PRELP^{-/-}$ and confirmed this finding using tracer dye injection. Analysis of BBB components indicated that constituents of the basement membrane laminin and perlecan were down-regulated in addition to a decrease in vessel coverage by pericytes and astrocyte end-feet. The staining pattern of cell-cell junction proteins also indicated that there were abnormalities in $PRELP^{-/-}$ vessels which were notably more punctate compared to wild-type. Finally, I analysed immune components of the brain and found an increase in microglial number and activation state. No differences were observed when quantifying the number of astrocytes and staining intensity of GFAP, indicative of mild BBB breakdown.

No differences were observed between $OMD^{-/-}$ and wild-type in any of the experiments described above.

7.1.3 Chapter 5

A microarray experiment comparing the gene expression profiles of large ventral vessels was performed prior to the commencement of this PhD project. I obtained raw data files and analysed them using R. Data was normalised to GC-RMA and statistically-significant genes were obtained. I attempted to perform ontology analysis, however the results were inconclusive due to a limited number of differentially-expressed genes.

In order to obtain a more refined and relevant dataset, I isolated RNA from brain meningeal vessels for RNA seq. Raw gene counts were analysed in R and a list of significant genes was obtained. Ontology analysis using tools provided by the GO consortium indicated that cytokine signalling is affected in $OMD^{-/-}$. Analysis of $PRELP^{-/-}$ data indicated that many differentially expressed genes had gene products localised to the ECM, including SLRPs and BM components. Finally, using GSEA, I determined that genes related to interferon signalling were up-regulated in both $OMD^{-/-}$ and $PRELP^{-/-}$. From this gene expression study, it is still unclear which pathways are affected in $PRELP^{-/-}$ to produce the phenotype of BBB dysfunction.

7.1.4 Chapter 6

I created MEF cell lines from our transgenic mice and analysed their responsiveness to a variety of signalling molecules. No changes were detected in the relative phosphorylation in wild-type, $OMD^{-/-}$ and $PRELP^{-/-}$ MEFs.

By supplementing HUVECs with OMD and PRELP produced by transfected HEK293 cells, I assayed their ability to form tubules in response to various growth factors. Tubule formation in the presence of PRELP-CM was inhibited when TGF-β and VEGFA-165 were added. The tubule formation assay was then repeated using constructs of PRELP lacking its signal sequence and/or HS-binding domain. Unfortunately, the validity of these experiments is difficult to determine given the problems related to protein stability and expression in HEK293 CM. IP experiments indicated that PRELP binds to TGF-β, dependent on the PR-rich region whereas there was no binding to VEGFA isoforms. There was no effect of OMD-CM on tubule formation.

Next, HUVECs were grown on transwell monolayers in the presence of CM and TEER was assessed. While there were no changes in TEER when cells were grown with OMD-CM, there was a small increase in TEER with PRELP-CM. The permeability of the monolayer was assessed using 70kDa dextran, and no differences were detected with respect to CM.

Finally, I attempted to characterise the properties of MBECs isolated from our transgenic animals. The conditions for MBEC purification was optimised using wild-type mice. Unfortunately, attempts to purify cells from PRELP$^{-/-}$ mice were unsuccessful.

7.2 Proposed roles of PRELP on brain capillary stability

7.2.1 PRELP acts to stabilise the basement membrane

This work highlights the importance of PRELP in maintaining cerebral vasculature. While there are many studies describing the role of SLRPs in regulating angiogenesis, this study represents the first description of an SLRP being involved in the maintenance the BBB. In particular, this effect seems to be dependent on the role of PRELP in stabilising ECM architecture. This is supported by evidence of vascular leakage in PRELP$^{-/-}$, as shown by IgG staining, injection of fluorophore-conjugated dextran and immunostaining of a variety of BBB constituents. I also demonstrated that microglia in PRELP$^{-/-}$ are shifted towards a more activated state, further supporting the finding of BBB degeneration in PRELP$^{-/-}$. In particular, I noted that the components of the BM are the most strongly downregulated element of the BBB. This is also supported by my RNA seq analysis, where a large proportion of differentially-expressed genes encode ECM proteins, including other SLRP members and BM constituents.

Bengtsson and colleagues proposed a role for PRELP to anchor perlecan to the BM (Bengtsson et al., 2002). In this study, there is a decrease in perlecan staining intensity in PRELP$^{-/-}$, supporting this proposition. Perlecan has a variety of roles in maintaining the BM, notably bridging laminin-collagen IV lattices. Therefore, the loss of perlecan could also lead to decreased retention of laminin. As discussed in Chapter 4, loss of laminin is detrimental to the BBB. The knock-out systems analysed in these studies looked at total loss of laminin α2, astrocyte-specific laminin and pericyte-specific laminin, where the most severe phenotype was observed in laminin α2 deletion (Gautam et al., 2016; Menezes et al., 2014; Yao et al., 2014).

These laminin mouse models and PRELP$^{-/-}$ mice exhibited defects in astrocyte end-foot and pericyte coverage, in addition to diminished cell-cell junction proteins. A perturbed BM leads to reduced attachment of astrocyte end-feet and pericytes. This in turn leads to decreased stabilising interactions from astrocytes and pericytes, leading to decreased endothelial barrier function. Shh, TGF-β and Wnt ligands secreted by astrocytes have been shown to bind to receptors on endothelial cells and induce the expression of tight junction proteins (Alvarez et al., 2011; Liebner et al., 2008; Obermeier et al., 2013). Similarly,

cross-talk between pericytes and endothelial cells via Ang-1 have been shown to be essential for maintaining the BBB (Lee et al., 2003).

In addition, I have demonstrated in Chapter 3 that PRELP is expressed in pericytes. It is therefore possible that pericytic laminin is most strongly affected in PRELP$^{-/-}$ mice. This is supported by the fact that PRELP$^{-/-}$ mice and pericyte-specific knock-out of laminin γ1 seem to share similarities in the severity of the phenotype, where there are clearly defects in the BBB, but the leakage is relatively mild.

I therefore propose that PRELP acts to maintain the integrity of the BBB by stabilising and facilitating the assembly of the basement membrane, by providing additional bridging interactions between HSPGs such as perlecan and the collagen network. Loss of PRELP results in a perturbed basement membrane, with reduced laminin, perlecan and possibly other proteins, leading to decreased attachment of critical perivascular cells. This then leads to down-stream consequences due to decreased cross-talk between endothelial cells and pericytes and astrocytes resulting in increased vascular leakage.

7.3 Future work

7.3.1 The addition of stresses on the PRELP$^{-/-}$ BBB

Many studies regarding the BBB are performed investigating the effect of stroke and ischaemia (Brown & Davis, 2002; Dénes et al., 2011; Engelhardt, 2011; Gidday et al., 2005; Kangwantas et al., 2016; Mckittrick et al., 2015; Zhang et al., 2000). Some interesting genetic models, such as the various laminin knock-out mice, are performed without inducing ischaemia, although defects in the BBB are more obvious and severe when obtained with stimulation. As discussed previously, the phenotype observed in PRELP$^{-/-}$ brains is not severe; there is no embryonic lethality, mice seem to have a normal lifespan and astrocyte activation is comparable to wild-type. The introduction of a challenge such as stroke or injection of neuroinflammatory compounds, e.g. LPS, could be interesting to investigate in PRELP$^{-/-}$. This would be interesting to study from the perspective of the BBB, as well as the inflammatory response in PRELP$^{-/-}$, given the ubiquitous expression of PRELP in microglia.

7.3.2 Studying the BBB of double knock-out mice

Given the structural similarity between SLRP members, it is not surprising that they are capable of compensating loss-of-function of one member. For example, in fibromodulin-deficient mice, there is an increase in lumican expression in the tendon (Svensson et al., 1999). Given the relatively mild phenotype of PRELP$^{-/-}$ mice, it is entirely possible that an

up-regulation of another SLRP member is compensating for PRELP loss. It would therefore be interesting to study double knock-out mice.

In Chapter 3, I analysed transcriptome data in order to confirm the cell-type expressing PRELP. When investigating the list of pericyte-specific gene expression provided by (He et al., 2016), I found that other SLRPs were also expressed in the mural cell transcriptome. Biglycan, asporin and osteoglycin were all expressed at higher levels compared to PRELP. When analysing our own transcriptome data of meningeal vessels, I observed that other SLRPs are up-regulated. I notably observed that osteoglycin is up-regulated. As outlined in Chapter 1, osteoglycin has an anti-angiogenic function, where it inhibits VEGFA-VEGFR2 signalling. I have also concluded from experiments in Chapter 6 that PRELP also inhibits this signalling pathway. Therefore, it is quite possible that the up-regulation of osteoglycin in PRELP$^{-/-}$ mice is compensating for PRELP loss. The study of PRELP and osteoglycin double knock-out mice could be of interest.

7.3.3 The role of PRELP in neurodegenerative disorders

Throughout this PhD project, I have attempted to determine whether there is neurodegeneration in PRELP$^{-/-}$, given that BBB and neurodegenerative disorders are commonly associated. Staining of proteins associated with neurodegeneration, such as Aβ-42 in the case of Alzheimer's disease, was negative, indicating that there was no evidence of disease progression. As described above, the BBB of PRELP$^{-/-}$ mice housed in conditions of little to no stress only exhibited mild BBB breakdown. It would, however, be interesting to cross PRELP$^{-/-}$ with other lines or induce CNS insults by administration of specific compounds and study the effect of PRELP loss in the context of neurodegeneration. For example, APP (SW) mice overexpress a familial version of the Aβ precursor protein (Games et al., 1995); crossing them with pericyte-deficient PDGFR-β$^{+/-}$ mice results in accelerated Alzheimer's disease pathology (Sagare et al., 2013). Production and optimisation of an in vitro BBB model from PRELP$^{-/-}$ mice

In order to further understand the properties of the PRELP$^{-/-}$ BBB, an elaborate *in vitro* model could be produced. Just as described above, the different constituents of the BBB could be purified from brain homogenates and assembled *in vitro*. Endothelial cells and pericytes could be cultured on different sides of a transwell insert, whereas astrocytes and/or microglia could be grown at the bottom of the dish. The use of a transwell insert establishes cell polarity and is an important feature of vascular models. For example, there is higher expression of VEGFR2 in the abluminal side of brain endothelial cells – a property which is not conserved in peripheral vessels (Hudson et al., 2014).

As I found out in Chapter 6, the best approach to this experiment would be to purify cells using a method such as FACs, to avoid difficulties purifying cells from the knock-out. Alternatively, in order to circumvent this complex procedure of purifying and culturing multiple cell-types in a single well, commercial BBB models are available. For example, the Ready-To-Use BBB Kit produced by PharmaCo-Cell (Japan) is a triple co-culture of endothelial cells, pericytes and astrocytes from rat or monkey. PRELP can be added to these cells in culture in the form of CM, just as was done in my experiments. To further optimise this, a stable-cell line overexpressing PRELP may be more appropriate to reduce fluctuations in PRELP concentration in the CM.

These *in vitro* models could then be used to assess the changes in the permeability of the BBB in response to different treatments in the presence or absence of PRELP. As done previously, the integrity of the endothelial cell monolayer in this culture system could be assessed by TEER measurements and permeability to tracer dyes. For example, I would expect that the response to VEGFA would be altered in PRELP$^{-/-}$ cells or cells supplemented with PRELP-CM. Other molecules could be screened using this BBB model – for example, I could investigate the relationship between inflammatory molecules, PRELP and BBB breakdown.

7.3.4 Investigating immune functions of OMD

In this study, I was unable to determine any differences between OMD$^{-/-}$ and wild-type vasculature – angiogenesis, BBB function and inflammatory state were comparable. I did, however, determine using microarray and RNA seq analysis that many pathways linked to innate immunity and inflammation are likely to be up-regulated in OMD$^{-/-}$. Ontology analysis indicated that many GO Biological Processes associated with immunity were altered in OMD$^{-/-}$. In addition, when visualising the protein-protein interactions of the genes detected using RNA seq, almost all gene products were involved in cytokine and chemokine signalling. GSEA analysis also detected gene sets up-regulated during interferon-γ, interferon-α and interleukin-6-JAK-STAT signalling. It could therefore be extremely interesting to study OMD$^{-/-}$ mice in the context of auto-immune disease, perhaps using an adjuvant such as LPS.

Appendix A Appendix

A.1 Multiple sequence alignment of OMD and PRELP

Amino acid sequences of human, mouse and rat OMD and PRELP were aligned using Clustal Omega (Sievers et al., 2011) (Figure A.1, Figure A.2). Alignment clearly shows that there is considerable homology, particularly with regards to PRELP.

```
CLUSTAL O(1.2.4) multiple sequence alignment


sp|Q99983|OMD_HUMAN      MGFLSPIYVIFFFFGVKVHCQYETYQWDEDYDQEPDDDYQTGFPFRQNVDYGVPFHQYTL
sp|O35103|OMD_MOUSE      MGFLSPIYVLFFCFGVRVYCQYEAYRWDDDYDQEPNEDYDPEFQFHQNIEYGVPFYNNIL
sp|Q9Z1S7|OMD_RAT        MGCLRPIYVLFFCFVVRVYGQYEAYQWDEDYEQEPSEDYEPEFQFHQNIEYGAPFYQNIL
                         ** * ****:** * *:*: ***:*:**:**:***.:**:  * *:**::**.**::  *

sp|Q99983|OMD_HUMAN      GCVSECFCPTNFPSSMYCDNRKLKTIPNIPMHIQQLYLQFNEIEAVTANSFINATHLKEI
sp|O35103|OMD_MOUSE      GCAKECFCPTNFPTSMYCDNRKLKTIPIIPMHIQQLNLQFNDIEAVTANSFINATHLKEI
sp|Q9Z1S7|OMD_RAT        GCAKECFCPTNFPTSMYCDNRKLKTIPDIPMHIQQLNLQFNDIEAVTADSFINATHLKEI
                         **..*********:************* ******** ****:******:***********

sp|Q99983|OMD_HUMAN      NLSHNKIKSQKIDYGVFAKLPNLLQLHLEHNNLEEFPFPLPKSLERLLLGYNEISKLQTN
sp|O35103|OMD_MOUSE      NLSHNKIKSQKIDYGVFAKLSNLQQLHLEHNNLEEFPFPLPKSLERLLLGYNEISILPTN
sp|Q9Z1S7|OMD_RAT        NLSHNKIKSQKIDYGVFAKLSNLQQLHLDHNNLEEFPFPLPKSLERLLLGYNEISTLPTH
                         ******************** ** ****:************************** * *:

sp|Q99983|OMD_HUMAN      AMDGLVNLTMLDLCYNYLHDSLLKDKIFAKMEKLMQLNLCSNRLESMPPGLPSSLMYLSL
sp|O35103|OMD_MOUSE      AMDGLVNVTMLDLCYNHLSDSMLKEKTLSKMEKLMQLNLCNNRLESMPLGLPSSLMYLSL
sp|Q9Z1S7|OMD_RAT        AMDGLVNVTMLDLCYNHLSDSTLKGKILSKLEKLMQLNLCNNRLESMPPGLPLSLMYLSL
                         *******:********:* ** ** * ::*:*********.******* *** *******

sp|Q99983|OMD_HUMAN      ENNSISSIPEKYFDKLPKLHTLRMSHNKLQDIPYNIFNLPNIVELSVGHNKLKQAFYIPR
sp|O35103|OMD_MOUSE      ENNSISSIPDNYFDKLPKLHALRISHNKLEDIPYDIFNLSNLIELNVGHNKLKQAFYIPR
sp|Q9Z1S7|OMD_RAT        ENNSISSIPEDYFQKLPKLHALRISHNKLEDIPYDIFNLSNLIELNVGHNKLKQAFYIPR
                         *********:.**:******:**:*****:****:**** *::**.**************

sp|Q99983|OMD_HUMAN      NLEHLYLQNNEIEKMNLTVMCPSIDPLHYHHLTYIRVDQNKLKEPISSYIFFCFPHIHTI
sp|O35103|OMD_MOUSE      NLEHLYLQNNEIESINVTMICPSPDPVHHHHLTYLRVDQNKLKEPISSYIFFCFPRIHSI
sp|Q9Z1S7|OMD_RAT        NLEHLYLQNNEIQSINVTMMCPSLDPLHHHHLTYLRVDQNKLKEPISSYIFFCFPRIHSI
                         ************:.:*:*::*** **:*:*****:*********************:**:*

sp|Q99983|OMD_HUMAN      YYGEQRSTNGQTIQLKTQVFRRFPDDDDESEDHDDPDNAHESPEQEGAEGHFDLHYYENQ
sp|O35103|OMD_MOUSE      YYGEQRSTNGETIQLKTQVFRSYQEEEEED-DHDSQDNTL--EGQEVSDEHYNSHYYEMQ
sp|Q9Z1S7|OMD_RAT        YYGEQRSTNGETIQLKTQVFRRYQDEEEEE-EDDSQDHTL--EGQEETEEHFNSHYYEMQ
                         **********:********** : ::::*. :.*. *::     ** :: *:: **** *

sp|Q99983|OMD_HUMAN      E-----
sp|O35103|OMD_MOUSE      EWQDTI
sp|Q9Z1S7|OMD_RAT        AWQNTI
```

Figure A.1. Alignment of human, mouse and rat OMD protein sequence.

```
CLUSTAL O(1.2.4) multiple sequence alignment


sp|P51888|PRELP_HUMAN      MRSPLCWLLPLL-ILASVAQGQPTRRPRPGTGPGRRPRPRPRPTPSFPQPDEPAEPTDLP
sp|Q9JK53|PRELP_MOUSE      MRASFFWLLPLLLILASVAQGQPTRP-----KPGIRRKPKPRPTPRFPQAPEPAEPTDLP
sp|Q9EQP5|PRELP_RAT        MRASFFWFLPLLLILASVAQGQP-RP-----KPGIRRKPKPRPTPSFPQPHEPAEPTDLP
                           **: : *:**** ********** *       ** * :*:***** ***  *********

sp|P51888|PRELP_HUMAN      PPLPPGPPSIFPDCPRECYCPPDFPSALYCDSRNLRKVPVIPPRIHYLYLQNNFITELPV
sp|Q9JK53|PRELP_MOUSE      PPLPPGPPSVFPDCPRECYCPPDFPSALYCDSRNLRRVPVIPPRIHYLYLQNNFITELPL
sp|Q9EQP5|PRELP_RAT        PPLPPGPPSVFPDCPRECYCPPDFPSALYCDSRNLRKVPIIPPRIHYLYLQNNFITELPV
                           *********:**************************:**:*******************:

sp|P51888|PRELP_HUMAN      ESFQNATGLRWINLDNNRIRKIDQRVLEKLPGLVFLYMEKNQLEEVPSALPRNLEQLRLS
sp|Q9JK53|PRELP_MOUSE      ESFQNATGLRWVNLDNNRIRKVDQRVLGKLPSLAFLYMEKNQLEEVPSALPRNLEQLRLS
sp|Q9EQP5|PRELP_RAT        ESFKNATGLRWINLDNNRIRKVDQRVLEKLPGLAFLYMDKNQLEEVPSALPRNLEQLRLS
                           ***:********:*********:***** ***.*.****:**********************

sp|P51888|PRELP_HUMAN      QNHISRIPPGVFSKLENLLLLDLQHNRLSDGVFKPDTFHGLKNLMQLNLAHNILRKMPPR
sp|Q9JK53|PRELP_MOUSE      QNLISRIPPGVFSKLENLLLLDLQHNRLSDGVFKADTFQGLKNLMQLNLAHNILRKMPPK
sp|Q9EQP5|PRELP_RAT        QNLISRIPPGVFSKLENLLLLDLQHNRLSDGVFKADTFQGLKNLMQLNLAHNILRRMPPK
                           ** ******************************** ***:****************:***:

sp|P51888|PRELP_HUMAN      VPTAIHQLYLDSNKIETIPNGYFKSFPNLAFIRLNYNKLTDRGLPKNSFNISNLLVLHLS
sp|Q9JK53|PRELP_MOUSE      VPQAIHQLYLDSNKIETIPNGYFKDFPNLAFIRMNYNKLSDRGLPKNSFNISNLLVLHLS
sp|Q9EQP5|PRELP_RAT        VPPAIHQLYLDSNKIETIPSGYFKDFPNLAFIRMNYNKLSDRGLPKNSFNISNLLVLHLS
                           ** ****************.****.********:*****:**********************

sp|P51888|PRELP_HUMAN      HNRISSVPAINNRLEHLYLNNNSIEKINGTQICPNDLVAFHDFSSDLENVPHLRYLRLDG
sp|Q9JK53|PRELP_MOUSE      HNKISNVPAISNKLEHLYLNNNSIEKINGTQICPNNLVAFHDFSSDLENVPHLRYLRLDG
sp|Q9EQP5|PRELP_RAT        HNKISNVPAISNKLEHLYLNNNSIEKINGTQICPSNLVAFHDFSSDLENVPHLRYLRLDG
                           **:**.****.*:*********************.:************************

sp|P51888|PRELP_HUMAN      NYLKPPIPLDLMMCFRLLQSVVI
sp|Q9JK53|PRELP_MOUSE      NFLKPPIPLDLMMCFRLLQSVVI
sp|Q9EQP5|PRELP_RAT        NFLKPPIPLDLMMCFRLLQSVVI
                           *:**********************
```

Figure A.2. Alignment of human, mouse and rat PRELP protein sequence.

A.2 Microarray R codes

A.2.1 Normalisation of microarray data

```
###############################################################################
#
# Start-up!
#
###############################################################################

#What is this?
#Need to check which normalisation method works best.

#Method
#1) Normalise data with various techniques.
#2) Intensity plots
#3) MVA plots

#Date edited: 22-02-17

#Working at the Institute?
setwd("/Users/shin-ichiohnuma/Desktop/Hongorzul/Quantification/Hamamoto Microarray/CEL
files/Bayes")

#Working from home?
setwd("C:/Users/hd/Desktop/Hamamoto Microarray/CEL files/Bayes")

#Working from harddrive?
setwd("D:/Quantification/Hamamoto Microarray/CEL files") #laptop
```

```
setwd("/Volumes/Hongorzul/Quantification/Hamamoto Microarray/CEL files") #Mac
computers..... !!!!

source("http://www.bioconductor.org/biocLite.R")
biocLite("affy")
biocLite("mouse430a2.db") ###Mouse genome annotation library
biocLite("gcrma")
biocLite("RColorBrewer")
biocLite("affyPLM")
biocLite("affyQCReport")

library(affy)
library("mouse430a2.db")
library("gcrma")
library("RColorBrewer")
library("affyPLM")
library("affyQCReport")
library("affydata")

load("mas5.rda")
load("rma.rda")
load("gcrma.rda")
load("raw.rda")
load("affydata.rda")
load("datamas5.rda")
load("datarma.rda")
load("datagcrma.rda")

###########################################################################
#
# Initial
#
###########################################################################

affy.data<-ReadAffy()   ###reads CEL files
#save(affy.data, file="affydata.rda")
raw<-exprs(affy.data)
#save(raw, file="raw.rda")

#Colours and labels for easy graphing !
animalcodes<-c("OMD-/- (1)", "OMD-/- (2)", "PRELP-/- (1)", "PRELP-/- (2)", "Wild-type (1)",
"Wild-type (2)")
colours<-c("dodgerblue","slateblue1","red","firebrick","forestgreen","seagreen3") #for
histogram
colours2<-c("skyblue","skyblue","salmon","salmon","palegreen3","palegreen3") #for
boxplot; colours correspond to those I use in my thesis - yay for consistency !!

###########################################################################
#
# Un-normalised data
#
###########################################################################

boxplot(affy.data, ylim=c(0,14), names=animalcodes, col=colours2,
ylab="Log2(intensity)", main="PM-MM intensities of raw data",cex.axis=0.8)

hist(affy.data, col=colours, xlab="Log2(intensity)", main="Distribution of raw PM
probe data",cex=0.7)
legend(12,1.3,animalcodes, fill=colours,box.lty=0)

par(mar=c(1,1,1,1))
MAplot(affy.data,pairs=TRUE,plot.method="smoothScatter",main="MVA plots for raw data")

correlationPlot(affy.data)

###########################################################################
#
# Mas5 normalisation
#
###########################################################################

data.mas5<-mas5(affy.data)
#save(data.mas5, file="datamas5.rda")
mas5<-exprs(data.mas5)
#save(mas5,file="mas5.rda")
```

```
boxplot(data.mas5, names=animalcodes, col=colours2, ylab="Log2(intensity)", main="PM
intensities of MAS5-normalised data",cex.axis=0.8)

hist(data.mas5, col=colours, xlab="Log2(intensity)", main="Distribution of intensities
of MAS5-normalised data")
legend(12,1,animalcodes, fill=colours,box.lty=0)

MAplot(data.rma,pairs=TRUE,plot.method="smoothScatter",cex=0.6,main="MVA plots for
MAS5-normalised data")

correlationPlot(data.mas5)

###############################################################################
#
# RMA normalisation
#
###############################################################################

data.rma<-rma(affy.data)   ###RMA normalisation on data
#save(data.rma,file="datarma.rda")
rma<-exprs(data.rma)
#save(rma,file="rma.rda")

boxplot(data.rma, ylim=c(0,14), names=animalcodes, col=colours2,
ylab="Log2(intensity)", main="Probe set intensities after RMA normalisation",
cex.axis=0.8)

hist(data.rma, col=colours, xlab="Log2(intensity)", main="Distribution of intensities
after RMA normalisation")
legend(11.3,0.22,animalcodes, fill=colours,box.lty=0)

MAplot(data.rma,pairs=TRUE,plot.method="smoothScatter",cex=0.6,main="MVA plots for
RMA-normalised data")

correlationPlot(data.rma)

###############################################################################
#
# gcRMA normalisation
#
###############################################################################

data.gcrma<-gcrma(affy.data)
#save(data.gcrma, file="datagcrma.rda")
gcrma<-exprs(data.gcrma)
#save(gcrma,file="gcrma.rda")

boxplot(data.gcrma, ylim=c(0,14), names=animalcodes, col=colours2,
ylab="Log2(intensity)", main="Probe set intensities after GC-RMA normalisation",
cex.axis=0.8)

hist(data.gcrma, col=colours, xlab="Log2(intensity)", main="Distribution of
intensities after GC-RMA normalisation")
legend(12.5,0.65,animalcodes, fill=colours,box.lty=0)

MAplot(data.gcrma,pairs=TRUE,plot.method="smoothScatter",cex=0.6,main="MVA plots for
GC-RMA-normalised data")

correlationPlot(data.gcrma)
```

A.2.2 Obtaining lists of significant genes & drawing heatmaps

```
###############################################################################
#
# Start-up!
#
###############################################################################

#What is this?
#Clean code for analysing GC-RMA normalised data

#Date edited: 22-02-17

#Working from harddrive?
setwd("D:/Quantification/Hamamoto Microarray/CEL files") #laptop
```

```
setwd("/Volumes/Hongorzul/Quantification/Hamamoto Microarray/CEL files") #Mac
computers..... !!!!

source("http://www.bioconductor.org/biocLite.R")
biocLite("affy")
biocLite("mouse430a2.db") ###Mouse genome annotation library
biocLite("gcrma")
biocLite("affyPLM")
biocLite("sigPathway")
biocLite("ggplot2")
biocLite("biomaRt")
biocLite("pheatmap")
biocLite("RColorBrewer")

library("affy")
library("mouse430a2.db")
library("gcrma")
library("affyPLM")
library("sigPathway")
library("ggplot2")
library("biomaRt")
library("pheatmap")
library("RColorBrewer")

load("raw.rda")
load("affydata.rda")
load("gcrma.rda")
load("datagcrma.rda")

###########################################################################
#
# Extracting datasets
#
###########################################################################

affy.data<-ReadAffy()   ###reads CEL files
#save(affy.data, file="affydata.rda")
raw<-exprs(affy.data)
#save(raw, file="raw.rda")

data.gcrma<-gcrma(affy.data)
#save(data.gcrma, file="datagcrma.rda")
gcrma<-exprs(data.gcrma)
#save(gcrma,file="gcrma.rda")

###########################################################################
#
# OMD-/-
#
###########################################################################

data<-exprs(data.gcrma)
data.ok<-data[,c(5,6,1,2)] # Create subset with only OMD and WT data; no PRELP
phen.ok<-as.character(c("0_WT","0_WT","1_OK","1_OK"))

statList.ok<-calcTStatFast(data.ok,phen.ok,ngroups=2) # unpaired 2-sample t-test
(unequal variance) since n=2
ok.pval<-data.frame(statList.ok$pval) # Extract list of p-values only

# Drawing histograms to show distribution of p-values
ok.hist<-data.frame(x=statList.ok$pval, above=statList.ok$pval > 0.05)
ok.sig<-qplot(x,data=ok.hist,geom="histogram",fill=above, xlab="p-
value",ylab="Frequency")

ok.sig +
  scale_fill_manual(values=c("red","grey")) +
  theme(legend.position='none') +
  labs(title = "Distribution of p-values (OMD-/- vs. wild-type)") +
  theme(plot.title = element_text(hjust = 0.5)) +
  scale_x_continuous(breaks = round(seq(min(dat$x), max(dat$x), by = 0.1),1))


data.ok.pval<-cbind(data.ok,ok.pval) # Combine p-vals with probe intensities

data.ok.0.05<-subset(data.ok.pval,data.ok.pval$statList.ok.pval<0.05) #subsetting data
to remove all rows when p>0.05
```

```
# Need to convert probe ID -> gene name
# If need to change gene ID format, just change the "attribute" below !

ensembl<-useMart("ensembl")
mouse<-useMart("ensembl", dataset = "mmusculus_gene_ensembl")

attributes<-listAttributes(mouse)
attributes[1:150,]

genes_omd<-getBM(filters= "affy_mouse430a_2",
          attributes= c("affy_mouse430a_2","external_gene_name"),
          values= rownames(data.ok.0.05), mart= mouse, uniqueRows=TRUE)

# Need to combine gene and probe data & ensure that everything is in the correct order
!
probes_omd<-data.frame(rownames(data.ok.0.05))
data.ok.0.05.2<-data.frame(c(probes_omd,data.ok.0.05))

ok_final<-merge(genes_omd,data.ok.0.05.2, by.x=1, by.y=1)
ok_final<-ok_final[!duplicated(ok_final$external_gene_name), ] # Remove duplicated
rows

write.csv(ok_final,file="OK_p0.05_final.csv")

# Draw a heatmap !
ok.hm<-data.frame(ok_final[,c(3,4,5,6)])
rownames(ok.hm)<-ok_final[,2]
colnames(ok.hm)<-c("WT1","WT2","OK1","OK2")

df <- data.frame(c("WT","WT","OK","OK"))
rownames(df)<-c("WT1","WT2","OK1","OK2")
colnames(df)<-"Genotype"

breaksList<- seq(0, 15, by = 0.5) #scale goes from 0 to 15 in increments of 0.5. Done
to keep all the heatmaps the same

annot<- list(Genotype = c(OK = "lightcoral", WT="palegreen3"))

pheatmap(ok.hm,
         annotation_col=df,
         annotation_colors = annot,
         gaps_col=2,
         cluster_rows=TRUE,
         show_rownames=FALSE,
         cluster_cols = FALSE,
         color = colorRampPalette(rev(brewer.pal(n = 7, name =
"RdYlBu")))(length(breaksList)),
         breaks = breaksList,
         display_numbers=FALSE)

################################################################################
#
# PRELP-/-
#
################################################################################

data<-exprs(data.gcrma)
data.pk<-data[,c(5,6,3,4)]
phen.pk<-as.character(c("0_WT","0_WT","1_PK","1_PK"))

statList.pk<-calcTStatFast(data.pk,phen.pk,ngroups=2)
pk.pval<-data.frame(statList.pk$pval)

# Drawing histograms to show distribution of p-values
pk.hist<-data.frame(x=statList.pk$pval, above=statList.pk$pval > 0.05)
pk.sig<-qplot(x,data=pk.hist,geom="histogram",fill=above, xlab="p-
value",ylab="Frequency")

pk.sig +
  scale_fill_manual(values=c("red","grey")) +
  theme(legend.position='none') +
  labs(title = "Distribution of p-values (PRELP-/- vs. wild-type)") +
  theme(plot.title = element_text(hjust = 0.5)) +
  scale_x_continuous(breaks = round(seq(min(dat$x), max(dat$x), by = 0.1),1))

hist(statList.pk$pval, main="Distribution of p-values (PRELP-/- vs. wild-type)",
xlab="p-value")
```

```
data.pk.pval<-cbind(data.pk,pk.pval)

data.pk.0.05<-subset(data.pk.pval,data.pk.pval$statList.pk.pval<0.05) #subsetting data
to remove all rows when p>0.05


# Need to convert probe ID -> gene name
# If need to change gene ID format, just change the "attribute" below !

ensembl<-useMart("ensembl")
mouse<-useMart("ensembl", dataset = "mmusculus_gene_ensembl")

attributes<-listAttributes(mouse)
attributes[1:150,]

genes_pk<-getBM(filters= "affy_mouse430a_2",
                attributes= c("affy_mouse430a_2","external_gene_name"),
                values= rownames(data.pk.0.05), mart= mouse, uniqueRows=TRUE)

# Need to combine gene and probe data & ensure that everything is in the correct order
!
probes_pk<-data.frame(rownames(data.pk.0.05))
data.pk.0.05.2<-data.frame(c(probes_pk,data.pk.0.05))

pk_final<-merge(genes_pk,data.pk.0.05.2, by.x=1, by.y=1)
pk_final<-pk_final[!duplicated(pk_final$external_gene_name), ] # Remove duplicated
rows

write.csv(pk_final,file="PK_p0.05_final.csv")

# Draw a heatmap !
pk.hm<-data.frame(pk_final[,c(3,4,5,6)])
rownames(pk.hm)<-pk_final[,2]
colnames(pk.hm)<-c("WT1","WT2","PK1","PK2")

df <- data.frame(c("WT","WT","PK","PK"))
rownames(df)<-c("WT1","WT2","PK1","PK2")
colnames(df)<-"Genotype"

breaksList<- seq(0, 15, by = 0.5) #scale goes from 0 to 15 in increments of 0.5. Done
to keep all the heatmaps the same

annot<- list(Genotype = c(PK = "lightcoral", WT="palegreen3"))

pheatmap(pk.hm,
         annotation_col=df,
         annotation_colors = annot,
         gaps_col=2,
         cluster_rows=TRUE,
         show_rownames=FALSE,
         cluster_cols = FALSE,
         color = colorRampPalette(rev(brewer.pal(n = 7, name =
"RdYlBu")))(length(breaksList)),
         breaks = breaksList,
         display_numbers=FALSE)
```

A.2.3 SAM analysis

```
################################################################################
#Start-up!
################################################################################

#What is this?
#Given how stringent t-test statistics can be, especially with small sample size,
decided to attempt to look at SAM to determine the list of interesting genes
#For more information on the method from ExpressSet: https://cran.r-
project.org/doc/Rnews/Rnews_2006-5.pdf
#More information: http://statweb.stanford.edu/~tibs/SAM/sam.pdf
#Original paper: http://www.ncbi.nlm.nih.gov/pmc/articles/PMC33173/

#Date edited: 19-05-16

#Working at the Institute?
```

```
setwd("/Users/shin-ichiohnuma/Desktop/Hongorzul/Quantification/Hamamoto Microarray/CEL
files/Bayes")

#Working from home?
setwd("C:/Users/hd/Desktop/Hamamoto Microarray/CEL files/Bayes")

#Working from harddrive?
setwd("D:/Quantification/Hamamoto Microarray/CEL files/Bayes")

source("http://www.bioconductor.org/biocLite.R")
biocLite("affy")
biocLite("mouse430a2.db") ###Mouse genome annotation library
biocLite("siggenes")
biocLite("biomaRt")
biocLite("pheatmap")
biocLite("RColorBrewer")

library(affy)
library("mouse430a2.db")
library("siggenes")
library("biomaRt")
library("pheatmap")
library("RColorBrewer")

load("gcrma.rda")
load("ok.sam.rda")
load("pk.sam.rda")

##############################################################################
#OMD
##############################################################################

data<-exprs(data.gcrma) #create matrix from GC-RMA normalised data
data.ok<-data[,c(5,6,1,2)]
probes<-rownames(data.ok)

cl<-c(0,0,1,1)

res.ok <- sam(data.ok, cl, var.equal = TRUE, gene.names = probes, rand = 123456)
#save(res.ok,file="ok.sam.rda")


print(res.ok, seq(0.5, 10, 0.5))
ok.final<-print(res.ok, seq(0.5, 10, 0.5))

write.csv(ok.final,file="OK_sam.csv")

ok.10<-summary(res.ok,10) #Delta = 10
genes.ok<-data.frame(ok.10@row.sig.genes)

ok.sam<-merge(data.ok,genes.ok,by=0)

# Need to convert probe ID -> gene name
# If need to change gene ID format, just change the "attribute" below !

ensembl<-useMart("ensembl")
mouse<-useMart("ensembl", dataset = "mmusculus_gene_ensembl")

genes_omd<-getBM(filters= "affy_mouse430a_2",
                 attributes= c("affy_mouse430a_2","external_gene_name"),
                 values=ok.sam$Row.names, mart= mouse, uniqueRows=TRUE)


# Draw a heatmap !
ok_heatmapdata<-merge(genes_omd,ok.sam, by.x=1, by.y=1)
rownames(ok_heatmapdata)<-ok_heatmapdata$external_gene_name
ok_heatmapdata<-ok_heatmapdata[,c(3,4,5,6)]
colnames(ok_heatmapdata)<-c("WT1","WT2","OK1","OK2")

df <- data.frame(c("WT","WT","OK","OK"))
rownames(df)<-c("WT1","WT2","OK1","OK2")
colnames(df)<-"Genotype"

breaksList<- seq(0, 15, by = 0.5) #scale goes from 0 to 15 in increments of 0.5. Done
to keep all the heatmaps the same

annot<- list(Genotype = c(OK = "lightcoral", WT="palegreen3"))
```

```
pheatmap(ok_heatmapdata,
         annotation_col=df,
         annotation_colors = annot,
         gaps_col=2,
         cluster_rows=TRUE,
         show_rownames=TRUE,
         cluster_cols = FALSE,
         color = colorRampPalette(rev(brewer.pal(n = 7, name =
"RdYlBu")))(length(breaksList)),
         breaks = breaksList,
         display_numbers=FALSE)

################################################################################
#PRELP
################################################################################

data<-exprs(data.gcrma) #create matrix from GC-RMA normalised data
data.pk<-data[,c(5,6,3,4)]
probes<-rownames(data.ok)

cl<-c(0,0,1,1)

res.pk <- sam(data.pk, cl, var.equal = TRUE, gene.names = probes, rand = 123456)
#save(res.pk,file="pk.sam.rda")

print(res.pk, seq(0.5, 10, 0.5))
pk.final<-print(res.pk, seq(0.5, 10, 0.5))
write.csv(pk.final,file="PK_sam.csv")

summary(res.pk,10)

pk.10<-summary(res.pk,10) #Delta = 10
genes.pk<-data.frame(pk.10@row.sig.genes)

pk.sam<-merge(data.pk,genes.pk,by=0)

# Need to convert probe ID -> gene name
# If need to change gene ID format, just change the "attribute" below !

ensembl<-useMart("ensembl")
mouse<-useMart("ensembl", dataset = "mmusculus_gene_ensembl")

genes_prelp<-getBM(filters= "affy_mouse430a_2",
                 attributes= c("affy_mouse430a_2","external_gene_name"),
                 values=pk.sam$Row.names, mart= mouse, uniqueRows=TRUE)


# Draw a heatmap !
pk_heatmapdata<-merge(genes_prelp,pk.sam, by.x=1, by.y=1)
rownames(pk_heatmapdata)<-pk_heatmapdata$external_gene_name
pk_heatmapdata<-pk_heatmapdata[,c(3,4,5,6)]
colnames(pk_heatmapdata)<-c("WT1","WT2","PK1","PK2")

df <- data.frame(c("WT","WT","PK","PK"))
rownames(df)<-c("WT1","WT2","PK1","PK2")
colnames(df)<-"Genotype"

breaksList<- seq(0, 15, by = 0.5) #scale goes from 0 to 15 in increments of 0.5. Done
to keep all the heatmaps the same

annot<- list(Genotype = c(PK = "lightcoral", WT="palegreen3"))

pheatmap(pk_heatmapdata,
         annotation_col=df,
         annotation_colors = annot,
         gaps_col=2,
         cluster_rows=TRUE,
         show_rownames=TRUE,
         cluster_cols = FALSE,
         color = colorRampPalette(rev(brewer.pal(n = 7, name =
"RdYlBu")))(length(breaksList)),
         breaks = breaksList,
         display_numbers=FALSE)
```

A.3 RNA seq R codes

A.3.1 DeSEQ2 analysis

```
##############################################################################
#
#  Analysis of RNA seq data : comparison of WT vs OK
#
##############################################################################

# What is this?
# Counts obtained from Illumina software; want to find differentially-expressed genes
in OK. Unfortunately, only 2 samples seemed to come from OMD--; a third sample was
prepared later (May 2017)

# Last edit date : 24-10-16

# Working at the institute?
setwd("~/Desktop/Hongorzul/RNA-seq/deseq2/Global/Manual analysis OK WT")

# Working from home?

# Installing packages
# source("http://www.bioconductor.org/biocLite.R")
# biocLite("DESeq2")
# biocLite("GenomicAlignments")
# biocLite("genefilter")
# biocLite("pheatmap")

# Loading files & packages
library("DESeq2")
library("GenomicAlignments")
library("genefilter")
library("pheatmap")
library("RColorBrewer")

load("global.rda")
load("wtok.rda")
load("res.rda")
load("res2.rda")
load("res05.rda")
load("results.rda")

##############################################################################
#
# Importing raw counts into DESeq2
#
##############################################################################

global<-read.csv("Global.genes.counts.csv")
colnames(global)<-c("genes","OK1","OK2","OK3","PK1","PK2","PK3","WT1","WT2","WT3")
#OK2 was removed because not actually knockout from OMD gene count !!
# save(global,file="global.rda")

#May 2017 change: OK2 added
ok2<-read.csv("May_2017_OK2.csv")
global2<-merge(global,ok2,by.x=1,by.y=1)
global2<-global2[,c(1,2,11,4,5,6,7,8,9,10)]
colnames(global2)<-c("genes","OK1","OK2","OK3","PK1","PK2","PK3","WT1","WT2","WT3")

wtok<-global2[,c(8,9,10,2,3,4)] # create subset containing only WT and PK counts
rownames(wtok)<-global2[,1]

# save(wtok,file="wtok.rda")

genotype<-factor(c("WT","WT","WT","OK","OK","OK"))

# Set of results which include all genes
dds<-DESeqDataSetFromMatrix(wtok,DataFrame(genotype),~genotype)
dds <- DESeq(dds)
res <- results(dds)
# save(res,file="res.rda")

# Set of results which excludes genes with few or no reads
dds2<-DESeqDataSetFromMatrix(wtok,DataFrame(genotype),~genotype)
```

```
dds2 <- dds2[ rowSums(counts(dds2)) > 1, ]
dds2 <- DESeq(dds2)
res2 <- results(dds2)
# save(res2,file="res2.rda")

# Use summary(res) to print summary of results

resOrdered <- res[order(res$padj),] #orders results by adjusted p-value
resOrdered2 <- res2[order(res2$padj),]

sum(res$padj < 0.05, na.rm=TRUE) #how many genes have padj < 0.05?
sum(res2$padj < 0.05, na.rm=TRUE)

# Interesting, both res and res2 yield 56 genes which are significant (padj); hence,
removing low-count genes is not important for this particular analysis?

res.padj0.05<-subset(res,padj<0.05)
res2.padj0.05<-subset(res2,padj<0.05)

# Seems to be true; both res and res2 give the same subset of genes! Will continue to
use un-cut set of genes

# write.csv(as.data.frame(resOrdered), file="wt_vs_ok_results.csv")
# results<-read.csv("wt_vs_ok_results.csv")
# save(results,file="results.rda")

#########################################################################
#
# Visualising and evaluating the results : p-value <0.01
#
#########################################################################

plotMA(results, main="MA plot of WT vs OK", ylim=c(-2,2))

results.sig<-subset(results,pvalue<0.01) # Decided to use unadjusted p-value < 0.01 as
cut-off ; have 90 genes

sig.genes<-data.frame(results.sig[,1])
rownames(sig.genes)<-sig.genes[,1]

sig.pval<-results.sig[,c(1,6)]

results.sig.genes<-merge(global2, sig.pval, by.x=1, by.y=1, all.x=TRUE)
results.sig.genes<-na.omit(results.sig.genes)
rownames(results.sig.genes)<-results.sig.genes[,1]
results.sig.genes<-results.sig.genes[,c(2,3,4,8,9,10)]

log2.results<-log2(results.sig.genes)
log2.results[mapply(is.infinite,log2.results)]<-0 # Replaces all Inf to 0

df <- data.frame(c("OK","OK","OK","WT","WT","WT"))
rownames(df)<-c("OK1","OK2","OK3","WT1","WT2","WT3")
colnames(df)<-"Genotype"

breaksList<- seq(0, 16, by = 1) #scale goes from 0 to 16 in increments of 1. Done to
keep all the heatmaps the same

annot<- list(Genotype = c(OK = "sandybrown", WT="palegreen3"))

pheatmap(log2.results,
         border_color=NA,
         annotation_col=df,
         annotation_colors = annot,
         gaps_col=3,
         cluster_rows=TRUE,
         show_rownames=FALSE,
         cluster_cols = FALSE,
         color = colorRampPalette(rev(brewer.pal(n = 7, name =
"RdYlBu")))(length(breaksList)),
         breaks = breaksList,
         display_numbers=FALSE)


write.csv(results.sig.genes, file="wt_vs_ok_p0.01_may2017.csv")

#########################################################################
#
```

```
# Importing raw counts into DESeq2 (old code; pre-May 2017 where OMD n=2)
#
################################################################################

global<-read.csv("Global.genes.counts.csv")
colnames(global)<-c("genes","OK1","OK2","OK3","PK1","PK2","PK3","WT1","WT2","WT3")
#OK2 was removed because not actually knockout from OMD gene count !!
# save(global,file="global.rda")

wtok<-global[,c(2,4,8,9,10)] # create subset containing only WT and PK counts
rownames(wtok)<-global[,1]

wtok2<-global[,c(1,2,4,8,9,10)] #useful to have the genes in another column too!

# save(wtok,file="wtok.rda")


genotype<-factor(c("OK","OK","WT","WT","WT"))

# Set of results which include all genes
dds<-DESeqDataSetFromMatrix(wtok,DataFrame(genotype),~genotype)
dds <- DESeq(dds)
res <- results(dds)
# save(res,file="res.rda")

# Set of results which excludes genes with few or no reads
dds2<-DESeqDataSetFromMatrix(wtok,DataFrame(genotype),~genotype)
dds2 <- dds2[ rowSums(counts(dds2)) > 1, ]
dds2 <- DESeq(dds2)
res2 <- results(dds2)
# save(res2,file="res2.rda")

# Use summary(res) to print summary of results

resOrdered <- res[order(res$padj),] #orders results by adjusted p-value
resOrdered2 <- res2[order(res2$padj),]

sum(res$padj < 0.05, na.rm=TRUE) #how many genes have padj < 0.05?
sum(res2$padj < 0.05, na.rm=TRUE)

# Interesting, both res and res2 yield 56 genes which are significant (padj); hence,
removing low-count genes is not important for this particular analysis?

res.padj0.05<-subset(res,padj<0.05)
res2.padj0.05<-subset(res2,padj<0.05)

# Seems to be true; both res and res2 give the same subset of genes! Will continue to
use un-cut set of genes

# write.csv(as.data.frame(resOrdered), file="wt_vs_ok_results.csv")
# results<-read.csv("wt_vs_ok_results.csv")
# save(results,file="results.rda")

################################################################################
#
# Visualising and evaluating the results : p-value <0.01
#
################################################################################

plotMA(results, main="MA plot of WT vs OK", ylim=c(-2,2))

results.sig<-subset(results,pvalue<0.01) # Decided to use unadjusted p-value < 0.01 as
cut-off ; have 189 genes instead of only 56

sig.genes<-data.frame(results.sig[,1])
rownames(sig.genes)<-sig.genes[,1]

sig.pval<-results.sig[,c(1,6)]

results.sig.genes<-merge(wtok2, sig.pval, by.x=1, by.y=1, all.x=TRUE)
results.sig.genes<-na.omit(results.sig.genes)
rownames(results.sig.genes)<-results.sig.genes[,1]
results.sig.genes<-results.sig.genes[,c(2,3,4,5,6)]

log2.results<-log2(results.sig.genes)
log2.results[mapply(is.infinite,log2.results)]<-0 # Replaces all Inf to 0
```

```
df <- data.frame(c("OK","OK","WT","WT","WT"))
rownames(df)<-c("OK1","OK3","WT1","WT2","WT3")
colnames(df)<-"Genotype"

breaksList<- seq(0, 16, by = 1) #scale goes from 0 to 16 in increments of 1. Done to
keep all the heatmaps the same

annot<- list(Genotype = c(OK = "sandybrown", WT="palegreen3"))

pheatmap(log2.results,
         annotation_col=df,
         annotation_colors = annot,
         gaps_col=2,
         cluster_rows=TRUE,
         show_rownames=FALSE,
         cluster_cols = FALSE,
         color = colorRampPalette(rev(brewer.pal(n = 7, name =
"RdYlBu")))(length(breaksList)),
         breaks = breaksList,
         display_numbers=FALSE)


write.csv(results.sig.genes, file="wt_vs_ok_p0.01_n2.csv")


#########################################################################
#
# Visualising and evaluating the results : p-adj <0.05
#
#########################################################################


results.sig.adj<-subset(results,padj<0.05)

sig.genes.adj<-data.frame(results.sig.adj[,1])
rownames(sig.genes.adj)<-sig.genes.adj[,1]

sig.pval.adj<-results.sig.adj[,c(1,6)]

results.sig.genes.adj<-merge(wtok2, sig.pval.adj, by.x=1, by.y=1, all.x=TRUE)
results.sig.genes.adj<-na.omit(results.sig.genes.adj)
rownames(results.sig.genes.adj)<-results.sig.genes.adj[,1]
results.sig.genes.adj<-results.sig.genes.adj[,c(2,3,4,5,6,7)]

log2.results.adj<-log2(results.sig.genes.adj)
log2.results.adj[mapply(is.infinite,log2.results.adj)]<-0 # Replaces all Inf to 0
log2.results.adj<-log2.results.adj[,c(1,2,3,4,5)]

pheatmap(log2.results.adj,
         annotation_col=df,
         annotation_colors = annot,
         gaps_col = 2,
         cluster_rows=TRUE,
         show_rownames=TRUE,
         cluster_cols = FALSE,
         color = colorRampPalette(rev(brewer.pal(n = 7, name =
"RdYlBu")))(length(breaksList)),
         breaks = breaksList,
         display_numbers=TRUE)

write.csv(results.sig.genes.adj, file="wt_vs_ok_padj0.05.csv")

#########################################################################
#
# KEGGprofile
#
#########################################################################

#To use KEGGprofile, need to convert genes to NCBI gene id (numerical)

data.MGI<-read.csv("wt_vs_ok_p0.05_with_MGI.csv")
genes<-as.data.frame(data.MGI[,7])

ensembl<-useMart("ensembl")
mouse<-useMart("ensembl", dataset = "mmusculus_gene_ensembl")

attributes<-listAttributes(mouse)
```

```
attributes[1:150,]

g<-getBM(filters="mgi_id",
         attributes= c("mgi_id","entrezgene","mgi_description"),
         values=genes, mart=mouse, uniqueRows=TRUE)

# save(g,file="entrez.rda")

data<-merge(data.MGI,g,by.x=7,by.y=1)
write.csv(data,file="final.csv")


KEGGgenes<-data[,8]

KEGGresult <- find_enriched_pathway(KEGGgenes, species = "mmu")

x <- find_enriched_pathway(KEGGgenes, species = "mmu",returned_pvalue =
0.05,returned_adjpvalue = 0.05,returned_genenumber = 2)
################################################################################
#
#  Analysis of RNA seq data : comparison of WT vs PK
#
################################################################################

# What is this?
# Counts obtained from Illumina software; want to find differentially-expressed genes
in PK

# Last edit date : 31-10-16

# Working at the institute?
setwd("~/Desktop/Hongorzul/RNA-seq/deseq2/Global/Manual analysis PK WT")

# Working from home?

# Installing packages
# source("http://www.bioconductor.org/biocLite.R")
# biocLite("DESeq2")
# biocLite("GenomicAlignments")
# biocLite("genefilter")
# biocLite("pheatmap")
# biocLite("biomaRt")
# biocLite("KEGGprofile")

# Loading files & packages
library("DESeq2")
library("GenomicAlignments")
library("genefilter")
library("pheatmap")
library("biomaRt")
library("KEGGprofile")
library("RColorBrewer")

load("global.rda")
load("wtpk.rda")
load("res.rda")
load("res2.rda")
load("res05.rda")
load("results.rda")
load("results.sig.genes.rda") #load this file !
load("entrez.rda")

################################################################################
#
# Importing raw counts into DESeq2
#
################################################################################

global<-read.csv("Global.genes.counts.csv")
colnames(global)<-c("genes","OK1","OK2","OK3","PK1","PK2","PK3","WT1","WT2","WT3")
# save(global,file="global.rda")

wtpk<-global[,c(8,9,10,5,6,7)] # create subset containing only WT and PK counts
rownames(wtpk)<-global[,1]
wtpk<-wtpk[,c(4,5,6,1,2,3)] # just need to invert order of WT and PK for fold-change!

wtpk2<-global[,c(1,5,6,7,8,9,10)] #useful to have the genes in another column too!
```

```
# save(wtpk,file="wtpk.rda")


genotype<-factor(c("PK","PK","PK","WT","WT","WT"))

# Set of results which include all genes
dds<-DESeqDataSetFromMatrix(wtpk,DataFrame(genotype),~genotype)
dds <- DESeq(dds)
res <- results(dds)
# save(res,file="res.rda")

# Set of results which excludes genes with few or no reads
dds2<-DESeqDataSetFromMatrix(wtpk,DataFrame(genotype),~genotype)
dds2 <- dds2[ rowSums(counts(dds2)) > 1, ]
dds2 <- DESeq(dds2)
res2 <- results(dds2)
# save(res2,file="res2.rda")

# Use summary(res) to print summary of results

resOrdered <- res[order(res$padj),] #orders results by adjusted p-value
resOrdered2 <- res2[order(res2$padj),]

sum(res$padj < 0.05, na.rm=TRUE) #how many genes have padj < 0.05?
sum(res2$padj < 0.05, na.rm=TRUE)

# Interesting, both res and res2 yield 39 genes which are significant (padj); hence,
removing low-count genes is not important for this particular analysis?

res.padj0.05<-subset(res,padj<0.05)
res2.padj0.05<-subset(res2,padj<0.05)

# Seems to be true; both res and res2 give the same subset of genes! Will continue to
use un-cut set of genes

write.csv(as.data.frame(resOrdered), file="wt_vs_pk_results.csv")
results<-read.csv("wt_vs_pk_results.csv")
# save(results,file="results.rda")

#############################################################################
#
# Visualising and evaluating the results : p-value <0.01
#
#############################################################################

plotMA(results, main="MA plot of WT vs PK", ylim=c(-2,2))

results.sig<-subset(results,pvalue<0.01) # Decided to use unadjusted p-value < 0.01 as
cut-off ; have 288 genes instead of only 39

sig.genes<-data.frame(results.sig[,1])
rownames(sig.genes)<-sig.genes[,1]

sig.pval<-results.sig[,c(1,6)]

results.sig.genes<-merge(wtpk2, sig.pval, by.x=1, by.y=1, all.x=TRUE)
results.sig.genes<-na.omit(results.sig.genes)
rownames(results.sig.genes)<-results.sig.genes[,1]
results.sig.genes<-results.sig.genes[,c(2,3,4,5,6,7)]

log2.results<-log2(results.sig.genes)
log2.results[mapply(is.infinite,log2.results)]<-0 # Replaces all Inf to 0

df <- data.frame(c("PK","PK","PK","WT","WT","WT"))
rownames(df)<-c("PK1","PK2","PK3","WT1","WT2","WT3")
colnames(df)<-"Genotype"

breaksList<- seq(0, 16, by = 1) #scale goes from 0 to 16 in increments of 1. Done to
keep all the heatmaps the same

annot<- list(Genotype = c(PK = "lightcoral", WT="palegreen3"))

pheatmap(log2.results,
         annotation_col=df,
         annotation_colors = annot,
         gaps_col=3,
```

```
         cluster_rows=TRUE,
         show_rownames=FALSE,
         cluster_cols = FALSE,
         color = colorRampPalette(rev(brewer.pal(n = 7, name =
"RdYlBu")))(length(breaksList)),
         breaks = breaksList,
         display_numbers=FALSE)



write.csv(results.sig.genes, file="wt_vs_pk_p0.05.csv")
# save(results.sig.genes,file="results.sig.genes.rda")


###############################################################################
#
# Visualising and evaluating the results : p-adj <0.05
#
###############################################################################


results.sig.adj<-subset(results,padj<0.05)

sig.genes.adj<-data.frame(results.sig.adj[,1])
rownames(sig.genes.adj)<-sig.genes.adj[,1]

sig.pval.adj<-results.sig.adj[,c(1,6)]

results.sig.genes.adj<-merge(wtpk2, sig.pval.adj, by.x=1, by.y=1, all.x=TRUE)
results.sig.genes.adj<-na.omit(results.sig.genes.adj)
rownames(results.sig.genes.adj)<-results.sig.genes.adj[,1]
results.sig.genes.adj<-results.sig.genes.adj[,c(2,3,4,5,6,7)]

log2.results.adj<-log2(results.sig.genes.adj)
log2.results.adj[mapply(is.infinite,log2.results.adj)]<-0 # Replaces all Inf to 0

breaksList<- seq(0, 16, by = 1) #scale goes from 0 to 16 in increments of 1. Done to
keep all the heatmaps the same

pheatmap(log2.results.adj,
         annotation_col=df,
         annotation_colors = annot,
         gaps_col = 3,
         cluster_rows=TRUE,
         show_rownames=TRUE,
         cluster_cols = FALSE,
         color = colorRampPalette(rev(brewer.pal(n = 7, name =
"RdYlBu")))(length(breaksList)),
         breaks = breaksList,
         display_numbers=TRUE)


write.csv(results.sig.genes.adj, file="wt_vs_pk_padj0.05.csv")


###############################################################################
#
# KEGGprofile
#
###############################################################################

#To use KEGGprofile, need to convert genes to NCBI gene id (numerical)

data.MGI<-read.csv("wt_vs_pk_p0.05_with_MGI.csv")
genes<-as.data.frame(data.MGI[,2])

ensembl<-useMart("ensembl")
mouse<-useMart("ensembl", dataset = "mmusculus_gene_ensembl")

attributes<-listAttributes(mouse)
attributes[1:150,]

g<-getBM(filters="mgi_id",
        attributes= c("mgi_id","entrezgene","mgi_description"),
        values=genes, mart=mouse, uniqueRows=TRUE)

# save(g,file="entrez.rda")
```

```
data<-merge(data.MGI,g,by.x=2,by.y=1)
write.csv(data,file="final.csv")


KEGGgenes<-data[,9]

KEGGresult <- find_enriched_pathway(KEGGgenes, species = "mmu")

x <- find_enriched_pathway(KEGGgenes, species = "mmu",returned_pvalue =
0.05,returned_adjpvalue = 0.05,returned_genenumber = 2)
```

A.4 Molecular cloning

A.4.1.1 Designing primers for VEGFA-121 cDNA amplification

I analysed the sequence of pPICZalphaA_VEGF-A121_Nhis and obtained the cDNA sequence (Box A.1). Using ExPASy (Gasteiger et al., 2003), I translated the mRNA sequence and continued to work with the longest coding frame (Box A.2). I compared the protein sequence in Box A.1 with that of *vascular endothelial growth factor A isoform n precursor [Homo sapiens]* (NP_001165099.1) from the RefSeq protein database and performed multiple sequence alignment using Clustal Omega (Sievers et al., 2011) to determine how similar the sequences are (Figure A.3). The translated cDNA sequence is almost a perfect match for the RefSeq sequence, however it is truncated at the N-terminus where it is missing the first 28 amino acids, which correspond to the signal peptide of VEGFA as assessed by sequence analysis in UniProt. Given that the insert sequence corresponds to VEGFA-121, I proceeded to design PCR amplification primers.

5'ggttctcatcaccatcaccatcacggttctgcaccc**atg**gcagaaggaggagggcagaatcatcacgaagtg
gtgaagttcatggatgtctatcagcgcagctactgccatccaatcgagaccctggtggacatcttccaggagta
ccctgatgagatcgagtacatcttcaagccatcctgtgtgcccctgatgcgatgcgggggctgctgcaatgacg
agggcctggagtgtgtgcccactgaggagtccaacatcaccatgcagattatgcggatcaaacctcaccaaggc
cagcacataggagagatgagcttcctacagcacaacaaatgtgaatgcagaccaaagaaagatagagcaagaca
agaaaattgtgacaagccgaggcggtgatga**3'**

Box A.1. Insert sequence from pPICZalphaA_VEGF-A121_Nhis. Initiating methionine codon in bold red; stop codons in red.

MAEGGGQNHHEVVKFMDVYQRSYCHPIETLVDIFQEYPDEIEYIFKPSCVPLMRCGGCCNDEGLECVPTEESNI
TMQIMRIKPHQGQHIGEMSFLQHNKCECRPKKDRARQENCDKPRR**

Box A.2. Translated protein sequence of insert from pPICZalphaA_VEGF-A121_Nhis. Initiating methionine residue in bold red; stop codons in red.

```
cDNA              ----------------------------MAEGGGQNHHEVVKFMDVYQRSYCHPIETLVD
NP_001165099.1    MNFLLSWVHWSLALLLYLHHAKWSQAAPMAEGGGQNHHEVVKFMDVYQRSYCHPIETLVD
                                               ********************************

cDNA              IFQEYPDEIEYIFKPSCVPLMRCGGCCNDEGLECVPTEESNITMQIMRIKPHQGQHIGEM
NP_001165099.1    IFQEYPDEIEYIFKPSCVPLMRCGGCCNDEGLECVPTEESNITMQIMRIKPHQGQHIGEM
                  ************************************************************

cDNA              SFLQHNKCECRPKKDRARQENCDKPRR
NP_001165099.1    SFLQHNKCECRPKKDRARQEKCDKPRR
                  ********************:******
```

Figure A.3. Alignment of translated sequence from plasmid and VEGFA-121 protein from the RefSeq database. The translated cDNA sequence is missing the first 28 amino acids compared to the database sequence.

A.4.1.2 Designing primers for VEGFA-165 cDNA amplification

I analysed the sequence of pPICZalphaA_VEGF-A165_Nhis and obtained the cDNA sequence (Box A.3). Using ExPASy, I translated the mRNA sequence and continued to work with the longest coding frame (Box A.4). I compared the protein sequence in Box A.3 with that of *vascular endothelial growth factor A isoform l precursor [Homo sapiens]* (NP_001165097.1) from the RefSeq protein database and performed multiple sequence alignment using Clustal Omega to determine how similar the sequences are (Figure A.4). The translated cDNA sequence is a perfect match for the RefSeq sequence, however it is truncated at the N-terminus where it is missing the first 28 amino acids, which correspond to the signal peptide of VEGFA. Given that the insert sequence corresponds to VEGFA-165, I proceeded to design PCR amplification primers.

```
5'ggttctcatcaccatcaccatcacggttctgcacccatggcagaaggaggagggcagaatcatcacgaagtg
gtgaagttcatggatgtctatcagcgcagctactgccatccaatcgagaccctggtggacatcttccaggagta
ccctgatgagatcgagtacatcttcaagccatcctgtgtgcccctgatgcgatgcgggggctgctgcaatgacg
agggcctggagtgtgtgcccactgaggagtccaacatcaccatgcagattatgcggatcaaacctcaccaaggc
cagcacataggagagatgagcttcctacagcacaacaaatgtgaatgcagaccaaagaaagatagagcaagaca
agaaaatccctgtgggccttgctcagagcggagaaagcatttgtttgtacaagatccgcagacgtgtaaatgtt
cctgcaaaaacacagactcgcgttgcaaggcgaggcagcttgagttaaacgaacgtacttgcagatgtgacaag
ccgaggcggtgatga 3'
```

Box A.3. Insert sequence from pPICZalphaA_VEGF-A165_Nhis. Initiating methionine codon in bold red; stop codons in red.

```
MAEGGGQNHHEVVKFMDVYQRSYCHPIETLVDIFQEYPDEIEYIFKPSCVPLMRCGGCCNDEGLECVPTEESNI
TMQIMRIKPHQGQHIGEMSFLQHNKCECRPKKDRARQENPCGPCSERRKHLFVQDPQTCKCSCKNTDSRCKARQ
LELNERTCRCDKPRR**
```

Box A.4. Translated protein sequence of insert from pPICZalphaA_VEGF-A165_Nhis. Initiating methionine residue in bold red; stop codons in red.

```
cDNA              ----------------------------MAEGGGQNHHEVVKFMDVYQRSYCHPIETLVD
NP_001165097.1    MNFLLSWVHWSLALLLYLHHAKWSQAAPMAEGGGQNHHEVVKFMDVYQRSYCHPIETLVD
                                               ********************************

cDNA              IFQEYPDEIEYIFKPSCVPLMRCGGCCNDEGLECVPTEESNITMQIMRIKPHQGQHIGEM
NP_001165097.1    IFQEYPDEIEYIFKPSCVPLMRCGGCCNDEGLECVPTEESNITMQIMRIKPHQGQHIGEM
                  ************************************************************

cDNA              SFLQHNKCECRPKKDRARQENPCGPCSERRKHLFVQDPQTCKCSCKNTDSRCKARQLELN
NP_001165097.1    SFLQHNKCECRPKKDRARQENPCGPCSERRKHLFVQDPQTCKCSCKNTDSRCKARQLELN
                  ************************************************************

cDNA              ERTCRCDKPRR
NP_001165097.1    ERTCRCDKPRR
                  ***********
```

Figure A.4. Alignment of translated sequence from plasmid and VEGFA-165b protein from the RefSeq database. The translated cDNA sequence is missing the first 28 amino acids compared to the database sequence.

A.4.1.3 Designing primers for VEGFA-165b cDNA amplficiation

I analysed the sequence of pPICZalphaA_VEGF-A165b_Nhis and obtained the cDNA sequence (Box A.5). Using ExPASy, I translated the mRNA sequence and continued to work with the longest coding frame (Box A.6). I compared the protein sequence in Box A.5 with that of *vascular endothelial growth factor A isoform o precursor [Homo sapiens]* (NP_001165100.1) from the RefSeq protein database and performed multiple sequence alignment using Clustal Omega to determine how similar the sequences are (Figure A.5). The translated cDNA sequence is a perfect match for the RefSeq sequence, however it is truncated at the N-terminus where it is missing the first 28 amino acids, which correspond to the signal peptide of VEGFA. Given that the insert sequence corresponds to VEGFA-165b, I proceeded to design PCR amplification primers.

5'ggttctcatcaccatcaccatcacggttctgcaccc**atg**gcagaaggaggagggcagaatcatcacgaagtg
gtgaagttcatggatgtctatcagcgcagctactgccatccaatcgagaccctggtggacatcttccaggagta
ccctgatgagatcgagtacatcttcaagccatcctgtgtgcccctgatgcgatgcgggggctgctgcaatgacg
agggcctggagtgtgtgcccactgaggagtccaacatcaccatgcagattatgcggatcaaacctcaccaaggc
cagcacataggagagatgagcttcctacagcacaacaaatgtgaatgcagaccaaagaaagatagagcaagaca
agaaaatccctgtgggccttgctcagagcggagaaagcatttgtttgtacaagatccgcagacgtgtaaatgtt
cctgcaaaaacacagactcgcgttgcaaggcgaggcagcttgagttaaacgaacgtacttgcagatctctcacc
aggaaagactgatga **3'**

Box A.5. Insert sequence from pPICZalphaA_VEGF-A165b_Nhis. Initiating methionine codon in bold red; stop codons in red.

MAEGGGQNHHEVVKFMDVYQRSYCHPIETLVDIFQEYPDEIEYIFKPSCVPLMRCGGCCNDEGLECVPTEESNI
TMQIMRIKPHQGQHIGEMSFLQHNKCECRPKKDRARQENPCGPCSERRKHLFVQDPQTCKCSCKNTDSRCKARQ
LELNERTCRSLTRKD**

Box A.6. Translated protein sequence of insert from pPICZalphaA_VEGF-A165b_Nhis. Initiating methionine residue in bold red; stop codons in red.

```
cDNA              ----------------------------MAEGGGQNHHEVVKFMDVYQRSYCHPIETLVD
NP_001165100.1    MNFLLSWVHWSLALLLYLHHAKWSQAAPMAEGGGQNHHEVVKFMDVYQRSYCHPIETLVD
                                               ********************************

cDNA              IFQEYPDEIEYIFKPSCVPLMRCGGCCNDEGLECVPTEESNITMQIMRIKPHQGQHIGEM
NP_001165100.1    IFQEYPDEIEYIFKPSCVPLMRCGGCCNDEGLECVPTEESNITMQIMRIKPHQGQHIGEM
                  ************************************************************

cDNA              SFLQHNKCECRPKKDRARQENPCGPCSERRKHLFVQDPQTCKCSCKNTDSRCKARQLELN
NP_001165100.1    SFLQHNKCECRPKKDRARQENPCGPCSERRKHLFVQDPQTCKCSCKNTDSRCKARQLELN
                  ************************************************************

cDNA              ERTCRSLTRKD
NP_001165100.1    ERTCRSLTRKD
                  ***********
```

Figure A.5. Alignment of translated sequence from plasmid and VEGFA-165b protein from the RefSeq database. The translated cDNA sequence is missing the first 28 amino acids compared to the database sequence.

References

Abbott, N. J., Rönnbäck, L., & Hansson, E. (2006). Astrocyte–endothelial interactions at the blood–brain barrier. *Nature Reviews Neuroscience*, *7*(1), 41–53. https://doi.org/10.1038/nrn1824

Abramsson, A., Kurup, S., Busse, M., Yamada, S., Ringvall, M., Landegren, U., … Lindahl, U. (2007). PDGF-BB binding and pericyte recruitment in vascular development Defective N -sulfation of heparan sulfate proteoglycans limits PDGF-BB binding and pericyte recruitment in vascular development. *Genes & Development*, *21*(3), 316–331. https://doi.org/10.1101/gad.398207

Acton, Q. A. (2013). *Cell Adhesion Molecules—Advances in Research and Application: 2013 Edition*. Atlanta, Georgia: Scholarly Editions.

Adair, T., & Montani, J. (2010). Overview of Angiogenesis. In *Angiogenesis*. San Rafael: Morgan & Claypool Life Sciences.

Ahmed, Z., Bansal, D., Tizzard, K., Surey, S., Esmaeili, M., Gonzalez, A. M., … Logan, A. (2014). Decorin blocks scarring and cystic cavitation in acute and induces scar dissolution in chronic spinal cord wounds. *Neurobiology of Disease*, *64*, 163–176. https://doi.org/10.1016/j.nbd.2013.12.008

Alberts, B., Johnson, A., Lewis, J., Raff, M., Roberts, K., & Walter, P. (2002). *Molecular Biology of the Cell* (4th Editio). New York: Garland Science.

Allan, S. M., Tyrrell, P. J., & Rothwell, N. J. (2005). Interleukin-1 and neuronal injury. *Nature Reviews Immunology*, *5*(8), 629–640. https://doi.org/10.1038/nri1664

Alliot, F., Godin, I., & Pessac, B. (1999). Microglia derive from progenitors , originating from the yolk sac , and which proliferate in the brain.

Alvarez, J. I., Dodelet-Devillers, A., Kebir, H., Ifergan, I., Fabre, P. J., Terouz, S., … Prat, A. (2011). The Hedgehog Pathway Promotes Blood-Brain Barrier Integrity and CNS Immune Quiescence. *Science*, *334*(6063), 1727 LP-1731. Retrieved from http://science.sciencemag.org/content/334/6063/1727.abstract

Alvarez, J. I., Katayama, T., & Prat, A. (2013). Glial influence on the blood brain barrier. *Glia*, *61*(12), 1939–1958. https://doi.org/10.1002/glia.22575

Amenta, P. S., Scivoletti, N. A., Newman, M. D., Sciancalepore, J. P., Li, D., & Myers, J. C. (2005). Proteoglycan-Collagen XV in Human Tissues Is Seen Linking Banded Collagen Fibers Subjacent to the Basement Membrane. *Journal of Histochemistry & Cytochemistry*, *53*(2), 165–176. https://doi.org/10.1369/jhc.4A6376.2005

Ameye, L., & Young, M. F. (2002). Mice deficient in small leucine-rich proteoglycans: novel in vivo models for osteoporosis, osteoarthritis, Ehlers-Danlos syndrome, muscular dystrophy, and corneal diseases. *Glycobiology*, *12*(9), 107R–16R. https://doi.org/10.1093/glycob/cwf065

Anders, S., & Huber, W. (2010). Differential expression analysis for sequence count data. *Genome Biology*, *11*(10), R106. https://doi.org/10.1186/gb-2010-11-10-r106

Andrade, S. P., & Ferreira, M. A. N. D. (2016). The Sponge Implant Model of Angiogenesis. In S. G. Martin & P. W. Hewett (Eds.), *Angiogenesis Protocols* (pp. 333–343). New York, NY: Springer New York. https://doi.org/10.1007/978-1-4939-3628-1_23

Andrews, K. (2014). Intraperitoneal (IP) Injection in Rats and Mice.

Angel, P., & Karin, M. (1991). The role of Jun, Fos and the AP-1 complex in cell-proliferation and transformation. *BBA - Reviews on Cancer*, *1072*(2–3), 129–157. https://doi.org/10.1016/0304-419X(91)90011-9

Antonelli-Orlidge A, Saunders KB, S. S. (1989). An activated form of transforming growth factor beta is produced by cocultures of endothe- lial cells and pericytes. *Proc Natl Acad Sci USA*, *86*(86), 4544–8.

Arakawa, T., Wen, J., & Philo, J. S. (1994). Stoichiometry of heparin binding to basic fibroblast growth factor. *Archives of Biochemistry and Biophysics*.

Arganda-Carreras, I., Fernández-González, R., Muñoz-Barrutia, A., & Ortiz-De-Solorzano, C. (2010). 3D reconstruction of histological sections: Application to mammary gland tissue. *Microscopy Research and Technique*, *73*(11), 1019–1029. https://doi.org/10.1002/jemt.20829

Argaw, A. T., Gurfein, B. T., Zhang, Y., Zameer, A., & John, G. R. (2009). VEGF-mediated disruption of endothelial CLN-5 promotes blood-brain barrier breakdown. *Proceedings of the National Academy of Sciences*, *106*(6), 1977–1982. https://doi.org/10.1073/pnas.0808698106

Armulik, A., Abramsson, A., & Betsholtz, C. (2005). Endothelial/pericyte interactions. *Circulation Research*, *97*(6), 512–523. https://doi.org/10.1161/01.RES.0000182903.16652.d7

Armulik, A., Genove, G., & Betsholtz, C. (2011). Review Pericytes : Developmental , Physiological , and Pathological Perspectives , Problems , and Promises. *Developmental Cell*, *21*, 193–215. https://doi.org/10.1016/j.devcel.2011.07.001

Armulik, A., Genové, G., Mäe, M., Nisancioglu, M. H., Wallgard, E., Niaudet, C., … Betsholtz, C. (2010). Pericytes regulate the blood-brain barrier. *Nature*, *468*(V), 557–561. https://doi.org/10.1038/nature09522

Ashikari-Hada, S., Habuchi, H., Kariya, Y., & Kimata, K. (2005). Heparin Regulates Vascular Endothelial Growth Factor165-dependent Mitogenic Activity, Tube Formation, and Its Receptor Phosphorylation of Human Endothelial Cells: COMPARISON OF THE EFFECTS OF HEPARIN AND MODIFIED HEPARINS. *Journal of Biological Chemistry*, *280*(36), 31508–31515. https://doi.org/10.1074/jbc.M414581200

Au-Yeung, N., Mandhana, R., & Horvath, C. M. (2013). Transcriptional regulation by STAT1 and

STAT2 in the interferon JAK-STAT pathway. *Jak-Stat*, *2*(3), e23931. https://doi.org/10.4161/jkst.23931

Augustin, H. G., Koh, G. Y., Thurston, G., & Alitalo, K. (2009). Control of vascular morphogenesis and homeostasis through the angiopoietin-Tie system. *Nature Reviews. Molecular Cell Biology*, *10*(3), 165–177. https://doi.org/10.1038/nrm2639

Aumailley, M. (2013). The laminin family. *Cell Adhesion and Migration*, *7*(1), 48–55. https://doi.org/10.4161/cam.22826

Aumailley, M., Battaglia, C., Mayer, U., Reinhardt, D., Nischt, R., Timpl, R., & Fox, J. W. (1993). Nidogen mediates the formation of ternary complexes of basement membrane components. *Kidney International*, *43*(1), 7–12. https://doi.org/10.1007/s00018-010-0367-x

Aumailley, M., Wiedemann, H., Mann, K., & Timpl, R. (1989). Binding of nidogen and the laminin nidogen complex to basement membrane collagen type IV. *European Journal of Biochemistry*, *184*(1), 241–248.

Aviezer, D., Hecht, D., Safran, M., Eisinger, M., David, G., & Yayon, A. (1994). Perlecan, basal lamina proteoglycan, promotes basic fibroblast growth factor-receptor binding, mitogenesis, and angiogenesis. *Cell*, *79*(6), 1005–1013. https://doi.org/10.1016/0092-8674(94)90031-0

Azzam, M. E., & Algranati, I. D. (1973). Mechanism of puromycin action: fate of ribosomes after release of nascent protein chains from polysomes. *Proceedings of the National Academy of Sciences of the United States of America*, *70*(12), 3866–9. https://doi.org/10.1073/pnas.70.12.3866

Bader, B. L., Smyth, N., Nedbal, S., Baranowsky, A., Mokkapati, S., Miosge, N., … Nischt, R. (2005). Compound Genetic Ablation of Nidogen 1 and 2 Causes Basement Membrane Defects and Perinatal Lethality in Mice. *Molecular and Cellular Biology*, *25*(15), 6846–6856. https://doi.org/10.1128/MCB.25.15.6846

Baghy, K., Horváth, Z., Regos, E., Kiss, K., Schaff, Z., Iozzo, R. V., & Kovalszky, I. (2013). Decorin interferes with platelet-derived growth factor receptor signaling in experimental hepatocarcinogenesis. *FEBS Journal*, *280*(10), 2150–2164. https://doi.org/10.1111/febs.12215

Banks, W. A., Dohgu, S., Lynch, J. L., Fleegal-DeMotta, M. A., Erickson, M. A., Nakaoke, R., & Vo, T. Q. (2008). Nitric Oxide Isoenzymes Regulate Lipopolysaccharide-Enhanced Insulin Transport across the Blood-Brain Barrier. *Endocrinology*, *149*(4), 1514–1523. https://doi.org/10.1210/en.2007-1091

Bech-Hansen, N. T., Naylor, M. J., Maybaum, T. A., Sparkes, R. L., Koop, B., Birch, D. G., … Weleber, R. G. (2000). Mutations in NYX, encoding the leucine-rich proteoglycan nyctalopin, cause X-linked complete congenital stationary night blindness. *Nat Genet*, *26*(3), 319–323. Retrieved

from http://dx.doi.org/10.1038/81619

Beck, K., Dixon, T., Engel, J., & Parry, D. (1993). Ionic Interactions in the Coiled-coil Domain of Laminin Determine the Specificity of Chain Assembly. *Journal of Molecular Biology*, *231*, 311–323.

Beenken, A., & Mohammadi, M. (2009). The FGF family: biology, pathophysiology and therapy. *Nature Reviews Drug Discovery*, *8*(3), 235–253. https://doi.org/10.1021/nl061786n.Core-Shell

Begley, D. J., & Brightman, M. W. (2003). Structural and functional aspects of the blood-brain barrier BT - Peptide Transport and Delivery into the Central Nervous System. In L. Prokai & K. Prokai-Tatrai (Eds.) (pp. 39–78). Basel: Birkhäuser Basel. https://doi.org/10.1007/978-3-0348-8049-7_2

Behrens, D. T., Villone, D., Koch, M., Brunner, G., Sorokin, L., Robenek, H., … Hansen, U. (2012). The epidermal basement membrane is a composite of separate laminin- or collagen IV-containing networks connected by aggregated perlecan, but not by nidogens. *Journal of Biological Chemistry*, *287*(22), 18700–18709. https://doi.org/10.1074/jbc.M111.336073

Bell, R. D., Winkler, E. A., Sagare, A. P., Singh, I., LaRue, B., Deane, R., & Zlokovic, B. V. (2010). Pericytes Control Key Neurovascular Functions and Neuronal Phenotype in the Adult Brain and during Brain Aging. *Neuron*, *68*(3), 409–427. https://doi.org/10.1016/j.neuron.2010.09.043

Bellacen, K., & Lewis, E. C. (2009). Aortic ring assay. *Journal of Visualized Experiments : JoVE*, (33), 1–2. https://doi.org/10.3791/1564

Bengtsson, E., Aspberg, A., Heinegard, D., Sommarin, Y., & Spillmann, D. (2000). The amino-terminal part of PRELP binds to heparin and heparan sulfate. *The Journal of Biological Chemistry*, *275*(52), 40695–702. https://doi.org/10.1074/jbc.M007917200

Bengtsson, E., Lindblom, K., Tillgren, V., & Aspberg, A. (2016). The leucine-rich repeat protein PRELP binds fibroblast cell-surface proteoglycans and enhances focal adhesion formation. *Biochemical Journal*, *473*(9), 1153–1164. https://doi.org/10.1042/BCJ20160095

Bengtsson, E., Mörgelin, M., Sasaki, T., Timpl, R., Heinegård, D., & Aspberg, A. (2002). The leucine-rich repeat protein PRELP binds perlecan and collagens and may function as a basement membrane anchor. *The Journal of Biological Chemistry*, *277*(17), 15061–8. https://doi.org/10.1074/jbc.M108285200

Bengtsson, E., Neame, P. J., Heinegard, D., & Sommarin, Y. (1995). The Primary Structure of a Basic Leucine-rich Repeat Protein, PRELP, Found in Connective Tissues. *Journal of Biological Chemistry*, *270*(43), 25639–25644. https://doi.org/10.1074/jbc.270.43.25639

Bennett, M., Sinha, S., & Owens, G. (2016). Vascular smooth muscle cells in atherosclerosis.

Circulation Research, *118*(4), 692–702. https://doi.org/10.1146/annurev-immunol-032713-120240.Microglia

Berendsen, A. D., Fisher, L. W., Kilts, T. M., Owens, R. T., Robey, P. G., Gutkind, J. S., & Young, M. F. (2011). Modulation of canonical Wnt signaling by the extracellular matrix component biglycan. *Proceedings of the National Academy of Sciences of the United States of America*, *108*(41), 17022–7. https://doi.org/10.1073/pnas.1110629108

Bergers, G., & Song, S. (2005). The role of pericytes in blood-vessel formation and maintenance. *Neuro-Oncology*, *7*(4), 452–464. https://doi.org/10.1215/S1152851705000232

Berrier, A., & Yamada, K. M. (2007). Cell-Matrix Adhesion. *Journal of Cellular Physiology*, *213*, 565–573. https://doi.org/10.1002/JCP

Birke, M., Lipo, E., Adhi, M., Birke, K., & Kumar-Singh, R. (2014). AAV Mediated Expression of Human PRELP inhibits Complement Activation, Choroidal Neovascularization and Deposition of Membrane Attack Complex in Mice. *Gene Therapy*, *21*(5), 507–513. https://doi.org/10.1016/j.surg.2006.10.010.Use

Bix, G., Fu, J., Gonzalez, E. M., Macro, L., Barker, A., Campbell, S., … Iozzo, R. V. (2004). Endorepellin causes endothelial cell disassembly of actin cytoskeleton and focal adhesions through α2β1 integrin. *Journal of Cell Biology*, *166*(1), 97–109. https://doi.org/10.1083/jcb.200401150

Bjarnegård, M., Enge, M., Norlin, J., Gustafsdottir, S., Fredriksson, S., Abramsson, A., … Betsholtz, C. (2004). Endothelium-specific ablation of PDGFB leads to pericyte loss and glomerular, cardiac and placental abnormalities. *Development (Cambridge, England)*, *131*(8), 1847–57. https://doi.org/10.1242/dev.01080

Bonnans, C., Chou, J., & Werb, Z. (2014). Remodelling the extracellular matrix in development and disease. *Nature Publishing Group*, *15*(12), 786–801. https://doi.org/10.1038/nrm3904

Bosse, A., Schwarz, K., Vollmer, E., & Kresse, H. (1993). Divergent and co-localization of the two small proteoglycans decorin and proteoglycan-100 in human skeletal tissues and tumors. *J Histochem Cytochem*, *41*(1), 13–19. https://doi.org/10.1177/41.1.8417108

Boudier, H. (1999). Arteriolar and capillary remodelling in hypertension. *Drugs*, *58*, 37–40.

Bowyer, J. F., Thomas, M., Patterson, T. a, George, N. I., Runnells, J. a, & Levi, M. S. (2012). A visual description of the dissection of the cerebral surface vasculature and associated meninges and the choroid plexus from rat brain. *Journal of Visualized Experiments : JoVE*, (November), e4285. https://doi.org/10.3791/4285

Brachvogel, B., Pausch, F., Farlie, P., Gaipl, U., Etich, J., Zhou, Z., … Pöschl, E. (2007). Isolated Anxa5+/Sca-1+ perivascular cells from mouse meningeal vasculature retain their perivascular phenotype in vitro and in vivo. *Experimental Cell Research*, *313*(12), 2730–2743. https://doi.org/10.1016/j.yexcr.2007.04.031

Brakebusch, C., & Fässler, R. (2003). The integrin-actin connection, an eternal love affair. *EMBO Journal*, *22*(10), 2324–2333. https://doi.org/10.1093/emboj/cdg245

Bredrup, C., Knappskog, P. M., Majewski, J., Rødahl, E., & Boman, H. (2005). Congenital stromal dystrophy of the cornea caused by a mutation in the decorin gene. *Investigative Ophthalmology & Visual Science*, *46*(2), 420–426. https://doi.org/10.1167/iovs.04-0804

Brown, R. C., & Davis, T. P. (2002). Calcium modulation of adherens and tight junction function: A potential mechanism for blood-brain barrier disruption after stroke. *Stroke*, *33*(6), 1706–1711. https://doi.org/10.1161/01.STR.0000016405.06729.83

Buraschi, S., Neill, T., Goyal, A., Poluzzi, C., Smythies, J., Owens, R. T., … Iozzo, R. V. (2013). Decorin causes autophagy in endothelial cells via Peg3. *Proceedings of the National Academy of Sciences*, *110*(28), E2582–E2591. https://doi.org/10.1073/pnas.1305732110

Burgess, R. W., Skarnes, W. C., & Sanes, J. R. (2000). Agrin Isoforms with Distinct Amino Termini: Differential Expression, Localization, and Function. *The Journal of Cell Biology*, *151*(1), 41–52. Retrieved from http://jcb.rupress.org/content/151/1/41.long

Burri, P. H., Hlushchuk, R., & Djonov, V. (2004). Intussusceptive angiogenesis: Its emergence, its characteristics, and its significance. *Developmental Dynamics*, *231*(3), 474–488. https://doi.org/10.1002/dvdy.20184

Cabello, C. M., Bair, W. B., Lamore, S. D., Ley, S., Alexandra, S., Azimian, S., & Wondrak, G. T. (2010). Border Patrol: Insights into the Unique Role of Perlecan/Heparan Sulfate Proteoglycan2 at Cell and Tissue Borders Mary. *Matrix Biology*, *46*(2), 220–231. https://doi.org/10.1016/j.freeradbiomed.2008.10.025.The

Cailhier, J. F., Sirois, I., Laplante, P., Lepage, S., Raymond, M. A., Brassard, N., … Hébert, M. J. (2008). Caspase-3 activation triggers extracellular cathepsin L release and endorepellin proteolysis. *Journal of Biological Chemistry*, *283*(40), 27220–27229. https://doi.org/10.1074/jbc.M801164200

Carbon, S., Dietze, H., Lewis, S. E., Mungall, C. J., Munoz-Torres, M. C., Basu, S., … Westerfield, M. (2017). Expansion of the gene ontology knowledgebase and resources: The gene ontology consortium. *Nucleic Acids Research*, *45*(D1), D331–D338. https://doi.org/10.1093/nar/gkw1108

Carmeliet, P. (2003). Angiogenesis in health and disease. *Nature Medicine*, *9*(6), 653–660. https://doi.org/10.1016/S0306-3623(01)00111-2

Carmeliet, P., Ferreira, V., Breier, G., Pollefeyt, S., Kieckens, L., Gertsenstein, M., … Nagy, A. (1996). Abnormal blood vessel development and lethality in embryos lacking a single VEGF allele. *Nature*. https://doi.org/10.1038/380435a0

Chai, Q., He, W. Q., Zhou, M., Lu, H., & Fu, Z. F. (2014). Enhancement of Blood-Brain Barrier

Permeability and Reduction of Tight Junction Protein Expression Are Modulated by Chemokines/Cytokines Induced by Rabies Virus Infection. *Journal of Virology*, *88*(9), 4698–4710. https://doi.org/10.1128/JVI.03149-13

Chakravarti, S., Horchar, T., Jefferson, B., Laurie, G. W., & Hassell, J. R. (1995). Recombinant domain III of perlecan promotes cell attachment through its RGDS sequence. *Journal of Biological Chemistry*. https://doi.org/10.1074/jbc.270.1.404

Chakravarti, S., Stallings, R., Sundarraj, N., Cornuet, P., & Hassell, J. R. (1995). Primary Structure of Human Lumican (Keratan Sulfate Proteoglycan) and Localization of the Gene (LUM) to Chromosome 12q21.3-q22. *Genomics*. https://doi.org/10.1006/geno.1995.1080

Checchin, D., Sennlaub, F., Levavasseur, E., Leduc, M., & Chemtob, S. (2006). Potential role of microglia in retinal blood vessel formation. *Investigative Ophthalmology & Visual Science*, *47*(8), 3595–3602. https://doi.org/10.1167/iovs.05-1522

Chen, H., Bagri, A., Zupicich, J. A., Zou, Y., Stoeckli, E., Pleasure, S. J., … Tessier-Lavigne, M. (2000). Neuropilin-2 regulates the development of selective cranial and sensory nerves and hippocampal mossy fiber projections. *Neuron*, *25*(1), 43–56. https://doi.org/10.1016/S0896-6273(00)80870-3

Chen, Q., Zhang, H., Liu, Y., Adams, S., Eilken, H., Stehling, M., … Adams, R. H. (2016). Endothelial cells are progenitors of cardiac pericytes and vascular smooth muscle cells. *Nature Communications*, *7*, 12422. https://doi.org/10.1038/ncomms12422

Chen, S., Kulik, M., & Lechleider, R. J. (2003). Smad proteins regulate transcriptional induction of the SM22?? gene by TGF-?? *Nucleic Acids Research*, *31*(4), 1302–1310. https://doi.org/10.1093/nar/gkg224

Chen, S., Sun, M., Meng, X., Iozzo, R. V., Kao, W. W. Y., & Birk, D. E. (2011). Pathophysiological mechanisms of autosomal dominant congenital stromal corneal dystrophy: C-terminaltruncated decorin results in abnormal matrix assembly and altered expression of small leucine-rich proteoglycans. *American Journal of Pathology*, *179*(5), 2409–2419. https://doi.org/10.1016/j.ajpath.2011.07.026

Conesa, A., Madrigal, P., Tarazona, S., Gomez-Cabrero, D., Cervera, A., McPherson, A., … Mortazavi, A. (2016). A survey of best practices for RNA-seq data analysis. *Genome Biol*, *17*(1), 13. https://doi.org/10.1186/s13059-016-0881-8

Constantinescu, C. S., Farooqi, N., O'Brien, K., & Gran, B. (2011). Experimental autoimmune encephalomyelitis (EAE) as a model for multiple sclerosis (MS). *British Journal of Pharmacology*, *164*(4), 1079–1106. https://doi.org/10.1111/j.1476-5381.2011.01302.x

Corpuz, L. M., Funderburgh, J. L., Funderburgh, M. L., Bottomley, G. S., Prakash, S., & Conrad, G. W. (1996). Molecular cloning and tissue distribution of keratocan. *The Journal of Biological*

Chemistry, *271*(16), 9759–9763.

Costell, M., Gustafsson, E., Aszódi, A., Mörgelin, M., Bloch, W., Hunziker, E., … Fässler, R. (1999). Perlecan Maintains the Integrity of Cartilage and Some Basement Membranes. *The Journal of Cell Biology*, *147*(5), 1109–1122.

Costell, M., Sasaki, T., Mann, K., Yamada, Y., & Timpl, R. (1996). Structural characterization of recombinant domain II of the basement membrane proteoglycan perlecan. *FEBS Letters*, *396*(2–3), 127–131. https://doi.org/10.1016/0014-5793(96)01082-4

Cox, C. M., & Poole, T. J. (2000). Angioblast differentiation is influenced by the local environment: FGF-2 induces angioblasts and patterns vessel formation in the quail embryo. *Developmental Dynamics*, *218*(2), 371–382. https://doi.org/10.1002/(SICI)1097-0177(200006)218:2<371::AID-DVDY10>3.0.CO;2-Z

Crossin, K. L., & Krushel, L. a. (2000). Cellular signaling by neural cell adhesion molecules of the immunoglobulin superfamily. *Developmental Dynamics : An Official Publication of the American Association of Anatomists*, *218*(2), 260–279. https://doi.org/10.1002/(SICI)1097-0177(200006)218:2<260::AID-DVDY3>3.0.CO;2-9

Cuadros, M. A., Martin, C., Coltey, P., Almendros, A., & Navascués, J. (1993). First appearance, distribution, and origin of macrophages in the early development of the avian central nervous system. *Journal of Comparative Neurology*, *330*(1), 113–129. https://doi.org/10.1002/cne.903300110

Cuddapah, V. A., Robel, S., Watkins, S., & Sontheimer, H. (2014). A neurocentric perspective on glioma invasion. *Nat Rev Neurosci*, *15*(7), 455–465. Retrieved from http://dx.doi.org/10.1038/nrn3765

Cuevas, P., Gutierrez-Diaz, J. a, Reimers, D., Dujovny, M., Diaz, F. G., & Ausman, J. I. (1984). Pericyte endothelial gap junctions in human cerebral capillaries. *Anatomy and Embryology*, *170*(2), 155–9. https://doi.org/10.1007/BF00319000

Dalma-Weiszhausz, D. D., Warrington, J., Tanimoto, E. Y., & Miyada, C. G. (2006). [1] The Affymetrix GeneChip?? Platform: An Overview. *Methods in Enzymology*, *410*(6), 3–28. https://doi.org/10.1016/S0076-6879(06)10001-4

Dalmau, I., Finsen, B., Tønder, N., Zimmer, J., González, B., & Castellano, B. (1997). Development of microglia in the prenatal rat hippocampus. *Journal of Comparative Neurology*, *377*(1), 70–84. https://doi.org/10.1002/(SICI)1096-9861(19970106)377:1<70::AID-CNE7>3.0.CO;2-G

Daneman, R., Agalliu, D., Zhou, L., Kuhnert, F., Kuo, C. J., & Barres, B. A. (2009). Wnt/beta-catenin signaling is required for CNS, but not non-CNS, angiogenesis. *Proceedings of the National Academy of Sciences of the United States of America*, *106*(2), 641–6. https://doi.org/10.1073/pnas.0805165106

Daneman, R., Zhou, L., Kebede, A. a., & Barres, B. a. (2010). Pericytes are required for blood–brain barrier integrity during embryogenesis. *Nature*, *468*(7323), 562–566. https://doi.org/10.1038/nature09513

Danielson, K. G., Baribault, H., Holmes, D. F., Graham, H., Kadler, K. E., & Iozzo, R. V. (1997). Targeted disruption of decorin leads to abnormal collagen fibril morphology and skin fragility. *The Journal of Cell Biology*, *136*(3), 729–43. https://doi.org/10.1083/jcb.136.3.729

Davies, J. E., Tang, X., Bournat, J. C., & Davies, S. J. A. (2006). Decorin Promotes Plasminogen/Plasmin Expression within Acute Spinal Cord Injuries and by Adult Microglia In Vitro, *23*(3–4), 397–408. https://doi.org/10.1089/neu.2006.23.397

Davies, J. E., Tang, X., Denning, J. W., Archibald, S. J., & Davies, S. J. A. (2004). Decorin suppresses neurocan, brevican, phosphacan and NG2 expression and promotes axon growth across adult rat spinal cord injuries. *European Journal of Neuroscience*, *19*(5), 1226–1242. https://doi.org/10.1111/j.1460-9568.2004.03184.x

Deandrés-Galiana, E. J., Fernández-Martínez, J. L., Saligan, L. N., & Sonis, S. T. (2016). Impact of Microarray Preprocessing Techniques in Unraveling Biological Pathways. *Journal of Computational Biology : A Journal of Computational Molecular Cell Biology*, *0*(0), 1–12. https://doi.org/10.1089/cmb.2016.0042

Deguchi, J., Namba, T., Hamada, H., Nakaoka, T., Abe, J., Sato, O., … Makuuchi, M. (1999). Targeting endogenous platelet-derived growth factor B- chain by adenovirus-mediated gene transfer potently inhibits in vivo smooth muscle proliferation after arterial injury. *Gene Therapy*, *6*, 956–965.

Del Bigio, M. R., & Enno, T. L. (2008). Effect of hydrocephalus on rat brain extracellular compartment. *Cerebrospinal Fluid Research*, *5*, 12. https://doi.org/10.1186/1743-8454-5-12

Dellett, M., Hu, W., Papadaki, V., & Ohnuma, S. (2012). Small leucine rich proteoglycan family regulates multiple signalling pathways in neural development and maintenance. *Development, Growth & Differentiation*, *54*(3), 327–40. https://doi.org/10.1111/j.1440-169X.2012.01339.x

Dénes, A., Ferenczi, S., & Kovács, K. J. (2011). Systemic inflammatory challenges compromise survival after experimental stroke via augmenting brain inflammation, blood- brain barrier damage and brain oedema independently of infarct size. *Journal of Neuroinflammation*, *8*(1), 164. https://doi.org/10.1186/1742-2094-8-164

Dewi, B. E., Takasaki, T., & Kurane, I. (2004). In vitro assessment of human endothelial cell permeability: effects of inflammatory cytokines and dengue virus infection. *Journal of Virological Methods*, *121*(2), 171–180. https://doi.org/10.1016/j.jviromet.2004.06.013

Dickson, M. C., Martin, J. S., Cousins, F. M., Kulkarni, A. B., Karlsson, S., & Akhurst, R. J. (1995).

Defective haematopoiesis and vasculogenesis in transforming growth factor-beta 1 knock out mice. *Development*, *121*(6), 1845–1854.

Ding, I., Liu, W., Sun, J., Fenton, B., & Okunieff, P. (2002). Comparison and modulation of angiogenic responses by FGFs, VEGF and SCF in murine and human fibrosarcomas. *Comparative Biochemistry and Physiology - A Molecular and Integrative Physiology*, *132*(1), 17–25. https://doi.org/10.1016/S1095-6433(01)00524-4

Dobrogowska, D. H., Lossinsky, A. S., Tarnawski, M., & Vorbrodt, A. W. (1998). Increased blood-brain barrier permeability and endothelial abnormalities induced by vascular endothelial growth factor. *Journal of Neurocytology*, *27*(3), 163–173. https://doi.org/10.1023/A:1006907608230

Dohgu, S., Higuchi, S., Tsuruo, T., Kataoka, Y., Takata, F., Naito, M., … Yamauchi, A. (2004). Transforming growth factor-beta1 upregulates the tight junction and P-glycoprotein of brain microvascular endothelial cells. *Cellular and Molecular Neurobiology*, *24*(3), 491–497.

Dolan, M., Horchar, T., Rigatti, B., & Hassell, J. R. (1997). Identification of sites in domain I of perlecan that regulate heparan sulfate synthesis. *Journal of Biological Chemistry*, *272*(7), 4316–4322. https://doi.org/10.1074/jbc.272.7.4316

Domogatskaya, A., Rodin, S., & Tryggvason, K. (2012). Functional Diversity of Laminins. *Annual Review of Cell and Developmental Biology*, *28*(1), 523–553. https://doi.org/10.1146/annurev-cellbio-101011-155750

Douaiher, J., Succar, J., Lancerotto, L., Gurish, M. F., Orgill, D. P., Hamilton, M. J., … Stevens, R. L. (2014). *Development of mast cells and importance of their tryptase and chymase serine proteases in inflammation and wound healing*. *Advances in Immunology* (1st ed., Vol. 122). Elsevier Inc. https://doi.org/10.1016/B978-0-12-800267-4.00006-7

Dougher, A., Wasserstrom, H., Torley, L., Shridaran, L., Westdock, P., Hileman, R., … Terman, B. (1997). Identification of a heparin binding peptide on the extracellular domain of the KDR VEGF receptor. *Growth Factors*, *14*(4), 257–268.

Douglass, S., Goyal, A., & Iozzo, R. V. (2015). The role of perlecan and endorepellin in the control of tumor angiogenesis and endothelial cell autophagy. *Connect Tissue Res.*, *56*(5), 381–391. https://doi.org/10.1146/annurev-immunol-032713-120240.Microglia

Drake, C. J. (2003). Embryonic and adult vasculogenesis. *Birth Defects Research Part C - Embryo Today: Reviews*, *69*(1), 73–82. https://doi.org/10.1002/bdrc.10003

Drake, C. J., & Little, C. D. (1995). Exogenous vascular endothelial growth factor induces malformed and hyperfused vessels during embryonic neovascularization. *Proceedings of the National Academy of Sciences of the United States of America*, *92*(17), 7657–7661. https://doi.org/10.1073/pnas.92.17.7657

Dumont, D. J., Gradwohl, G., Fong, G. H., Puri, M. C., Gertsenstein, M., Auerbach, A., & Breitman, M. L. (1994). Dominant-negative and targeted null mutations in the endothelial receptor tyrosine kinase, tek, reveal a critical role in vasculogenesis of the embryo. *Genes and Development*, *8*(16), 1897–1909. https://doi.org/10.1101/gad.8.16.1897

Durbeej, M. (2010). Laminins. *Cell and Tissue Research*, *339*(1), 259–268. https://doi.org/10.1007/s00441-009-0838-2

Dyer, M. a, Farrington, S. M., Mohn, D., Munday, J. R., & Baron, M. H. (2001). Indian hedgehog activates hematopoiesis and vasculogenesis and can respecify prospective neurectodermal cell fate in the mouse embryo. *Development (Cambridge, England)*, *128*(10), 1717–1730.

Eilken, H. M., & Adams, R. H. (2010). Dynamics of endothelial cell behavior in sprouting angiogenesis. *Current Opinion in Cell Biology*, *22*(5), 617–625. https://doi.org/10.1016/j.ceb.2010.08.010

Eklund, L., Piuhola, J., Komulainen, J., Sormunen, R., Ongvarrasopone, C., Fassler, R., … Pihlajaniemi, T. (2001). Lack of type XV collagen causes a skeletal myopathy and cardiovascular defects in mice. *Proceedings of the National Academy of Sciences*, *98*(3), 1194–1199. https://doi.org/10.1073/pnas.98.3.1194

Enge, M., Bjarnega, M., Gerhardt, H., Gustafsson, E., Asker, N., Hammes, H., & Shani, M. (2002). Endothelium-specific platelet-derived growth factor-B ablation mimics diabetic retinopathy. *The EMBO Journal*, *21*(16), 4307–4316.

Engelhardt, B. (2011). β1-Integrin/matrix interactions support blood–brain barrier integrity. *Journal of Cerebral Blood Flow & Metabolism*, *31*(10), 1969–1971. https://doi.org/10.1038/jcbfm.2011.98

Ernst, C., & Christie, B. R. (2006). Isolectin-IB4 as a vascular stain for the study of adult neurogenesis. *Journal of Neuroscience Methods*, *150*(1), 138–142. https://doi.org/10.1016/j.jneumeth.2005.06.018

Errede, M., Girolamo, F., Ferrara, G., Strippoli, M., Morando, S., Boldrin, V., … Virgintino, D. (2012). Blood-brain barrier alterations in the cerebral cortex in experimental autoimmune encephalomyelitis. *Journal of Neuropathology and Experimental Neurology*, *71*(10), 840–854. https://doi.org/10.1097/NEN.0b013e31826ac110

Eskildsen, S., Justesen, J., Schierup, M. H., & Hartmann, R. (2003). Characterization of the 2′-5′-oligoadenylate synthetase ubiquitin-like family. *Nucleic Acids Research*, *31*(12), 3166–3173. https://doi.org/10.1093/nar/gkg427

Esko, J., Kimata, K., & Lindahl, U. (2009). Proteoglycans and Sulfated Glycosaminoglycans. In *Essentials of Glycobiology* (p. Chapter 16).

Ettner, N., Göhring, W., Sasaki, T., Mann, K., & Timpl, R. (1998). The N-terminal globular domain of

the laminin α1 chain binds to α1β1 and α2β1 integrins and to the heparan sulfate-containing domains of perlecan. *FEBS Letters*, *430*(3), 217–221. https://doi.org/10.1016/S0014-5793(98)00601-2

Evanko, S. P., Angello, J. C., & Wight, T. N. (1999). Formation of hyaluronan- and versican-rich pericellular matrix is required for proliferation and migration of vascular smooth muscle cells. *Arteriosclerosis, Thrombosis, and Vascular Biology*, *19*, 1004–1013. https://doi.org/10.1161/01.ATV.19.4.1004

Fantin, A., Vieira, J. M., Gestri, G., Denti, L., Schwarz, Q., Prykhozhij, S., … Ruhrberg, C. (2010). Tissue macrophages act as cellular chaperones for vascular anastomosis downstream of VEGF-mediated endothelial tip cell induction. *Blood*, *116*(5), 829–841. https://doi.org/10.1182/blood-2009-12-257832.

Fantin, A., Vieira, J. M., Plein, A., Maden, C. H., & Ruhrberg, C. (2013). The embryonic mouse hindbrain as a qualitative and quantitative model for studying the molecular and cellular mechanisms of angiogenesis. *Nature Protocols*, *8*(2), 418–429. https://doi.org/10.1038/nprot.2013.015

Farach-Carson, M. C., & Carson, D. D. (2007). Perlecan - A multifunctional extracellular proteoglycan scaffold. *Glycobiology*, *17*(9), 897–905. https://doi.org/10.1093/glycob/cwm043

Feingold, E., Good, P., Guyer, M., Kamholz, S., Liefer, L., Wetterstrand, K., … Consortium, E. P. (2004). The ENCODE (ENCyclopedia Of DNA Elements) Project. *Science*, *306*(5696), 636–40. https://doi.org/10.1126/science.1105136

Fisher, L. W., Termine, J. D., & Young, M. F. (1989). Deduced protein sequence of bone small proteoglycan I (biglycan) shows homology with proteoglycan II (decorin) and several nonconnective tissue proteins in a variety of species. *Journal of Biological Chemistry*, *264*(8), 4571–4576.

Fong, G.-H., Rossant, J., Gertsenstein, M., & Breitman, M. L. (1995). Role of the Flt-1 receptor tyrosine kinase in regulating the assembly of vascular endothelium. *Nature*. https://doi.org/10.1038/376066a0

Forsberg, E., Institutet, K., & Chemistry, P. (1988). Phenotypic Properties of Cultured Arterial Smooth Muscle Cells. *Cell*, *107*(July), 307–319.

Francavilla, C., Maddaluno, L., & Cavallaro, U. (2009). The functional role of cell adhesion molecules in tumor angiogenesis. *Seminars in Cancer Biology*, *19*(5), 298–309. https://doi.org/10.1016/j.semcancer.2009.05.004

Friedrich, M. V, Göhring, W., Mörgelin, M., Brancaccio, a, David, G., & Timpl, R. (1999). Structural basis of glycosaminoglycan modification and of heterotypic interactions of perlecan domain

V. *Journal of Molecular Biology*, *294*(1), 259–270. https://doi.org/10.1006/jmbi.1999.3259

Frieser, M., Nockel, H., Pausch, F., Roder, C., Hahn, A., Deutzmann, R., & Sorokin, L. M. (1997). Cloning of the mouse laminin alpha 4 cDNA. Expression in a subset of endothelium. *Eur J Biochem*, *246*(3), 727–735. https://doi.org/10.1111/j.1432-1033.1997.t01-1-00727.x

Fuh, G., Garcia, K. C., & de Vos, A. M. (2000). The interaction of neuropilin-1 with vascular endothelial growth factor and its receptor flt-1. *J Biol Chem*, *275*(35), 26690–26695. https://doi.org/10.1074/jbc.M003955200

Funderburgh, J. L., Corpuz, L. M., Roth, M. R., Funderburgh, M. L., Tasheva, E. S., & Conrad, G. W. (1997). Mimecan, the 25-kDa Corneal Keratan Sulfate Proteoglycan, Is a Product of the Gene Producing Osteoglycin, *272*(44), 28089–28095.

Furuse, M. (2010). Molecular Basis of the Core Structure of Tight Junctions. *Cold Spring Harbor Perspectives in Biology*, *2*(1), 1–14. https://doi.org/10.1101/cshperspect.a002907

Gaengel, K., Genové, G., Armulik, A., & Betsholtz, C. (2009). Endothelial-mural cell signaling in vascular development and angiogenesis. *Arteriosclerosis, Thrombosis, and Vascular Biology*, *29*(5), 630–638. https://doi.org/10.1161/ATVBAHA.107.161521

Gaillard, P. J., De Boer, A. G., & Breimer, D. D. (2003). Pharmacological investigations on lipopolysaccharide-induced permeability changes in the blood-brain barrier in vitro. *Microvascular Research*, *65*(1), 24–31. https://doi.org/10.1016/S0026-2862(02)00009-2

Games, D., Adams, D., Alessandrini, R., Barbour, R., Borthelette, P., Blackwell, C., … Zhao, J. (1995). Alzheimer-type neuropathology in transgenic mice overexpressing V717F [beta]-amyloid precursor protein. *Nature*, *373*(6514), 523–527. Retrieved from http://dx.doi.org/10.1038/373523a0

Gao, X., & Xu, Z. (2008). Mechanisms of action of angiogenin. *Acta Biochim Biophys Sin*, *40*(7), 619–624. https://doi.org/10.1111/j.1745-7270.2008.

Gasteiger, E., Gattiker, A., Hoogland, C., Ivanyi, I., Appel, R. D., & Bairoch, A. (2003). ExPASy: The proteomics server for in-depth protein knowledge and analysis. *Nucleic Acids Research*, *31*(13), 3784–3788. https://doi.org/10.1093/nar/gkg563

Gautam, J., Zhang, X., & Yao, Y. (2016). The role of pericytic laminin in blood brain barrier integrity maintenance. *Scientific Reports*, *6*(November), 1–13. https://doi.org/10.1038/srep36450

Gerhardt, H., Golding, M., Fruttiger, M., Ruhrberg, C., Lundkvist, A., Abramsson, A., … Betsholtz, C. (2003). VEGF guides angiogenic sprouting utilizing endothelial tip cell filopodia. *Journal of Cell Biology*, *161*, 1163–1177. https://doi.org/10.1083/jcb.200302047

Gerhardt, H., Wolburg, H., & Redies, C. (2000). N-cadherin mediates pericytic-endothelial interaction during brain angiogenesis in the chicken. *Developmental Dynamics*, *218*(3), 472–

479. https://doi.org/10.1002/1097-0177(200007)218:3<472::AID-DVDY1008>3.0.CO;2-#

Giannotta, M., Trani, M., & Dejana, E. (2013). VE-Cadherin and Endothelial Adherens Junctions: Active Guardians of Vascular Integrity. *Developmental Cell*, *26*(5), 441–454. https://doi.org/10.1016/j.devcel.2013.08.020

Giasson, B. I., Duda, J. E., Quinn, S. M., Zhang, B., Trojanowski, J. Q., & Lee, V. M. Y. (2002). Neuronal α-synucleinopathy with severe movement disorder in mice expressing A53T human α-synuclein. *Neuron*, *34*(4), 521–533. https://doi.org/10.1016/S0896-6273(02)00682-7

Gidday, J. M., Gasche, Y. G., Copin, J., Shah, A. R., Perez, R. S., Shapiro, S. D., … Leukocyte-derived, T. S. P. (2005). Leukocyte-derived matrix metalloproteinase-9 mediates blood-brain barrier breakdown and is proinflammatory after transient focal cerebral ischemia, *63110*, 558–568. https://doi.org/10.1152/ajpheart.01275.2004.

Giger, R. J., Cloutier, J. F., Sahay, a, Prinjha, R. K., Levengood, D. V, Moore, S. E., … Geppert, M. (2000). Neuropilin-2 is required in vivo for selective axon guidance responses to secreted semaphorins. *Neuron*, *25*(1), 29–41. https://doi.org/10.1016/S0896-6273(00)80869-7

Gluzman-Poltorak, Z., Cohen, T., Shibuya, M., & Neufeld, G. (2001). Vascular Endothelial Growth Factor Receptor-1 and Neuropilin-2 Form Complexes. *Journal of Biological Chemistry*, *276*(22), 18688–18694. https://doi.org/10.1074/jbc.M006909200

Godowski, P. J. (2005). A smooth operator for LPS responses. *Nature Immunology*, *6*(6), 544–6. https://doi.org/10.1038/ni0605-544

Goldman, C. K., Kim, J., Wong, W., King, V., Brock, T., & Gillespie, G. Y. (1993). Epidermal Growth Factor Stimulates Vascular Endothelial Growth Factor Production by Human Malignant Glioma Cells : A Model of Glioblastoma Multiforme Pathophysiology. *Molecular Biology of the Cell*, *4*(January), 121–133.

Gomperts, B., Kramer, I., & Tatham, P. (2009). *Signal transduction*. Elsevier.

Gospodarowicz, D., Greenburg, G., Foidart, J. M., & Savion, N. (1981). The production and localization of laminin in cultured vascular and corneal endothelial cells. *Journal of Cellular Physiology*, *107*(2), 171–83. https://doi.org/10.1002/jcp.1041070203

Gould, D. B., Phalan, F. C., & Breedveld, G. J. (2005). Mutations in Col4a1 Cause Perinatal Cerebral Hemorrhage and Porencephaly. *Science*, *308*(May), 1167–1172.

Goumans, M. J., Valdimarsdottir, G., Itoh, S., & Lebrin, F. (2003). Activin receptor-like kinase (ALK) 1 is an antagonistic mediator of lateral TGF [beta]/ALK5 signaling. *Molecular Cell*, *12*, 817–828. https://doi.org/10.1016/S1097-2765(03)00386-1

Goyal, A., Pal, N., Concannon, M., Paul, M., Doran, M., Poluzzi, C., … Iozzo, R. V. (2011). Endorepellin, the angiostatic module of perlecan, interacts with both the ??2??1 integrin and vascular

endothelial growth factor receptor 2 (VEGFR2): A dual receptor antagonism. *Journal of Biological Chemistry*, *286*(29), 25947–25962. https://doi.org/10.1074/jbc.M111.243626

Goyal, A., Poluzzi, C., Willis, C. D., Smythies, J., Shellard, A., Neill, T., & Iozzo, R. V. (2012). Endorepellin affects angiogenesis by antagonizing diverse vascular endothelial growth factor receptor 2 (VEGFR2)-evoked signaling pathways: Transcriptional repression of hypoxia-inducible factor 1?? and VEGFA and concurrent inhibition of nuclear factor of. *Journal of Biological Chemistry*, *287*(52), 43543–43556. https://doi.org/10.1074/jbc.M112.401786

Grainger, D. J., Metcalfe, J. C., Grace, a a, & Mosedale, D. E. (1998). Transforming growth factor-beta dynamically regulates vascular smooth muscle differentiation in vivo. *Journal of Cell Science*, *111 (Pt 1*, 2977–2988.

Grant, D. S., Yenisey, C., Rose, R. W., Tootell, M., Santra, M., & Iozzo, R. V. (2002). Decorin suppresses tumor cell-mediated angiogenesis. *Oncogene*, *21*(31), 4765–4777. https://doi.org/10.1038/sj.onc.1205595

Groeneveld, T. W. L., Oroszlan, M., Owens, R. T., Faber-Krol, M. C., Bakker, A. C., Arlaud, G. J., … Roos, A. (2005). Interactions of the Extracellular Matrix Proteoglycans Decorin and Biglycan with C1q and Collectins. *The Journal of Immunology*, *175*(7), 4715–4723. https://doi.org/10.4049/jimmunol.175.7.4715

Grover, J., & Roughley, P. (2001). Characterization and expression of murine PRELP. *Matrix Biology*, *109*(3), 555–564. https://doi.org/10.1172/JCI200213595.Introduction

Halfter, W., Dong, S., Schurer, B., & Cole, G. J. (1998). Collagen XVIII is a basement membrane heparan sulfate proteoglycan. *Journal of Biological Chemistry*, *273*(39), 25404–25412. https://doi.org/10.1074/jbc.273.39.25404

Hamill, K. J., Kligys, K., Hopkinson, S. B., & Jones, J. C. R. (2009). Laminin deposition in the extracellular matrix: a complex picture emerges. *Journal of Cell Science*, *122*(Pt 24), 4409–17. https://doi.org/10.1242/jcs.041095

Hamilton, N. B., Attwell, D., & Hall, C. N. (2010). Pericyte-mediated regulation of capillary diameter: a component of neurovascular coupling in health and disease. *Frontiers in Neuroenergetics*, *2*(May), 1–14. https://doi.org/10.3389/fnene.2010.00005

Hanemann, C. O., Kuhn, G., Lie, A., Gillen, C., Bosse, F., Spreyer, P., & Müller, H. W. (1993). Expression of decorin mRNA in the nervous system of rat. *The Journal of Histochemistry and Cytochemistry : Official Journal of the Histochemistry Society*, *41*(9), 1383–91. https://doi.org/10.1177/41.9.8354878

Hanna, R. N., Carlin, L. M., Hubbeling, H. G., Nackiewicz, D., Green, A. M., Punt, J. a, … Hedrick, C. C. (2011). The transcription factor NR4A1 (Nur77) controls bone marrow differentiation and the survival of Ly6C- monocytes. *Nature Immunology*, *12*(8), 778–785.

https://doi.org/10.1038/ni.2063

Hanske, S., Dyrna, F., Bechmann, I., & Krueger, M. (2016). Different segments of the cerebral vasculature reveal specific endothelial specifications, while tight junction proteins appear equally distributed. *Brain Structure and Function*, *222*(3), 1–14. https://doi.org/10.1007/s00429-016-1267-0

Hao, H., Ropraz, P., Verin, V., Camenzind, E., Geinoz, A., Pepper, M. S., … Bochaton-Piallat, M. L. (2002). Heterogeneity of smooth muscle cell populations cultured from pig coronary artery. *Arteriosclerosis, Thrombosis, and Vascular Biology*, *22*(7), 1093–1099. https://doi.org/10.1161/01.ATV.0000022407.91111.E4

Happonen, K. E., Fürst, C. M., Saxne, T., Heinegård, D., & Blom, A. M. (2012). PRELP protein inhibits the formation of the complement membrane attack complex. *Journal of Biological Chemistry*, *287*(11), 8092–8100. https://doi.org/10.1074/jbc.M111.291476

Harburger, D. S., & Calderwood, D. A. (2009). Integrin signalling at a glance. *Journal of Cell Science*, *122*(9), 1472–1472. https://doi.org/10.1242/jcs.052910

Haskill, S., Johnson, C., Eierman, D., Becker, S., & Warren, K. (1988). Adherence induces selective mRNA expression of monocyte mediators and proto-oncogenes. *The Journal of Immunology*, *140*(5), 1690 LP-1694. Retrieved from http://www.jimmunol.org/content/140/5/1690.abstract

Hautmann, M. B., Madsen, C. S., & Owens, G. K. (1997). A transforming growth factor beta (TGFbeta) control element drives TGFbeta-induced stimulation of smooth muscle alpha-actin gene expression in concert with two CArG elements. *The Journal of Biological Chemistry*, *272*(16), 10948–56. https://doi.org/10.1074/jbc.272.16.10948

He, L., Vanlandewijck, M., Raschperger, E., Andaloussi Mäe, M., Jung, B., Lebouvier, T., … Betsholtz, C. (2016). Analysis of the brain mural cell transcriptome. *Scientific Reports*, *6*(1), 35108. https://doi.org/10.1038/srep35108

Heidenreich, R., Röcken, M., & Ghoreschi, K. (2009). Angiogenesis drives psoriasis pathogenesis. *International Journal of Experimental Pathology*, *90*(3), 232–248. https://doi.org/10.1111/j.1365-2613.2009.00669.x

Heinegard, D., Larsson, T., Sommarin, Y., Franzén, A., Paulsson, M., & Hedbom, E. (1986). Two novel matrix proteins isolated from articular cartilage show wide distributions among connective tissues. *Journal of Biological Chemistry*, *261*(29), 13866–13872.

Heldin, C.-H. (2013). Targeting the PDGF signaling pathway in tumor treatment. *Cell Communication and Signaling*, *11*(1), 97. https://doi.org/10.1186/1478-811X-11-97

Heldin, C.-H., & Westermark, B. (1999). Mechanism of Action and In Vivo Role of Platelet-Derived Growth Factor. *Physiological Reviews*, *79*(4), 1283–1316. Retrieved from

http://physrev.physiology.org/cgi/content/abstract/79/4/1283

Hellström, M., Phng, L. K., Hofmann, J., Wallgard, E., Coultas, L., Lindblom, P., … Betsholtz, C. (2007). Dll4 signalling through Notch1 regulates formation of tip cells during angiogenesis. *Nature*, *445*(15), 776–780. https://doi.org/10.1038/nature05571

Helms, H. C., Abbott, N. J., Burek, M., Cecchelli, R., Couraud, P.-O., Deli, M. A., … Brodin, B. (2016). In vitro models of the blood–brain barrier: An overview of commonly used brain endothelial cell culture models and guidelines for their use. *Journal of Cerebral Blood Flow & Metabolism*, *36*(5), 862–890. https://doi.org/10.1177/0271678X16630991

Henry, S. P., Takanosu, M., Boyd, T. C., Mayne, P. M., Eberspaecher, H., Zhou, W., … Mayne, R. (2001). Expression Pattern and Gene Characterization of Asporin. *Biochemistry*, *276*(15), 12212–12221. https://doi.org/10.1074/jbc.M011290200

Herrmann, J., Lerman, L. O., Mukhopadhyay, D., Napoli, C., & Lerman, A. (2006). Angiogenesis in atherogenesis. *Arteriosclerosis, Thrombosis, and Vascular Biology*, *26*(9), 1948–1957. https://doi.org/10.1161/01.ATV.0000233387.90257.9b

Herzog, Y., Kalcheim, C., Kahane, N., Reshef, R., & Neufeld, G. (2001). Differential expression of neuropilin-1 and neuropilin-2 in arteries and veins. *Mechanisms of Development*, *109*(1), 115–119. https://doi.org/10.1016/S0925-4773(01)00518-4

Hildebrand, A., Romarís, M., Rasmussen, L. M., Heinegård, D., Twardzik, D. R., Border, W. A., & Ruoslahti, E. (1994). Interaction of the small interstitial proteoglycans biglycan, decorin and fibromodulin with transforming growth factor beta. *The Biochemical Journal*, *534*(Pt 2), 527–534. https://doi.org/10.1042/bj3020527

Hirsch, E. C., & Hunot, S. (2009). Neuroinflammation in Parkinson's disease: a target for neuroprotection? *The Lancet Neurology*, *8*(4), 382–397. https://doi.org/10.1016/S1474-4422(09)70062-6

Hirschi, K. K., Rohovsky, S. A., & D'Amore, P. A. (1998). PDGF, TGF-β, and heterotypic cell-cell interactions mediate endothelial cell-induced recruitment of 10T1/2 cells and their differentiation to a smooth muscle fate. *Journal of Cell Biology*, *141*(3), 805–814. https://doi.org/10.1083/jcb.141.3.805

Ho, M. S. P., Böse, K., Mokkapati, S., Nischt, R., & Smyth, N. (2008). Nidogens-extracellular matrix linker molecules. *Microscopy Research and Technique*, *71*(5), 387–395. https://doi.org/10.1002/jemt.20567

Hoettels, B. A., Wertz, T. S., Birk, D. E., Oxford, J. T., & Beard, R. S. (2017). The Extracellular Matrix Proteoglycan Decorin is Upregulated by Endothelial Cells During Inflammation and Contributes to Blood-Brain Barrier Dysfunction. *The FASEB Journal* , *31*(1 Supplement), 682.4-682.4. Retrieved from

http://www.fasebj.org/content/31/1_Supplement/682.4.abstract

Hoffmann, A., Bredno, J., Wendland, M., Derugin, N., Ohara, P., & Wintermark, M. (2011). High and Low Molecular Weight Fluorescein Isothiocyanate (FITC)-Dextrans to Assess Blood-Brain Barrier Disruption: Technical Considerations. *Translational Stroke Research*, *2*(1), 106–111. https://doi.org/10.1007/s12975-010-0049-x

Hohenester, E., & Yurchenco, P. D. (2013). Laminins in basement membrane assembly Laminins in basement membrane assembly. *Cell Adhesion and Migration*, *7*(1), 56–63. https://doi.org/10.4161/cam.21831

Holbro, T., & Hynes, N. E. (2004). ErbB Receptors : Directing Key Signaling Networks Throughout Life. *Annual Review of Pharmacology and Toxicology*, *44*, 195–217. https://doi.org/10.1146/annurev.pharmtox.44.101802.121440

Hopf, M., Göhring, W., Kohfeldt, E., Yamada, Y., & Timpl, R. (1999). Recombinant domain IV of perlecan binds to nidogens, laminin-nidogen complex, fibronectin, fibulin-2 and heparin. *European Journal of Biochemistry*, *259*(3), 917–925. https://doi.org/10.1046/j.1432-1327.1999.00127.x

Huang, D. W., Sherman, B. T., & Lempicki, R. a. (2009). Systematic and integrative analysis of large gene lists using DAVID bioinformatics resources. *Nature Protocols*, *4*(1), 44–57. https://doi.org/10.1038/nprot.2008.211

Huang, R. L., Teo, Z., Chong, H. C., Zhu, P., Tan, M. J., Tan, C. K., … Tan, N. S. (2011). ANGPTL4 modulates vascular junction integrity by integrin signaling and disruption of intercellular VE-cadherin and claudin-5 clusters. *Blood*, *118*(14), 3990–4002. https://doi.org/10.1182/blood-2011-01-328716

Hubbell, E., Liu, W. M., & Mei, R. (2002). Robust estimators for expression analysis. *Bioinformatics*, *18*(12), 1585–1592. https://doi.org/10.1093/bioinformatics/18.12.1585

Huber, R. E., Kurz, G., & Wallenfels, K. (1976). A Quantitation of the Factors Which Affect the Hydrolase and Transgalactosylase Activities of β-galactosidase. *Biochemistry*, *15*(9), 1994–2001.

Hudson, N., Powner, M. B., Sarker, M. H., Burgoyne, T., Campbell, M., Ockrim, Z. K., … Turowski, P. (2014). Differential apicobasal VEGF signaling at vascular blood-neural barriers. *Developmental Cell*, *30*(5), 541–552. https://doi.org/10.1016/j.devcel.2014.06.027

Hutchings, M., & Weller, R. (1986). Anatomical relationships of the pia mater to cerebral blood vessels in man. *Journal of Neurosurgery*, *65*(3), 316–325. https://doi.org/10.3171/jns.1986.65.3.0316

Huynh, H. K., & Dorovini-Zis, K. (1993). Effects of interferon-gamma on primary cultures of human brain microvessel endothelial cells. *The American Journal of Pathology*, *142*(4), 1265–78.

Retrieved from http://www.pubmedcentral.nih.gov/articlerender.fcgi?artid=1886858&tool=pmcentrez&rendertype=abstract

Ichii, T., Koyama, H., Tanaka, S., Kim, S., Shioi, A., Okuno, Y., … Nishizawa, Y. (2001). Fibrillar collagen specifically regulates human vascular smooth muscle cell genes involved in cellular responses and the pericellular matrix environment. *Circulation Research*, *88*(5), 460–7. https://doi.org/10.1161/01.RES.88.5.460

Iivanainen, A., Vuolteenaho, R., Sainio, K., Eddy, R., Shows, T. B., Sariola, H., & Tryggvason, K. (1995). The human laminin β2 chain (S-Laminin): Structure, expression in fetal tissues and chromosomal assignment of the LAMB2 gene. *Matrix Biology*, *14*(6), 489–497. https://doi.org/10.1016/0945-053X(95)90006-3

Iozzo, R. V. (1998). MATRIX PROTEOGLYCANS: From Molecular Design to Cellular Function. *Annual Review of Biochemistry*, *67*(1), 609–652. https://doi.org/10.1146/annurev.biochem.67.1.609

Iozzo, R. V., & Schaefer, L. (2015). Proteoglycan form and function: A comprehensive nomenclature of proteoglycans. *Matrix Biology*, *42*, 11–55. https://doi.org/10.1016/j.matbio.2015.02.003

Irizarry, R. A., Bolstad, B. M., Collin, F., Cope, L. M., Hobbs, B., & Speed, T. P. (2003). Summaries of Affymetrix GeneChip probe level data. *Nucleic Acids Research*, *31*(4), e15. https://doi.org/10.1093/nar/gng015

Irizarry, R. A., Hobbs, B., Collin, F., Beazer-Barclay, Y. D., Antonellis, K. J., Scherf, U., & Speed, T. P. (2003). Exploration, normalization, and summaries of high density oligonucleotide array probe level data. *Biostatistics*, *4*(2), 249–264. https://doi.org/10.1093/biostatistics/4.2.249

Isasi, E., Barbeito, L., & Olivera-Bravo, S. (2014). Increased blood-brain barrier permeability and alterations in perivascular astrocytes and pericytes induced by intracisternal glutaric acid. *Fluids and Barriers of the CNS*, *11*, 15. https://doi.org/10.1186/2045-8118-11-15

Ishijima, M., Suzuki, N., Hozumi, K., Matsunobu, T., Kosaki, K., Kaneko, H., … Yamada, Y. (2012). Perlecan modulates VEGF signaling and is essential for vascularization in endochondral bone formation. *Matrix Biology*, *31*(4), 234–245. https://doi.org/10.1016/j.matbio.2012.02.006

Jacobsen, F., Kraft, J., Schroeder, C., Hube-Magg, C., Kluth, M., Lang, D. S., … Melling, N. (2017). Up-regulation of Biglycan is Associated with Poor Prognosis and PTEN Deletion in Patients with Prostate Cancer. *Neoplasia (United States)*, *19*(9), 707–715. https://doi.org/10.1016/j.neo.2017.06.003

Jakobsson, L., Kreuger, J., Holmborn, K., Lundin, L., Eriksson, I., Kjellén, L., & Claesson-Welsh, L. (2006). Heparan Sulfate in trans Potentiates VEGFR-Mediated Angiogenesis. *Developmental Cell*, *10*(5), 625–634. https://doi.org/10.1016/j.devcel.2006.03.009

Jansson, D., Scotter, E. L., Rustenhoven, J., Coppieters, N., Smyth, L. C. D., Oldfield, R. L., … Dragunow, M. (2016). Interferon-γ blocks signalling through PDGFRβ in human brain pericytes. *Journal of Neuroinflammation*, *13*(1), 249. https://doi.org/10.1186/s12974-016-0722-4

Janzer, R. C., & Raff, M. C. (1987). Astrocytes induce blood-brain barrier properties in endothelial cells. *Nature*. https://doi.org/10.1038/325253a0

Jian, J., Zheng, Z., Zhang, K., Rackohn, T. M., Hsu, C., Levin, A., … Soo, C. (2013). Fibromodulin promoted in vitro and in vivo angiogenesis. *Biochemical and Biophysical Research Communications*, *436*(3), 530–535. https://doi.org/10.1016/j.bbrc.2013.06.005

Johnson, H. J., Rosenberg, L., Choi, H. U., Garza, S., Höök, M., & Neame, P. J. (1997). Characterization of epiphycan, a small proteoglycan with a leucine-rich repeat core protein. *Journal of Biological Chemistry*, *272*(30), 18709–18717. https://doi.org/10.1074/jbc.272.30.18709

Jozefczuk, J., Drews, K., & Adjaye, J. (2012). Preparation of mouse embryonic fibroblast cells suitable for culturing human embryonic and induced pluripotent stem cells. *Journal of Visualized Experiments : JoVE*, (64), e3854. https://doi.org/10.3791/3854

Jucker, M., Tian, M., Norton, D. D., Sherman, C., & Kusiaki, J. . (1996). Laminin α2 is a component of brain capillary basement membrane: reduced expression in dystrophic dy mice. *Neuroscience*, *71*(4), 1153–1161.

Juers, D. H., Matthews, B. W., & Huber, R. E. (2012). LacZ b -galactosidase : Structure and function of an enzyme of historical and molecular biological importance, *21*. https://doi.org/10.1002/pro.2165

Kang, D. H., Anderson, S., Kim, Y. G., Mazzalli, M., Suga, S., Jefferson, J. A., … Johnson, R. J. (2001). Impaired angiogenesis in the aging kidney: vascular endothelial growth factor and thrombospondin-1 in renal disease. *American Journal of Kidney Diseases : The Official Journal of the National Kidney Foundation*, *37*(3), 601–11. https://doi.org/10.1053/ajkd.2001.22087

Kangwantas, K., Pinteaux, E., & Penny, J. (2016). The extracellular matrix protein laminin-10 promotes blood-brain barrier repair after hypoxia and inflammation in vitro. *Journal of Neuroinflammation*, *13*(1), 25. https://doi.org/10.1186/s12974-016-0495-9

Kappler, J., Stichel, C. C., Gleichmann, M., Gillen, C., Junghans, U., Kresse, H., & Müller, H. W. (1998). Developmental regulation of decorin expression in postnatal rat brain. *Brain Research*, *793*(1–2), 328–332. https://doi.org/10.1016/S0006-8993(98)00260-1

Katsuno, T., Umeda, K., Matsui, T., Hata, M., Tamura, A., Itoh, M., … Tsukita, S. (2008). Deficiency of Zonula Occludens-1 Causes Embryonic Lethal Phenotype Associated with Defected Yolk Sac Angiogenesis and Apoptosis of Embryonic Cells. *Molecular Biology of the Cell*, *19*, 2465–2475. https://doi.org/10.1091/mbc.E07

Kawasaki, T., Kitsukawa, T., Bekku, Y., Matsuda, Y., Sanbo, M., Yagi, T., & Fujisawa, H. (1999). A

requirement for neuropilin-1 in embryonic vessel formation. *Development*, *126*(21), 4895–4902.

Kim, I., Kim, H. G., Moon, S.-O., Chae, S. W., So, J.-N., Koh, K. N., … Koh, G. Y. (2000). Angiopoietin-1 Induces Endothelial Cell Sprouting Through the Activation of Focal Adhesion Kinase and Plasmin Secretion. *Circulation Research*, *86*(9), 952–959. https://doi.org/10.1161/01.RES.86.9.952

Kizawa, H., Kou, I., Iida, A., Sudo, A., Miyamoto, Y., Fukuda, A., … Ikegawa, S. (2005). An aspartic acid repeat polymorphism in asporin inhibits chondrogenesis and increases susceptibility to osteoarthritis. *Nature Genetics*, *37*(2), 138–144. https://doi.org/10.1038/ng1496

Klagsbrun, M., & Bairdt, A. (1991). Growth Factor Activity. *Cell*, *67*, 229–231.

Kleinman, H. K., McGarvey, M. L., Hassell, J. R., Star, V. L., Cannon, F. B., Laurie, G. W., & Martin, G. R. (1986). Basement membrane complexes with biological activity. *Biochemistry*, *25*(2), 312–318. https://doi.org/10.1021/bi00350a005

Koch, S., & Claesson-Welsh, L. (2012). Signal transduction by vascular endothelial growth factor receptors. *Cold Spring Harbor Perspectives in Medicine*, *2*(7), 1–21. https://doi.org/10.1101/cshperspect.a006502

Koops, A., Kappler, J., Junghans, U., Kuhn, G., Kresse, H., & Müller, H. (1996). Cultured astrocytes express biglycan, a chondroitin/dermatan sulfate proteoglycan supporting the survival of neocortical neurons. *Brain Research: Molecular Brain Research*, *41*, 65–73.

Kragh, M., Hjarnaa, P. V., Bramm, E., Kristjansen, P. E., Rygaard, J., & Binderup, L. (2003). In vivo chamber angiogenesis assay: An optimized Matrigel plug assay for fast assessment of anti-angiogenic activity. *International Journal of Oncology*, *22*(2), 305–311.

Kubota, Y., Takubo, K., Shimizu, T., Ohno, H., Kishi, K., Shibuya, M., … Suda, T. (2009). M-CSF inhibition selectively targets pathological angiogenesis and lymphangiogenesis. *The Journal of Experimental Medicine*, *206*(5), 1089–1102. https://doi.org/10.1084/jem.20081605

Langmead, B., Trapnell, C., Pop, M., & Salzberg, S. (2009). Ultrafast and memory-efficient alignment of short DNA sequences to the human genome. *Genome Biology*, *10*(3), R25. https://doi.org/10.1186/gb-2009-10-3-r25

Larsson, J., Goumans, M. J., Sjöstrand, L. J., Van Rooijen, M. A., Ward, D., Levéen, P., … Karlsson, S. (2001). Abnormal angiogenesis but intact hematopoietic potential in TGF-β type I receptor-deficient mice. *EMBO Journal*, *20*(7), 1663–1673. https://doi.org/10.1093/emboj/20.7.1663

Lauder, R. M., Huckerby, T. N., & Nieduszynski, I. A. (1995). The structure of the keratan sulphate chains attached to fibromodulin isolated from bovine tracheal cartilage: Oligosaccharides generated by keratanase II digestion. *Glycoconjugate Journal*, *12*(5), 651–659. https://doi.org/10.1007/BF00731261

Lawson, L. J., Perry, V. H., Dri, P., & Gordon, S. (1990). Heterogeneity in the distribution and morphology of microglia in the normal adult mouse brain. *Neuroscience*, *39*(I), 151–170.

le Goff, M. M., Lu, H., Ugarte, M., Henry, S., Takanosu, M., Mayne, R., & Bishop, P. N. (2012). The vitreous glycoprotein opticin inhibits preretinal neovascularization. *Investigative Ophthalmology and Visual Science*, *53*(1), 228–234. https://doi.org/10.1167/iovs.11-8514

Le Goff, M. M., Sutton, M. J., Slevin, M., Latif, A., Humphries, M. J., & Bishop, P. N. (2012). Opticin exerts its anti-angiogenic activity by regulating extracellular matrix adhesiveness. *The Journal of Biological Chemistry*, *287*(33), 28027–36. https://doi.org/10.1074/jbc.M111.331157

LeBleu, V. S., Macdonald, B., & Kalluri, R. (2007). Structure and function of basement membranes. *Experimental Biology and Medicine (Maywood, N.J.)*, *232*(9), 1121–9. https://doi.org/10.3181/0703-MR-72

Lebrin, F., Deckers, M., Bertolino, P., & Ten Dijke, P. (2005). TGF-beta receptor function in the endothelium. *Cardiovascular Research*, *65*(3), 599–608. https://doi.org/10.1016/j.cardiores.2004.10.036

Lee, B., Clarke, D., Al Ahmad, A., Kahle, M., Parham, C., Auckland, L., … Bix, G. J. (2011). Perlecan domain V is neuroprotective and proangiogenic following ischemic stroke in rodents. *The Journal of Clinical Investigation*, *121*(8), 3005–3023. https://doi.org/10.1172/JCI46358

Lee, E. Y., Parry, G., & Bissell, M. J. (1984). Modulation of secreted proteins of mouse mammary epithelial cells by the collagenous substrata. *The Journal of Cell Biology*, *98*(1), 146–55. https://doi.org/10.1083/jcb.98.1.146

Lee, S.-W., Kim, W. J., Choi, Y. K., Song, H. S., Son, M. J., Gelman, I. H., … Kim, K.-W. (2003). SSeCKS regulates angiogenesis and tight junction formation in blood-brain barrier. *Nature Medicine*, *9*(7), 900–906. https://doi.org/10.1038/nm889

Lee, S., Jilan, S. M., Nikolova, G. V., Carpizo, D., & Luisa Iruela-Arispe, M. (2005). Processing of VEGF-A by matrix metalloproteinases regulates bioavailability and vascular patterning in tumors. *Journal of Cell Biology*, *169*(4), 681–691. https://doi.org/10.1083/jcb.200409115

Levéen, P., Pekny, M., Gebre-Medhin, S., Swolin, B., Larsson, E., & Betsholtz, C. (1994). Mice deficient for PDGF B show renal, cardiovascular, and hematological abnormalities. *Genes and Development*, *8*(16), 1875–1887. https://doi.org/10.1101/gad.8.16.1875

Lewis, M. (2003). PRELP, collagen, and a theory of Hutchinson-Gilford progeria. *Ageing Research Reviews*, *2*(1), 95–105. https://doi.org/10.1016/S1568-1637(02)00044-2

Li, H., Cui, Y., Luan, J., Zhang, X., Li, C., Zhou, X., … Han, J. (2016). PRELP (proline/arginine-rich end leucine-rich repeat protein) promotes osteoblastic differentiation of preosteoblastic MC3T3-E1 cells by regulating the β-catenin pathway. *Biochemical and Biophysical Research*

Communications, *470*(3), 558–562. https://doi.org/10.1016/j.bbrc.2016.01.106

Li, H., Ruan, J., Durbin, R., Li, H., Ruan, J., & Durbin, R. (2008). Mapping short DNA sequencing reads and calling variants using mapping quality scores Mapping short DNA sequencing reads and calling variants using mapping quality scores. *Genome Research*, 1851–1858. https://doi.org/10.1101/gr.078212.108

Li, X., Van Putten, V., Zarinetchi, F., Nicks, M. E., Thaler, S., Heasley, L. E., & Nemenoff, R. a. (1997). Suppression of smooth-muscle alpha-actin expression by platelet-derived growth factor in vascular smooth-muscle cells involves Ras and cytosolic phospholipase A2. *The Biochemical Journal*, *327 (Pt 3*(8), 709–716. https://doi.org/10.1042/bj3270709

Li, Y., Liu, W., Oo, T. F., Wang, L., Tang, Y., Jackson-Lewis, V., … Li, C. (2009). Mutant LRRK2(R1441G) BAC transgenic mice recapitulate cardinal features of Parkinson's disease. *Nature Neuroscience*, *12*(7), 826–828. https://doi.org/10.1038/nn.2349

Liebner, S., Corada, M., Bangsow, T., Babbage, J., Taddei, A., Czupalla, C. J., … Dejana, E. (2008). Wnt/β-catenin signaling controls development of the blood–brain barrier. *The Journal of Cell Biology*, *183*(3), 409–417. https://doi.org/10.1083/jcb.200806024

Lim, J. C., Kania, K. D., Wijesuriya, H., Chawla, S., Sethi, J. K., Pulaski, L., … Barrand, M. A. (2008). Activation of beta-catenin signalling by GSK-3 inhibition increases p-glycoprotein expression in brain endothelial cells. *Journal of Neurochemistry*, *106*(4), 1855–65. https://doi.org/10.1111/j.1471-4159.2008.05537.x

Lindahl, P., Johansson, B. R., Levéen, P., & Betsholtz, C. (1997). Pericyte loss and microaneurysm formation in PDGF-B-deficient mice. *Science (New York, N.Y.)*, *277*(5323), 242–245. https://doi.org/10.1126/science.277.5323.242

Lindblom, P., & Gerhardt, H. (2003). Endothelial PDGF-B retention is required for proper investment of pericytes in the microvessel wall. *Genes & …*, 1835–1840. https://doi.org/10.1101/gad.266803.hedgehog

Linnarsson, S. (2015). Single-cell analysis of mouse cortex. Retrieved from http://linnarssonlab.org/cortex/

llić, D., Furuta, Y., Kanazawa, S., Takeda, N., Sobue, K., Nakatsuji, N., … Aizawa, S. (1995). Reduced cell motility and enhanced focal adhesion contact formation in cells from FAK-deficient mice. *Nature*. https://doi.org/10.1038/377539a0

Logan, A., Baird, A., & Berry, M. (1999). Decorin attenuates gliotic scar formation in the rat cerebral hemisphere. *Exp.Neurol.*, *159*(0014–4886 (Print)), 504–510.

Lu, P., Takai, K., Weaver, V. M., & Werb, Z. (2011). Extracellular matrix degradation and remodeling in development and disease. *Cold Spring Harbor Perspectives in Biology*, *3*(12). https://doi.org/10.1101/cshperspect.a005058

Luca, A. De, Santra, M., Baldi, A., Giordano, A., Iozzo, V., & Iozzo, R. V. (1996). Cell Biology and Metabolism : Decorin-induced Growth Suppression Is Associated with Up-regulation of p21 , an Inhibitor of Cyclin-dependent Kinases Decorin-induced Growth Suppression Is Associated with Up-regulation of p21 , an Inhibitor of Cyclin-depende. *Cell Biology and Metabolism J. Biol. Chem*, *271*(31), 18961–18965. Retrieved from http://www.jbc.org/content/271/31/18961%5Cnhttp://www.jbc.org/content/271/31/18961.full.html#ref-list-1%5Cnhttp://www.jbc.org/

Lui, J. C. K., Andrade, A. C., Forcinito, P., Hegde, A., Chen, W., Baron, J., & Nilsson, O. (2010). Spatial and Temporal Regulation of Gene Expression in the Mammalian Growth Plate. *Bone*, *46*(5), 1380–1390. https://doi.org/10.1016/j.bone.2010.01.373.Spatial

Luttun, A., Tjwa, M., Moons, L., Wu, Y., Angelillo-Scherrer, A., Liao, F., … Carmeliet, P. (2002). Revascularization of ischemic tissues by PlGF treatment, and inhibition of tumor angiogenesis, arthritis and atherosclerosis by anti-Flt1. *Nat Med*, *8*(8), 831–840. Retrieved from http://dx.doi.org/10.1038/nm731

Majava, M., Bishop, P. N., Hagg, P., Scott, P. G., Rice, A., Inglehearn, C., … Mannikko, M. (2014). Novel Mutations in the Small Leucine-Rich Repeat Protein/Proteoglycan (SLRP) Genes in High Myopia. *Human Mutation*, *28*(4), 336–344. https://doi.org/10.1002/humu

Makanya, A. N., Hlushchuk, R., & Djonov, V. G. (2009). Intussusceptive angiogenesis and its role in vascular morphogenesis, patterning, and remodeling. *Angiogenesis*, *12*(2), 113–123. https://doi.org/10.1007/s10456-009-9129-5

Makki, N., Thiel, K. W., & Miller, F. J. (2013). The epidermal growth factor receptor and its ligands in cardiovascular disease. *International Journal of Molecular Sciences*, *14*(10), 20597–20613. https://doi.org/10.3390/ijms141020597

Manaenko, A., Chen, H., Kammer, J., Zhang, J. H., & Tang, J. (2011). Comparison Evans Blue Injection Routes: Intravenous vs. Intraperitoneal, for Measurement of Blood-Brain Barrier in a Mice Hemorrhage Model. *Journal of Neuroscience Methods*, *195*(2), 206–210. https://doi.org/10.1016/j.jneumeth.2010.12.013.Comparison

Mantione F, K. J., Kream F, R. M., Kuzelova, H. F., Ptacek, R. F., Raboch, J. E., Samuel E, J. M., … Mantione, K. J. (2014). Comparing Bioinformatic Gene Expression Profiling Methods: Microarray and RNA-Seq. *Med Sci Monit Basic Res*, *20*, 138–141. https://doi.org/10.12659/MSMBR.892101

Marconcini, L., Marchio, S., Morbidelli, L., Cartocci, E., Albini, A., Ziche, M., … Oliviero, S. (1999). c-fos-induced growth factor/vascular endothelial growth factor D induces angiogenesis in vivo and in vitro. *Proceedings of the National Academy of Sciences of the United States of America*, *96*(17), 9671–6. https://doi.org/10.1073/pnas.96.17.9671

Markovic, D. S., Glass, R., Synowitz, M., Rooijen, N. Van, & Kettenmann, H. (2005). Microglia stimulate the invasiveness of glioma cells by increasing the activity of metalloprotease-2. *Journal of Neuropathology and Experimental Neurology*, *64*(9), 754–62. https://doi.org/10.1097/01.jnen.0000178445.33972.a9

Martínez, P., Esbrit, P., Rodrigo, A., Alvarez-Arroyo, M. V, & Martínez, M. E. (2002). Age-Related Changes in Parathyroid Hormone-Related Protein and Vascular Endothelial Growth Factor in Human Osteoblastic Cells. *Osteoporosis International*, *13*(11), 874–881. https://doi.org/10.1007/s001980200120

Mathiisen, T. M., Lehre, K. P., Danbolt, N. C., & Ottersen, O. P. (2010). The perivascular astroglial sheath provides a complete covering of the brain microvessels: an electron microscopic 3D reconstruction. *Glia*, *58*(March), 1094–1103. https://doi.org/10.1002/glia.20990

Matsumoto, Y., Otsuka, F., Hino, J., Miyoshi, T., Takano, M., Miyazato, M., … Kangawa, K. (2012). Bone morphogenetic protein-3b (BMP-3b) inhibits osteoblast differentiation via Smad2/3 pathway by counteracting Smad1/5/8 signaling. *Molecular and Cellular Endocrinology*, *350*(1), 78–56. https://doi.org/10.1016/j.mce.2011.11.023

McCaffrey, T. A., Falcone, D. J., & Du, B. (1992). Transforming growth factor-β1 is a heparin-binding protein: Identification of putative heparin-binding regions and isolation of heparins with varying affinity for TGF-β1. *Journal of Cellular Physiology*, *152*(2), 430–440. https://doi.org/10.1002/jcp.1041520226

McEwan, P. a, Scott, P. G., Bishop, P. N., & Bella, J. (2006). Structural correlations in the family of small leucine-rich repeat proteins and proteoglycans. *Journal of Structural Biology*, *155*(2), 294–305. https://doi.org/10.1016/j.jsb.2006.01.016

Mckittrick, C. M., Lawrence, C. E., & Carswell, H. V. O. (2015). Mast cells promote blood brain barrier breakdown and neutrophil in fi ltration in a mouse model of focal cerebral ischemia. *Journal of Cerebral Blood Flow & Metabolism*, (August 2014), 1–10. https://doi.org/10.1038/jcbfm.2014.239

McMillin, M. a, Frampton, G. a, Seiwell, A. P., Patel, N. S., Jacobs, A. N., & DeMorrow, S. (2015). TGFβ1 exacerbates blood–brain barrier permeability in a mouse model of hepatic encephalopathy via upregulation of MMP9 and downregulation of claudin-5. *Laboratory Investigation*, *0*(April), 1–11. https://doi.org/10.1038/labinvest.2015.70

Menezes, M. J., Mcclenahan, F. K., Leiton, X. C. V, Aranmolate, A., Shan, X., & Colognato, H. (2014). The Extracellular Matrix Protein Laminin α2 Regulates the Maturation and Function of the Blood – Brain Barrier. *The Journal of Neuroscience*, *34*(46), 15260–15280. https://doi.org/10.1523/JNEUROSCI.3678-13.2014

Meredith, G. E., & Rademacher, D. J. (2012). MPTP Mouse Models of Parkinson ' s Disease: An

Update. *J Parkinsons Dis*, *1*(1), 19–33. https://doi.org/10.3233/JPD-2011-11023.MPTP

Mi, H., Huang, X., Muruganujan, A., Tang, H., Mills, C., Kang, D., & Thomas, P. D. (2017). PANTHER version 11: Expanded annotation data from Gene Ontology and Reactome pathways, and data analysis tool enhancements. *Nucleic Acids Research*, *45*(D1), D183–D189. https://doi.org/10.1093/nar/gkw1138

Miao, Z., Dong, Y., Fang, W., Shang, D., Liu, D., Zhang, K., … Chen, Y. H. (2014). VEGF increases paracellular permeability in brain endothelial cells via upregulation of EphA2. *Anatomical Record*, *297*(5), 964–972. https://doi.org/10.1002/ar.22878

Michael, J. (2012). Ovid: Clinical Neuroanatomy.

Mikaelsson, E., Danesh-Manesh, A. H., Luppert, A., Jeddi-Tehrani, M., Rezvany, M.-R., Sharifian, R. A., … Rabbani, H. (2005). Fibromodulin, an extracellular matrix protein: characterization of its unique gene and protein expression in B-cell chronic lymphocytic leukemia and mantle cell. *Blood*, *105*(12), 4828–4836. https://doi.org/10.1182/blood-2004-10-3941.Supported

Mikaelsson, E., Jeddi-Tehrani, M., Ã–Sterborg, A., Shokri, F., Rabbani, H., & Mellstedt, H. (2015). Small Leucine Rich Proteoglycans as Novel Tumor Markers In Chronic Lymphocytic Leukemia. *Blood*, *116*(21), 694 LP-694. Retrieved from http://www.bloodjournal.org/content/116/21/694.abstract

Mikaelsson, E., Osterborg, A., Tahmasebi Fard, Z., Mahmoudi, A., Mahmoudian, J., Jeddi-Tehrani, M., … Mellstedt, H. (2013). Opticin, a small leucine-rich proteoglycan, is uniquely expressed and translocated to the nucleus of chronic lymphocytic leukemia cells. *Experimental Hematology & Oncology*, *2*(1), 23. https://doi.org/10.1186/2162-3619-2-23

Minami, H., Tashiro, K., Okada, A., Hirata, N., Yamaguchi, T., Takayama, K., … Kawabata, K. (2015). Generation of brain microvascular endothelial-like cells from human induced pluripotent stem cells by co-culture with C6 glioma cells. *PLoS ONE*, *10*(6), 1–13. https://doi.org/10.1371/journal.pone.0128890

Miyagoe, Y., Hanaoka, K., Nonaka, I., Hayasaka, M., Nabeshima, Y., Arahata, K., & Nabeshima, Y. (1997). Laminin α2 chain-null mutant mice by targeted disruption of the Lama2 gene : a new model of merosin (laminin 2)-deficient congenital muscular dystrophy. *FEBS Letters*, *415*(1), 33–39. https://doi.org/10.1016/S0014-5793(97)01007-7

Mochida, Y., Kaku, M., Yoshida, K., Katafuchi, M., Atsawasuwan, P., & Yamauchi, M. (2011). Podocan-like protein: A novel small leucine-rich repeat matrix protein in bone. *Biochemical and Biophysical Research Communications*, *410*(2), 333–338. https://doi.org/10.1016/j.bbrc.2011.05.150

Mohammadi, M., Dikic, I., Sorokin, A., Burgess, W. H., Jaye, M., & Schlessinger, J. (1996). Identification of six novel autophosphorylation sites on fibroblast growth factor receptor 1

and elucidation of their importance in receptor activation and signal transduction. *Molecular and Cellular Biology*, *16*(3), 977–89. https://doi.org/10.1128/MCB.16.3.977

Mohan, H., Krumbholz, M., Sharma, R., Eisele, S., Junker, A., Sixt, M., … Meinl, E. (2010). Extracellular matrix in multiple sclerosis lesions: Fibrillar collagens, biglycan and decorin are upregulated and associated with infiltrating immune cells. *Brain Pathology*, *20*(5), 966–975. https://doi.org/10.1111/j.1750-3639.2010.00399.x

Mongiat, M., Sweeney, S. M., San Antonio, J. D., Fu, J., & Iozzo, R. V. (2003). Endorepellin, a novel inhibitor of angiogenesis derived from the C terminus of perlecan. *Journal of Biological Chemistry*, *278*(6), 4238–4249. https://doi.org/10.1074/jbc.M210445200

Moreno, M., Muñoz, R., Aroca, F., Labarca, M., Brandan, E., & Larraín, J. (2005). Biglycan is a new extracellular component of the Chordin-BMP4 signaling pathway. *The EMBO Journal*, *24*(7), 1397–1405. https://doi.org/10.1038/sj.emboj.7600615

Morrey, J. D., Olsen, A. L., Siddharthan, V., Motter, N. E., Wang, H., Taro, B. S., … Hall, J. O. (2008). Increased blood-brain barrier permeability is not a primary determinant for lethality of West Nile virus infection in rodents. *Journal of General Virology*, *89*(2), 467–473. https://doi.org/10.1099/vir.0.83345-0

Morrison, H. W., & Filosa, J. A. (2013). A quantitative spatiotemporal analysis of microglia morphology during ischemic stroke and reperfusion. *Journal of Neuroinflammation*, *10*(1), 4. https://doi.org/10.1186/1742-2094-10-4

Mortazavi, A., Williams, B. A., McCue, K., Schaeffer, L., & Wold, B. (2008). Mapping and quantifying mammalian transcriptomes by RNA-Seq. *Nature Methods*, *5*(7), 621–628. https://doi.org/10.1038/nmeth.1226

Moscatello, D. K., Santra, M., Mann, D. M., McQuillan, D. J., Wong, a. J., & Iozzo, R. V. (1998). Decorin suppresses tumor cell growth by activating the epidermal growth factor receptor. *J Clin Invest*, *101*(2), 406–12. https://doi.org/10.1172/JCI846

Murata, M., Nishiyori-Sueki, H., Kojima-Ishiyama, M., Carninci, P., Hayashizaki, Y., & Itoh, M. (2014). Transcription Factor Regulatory Networks. *Methods in Molecular Biology (Clifton, N.J.)*, *1164*, 67–85. https://doi.org/10.1007/978-1-4939-0805-9

Murshed, M., Smyth, N., Miosge, N., Karolat, J., Krieg, T., Paulsson, M., & Nischt, R. (2000). The absence of nidogen 1 does not affect murine basement membrane formation. *Molecular and Cellular Biology*, *20*(18), 7007–12. https://doi.org/10.1128/MCB.20.18.7007-7012.2000

Myers, R. M., Stamatoyannopoulos, J., Snyder, M., Dunham, I., Hardison, R. C., Bernstein, B. E., … Good, P. J. (2011). A user's guide to the Encyclopedia of DNA elements (ENCODE). *PLoS Biology*, *9*(4). https://doi.org/10.1371/journal.pbio.1001046

Myren, M., Kirby, D. J., Noonan, M. L., Maeda, A., Owens, R. T., Ricard-Blum, S., … Young, M. F. (2016).

Biglycan potentially regulates angiogenesis during fracture repair by altering expression and function of endostatin. *Matrix Biology*, *52–54*, 141–150. https://doi.org/10.1016/j.matbio.2016.03.008

Nachbar, M., & Oppenheim, J. (1982). Tomato (Lycopersicon esculentum) lectin. *Methods in Enzymology*, *83*, 363–368.

Nagelhus, E. a, Veruki, M. L., Torp, R., Haug, F. M., Laake, J. H., Nielsen, S., … Ottersen, O. P. (1998). Aquaporin-4 water channel protein in the rat retina and optic nerve: polarized expression in Müller cells and fibrous astrocytes. *The Journal of Neuroscience : The Official Journal of the Society for Neuroscience*, *18*(7), 2506–2519.

Naito, Y., Yoshioka, K., Tanaka, K., Tatsumi, K., Kimura, S., & Kasuya, Y. (2014). Endothelin B receptor-mediated encephalopathic events in mouse sepsis model. *Life Sciences*, *118*(2), 340–346. https://doi.org/10.1016/j.lfs.2014.03.012

Nakagawa, S., Deli, M. A., Kawaguchi, H., Shimizudani, T., Shimono, T., Kittel, Á., … Niwa, M. (2009). A new blood-brain barrier model using primary rat brain endothelial cells, pericytes and astrocytes. *Neurochemistry International*, *54*(3–4), 253–263. https://doi.org/10.1016/j.neuint.2008.12.002

Nakao, A., Imamura, T., Souchelnytskyi, S., Kawabata, M., Ishisaki, A., Oeda, E., … Ten Dijke, P. (1997). TGF-β receptor-mediated signalling through Smad2, Smad3 and Smad4. *EMBO Journal*, *16*(17), 5353–5362. https://doi.org/10.1093/emboj/16.17.5353

Navarro, P., Ruco, L., & Dejana, E. (1998). Differential localization of VE- and N-cadherins in human endothelial cells: VE-cadherin competes with N-cadherin for junctional localization. *Journal of Cell Biology*, *140*(6), 1475–1484. https://doi.org/10.1083/jcb.140.6.1475

Neame, P. J., Sommarin, Y., Boynton, R. E., & Heinegård, D. (1994). The structure of a 38-kDa leucine-rich protein (chondroadherin) isolated from bovine cartilage. *Journal of Biological Chemistry*, *269*(34), 21547–21554.

Nelimarkka, L., Salminen, H., Kuopio, T., Nikkari, S., Ekfors, T., Laine, J., … Järveläinen, H. (2001). Decorin is produced by capillary endothelial cells in inflammation-associated angiogenesis. *American Journal of Pathology*, *158*(2), 345–353. https://doi.org/10.1016/S0002-9440(10)63975-2

Neubauer, K., Kruger, M., Quondamatteo, F., Knittel, T., Saile, B., & Ramadori, G. (1999). Transforming growth factor-beta 1 stimulates the synthesis of basement membrane proteins laminin, collagen type IV and entactin in rat liver sinusoidal endothelial cells. *Journal of Hepatology*, *31*(4), 692–702. https://doi.org/Doi 10.1016/S0168-8278(99)80350-X

Niewiarowska, J., Brézillon, S., Sacewicz-Hofman, I., Bednarek, R., Maquart, F.-X., Malinowski, M., … Cierniewski, C. S. (2011). Lumican inhibits angiogenesis by interfering with α2β1 receptor

activity and downregulating MMP-14 expression. *Thrombosis Research*, *128*(5), 452–7. https://doi.org/10.1016/j.thromres.2011.06.011

Nikitovic, D., Aggelidakis, J., Young, M. F., Iozzo, R. V., Karamanos, N. K., & Tzanakakis, G. N. (2012). The biology of small leucine-rich proteoglycans in bone pathophysiology. *Journal of Biological Chemistry*, *287*(41), 33926–33933. https://doi.org/10.1074/jbc.R112.379602

Nishitsuji, K., Hosono, T., Nakamura, T., Bu, G., & Michikawa, M. (2011). Apolipoprotein E regulates the integrity of tight junctions in an isoform-dependent manner in an in vitro blood-brain barrier model. *Journal of Biological Chemistry*, *286*(20), 17536–17542. https://doi.org/10.1074/jbc.M111.225532

Nitta, T., Hata, M., Gotoh, S., Seo, Y., Sasaki, H., Hashimoto, N., … Tsukita, S. (2003). Size-selective loosening of the blood-brain barrier in claudin-5-deficient mice. *Journal of Cell Biology*, *161*(3), 653–660. https://doi.org/10.1083/jcb.200302070

Niu, G., Wright, K. L., Huang, M., Song, L., Haura, E., Turkson, J., … Yu, H. (2002). Constitutive Stat3 activity up-regulates VEGF expression and tumor angiogenesis. *Oncogene*, *21*(November 2001), 2000–2008. https://doi.org/10.1038/sj/onc/1205260

Noakes, P., Gautam, M., Mudd, J., Sanes, J., & Merlie, J. (1995). Aberrant differentiation of neuromuscular junctions in mice lacking s-laminin/laminin β2. *Nature*, *374*, 258–262.

Noakes, P., Miner, J., Gautam, M., Cunningham, J., Sanes, J., & Merlie, J. (1995). The renal glomerulus of mice lacking s-laminin/laminin β2: nephrosis despite molecular compensation by laminin β1. *Nature Genetics*, *10*, 400–406.

Nobes, C. D., & Hall, A. (1995). Rho, Rac, and Cdc42 GTPases regulate the assembly of multimolecular focal complexes associated with actin stress fibers, lamellipodia, and filopodia. *Cell*, *81*(1), 53–62. https://doi.org/10.1016/0092-8674(95)90370-4

Noell, S., Fallier-Becker, P., Deutsch, U., MacK, A. F., & Wolburg, H. (2009). Agrin defines polarized distribution of orthogonal arrays of particles in astrocytes. *Cell and Tissue Research*, *337*(2), 185–195. https://doi.org/10.1007/s00441-009-0812-z

Nolan, G. P., Fiering, S., Nicolas, J. F., & Herzenberg, L. A. (1988). Fluorescence-activated cell analysis and sorting of viable mammalian cells based on beta-D-galactosidase activity after transduction of Escherichia coli lacZ. *Proceedings of the National Academy of Sciences of the United States of America*, *85*(8), 2603–7. https://doi.org/10.1073/pnas.85.8.2603

Nonaka, R., Iesaki, T., de Vega, S., Daida, H., Okada, T., Sasaki, T., & Arikawa-Hirasawa, E. (2015). Perlecan deficiency causes endothelial dysfunction by reducing the expression of endothelial nitric oxide synthase. *Physiological Reports*, *3*(1), e12272. https://doi.org/10.14814/phy2.12272

Nooteboom, A., Hendriks, T., Ottehöller, I., & Van Der Linden, C. J. (2000). Permeability

characteristics of human endothelial monolayers seeded on different extracellular matrix proteins. *Mediators of Inflammation*, *9*(5), 235–241. https://doi.org/10.1080/09629350020025755

Norrby, K. (2006). In vivo models of angiogenesis. *J Cell Mol Med*, *10*(3), 588–612. https://doi.org/10.2755/jcmm010.003.01

Nuki, Y., Tsou, T.-L., Kurihara, C., Kanematsu, M., Kanematsu, Y., & Hashimoto, T. (2009). Elastase-Induced Intracranial Aneurysms in Hypertensive Mice. *Hypertension*, *54*(6), 1337–1344. https://doi.org/10.1161/HYPERTENSIONAHA.109.138297

Nyström, A., Shaik, Z. P., Gullberg, D., Krieg, T., Eckes, B., Zent, R., … Iozzo, R. V. (2009). Role of tyrosine phosphatase SHP-1 in the mechanism of endorepellin angiostatic activity. *Blood*, *114*(23), 4897–4906. https://doi.org/10.1182/blood-2009-02-207134

O'Callaghan, P., Li, J. P., Lannfelt, L., Lindahl, U., & Zhang, X. (2015). Microglial heparan sulfate proteoglycans facilitate the cluster-of-differentiation 14 (CD14)(WARNING)Toll-like receptor 4 (TLR4)-dependent inflammatory response. *Journal of Biological Chemistry*, *290*(24), 14904–14914. https://doi.org/10.1074/jbc.M114.634337

O'Neil, D., Glowatz, H., & Schlumpberge, M. (2013). Ribosomal RNA depletion for efficient use of RNA-seq capacity. *Current Protocols in Molecular Biology*, (SUPPL.103). https://doi.org/10.1002/0471142727.mb0419s103

O'Reilly, M. S., Boehm, T., Shing, Y., Fukai, N., Vasios, G., Lane, W. S., … Folkman, J. (1997). Endostatin: an endogenous inhibitor of angiogenesis and tumor growth. *Cell*, *88*(2), 277–285. https://doi.org/10.1016/S0092-8674(00)81848-6

Obermeier, B., Daneman, R., & Ransohoff, R. M. (2013). Development, maintenance and disruption of the blood-brain barrier. *Nature Medicine*, *19*(12), 1584–96. https://doi.org/10.1038/nm.3407

Oh, S. P., Seki, T., Goss, K. A., Imamura, T., Yi, Y., Donahoe, P. K., … Li, E. (2000). Activin receptor-like kinase 1 modulates transforming growth factor-beta 1 signaling in the regulation of angiogenesis. *Proceedings of the National Academy of Sciences of the United States of America*, *97*(6), 2626–31. https://doi.org/10.1073/pnas.97.6.2626

Ohta, K., Lupo, G., Kuriyama, S., Keynes, R., Holt, C. E., Harris, W. A., … Ohnuma, S. I. (2004). Tsukushi functions as an organizer inducer by inhibition of BMP activity in cooperation with chordin. *Developmental Cell*, *7*(3), 347–358. https://doi.org/10.1016/j.devcel.2004.08.014

Okroj, M., Heinegård, D., Holmdahl, R., & Blom, A. M. (2007). Rheumatoid arthritis and the complement system. *Annals of Medicine*, *39*(7), 517–530. https://doi.org/10.1080/07853890701477546

Ono, K., Hattori, H., & Takeshita, S. (1999). Structural features in heparin that interact with VEGF

165 and modulate its biological activity. *Glycobiology*, *9*(7), 705–711.

Ornitz, D. M., Yayon, A., Flanagan, J. G., Svahn, C. M., Levi, E., & Leder, P. (1992). Heparin is required for cell-free binding of basic fibroblast growth factor to a soluble receptor and for mitogenesis in whole cells. *Molecular and Cellular Biology*, *12*(1), 240–7. https://doi.org/10.1128/mcb.12.1.240

Oshima, M., Oshima, H., & Taketo, M. M. (1996). TGF-beta receptor type II deficiency results in defects of yolk sac hematopoiesis and vasculogenesis. *Developmental Biology*, *179*(259), 297–302. https://doi.org/10.1006/dbio.1996.0259

Ostman, a, Andersson, M., Betsholtz, C., Westermark, B., & Heldin, C. H. (1991). Identification of a cell retention signal in the B-chain of platelet-derived growth factor and in the long splice version of the A-chain. *Cell Regulation*, *2*(7), 503–12. Retrieved from http://www.pubmedcentral.nih.gov/articlerender.fcgi?artid=361840&tool=pmcentrez&rendertype=abstract

Owens, G. K., Kumar, M. S., & Wamhoff, B. R. (2004). Molecular Regulation of Vascular Smooth Muscle Cell Differentiation in Development and Disease PLAYS A KEY ROLE IN A NUMBER OF, 767–801. https://doi.org/10.1152/physrev.00041.2003

Ozerdem, U., Grako, K. a, Dahlin-Huppe, K., Monosov, E., & Stallcup, W. B. (2001). NG2 proteoglycan is expressed exclusively by mural cells during vascular morphogenesis. *Developmental Dynamics : An Official Publication of the American Association of Anatomists*, *222*(2), 218–27. https://doi.org/10.1002/dvdy.1200

Pardridge, W. M. (2005). The blood-brain barrier: Bottleneck in brain drug development. *NeuroRX*, *2*(1), 3–14. https://doi.org/10.1602/neurorx.2.1.3

Park, J. E., Keller, G. A., & Ferrara, N. (1993). The vascular endothelial growth factor (VEGF) isoforms: differential deposition into the subepithelial extracellular matrix and bioactivity of extracellular matrix-bound VEGF. *Molecular Biology of the Cell*, *4*(12), 1317–1326. https://doi.org/10.1091/mbc.4.12.1317

Park, K. M., Gerecht, S., Asahara, T., Murohara, T., Sullivan, A., Silver, M., … Basile, J. R. (2014). Harnessing developmental processes for vascular engineering and regeneration. *Development (Cambridge, England)*, *141*(14), 2760–9. https://doi.org/10.1242/dev.102194

Patan, S. (2000). Vasculogenesis and Angiogenesis as Mechanisms of Vascular Network Formation, Growth and Remodeling. *Journal of Neuro-Oncology*, *50*(1), 1–15. https://doi.org/10.1023/A:1006493130855

Patel-Hett, S., & D'Amore, P. A. (2011). Signal transduction in vasculogenesis and developmental angiogenesis. *International Journal of Developmental Biology*, *55*(4–5), 353–369. https://doi.org/10.1387/ijdb.103213sp

Peeters, A., Palay, S., & Webster, H. (1991). The Fine Structure of the Nervous System: the Neurons and Supporting Cells. In A. Peeters (Ed.) (3rd editio, pp. 395–406). Philadelphia: W.B. Saunders.

Pei, L., Castrillo, A., & Tontonoz, P. (2006). Regulation of macrophage inflammatory gene expression by the orphan nuclear receptor Nur77. *Molecular Endocrinology (Baltimore, Md.)*, *20*(4), 786–794. https://doi.org/10.1210/me.2005-0331

Peng, X., Karna, P., Cao, Z., Jiang, B., Zhou, M., & Yang, L. (2006). Cross-talk between Epidermal Growth Factor Receptor and Hypoxia-inducible Factor-1 Signal Pathways Increases Resistance to Apoptosis by Up-regulating Survivin Gene Expression *. *The Journal of Biological Chemistry*, *281*(36), 25903–25914. https://doi.org/10.1074/jbc.M603414200

Perez, F. (2013). Serial Cloner 2.6. Retrieved from http://serialbasics.free.fr/Serial_Cloner.html

Pfeiffer, B., Norman, A. W., & Hamprecht, B. (1989). Immunocytochemical characterization of neuron-rich rat brain primary cultures: calbindin D28K as marker of a neuronal subpopulation. *Brain Research*, *476*(1), 120–128. https://doi.org/https://doi.org/10.1016/0006-8993(89)91543-6

Politis, M., Lahiri, N., Niccolini, F., Su, P., Wu, K., Giannetti, P., … Piccini, P. (2015). Increased central microglial activation associated with peripheral cytokine levels in premanifest Huntington's disease gene carriers. *Neurobiology of Disease*, *83*, 115–121. https://doi.org/10.1016/j.nbd.2015.08.011

Polito, A., & Reynolds, R. (2005). NG2-expressing cells as oligodendrocyte progenitors in the normal and demyelinated adult central nervous system. *Journal of Anatomy*, *207*, 707–716.

Pollex, R. L., & Hegele, R. A. (2004). Hutchinson–Gilford progeria syndrome. *Clinical Genetics*, *66*(5), 375–381. https://doi.org/10.1111/j.1399-0004.2004.00315.x

Polte, T. R., Hanks, S. K., & Naftilan, A. J. (1994). Focal adhesion kinase is abundant in developing blood vessels and elevation of its phosphotyrosine content in vascular smooth muscle cells is a rapid response to angiotensin II. *Journal of Cellular Biochemistry*, *55*(1), 106–119. https://doi.org/10.1002/jcb.240550113

Poopalasundaram, S., Knott, C., Shamotienko, O. G., Foran, P. G., Dolly, J. O., Ghiani, C. a., … Wilkin, G. P. (2000). Glial heterogeneity in expression of the inwardly rectifying K+ channel, Kir4.1, in adult rat CNS. *Glia*, *30*(4), 362–372. https://doi.org/10.1002/(SICI)1098-1136(200006)30:4<362::AID-GLIA50>3.0.CO;2-4

Pore, N., Jiang, Z., Gupta, A., Cerniglia, G., Kao, G. D., & Maity, A. (2006). EGFR Tyrosine Kinase Inhibitors Decrease VEGF Expression by Both Hypoxia-Inducible Factor (HIF) -1 – Independent and HIF-1 – Dependent Mechanisms. *Cancer Research*, *66*(6), 3197–3205. https://doi.org/10.1158/0008-5472.CAN-05-3090

Poschl, E., Schlötzer-Schrehardt, U., Brachvogel, B., Saito, K., Ninomiya, Y., & Mayer, U. (2004). Collagen IV is essential for basement membrane stability but dispensable for initiation of its assembly during early development. *Development*, *131*(7), 1619–1628. https://doi.org/10.1242/dev.01037

Pusch, C. M., Zeitz, C., Brandau, O., Pesch, K., Achatz, H., Feil, S., … Meindl, A. (2000). The complete form of X-linked congenital stationary night blindness is caused by mutations in a gene encoding a leucine-rich repeat protein. *Nat Genet*, *26*(3), 324–327. Retrieved from http://dx.doi.org/10.1038/81627

Qi, J. H., & Claesson-Welsh, L. (2001). VEGF-Induced Activation of Phosphoinositide 3-Kinase Is Dependent on Focal Adhesion Kinase. *Experimental Cell Research*, *263*(1), 173–182. https://doi.org/10.1006/excr.2000.5102

Qin, L., Zhao, D., Xu, J., Ren, X., Terwilliger, E. F., Parangi, S., … Zeng, H. (2013). The vascular permeabilizing factors histamine and serotonin induce angiogenesis through TR3/Nur77 and subsequently truncate it through thrombospondin-1. *Blood*, *121*(11), 2154–2164. https://doi.org/10.1182/blood-2012-07-443903

Raghu, H., Lepus, C. M., Wang, Q., Wong, H. H., Lingampalli, N., Oliviero, F., … Robinson, W. H. (2017). CCL2/CCR2, but not CCL5/CCR5, mediates monocyte recruitment, inflammation and cartilage destruction in osteoarthritis. *Annals of the Rheumatic Diseases*, *76*(5), 914 LP-922. Retrieved from http://ard.bmj.com/content/76/5/914.abstract

Ramjaun, A. R., & Hodivala-Dilke, K. (2009). The role of cell adhesion pathways in angiogenesis. *International Journal of Biochemistry and Cell Biology*, *41*(3), 521–530. https://doi.org/10.1016/j.biocel.2008.05.030

Raper, D., Louveau, A., & Kipnis, J. (2016). How Do Meningeal Lymphatic Vessels Drain the CNS? *Trends in Neurosciences*, *39*(9), 581–586. https://doi.org/10.1016/j.tins.2016.07.001

Rapraeger, A. C., Krufka, A., & Olwin, B. B. (1991). Requirement of Heparan Sulfate for bFGF-Mediated Fibroblast Growth and Myoblast Differentiation. *Science*, *252*(June 1989), 1705–1708.

Rascher, G., Fischmann, A., Kröger, S., Duffner, F., Grote, E. H., & Wolburg, H. (2002). Extracellular matrix and the blood-brain barrier in glioblastoma multiforme: Spatial segregation of tenascin and agrin. *Acta Neuropathologica*, *104*(1), 85–91. https://doi.org/10.1007/s00401-002-0524-x

Reagan, F. P. (1915). Vascularization phenomena in fragments of embryonic bodies completely isolated from yolk-sac blastoderm. *The Anatomical Record*, *9*(4), 329–341. https://doi.org/10.1002/ar.1090090406

Reardon, A. J., Le Goff, M. L., Briggs, M. D., McLeod, D., Sheehan, J. K., Thornton, D. J., & Bishop, P. N.

(2000). Identification in vitreous and molecular cloning of opticin, a novel member of the family of leucine-rich repeat proteins of the extracellular matrix. *Journal of Biological Chemistry*, *275*(3), 2123–2129. https://doi.org/10.1074/jbc.275.3.2123

Reed, C. C., & Iozzo, R. V. (2002). The role of decorin in collagen fibrillogenesis and skin homeostasis. *Glycoconjugate Journal*, *19*(4–5), 249–255. https://doi.org/10.1023/A:1025383913444

Rehn, A. P., Cerny, R., Sugars, R. V, Kaukua, N., & Wendel, M. (2008). Osteoadherin is upregulated by mature osteoblasts and enhances their in vitro differentiation and mineralization. *Calcified Tissue International*, *82*(6), 454–64. https://doi.org/10.1007/s00223-008-9138-1

Rehn, A. P., Chalk, A. M., & Wendel, M. (2006). Differential regulation of osteoadherin (OSAD) by TGF-beta1 and BMP-2. *Biochemical and Biophysical Research Communications*, *349*(3), 1057–1064. https://doi.org/10.1016/j.bbrc.2006.08.133

Reich-Schupke, S., Mumme, A., Altmeyer, P., & Stuecker, M. (2011). Decorin Expression with Stump Recurrence and Neovascularization after Varicose Vein Surgery—a Pilot Study. *Dermatologic Surgery*, *37*(4). Retrieved from http://journals.lww.com/dermatologicsurgery/Fulltext/2011/04000/Decorin_Expression_with_Stump_Recurrence_and.12.aspx

Rensen, S. S. M., Doevendans, P. A. F. M., & van Eys, G. J. J. M. (2007). Regulation and characteristics of vascular smooth muscle cell phenotypic diversity. *Netherlands Heart Journal : Monthly Journal of the Netherlands Society of Cardiology and the Netherlands Heart Foundation*, *15*(3), 100–8. https://doi.org/10.1007/BF03085963

Ribatti, D., Nico, B., & Crivellato, E. (2011). The role of pericytes in angiogenesis. *International Journal of Developmental Biology*, *55*(3), 261–268. https://doi.org/10.1387/ijdb.103167dr

Rigato, C., Buckinx, R., Le-Corronc, H., Rigo, J. M., & Legendre, P. (2011). Pattern of invasion of the embryonic mouse spinal cord by microglial cells at the time of the onset of functional neuronal networks. *Glia*, *59*(4), 675–695. https://doi.org/10.1002/glia.21140

Risau, W. (1997). Mechanisms of angiogenesis. *Nature*. https://doi.org/10.1146/annurev.physiol.49.1.453

Risau, W., & Wolburg, H. (1990). Development of the blood-brain barrier. *Trends in Neurosciences*, *13*(5), 174–178. https://doi.org/10.1007/s00441-003-0751-z

Robertson, R. T., Levine, S. T., Haynes, S. M., Gutierrez, P., Baratta, J. L., Tan, Z., & Longmuir, K. J. (2014). Use of labeled tomato lectin for imaging vasculature structures. *Histochemistry and Cell Biology*, *143*(2), 225–234. https://doi.org/10.1007/s00418-014-1301-3

Robinson, D. (2014). How to interpret a p-value histogram. Retrieved March 13, 2017, from http://varianceexplained.org/statistics/interpreting-pvalue-histogram/

Rogers, M. S., Birsner, A. E., & Amato, R. J. D. (2007). The mouse cornea micropocket angiogenesis assay. *Nature Protocols*, *2*(10), 2545–2550. https://doi.org/10.1038/nprot.2007.368

Romer, L. H., McLean, N., Turner, C. E., & Burridge, K. (1994). Tyrosine kinase activity, cytoskeletal organization, and motility in human vascular endothelial cells. *Molecular Biology of the Cell*, *5*(3), 349–61. https://doi.org/10.1091/mbc.5.3.349

Ronaldson, P. T., Demarco, K. M., Sanchez-Covarrubias, L., Solinsky, C. M., & Davis, T. P. (2009). Transforming growth factor-beta signaling alters substrate permeability and tight junction protein expression at the blood-brain barrier during inflammatory pain. *Journal of Cerebral Blood Flow and Metabolism : Official Journal of the International Society of Cerebral Blood Flow and Metabolism*, *29*(6), 1084–98. https://doi.org/10.1038/jcbfm.2009.32

Rosenstein, J. M., Mani, N., Silverman, W. F., & Krum, J. M. (1998). Patterns of brain angiogenesis after vascular endothelial growth factor administration in vitro and in vivo. *Proceedings of the National Academy of Sciences of the United States of America*, *95*(June), 7086–7091.

Ross, M. D., Bruggeman, L. A., Hanss, B., Sunamoto, M., Marras, D., Klotman, M. E., & Klotman, P. E. (2003). Podocan, a novel small leucine-rich repeat protein expressed in the sclerotic glomerular lesion of experimental HIV-associated nephropathy. *Journal of Biological Chemistry*, *278*(35), 33248–33255. https://doi.org/10.1074/jbc.M301299200

Rozakis-Adcock, M., Fernley, R., Wade, J., Pawson, T., & Bowtell, D. (1993). The SH2 and SH3 domains of mammalian Grb2 couple the EGF receptor to the Ras activator mSos1. *Nature*, *363*(6 May), 83–85.

Rucci, N., Rufo, A., Alamanou, M., Capulli, M., Del Fattore, A., Ahrman, E., … Teti, A. (2009). The glycosaminoglycan-binding domain of PRELP acts as a cell type-specific NF-kappaB inhibitor that impairs osteoclastogenesis. *The Journal of Cell Biology*, *187*(5), 669–83. https://doi.org/10.1083/jcb.200906014

Ruhrberg, C., & Bautch, V. L. (2013). Neurovascular development and links to disease. *Cellular and Molecular Life Sciences*, *70*(10), 1675–1684. https://doi.org/10.1007/s00018-013-1277-5

Rymo, S. F., Gerhardt, H., Sand, F. W., Lang, R., Uv, A., & Betsholtz, C. (2011). A two-way communication between microglial cells and angiogenic sprouts regulates angiogenesis in aortic ring cultures. *PLoS ONE*, *6*(1). https://doi.org/10.1371/journal.pone.0015846

Sabin, F. (1920). Studies on the origin of blood-vessels and of red blood-corpuscles as seen in the living blastoderm of chicks during the second day of incubation. *Contrib Embryol*, *26*, 213–259.

Sagare, A. P., Bell, R. D., Zhao, Z., Ma, Q., Winkler, E. A., Ramanathan, A., & Zlokovic, B. V. (2013). Pericyte loss influences Alzheimer-like neurodegeneration in mice. *Nat Commun*, *4*, 2932. https://doi.org/10.1038/ncomms3932

Saitou, M., Furuse, M., Sasaki, H., Schulzke, J.-D., Fromm, M., Takano, H., … Tsukita, S. (2000). Complex Phenotype of Mice Lacking Occludin, a Component of Tight Junction Strands. *Molecular Biology of the Cell*, *11*(12), 4131–4142. https://doi.org/10.1091/mbc.11.12.4131

Samuel, M. A., Valdez, G., Tapia, J. C., Lichtman, J. W., & Sanes, J. R. (2012). Agrin and Synaptic Laminin Are Required to Maintain Adult Neuromuscular Junctions. *PLoS ONE*, *7*(10). https://doi.org/10.1371/journal.pone.0046663

Schaefer, L., Babelova, A., Kiss, E., Hausser, H. J., Baliova, M., Krzyzankova, M., … Gröne, H. J. (2005). The matrix component biglycan is proinflammatory and signals through Toll-like receptors 4 and 2 in macrophages. *Journal of Clinical Investigation*, *115*(8), 2223–2233. https://doi.org/10.1172/JCI23755

Schellenberg, A. E., Buist, R., Del Bigio, M. R., Toft-Hansen, H., Khorooshi, R., Owens, T., & Peeling, J. (2012). Blood-brain barrier disruption in CCL2 transgenic mice during pertussis toxin-induced brain inflammation. *Fluids and Barriers of the CNS*, *9*(1), 10. https://doi.org/10.1186/2045-8118-9-10

Schlessinger, J. (2000). Cell Signaling by Receptor Tyrosine Kinases A large group of genes in all eukaryotes encode for. *October*, *103*(2), 211–225. https://doi.org/10.1016/j.cell.2010.06.011

Schlessinger, J., Plotnikov, A. N., Ibrahimi, O. A., Eliseenkova, A. V., Yeh, B. K., Yayon, A., … Mohammadi, M. (2000). Crystal Structure of a Ternary FGF-FGFR-Heparin Complex Reveals a Dual Role for Heparin in FGFR Binding and Dimerization. *Molecular Cell*, *6*(3), 743–750. https://doi.org/10.1016/S1097-2765(00)00073-3

Schönherr, E., Broszat, M., Brandan, E., Bruckner, P., & Kresse, H. (1998). Decorin core protein fragment Leu155-Val260 interacts with TGF-beta but does not compete for decorin binding to type I collagen. *Arch. Biochem. Biophys.*, *355*(2), 241–8. https://doi.org/10.1006/abbi.1998.0720

Schönherr, E., Sunderkötter, C., Schaefer, L., Thanos, S., Grässel, S., Oldberg, Å., … Kresse, H. (2004). Decorin Deficiency Leads to Impaired Angiogenesis in Injured Mouse Cornea. *Journal of Vascular Research*, *41*(6), 499–508. Retrieved from http://www.karger.com/DOI/10.1159/000081806

Schroeder, A., Mueller, O., Stocker, S., Salowsky, R., Leiber, M., Gassmann, M., … Ragg, T. (2006). The RIN: an RNA integrity number for assigning integrity values to RNA measurements. *BMC Molecular Biology*, *7*(1), 3. https://doi.org/10.1186/1471-2199-7-3

Schwaninger, M., Sallmann, S., Petersen, N., Schneider, A., Prinz, S., Libermann, T. A., & Spranger, M. (1999). Bradykinin induces interleukin-6 expression in astrocytes through activation of nuclear factor-??B. *Journal of Neurochemistry*, *73*(4), 1461–1466.

https://doi.org/10.1046/j.1471-4159.1999.0731461.x

Schymeinsky, J., Nedbal, S., Miosge, N., Pöschl, E., Rao, C., Beier, D. R., … Bader, B. L. (2002). Gene structure and functional analysis of the mouse nidogen-2 gene: nidogen-2 is not essential for basement membrane formation in mice. *Molecular and Cellular Biology*, *22*(19), 6820–30. https://doi.org/10.1128/MCB.22.19.6820

Scott, J. E., & Orford, C. R. (1981). Dermatan sulphate-rich proteoglycan associates with rat tail-tendon collagen at the d band in the gap region. *Biochemical Journal*, *197*(1), 213–216. https://doi.org/10.1042/bj1970213

Segawa, Y., Muneta, T., Makino, H., Nimura, A., Mochizuki, T., Ju, Y. J., … Sekiya, I. (2009). Mesenchymal stem cells derived from synovium, meniscus, anterior cruciate ligament, and articular chondrocytes share similar gene expression profiles. *Journal of Orthopaedic Research*, *27*(4), 435–441. https://doi.org/10.1002/jor.20786

Senger, D., Galli, S., Dvorak, A., Perruzzi, C., Harvey, V., & Dvorak, H. (1983). Tumor cells secrete a vascular permeability factor that promotes accumulation of ascites fluid. *Science*, *219*, 983–986. https://doi.org/10.1126/science.6823562

Shalaby, F., Rossant, J., Yamaguchi, T. P., Gertsenstein, M., Wu, X. F., Breitman, M. L., & Schuh, a C. (1995). Failure of blood-island formation and vasculogenesis in Flk-1-deficient mice. *Nature*. https://doi.org/10.1038/376062a0

Sharma, B., Ramus, M. D., Kirkwood, C. T., Sperry, E. E., Chu, P. H., Kao, W. W., & Albig, A. R. (2013). Lumican exhibits anti-angiogenic activity in a context specific manner. *Cancer Microenvironment*, *6*(3), 263–271. https://doi.org/10.1007/s12307-013-0134-2

Shibuya, M. (2011). Vascular Endothelial Growth Factor (VEGF) and Its Receptor (VEGFR) Signaling in Angiogenesis: A Crucial Target for Anti- and Pro-Angiogenic Therapies. *Genes & Cancer*, *2*(12), 1097–1105. https://doi.org/10.1177/1947601911423031

Sievers, F., Wilm, A., Dineen, D., Gibson, T. J., Karplus, K., Li, W., … Higgins, D. G. (2011). Fast, scalable generation of high-quality protein multiple sequence alignments using Clustal Omega. *Molecular Systems Biology*, *7*(539), 1–6. https://doi.org/10.1038/msb.2011.75

Simon-Assmann, P., Orend, G., Mammadova-Bach, E., Spenle, C., & Lefebvre, O. (2011). Role of laminins in physiological and pathological angiogenesis. *The International Journal of Developmental Biology*, *55*(4–5), 455–465. https://doi.org/10.1387/ijdb.103223ps

Sixt, M., Engelhardt, B., Pausch, F., Hallmann, R., Wendler, O., & Sorokin, L. M. (2001). Roles in T Cell Recruitment Across the Blood – Brain Barrier in Experimental Autoimmune Encephalomyelitis. *The Journal of Cell Biology*, *153*(5), 933–945.

Sjöberg, A., Önnerfjord, P., Mörgelin, M., Heinegård, D., & Blom, A. M. (2005). The extracellular matrix and inflammation: Fibromodulin activates the classical pathway of complement by

directly binding C1q. *Journal of Biological Chemistry*, *280*(37), 32301–32308. https://doi.org/10.1074/jbc.M504828200

Sjöberg, A. P., Manderson, G. A., Mörgelin, M., Day, A. J., Heinegård, D., & Blom, A. M. (2009). Short leucine-rich glycoproteins of the extracellular matrix display diverse patterns of complement interaction and activation. *Molecular Immunology*, *46*(5), 830–839. https://doi.org/10.1016/j.molimm.2008.09.018

Sofroniew, M. V., & Vinters, H. V. (2010). Astrocytes: Biology and pathology. *Acta Neuropathologica*, *119*(1), 7–35. https://doi.org/10.1007/s00401-009-0619-8

Soltoff, S. P., & Cantley, L. C. (1996). p120 cbl Is a Cytosolic Adapter Protein That Associates with Phosphoinositide 3-Kinase in Response to Epidermal Growth Factor in PC12 and Other Cells *. *The Journal of Biological Chemistry*, *271*(1), 563–567.

Sommarin, Y., Wendel, M., Hellman, U., Heinegård, D., & Shen, Z. (1998). PROTEIN CHEMISTRY AND STRUCTURE : Osteoadherin , a Cell-binding Keratan Sulfate Proteoglycan in Bone , Belongs to the Family of Leucine-rich Repeat Proteins of the Extracellular Matrix Osteoadherin , a Cell-binding Keratan Sulfate Proteoglycan in Bone , B. *The Journal of Biological Chemistry*, *273*(27), 16723–16729. https://doi.org/10.1074/jbc.273.27.16723

Song, J., Zhang, X., Buscher, K., Wang, Y., Wang, H., Di Russo, J., … Sorokin, L. (2017). Endothelial Basement Membrane Laminin 511 Contributes to Endothelial Junctional Tightness and Thereby Inhibits Leukocyte Transmigration. *Cell Reports*, *18*(5), 1256–1269. https://doi.org/10.1016/j.celrep.2016.12.092

Soriano, P. (1994). Abnormal kidney development and hematological disorders in PDGF beta-receptor mutant mice. *Genes & Development*, *8*(16), 1888–1896. https://doi.org/10.1101/gad.8.16.1888

Sorokin, L. M., Pausch, F., Frieser, M., Kröger, S., Ohage, E., & Deutzmann, R. (1997). Developmental regulation of the laminin alpha5 chain suggests a role in epithelial and endothelial cell maturation. *Developmental Biology*, *189*(2), 285–300. https://doi.org/10.1006/dbio.1997.8668

Srinivasan, B., Kolli, A. R., Esch, M. B., Abaci, H. E., Shuler, M. L., & Hickman, J. J. (2015). TEER Measurement Techniques for In Vitro Barrier Model Systems. *Journal of Laboratory Automation*, *20*(2), 107–126. https://doi.org/10.1177/2211068214561025

Stafford, P., & Brun, M. (2007). Three methods for optimization of cross-laboratory and cross-platform microarray expression data. *Nucleic Acids Research*, *35*(10). https://doi.org/10.1093/nar/gkl1133

Stenman, J. M., Rajagopal, J., Carroll, T. J., Ishibashi, M., McMahon, J., & McMahon, A. P. (2008). Canonical Wnt Signaling Regulates Organ-Specific Assembly and Differentiation of CNS

Vasculature. *Science*, *322*(5905), 1247 LP-1250. Retrieved from http://science.sciencemag.org/content/322/5905/1247.abstract

Stichel, C. C., Kappler, J., Junghans, U., Koops, a, Kresse, H., & Müller, H. W. (1995). Differential expression of the small chondroitin/dermatan sulfate proteoglycans decorin and biglycan after injury of the adult rat brain. *Brain Research*, *704*(2), 263–74. Retrieved from http://www.ncbi.nlm.nih.gov/pubmed/8788923

Strachan, R., Wood, J., & Hirschmann, R. (1961). Synthesis and Properties of 4-Methyl-2-oxo-1,2-benzopyran-7-yl β-D-Galactosidase (Galactosidase of 4-Methylumbelliferone). *Journal of Organic Chemistry*, *27*, 1074–1075.

Streit, W. J., Braak, H., Xue, Q. S., & Bechmann, I. (2009). Dystrophic (senescent) rather than activated microglial cells are associated with tau pathology and likely precede neurodegeneration in Alzheimer's disease. *Acta Neuropathologica*, *118*(4), 475–485. https://doi.org/10.1007/s00401-009-0556-6

Stuurman, N., Edelstein, A. D., Amodaj, N., Hoover, K. H., & Ronald, D. (2011). Computer Control of Microscopes using μ Manager, 1–22. https://doi.org/10.1002/0471142727.mb1420s92.Computer

Subramanian, A., Tamayo, P., Mootha, V. K., Mukherjee, S., Ebert, B. L., Gillette, M. A., … Mesirov, J. P. (2005). Gene set enrichment analysis: A knowledge-based approach for interpreting genome-wide expression profiles. *Proceedings of the National Academy of Sciences*, *102*(43), 15545–15550. https://doi.org/10.1073/pnas.0506580102

Sugimoto, M., Cutler, A., Shen, B., Moss, S. E., Iyengar, S. K., Klein, R., & Folkman, J. (2013). Inhibition of EGF Signaling Protects the Diabetic Retina from Insulin-Induced Vascular Leakage. *The American Journal of Pathology*, *183*(3), 987–995. https://doi.org/10.1016/j.ajpath.2013.05.017

Sulochana, K. N., Fan, H., Jois, S., Subramanian, V., Sun, F., Kini, R. M., & Ge, R. (2005). Peptides derived from human decorin leucine-rich repeat 5 inhibit angiogenesis. *Journal of Biological Chemistry*, *280*(30), 27935–27948. https://doi.org/10.1074/jbc.M414320200

Sumi, N., Nishioku, T., Takata, F., Matsumoto, J., Watanabe, T., Shuto, H., … Kataoka, Y. (2010). Lipopolysaccharide-activated microglia induce dysfunction of the blood-brain barrier in rat microvascular endothelial cells co-cultured with microglia. *Cellular and Molecular Neurobiology*, *30*(2), 247–253. https://doi.org/10.1007/s10571-009-9446-7

Suri, C., Jones, P. F., Patan, S., Bartunkova, S., Maisonpierre, P. C., Davis, S., … Yancopoulos, G. D. (1996). Requisite Role of Angiopoietin-1 , a Ligand for the TIE2 Receptor , during Embryonic Angiogenesis. *CELL*, *87*(7), 1171–1180. https://doi.org/10.1016/S0092-8674(00)81813-9

Svensson, L., Aszódi, A., Reinholt, F. P., Fässler, R., Heinegård, D., & Oldberg, Å. (1999).

Fibromodulin-null mice have abnormal collagen fibrils, tissue organization, and altered lumican deposition in tendon. *Journal of Biological Chemistry*, *274*(14), 9636–9647. https://doi.org/10.1074/jbc.274.14.9636

Szklarczyk, D., Franceschini, A., Wyder, S., Forslund, K., Heller, D., Huerta-Cepas, J., … Von Mering, C. (2015). STRING v10: Protein-protein interaction networks, integrated over the tree of life. *Nucleic Acids Research*, *43*(D1), D447–D452. https://doi.org/10.1093/nar/gku1003

Taddei, A., Giampietro, C., Conti, A., Orsenigo, F., Breviario, F., Pirazzoli, V., … Dejana, E. (2008). Endothelial adherens junctions control tight junctions by VE-cadherin-mediated upregulation of claudin-5. *Nature Cell Biology*, *10*(8), 923–934. https://doi.org/10.1038/ncb1752

Takashima, S., Kitakaze, M., Asakura, M., Asanuma, H., Sanada, S., Tashiro, F., … Hori, M. (2002). Targeting of both mouse neuropilin-1 and neuropilin-2 genes severely impairs developmental yolk sac and embryonic angiogenesis. *Proceedings of the National Academy of Sciences*, *99*(6), 3657–3662. https://doi.org/10.1073/pnas.022017899

Tanaka, Y., & Okada, S. N. and Y. (2005). Osteoblasts and Osteoclasts in Bone Remodeling and Inflammation. *Current Drug Targets - Inflammation & Allergy*. https://doi.org/http://dx.doi.org/10.2174/1568010054022015

Tashima, T., Nagatoishi, S., Sagara, H., Ohnuma, S., & Tsumoto, K. (2015). Osteomodulin regulates diameter and alters shape of collagen fibrils. *Biochemical and Biophysical Research Communications*, *463*(3), 292–296. https://doi.org/10.1016/j.bbrc.2015.05.053

Tau, G., & Rothman, P. (1999). Biologic functions of the IFN-gamma receptors. *Allergy*, *54*(12), 1233–51. https://doi.org/10.1016/j.drudis.2011.09.009

Tenu, J.-P., Viratelle, O. M., & Yon, J. (1972). Kinetic Study of the Activation Process of b-Galactosidase from Escherichia coli by Mg2+. *European Journal of Biochemistry / FEBS*, *26*, 112–118.

Thurston, G., Suri, C., Smith, K., Mcclain, J., Sato, T. N., Yancopoulos, G. D., & Mcdonald, D. M. (1999). Leakage-Resistant Blood Vessels in Mice Transgenically Overexpressing Angiopoietin-1. *Science*, *286*(December), 2511–2515.

Thyberg, J., & Hultgårdh-Nilsson, A. (1994). Fibronectin and the basement membrane components laminin and collagen type IV influence the phenotypic properties of subcultured rat aortic smooth muscle cells differently. *Cell and Tissue Research*, *276*(2), 263–271. https://doi.org/10.1007/BF00306112

Thyboll, J., Kortesmaa, J., Cao, R., Soininen, R., Wang, L., Iivanainen, A., … Tryggvason, K. (2002). Deletion of the Laminin α4 Chain Leads to Impaired Microvessel Maturation. *Molecular and Cellular Biology*, *22*(4), 1194–1202. https://doi.org/10.1128/MCB.22.4.1194

Tietz, S., & Engelhardt, B. (2015). Brain barriers: Crosstalk between complex tight junctions and adherens junctions. *Journal of Cell Biology*, *209*(4), 493–506. https://doi.org/10.1083/jcb.201412147

Too, L. K., Ball, H. J., McGregor, I. S., & Hunt, N. H. (2014). The pro-inflammatory cytokine interferon-gamma is an important driver of neuropathology and behavioural sequelae in experimental pneumococcal meningitis. *Brain, Behavior, and Immunity*, *40*, 252–268. https://doi.org/10.1016/j.bbi.2014.02.020

Tran, P. K., Tran-Lundmark, K., Soininen, R., Tryggvason, K., Thyberg, J., & Hedin, U. (2004). Increased Intimal Hyperplasia and Smooth Muscle Cell Proliferation in Transgenic Mice with Heparan Sulfate-Deficient Perlecan. *Circulation Research*, *94*(4), 550–558. https://doi.org/10.1161/01.RES.0000117772.86853.34

Trapnell, C., Pachter, L., & Salzberg, S. L. (2009). TopHat: Discovering splice junctions with RNA-Seq. *Bioinformatics*, *25*(9), 1105–1111. https://doi.org/10.1093/bioinformatics/btp120

Trapnell, C., & Salzberg, S. L. (2009). How to map billions of short reads onto genomes. *Nature Biotechnology*, *27*(5), 455–457. https://doi.org/10.1038/nbt0509-455.How

Trapnell, C., Williams, B. A., Pertea, G., Mortazavi, A., Kwan, G., van Baren, M. J., … Pachter, L. (2010). Transcript assembly and quantification by RNA-Seq reveals unannotated transcripts and isoform switching during cell differentiation. *Nature Biotechnology*, *28*(5), 511–515. https://doi.org/10.1038/nbt.1621

Tsukita, S., & Furuse, M. (2002). Claudin-based barrier in simple and stratified cellular sheets. *Current Opinion in Cell Biology*, *14*(5), 531–536. https://doi.org/10.1016/S0955-0674(02)00362-9

Tulchinsky, E. (2000). Fos family members: Regulation, structure and role in oncogenic transformation. *Histology and Histopathology*, *15*(3), 921–928.

Ujie, M., Dickenstein, D. L., Carlow, D. A., & Jefferies, W. A. (2003). Blood–Brain Barrier Permeability Precedes Senile Plaque Formation in an Alzheimer Disease Model. *Microcirculation*, *10*(6), 463–470. https://doi.org/10.1080/mic.10.6.463.470

Utriainen, A., Sormunen, R., Kettunen, M., Carvalhaes, L. S., Sajanti, E., Eklund, L., … Pihlajaniemi, T. (2004). Structurally altered basement membranes and hydrocephalus in a type XVIII collagen deficient mouse line. *Human Molecular Genetics*, *13*(18), 2089–2099. https://doi.org/10.1093/hmg/ddh213

van Beijnum, J. R., Rousch, M., Castermans, K., van der Linden, E., & Griffioen, A. W. (2008). Isolation of endothelial cells from fresh tissues. *Nature Protocols*, *3*(6), 1085–1091. https://doi.org/10.1038/nprot.2008.71

Van Gansen, P., & Van Lerberghe, N. (1988). Potential and limitations of cultivated fibroblasts in

the study of senescence in animals. A review on the murine skin fibroblasts system. *Archives of Gerontology and Geriatrics*, *7*(1), 31–74. https://doi.org/10.1016/0167-4943(88)90021-0

Van Hinsbergh, V. W. M., & Koolwijk, P. (2008). Endothelial sprouting and angiogenesis: Matrix metalloproteinases in the lead. *Cardiovascular Research*, *78*(2), 203–212. https://doi.org/10.1093/cvr/cvm102

Verrecchia, F., Chu, M. L., & Mauviel, A. (2001). Identification of Novel TGF-β/Smad Gene Targets in Dermal Fibroblasts using a Combined cDNA Microarray/Promoter Transactivation Approach. *Journal of Biological Chemistry*, *276*(20), 17058–17062. https://doi.org/10.1074/jbc.M100754200

Villacampa, N., Almolda, B., González, B., & Castellano, B. (2013). Microglia, *1041*, 261–279. https://doi.org/10.1007/978-1-62703-520-0

Vokes, S. a, Yatskievych, T. a, Heimark, R. L., McMahon, J., McMahon, A. P., Antin, P. B., & Krieg, P. a. (2004). Hedgehog signaling is essential for endothelial tube formation during vasculogenesis. *Development (Cambridge, England)*, *131*(17), 4371–4380. https://doi.org/10.1242/dev.01304

Wallquist, W., Plantman, S., Thams, S., Thyboll, J., Kortesmaa, J., La, J., … Tryggvason, K. (2005). Impeded Interaction between Schwann Cells and Axons in the Absence of Laminin α4. *The Journal of Neuroscience*, *25*(14), 3692–3700. https://doi.org/10.1523/JNEUROSCI.5225-04.2005

Wang, B., Li, G.-X., Zhang, S.-G., Wang, Q., Wen, Y.-G., Tang, H.-M., … Peng, Z.-H. (2011). Biglycan expression correlates with aggressiveness and poor prognosis of gastric cancer. *Experimental Biology and Medicine (Maywood, N.J.)*, *236*(11), 1247–53. https://doi.org/10.1258/ebm.2011.011124

Wang, D., Cheng, L., Zhang, Y., Wu, R., Wang, M., Gu, Y., … Guo, Z. (2012). Extensive up-regulation of gene expression in cancer: the normalised use of microarray data. *Molecular bioSystems*, *8*(3), 818–27. https://doi.org/10.1039/c2mb05466c

Wang, Y., Wang, N., Cai, B., Wang, G. Y., Li, J., & Piao, X. X. (2015). In vitro model of the blood-brain barrier established by co-culture of primary cerebral microvascular endothelial and astrocyte cells. *Neural Regeneration Research*, *10*(12), 2011–2017. https://doi.org/10.4103/1673-5374.172320

Wang, Z., Gerstein, M., & Snyder, M. (2009). RNA-Seq: a revolutionary tool for transcriptomics. *Nature Reviews. Genetics*, *10*(1), 57–63. https://doi.org/10.1038/nrg2484.RNA-Seq

Weiss, A., & Attisano, L. (2013). The TGFbeta superfamily signaling pathway. *Wiley Interdisciplinary Reviews: Developmental Biology*, *2*(1), 47–63. https://doi.org/10.1002/wdev.86

Welser-alves, J. V, Boroujerdi, A., & Milner, R. (2014). Isolation and Culture of Primary Mouse Brain Endothelial Cells. *Cerebral Angiogenesis: Methods and Protocols*, *1135*, 345–356. https://doi.org/10.1007/978-1-4939-0320-7

Welser, J. V, Li, L., & Milner, R. (2010). Microglial activation state exerts a biphasic influence on brain endothelial cell proliferation by regulating the balance of TNF and TGF-β1. *Journal of Neuroinflammation*, *7*(1), 89. https://doi.org/10.1186/1742-2094-7-89

Wendel, M., Sommarin, Y., & Heinegard, D. (1998). Bone matrix proteins: isolation and characterization of a novel cell-binding keratan sulfate proteoglycan (osteoadherin) from bovine bone. *J Cell Biol*, *141*(3), 839–847. https://doi.org/10.1083/jcb.141.3.839

Wessel, F., Winderlich, M., Holm, M., Frye, M., Rivera-Galdos, R., Vockel, M., … Vestweber, D. (2014). Leukocyte extravasation and vascular permeability are each controlled in vivo by different tyrosine residues of VE-cadherin. *Nat Immunol*, *15*(3), 223–230. https://doi.org/10.1038/ni.2824

Whitelock, J. M., Graham, L. D., Melrose, J., Murdoch, A. D., Iozzo, R. V., & Anne Underwood, P. (1999). Human perlecan immunopurified from different endothelial cell sources has different adhesive properties for vascular cells. *Matrix Biology*, *18*(2), 163–178. https://doi.org/10.1016/S0945-053X(99)00014-1

Winger, R. C., Koblinski, J. E., Kanda, T., Ransohoff, R. M., & Muller, W. A. (2014). Rapid Remodeling of Tight Junctions during Paracellular Diapedesis in a Human Model of the Blood–Brain Barrier. *The Journal of Immunology*, *193*(5), 2427–2437. https://doi.org/10.4049/jimmunol.1400700

Wisniewska-kruk, J., Klaassen, I., Vogels, I. M. C., Magno, A. L., Lai, C., Noorden, C. J. F. Van, … Rakoczy, E. P. (2014). Molecular analysis of blood e retinal barrier loss in the Akimba mouse , a model of advanced diabetic retinopathy. *Experimental Eye Research*, *122*, 123–131. https://doi.org/10.1016/j.exer.2014.03.005

Wolburg-Buchholz, K., Mack, A. F., Steiner, E., Pfeiffer, F., Engelhardt, B., & Wolburg, H. (2009). Loss of astrocyte polarity marks blood-brain barrier impairment during experimental autoimmune encephalomyelitis. *Acta Neuropathologica*, *118*(2), 219–233. https://doi.org/10.1007/s00401-009-0558-4

Wrana, J. L., Attisano, L., Cárcamo, J., Zentella, A., Doody, J., Laiho, M., … Massagué, J. (1992). TGFb signals through a heteromeric protein kinase receptor complex. *Cell*, *71*, 1003–1014.

Wu, C. (2007). Focal Adhesion. *Cell Adhesion & Migration*, *1*(March), 13–18. https://doi.org/10.1074/jbc.M310739200

Wu, Q.-H., Ma, Y., Ruan, C.-C., Yang, Y., Liu, X.-H., Ge, Q., … Gao, P.-J. (2017). Loss of osteoglycin promotes angiogenesis in limb ischaemia mouse models via modulation of vascular

endothelial growth factor and vascular endothelial growth factor receptor 2 signalling pathway. *Cardiovascular Research*, *113*(1), 70–80. https://doi.org/10.1093/cvr/cvw220

Xing, X., Gu, X., Ma, T., & Ye, H. (2014). Biglycan up-regulated vascular endothelial growth factor (VEGF) expression and promoted angiogenesis in colon cancer. *Tumour Biology : The Journal of the International Society for Oncodevelopmental Biology and Medicine*. https://doi.org/10.1007/s13277-014-2779-y

Xu, J., Mcrae, M. A. A., Harron, S., Rob, B., & Huber, R. E. (2004). A study of the relationships of interactions between Asp-201 , Na + or K + , and galactosyl C6 hydroxyl and their effects on binding and reactivity of β-galactosidase. *Biochemistry and Cell Biology*, *82*, 275–284. https://doi.org/10.1139/O04-004

Xu, T., Bianco, P., Fisher, L. W., Longenecker, G., Smith, E., Goldstein, S., … Young, M. F. (1998). Targeted disruption of the biglycan gene leads to an osteoporosis-like phenotype in mice. *Nat Genet*, *20*(1), 78–82. Retrieved from http://dx.doi.org/10.1038/1746

Xue, Y., Gao, X., Lindsell, C. E., Norton, C. R., Chang, B., Hicks, C., … Gridley, T. (1999). Embryonic lethality and vascular defects in mice lacking the Notch ligand Jagged1. *Human Molecular Genetics*, *8*(5), 723–730. https://doi.org/ddc089 [pii]

Yamaguchi, Y., Mann, D. M., & Ruoslahti, E. (1990). Negative regulation of transforming growth factor-[beta] by the proteoglycan decorin. *Nature*, *346*(6281), 281–284. Retrieved from http://dx.doi.org/10.1038/346281a0

Yamamoto, K., Ohga, N., Hida, Y., Maishi, N., Kawamoto, T., Kitayama, K., … Hida, K. (2012). Biglycan is a specific marker and an autocrine angiogenic factor of tumour endothelial cells. *British Journal of Cancer*, *106*(6), 1214–23. https://doi.org/10.1038/bjc.2012.59

Yao, Y., Chen, Z.-L., Norris, E. H., & Strickland, S. (2014). Astrocytic laminin regulates pericyte differentiation and maintains blood brain barrier integrity. *Nature Communications*, *5*, 3413. https://doi.org/10.1038/ncomms4413

Yayon, A., Klagsbrun, M., Leder, P., & Ornitz, D. M. (1991). Cell Surface , Heparin-like Molecules Are Required for Binding of Basic Fibroblast Growth Factor to Its High Affinity Receptor. *Cell*, *64*, 841–848.

Yousif, L. F., Di Russo, J., & Sorokin, L. (2013). Laminin isoforms in endothelial and perivascular basement membranes. *Cell Adhesion and Migration*, *7*(1), 101–110. https://doi.org/10.4161/cam.22680

Yu, C.-Y., Wang, L., Khaletskiy, A., Farrar, W. L., Larner, A., Colburn, N. H., & Li, J. J. (2002). STAT3 activation is required for interleukin-6 induced transformation in tumor-promotion sensitive mouse skin epithelial cells. *Oncogene*, *21*(25), 3949–3960. https://doi.org/10.1038/sj.onc.1205499

Yurchenco, P. D. (2011). Basement membranes: Cell scaffoldings and signaling platforms. *Cold Spring Harbor Perspectives in Biology*, *3*(2), 1–27. https://doi.org/10.1101/cshperspect.a004911

Yurchenco, P. D., & Ruben, G. C. (1987). Basement-Membrane Structure Insitu - Evidence for Lateral Associations in the Type-Iv Collagen Network. *Journal of Cell Biology*, *105*(6), 2559–2568. https://doi.org/10.1083/jcb.105.6.2559

Yurchenco, P. D., Tsilibary, E. C., Charonis, A. S., & Furthmayr, H. (1986). Models for the self-assembly of basement membrane. *Journal of Histochemistry and Cytochemistry*, *34*(1), 93–102. https://doi.org/10.1177/34.1.3510247

Zeisel, A., Muñoz-Manchado, A. B., Codeluppi, S., Lönnerberg, P., La Manno, G., Juréus, A., … Linnarsson, S. (2015). Cell types in the mouse cortex and hippocampus revealed by single-cell RNA-seq. *Science*, *347*(6226), 1138 LP-1142. Retrieved from http://science.sciencemag.org/content/347/6226/1138.abstract

Zeng, H., Qin, L., Zhao, D., Tan, X., Manseau, E. J., Van Hoang, M., … Dvorak, H. F. (2006). Orphan nuclear receptor TR3/Nur77 regulates VEGF-A-induced angiogenesis through its transcriptional activity. *The Journal of Experimental Medicine*, *203*(3), 719–29. https://doi.org/10.1084/jem.20051523

Zhang, G., Chen, S., Goldoni, S., Calder, B. W., Simpson, H. C., Owens, R. T., … Birk, D. E. (2009). Genetic evidence for the coordinated regulation of collagen fibrillogenesis in the cornea by decorin and biglycan. *Journal of Biological Chemistry*, *284*(13), 8888–8897. https://doi.org/10.1074/jbc.M806590200

Zhang, Z. G., Zhang, L., Jiang, Q., Zhang, R., Davies, K., Powers, C., … Chopp, M. (2000). VEGF enhances angiogenesis and promotes blood-brain barrier leakage in the ischemic brain. *Journal of Clinical Investigation*, *106*(7), 829–838. https://doi.org/10.1172/JCI9369

Zhao, S., Fung-Leung, W. P., Bittner, A., Ngo, K., & Liu, X. (2014). Comparison of RNA-Seq and microarray in transcriptome profiling of activated T cells. *PLoS ONE*, *9*(1). https://doi.org/10.1371/journal.pone.0078644

Zhou, Y., & Nathans, J. (2014). Gpr124 controls CNS angiogenesis and blood-brain barrier integrity by promoting ligand-specific canonical Wnt signaling. *Dev Cell*, *31*(2), 248–256. https://doi.org/10.1086/498510.Parasitic

Zhu, Y.-H., Yang, F., Zhang, S.-S., Zeng, T.-T., Xie, X., & Guan, X.-Y. (2013). High expression of biglycan is associated with poor prognosis in patients with esophageal squamous cell carcinoma. *International Journal of Clinical and Experimental Pathology*, *6*(11), 2497–505. Retrieved from http://www.pubmedcentral.nih.gov/articlerender.fcgi?artid=3816819&tool=pmcentrez&r

endertype=abstract

Zoeller, J. J., Whitelock, J. M., & Iozzo, R. V. (2009). Perlecan regulates developmental angiogenesis by modulating the VEGF-VEGFR2 axis. *Matrix Biology*, *28*(5), 284–291. https://doi.org/10.1016/j.matbio.2009.04.010

Zudaire, E., Gambardella, L., Kurcz, C., & Vermeren, S. (2011). A computational tool for quantitative analysis of vascular networks. *PLoS ONE*, *6*(11), 1–12. https://doi.org/10.1371/journal.pone.0027385